RUTHENIUM AND SILVER COMPLEXES OF POTENTIALLY BINUCLEATING PHOSPHORUSPYRIDYL AND PHOSPHORUSBIPYRIDYL LIGANDS

By

CAMPBELL JOHN PARRY B.Sc. (Hons.) (Natal)

A thesis submitted in partial fulfillment of the requirements for the degree of
Doctor of Philosophy in the Faculty of Science
University of Natal, Pietermaritzburg

Department of Chemistry
University of Natal
Pietermaritzburg
November 1994

FOR MY FAMILY

"Every great and commanding moment is the triumph of some enthusiasm"

- RUNNER'S WORLD

ACKNOWLEDGEMENTS

I wish to express my sincere gratitude to **Professors R.J.Haines** and **J.S.Field** for invaluable discussions and expert advice concerning this research project and for their continued interest and encouragement offered to me during the course of this investigation.

I also have a number of other people to thank :

Mr. Martin Watson, for his tireless assistance with regards to the ^1H and $^{31}P\{^1H\}$ nmr spectroscopy discussed in this thesis and in particular for the training received in the operation of nmr spectrometers;
Miss Niyum Ramesar, for her help and guidance during the solving of the X-ray structures discussed herein;
Mr. Paul Forder, for always being available when glassware was urgently required;
Mssrs. Les Mayne, Dave Gregory, Darryl Leibrandt and Chris Morewood, of the Mechanical Instrument Workshop, without whose technical assistance the progress of work would have been substantially slowed;
Mr. Dave Crawley, with whom I worked closely with regards to the ordering of chemicals and who has drawn a number of the diagrams presented in this thesis;
Mrs. Diane Monteiro, for her speed-typing;
Mssrs. Hashim Desai and Raj Somaru, for technical help and elemental analysis;
Dr. Florence Ajulu and the University of Sussex, for collaboration with regards to the high resolution recording of the $^{31}P\{^1H\}$ nmr spectra discussed in Chapter 5;
The Foundation of Research Development and the **University of Natal**, for financial assistance.
My colleagues of the Inorganic Laboratory, what a crazy bunch. Sss sss sss.

Finally, I would not have accomplished anything if it hadn't been for the undying patience and support of my parents and sister in Cape Town. This is for them.

LIST OF ABBREVIATIONS AND SYMBOLS

Å	angstrom
bipy	bipyridyl
Bu	butyl
C	Celsius
cm	centimetre
cod	1,5-cyclooctadiene
C_p	cyclopentadienyl
D_c	calculated density
dmpm	bis(dimethylphosphino)methane
dppa	bis(diphenylphosphino)amine
dppe	bis(diphenylphosphino)ethane
dppm	bis(diphenylphosphino)methane
dppp	bis(diphenylphosphino)pyridine
Et	ethyl
EtOH	ethanol
ν	frequency
g	gram
$\{^1H\}$	proton noise decoupled
H_3PO_4	85% phosphoric acid
i	iso
IR	infra-red
K	Kelvin
λ	radiation wavelength
L	ligand, unless otherwise specified
M	transition metal
M^+	molecular ion
Me	methyl
mg	milligram
mmol	millimole
NCMe	acetonitrile

nmr	nuclear magnetic resonance
Ph	phenyl
Ph_2Pbipy	6-diphenylphosphino-2,2'-bipyridine
Ph_2Ppy	2-diphenylphosphino-pyridine
Ph_2Pquin	2-diphenylphosphino-quinoline
ppm	parts per million
Pr	propyl
py	pyridine
quin	quinoline
R	alkyl group
S	solvent
thf	tetrahydrofuran
tpdo	tetraphenyldiphosphoxane
uv	ultra-violet
X	halide, unless otherwise specified
Xylyl	2,6-dimethylphenyl

SUMMARY

Chapter One outlines the possible modes of coordination of bidentate, potentially binucleating ligands which can be regarded as substituted derivatives of triphenylphosphine *i.e.* ligands such as Ph_2PX [where X = CH_2PPh_2, $(CH_2)_2PPh_2$, $N(R)PPh_2$ (R = alkyl group), $OPPh_2$, pyridine and quinoline] in which substitution of one phenyl group of triphenylphosphine, by a moiety containing another donor atom, has occurred. This serves as an introduction to the coordination chemistry of the 2-diphenylphosphinopyridine (Ph_2Ppy) and 2-diphenylphosphinoquinoline (Ph_2Pquin) ligands discussed in later chapters, as well as to that of the novel tridentate 6-diphenylphosphino-2,2′-bipyridine (Ph_2Pbipy) ligand. The synthesis, characterisation and X-ray crystal structure of the latter ligand is described in Chapter Two; the compound has been shown to crystallise with the bipyridyl fragment in a trans orientation.

In Chapter Three, the reactions of the potentially bridging Ph_2Ppy, Ph_2Pquin and Ph_2Pbipy ligands with diruthenium(I) precursors are described, the aim being to develop diruthenium(I) systems stabilised to fragmentation through the bridging coordination of the ligand. Two suitable precursors have been used. The first, the polymeric carboxylate $[Ru\{\mu\text{-}\eta^2\text{-}OC(R)O\}(CO)_2]_n$, reacts with all three ligands under fairly forcing conditions, affording two types of products for R = H, CH_3 and C_2H_5. One contains the phosphorus-pyridyl or -bipyridyl ligand bound in a monodentate fashion in an axial position (with respect to the Ru-Ru vector) through its phosphorus atom alone *i.e.* $[Ru_2\{\mu\text{-}\eta^2\text{-}OC(R)O\}_2(CO)_4(\eta^1\text{-}L)_2]$ (L = Ph_2Ppy, Ph_2Pquin or Ph_2Pbipy), as confirmed X-ray crystallographically for R = Me and L = Ph_2Ppy. The other is formed from the η^1 species of the above type by refluxing a solution of the compound in the presence of NH_4PF_6. This results in the systematic abstraction of one carboxylate group and subsequent migration of the ligand from a terminal into a bridging position *i.e.* $[Ru_2\{\mu\text{-}\eta^2\text{-}OC(R)O\}(CO)_4(\mu\text{-}L)_2](PF_6)$, as confirmed X-ray crystallographically for R = H and L = Ph_2Ppy. The second precursor used is the novel diruthenium(I) complex $[Ru_2(CO)_4(NCMe)_6](PF_6)_2$, which reacts with the Ph_2Ppy and Ph_2Pbipy ligands, affording synthetically useful ligand-bridged dimers; the former

ligand bridges the dimer in a trans-fashion, as confirmed crystallographically for $[Ru_2(\mu\text{-}Ph_2Ppy)_2(\mu\text{-}CO)_2(NCMe)_4](PF_6)_2$, whereas the latter ligand bridges in a cis-fashion, as found in $[Ru_2(\mu\text{-}Ph_2Pbipy)_2(CO)_2(NCEt)_2](PF_6)_2$, also confirmed crystallographically. In addition, the trans-bridged Ph$_2$Pbipy complex $[Ru_2(\mu\text{-}Ph_2Pbipy)_2(CO)_4](PF_6)_2$ has been synthesised by carrying out the reaction in refluxing acetone, its formula being based on spectroscopic and microanalytical data. Presumably as a result of steric problems, the Ph$_2$Pquin ligand forms only the η^1 species $[Ru_2(CO)_4(NCMe)_4(\eta^1\text{-}Ph_2Pquin)_2](PF_6)_2$ in which the phosphine ligand is bound through its phosphorus atom alone in an axial position with respect to the Ru-Ru vector.

In Chapter Four, the synthesis of mononuclear complexes of ruthenium, in which the Ph$_2$Ppy and Ph$_2$Pbipy ligands bind to the metal atom through their phosphorus atom alone, is described. It has been found that the formation of such species is favoured when the oxidation state of the ruthenium is 0 or +2 and in line with this, $[Ru_3(CO)_{12}]$ and $[Ru_2(\mu\text{-}Cl)_2Cl_2(CO)_6]$ respectively, have been used as precursors. Species of the type $[Ru(CO)_4(\eta^1\text{-}L)]$ and $[Ru(CO)_3(\eta^1\text{-}L)_2]$ (where L = Ph$_2$Ppy and Ph$_2$Pbipy) have been synthesised through a number of routes, as well as such species such as $[Ru(CO)_2Cl_2(\eta^1\text{-}L)_2]$ (L = Ph$_2$Ppy and Ph$_2$Pbipy). The pendant mode of coordination of the phosphine ligands has been confirmed by means of X-ray diffraction studies on the $[Ru(CO)_2Cl_2(\eta^1\text{-}Ph_2Ppy)_2]$ complex. These η^1 derivatives have been reacted with other transition metal precursors, with the aim of producing heterodinuclear derivatives bridged by the phosphine ligand. Although largely unsuccessful, these latter reactions did lead to the serendipitous discovery that silver(I) has a strong affinity for phosphoruspyridyl and phosphorusbipyridyl ligands.

In Chapter Five, the results of an investigation into the coordination of Ph$_2$Pbipy to silver(I) are descibed. It has been shown that Ph$_2$Pbipy reacts with suitable Ag(I) precursors *viz.* $[Ag(NCMe)_4]^+$ or $[Ag(1,5\text{-}cod)_2]^+$ to form the versatile dimeric $[Ag_2(\mu\text{-}Ph_2Pbipy)_2(NCMe)_2]^{2+}$ complex cation containing a pair of bridging Ph$_2$Pbipy ligands; the structure of the PF_6^- salt of this complex has been determined X-ray crystallographically. The chemistry of this complex has been extensively studied; the acetonitrile ligands have been shown to be labile towards substitution by various anionic and N-heterocyclic nucleophiles resulting in a range of neutral, mono- and di-cationic complexes. Certain of these complexes, depending on the nature of the substituting ligand, are polymeric in the solid state, for example as determined X-ray crystallographically for $\{[Ag_2(\mu\text{-}Ph_2Pbipy)_2(\mu'\text{-}4,4'\text{-bipy})](PF_6)_2\}_n$. When the substituting ligand has chelating properties *e.g.* 2,2′-bipyridine, systematic rearrangement of the Ph_2Pbipy ligands around the dimer is induced, such that the phosphorus atoms of both ligands bond to the same silver atom while both bipyridyl fragments chelate at the other. This has been confirmed by the crystal structure determination of $[Ag_2(\mu\text{-}Ph_2Pbipy)_2(\eta^2\text{-}2,2'\text{-bipy})](BF_4)_2$. A comparison of the molecular structures of a number of closely related disilver Ph_2Pbipy ligand-bridged complexes has allowed trends to be discerned in certain bonding parameters. For example, with reference to the bridging Ph_2Pbipy ligand, an inverse relationship exists between the P-Ag-Ag-N(β to P) torsion angles and the dihedral angle between the planes of the pyridine rings.

CONTENTS

Acknowledgements i
List of Abbreviations and Symbols ii
Summary iv

CHAPTER ONE : COORDINATION CHEMISTRY OF SUBSTITUTED DERIVATIVES OF TRIPHENYLPHOSPHINE 1
1.1 Complexes of bis(diphenylphosphino)methane (dppm) 2
1.2 Complexes of bis(diphenylphosphino)ethane (dppe) 10
1.3 Complexes of bis(diphenylphosphino)amines (dppa) 14
1.4 Complexes of tetraphenyldiphosphoxane (tpdo) 20
1.5 Complexes of diphenylphosphinopyridine (dppp) 22
1.6 Complexes of diphenylphosphinoquinoline (dppq) 28
1.7 Objectives of this study 29

CHAPTER TWO : SYNTHESIS AND STRUCTURAL CHARACTERISATION OF THE NOVEL 6-DIPHENYLPHOSPHINO-2,2′-BIPYRIDINE (Ph_2Ppy) LIGAND 32
2.1 Introduction 32
2.2 Synthesis and characterisation of 6-diphenylphosphino-2,2′-bipyridine 33
2.3 Crystal structure determination of 6-diphenylphosphino-2,2′-bipyridine 36
2.4 Experimental 38

CHAPTER THREE : DINUCLEAR PHOSPHORUSPYRIDYL AND PHOSPHORUSBIPYRIDYL LIGAND-BRIDGED DERIVATIVES OF RUTHENIUM(I) 47
3.1 Introduction 47
3.2 Reactions of Ph_2Ppy, Ph_2Pquin and Ph_2Pbipy with $[Ru\{\mu\text{-}\eta^2\text{-}OC(R)O\}(CO)_2]_n$ 50
3.3 Reactions of Ph_2Ppy, Ph_2Pquin and Ph_2Pbipy with $[Ru_2(CO)_4(NCMe)_6](PF_6)_2$ 70
3.4 Conclusion 85
3.5 Experimental 86

CHAPTER FOUR : MONONUCLEAR RUTHENIUM COMPLEXES CONTAINING PENDANT PHOSPHORUSPYRIDYL AND PHOSPHORUSBIPYRIDYL LIGANDS : POTENTIAL PRECURSORS FOR THE SYNTHESIS OF LIGAND-BRIDGED HETERODINUCLEAR COMPOUNDS 133

4.1 Introduction 133

4.2 Synthesis of mononuclear ruthenium(0) complexes of Ph_2Ppy and Ph_2Pbipy 134

4.3 Synthesis of mononuclear ruthenium(II) complexes of dppm, Ph_2Ppy and Ph_2Pbipy 139

4.4 Attempted synthesis of heterodinuclear complexes of ruthenium(0) and ruthenium(II) 145

4.5 Conclusion 151

4.6 Experimental 152

CHAPTER FIVE : DINUCLEAR Ph_2Pbipy LIGAND-BRIDGED DERIVATIVES OF SILVER(I) 172

5.1 Introduction 172

5.2 Reactions of Ph_2Pbipy with silver(I) precursors 172

5.3 The chemistry of $[Ag_2(\mu\text{-}Ph_2Pbipy)_2(NCMe)_2](PF_6)_2$ **[33]** 180

  5.3.1 The substitution behaviour of $[Ag_2(\mu\text{-}Ph_2Pbipy)_2(NCMe)_2]^{2+}$ 180

  5.3.2 Reactions of $[Ag_2(\mu\text{-}Ph_2Pbipy)_2(NCMe)_2]^{2+}$ with anionic ligands 189

  5.3.3 Reactions of $[Ag_2(\mu\text{-}Ph_2Pbipy)_2(NCMe)_2]^{2+}$ with substituted pyridines 207

  5.3.4 Reactions of $[Ag_2(\mu\text{-}Ph_2Pbipy)_2(NCMe)_2]^{2+}$ with bipyridines and substituted bipyridines 216

5.4 Structural trends in dimeric $Ag_2(\mu\text{-}Ph_2Pbipy)_2$ units 231

5.5 Conclusion 233

5.6 Experimental 234

Appendix A General experimental details 345

Appendix B Sources of chemicals 348

Appendix C Publication list 350

References 351

CHAPTER ONE

COORDINATION CHEMISTRY OF SUBSTITUTED DERIVATIVES OF TRIPHENYLPHOSPHINE

Triphenylphosphine is one of the most widely utilised ligands in organometallic and coordination chemistry. It is referred to as a π-acid or π-acceptor ligand[1] and is classified in this way because, in addition to the lone-pair on the phosphorus atom available for σ-donation, there are vacant *3d*π-orbitals of low energy on the phosphorus atom which can accept electron density from filled metal *d*-orbitals of the same symmetry; as such it forms a wide range of complexes with transition metals.[2a] The bonding scheme is illustrated below. Note that it is a soft donor ligand and for this reason, as well as the fact that it is capable of accepting electron density from the metal, it tends to form complexes with transition metals in low formal oxidation states.

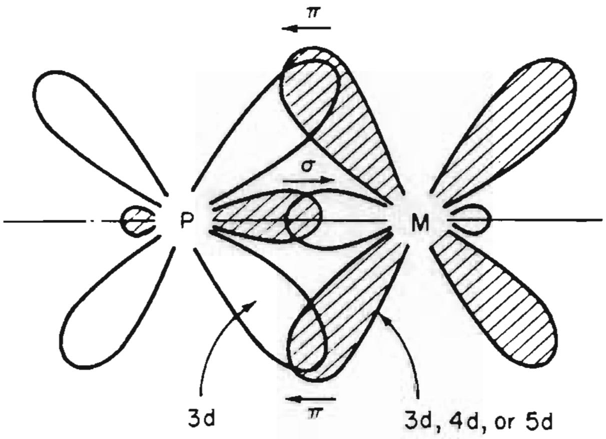

Figure 1.1 The bonding mode of metal-triphenylphosphine complexes

Triphenylphosphine is a sterically demanding ligand because of the presence of the three bulky phenyl substituents on the phosphorus atom. This is reflected by a large Tolman cone angle of 145° for the ligand.[1] As a result the triphenylphosphine ligands in metal complexes tend to dissociate in solution, a property which can be employed in the design of transition metal complexes as homogeneous catalysts. The complex [RhCl(PPh$_3$)$_3$], known as Wilkinson's catalyst,[3] is a good example, being extensively used to catalyse the hydrogenation of unsaturated compounds at ambient temperatures and pressures.[2b]

Although it has been known to coordinate through one of its phenyl rings, either in a σ- mode (orthometallation) or through the π-system[4], triphenylphosphine is essentially a monofunctional inflexible ligand in the sense that it is monodentate and can only bond to a metal through the phosphorus atom; also the geometry at the coordinated phosphorus atom is invariably approximately tetrahedral. However, by substituting a phenyl group for a moiety containing another donor atom, a bidentate ligand is produced which can show greater flexibility in its modes of coordination but which will, nevertheless, still possess the properties of triphenylphosphine which make it such a useful ligand. The purpose of this chapter is to outline possible modes of coordination of bidentate ligands of general formula Ph_2PX where X = CH_2PPh_2, $(CH_2)_2PPh_2$, $N(R)PPh_2$ (R = alkyl group), $OPPh_2$, pyridine and quinoline *i.e.*, ligands which can be regarded as substituted derivatives of triphenylphosphine. This survey will serve as an introduction to the coordination chemistry of the Ph_2Ppy (py = pyridine) and Ph_2Pquin (quin = quinoline) ligands described in later chapters, as well as to that of the new phophorusbipyridyl ligand 6-diphenylphosphino-2,2′-bipyridine (Ph_2Pbipy), the synthesis, structural characterisation and coordination chemistry of which is also described in this thesis.

1.1 Complexes of bis(diphenylphosphino)methane (dppm)

There are essentially three possible modes of coordination for dppm:

i) Monodentate coordination through one phosphorus atom only;

ii) Chelating coordination where both phosphorus atoms bond to the same metal atom and

iii) Bridging coordination where the two phosphorus atoms bond to separate metal atoms.

Selected examples will be given of complexes containing the ligand in each of above modes of coordination followed by a brief discussion of trends that can be discerned in the coordination chemistry of the dppm ligand. The coordination chemistry of dppm has been discussed in several reviews.[5-7]

1.1.1. Monodentate coordination

The seven - coordinate molybdenum complex $[Mo(CO)_2Cl_2(\eta^1\text{-dppm})(\eta^2\text{-dppm})_2]$[8] was the first reported complex shown by crystal structure analysis to possess a pendant dppm *i.e.*, one coordinated in a monodentate manner; also present in the complex is a chelating dppm.

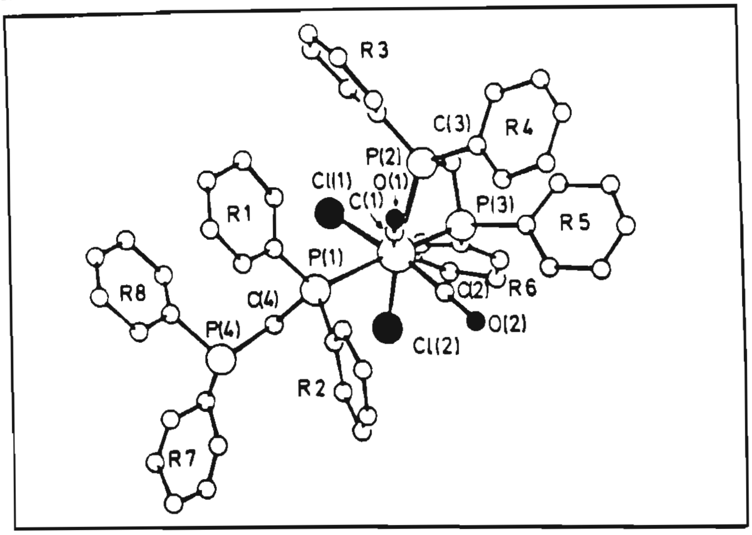

Figure 1.2: Crystal Structure of $[Mo(CO)_2Cl_2(\eta^1\text{-dppm})(\eta^2\text{-dppm})]$

A similar example, but containing two bridging instead of one chelating ligand is the square-planar platinum(II) dimeric complex cation $[Pt_2H(\mu\text{-dppm})_2(\eta^1\text{-dppm})]^+$.[9]

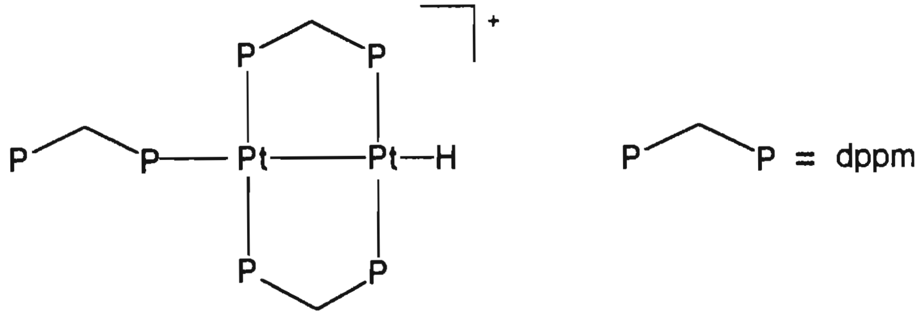

$[Pt_2H(\mu\text{-dppm})_2(\eta^1\text{-dppm})]^+$

A number of complexes have been synthesised in which the ligand is only found coordinated in a pendant fashion *e.g.* the cation of trans-$[Pd(^tBuNC)_2(\eta^1\text{-dppm})_2](BF_4)_2$[10] contains two pendant dppm ligands which are trans-disposed with respect to one another and which are fluxional on the nmr time scale at ambient temperature.

Metal halides and metal carbonyls are also known to give complexes with pendant dppm. Examples of metal halide derivatives include the unstable complex [NiCl$_2$(η^1-dppm)$_2$] and the cations [MCl$_2$O(η^1-dppm)$_2$]$^+$(M = Mo or W)[11-13]. Metal carbonyl-derivatives include the octahedral chromium complex [Cr(CO)$_5$(η^1-dppm)][14]. The free phosphorus atom of the bidentate dppm in this complex may be induced to react with the central metal atom via the following reaction.

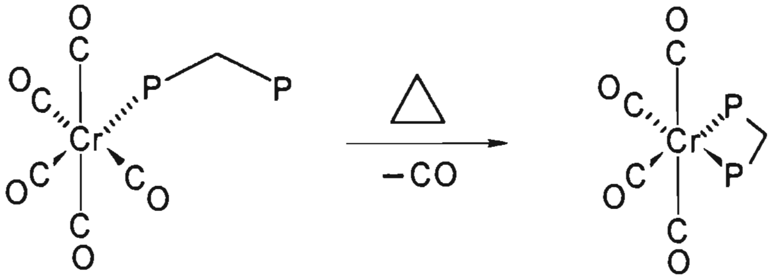

[Cr(CO)$_5$(dppm)]

1.1.2. Chelate coordination

The square-planar complexes [Ni(η^2-dppm)X$_2$](X = Cl, Br and I) are formed by reaction of anhydrous NiX$_2$ with a deficiency of dppm in a variety of solvents[11,12] and contain chelating dppm. An example of a complex containing two chelating dppm ligands is the square-planar [Pt(η^2-dppm)$_2$]Cl$_2$[15]. This species has been used extensively as a precursor for the synthesis of mixed-metal platinum-mercury(II) and platinum-silver(I) systems,[15,16] in which the two previously chelating dppms are now present as bridging ligands.

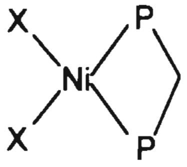

[Ni(η^2-dppm)X$_2$]

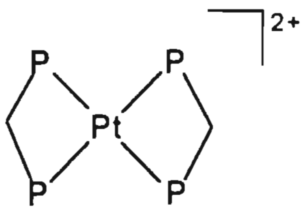

[Pt(η^2-dppm)$_2$]$^{2+}$

Although there are numerous square-planar transition metal analogues of the above two complexes, such as [Pt(η^2-dppm)X$_2$][17,18] and [Rh(η^2-dppm)$_2$]BF$_4$ [19] respectively, there are noticeably fewer complexes with dppm chelating to a metal atom that has octahedral geometry. Perhaps a reason for this paucity is the greater steric hindrance introduced by the increased number of groups attached to the metal atom. However, an interesting series of Group 6 metal carbonyl derivatives containing chelating dppm have been synthesised[20]. At one end of this series are [M(CO)$_4$(η^2-dppm)] (M = Cr, Mo or W) which contain one chelating dppm ligand. The crystal structure of the molybdenum derivative is shown in Figure 1.3 and it is interesting to note that the two mutually trans carbonyl groups have longer Mo-C distances than the two trans to the phosphorus atom, attributed to the difference in the degree of π-back bonding.

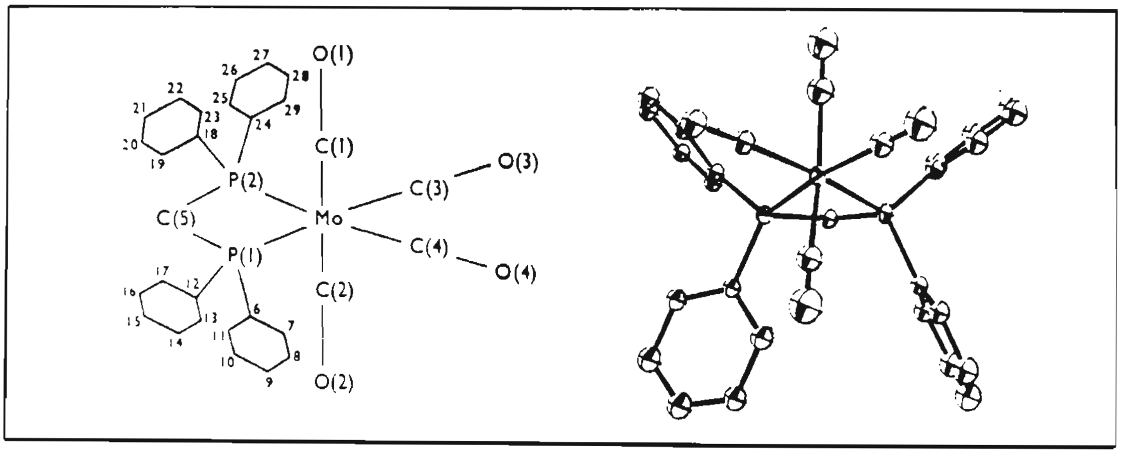

Figure 1.3 Structural formula and perspective view of cis-[Mo(CO)$_4$(η^2-dppm)]

The molybdenum series is completed by cis-[Mo(CO)$_2$(η^2-dppm)$_2$] and the unstable, reddish-brown tris-chelate [Mo(η^2-dppm)$_3$].

The dinuclear complex [Pt$_2$(η^2-dppm)$_2$(μ-Cl)$_2$]Cl$_2$ contains a weak Pt-Pt bond, chloride bridges and chelating dppm's.[21]

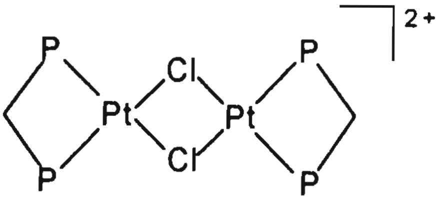

[Pt$_2$(η^2-dppm)$_2$(μ-Cl)$_2$]$^{2+}$

1.1.3. Bridging coordination

The ability of complexes with the M$_2$(μ-dppm)$_2$ skeleton to activate small molecules by their coordination in a position bridging the two metal atoms has led to several attempts to develop catalytic systems based on this skeleton; one such system has been used for the hydrogenation of acetylene to ethylene.[22]

Of the vast range of ligand-bridged derivatives thus far synthesised, most contain two dppm ligands bridging two metal atoms in a dimer in one of two possible arrangements, *viz.* cis or trans. There are only a few complexes containing cis-dppm bridges, $[Pt_2Me_4(\mu\text{-dppm})_2]$ [23] being an example. Trans-disposition of the dppm ligand occurs most frequently and an analysis of complexes of this type will now be made in terms of the geometries of the metal atoms.

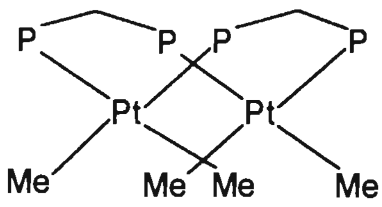

cis-$[Pt_2Me_4(\mu\text{-dppm})_2]$

a) Linear geometries: Au(I) commonly exhibits linear coordination (but also trigonal and tetrahedral coordination - see b) and c). By far the most important dppm bridged complex of Au(I) is the coordinatively unsaturated d^{10}-d^{10} complex $[Au_2(\mu\text{-dppm})_2](PF_6)_2$ which boasts novel photophysical and photochemical properties.[24]

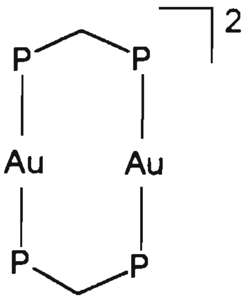

$[Au_2(\mu\text{-dppm})_2]^{2+}$

The structure consists of two trans-bound, bridging dppm ligands defining a planar M_2P_4 core structure with the two metal atoms held in close proximity (regardless of whether or not a metal-metal bond is present); the geometry at each gold atom is linear.

b) Trigonal geometries: The tris-dppm bridged dimer $[Au_2(\mu\text{-dppm})_3](PF_6)_2$ [25] can be regarded as a derivative of the di-bridged complex in a part a) and displays trigonal geometry at each gold atom, a type of structure commonly referred to by the term "manxane".

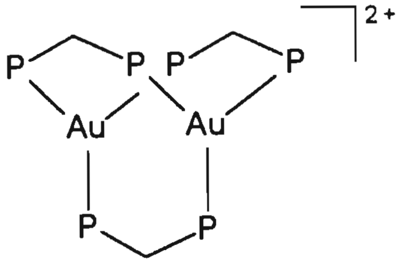

$[Au_2(\mu\text{-dppm})_3]^{2+}$

Other examples with three bridging dppm ligands are the complex cations $[M_2(\mu\text{-dppm})_3]^{2+}$ (M = Pd or Pt) both of which exhibit weak metal-metal interactions and a prolific chemistry.[26,27]

c) Tetrahedral geometries: Au(I) extends its coordination geometries to include tetrahedral coordination, albeit seldom, and the polymeric complex $\{[Au_2(\mu\text{-dppm})_3(\mu'\text{-dppm})](ClO_4)_2\}_n$ has the Au atoms tetrahedrally coordinated as shown.[25] On the other hand silver(I) and copper(I) prefer tetrahedral coordination geometries. The labile complex $[Ag_2(\mu\text{-dppm})_2(NO_3)_2]$[28] possesses two dppm bridges and in addition, each silver atom is terminally bound by a single nitrate anion in an asymmetric bidentate fashion.

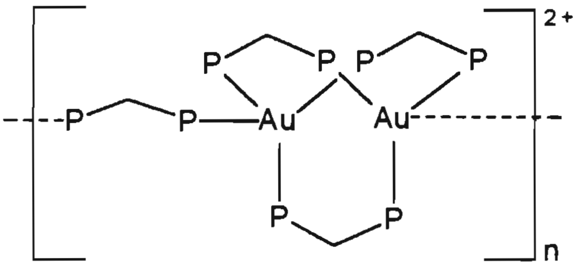

$\{[Au_2(\mu\text{-dppm})_3(\mu'\text{-dppm})]^{2+}\}_n$

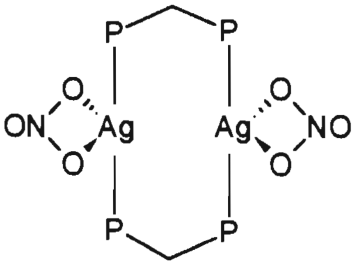

$[Ag_2(\mu\text{-dppm})_2(NO_3)_2]$

d) Square-planar geometries: There are a great number of complexes in which dppm bridges across two metal atoms that have square-planar geometries. Face-to-face rhodium(I) dimers are common, $[Rh_2(\mu\text{-dppm})_2(CO)_2Cl_2]$ [29] and $[Rh_2(\mu\text{-dppm})_2(NCMe)_4](PF_6)_2$ [30] being examples.

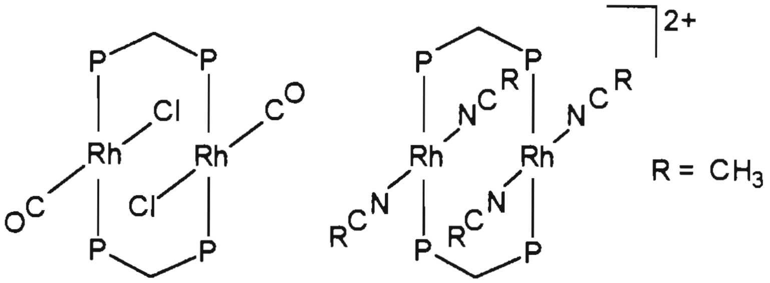

$[Rh_2(\mu\text{-dppm})_2(CO)_2Cl_2]$ $[Rh_2(\mu\text{-dppm})_2(NCMe)_4]^{2+}$

Face-to-face square-planar dimers of other metals are less common, a recent example being $[Pt_2(\mu\text{-dppm})_2(C{\equiv}CR)_4]$ (R = Me, CF_3, Ph or 4-tolyl),[31,32] which has the same structure as $[Rh_2(\mu\text{-dppm})_2(NCMe)_4]^{2+}$. Treatment of $[Pd_2(\mu\text{-dppm})_3]$ (see b)) with I_2 affords the side-by-side complex $[Pd_2(\mu\text{-dppm})_2I_2]$ [33] which contains a Pd-Pd bond and a square planar geometry at each Pd atom.

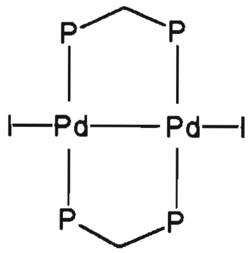

$[Pd_2(\mu\text{-dppm})_2I_2]$

A-frame complexes, usually derived from square-planar side-by-side derivatives exhibit a rich chemistry. The reaction below shows an example of this type of conversion [34] while the dirhodium complex $[Rh_2(\mu\text{-dppm})_2(\mu\text{-CO})Cl_2]$ [30], also illustrated below, provides an example of an A-frame complex that contains a metal-metal bond.

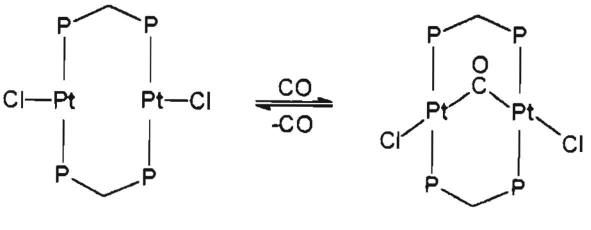

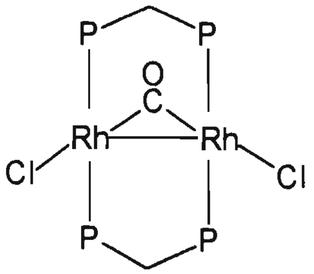

$[Ru_2(\mu\text{-dppm})_2(\mu\text{-CO})Cl_2]$

e) Square-pyramidal geometries: dppm is also known to bridge across two metal atoms that have face-to-face square-pyramidal geometries. One such example is $[Rh_2(\mu\text{-dppm})_2(CO)_4(CN)_2]$ [35] while $[Re_2(\mu\text{-dppm})_2Cl_4(CN^tBu)]$ [36] with its metal-metal bond, is an A-frame representative of this type of metal atom geometry.

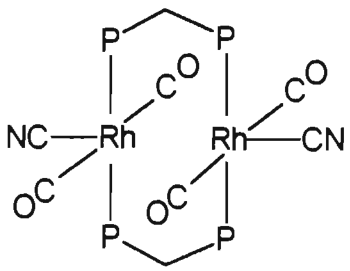

$[Rh_2(\mu\text{-dppm})_2(CO)_4(CN)_2]$

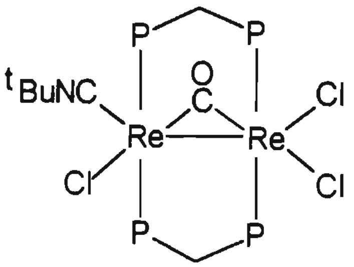

$[Re_2(\mu\text{-dppm})_2Cl_4(CN^tBu)]$

f) Octahedral geometries: The symmetric complex $[Mn_2(\mu\text{-dppm})_2(CO)_6]$ is a good example in this regard, formed from the extensively studied A-frame square-pyramidal dimeric complex $[Mn_2(\mu\text{-dppm})_2(\mu\text{-CO})(CO)_4]$.[37-39]

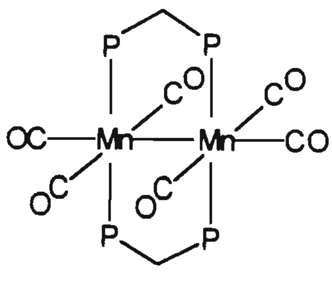

$[Mn_2(\mu\text{-dppm})_2(CO)_6]$

Pseudo A-frame octahedral geometries are found in compounds like $[Re_2(\mu\text{-}dppm)_2(\mu\text{-}CO)(\mu\text{-}Cl)(CN^tBu)(CO)Cl_2]$ [40] which possesses an unsymmetrical arrangement of ligands in the equatorial plane.

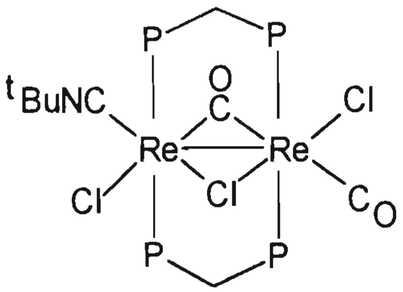

$[Re_2(\mu\text{-}dppm)_2(\mu\text{-}CO)(\mu\text{-}Cl)(CN^tBu)(CO)Cl_2]$

1.1.4 Concluding remarks

It is clear from the above overview that the bidentate dppm ligand has a propensity to bind two metal atoms together in a bridging fashion rather than to chelate at a single metal atom or to function as a monodentate ligand. The reason for this preference is that when dppm chelates to a single metal atom, the four-membered ring so produced is considerably strained. The P-M-P angles that result generally range in size from 67-74° and the P-C-P angles are usually about 95° with the normal stable, unstrained angles being 90° and 109,5° respectively. It is also clear that when dppm chelates to a transition metal, this chelation is found predominantly for those metal atom geometries for which the least angle strain would be introduced *i.e.* square-planar and, to a lesser extent, octahedral geometries . Indeed no complexes have been reported containing dppm chelating to a metal atom in a trigonal or tetrahedral environment. On the other hand, when dppm bridges across two metal atoms, the five-membered M_2P_2 core that results has normal unstrained bond angles and the complex as a whole is very stable. Hence the proliferation of di-bridged dppm complexes of transition metals; indeed, complexes of this sort find widespread application as far as the activation of small molecules at the dinuclear centre is concerned.

1.2 Complexes of bis(diphenylphosphino)ethane (dppe)

The bis(diphenylphosphino)ethane (dppe) ligand is closely related to the dppm ligand the only difference being the inclusion of an additional methylene group between the two phosphorus atoms. The same modes of coordination are possible as for dppm, but the presence of the additional methylene group does have the result that dppm and dppe frequently exhibit different coordination behaviour; in particular the chelating mode is found to occur more often for dppe for reasons which are discussed below. The coordination chemistry of dppe has been discussed in several reviews.[6,41,42]

1.2.1 Monodentate coordination

The complexes [M(η^1-dppe)(η^2-dppe)$(CO)_2X_2$] (M = Mo or W; X = Cl, Br) are neutral, diamagnetic seven coordinate complexes in which one of the dppe ligands behaves as a pendant, monodentate ligand.[43]

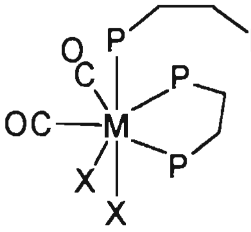

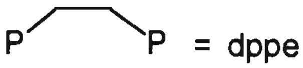

[M(η^1-dppe)(η^2-dppe)$(CO)_2X_2$]

Tentative assignments of pendant dppe ligands have been made by various other researchers,[44,45] based mainly on $^{31}P\{^1H\}$ nmr and infra-red evidence, but there are as yet no crystal structures to support their arguments.

1.2.2 Chelating Coordination

For reasons laid out in the concluding remarks section (1.2.4), this is the predominant coordination mode of dppe and numerous complexes containing chelating dppe have been reported. As for bridging dppm, dppe can chelate to a range of different metal atom geometries.

a) Square-planar and tetrahedral geometries: These are grouped together since interesting comparisons can be drawn with respect to the steric problems introduced upon chelation of dppe. Mono-chelates are generally of the cis-form (Fig 1.4a)) as opposed to the trans-form (Fig 1.4b)), since dppe's 'backbone" is still too short to span the distance required for the latter mode of coordination.

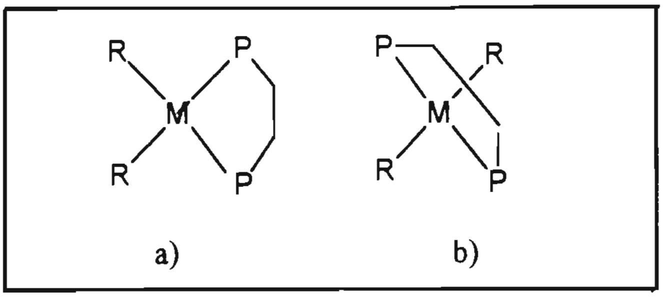

Figure 1.4: Cis and trans-coordination of dppe monochelates

Complexes like $[Ni(\eta^2\text{-dppe})Cl_2]$,[46] $[Pd(\eta^2\text{-dppe})Br_2]$ [47] and $[Rh(\eta^2\text{-dppe})(CO)Cl]$ [48] are examples in point. A review by Minahan *et al* [42] gives a comprehensive listing of dppe complexes for square-planar d^8 metal systems such as Rh(I), Ir(I), Pd(II), Pt(II) and Au(III).

Bis-chelates, of the form $[M(\eta^2\text{-dppe})_2]$ are, it appears, more common for tetrahedral metal atom geometries. The shorter 'bite" of the dppe ligand pulls the phosphorus atoms (and their phenyl substituents) of each ligand closer together such that steric strain is anticipated for square-planar bis-chelates while relief of this strain occurs by rotation into a tetrahedral environment. The tetrahedral cations $[M(\eta^2\text{-dppe})_2]^+$ [42] (M = Ag or Au) are both known along with numerous other tetrahedral bis-chelates while the highly strained $[Rh(\eta^2\text{-dppe})_2]Cl$ [50] is one of a few examples of square-planar bis-chelates.

b) Square-pyramidal geometries: $[Fe_2(\eta^2\text{-dppe})(\mu\text{-SR})_2(CO)_4]$ [51] and the complex cation $[Ir(\eta^2\text{-dppe})_2(CO)]^+$ [48] are two representative examples, both possessing dppe in a chelating mode of coordination in equatorial positions for the mono- and bis-chelate respectively, with a carbonyl group coordinated in the apical position.

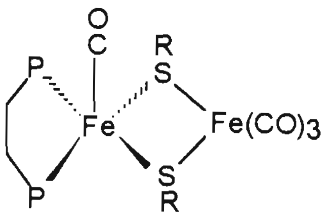

[Fe$_2$(η^2-dppe)(μ-SR)$_2$(CO)$_4$]

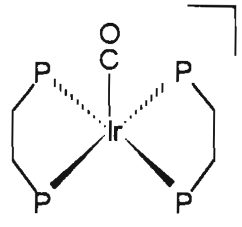

[Ir(η^2-dppe)$_2$(CO)]$^+$

c) Octahedral geometries: Early octahedral complexes include [Mo(η^2-dppe)$_3$],[52] [Cr(η^2-dppe)$_3$] [53] and [Mo(η^2-dppe)Cl$_4$] [54]. More conventional octahedral geometries, like those required for Ru(II) and Os(II) are found in complexes such as cis- [Ru(η^2-dppe)$_2$Me$_2$] and trans- [Os(η^2-dppe)$_2$HCl]. C_6H_6[55a) - c)]

1.2.3 Bridging Coordination

A well known example of a dppe-bridged complex is the iron carbonyl complex [Fe(μ-dppe)(μ-CO)$_2$(π-C$_5$H$_5$)$_2$], containing π-C$_5$H$_5$ ligands.[56]

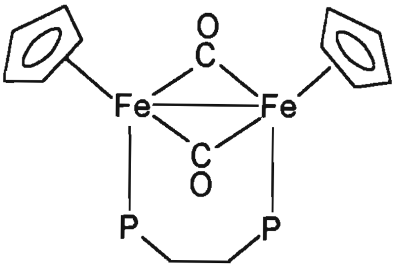

[Fe(μ-dppe)(μ-CO)$_2$(π-C$_5$H$_5$)$_2$]

McAuliffe *et al* have prepared a series of complexes using Au(I), one of which is [{AuCl}$_2$(μ-dppe)],[57] a conventional, linear two coordinate complex in which the bidentate ligand bridges the two gold(I) atoms i.e. [ClAu(μ-dppe)AuCl]. The di-bridged dppe complex [Re$_2$(μ-dppe)$_2$Cl$_4$],[58] synthesised by Cotton *et al*, comprises two bridging dppe ligands and a rhenium-rhenium triple bond. A crystal structure (Fig 1.5) shows the eclipsed conformation and the cis-decalin like fusion of the two trans-form rings.

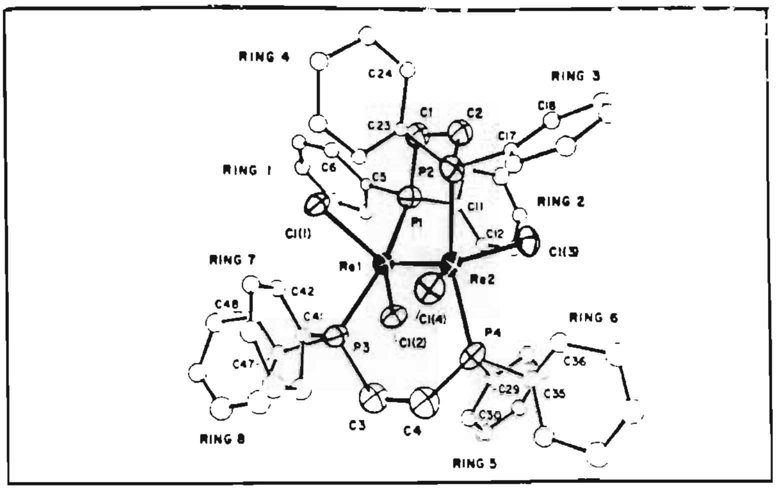

Figure 1.5: Crystal structure of $[Re_2(\mu\text{-dppe})_2Cl_4]$

1.2.4 Concluding Remarks

In forming chelate complexes, the optimum ring size for a metal having natural bond angles at 90° to one another is five. For this reason, dppe forms predominantly chelated complexes with transition metals, and in so doing forms stable five-membered rings. This is in contrast to dppm's tendency to bridge across two metal atoms.

Although bridged complexes of dppe are known, it is obvious that the shorter 'bite" of the ligand is detrimental to their formation. In addition to this, the short 'bite" means that the phosphorus atoms are closer together and this almost entirely precludes the possibility of dppe behaving as a monodentate ligand.

1.3 Complexes of bis(diphenylphosphino)amines (dppa)

These are ligands of general formula $Ph_2PN(R)PPh_2$ (R = alkyl group). While interest in binucleating diphosphine ligands with a P-(C)$_n$-P framework has been great over the last few decades, interest has been growing in their analagous diphosphinoamine ligands. These can also be considered to be substituted derivatives of triphenylphosphine; instead they possess another phosphorus donor connected through a nitrogen atom rather than a carbon, resulting in a P-N(R)-P framework. Substituents on the nitrogen atom (generally alkyl groups) can be varied with attendant changes in the P-N-P bond angle and the conformation around the phosphorus centre. Furthermore, fairly small differences in these ligands can cause significant changes in their coordination behaviour and the structural features of the resulting complexes. As such, dppa ligands exhibit all three modes of coordination (i.e. monodentate, chelating and bridging) and for reasons discussed below they are most likely found to bridge across two metal atoms in much the same way as dppm.

1.3.1 Monodentate coordination

There are only a few examples of transition metal complexes containing pendant dppa acting as a monodentate ligand. The complex [Ni(η^1-dppa)(Cp)(CN)] is highly reactive and contains the ligand bound in a monodentate fashion.[59]

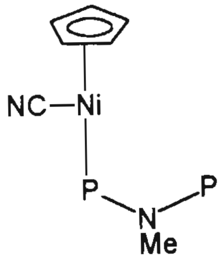

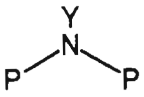

= dppa ligand (Y = aryl or alkoxy group)

[Ni(η^1-dppa)(Cp)(CN)]

Dppa ligands also react with square-planar metal precursors to produce complexes in which the pendant ligand is either cis- or trans-bound; [M(η^1-dppa)$_2$(C_6X_5)$_2$] (M = Pd or Pt; X = Cl or F) is found as both structural forms.[60]

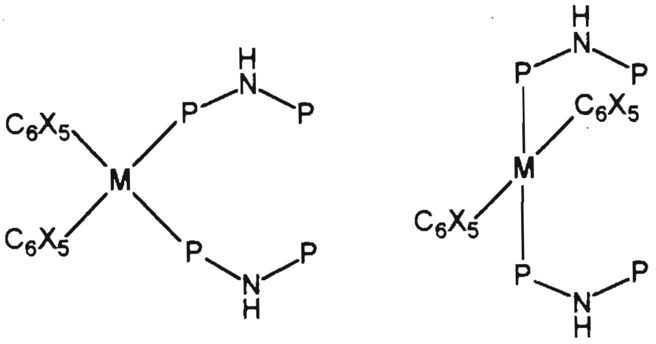

[M(η^1-dppa)$_2$(C_6X_5)$_2$]

1.3.2 Chelating Coordination

The thermal reactions of [M(CO)$_6$] (M = Mo or W) with diphosphinoamines afford the cis-chelate complexes [M(CO)$_4$(η^2-dppa)]. An X-ray crystallographic study [61] of the molybdenum analogue (Fig 1.6) has confirmed that these complexes have the expected cis-configuration of carbonyl ligands and a chelating dppa.

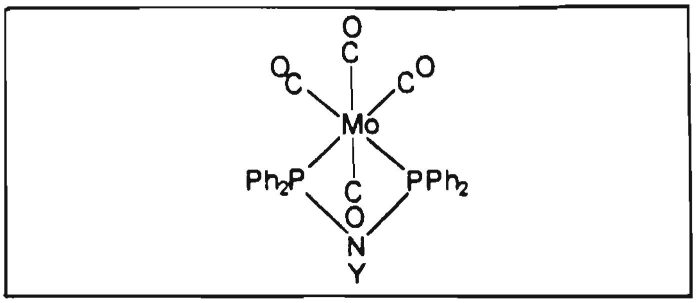

Figure 1.6: Structure of $[Mo(CO)_4(\eta^2\text{-dppa})]$

For Y = ^{i}Pr, it has been possible thermally to effect complete substitution of the carbonyl groups to obtain $[M(\eta^2\text{-dppa})_3]$ (M = Mo or W) in which there are three chelating dppa ligands.[62]

For lower metal atom coordination numbers, iridium(I) and nickel(II) respectively form simple square-planar and trigonal chelates with dppa ligands. The complex $[Ir(\eta^2\text{-dppa})_2]Cl$ has been isolated as a solvate,[63] while the complex $[Ni(\eta^2\text{-dppa})(Cp)]BF_4$ [59] has also been isolated, but is very unstable and usually reverts back to $[Ni(\eta^1\text{-dppa})(Cp)(CN)]$, which contains a pendant dppa ligand(section 1.3.1), in the presence of NaCN.

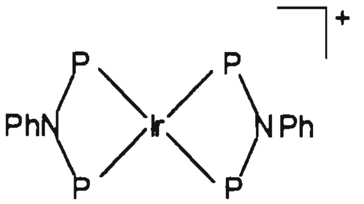

$[Ir(\eta^2\text{-dppa})_2]^+$

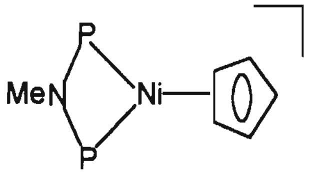

$[Ni(\eta^1\text{-dppa})(Cp)]$

1.3.3 Bridging Coordination

Like dppm, there are numerous transition metal complexes in which dppa ligands bridge across two metal atoms and these atoms can be present in a range of coordination geometries.

a) Linear geometries: Reaction of dppa (Y = H or Me) with $[Au(CO)Cl]_n$ yields the dinuclear gold(I) complex $[\{AuCl\}_2(\mu\text{-dppa})]$ which, on treatment with excess ligand, yields $[Au_2(\mu\text{-dppa})_2Cl_2]$ which has weak Au-Cl bonds.[64]

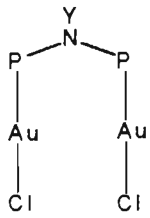

[{AuCl}$_2$(μ-dppa)]

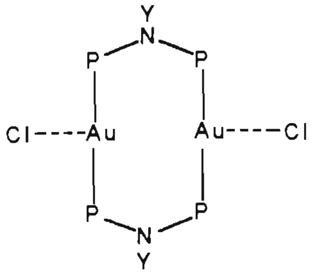

[Au$_2$(μ-dppa)$_2$Cl$_2$]

b) Tetrahedral geometries: Although the coordination chemistry of Group 11 transition metals with dppa ligands has received only slight attention, recent work by Ellermann *et al.* on the reactions of copper(I) and silver(I) halides with dppa (Y = H) has yielded the trinuclear complexes [M$_3$(μ-dppa)$_3$(μ-X)$_2$]X (M = Cu or Ag; X = Cl, Br or I) which have tetrahedral geometry at each metal-atom.[65,66]

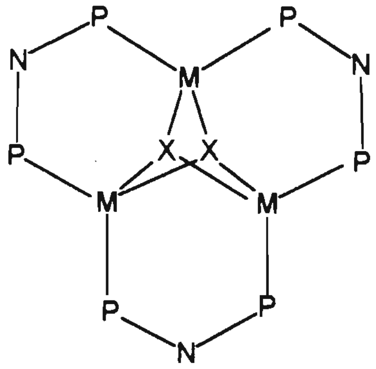

[M$_3$(μ-dppa)$_3$(μ-X)$_2$]$^+$

c) Square-planar geometries: Numerous bimetallic complexes containing bridging dppa ligands and square-planar, four coordinate metals have been reported. A-frame derivatives, such as [Rh$_2$(μ-dppa)(μ-CO)Cl$_2$] CH$_3$OH.Et$_2$O are common[67] while side-by-side dimers such as [Pd$_2$(μ-dppa)$_2$Cl$_2$] [68] have also been reported.

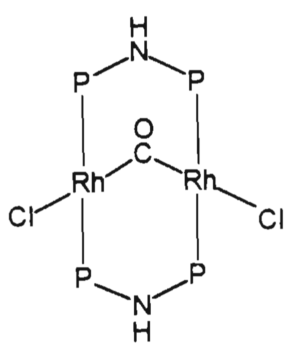

[Rh$_2$(μ-dppa)(μ-CO)Cl$_2$]

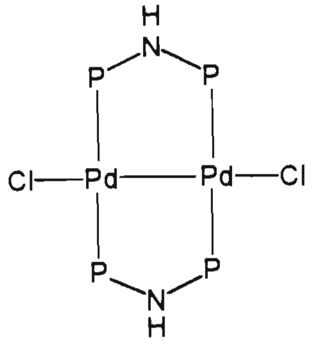

[Pd$_2$(μ-dppa)$_2$Cl$_2$]

Heterobimetallic compounds, in which dppa bridges two unlike metal atoms having square-planar geometry, have also been reported, usually synthesised from monomeric metal precursors containing pendant ligands. The complex [PdPt(μ-dppa)$_2$Cl$_2$][62] is one example hereof.

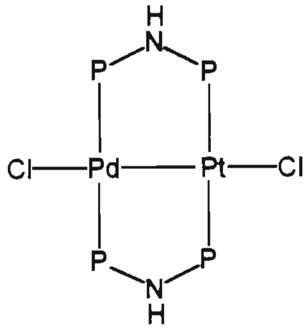

[PdPt(μ-dppa)$_2$Cl$_2$]

d) Octahedral geometries: Although Haines and co-workers have extensively explored the reactions of alkoxy/aryloxy-substituted dppa ligands with transition metal derivatives, only a limited amount of work involving the coordination of phenyl-substituted phosphinoamines to octahedral metal atoms has been reported in literature. However, thermal reaction of $Ru_3(CO)_{12}$ with dppa in varying stoichiometric proportions follows a complex course and yields a variety of products in which the Ru_3 framework remains intact [69a) - c)] and substitution of carbonyl groups only occurs when the dppa ligand has Y = Et. Figure 1.7 illustrates the range of dppa bridged trimers reported, with octahedral or near-octahedral geometry being preserved at the metal centres.

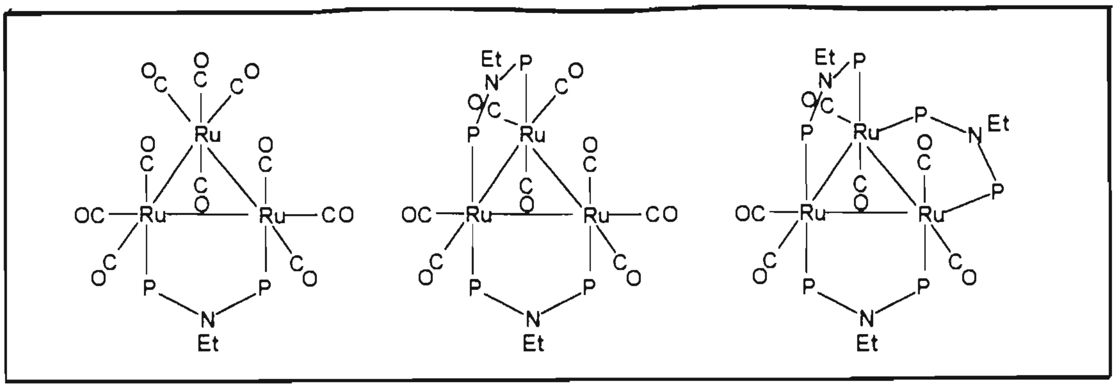

Figure 1.7: Triruthenium derivatives of dppa ligands

Dppa ligands form dimeric cis- and trans-bridged dirhenium(III) carboxylate derivatives; one such example is the complex $[Re_2(\mu\text{-dppa})_2(\mu\text{-}O_2CMe)_2X_2]$ (X = Cl) which contains a rhenium-rhenium triple bond.[70] An ORTEP representation of the structure of octahedral cis-$[Re_2(\mu\text{-dppa})_2(\mu\text{-}O_2CMe)_2Cl_2]$, as viewed down the Re-Re axis, is given in Figure 1.8.

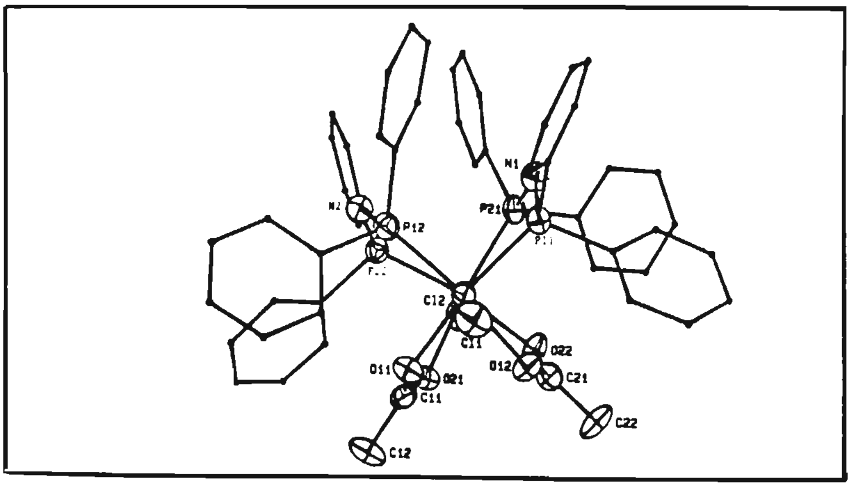

Figure 1.8: X-ray structure of cis-$[Re_2(\mu\text{-dppa})_2(\mu\text{-}O_2CMe)_2Cl_2]$

e) Higher geometries: The eight-coordinate complex $[M_2(\mu\text{-dppa})_2(\mu\text{-CO})_2](CO)_6]$ (M = Mo or W)[62] is a good example of dppa (Y = ^{i}Pr) bridging a metal of higher coordination number.

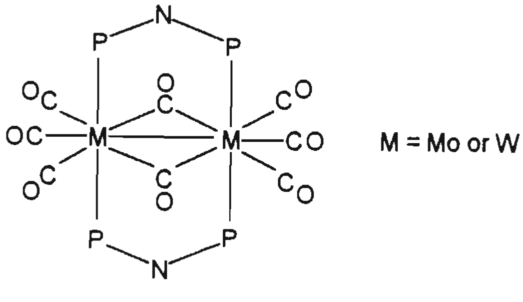

M = Mo or W

$[M_2(\mu\text{-dppa})_2(\mu\text{-CO})_2(CO)_6]$

1.3.4 Concluding Remarks

Though a monodentate mode of coordination of dppa ligands has been reported and is feasible, it is apparent that the choice of substituents on the nitrogen will favour mutual orientation of the phosphorus lone pairs suitable to allow bidentate ligand behaviour. As such, it is expected that, like dppm, dppa ligands will more likely bridge across two metal atoms than chelate to one, although the latter mode of coordination is well established. The five-membered dppa bridge is structurally more rigid than that for dppm, presumably due to the relatively inflexible nature of the P-N-P bond angle as opposed to that for P-C-P. Hence, dppa appears to have an even greater tendency than dppm to bridge rather than chelate. Thus it appears that all three bonding modes are once again possible, but that in the case of dppa ligands there is an even greater tendency to bridge across two metal atoms.

1.4 Complexes of tetraphenyldiphosphoxane (tpdo)

The ligand Ph_2POPPh_2 can also be considered as being derived from triphenylphosphine, by replacing a phenyl group with $OPPh_2$. It has not proved as versatile as those ligands mentioned above on account of the lower flexibility of the P-O-P backbone and the tendency for oxygen to adopt near linear linkages with the phosphorus atoms. There is thus very little reported work on the coordination of this ligand to transition metals. However, Wong and co-workers have recently been investigating the coordination chemistry of diphosphine monoxide (OP_2R_4) (R = Ph) and its diphosphoxane tautomer (R_2POPR_2) [71 a) - b)] and their results involving molybdenum precursors shows that all three coordination modes are possible. [72]

1.4.1 Monodentate coordination

Reaction of tpdo with $Mo(CO)_6$ yields the useful complex $[Mo(CO)_5(\eta^1\text{-tpdo})]$ in which the phosphoxane ligand behaves as a monodentate ligand.

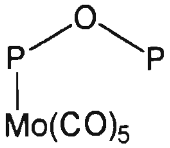

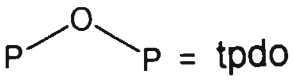

[Mo(CO)$_5$(η^1-tpdo)]

1.4.2 Chelating coordination

The unstable complex cis-[Mo(CO)$_4$(η^2-tpdo)], below, has been reported by the same group and is formed by the pyrolysis of the pentacarbonyl complex shown above. The P-O-P chelated angle is 103.3(1)° and hence is significantly strained.

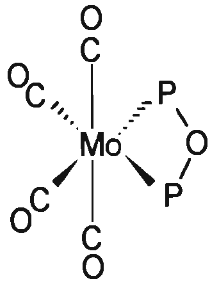

[Mo(CO)$_4$(η^2-tpdo)]

1.4.3 Bridging coordination

The monodentate tetraphenyldiphosphoxane ligand in [Mo(CO)$_5$(η^1-tpdo)] readily displaces labile donors on other metals to give bridged dinuclear products. Two similar reactions have been reported and these are shown below.

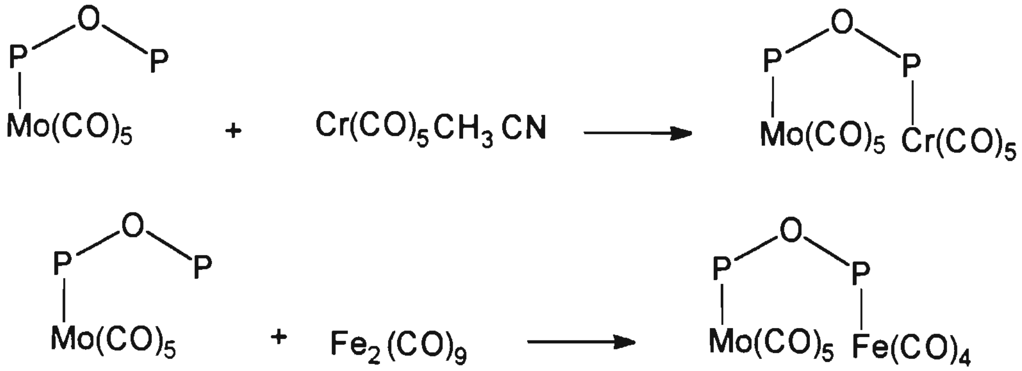

An X-ray structural study on the Fe compound[72] showed that angles around the molybdenum atoms are slightly distorted from an octahedral geometry with the bridging P-O-P angle being large at 146.4(2)°; this is in contrast with the small chelating P-O-P angle mentioned in 1.4.2.

1.4.4 Concluding Remarks

It is difficult to establish trends in tpdo's coordination behaviour simply due to the fact that so little work has been done in this area. However, by making an intelligent comparison with the coordination behaviour of an analogous tetrahedral diphosphite ligand (tedip), $(EtO)_2POP(OEt)_2$,[73] it is possible to establish that tpdo should preferentially bridge across two metal atoms, the expected reluctance to form chelated complexes being ascribed to the relatively large P-O-P angle. Indeed, chelate complexes seem to be much more common with ligands containing less open chains such as P-N(R)-P and $P\text{-}CH_2\text{-}P$, discussed in the preceeding schemes.

1.5 Complexes of diphenylphosphinopyridine (dppp)

Dppp can be regarded as a further branch of the derivatisation of triphenylphosphine in which one phenyl group has been replaced by an aromatic pyridine group. As such, it possesses a binucleating potential in the same way as the biphosphine ligands discussed above but in contrast comprises two *different* donor atoms, the harder nitrogen and the softer phosphorus.

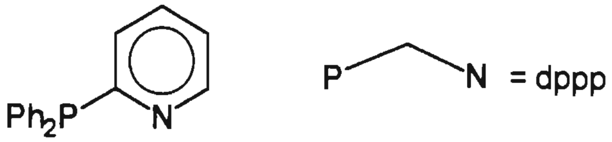

Generally, dppp acts as a P-monodentate ligand in much the same way as triphenylphosphine. However, N-monodentate coordination and P-N chelation of a single metal ion are also possible. There are, of course, numerous dppp bridged complexes as well, both homo- and heterodinuclear.

1.5.1 Monodentate coordination

a) P-bonded: For many transition metals, dppp preferentially binds through the phosphorus atom to give mononuclear complexes that are similar in properties to their well known triphenylphosphine analogues. Simple reaction conditions afford the rhodium complexes $[Rh(\eta^1\text{-dppp})(\pi\text{-}C_5H_5)(CO)]$[74] and $[Rh(\eta^1\text{-dppp})_2(CO)Cl]$,[75] containing one and two pendant dppp ligands respectively.

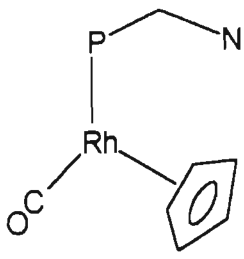

$[Rh(\eta^1\text{-dppp})(\pi\text{-}C_5H_5)(CO)]$

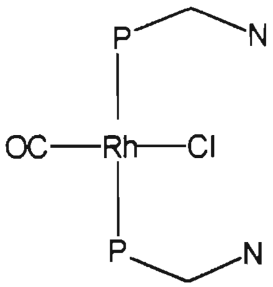

$[Rh(\eta^1\text{-dppp})_2(CO)Cl]$

There are numerous other mononuclear complexes containing one or more pendant dppp ligands.[76,77] An interesting example of a dinuclear complex containing two monodentate P-bonded dppp ligands is the "piano-stool" dimer $[Mo_2(\pi\text{-}C_5H_5)_2(CO)_4(dppp)_2]$. Figure 1.9 shows the crystal structure of this complex to contain trans disposed phosphinopyridine ligands and a metal-metal bond.[78]

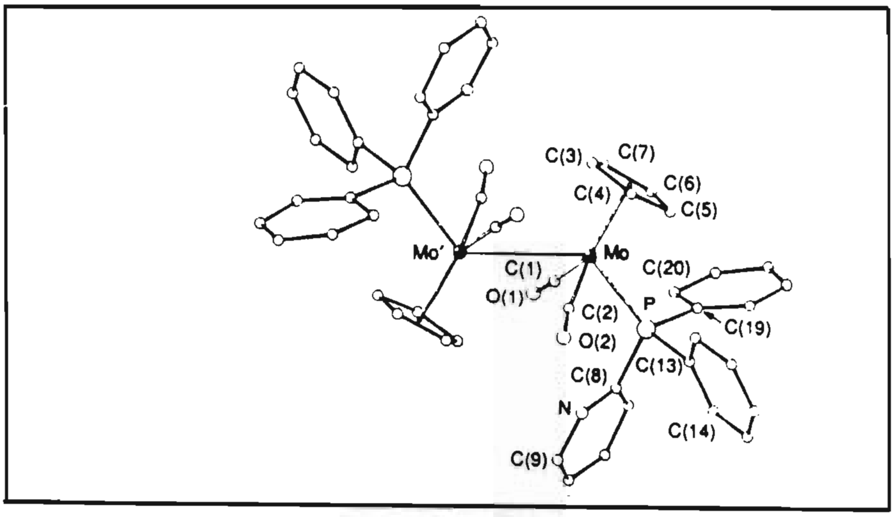

Figure 1.9 : Crystal structure of $[Mo_2(\pi\text{-}C_5H_5)_2(CO)_4(dppp)_2]$ showing the atom numbering scheme.

b) N-bonded: Although no specific references are made, Newkome has reported in his review that this mode of coordination is indeed feasible.[79]

1.5.2 Chelating coordination

As with ligands discussed above, chelation of dppp at a single metal atom introduces a considerable amount of strain into the complex as a whole due to the strained four-membered ring it involves. However, a number of complexes are known. Figure 1.10 shows the X-ray crystal structures of octahedral cis-[Ru(η^2-dppp)(CO)$_2$Cl$_2$] [80] and the highly unusual thirteen-coordinate U(III) complex [U(η^2-dppp)$_2$(BH$_4$)$_3$].[81]

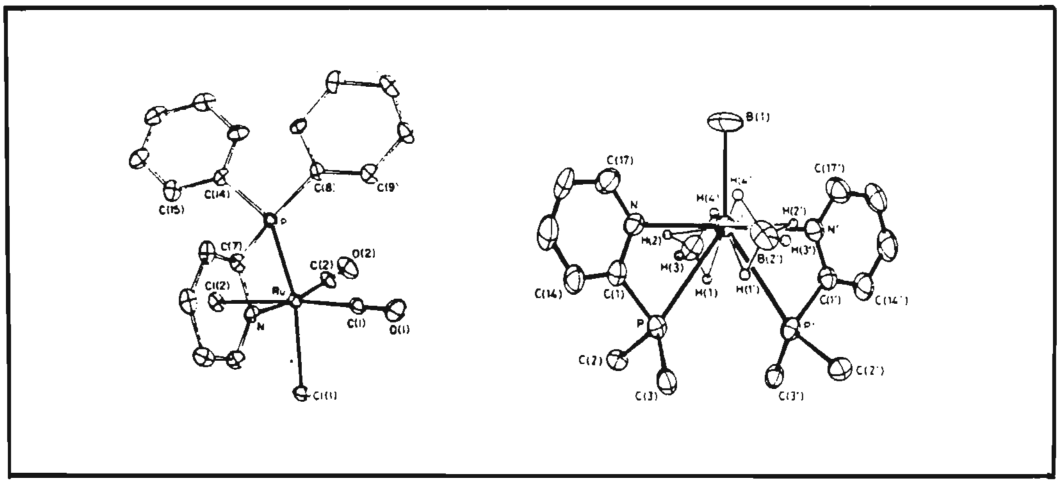
C(15)
C(14)
C(8)
C(9)
P
C(7)
Cl(2)
Ru
C(2)
O(2)
N
C(1)
O(1)
Cl(1)
B(1)
C(17)
H(4)
H(4')
C(17')
N
H(2')
H(2)
N'
H(3')
H(3)
B(2')
C(14)
C(1)
H(1)
H(1')
C(1')
C(14')
P
P'
C(2)
C(3)
C(3')
C(2')

a) b)

Figure 1.10: Perspective views of a) cis-[Ru(η^2-dppp)(CO)$_2$Cl$_2$] and b) [U(η^2-dppp)$_2$(BH$_4$)$_3$]

In order to alleviate some of the strain of a dppp chelate, oxygenation of the phosphorus atom sometimes occurs, with subsequent coordination of the oxygen atom to the metal. In this way a more stable O-N five-membered chelate is produced. The octahedral complex [Ni{η^2-(O)dppp}$_2$Cl$_2$] is a case in point.[82]

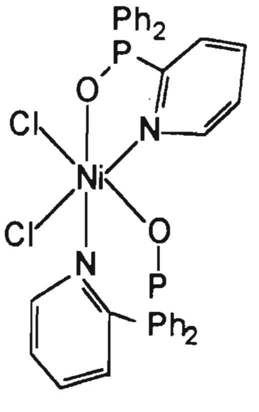
Ph2
P
O
Cl
N
Ni
Cl
O
N
P
Ph2

[Ni{η^2-(O)dppp}Cl$_2$]

1.5.3 Bridging coordination

a) Simple dinuclear dppp bridged complexes: By reaction of $[Cu(NCMe)_4]BF_4$ with dppp, Gimeno *et al*[83] have prepared a series of dinuclear complexes of the type $[Cu_2(\mu\text{-dppp})_2(NCMe)_n](BF_4)_2$ (n = 2 or 4) and $[Cu_2(\mu\text{-dppp})_3L_n](BF_4)_2$ (n = 0,1 or 2; L = N or P monodentate ligand) in which the copper atoms are bridged by the dppp ligands.

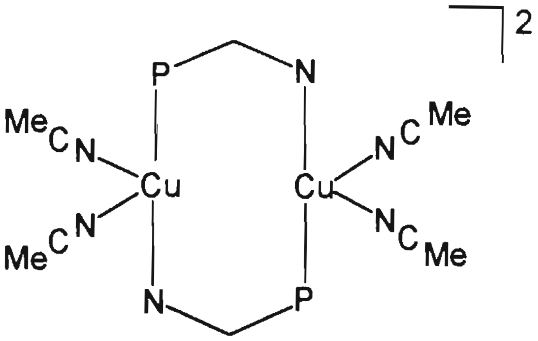

$[Cu_2(\mu\text{-dppp})_2(NCMe)_4]^{2+}$

Likewise, linear $[Au_2(\mu\text{-dppp})_2](PF_6)_2$ [84] and tetrahedral $[Ag_2(\mu\text{-dppp})(\eta^1\text{-dppp})_2(\mu\text{-Cl})_2]$ [85] have been prepared via the simple interaction between the dppp ligand and suitable metal precursors.

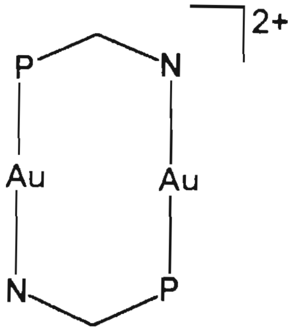

$[Au_2(\mu\text{-dppp})_2]^{2+}$

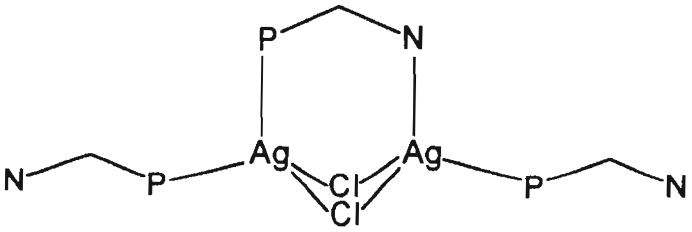

$[Ag_2(\mu\text{-dppp})(\eta^1\text{-dppp})_2(\mu\text{-Cl})_2]$

b) Dinuclear dppp bridged complexes derived from mononuclear precursors containing pendant dppp ligands: A metal-containing complex possessing a trans pair of pendant dppp ligands should be capable of chelating a second metal atom via the following reaction

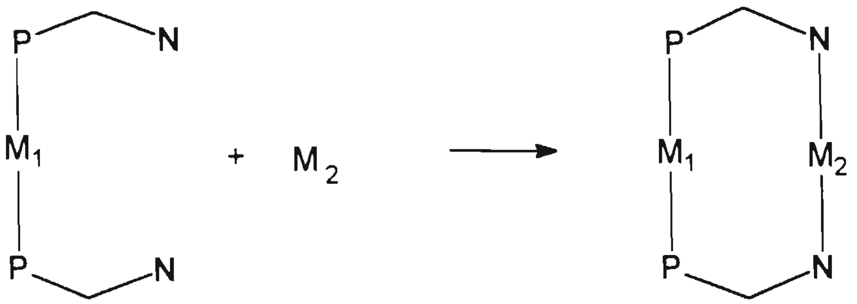

There have been extensive studies on reactions of this type, especially for metals of Group 8, in which homodinuclear (Rh-Rh, Pd-Pd, Pt-Pt) and hetero-dinuclear (Pd-Pt, Rh-Pd, Pd-Ru) species have been afforded.[75]

i) Homonuclear products: Treatment of $[Rh(\eta^1\text{-dppp})_2(CO)Cl]$ with a half molar equivalent of $[Rh_2(\mu\text{-Cl})_2(CO)_4]$ affords the well known dinuclear A-frame complex $[Rh_2(\mu\text{-dppp})_2(\mu\text{-CO})Cl_2]$ as shown by the following reaction.[86]

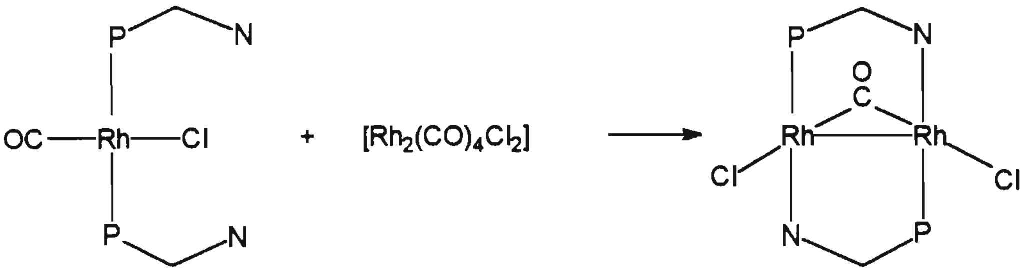

(ii) Heterodinuclear products: Numerous compounds of this type have been synthesised. An important example is the reaction of $[Rh(\eta^1\text{-dppp})_2(CO)Cl]$ (above) with $[(1,5\text{-cod})PdCl_2]$ to produce $[RhPd(\mu\text{-dppp})_2(CO)Cl_3]$,[75,87] shown below. Not only has the rhodium compound captured the palladium atom by complexation but it has undergone oxidative addition of a palladium-chloride bond. Formally, we can consider the product as a complex of Rh(II) and Pd(I). In addition, the orientation of the dppp ligands has changed to give a "head-to-tail" arrangement of phosphorus and nitrogen atoms.

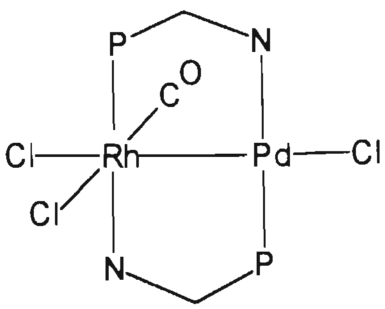

[RhPd(μ-dppp)$_2$(CO)Cl$_3$]

Rearrangements of this type are common. However, an example of a reaction in which reorientation of dppp does not occur is the reaction between [Fe(η^1-dppp)$_2$(CO)$_3$] and metal species such as Ni(NCS)$_2$, CuCl and Hg(SCN)$_2$.[88] The reaction below shows how the phosphorus atoms remain bonded to the iron centre while the nitrogens coordinate to the second metal, in this case Ni(II).

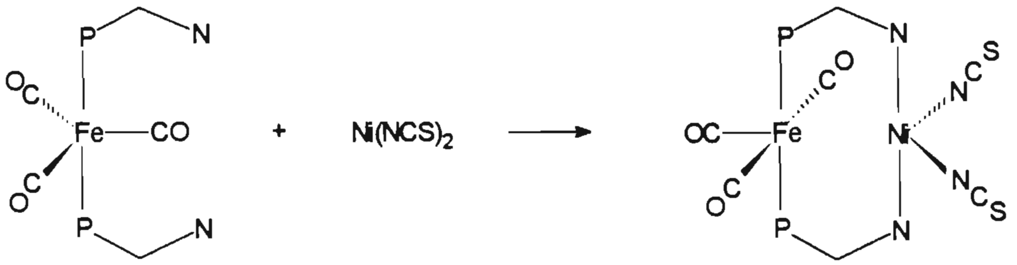

1.5.4 Concluding remarks

As with dppm, dppa and tpdo, the most common mode of coordination adopted by the dppp ligand is that of bridging, whereby the ligand spans two like or unlike metal centres to form homo- or heterodinuclear metal complexes. With regards to this coordination mode, because the bite size of dppp is smaller than that of dppm, dppa and tpdo, it cannot accommodate as wide a range of metal-metal distances. In fact, the small bite size of dppp favours metal-metal distances in the metal-metal single bond range. Thus, for example, where many Rh(I)-Rh(I) dppm complexes contain no formal Rh-Rh bond, Rh(I)-Rh(I) dppp complexes are generally found to contain metal-metal bonds. Complexes which contain pendant dppp ligands, of which only a few have been structurally characterised, resemble their triphenylphosphine analogues and are generally stable.

Least likely for dppp is for it to chelate at a single metal atom. The inherent ring strain generally distorts normally stable coordination geometries at the metal centre. Hence, very few examples of these complexes have been reported.

1.6 Complexes of diphenylphosphinoquinoline (dppq)

This new ligand provides an extension to the dppp ligand described above since it is envisaged to be a more efficient electron reservoir capable of increased π-back bonding.

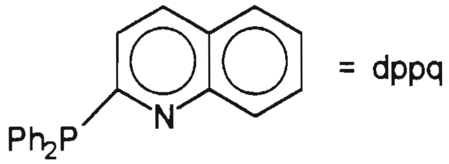

Its coordination chemistry has yet to be studied in detail and in later chapters, it is seen to coordinate in a P-monodentate fashion as well as in a bridging fashion. Of the work that has been carried out to date,[89] it is known only to bridge across two metal atoms. Reaction of dppq with Group 11 metal precursors affords the coordinatively unsaturated dimers $[Cu_2(\mu\text{-dppq})_2(NCMe)_2](PF_6)_2$ and $[Au_2(\mu\text{-dppq})_2](PF_6)_2$,[90] the latter of which has been stucturally characterised.

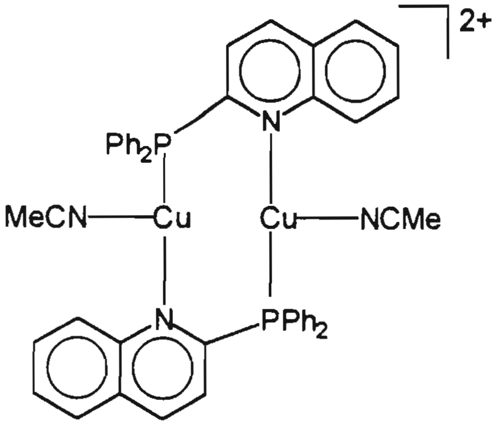

$[Cu_2(\mu\text{-dppq})_2(NCMe)_2]^{2+}$

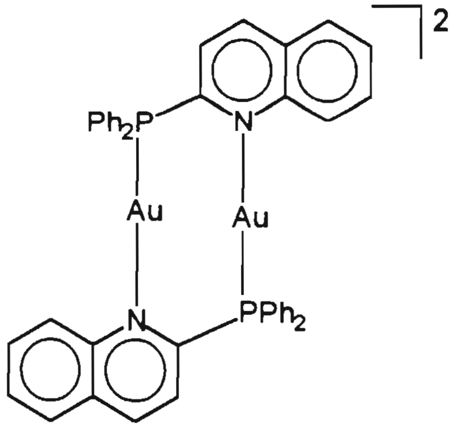

$[Au_2(\mu\text{-dppq})_2]^{2+}$

1.7 Objectives of this study

The initial aim of this work was to develop the synthesis of the new ligand 6-diphenylphosphino-2,2′-bipyridyl (Ph_2Pbipy) and to study its coordination to a range of low oxidation state ruthenium precursors as well as to investigate the chemistry of the resultant products. This ligand can also be regarded as being related to triphenylphosphine, but is distinguished from the ligands discussed in the previous sections by the presence of a *bidentate* substituent (the bipyridyl fragment) rather than a *monodentate* substituent for the phenyl group; as such the Ph_2Pbipy ligand is a *tridentate* potentially binucleating ligand. The bipyridyl (bipy) ligand itself is one of the most widely used ligands in coordination chemistry.[91] Its importance stems in the first instance from its ability to stabilise transition metals in a wide range of oxidation states. Furthermore, as a consequence of the presence of low lying π*-orbitals on the ligand a number of bipyridyl complexes *e.g.*, $[Os(bipy)_2(CO)H]PF_6$ [92], $[Ru(bipy)_2(CO)H]PF_6$ [93], and $[Rh(bipy)_2Cl_2]PF_6$ [94], have been found to be effective electrocatalysts for processes such as the reduction of carbon dioxide. Also, a number of these complexes *e.g.*, $[Ru(bipy)_3]Cl_2$ [95,96] and$[ReX(bipy)(CO)_3]$ (X = Cl, Br, I)[97] have proved to be very effective light sensitisers with their long-lived excited states being derived from d_π(metal)-π\*(bipyridine) metal to ligand charge-transfer (MLCT) transitions. Thus, in Ph_2Pbipy, the properties of two of the most important ligands in coordination and organometallic chemistry have been combined.

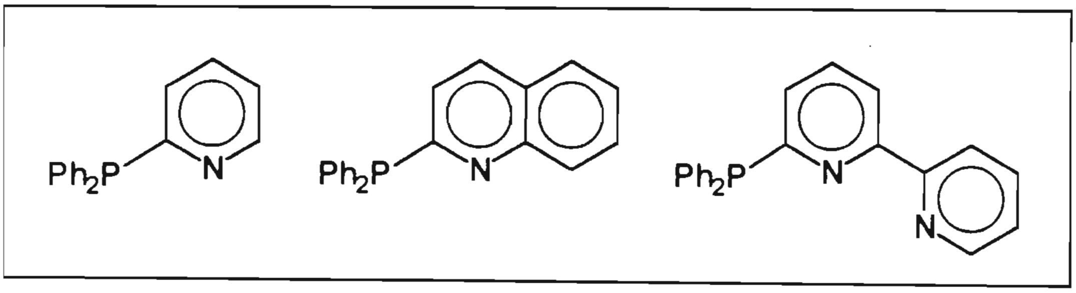

The coordination chemistry of 2-diphenylphosphinopyridine (Ph_2Ppy or dppp-section 1.5) and 2-diphenylphosphinoquinoline (Ph_2Pquin or dppq - section 1.6) ligands has also been studied, partly to extend the work on the Ph_2Ppy ligand, but also to allow comparisons to be made between the coordination behaviour of all three ligands. The Ph_2Ppy ligand was discussed in Section 1.5, the conclusion being that it is likely to adopt the bridging coordination mode. The synthesis of the Ph_2Pquin ligand has only very recently been reported [89] but, by analogy with the pyridyl analogue, it is also expected to adopt the bridging coordination mode in its complexes. Of relevance to the possible modes of coordination of the Ph_2Pbipy ligand is the observation that the bipyridyl ligand coordinates to the metal atom in a chelating fashion in virtually all its complexes. [91] Assuming that the bipyridyl fragment in Ph_2Pbipy will also bond in this way, there are three likely modes of coordination for the Ph_2Pbipy ligand *viz.* monodentate coordination through the phosphorus atom, chelation through the nitrogen atoms of the bipyridyl fragment and bridging where the phosphorus atom bonds to one metal atom and the bipyridyl fragment chelates to a second metal atom. These are illustrated below.

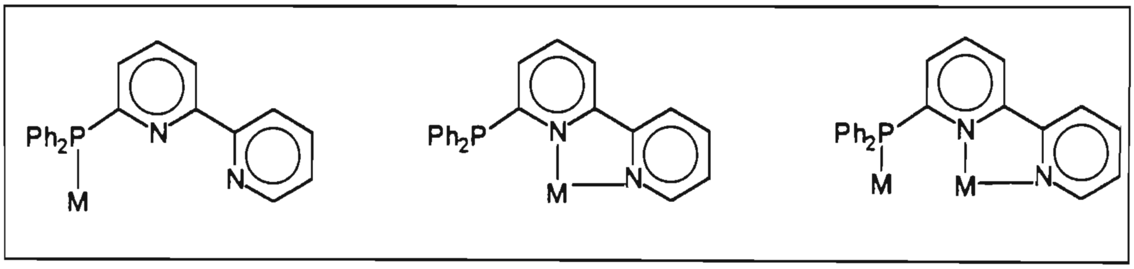

Figure 1.11: The feasible coordination modes of Ph_2Pbipy

A fourth mode of coordination is also possible *viz* coordination by all three donor atoms to the same metal atom. This mode is considered less likely than the three illustrated above in view of the considerable angle strain that would be involved. Of all the above possibilities the bridging mode of coordination appears most likely for Ph_2Pbipy. This can be understood by noting that Ph_2Pbipy can be considered as a tridentate equivalent of the bidentate Ph_2Ppy ligand, the bridging properties of which are well established (see section 1.5). With this expectation in mind, a further aim of this study can be stated; to employ the Ph_2Pbipy ligand in the synthesis of *dinuclear* transition metal complexes of ruthenium which are stabilised to fragmentation by the presence of the bridging ligand. As the work in subsequent chapters shows, this aim has been largely realised. During the course of the investigation the serendipitous discovery was made the Ph_2Pbipy ligand has a high affinity for silver in the +I oxidation state. As a consequence the coordination behaviour of Ph_2Pbipy towards precursors of silver(I) has also been studied. A further aim was to develop procedures for the synthesis of Ph_2Ppy and Ph_2Pbipy ligand-bridged dinuclear complexes containing ruthenium and one other metal atom. These procedures were based on the use of mononuclear complexes of ruthenium containing the ligand coordinated in a pendant fashion *i.e.*, bonded to the ruthenium through the phosphorus atom only. Though the synthesis of the mononuclear precursors has been achieved attempts to produce the mixed-metal dimers were not successful.

CHAPTER TWO

SYNTHESIS AND STRUCTURAL CHARACTERISATION OF THE NOVEL 6-DIPHENYLPHOSPHINO-2,2′-BIPYRIDINE (Ph_2Pbipy) LIGAND

2.1 Introduction

The general preparation of phosphines as well as the known metal complexes of the pyridylphosphines has recently been overviewed by Newkome.[79] The review highlights the increased usage of pyridylphosphines in metal ion coordination over the last decade. Indeed, this field in expanding as new structural combinations are prepared. The use of *poly*pyridine ligands has already been motivated (Chapter 1) and by coupling these polypyridines with diphenylphosphide nucleophiles, Ziessel[98] has reported a series of new heterodifunctional ligands shown in Figure 2.1.

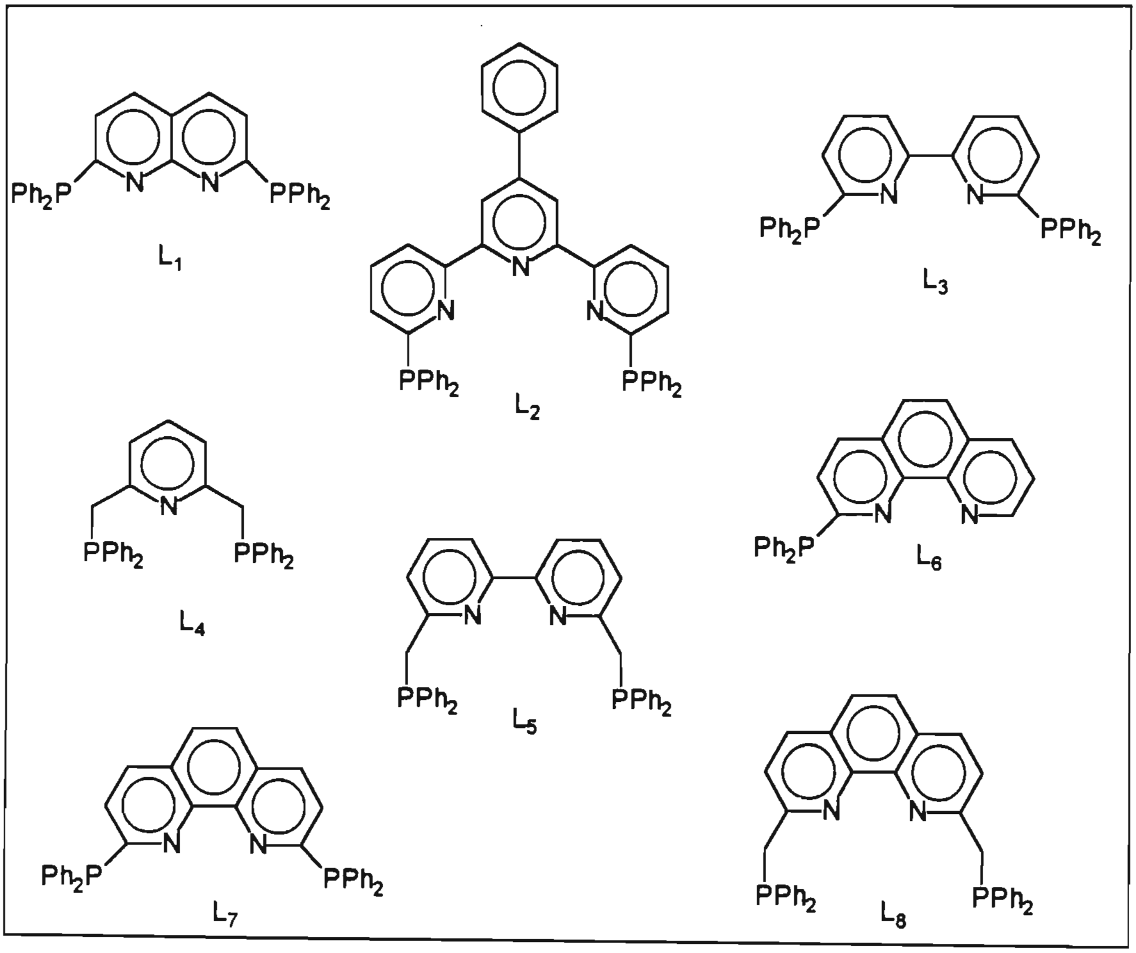

Figure 2.1

Ziessel's paper, which is at best sketchy, describes the coordination of L_1 to rhodium (I) precursors and does not discuss in any sort of detail analogous reactions with the other ligands. Furthermore, no subsequent reports on work of this nature have been forthcoming from his group.

No attempts have been made to synthesise and characterise monosubstituted analogues of the ligands above and to this end, we have synthesised the novel monosubstituted polypyridine ligand 6-diphenylphospino-2,2'-bipyridine (Ph_2Pbipy). In this chapter, a substantially modified synthesis of the 6-chloro precursor[99] is reported together with its conversion to the diphenylphosphine, based on methods used by Balch *et al.*[80] for the synthesis of the diphenylphosphinopyridine (dppp) ligand.

2.2 Synthesis and characterisation of 6-diphenylphosphino- 2,2'-bipyridine

Figure 2.2 shows a schematic representation of the synthesis of the Ph_2Pbipy ligand.

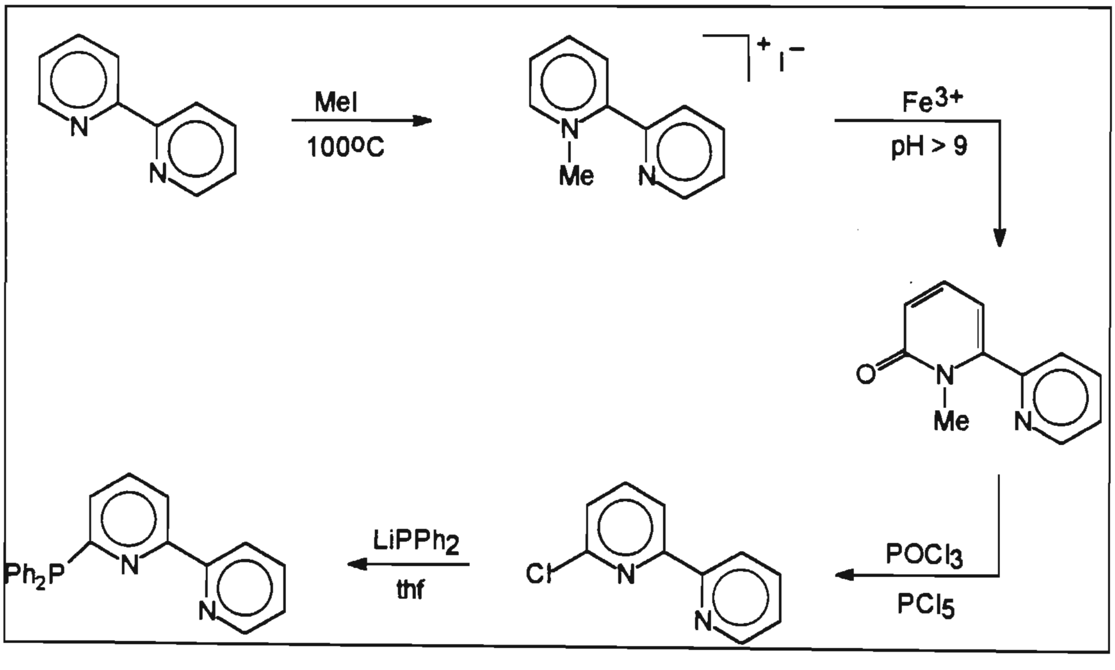

Figure 2.2: The synthesis of 6-diphenylphosphino-2,2'-bipyridine

The first step involves the methylation by methyl iodide of one of the nitrogen atoms of bipyridine to afford 2,2′-bipyridylmonomethiodide in good yield. In the second step a strongly alkaline solution of ferric salts is used to oxidise the monomethiodide to 1-methyl-2,2′-bipyridin-6-one, a high yield again being obtained. The third step involves the chlorination of the keto-group by PCl_5 and $POCl_3$ to afford 6-chloro-2,2′-bipyridine but, in this step, a low yield of only *ca.* 30% is obtained. The latter compound is reacted with lithium diphenylphosphide to afford the required product, a good yield in this final step also being obtained. The overall yield of 22% is limited by the poor yield of the product in the third step but, although numerous attempts were made to improve the yield for this stage by repeating it under a variety of different conditions, they were not successful. The Ph_2Pbipy ligand is air-sensitive being readily oxidised to the corresponding oxide; evidence for this is the appearance in the $^{31}P\{^1H\}$ n.m.r. spectrum of a singlet at δ 19.98 characteristic of the oxidised product. Fortunately, the phosphine oxide is readily separated from Ph_2Pbipy by extraction into cold methanol; in fact the ligand is soluble in alcohols but only at temperatures above 30°C. It is soluble at room temperature in most other organic solvents, however. The ligand is stable up to temperatures of *ca.* 130°C, but rapidly degrades on exposure to ultraviolet light.

Figure 2.3 shows the ^1H n.m.r. spectrum while Table 2.1 lists the salient characterisation data for the Ph_2Pbipy ligand. The $^{31}P\{^1H\}$n.m.r. spectrum consists of a sharp singlet at δ -3.71, a chemical shift which clearly distinguishes the free ligand from the oxide (*vide supra*) and the coordinated ligand,[100] both of which have ^{31}P chemical shifts downfield of that for the free ligand. The high field value is indicative of high electron density on the phosphorus atom of the free ligand. As indicated in Table 2.1, the peaks in the ^1H n.m.r. spectrum of Ph_2Pbipy can be assigned to individual protons but the complex coupling effects in the $^{13}C\{^1H\}$ n.m.r. spectrum do not allow an equivalent assignment of the individual carbon atoms. The remaining spectroscopic data require no further comment, except to note that the UV/vis spectrum of bipyridine was also recorded and under the same conditions as that for Ph_2Pbpy; an intense band corresponding to a π-π* transition is also observed at 285 nm.

Table 2.1 : Spectroscopic data for 6-diphenylphosphino-2,2′-bipyridine

$^{31}P\{^{1}H\}$ nmr [a]	-3.71
^{1}H nmr [b]	8.62(1H, dbrm, $H_{6'}$) 8.31(2H, dbrm, $H_{3,3'}$) 7.65(2H, tbrm, $H_{4.4'}$) 7.39(10H,m,Ph) 7.19(2H,m,$H_{5,5'}$)
^{13}C nmr [c]	120-150(17C,d, aromatic CH's) 150-164(5C,s, quat.C's)
Infrared [d]	1421s, 1431m, 1472w, 1477w, 1550m, 1565m, 1572m, 1583w
UV/vis [e]	285 (π-π*)
GC-MS	*m/z* 340.3

[a] δ Scale: ppm values measured relative to $P(OMe)_3$ as internal standard at 303 K in CD_2Cl_2. [b] Measured at 303 K in $CDCl_3$: dbrm = doublet of broad multiplets, tbrm = triplet of broad multiplets, m = mulitplet. [c] Measured at 303 K in $CDCl_3$. [d] KBr disc; cm^{-1}. [e] Measured in CH_2Cl_2.

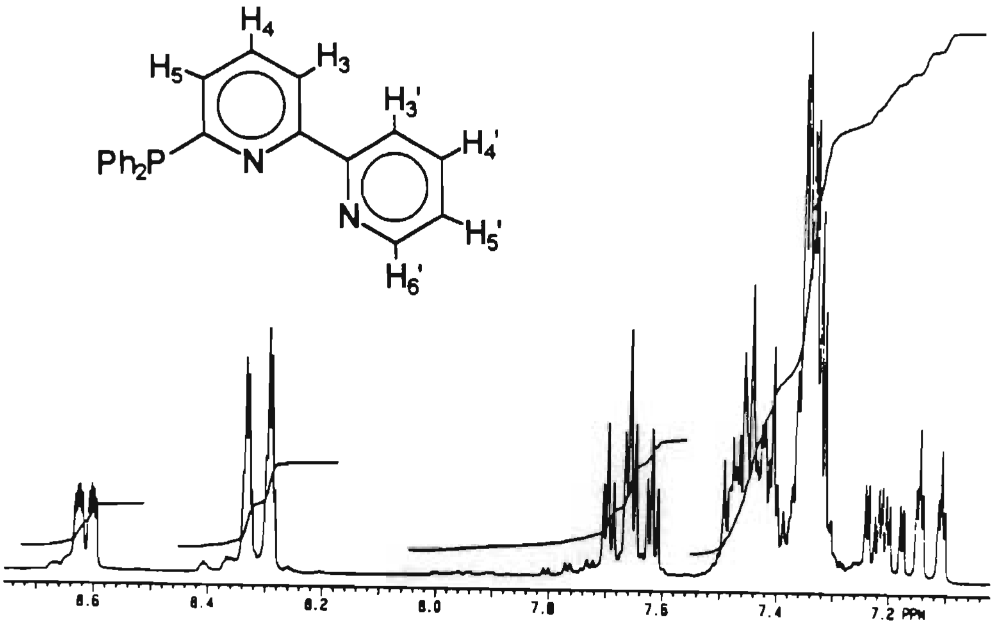

Figure 2.3: The ^{1}H nmr spectrum of 6-diphenylphosphino-2,2′-bipyridine ($CDCl_3$)

2.3 Crystal structure determination of 6-diphenylphosphino-2,2'-bipyridine

Figure 2.4 gives a perspective view of the ligand and also shows the atom labelling scheme. Tables 2.3 and 2.4 list the interatomic distances and angles respectively. The ligand molecules exist as discrete entities in the crystal, there being no non-bonded contact distances less than the sum of the van der Waals radii for the two atoms concerned.

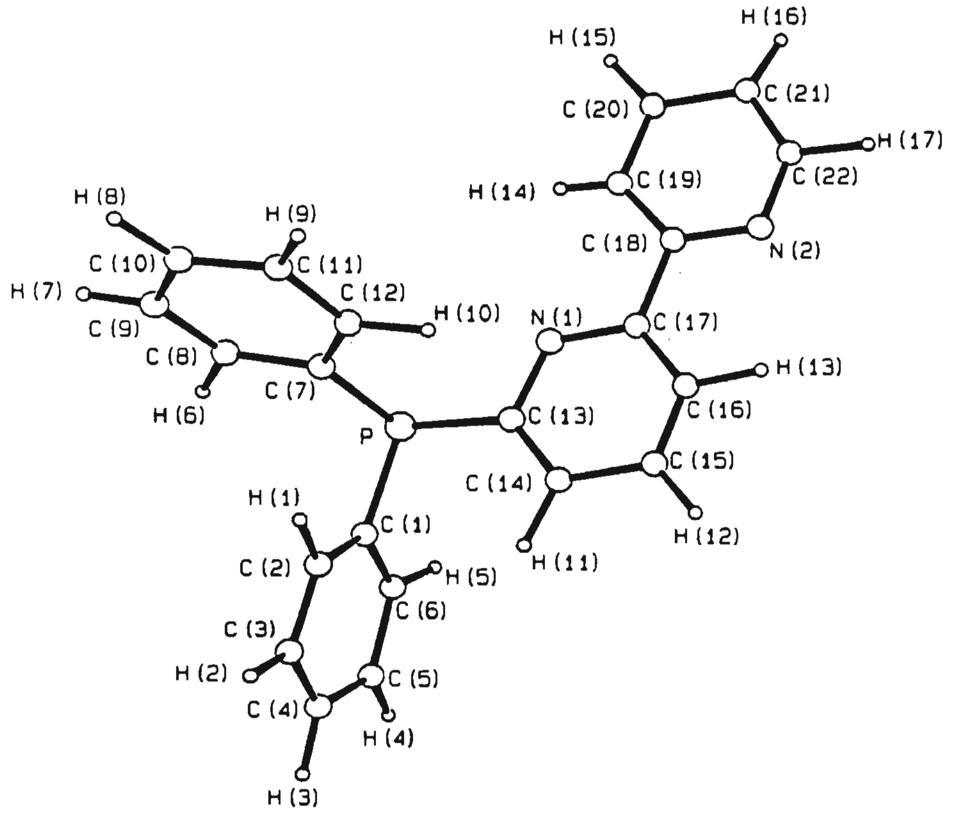
H (16)
H (15)
C (21)
C (20)
H (17)
C (19)
C (22)
H (14)
H (8)
H (9)
C (18)
N (2)
C (10)
C (11)
H (7)
C (12)
C (9)
H (10)
N (1)
C (17)
C (8)
H (13)
C (7)
C (16)
H (6)
C (13)
P
C (15)
C (14)
H (1)
C (1)
H (12)
C (2)
H (5)
H (11)
C (6)
C (3)
H (2)
C (5)
C (4)
H (4)
H (3)

Figure 2.4: A perspective view of 6-diphenylphosphino-2,2'-bipyridine, showing the atom numbering scheme

The bipyridyl fragment of the Ph_2Pbipy ligand adopts a near-planar *transoid* arrangement in the solid state as found for 2,2′-bipyridine itself.[101] The dihedral angle between the mean-planes through the non-hydrogen atoms of each pyridine ring is 7,7(3)° and the distance of the phosphorus atom from the mean-plane through all the non-hydrogen atoms of the bipyridyl fragment is 0,25(1)Å. The geometry at the phosphorus atom is pyramidal, with the C-P-C angles all close to 102° and with the phenyl rings adopting orientations such that their planes are at dihedral angles of 90,0(2) [C(1) to C(6)] and 104,5(2)° [C(7) to C(12)] to that of the bipyridyl fragment. Although the free Ph_2Pbipy ligand has the expected *transoid* arrangement in the solid state there is the possibility of free rotation about the interannular C-C bond in solution. Indeed, the chelating bonding mode of 2,2′-bipyridine found in the vast majority of its complexes [91] requires a *cisoid* arrangement about the interannular bond. In general, a near-planar configuration of the two pyridyl rings is observed in these complexes,[91] the implication being that there is little difference in stability between the *transoid* and *cisoid* forms of the bipyridyl moiety. Several crystal structures of complexes of the Ph_2Pbipy ligand are now known and in all of these the bipyridyl fragment adopts the chelating bonding mode with a near-planar configuration for the two pyridyl rings.[100] Given that the bipyridyl fragment of the Ph_2Pbipy ligand will chelate at a single metal atom the coordination of the phosphorus may be either at the same metal atom or at a second metal atom. In view of the known propensity of the 2-diphenylphosphinopyridine (Ph_2Ppy) ligand to bridge two metal atoms rather than to chelate at one metal atom, the latter mode of coordination is more likely; in fact all the crystal structures of complexes of the Ph_2Pbipy ligand determined so far show the ligand bridging two metal atoms.[100] The P...N(1) distance of 2,655(2)Å in the free Ph_2Pbipy ligand defines the bite of the potentially bridging moiety.

Remaining bond lengths and angles in the Ph_2Pbipy ligand are as expected (see Tables 2.3 and 2.4). Interestingly, there are no significant differences between the C-C and C-N bond lengths in the two pyridyl rings which might have been brought about by the presence of the bulky diphenylphosphido substituent in the 6-position. This is consistent with the observation that the UV/vis absorption spectra of Ph_2Pbipy and bipyridine itself are identical (*vide supra*) and also with our aim of employing the diphenylphosphido group simply as a means of anchoring the bipyridyl moiety to a second metal atom *i.e.*, without disturbing its electronic structure.

2.4 Experimental

All reactions were carried out in air unless otherwise specified. Solvents were dried and redistilled prior to use by the usual methods.[102] The thf used in the final step was first distilled from sodium and benzophenone and then redistilled from calcium hydride under an argon atmosphere to ensure absolute dryness.

2.4.1 Synthesis of 2,2′-bipyridyl-monomethiodide

A solution of 2,2′-bipyridyl (97g: 0.62mol) and methyl iodide (38.7cm^3; 0.62mol) in methanol (200cm^3) was refluxed in a vacuum-sealed Schlenk tube (500cm^3) at 100°C for 15 hours. The solution was filtered to remove the yellow dimethiodide by-product and the filtrate evaporated to yield an orange/yellow crystalline residue. 2,2′-Bipyridine was extracted from this residue using petroleum ether (60-80°C) (250cm^3) as extractant. The residual monomethiodide was found to be sufficiently pure for the next stage of synthesis. Yield 156 g (84%). Mpt 146°C. [Found: C, 44.3; H, 3.9; N, 9.3. Calc. for $C_{11}H_{11}N_2I$: C, 44.3; H, 3.7; N, 9.4%].

2.4.2 Synthesis of 1-methyl-2,2′-bipyridin-6-one

Solid 2-2′-bipyridyl-monomethiodide (156g; 0.52mol) was added in small portions to a saturated aqueous solution (800cm^3) of $K_3[Fe(CN)_6]$ (341g; 1.04mol) and NaOH (83g; 2.08mol) and at a rate such that the temperature of the solution did not exceed 10°C (ice-water bath). Following complete addition the reaction mixture was stirred at 10°C for 2 hours and subsequently at room temperature for a further 15 hours. The resulting black solution was extracted with ten 350cm^3 aliquots of $CHCl_3$ and the aliquots combined and dried over anhydrous magnesium sulphate for 3 hours. The solution was filtered and the filtrate evaporated to dryness. The residue was dried further in vacuo for at least 5 hours to afford the product sufficiently pure not to require crystallisation. Yield 86 g (88%). Mpt. 76°C. [Found: C, 70.7; H, 5.5; N, 14.9. Calc. for $C_{11}H_{10}N_2O$: C, 71.0; H, 5.4; N, 15.0%]

2.4.3 Synthesis of 6-chloro-2,2′-bipyridine

A one-litre round-bottomed flask, fitted with a reflux condenser and a DMSO bubbler or a $CaCl_2$ drying tube, was charged with 1-methyl-2,2′-bipyridin-6-one (86g; 0.46 mol), PCl_5 (96g; 0.46mol) and $POCl_3$ (ca. 200cm^3). The solution was refluxed at 130°C for 3 hours and then cooled to room temperature. Ice was added in small pieces down the condenser, producing a large quantity of HCl gas. Once evolution of gas had ceased, the resulting solution was basified with ammonia to a pH of *ca.* 10 and then allowed to stand at room temperature for 24 hours. The black precipitate which separated was filtered, dried in air and extracted into boiling petroleum ether (500cm^3; 60-80°C). The yellow petroleum ether extract was decanted and filtered, and then treated with activated charcoal. After filtering and evaporation of the filtrate under reduced pressure, the pale yellow product was dried in vacuo. Yield 28.5g (32%). Mpt. 59°C. GC-MS studies revealed a molecular ion peak (M^+) at 190. [Found: C, 63.6; H, 4.1; N,14,2. Calc. for $C_{10}H_7N_2Cl$; C, 63.0; H, 4.1; N, 14.7%]

2.4.4 Synthesis of 6-diphenylphosphino-2,2′-bipyridine

All manipulations in this preparation were performed under an atmosphere of argon. A solution of $ClPPh_2$ (27cm^3; 150mol) in thf (90cm^3) was added dropwise to a stirred suspension of freshly cut lithium (2.1g; 300mmol) in thf (78cm^3). On appearance of the characteristic red colour of $LiPPh_2$ stirring was continued for a further one hour. The red solution was then filtered to remove excess lithium and lithium chloride. The filtrate was cooled to -75°C and continuously stirred while a solution of 6-chloro-2,2′-bipyridine (28.5g; 150mmol) in thf (84cm^3) was added dropwise. The resulting black solution was stirred at room temperature for 15 hours. Hydrochloric acid was first added (initially 100cm^3 3*M* HCl followed by 40cm^3 concentrated HCl) to hydrolyse any free $LiPPh_2$, followed by aqueous ammonia to bring the pH to *ca.* 10. The resulting yellow solution was extracted with diethyl ether (5 x 100cm^3), the combined extracts dried over $MgSO_4$, and the solvent removed under reduced pressure to afford the product as a light-yellow residue. Recrystallisation from $CHCl_3$/methanol at -25°C gave a microcrystalline pale-yellow solid. Yield 52 g (94%). Mpt. 116-118°C. [Found: C, 77.8; H, 5.2; N, 7.9. Calc. for $C_{22}H_{17}N_2P$: C, 77.6; H, 5.0; N, 8.2%]

2.4.5 Single crystal X-ray diffraction study of 6-diphenylphosphino-2,2′-bipyridine

Pale yellow crystals of Ph_2Pbipy were grown by slow evaporation of a saturated CH_3CN solution of the compound. The general approach used for the intensity data collection is described in Appendix A. The crystallographic data are given in Table 2.2, the interatomic distances in Table 2.3, the interatomic angles in Table 2.4, the fractional coordinates in Table 2.5 and the anisotropic thermal parameters in Table 2.6. The observed and calculated structure factors may be found on microfiche in an envelope fixed to the inside back cover.

Table 2.2

Crystal data and details of the crystallographic analysis for 6-diphenylphosphino-2,2′-bipyridine

Formula	$C_{22}H_{17}N_2P$
Molecular Mass	340.36
Crystal System	monoclinic
Space Group	$P2_1/c$
a(Å)	10.446(1)
b(Å)	9.306(1)
c(Å)	19.016(1)
β(°)	91.68(1)
$V(Å^3)$	1848.0(4)
Z	4
$D_c(g.cm^{-3})$	1.23
F(000)	652
λ(Mo-Kα)(Å)	0.71069
Scan mode	ω-2θ
ω scan angle	$0.80 + 0.35 \tan\theta$
Horizontal Aperture width (mm)	$2.70 + 0.4 \tan\theta$
Scattering range (°)	$2 \leq \theta \leq 23$
$\mu\ (cm^{-1})$	1.59
Absorption corrections	Semi-empirical[103]
Measured intensities	2425
Unique intensities	2326
Unique intensities with $[I > 3\sigma(I)]$	1952
Structure solution	Direct methods
Weighting scheme	$1/[\sigma^2(F)+0{,}01F^2]$
$R = \Sigma(F_o-F_c)/\Sigma F_o$	0.036
$R_w = \Sigma_w½\,(F_o-F_c)/\ \Sigma_w½F_o$	0.044
$(\Delta/\sigma)_{max}$	0.017
$\Delta\rho_{max}(eÅ^{-3})$	0.15
Number of parameters	278

Table 2.3 Interatomic distances (Å) for Ph_2Pbipy

P-C(1)	1.833(2)	P-C(7)	1.834(2)
P-C(13)	1.842(2)	N(1)-C(13)	1.341(3)
N(1)-C(17)	1.342(3)	N(2)-C(18)	1.335(3)
N(2)-C(22)	1.338(3)	C(1)-C(2)	1.384(3)
C(1)-C(6)	1.386(4)	C(2)-C(3)	1.387(4)
C(2)-H(1)	.92(3)	C(3)-C(4)	1.362(4)
C(3)-H(2)	.92(3)	C(4)-C(5)	1.364(4)
C(4)-H(3)	.93(3)	C(5)-C(6)	1.370(4)
C(5)-H(4)	.90(3)	C(6)-H(5)	.81(3)
C(7)-C(8)	1.382(3)	C(7)-C(12)	1.380(3)
C(8)-C(9)	1.383(5)	C(8)-H(6)	1.02(3)
C(9)-C(10)	1.378(5)	C(9)-H(7)	.81(3)
C(10)-C(11)	1.353(4)	C(10)-H(8)	.98(3)
C(11)-C(12)	1.380(4)	C(11)-H(9)	.93(3)
C(12)-H(10)	.95(3)	C(13)-C(14)	1.385(3)
C(14)-C(15)	1.381(4)	C(14)-H(11)	.99(3)
C(15)-C(16)	1.385(4)	C(15)-H(12)	.99(3)
C(16)-C(17)	1.395(3)	C(16)-H(13)	.97(3)
C(17)-C(18)	1.491(3)	C(18)-C(19)	1.385(4)
C(19)-C(20)	1.381(4)	C(19)-H(14)	.89(3)
C(20)-C(21)	1.363(4)	C(20)-H(15)	.84(3)
C(21)-C(22)	1.362(4)	C(21)-H(16)	.92(3)
C(22)-H(17)	.95(3)		

Table 2.4 Interatomic angles (°) for Ph_2Pbipy

C(1)-P-C(7)	101.9(1)	C(1)-P-C(13)	102.1(1
C(7)-P-C(13)	101.4(1)	C(13)-N(1)-C(17)	118.2(2
C(18)-N(2)-C(22)	116.4(2)	P-C(1)-C(2)	124.9(2
P-C(1)-C(6)	117.4(2)	C(2)-C(1)-C(6)	117.7(2
C(1)-C(2)-C(3)	120.3(2)	C(1)-C(2)-H(1)	119(2)
C(3)-C(2)-H(1)	121(2)	C(2)-C(3)-C(4)	120.9(3
C(2)-C(3)-H(2)	118(2)	C(4)-C(3)-H(2)	122(2)
C(3)-C(4)-C(5)	119.0(3)	C(3)-C(4)-H(3)	120(2)
C(5)-C(4)-H(3)	121(2)	C(4)-C(5)-C(6)	120.9(3
C(4)-C(5)-H(4)	118(2)	C(6)-C(5)-H(4)	121(2)
C(1)-C(6)-C(5)	121.1(3)	C(1)-C(6)-H(5)	110(2)
C(5)-C(6)-H(5)	129(2)	P-C(7)-C(8)	117.0(2
P-C(7)-C(12)	125.0(2)	C(8)-C(7)-C(12)	118.0(2
C(7)-C(8)-C(9)	120.2(3)	C(7)-C(8)-H(6)	115(2)
C(9)-C(8)-H(6)	124(2)	C(8)-C(9)-C(10)	120.8(3
C(8)-C(9)-H(7)	120(2)	C(10)-C(9)-H(7)	119(2)
C(9)-C(10)-C(11)	119.1(3)	C(9)-C(10)-H(8)	116(2)
C(11)-C(10)-H(8)	124(2)	C(10)-C(11)-C(12)	120.5(3
C(10)-C(11)-H(9)	118(2)	C(12)-C(11)-H(9)	121(2)
C(7)-C(12)-C(11)	121.3(3)	C(7)-C(12)-H(10)	118(2)
C(11)-C(12)-H(10)	120(2)	P-C(13)-N(1)	112.1(2
P-C(13)-C(14)	125.2(2)	N(1)-C(13)-C(14)	122.7(2
C(13)-C(14)-C(15)	118.8(2)	C(13)-C(14)-H(11)	121(2)
C(15)-C(14)-H(11)	120(2)	C(14)-C(15)-C(16)	119.3(2
C(14)-C(15)-H(12)	124(2)	C(16)-C(15)-H(12)	117(2)
C(15)-C(16)-C(17)	118.3(2)	C(15)-C(16)-H(13)	121(2)
C(17)-C(16)-H(13)	121(2)	N(1)-C(17)-C(16)	122.6(2
N(1)-C(17)-C(18)	116.2(2)	C(16)-C(17)-C(18)	121.1(2
N(2)-C(18)-C(17)	116.2(2)	N(2)-C(18)-C(19)	122.8(2
C(17)-C(18)-C(19)	120.9(2)	C(18)-C(19)-C(20)	118.6(3
C(18)-C(19)-H(14)	121(2)	C(20)-C(19)-H(14)	121(2)
C(19)-C(20)-C(21)	119.2(3)	C(19)-C(20)-H(15)	118(2)
C(21)-C(20)-H(15)	123(2)	C(20)-C(21)-C(22)	118.3(3
C(20)-C(21)-H(16)	127(2)	C(22)-C(21)-H(16)	114(2)
N(2)-C(22)-C(21)	124.7(3)	N(2)-C(22)-H(17)	114(2)
C(21)-C(22)-H(17)	121(2)		

Table 2.5 Fractional coordinates (x10^4) and isotropic thermal factors (Å^2,x10^3) for Ph_2Pbipy

	x/a	y/b	z/c	U_{eq}
P	7145(1)	867(1)	5797(1)	52(1)
N(1)	6837(2)	2345(2)	4610(1)	49(1)
N(2)	6182(2)	4267(2)	3003(1)	68(1)
C(1)	7656(2)	-998(2)	5939(1)	47(1)
C(2)	8917(2)	-1450(3)	6004(1)	54(1)
C(3)	9200(3)	-2889(3)	6116(1)	62(1)
C(4)	8249(3)	-3881(3)	6174(2)	72(1)
C(5)	7006(3)	-3445(3)	6104(2)	86(1)
C(6)	6707(3)	-2030(3)	5989(2)	70(1)
C(7)	8585(2)	1869(2)	6073(1)	51(1)
C(8)	8817(3)	2026(3)	6788(1)	76(1)
C(9)	9882(4)	2777(4)	7035(2)	96(1)
C(10)	10718(3)	3391(3)	6575(2)	80(1)
C(11)	10492(3)	3245(3)	5875(2)	71(1)
C(12)	9435(2)	2493(3)	5623(2)	58(1)
C(13)	7192(2)	1033(2)	4833(1)	50(1)
C(14)	7512(2)	-61(3)	4376(1)	62(1)
C(15)	7467(3)	208(3)	3661(1)	67(1)
C(16)	7106(2)	1558(3)	3421(1)	60(1)
C(17)	6799(2)	2601(2)	3915(1)	48(1)
C(18)	6375(2)	4065(2)	3693(1)	51(1)
C(19)	6152(2)	5126(3)	4186(1)	59(1)
C(20)	5682(3)	6436(3)	3955(2)	72(1)
C(21)	5455(3)	6644(3)	3252(2)	79(1)
C(22)	5736(3)	5557(3)	2803(2)	77(1)
H(1)	9555(30)	-781(32)	5980(15)	81(2)*
H(2)	10047(30)	-3138(33)	6171(14)	81(2)*
H(3)	8456(27)	-4828(34)	6279(14)	81(2)*
H(4)	6400(30)	-4127(33)	6095(15)	81(2)*
H(5)	6011(31)	-1660(34)	5926(15)	81(2)*
H(6)	8106(28)	1654(31)	7099(14)	81(2)*
H(7)	9988(31)	2909(33)	7455(17)	81(2)*
H(8)	11411(29)	3972(31)	6787(14)	81(2)*
H(9)	11072(30)	3654(34)	5571(15)	81(2)*
H(10)	9244(29)	2447(30)	5129(16)	81(2)*

Table 2.5 / cont.

H(11)	7772(28)	-1021(32)	4552(15)	81(2)*
H(12)	7713(27)	-501(33)	3304(15)	81(2)*
H(13)	7125(27)	1797(32)	2925(14)	81(2)*
H(14)	6331(28)	4979(32)	4642(16)	81(2)*
H(15)	5606(29)	7096(36)	4252(15)	81(2)*
H(16)	5171(29)	7470(34)	3035(15)	81(2)*
H(17)	5626(28)	5665(31)	2308(16)	81(2)*

* isotropic temperature factor.

$$U_{eq} = \frac{1}{3} \Sigma_i \Sigma_j U_{ij} a_i^* a_j^* (a_i . a_j)$$

Table 2.6 Anisotropic thermal factors (Å^2, x10^3) for Ph_2Pbipy

	U(11)	U(22)	U(33)	U(23)	U(13)	U(12)
P	48(1)	49(1)	59(1)	2(1)	7(1)	8(1)
N(1)	41(1)	49(1)	57(1)	1(1)	-3(1)	5(1)
N(2)	74(1)	67(1)	61(1)	9(1)	-3(1)	10(1)
C(1)	47(1)	46(1)	48(1)	1(1)	5(1)	-1(1)
C(2)	46(1)	50(1)	66(1)	5(1)	4(1)	0(1)
C(3)	60(2)	55(1)	70(2)	0(1)	-2(1)	11(1)
C(4)	81(2)	42(1)	92(2)	4(1)	8(1)	1(1)
C(5)	73(2)	51(2)	135(3)	-4(2)	15(2)	-17(1)
C(6)	47(1)	60(2)	102(2)	-2(1)	6(1)	-6(1)
C(7)	62(1)	38(1)	54(1)	-1(1)	1(1)	9(1)
C(8)	102(2)	70(2)	56(2)	3(1)	-1(1)	-11(2)
C(9)	130(3)	93(2)	64(2)	-8(2)	-35(2)	-4(2)
C(10)	74(2)	68(2)	97(2)	-11(2)	-21(2)	0(2)
C(11)	59(2)	66(2)	88(2)	-6(1)	2(1)	-1(1)
C(12)	55(1)	59(1)	61(1)	-8(1)	2(1)	1(1)
C(13)	39(1)	47(1)	63(1)	0(1)	-3(1)	6(1)
C(14)	67(1)	49(1)	68(2)	-2(1)	-6(1)	9(1)
C(15)	80(2)	58(2)	64(2)	-14(1)	1(1)	11(1)
C(16)	59(1)	62(2)	57(1)	-4(1)	-2(1)	3(1)
C(17)	38(1)	50(1)	57(1)	-1(1)	-4(1)	-1(1)
C(18)	40(1)	54(1)	59(1)	4(1)	0(1)	-2(1)
C(19)	58(1)	52(1)	66(2)	3(1)	-3(1)	1(1)
C(20)	72(2)	51(2)	91(2)	-3(1)	-4(1)	5(1)
C(21)	76(2)	61(2)	101(2)	25(2)	-8(2)	8(1)
C(22)	85(2)	75(2)	71(2)	18(2)	-5(1)	15(2)

CHAPTER THREE

DINUCLEAR PHOSPHORUSPYRIDYL AND PHOSPHORUSBIPYRIDYL LIGAND-BRIDGED DERIVATIVES OF RUTHENIUM(I)

3.1 Introduction

Cluster chemistry has, during the last two decades, become a wide-spread and well documented area of research. Impetus for the plethora of studies that have resulted arises from the potential involvement of metal cluster complexes in homogeneous catalysis. Moreover, the arrangement of metal atoms in a cluster molecule is often similar to that believed to occur for the metal atoms at the surfaces of bulk metals and thus a study of cluster chemistry could provide insights into catalytic processes which take place at metal surfaces.

Of all metal clusters, dimers are the simplest. The involvement of dimetal centres in certain catalytic processes [104-106] is probably the consequence of (i) the stabilisation of unusual metal oxidation states through metal-metal bonding as well as (ii) the fact that certain ligand bonding modes (the most obvious being the bridging mode) not feasible in monometallic complexes, are possible. Metal dimers can be stabilised through the use of bridging bidentate ligands (see chapter 1) which hold the two metal atoms in close proximity to each other as well as promoting bridging by other groups. Metal-metal bonds are intrinsically weak but can be reversibly cleaved in the presence of bridging ligands without leading to cluster fragmentation.

Extensive use has been made of the bis(diphenylphosphino)methane (dppm) ligand for the stabilisation of dinuclear compounds to fragmentation.[7, 108] The propensity to bridge is also exhibited by the diphosphazane ligands $(RO)_2PNEtP(OR)_2$ (R = Me, Et, ^iPr or Ph) which have been used to stabilise substituted derivatives of the unstable diruthenium(O) nonacarbonyl $[Ru_2(CO)_9]^{69a),b)}$ to fragmentation. Thus an extensive chemistry of the Ru(O) species $[Ru_2(\mu\text{-}CO)(CO)_4\{\mu\text{-}(RO)_2PNEtP(OR)_2\}_2]$ has been developed.[109,110]

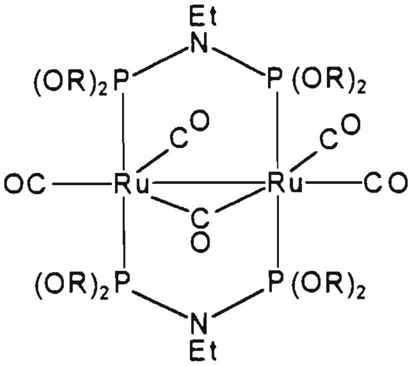

$[Ru_2(\mu\text{-}CO)(CO)_4\{\mu\text{-}(RO)_2PNEtP(OR)_2\}_2]$ (R = Me, Et, ^{i}Pr or Ph)

In this chapter, the reactions of the potentially bridging Ph_2Ppy, Ph_2Pquin and Ph_2Pbipy ligands (see chapter 1) with ruthenium(I) precursors are described, the aim being to develop stable diruthenium(I) ligand-bridged systems. Attempts were made to synthesise derivatives of Ru(O) similar to those mentioned and illustrated above. These were unsuccessful because the conditions required for their synthesis *viz.* the reaction of $Ru_3(CO)_{12}$ with the ligand under forcing conditions such as high temperatures and/or pressures as well as UV irradiation, lead to decomposition of the ligand. A further advantage of the use of a Ru(I), rather than Ru(O), precursor is that the former is slightly harder [111] with the result that coordination of the pyridyl nitrogen donor atoms of the Ph_2Ppy, Ph_2Pquin and Ph_2Pbipy ligands is facilitated; the softer P donor atoms are also expected to coordinate to Ru(I).

A thorough search for suitable Ru(I) precursors yielded two complexes.

a) **$[Ru_2(\mu\text{-}CO)_2(CO)_2(Cp)_2]$** : Complexes based on and derived from this complex constitute by far the largest class of dinuclear compounds of ruthenium(I)[112]. The decision was, however, that this would not be an ideal precursor due to the blocking effect of the cyclopentadienyl rings to ligand entry as well as the thermodynamic stability of the metal-carbon bond.

b) **$[Ru\{\mu\text{-}\eta^2\text{-}OC(R)O\}(CO)_2]_n$** : These insoluble ruthenium(I) carboxylate polymers, first synthesised by Lewis and Johnson,[113] have been shown to be excellent precursors for the synthesis of carboxylate-bridged diruthenium complexes affording products of the type $[Ru_2\{\mu\text{-}\eta^2\text{-}OC(R)O\}_2(CO)_4L_2]$ on treatment with excess of monodentate ligands such as CO, pyridine and tertiary phosphines.[114, 115] The polymer can be solubilised in donor solvents such as acetonitrile,[113] thf [116] or hot alcohols [117] since cleavage of the Ru-O-Ru bridges occurs, affording the labile solvento species $[Ru_2\{\mu\text{-}\eta^2\text{-}OC(R)O\}_2(CO)_4(solv)_2]$. This species, together with the polymer, make convenient synthons for an unusual series of dinuclear Ru(I) complexes, either through the replacement of the carboxylate groups by other bridging anionic ligands or by substitution of the labile solvento groups by bidentate neutral donor ligands.[117-119] For example, reaction of the polymer with 2 equivalents (per dimer unit) of bis(diphenylphosphino)methane (dppm) or bis(dimethylphosphino)methane (dmpm) affords the complex $[Ru_2\{\mu\text{-}\eta^2\text{-}OC(Me)O\}_2(CO)_4\{\eta^1\text{-}(L\text{-}L)\}_2]$ (L-L = dppm or dmpm) in which the dinuclear units contain pendant diphosphine ligands bonded trans to the Ru-Ru bond. Subsequent treatment with NH_4PF_6 under reflux conditions affords the cationic, ligand-bridged derivative $[Ru_2\{\mu\text{-}\eta^2\text{-}OC(Me)O\}(CO)_4\{\mu\text{-}(L\text{-}L)\}_2]^+$ through displacement of a carboxylate ligand in addition to the solvento ligands.[118]

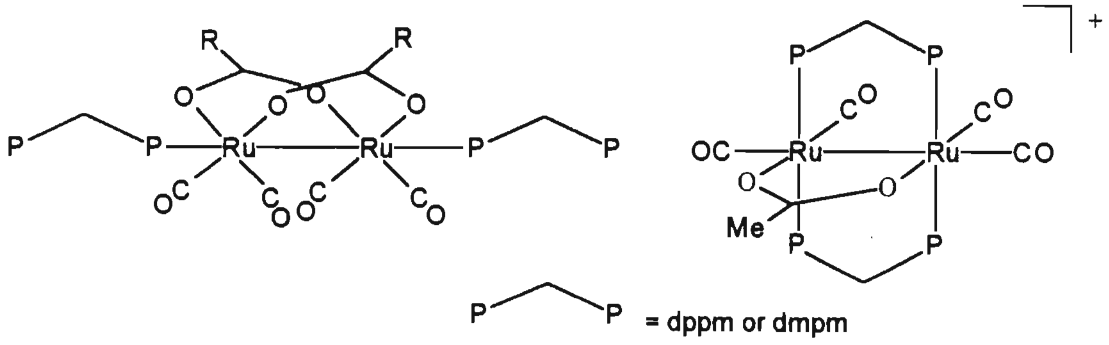

$[Ru_2\{\mu\text{-}\eta^2\text{-}OC(Me)O\}_2(CO)_4\{\eta^1\text{-}(L\text{-}L)\}_2]$ **$[Ru_2\{\mu\text{-}\eta^2\text{-}OC(R)O\}(CO)_4\{\eta^1\text{-}(L\text{-}L)\}_2]^+$**

The expectation was thus that the polymeric carboxylate precursor, or its solvento derivative would be suitable precursors for reaction with phosphoruspyridyl and phosphorusbipyridyl ligands, affording dinuclear ligand-bridged derivatives of ruthenium(I).

Towards the end of this project a further potentially useful ruthenium(I) precursor was reported.[120]

c) **$[Ru_2(CO)_4(NCMe)_6]^{2+}$**: During studies aimed at synthesising polyoxoanion-supported organoruthenium complexes that are reactive towards oxygen under mild condition, this reactive complex, with a core structure corresponding to the as yet unknown $[Ru_2(CO)_{10}]^{2+}$, was prepared. It is extremely substitution labile, as witnessed by the fact that diethyl ether readily substitutes for the acetonitrile in the complex.

Our expectation was thus that it would be an excellent precursor for reaction with the Ph_2Ppy, Ph_2Pquin and Ph_2Pbipy ligands. These reactions are expected to afford products which are distinguished from the ligand-bridged carboxylate diruthenium complexes shown above by the presence of terminal carbonyl and/or acetonitrile ligands, instead of carboxylato bridging ligands. Such complexes would be far more versatile than the carboxylato derivatives in terms of their potential for further chemistry because of the presence of labile acetonitrile ligands.

3.2 Reactions of Ph_2Ppy, Ph_2quin and Ph_2Pbipy with $[Ru\{\mu\text{-}\eta^2\text{-}OC(R)O\}(CO)_2]_n$

3.2.1 Synthesis and characterisation of $[Ru_2\{\mu\text{-}\eta^2\text{-}OC(R)O\}_2(CO)_4(\eta^1\text{-}L)_2]$ (R = H, Me or Et; L = Ph_2Ppy, Ph_2Pquin or Ph_2Pbipy) [1]-[9]

Treatment of the polymeric precursor $[Ru\{\mu\text{-}\eta^2\text{-}OC(R)O\}(CO)_2]_n$ or its acetonitrile adduct $[Ru_2\{\mu\text{-}\eta^2\text{-}OC(R)O\}_2(CO)_4(NCMe)_2]$ (R = H, Me or Et) with two molar equivalents of ligand (per dimer unit) in refluxing alcohols or toluene for short periods of time (< 4 hours) affords, in moderate to high yields, the air-stable, sparingly soluble neutral compounds $[Ru_2\{\mu\text{-}\eta^2\text{-}OC(R)O\}_2(CO)_4(\eta^1\text{-}L)_2]$ (R = H, Me or Et; L = Ph_2Ppy, Ph_2Pquin or Ph_2Pbipy) **[1]-[9]**. All of the products precipitate from the solution at room temperature, except for those involving the Ph_2Pbipy ligand, which precipitate out on reduction of the solvent volume and subsequent cooling to -25°C. Each ligand attacks the ruthenium, cleaving the polymer into dimeric units in which the acetate bridges remain in a cis configuration relative to one another and in which the P-Ru-Ru-P interaction is in a linear fashion along the Ru-Ru bond such that each ligand is bound in a monodentate fashion through the phosphorus atom. The colours of the products range from yellow (in the case of Ph_2Pquin) to orange (in the case of Ph_2Pbipy). All products have microanalyses consistent with their formulation (Table 3.1) while their infrared spectra (Table 3.2) in the C-O stretching region closely resemble those of the axially substituted compounds $[M_2\{\mu\text{-}\eta^2\text{-}OC(Me)O\}_2(CO)_2L]_2$ (M = Ru or Os; L = PPh_3, $AsPh_3$. PMe_2Ph, $PMePh_2$, C_5H_5N and MeCN),[118, 127] as well as those of Singleton *et al*, involving bidentate phosphine ligands such as dppm, formulated as $[Ru_2\{\mu\text{-}\eta^2\text{-}OC(R)O\}_2(CO)_4(\eta^1\text{-}L)_2]$ (L = dppm, for example).[119, 122] This suggests a similar core structure with two axial carbonyls having been displaced by the respective ligand behaving as a monodentate ligand. The ^1H nmr spectra have the expected integration ratios of carboxylate: ligand protons whilst the $^{31}P\{^1H\}$ nmr spectra exhibit well resolved singlets at ~18ppm downfield from H_3PO_4, external standard, indicating identical environments for the two phosphorus atoms (Table 3.3). Consequently, the following structure, having the ligands coordinated in an η^1 manner trans to the metal-metal bond, is proposed.

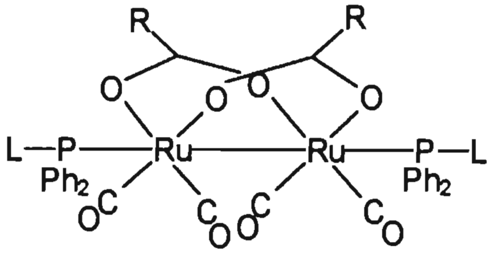

[1]-[9]: R = H, Me or Et; L = pyridine, quinoline or 2,2'-bipyridine

An X-ray crystallographic study of $[Ru_2\{\mu\text{-}\eta^2\text{-}OC(Me)O\}_2(CO)_4(\eta^1\text{-}Ph_2Ppy)_2]$ **[2]** has subsequently confirmed this expectation.

Table 3.1 Physical and microanalytical data

	Complex	Colour	M:g.mol^{-1}	Analysis : Found (Calculated) %		
				%C	%H	%N
[1]	$[Ru\{\mu\text{-}\eta^2\text{-}OC(H)O\}_2(CO)_4(\eta^1\text{-}Ph_2Ppy)_2]$	orange-yellow	930.17	51.22(51.62)	3.68(3.25)	2.87(3.01)
[2]	$[Ru\{\mu\text{-}\eta^2\text{-}OC(Me)O\}_2(CO)_4(\eta^1\text{-}Ph_2Ppy)_2]$	orange-yellow	958.83	52.70(52.61)	4.07(3.57)	2.58(2.92)
[3]	$[Ru\{\mu\text{-}\eta^2\text{-}OC(Et)O\}_2(CO)_4(\eta^1\text{-}Ph_2Ppy)_2]$	orange-yellow	986.88	53.37(53.55)	4.23(3.88)	2.58(2.84)
[4]	$[Ru\{\mu\text{-}\eta^2\text{-}OC(H)O\}_2(CO)_4(\eta^1\text{-}Ph_2Pquin)_2]$	yellow	1030.89	55.62(55.93)	3.48(3.32)	2.51(2.72)
[5]	$[Ru\{\mu\text{-}\eta^2\text{-}OC(Me)O\}_2(CO)_4(\eta^1\text{-}Ph_2Pquin)_2]$	yellow	1058.95	57.13(56.71)	3.47(3.62)	2.78(2.65)
[6]	$[Ru\{\mu\text{-}\eta^2\text{-}OC(Et)O\}_2(CO)_4(\eta^1\text{-}Ph_2Pquin)_2]$	yellow	1087.00	57.18(57.46)	3.69(3.89)	2.53(2.58)
[7]	$[Ru\{\mu\text{-}\eta^2\text{-}OC(H)O\}_2(CO)_4(\eta^1\text{-}Ph_2Pbipy)_2]$	orange	1084.95	55.83(55.35)	3.49(3.34)	5.41(5.16)
[8]	$[Ru\{\mu\text{-}\eta^2\text{-}OC(Me)O\}_2(CO)_4(\eta^1\text{-}Ph_2Pbipy)_2]$	orange	1112.08	55.92(56.11)	3.74(3.60)	4.66(5.04)
[9]	$[Ru\{\mu\text{-}\eta^2\text{-}OC(Et)O\}_2(CO)_4(\eta^1\text{-}Ph_2Pbipy)_2]$	orange	1141.05	56.72(56.84)	3.58(3.89)	4.63(4.91)

Table 3.2 Infrared spectroscopic data[(a)]

Complex	ν(CO), cm^{-1}	ν(CO_2), cm^{-1}
[1]	2025(s) 1981(m) 1952(vs) 1914(w,sh)	1572(s)
[2]	2027(s) 1981(m) 1953(vs) 1913(w,sh)	1571(s)
[3]	2027(s) 1977(m) 1952(vs) 1912(w,sh)	1574(s)
[4]	2033(s) 1978(m) 1945(vs) 1913(w,sh)	1567(s)
[5]	2032(s) 1978(m) 1950(vs) 1913(w,sh)	1568(s)
[6]	2034(s) 1978(m) 1950(vs) 1912(w,sh)	1570(s)
[7]	2026(s) 1989(m) 1952(vs) 1912(w,sh)	1575(s)
[8]	2025(s) 1989(m) 1953(vs) 1914(w,sh)	1572(s)
[9]	2025(s) 1981(m) 1952(vs) 1913(w,sh)	1566(s)

(a) : Recorded in CH_2Cl_2 solution unless otherwise specified. Intensity designation: vs = very strong, s = strong, m = medium, w = weak, w,sh = weak, shoulder.

Table 3.3 ^{1}H and ^{31}P{^{1}H} nmr spectroscopic data$^{(a)}$

Complex	δ ^{1}H (ppm)	δ ^{31}P {^{1}H} (ppm)
[1]	8.60-7.20(m, 28H, Ph_2Ppy)$^{(b)}$	16.91(s)
[2]	8.63-7.21(m, 28H, Ph_2Ppy) 1.63(s, 6H, $C\underline{H}_3CO_2$-)	16.88(s)
[3]	8.60-7.18(m, 28H, Ph_2Ppy) 2.78(q, 4H, $CH_3C\underline{H}_2CO_2$-) 1.56(t, 6H, $C\underline{H}_3CH_2CO_2$-)	17.02(s)
[4]	8.25-7.40(m, 32H, Ph_2Pquin)$^{(b)}$	18.09(s)
[5]	8.20-7.35(m, 32H, Ph_2Pquin) 1.62(s, 6H, $C\underline{H}_3CO_2$-)	17.50(s)
[6]	8.21-7.21(m, 32H, Ph_2Pquin) 2.69(q, 4H, $CH_3C\underline{H}_2CO_2$-) 1.50(t, 6H, $C\underline{H}_3CH_2CO_2$-)	17.53(s)
[7]	8.62-7.24(m, 34H, Ph_2Pbipy)$^{(c)}$	17.62(s)
[8]	8.63-7.22(m, 34H, Ph_2Pbipy) 1.74(s, 6H, $C\underline{H}_3CO_2$-)$^{(c)}$	17.79(s)
[9]	8.65-7.20(m, 34H, Ph_2Pbipy) 2.62(q, 4H, $CH_3C\underline{H}_2CO$-) 1.49(t, 6H, $C\underline{H}_3CH_2CO_2$-)$^{(c)}$	17.80(s)

(a) : Recorded in CD_2Cl_2 unless otherwise specified.
(b) : $\underline{H}CO_2$ - resonance obscured by multiplet corresponding to ligand protons.
(c) : Recorded in acetone - d_6.

3.2.2 Crystal Structure determination of $[Ru_2\{\mu-\eta^2-OC(Me)O\}_2(CO)_4(\eta^1-Ph_2Ppy)_2]$ [2]

Figure 3.1 gives a perspective view of $[Ru_2\{\mu-\eta^2-OC(Me)O\}_2(CO)_4(\eta^1-Ph_2Ppy)_2]$ **[2]** and shows the atom numbering scheme. The complex adopts a sawhorse or cis-eclipsed structure in which the two carbonyl groups on each metal are mutually cis and opposite the bridging groups, with the phosphoruspyridyl ligands bonded in a monodentate fashion in the axial sites opposite the Ru-Ru bond. The ruthenium atoms retain essentially octahedral geometry.

The stucture illustrated in Figure 3.1 is similar to that reported for the bridged compounds $[Ru_2\{\mu-\eta^2-OC(R)O\}_2(CO)_4L_2]$ (L = py, CO, H_2O, $PhCO_2H$ or P^tBu_3; R = Me, ^nPr, 4-F-C_6H_4 or Ph),[123-126] as well as that for the anionic ligand-bridged derivatives $[Ru_2(\mu-X)_2(CO)_4(\eta^1-PR_3)_2]$ (R = Ph, ^tBu or *p*-tol; X = Cl^-, 3,5-dimethylpyrazolato (pz'^-) or 2-oxypyridinato ($NC_5H_4O^-$))[127-129] It is however, different from the cis-staggered structure observed for the unbridged dinuclear compounds $[Ru_2\{\eta^3-HB(Rz)_3\}_2(CO)_4]$ (Rz = pyrazolato or 1,2,4-triazolyl)[130, 131]

The Ru-Ru bond length of 2.719(1)Å is consistent with a single bond expected for a Ru(I)-Ru(I) dimer but this bonding distance does give rise to a very slight twist of the carbonyl and acetate substituents on each metal from an exactly eclipsed conformation, as would be expected for the non-ligand containing polymer, resulting in the relatively small range of torsion angles of 8.9° [for C(39)-Ru(1)-Ru(2)-C(41)] to 2.5° [for O(1)-Ru(1)-Ru(2)-O(2)]. The P(1)-Ru(1)-Ru(2) angle is 169.5(1)° while that of P(2)-Ru(2)-Ru(1) is 176.6(1)°, confirming the linear, axial arrangement of the ligands. The axial phosphorus has a direct influence on the Ru-Ru bond distance and this can perhaps best be illustrated if comparisons are drawn between **[2]** and a few other similar structures obtained from the literature. Table 3.4 compares Ru-Ru bond lengths from various reported structures of $[Ru_2\{\mu-\eta^2-OC(R)O\}_2(CO)_4L_2]$. The observation that complex **[2]** has a longer Ru-Ru bond than that for R = Me and L = CO can be rationalised as follows. When π acids such

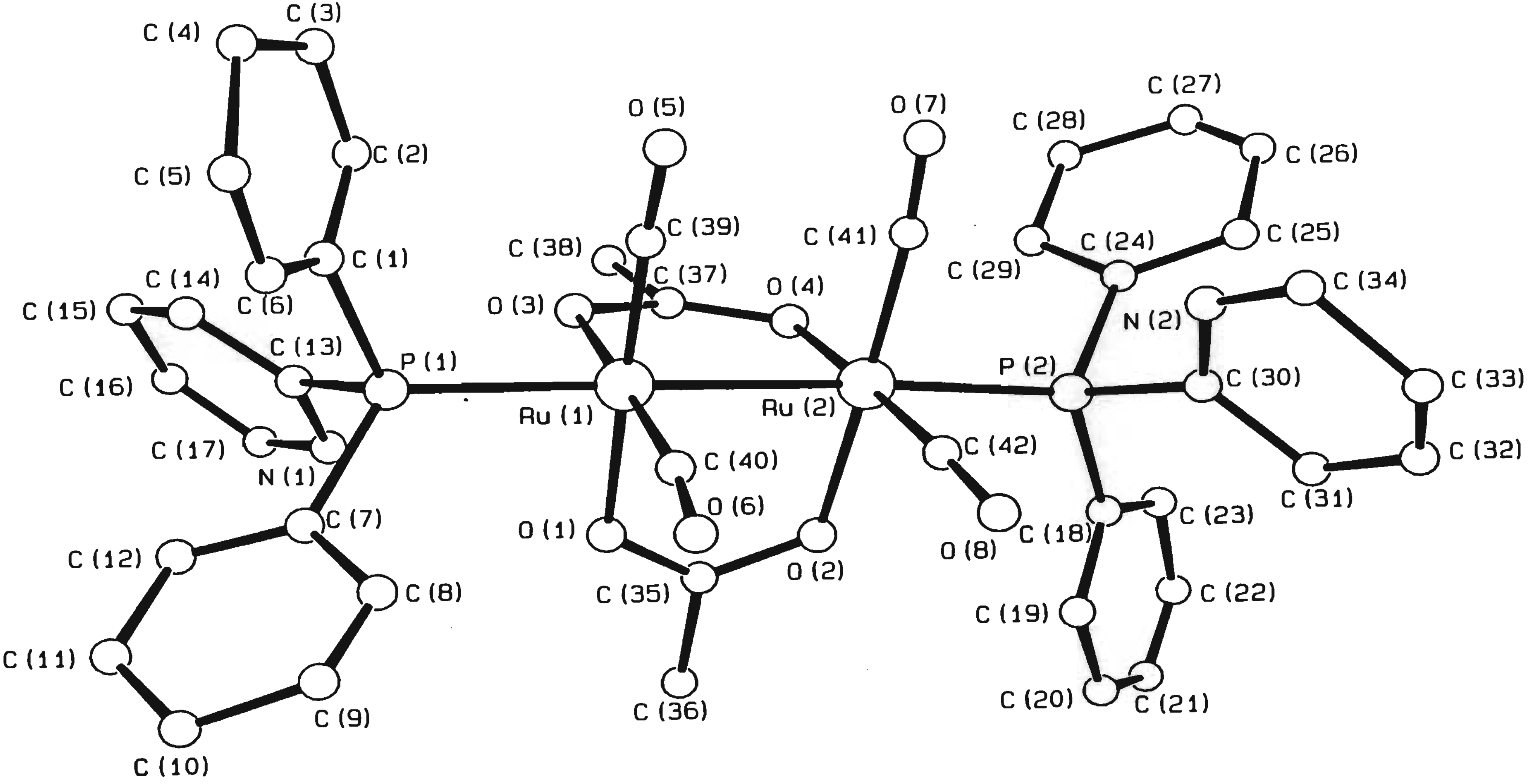
C (4)
C (3)
C (2)
C (5)
C (1)
C (6)
C (14)
C (15)
C (13)
C (16)
C (17)
N (1)
P (1)
C (7)
C (12)
C (8)
C (11)
C (9)
C (10)
O (5)
C (39)
C (38)
C (37)
O (3)
Ru (1)
C (40)
O (6)
O (1)
C (35)
C (36)
O (2)
O (4)
Ru (2)
O (7)
C (41)
C (42)
O (8)
C (28)
C (27)
C (26)
C (29)
C (24)
C (25)
C (34)
N (2)
P (2)
C (30)
C (33)
C (32)
C (31)
C (18)
C (23)
C (22)
C (19)
C (20)
C (21)

as CO coordinate axially with the Ru_2 dimer, electron transfer from the filled M-M antibonding orbitals (δ^* or π^*) to the CO π^* orbitals strengthens the M-M bonding interaction by increasing the M-M bond order (Ru-Ru shortening). However, when phosphorus, a strong σ donor coordinates, the M-M bond order decreases (Ru-Ru lengthening) by bonding interactions through the empty M-M antibonding orbitals (σ^*). Also noticeable is the longer Ru-Ru bond distances in the compounds that have L = PPh_3 (R = Me or Ph). This may reflect the stronger donor character of PPh_3 when compared to Ph_2Ppy.

Table 3.4 Structural comparisons in known complexes of the general formula $[Ru_2\{\mu\text{-}\eta^2\text{-}OC(R)O\}_2(CO)_4(\eta\text{-}L)_2]$

Compound		Avg. Interatomic Dist.(Å)		Reference
R	L	Ru-L	**Ru-Ru**	
Me	CO	1.976	2.689	123
Me	PPh_3	2.451	2.736	132
Ph	CO	2.013	2.704	123
Ph	PPh_3	2.437	2.741	132
[2] **Me**	**Ph_2Ppy**	**2.410**	**2.719**	**This work**

3.2.3 Synthesis and Characterisation of $[Ru_2\{\mu\text{-}\eta^2\text{-}OC(R)O\}(CO)_4(\mu\text{-}L)_2](PF_6)$ (R = H, Me or Et; L = Ph_2Ppy or Ph_2Pquin) **[10]-[15]**

The ligand-bridged complexes $[Ru_2\{\mu\text{-}\eta^2\text{-}OC(R)O\}(CO)_4(\mu\text{-}L)_2](PF_6)$ (R = H, Me or Et; L = Ph_2Ppy or Ph_2Pquin) **[10]-[15]** are synthesised by the reaction of the $[Ru\{\mu\text{-}\eta^2\text{-}OC(R)O\}(CO)_2]_n$ polymer with two equivalents (per dimeric unit) of the relevant ligand and two equivalents (per dimeric unit) of NH_4PF_6 in refluxing toluene under slight CO pressure. The product, in all cases, precipitates from solution and is isolated by filtration, the only difference being that the Ph_2Pquin complexes take approximately twice as long to form as the analogous Ph_2Ppy complexes. This is presumably due to steric problems introduced by the more bulky quinoline moiety. Yields of the yellow, crystalline products range from 4% (for one of the Ph_2Pquin complexes) to 72%. It is also possible to synthesise these ligand bridged derivatives from the relevant η^1-pendant precursor (**[1]-[6]**) by addition of excess NH_4PF_6 to a refluxing toluene suspension of the η^1 species under mild CO pressure. For this reason, it is presumed that the η^1 variety is an intermediate in the formation of the cationic ligand-bridged complex, whose presumed structure is shown below.

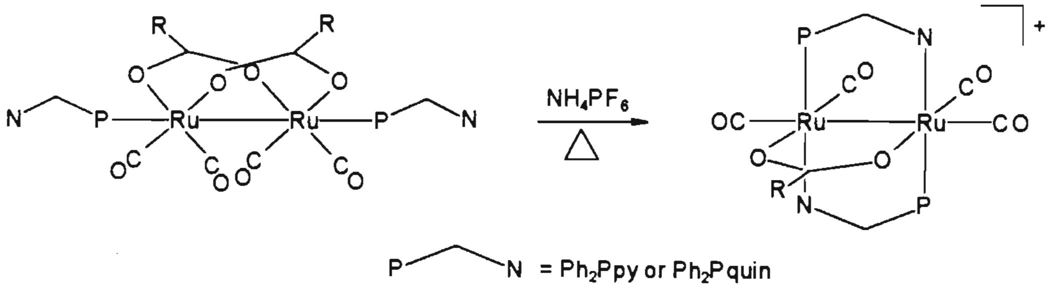

This conversion involves the migration of the ligand from an axial position into an equatorial one, with concomitant cleavage of a carboxylate bridge across the Ru-Ru bond and coordination of the nitrogen atom of the ligand to the second ruthenium atom. All complexes show satisfactory microanalyses (Table 3.5) while the band envelopes in the terminal carbonyl region of all infra-red spectra correspond closely with those found in the literature for the analogous dppm and dmpm bridged complexes[117, 122] (ie. four bands having a relative intensity, starting from largest wavenumber, of m, vs, s, w - see Table

Table 3.5 Physical and microanalytical data

	Complex	Colour	M:g.mol^{-1}	Analysis : Found (Calculated) %		
				%C	%H	%N
[10]	$[Ru_2\{\mu\text{-}\eta^2\text{-}OC(H)O\}(CO)_4(\mu\text{-}Ph_2Ppy)_2](PF_6)$	Yellow	1030.72	45.90(45.45)	2.92(2.84)	2.68(2.72)
[11]	$[Ru_2\{\mu\text{-}\eta^2\text{-}OC(Me)O\}(CO)_4(\mu\text{-}Ph_2Ppy)_2](PF_6)$	Yellow	1044.75	45.71(45.99)	3.23(2.99)	2.77(2.68)
[12]	$[Ru_2\{\mu\text{-}\eta^2\text{-}OC(Et)O\}(CO)_4(\mu\text{-}Ph_2Ppy)_2](PF_6)$	Yellow	1058.77	46.31(46.51)	3.41(3.14)	2.84(2.65)
[13]	$[Ru_2\{\mu\text{-}\eta^2\text{-}OC(H)O\}(CO)_4(\mu\text{-}Ph_2Pquin)_2](PF_6)$	Yellow	1130.84	49.87(49.92)	2.78(2.94)	2.45(2.48)
[14]	$[Ru_2\{\mu\text{-}\eta^2\text{-}OC(Me)O\}(CO)_4(\mu\text{-}Ph_2Pquin)_2](PF_6)$	Yellow	1144.87	50.50(50.36)	3.61(3.08)	2.51(2.45)
[15]	$[Ru_2\{\mu\text{-}\eta^2\text{-}OC(Et)O\}(CO)_4(\mu\text{-}Ph_2Pquin)_2](PF_6)$	Yellow	1158.89	50.52(50.78)	3.28(3.22)	2.58(2.42)

Table 3.6 Infrared spectroscopic data(a)

Complex	ν(CO), cm^{-1}	ν(CO$_2$),cm^{-1}	ν(P-F),cm^{-1}
[10]	2021(m) 1995(vs) 1964(s) 1942(w)	1557(w)	839(vs)
[11]	2027(m) 2004(vs) 1969(s) 1950(w)	1541(m)	847(vs)
[12]	2023(m) 1999(vs) 1968(s) 1951(w)	1550(m)	841(vs)
[13]	2060(m) 1986(vs) 1947(s) 1920(w)	1556(w)	836(vs)
[14]	2056(m) 1992(vs) 1953(s) 1920(w)	1553(m)	839(vs)
[15]	2061(m) 1982(vs) 1951(s) 1926(w)	1552(m)	840(vs)

(a) : Recorded in CH_2Cl_2 unless otherwise specified. Designation: vs = very strong, s = strong, m = medium, w = weak.

Table 3.7 ^{1}H and ^{31}P{^{1}H} nmr spectroscopic data(a)

Complex	δ^{1}H(ppm)	δ ^{31}P{^{1}H}(ppm)
[10]	9.30-6.88(m, 28H, Ph_2Ppy)(b)	45.03(s)
[11]	9.28-6.93(m, 28H, Ph_2Ppy) 1.58(s, 3H, $C\underline{H}_3CO_2$-)	45.24(s)
[12]	9.19-7.01(m, 28H, Ph_2Ppy) 2.72(q, 2H, $CH_3C\underline{H}_2CO_2$-) 1.43(t, 3H, $C\underline{H}_3CH_2CO_2$-)	45.91(s)
[13]	8.95-6.50(m, 32H, Ph_2Pquin)(b)	47.22(s)
[14]	9.00-6.35(m, 32H, Ph_2Pquin) 1.57(s, 3H, $C\underline{H}_3CO_2$-)	47.34(s)
[15]	8.95-6.40(m, 32H, Ph_2Pquin) 2.63(q, 2H, $CH_3C\underline{H}_2CO_2$-) 1.513(t, 3H, $C\underline{H}_3CH_2CO_2$-)	47.31(s)

(a) : recorded in CD_2Cl_2.

(b) : $\underline{H}CO_2$- resonance obscured by multiplet corresponding to ligand protons.

3.6). The IR spectra also exhibit characteristic carboxylate stretches and are distinguished from those of the η^1 complexes by the appearance of a ν(P-F) stretch at ~840cm^{-1} for the PF_6^- counter anion. ^{1}H nmr spectra (Table 3.7) show the correct integration ratios for ligand : carboxylate protons, except that for the formate derivatives, whose proton resonances are obscured by complex resonance patterns attributable to ligand protons, as was the case for the η^1 pendant derivatives **[1]**, **[4]** and **[7]** (section 3.2.1). The $^{31}P\{^1H\}$ nmr spectra (Table 3.7) of all complexes exhibit well resolved singlets well downfield of their η^1 analogues. These singlets are within the range expected for bridging Ph_2Ppy[79] and Ph_2Pquin ligands.[89] The structure of compound **[10]** has been elucidated by an X-ray crystal structure determination.

3.2.4 Crystal structure determination of $[Ru_2\{\mu\text{-}\eta^2\text{-}OC(H)O\}(CO)_4(\mu\text{-}Ph_2Ppy)_2](PF_6)$ [10]

A perspective view of the cation of $[Ru_2\{\mu\text{-}\eta^2\text{-}OC(H)O\}(CO)_4(\mu\text{-}Ph_2Ppy)_2](PF_6)$ **[10]** is shown in Figure 3.2. Both metals have nearly regular octahedral geometries and are bridged by the two Ph_2Ppy ligands in a mutually trans arrangement and by the formate group. Other octahedral positions on each metal are occupied by two carbon atoms of terminal carbonyls and the other ruthenium atom.

This structure is analogous to that for $[Ru_2\{\mu\text{-}\eta^2\text{-}OC(Me)O\}(CO)_4(\mu\text{-}dppm)_2]^+$.[117, 122] For complex **[10]**, octahedral angles about the ruthenium atom range from 80.6(2)° to 98.5(3)°. The ruthenium-ruthenium bond length of 2.731(1)Å is consistent with a ruthenium-ruthenium bond. Of all the similar diruthenium structures reported in the literature it does, however, have the shortest Ru-Ru bond, presumably due to the larger M-M bond order resulting from coordination of a harder σ donor (i.e. the nitrogen). This has the result that the substituents on each metal atom twist to a relatively large degree out of an exactly eclipsed conformation, yielding relatively substantial torsion angles about the Ru-Ru bond of 20.1°[C(36)-Ru(1)-Ru(2)-C(38)], 22.2° [O(3)-Ru(1)-Ru(2)-O(6)] and 38.4° [P(1)-Ru(1)-Ru(2)-N(1)]. These are in marked contrast to the analogous $[Ru_2\{\mu\text{-}\eta^2\text{-}$

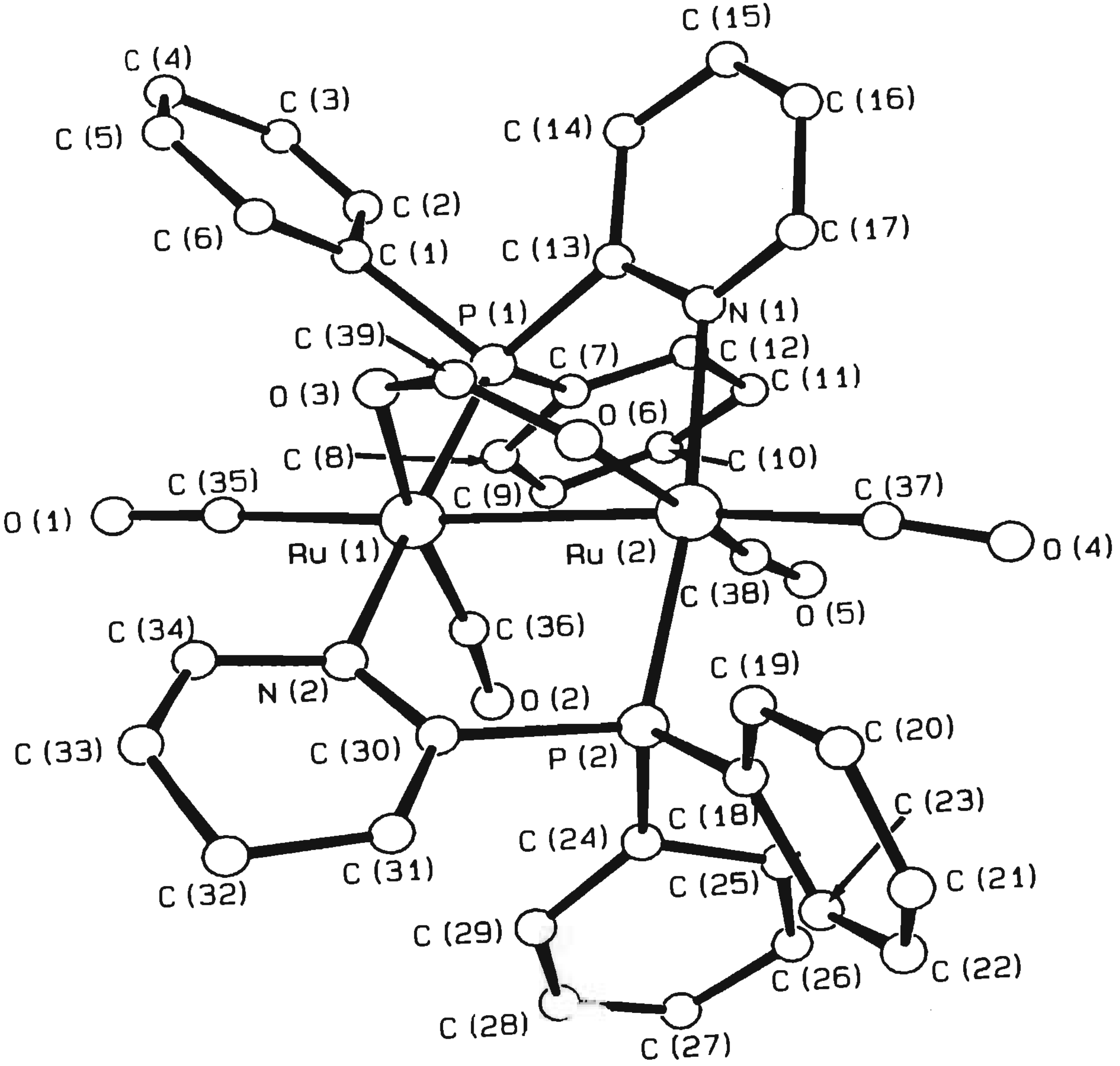
C (15)
C (4)
C (3)
C (16)
C (14)
C (5)
C (2)
C (6)
C (1)
C (13)
C (17)
N (1)
P (1)
C (39)
C (7)
C (12)
C (11)
O (3)
O (6)
C (8)
C (10)
C (35)
C (9)
C (37)
O (1)
Ru (1)
Ru (2)
O (4)
C (38)
O (5)
C (34)
C (36)
C (19)
N (2)
O (2)
C (20)
C (33)
C (30)
P (2)
C (23)
C (18)
C (24)
C (25)
C (21)
C (31)
C (32)
C (29)
C (26)
C (22)
C (28)
C (27)

OC(Me)O}(CO)$_4$(μ-dppm)$_2$]$^+$ complex,[117] whose torsion angles range from 17.3(2)° and 20.6(4)°, owing to the more symmetrical nature of the bidentate ligand and the relative absence of steric crowding. The torsion is also significantly increased from the previously discussed [Ru$_2${μ-η^2-OC(Me)O}$_2$(CO)$_4$(η^1-Ph$_2$Ppy)$_2$] complex. There is also a pronounced difference in the Ru-C distances of complex **[10]** for the axial [1.949(9)Å] and equatorial [1.831(9)Å] carbonyl ligands, which reflects either the weak π-donor ability of the formato groups opposite the equatorial carbonyls or the large trans influence of the metal-metal bond on the axial carbonyls.[133, 134]

3.2.5 Synthesis and characterisation of [Ru$_2${μ-η^2-OC(R)O}(CO)$_2$(μ-Ph$_2$Pbipy)$_2$](PF$_6$) (R= H, Me, Et) [16]-[18]

The reaction of the Ph$_2$Pbipy ligand with [Ru{μ-η^2-OC(R)O}(CO)$_2$]$_n$ requires that, in addition to a carboxylato group, two carbonyl groups are substituted in order to facilitate the ligands coordination. Thus, fairly vigorous conditions are utilised. The compounds are prepared by treating the polymer with two equivalents (per dimeric unit) of ligand in refluxing 1-butanol. The temperature of this reaction is carefully maintained at 120°C so as not to affect the ligand in any way (its decomposition temperature is 135°C). Subsequent treatment with excess NH$_4$PF$_6$ affords the product as a medium-brown powder readily soluble in most organic solvents. Again, it appears that the η^1 pendant species is an intermediate in the formation of [Ru$_2${μ-η^2-OC(R)O}(CO)$_2$(μ-Ph$_2$Pbipy)$_2$](PF$_6$) (R= H, Me or Et) **[16]-[18]** as the colour changes from orange through to dark brown during the course of the reaction; this corresponds to the migration of the ligand from an axial into an equatorial position, with the concomitant cleavage of one carboxylato and two carbonyl moieties that are necessarily mutually trans disposed with respect to one another. Correct microanalyses have been obtained (Table 3.8) for the formulation proposed below while the infra-red spectroscopic data confirm the presence of two mutually cis but slightly staggered carbonyl ligands (i.e. a strong terminal carbonyl band with a shoulder assigned to the asymmetric stretch). These two bands occur at relatively low wavenumbers, confirming the electron-rich nature of the product. Also observed are characteristic stretches for

Table 3.8 Physical and microanalytical data

	Complex	Colour	M:g.mol^{-1}	Analysis : Found (Calculated) % %C	%H	%N
[16]	$[Ru_2\{\mu\text{-}\eta^2\text{-}OC(H)O\}(CO)_2(\mu\text{-}Ph_2Pbipy)_2]PF_6$	dark brown	1128.87	49.91(50.01)	3.02(3.13)	4.68(4.96)
[17]	$[Ru_2\{\mu\text{-}\eta^2\text{-}OC(Me)O\}(CO)_2(\mu\text{-}Ph_2Pbipy)_2]PF_6$	dark brown	1142.90	49.99(50.44)	3.66(3.26)	4.70(4.90)
[18]	$[Ru_2\{\mu\text{-}\eta^2\text{-}OC(Et)O\}(CO)_2(\mu\text{-}Ph_2Pbipy)_2]PF_6$	dark brown	1156.92	50.39(50.87)	3.10(3.40)	4.72(4.84)

Table 3.9 Infrared spectroscopic data[(a)]

Complex	ν(CO), cm^{-1}	ν(CO_2),cm^{-1}	ν(P-F),cm^{-1}
[16]	1934(vs) 1899(m,sh)	1557(m)	841(vs)
[17]	1930(vs) 1890(m, sh)	1551(m)	847(vs)
[18]	1942(vs) 1903(m, sh)	1576(m)	839(vs)

(a) : Recorded in CH_2Cl_2 unless otherwise specified. Designation: vs = very strong, m, sh = medium, shoulder

Table 3.10 **^{1}H and ^{31}P{^{1}H} nmr spectroscopic data[(a)]**

Complex	δ^{1}H(ppm)	δ ^{31}P{^{1}H}(ppm)
[16]	8.34-7.05(m, 34H, Ph_2Pbipy)[(b)]	45.03(s)
[17]	8.40-7.12(m, 34H, Ph_2Pbipy) 1.53(s, 3H, $C\underline{H}_3CO_2$-)	45.24(s)
[18]	8.39-7.01(m, 34H, Ph_2Ppy) 2.47(q, 2H, $CH_3C\underline{H}_2CO_2$-) 1.41(t, 3H, $CH_3C\underline{H}_2CO_2$-)	45.91(s)

(a) : Recorded in CD_2Cl_2 unless otherwise specified.
(b) : $\underline{H}CO_2$ - resonance obscured by ligand multiplet

carboxylate and carbonyl moieties. The ^1H nmr data (Table 3.10) contain the usual ligand shifts in the aromatic region which can be correctly integrated against the acetate or propionate shifts occurring further upfield while the $^{31}P\{^1H\}$ nmr spectra comprise singlets, again well downfield of those obtained for the η^1-intermediates and, at the same time, slightly more downfield of those obtained for the Ph_2Ppy and Ph_2Pquin complexes, as would be expected for more electron-rich products. The following core structure for these complexes has thus been proposed and this has subsequently been confirmed by an X-ray crystallographic study on complex **[17]**.

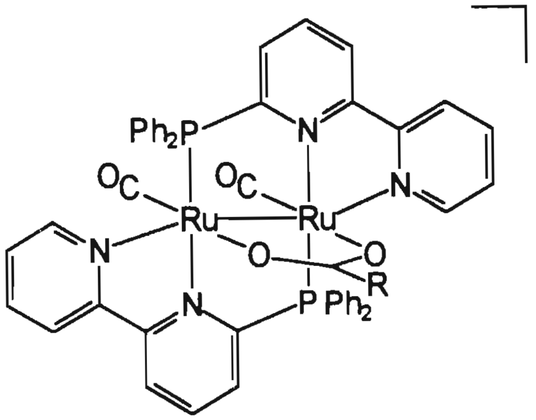

R = H, Me or Et

3.2.6 Crystal structure determination of [$Ru_2\{\mu$-η^2-$OC(Me)O\}(CO)_2(\mu$-$Ph_2Pbipy)_2](PF_6)$ [17]

A perspective view of the cation of [$Ru_2\{\mu$-η^2-$OC(Me)O\}(CO)_2(\mu$-$Ph_2Pbipy)_2]PF_6$ **[17]** is shown in Figure 3.3. Both metal atoms have distorted octahedral geometry and are bridged by two mutually trans Ph_2Pbipy ligands, as well as an acetate moiety. One carbonyl group and a bond to the other ruthenium complete the octahedron around each metal atom. The two carbonyl ligands adopt a near cis-eclipsed conformation trans to the acetate bridge. Angles around each ruthenium atom are in the range 75.7(6)° [N(1)-Ru(2)-N(2)] to 106.4(4)° [P(2)-Ru(2)-N(2)] and this gives an idea of the significant amount of distortion at each metal atom. This no doubt arises from the restriction which the bite of the bipyridyl fragment imposes upon its coordination in the manner observed, pulling the Ru(1)-N(4)

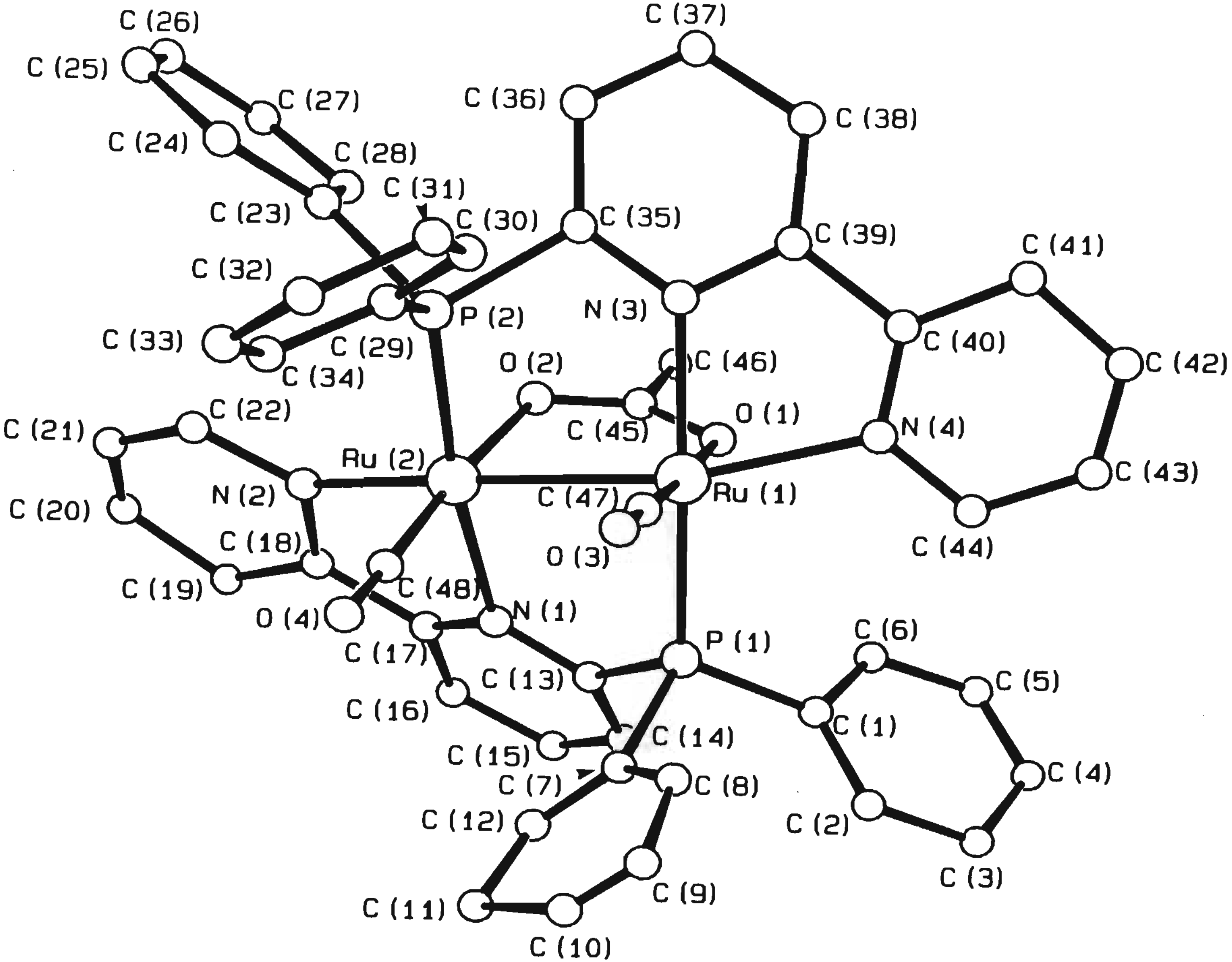
C (26)
C (37)
C (25)
C (27)
C (36)
C (38)
C (24)
C (28)
C (31)
C (23)
C (30)
C (35)
C (39)
C (41)
C (32)
N (3)
P (2)
C (33)
C (29)
C (40)
C (42)
C (34)
O (2)
C (46)
C (22)
O (1)
C (21)
C (45)
N (4)
Ru (2)
C (43)
N (2)
C (47)
Ru (1)
C (20)
C (18)
O (3)
C (44)
C (19)
C (48)
O (4)
N (1)
C (6)
C (17)
P (1)
C (13)
C (5)
C (16)
C (1)
C (14)
C (15)
C (4)
C (7)
C (8)
C (12)
C (2)
C (3)
C (9)
C (11)
C (10)

bond approximately 17° away from an exactly axial position and towards the ligand itself. All other torsion angles are probably as a direct result of this restriction, but all are fairly small angles of 19.0° [C(47)-Ru(1)-Ru(2)-C(48)], 14.9° [O(1)-Ru(1)-Ru(2)-O(2)] and 22.7° [P(1)-Ru(1)-Ru(2)-N(1)], corresponding more closely than those of **[10]** to examples in the literature. These restrictions and the distortions that result therefrom, may also be in part responsible for the short Ru-Ru bond length [2.687(2)Å], which is towards the bottom end of the range expected for diruthenium(I) metal-bonded complexes (2.683 - 2.841Å).[117-119] Within the ligands, the dihedral angles between the hexagonal planes defined by the pyridyl groups containing N(1) and N(2) and that between N(3) and N(4) are 13.5° and 12.3° respectively, neatly showing how the uniform planarity of the Ph_2Pbipy ligand is not preserved upon dinuclear coordination and that a certain degree of rotation can occur about the inter-annular C(17)-C(18) and C(39)-C(40) bonds. The remaining bond lengths and angles are as expected.

3.3 Reactions of Ph_2Ppy, Ph_2Pquin and Ph_2Pbipy with $[Ru_2(CO)_4(NCMe)_6](PF_6)_2$

The isolation, in low yields, of the homoleptic isocyanide derivative $[Ru_2(CNXylyl)_{10}](PF_6)_2$ by Singleton *et al.*[135] represented the first synthesis of a derivative of the unknown $[Ru_2(CO)_{10}]^{2+}$ species. This prompted an investigation into new routes to isocyanide and similar complexes based on the $[Ru_2(CO)_{10}]^{2+}$ framework. However, these investigations were hindered to some extent by the relative stability of the Ru-isocyanide bond. A considerably more versatile precursor, also based on the $[Ru_2(CO)_{10}]^{2+}$ core, is the complex $[Ru_2(CO)_4(NCMe)_6](PF_6)_2$, synthesised recently by Klemperer and Zhong[120] which contains substitutionally labile acetonitrile ligands. Due to this latter feature, it has been shown to be reactive towards a number of polyoxoanion ligands as well as triphenylphosphine itself, affording the complex $[Ru_2(CO)_4(NCMe)_4(PPh_3)_2](PF_6)_2$ whose cation structure is shown below.

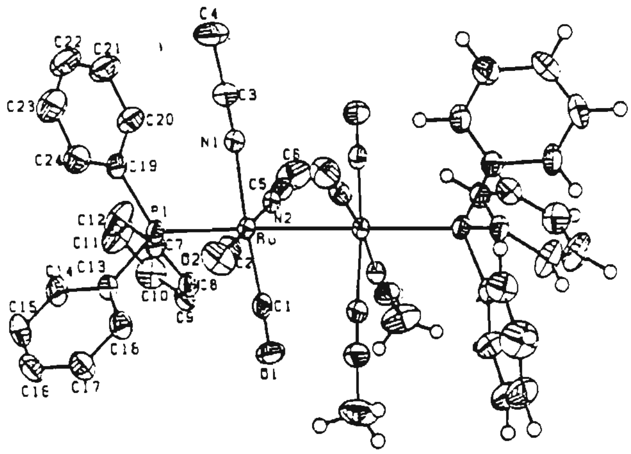
C4
C22
C21
C23
C20
C3
N1
C24
C19
C6
C5
N2
P1
C12
C11
C7
Ru
O2
C2
C14
C13
C8
C10
C9
C15
C1
C16
O1
C18
C17

$[Ru_2(CO)_4(NCMe)_4(PPh_3)_2]^{2+}$

In addition, current studies[136] in our laboratories on the coordination of chelating ligands such as 2,2′-bipyridine to the diruthenium precursor have produced two isomeric products, the first of which slowly reverts, in the absence of light and air, to the second. Both of these, essentially dinuclear fragments of the blue, neutral $[Ru_2(CO)_4(bipy)_2]_{n/2}$ polymer[137], are shown below.

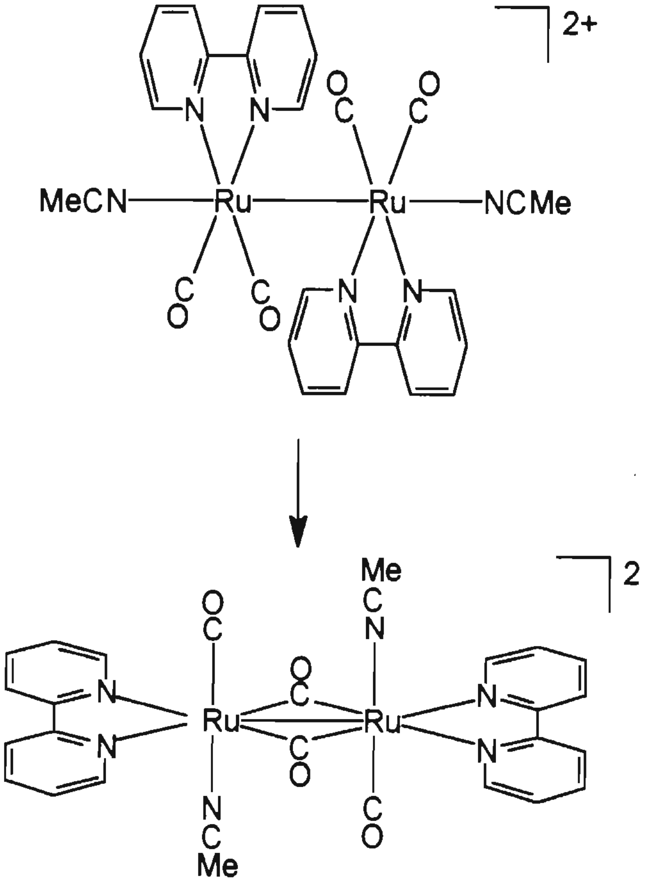
2+
MeCN
Ru
Ru
NCMe
N
N
O
C
2
Me
C
N

In view of these results, related ligands such as Ph_2Ppy, Ph_2Pquin and Ph_2Pbipy should afford dinuclear products bridged by the respective phosphine ligand, since the phosphorus atom of each ligand should coordinate at one ruthenium atom whilst the pyridine, quinoline or bipyridine substituent should coordinate at the other in a manner characteristic of the substituent. This would ultimately stabilise the Ru(I) dimer to fragmentation whilst at the same time provide labile nitrile sites for further chemistry.

3.3.1 Synthesis of the Ph_2Ppy complex $[Ru_2(\mu\text{-}Ph_2Ppy)_2(\mu\text{-}CO)_2(NCMe)_4](PF_6)_2$ [19]

When two equivalents of Ph_2Ppy are added to $[Ru_2(CO)_4(NCMe)_6](PF_6)_2$ in acetonitrile and the solution refluxed overnight, a clear orange-red solution results. From this, through addition of diethyl ether and cooling to -25°C, the orange-red crystalline product $[Ru_2(\mu\text{-}Ph_2Ppy)_2(\mu\text{-}CO)_2(NCMe)_4](PF_6)_2$ **[19]** is isolated in moderate yield. Alternatively, reaction of two equivalents of Ph_2Ppy with $[Ru_2(CO)_4(NCMe)_6](PF_6)_2$ in refluxing ethanol produces, after four hours, an ochre-coloured precipitate from which **[19]** is afforded by recrystallisation from CH_3CN/Et_2O.

The complex has an infra-red spectrum (Table 3.12) which contains two sharp, intense bands at 1715 and 841cm^{-1}. The former is due to the bridging carbonyl(s) stretch while the latter is attributable to P-F stretches within the PF_6^- counter-anion. There are no terminal carbonyl bands. The value of 1715cm^{-1} for the bridging carbonyls corresponds well with the 1710cm^{-1} observed in the infra-red spectrum of $[Ru_2\{\mu\text{-}(Pr^iO)_2PN(Et)P(OPr^i)_2\}_2(\mu\text{-}CO)(CO)_4]$ [69b)]. The ^1H nmr spectrum of the compound (Table 3.13) comprises complex resonance patterns assigned to the aromatic protons of the Ph_2Ppy as well as a sharp singlet at δ 2.27 attributable to the methyl protons of the acetonitrile ligands. When the two features are integrated against each other, a ratio of 2.42:1 is obtained; this is consistent with four acetonitrile and two Ph_2Ppy ligands. That these two Ph_2Ppy ligands are in equivalent environments is confirmed by the sharp singlet at δ 68.9 (relative to H_3PO_4, external standard) in the compound's $^{31}P\{^1H\}$ nmr spectrum (Table 3.13). The

Table 3.11 Physical and microanalytical data

	Complex	Colour	M:g.mol^{-1}	Analysis : Found (Calculated) % %C	%H	%N
[19]	$[Ru_2(\mu\text{-}Ph_2Ppy)_2(\mu\text{-}CO)_2(NCMe)_4](PF_6)_2$	Orange-red	1238.86	43.00(42.66)	3.21(3.25)	6.93(6.78)
[20]	$[Ru_2(CO)_4(NCMe)_4(\eta^1\text{-}Ph_2Pquin)_2](PF_6)_2$	Yellow	1395.00	47.01(46.49)	3.21(3.18)	6.71(6.02)
[21]	$[Ru_2(\mu\text{-}Ph_2Pbipy)_2(CO)_2(NCMe)_2](PF_6)_2$	Purple	1286.90	44.88(44.80)	3.11(3.13)	6.14(6.53)
[22]	$[Ru_2(\mu\text{-}Ph_2Pbipy)_2(CO)_2(NCEt)_2](PF_6)_2$	Purple	1338.98	46.65(46.30)	3.31(3.62)	6.28(6.12)
[23]	$[Ru_2(\mu\text{-}Ph_2Pbipy)_2(CO)_2(NCPh)_2](PF_6)_2$	Purple	1435.06	49.61(50.22)	3.41(3.09)	6.22(5.86)
[24]	$[Ru_2(\mu\text{-}Ph_2Pbipy)_2(CO)_4](PF_6)_2$	Purple-red	1284.84	44.60(44.87)	3.08(2.67)	4.51(4.36)

Table 3.12 Infra-red spectroscopic data[a]

Complex	ν(CO), cm^{-1}	ν(μ-CO),cm^{-1}	ν(P-F),cm^{-1}
[19]		1715(vs)	841(vs)
[20][b]	2052(m) 2030(s) 1992(s) 1912(m, sh)		839(vs)
[21]	1936(s) 1913(m, sh)		841(vs)
[22]	1938(s) 1914(m,sh)		839(vs)
[23]	1934(s) 1914(m, sh)		839(vs)
[24]	2019(s) 1948(s)		841(vs)

(a) : Recorded in the solid state as KBr disks unless otherwise stated. Designation : vs = very strong, s = strong, m, sh = medium, shoulder.
(b) : Recorded as a nujol mull.

Table 3.13 ^{1}H and $^{31}P\{^{1}H\}$ nmr spectroscopic data$^{(a)}$

Complex	$\delta^{1}H$(ppm)	$\delta\ ^{31}P\{^{1}H\}$(ppm)
[19]	8.85-7.39(m, 28H, Ph_2Ppy) 2.27(s, 12H, $C\underline{H}_3CN$)	68.90(s)
[20]	8.25-7.40(m, 32H, Ph_2Pquin) 2.17(s, 12H, $C\underline{H}_3CN$)	27.65(s)
[21]	9.61-6.50(m, 34H, Ph_2Pbipy) 2.81(s, 6H, $C\underline{H}_3CN$)	55.51(s)
[22]	9.50-6.38(m, 34H, Ph_2Pbipy) 2.36(q, 4H, $CH_3C\underline{H}_2CN$) 1.15(t, 6H, $C\underline{H}_3CH_2CN$)	55.20(s)
[23]	9.41-6.71(m, 34H, Ph_2Pbipy)$^{(b)}$	55.01(s)
[24]	9.55-6.40(m, 34H, Ph_2Pbipy)	55.47(s)

(a) : Recorded in CD_3CN unless otherwise specified.
(b) : Benzonitrile proton shifts obscured by multiplet corresponding to Ph_2Pbipy ligand protons.

following proposed structure, for which correct microanalysis has been obtained (Table 3.11), has subseqently been confirmed through the use of X-ray diffraction techniques.

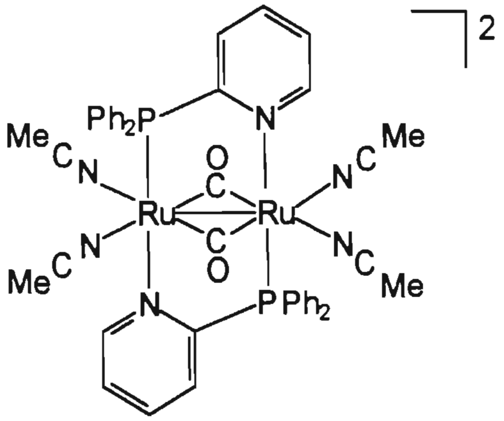

3.3.2 Crystal structure determination of [Ru_2(μ-Ph_2Ppy)$_2$(μ-CO)$_2$(NCMe)$_4$](PF_6)$_2$ [19]

The molecular geometry of the cation of [Ru_2(μ-Ph_2Ppy)$_2$(μ-CO)$_2$(NCMe)$_4$](PF_6)$_2$ **[19]**, which contains a crystallographically imposed centre of symmetry midway between the two ruthenium atoms along the Ru-Ru bond, is depicted in Figure 3.4. The two ruthenium atoms, each of which is approximately octahedral, are not only linked through two bridging Ph_2Ppy ligands trans disposed with respect to each other, but also by a formal ruthenium-ruthenium bond [Ru-Ru' = 2.677(0)Å]; because of the bridged nature of **[19]**, this Ru-Ru bond length is substantially shorter than the 2.873(8)Å found in the unbridged complex [Ru_2(CO)$_4$(NCMe)$_4$(PPh_3)$_2$](PF_6)$_2$ [120].

The entire molecule is highly symmetrical, with angles about each ruthenium atom very close to that required by octahedral coordination (90°). The two Ph_2Ppy ligands are in an almost exact axial plane, exhibiting only a very slight P(1)-Ru-Ru'-N(1) torsion angle of 1.9° within each ligand. More substantial torsion (10.8°) occurs about the C(20)-N(3)-N(2)-C(18) angle, where the acetonitrile ligand containing N(2) is bent away from the equatorial plane.

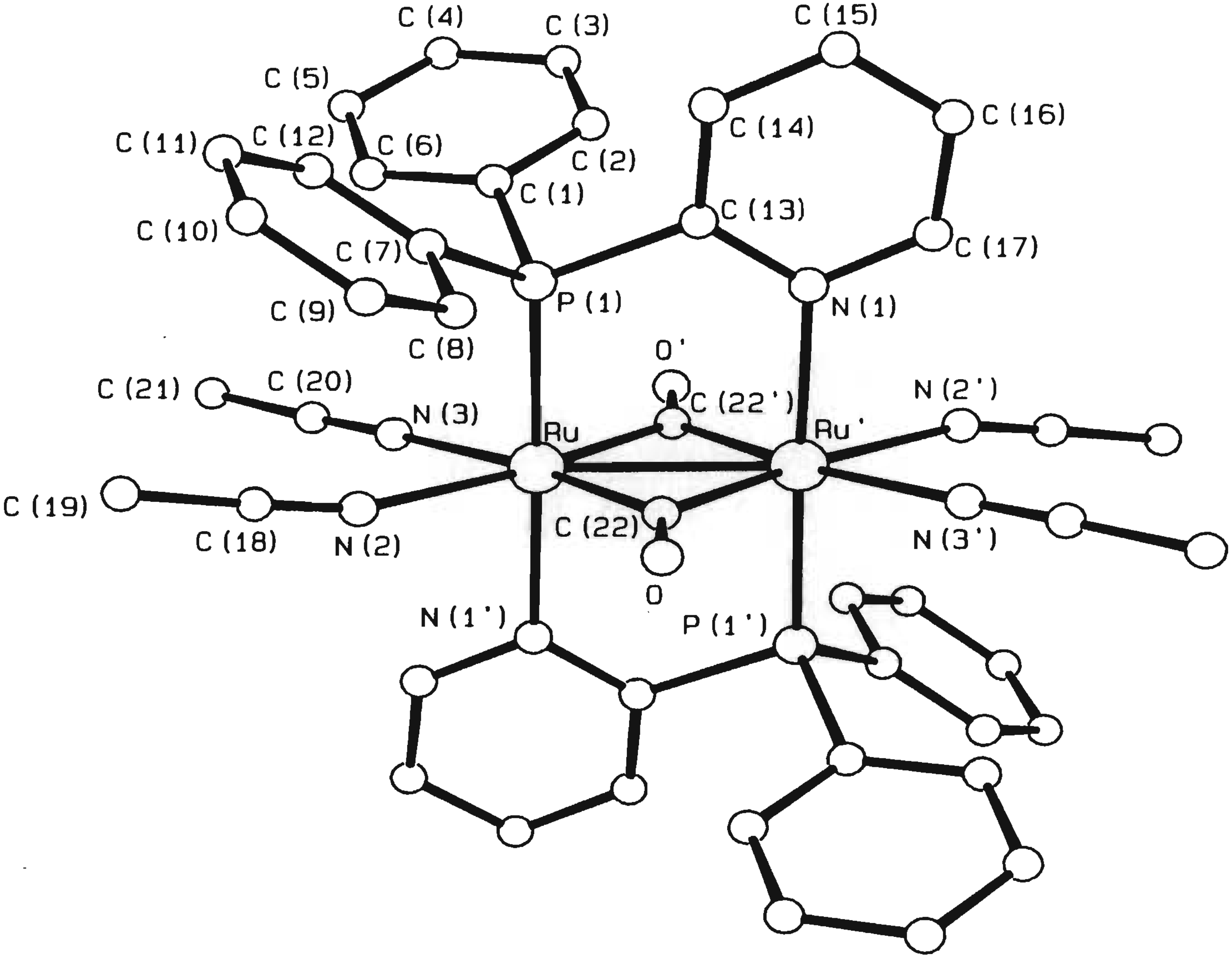
C (4)
C (3)
C (15)
C (5)
C (14)
C (16)
C (11)
C (12)
C (6)
C (2)
C (1)
C (13)
C (10)
C (7)
C (17)
P (1)
N (1)
C (9)
C (8)
O'
C (21)
C (20)
N (3)
C (22')
N (2')
Ru
Ru'
C (19)
C (18)
N (2)
C (22)
N (3')
O
N (1')
P (1')

The Ru-P(1) bond distance of 2.272(1)Å is noticeably shorter than that for $[Ru_2(CO)_4(NCMe)_4(PPh_3)_2](PF_6)_2$ [2.438(2)Å]^{120}. In contrast, the Ru-N(nitrile) bond distances (average = 2.168Å) are all longer than those in the latter compound (average = 2.104Å).

3.3.3 Synthesis of the Ph₂Pquin complex $[Ru_2(CO)_4(NCMe)_4(\eta^1\text{-}Ph_2Pquin)_2](PF_6)_2$ [20]

It was anticipated that the Ph_2Pquin ligand would react in a similar fashion to Ph_2Ppy with $[Ru_2(CO)_4(NCMe)_6](PF_6)_2$, producing the Ph_2Pquin ligand-bridged analogue of **[19]**. However, reaction of two equivalents of Ph_2Pquin with $[Ru_2(CO)_4(NCMe)_6](PF_6)_2$ in refluxing acetonitrile produces a deep-yellow solution from which a yellow-orange powder separates upon addition of diethyl ether. This powder exhibits four terminal CO stretching frequencies in its infra-red spectrum (Table 3.12) which, firstly, are located at lower wavenumbers [2052(m) 2030(s) 1992(s) 1912(m,sh)] than those of the $[Ru_2(CO)_4(NCMe)_6]^{2+}$ precursor [2064(m) 2031(vs) 1987(vs) 1968(s,sh)]^{120}and secondly, have a different band envelope. Both the structure of this band envelope and the wavenumbers of the bands therein correlate well with the four $\nu(C\equiv O)$ bands which appear in the infra-red spectrum of $[Ru_2(CO)_4(NCMe)_4(PPh_3)_2]^{2+}$ [2040(m) 2017(s) 1983(s) 1968(m,sh)]^{120}. The $^{31}P\{^1H\}$ nmr spectrum (CD_3CN, Table 3.13) exhibits a sharp singlet at δ 27.65, comparing well with the δ 22.4 observed in the corresponding spectrum of the above triphenylphosphine complex. The integrals on the relevant shifts in the ^1H nmr spectrum (Table 3.13) correspond approximately to two Ph_2Pquin and four acetonitrile ligands. Thus, the following structure is proposed for the cation in $[Ru_2(CO)_4(NCMe)_4(\eta^1\text{-}Ph_2Pquin)_2](PF_6)_2$, containing the Ph_2Pquin ligand bound in a monodentate fashion through its phosphorus atom only. The dimer is left unbridged as in the triphenylphosphine analogue.

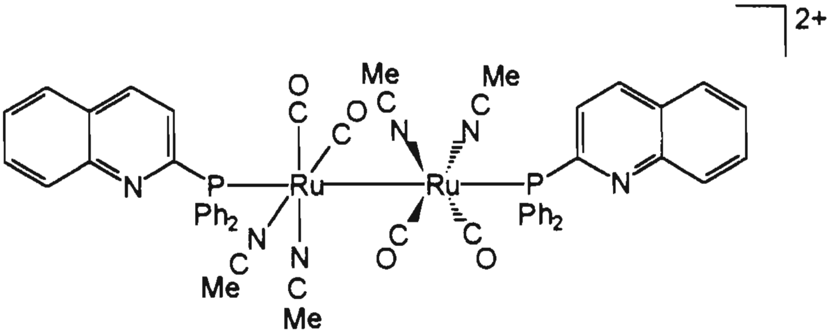

As in the triphenylphosphine analogue, the crystal structure of which is shown in section 3.3, the carbonyl and nitrile substituents on one ruthenium atom are most likely staggered relative to those on the other ruthenium atom while the Ph_2Pquin ligands are bonded in a monodentate fashion collinear with the Ru-Ru vector.

All attempts at shifting the Ph_2Pquin ligand into a position bridging the dimer, similar to that in **[19]**, failed. This included using higher boiling nitrile and other solvents and elevated ligand:dimer ratios. Presumably, the inflexible nature of the quinoline fragment prevents substitution of an acetonitrile ligand at the second ruthenium atom. The exact reasoning, however, remains unclear.

3.3.4 Synthesis of the Ph_2Pbipy complexes $[Ru_2(\mu\text{-}Ph_2Pbipy)_2(CO)_2(NCR)_2](PF_6)_2$ (R = Me [21], Et [22] and Ph [23])

Reaction of two equivalents of Ph_2Pbipy with $[Ru_2(CO)_4(NCMe)_6](PF_6)_2$ in refluxing (90°) acetonitrile for 24 hours produces a deep purple solution from which purple needle-like crystals are formed through the careful addition of diethyl ether and cooling of the resultant mixture to -25°C. After this initial crystallisation, the product is recrystallised a second time by slow diffusion of diethyl ether into an acetonitrile solution of the complex, affording single, needle-like crystals. During the course of the initial reflux, the solution changes colour from yellow, through purple-brown after approximately 4 hours and finally to the deep purple characteristic of the final product. By monitoring these changes using infra-red and $^{31}P\{^1H\}$ nmr spectroscopy, it is evident that the purple-brown solution contains an intermediate possessing both terminal and bridging carbonyl ligands. Its $^{31}P\{^1H\}$ nmr spectrum exhibits a singlet at δ 57.54. As the solution changes colour to deep purple, the bridging carbonyl bands disappear while the terminal carbonyl bands remain essentially unaffected; at the same time, the singlet in the $^{31}P\{^1H\}$ nmr spectrum shifts upfield to δ 55.20, corresponding to that for the complex isolated from the deep purple solution (see later, as well as Table 3.13). The exact nature of this intermediate is unclear, and the above evidence suggests that it slowly reverts to the final product. This conversion is apparently spontaneous, even at room temperature in nitrile solvents.

A solid state (KBr disk) infra-red spectrum (Table 3.12) of the purple crystals exhibits a single, intense terminal carbonyl band at 1936cm^{-1} with a shoulder at 1913cm^{-1}. In view of the similar band pattern observed for two cis-disposed terminal carbonyl groups in $[Ru_2\{\mu\text{-}\eta^2\text{-}OC(Me)O\}(CO)_2(\mu\text{-}Ph_2Pbipy)_2]PF_6$ **[17]** [1930(vs) 1890(m,sh)], it is presumed that there are two mutually cis carbonyl ligands in the complex. The singlet at δ 55.20 in its $^{31}P\{^1H\}$ nmr spectrum (Table 3.13) indicates chemically equivalent phosphorus atoms; moreover, this value is within the region expected for $^{31}P\{^1H\}$ nmr shifts resulting from dinuclear Ph_2Pbipy ligand-bridged ruthenium(I) complexes (see, for example, Table 3.10). A singlet at δ 2.81 in the ^1H nmr spectrum of the complex (Table 3.13) confirms the presence of coordinated acetonitrile ligand(s). When its integral is compared with that of the complex resonance patterns arising from aromatic Ph_2Pbipy ligand protons, a ratio of approximately 6:1 is observed; this indicates two acetonitrile and two Ph_2Pbipy ligands. On the basis of this evidence, and a correct microanalysis (Table 3.11), the following structure is proposed for the acetonitrile cation $[Ru_2(\mu\text{-}Ph_2Pbipy)_2(CO)_2(NCMe)_2]^{2+}$, as well as the propionitrile and benzonitrile analogues $[Ru_2(\mu\text{-}Ph_2Pbipy)_2(CO)_2(NCEt)_2]^{2+}$ and $[Ru_2(\mu\text{-}Ph_2Pbipy)_2(CO)_2(NCPh)_2]^{2+}$ respectively.

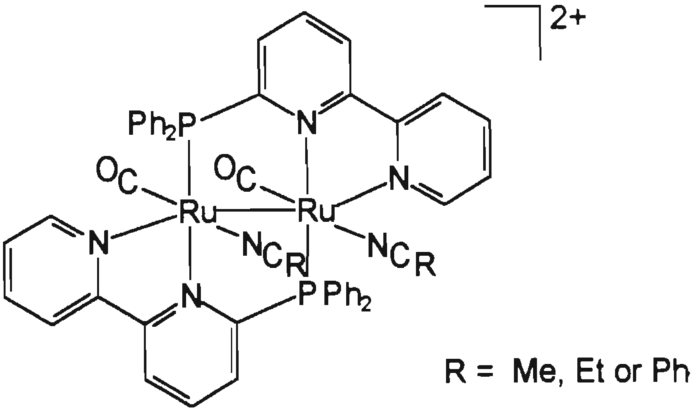

Through the use of single crystal X-ray diffraction studies on the propionitrile analogue **[22]**, the precise stereochemistry has been determined and the complex shown to be a different isomer to that above, with the ruthenium dimer bridged by two mutually *cis*, rather than trans, Ph_2Pbipy ligands.

3.3.5 Crystal structure determination of $[Ru_2(\mu\text{-}Ph_2Pbipy)_2(CO)_2(NCEt)_2](PF_6)_2$ [22]

The crystal structure of $[Ru_2(\mu\text{-}Ph_2Pbipy)_2(CO)_2(NCEt)_2](PF_6)_2$**[22]** consists of well separated cations and anions. The molecular geometry of the $[Ru_2(\mu\text{-}Ph_2Pbipy)_2(CO)_2(NCEt)_2]^{2+}$ cation of **[22]** is depicted in Figure 3.5. The complex cation possesses a crystallographically imposed two-fold axis which bisects the Ru-Ru bond.

The ruthenium atoms are held together by two mutually cis Ph_2Pbipy ligands which bridge in a "head-to-tail" fashion as well as a formal ruthenium-ruthenium bond. The geometry about each ruthenium atom is approximately octahedral [ranging from 74.7(2)° for N(2′)-Ru-N(1′) to 107.5(2)° for N(1′)-Ru-P(1)] , with the final two sites on each atom being occupied by one carbonyl and one propionitrile ligand, each orthogonal to the Ru-Ru vector.

The Ru-Ru bond length of 2.765(2)Å is slightly longer than that of the Ph_2Ppy ligand-bridged complex $[Ru_2(\mu\text{-}Ph_2Ppy)_2(\mu\text{-}CO)_2(NCMe)_4](PF_6)_2$ **[19]** [2.677(0)Å] and the carboxylate-bridged, Ph_2Pbipy ligand-bridged complex $[Ru_2\{\mu\text{-}\eta^2\text{-}OC(Me)O\}(CO)_2(\mu\text{-}$

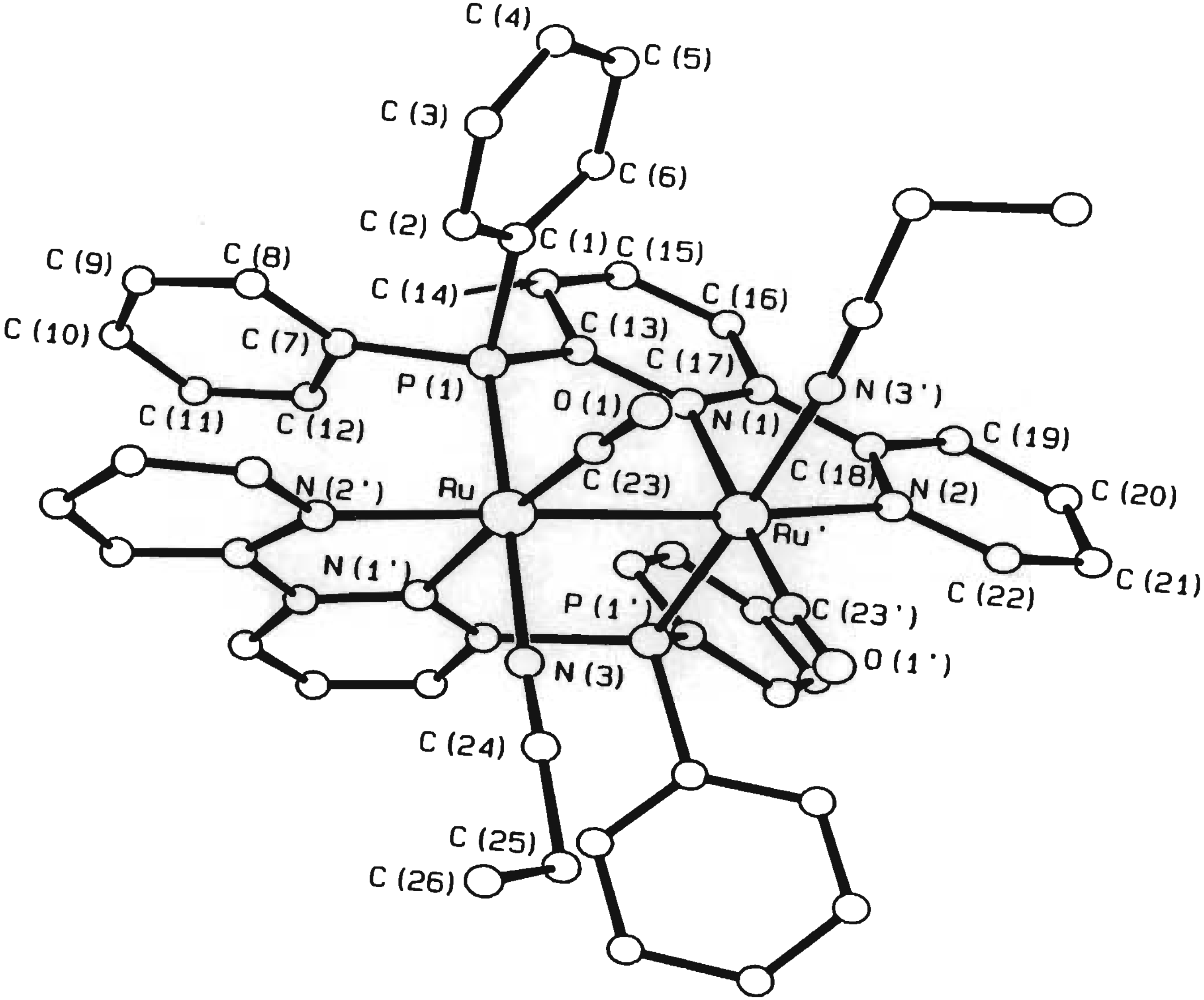
C (4)
C (5)
C (3)
C (6)
C (2)
C (1)
C (15)
C (9)
C (8)
C (14)
C (16)
C (10)
C (7)
C (13)
C (17)
P (1)
N (3')
C (11)
C (12)
O (1)
N (1)
C (19)
C (18)
N (2')
Ru
C (23)
N (2)
C (20)
Ru'
N (1')
C (21)
C (22)
P (1')
C (23')
O (1')
N (3)
C (24)
C (25)
C (26)

$Ph_2Pbipy)_2](PF_6)$ **[17]** [2.687(2)Å], but is shorter than the unbridged Ru-Ru bond distance of 2.873(8)Å observed in $[Ru_2(CO)_4(NCMe)_4(PPh_3)_2](PF_6)_2$.[120] The Ru-P and Ru-N bond distances correlate well with those observed in **[19]**.

The carbonyl and propionitrile ligands are staggered to different extents with respect to each other. The C(23)-Ru-Ru'-C(23') torsion angle of 82.3° is almost half of that involving the propionitrile ligands [N(3)-Ru-Ru'-N(3') = 130.4°]. Within the Ph_2Pbipy ligands, the fairly large degree of torsion [P(1)-Ru-Ru'-N(1) = 16.8°] is in contrast with the low dihedral angle of 8.3° between the mean planes defined by the non-hydrogen atoms of each pyridine ring of the bipyridyl fragment. Figure 3.6 shows a view down the Ru-Ru' axis and shows the cis orientation of the Ph_2Pbipy ligands, the staggering of the carbonyl and propionitrile ligands and the position of the two-fold axis bisecting the cation through the Ru-Ru vector.

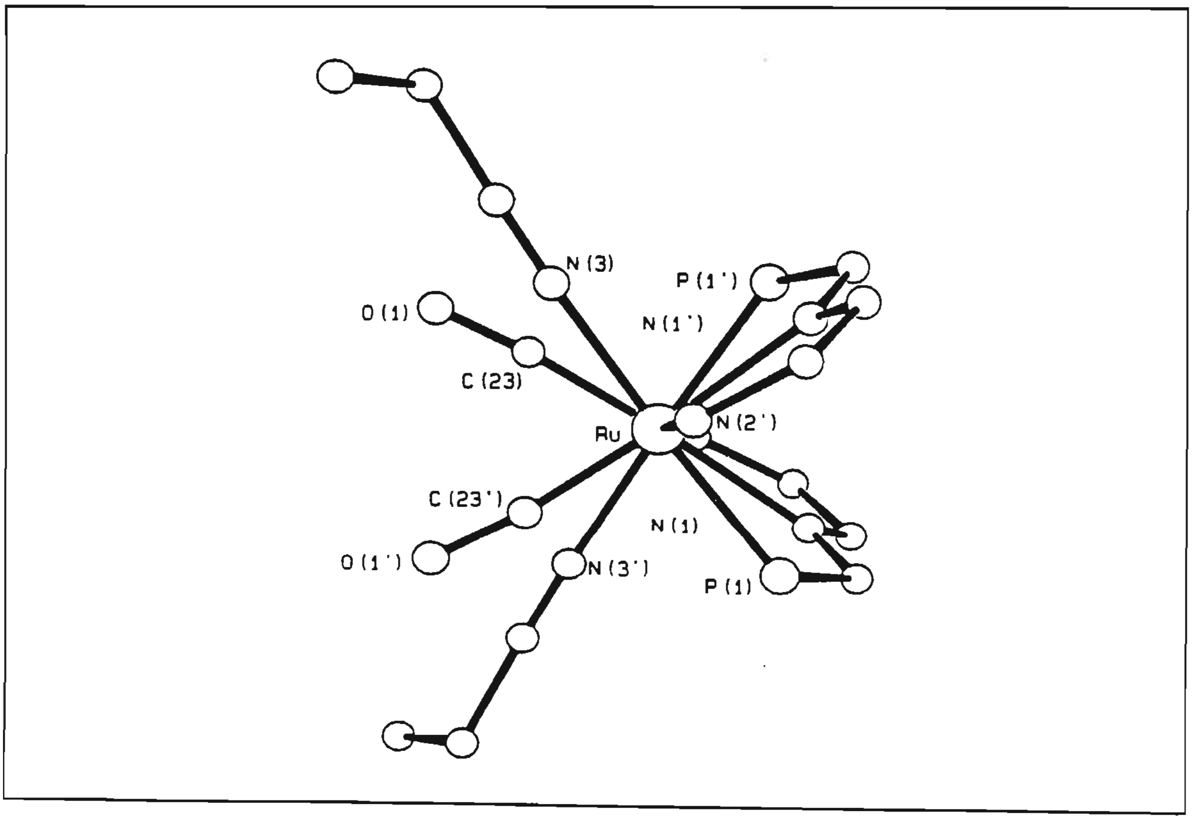

Figure 3.6 : Central portion of the $[Ru_2(\mu\text{-}Ph_2Pbipy)_2(CO)_2(NCEt)_2]^{2+}$ cation viewed along the Ru-Ru' axis

As viewed in Figure 3.6, the left hand side of the dimer is less sterically congested than the right hand side. Studies are currently under way to investigate this feature of the complex, since the relative lack of steric crowding might facilitate the substitution of the labile propionitrile groups.

3.3.6 Synthesis of [Ru_2(μ-Ph_2Pbipy)$_2$(CO)$_4$](PF_6)$_2$ [24]

Reaction of two equivalents of Ph_2Pbipy with [Ru_2(CO)$_4$(NCMe)$_6$](PF_6)$_2$ in refluxing acetone, rather than refluxing nitrile solvents as described above, produces, after 24 hours, a clear, purple-red solution. By slow diffusion of diethyl ether vapour into the cooled resultant solution, an amorphous purple-red solid is precipitated. After isolation, a solid state (KBr disk) infra-red spectrum (Table 3.12) of the product exhibits two equally intense terminal carbonyl bands at 2019 and 1948cm^{-1}, as well as the characteristic ν(P-F) band at 841cm^{-1} attributable to the PF_6^- counter-anion. The terminal carbonyl pattern is typical of that expected for a molecule possessing C_{2h} symmetry. That the Ph_2Pbipy ligands are in equivalent environments is confirmed by the singlet at δ 55.47 in its $^{31}P\{^1H\}$ nmr spectrum (Table 3.13), corresponding to equivalent phosphorus atoms. Unfortunately, despite numerous attempts, single crystals of the PF_6^- salt could not be grown. Thus, the spectroscopic evidence, coupled with an accurate microanalysis (Table 3.11), suggests the following structure for the cation. It is presumed that the use of the essentially non-coordinating acetone solvent (of markedly different polarity to that of nitriles) effects the substitution of the acetonitrile ligands on the starting material in preference to the carbonyl groups.

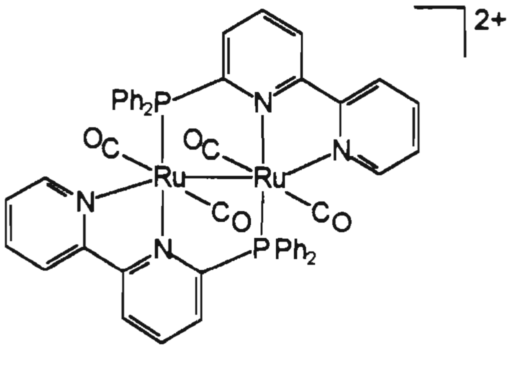

3.4 Conclusion

The work described in this chapter significantly extends the known types of diruthenium(I) complexes. It has been shown that bidentate, asymmetric ligands such as Ph_2Ppy and Ph_2Pquin, aside from coordinating to ruthenium(I) in a monodentate fashion through their phosphorus atoms alone, also possess the ability to bridge the ruthenium(I) dimer, thereby stabilising it to fragmentation. In so doing, the dimer's potential to promote reactions involving formation and cleavage of metal-metal bonds is enhanced. The novel, tridentate Ph_2Pbipy ligand possesses similar coordinating properties; in cases where it bridges ruthenium(I) dimers, chelation of its bipyridyl fragment at the second metal atom, as anticipated, is observed. In order to bring about these modes of coordination, two principal precursors have been utilised.

The ability of alcohols and toluene to labilise the carboxylate bridge of the $[Ru\{\mu\text{-}\eta^2\text{-}OC(R)O\}(CO)_2]_n$ polymer in the presence of the relevant ligand has been effectively demonstrated by the stepwise formation of cationic ligand-bridged derivatives from the η^1-species containing the relevant ligand bound in a monodentate manner. With regard to the Ph_2Pbipy ligand, this labilisation extends to carbonyl groups as well, since formation of the ligand-bridged complexes **[16]** - **[18]** involves cleavage of the M-C(O) bond in addition to a carboxylato group.

The more versatile precursor $[Ru_2(CO)_4(NCMe)_6](PF_6)_2$ contains labile acetonitrile ligands which have been shown to be easily substituted by all the ligands used in this work resulting, in the case of Ph_2Ppy and Ph_2Pbipy, in ligand-bridged derivatives. Steric restrictions within the rigid quinoline fragment prevent similar coordination of the Ph_2Pquin ligand and it forms instead dinuclear, unbridged complexes containing pendant ligands. Interesting features of the ligand-bridged derivatives include the presence of labile nitrile ligands, providing sites for further reaction and, in the case of the Ph_2Pbipy ligand-bridged derivative **[22]**, ligands bound in a cis configuration with respect to each other, the first of its kind for ruthenium dimers. Moreover, this cis orientation is very stable and creates a potential surface at which further reactions can occur in view of the less sterically conjested side of the dimer opposite the bridging ligands. Trans-dispositon of Ph_2Pbipy, like that observed in the analogous carboxylate complexes, is also observed and this reaffirms its coordinative versatility.

Crucial in understanding how these phosphorus-pyridyl and -bipyridyl ligands coordinate has been the use of X-ray diffraction structure solution techniques and a number of structures have been elucidated through such means. It is anticipated that with these new phosphoruspyridyl and phosphorusbipyridyl ligand-bridged species, the chemistry associated with adjacent ruthenium(I) centres can be probed.

3.5 Experimental

General experimental details and sources of chemicals are outlined in Appendices A and B respectively.

3.5.1 Synthesis of $[Ru_2\{\mu\text{-}\eta^2\text{-}OC(R)O\}_2(CO)_4(\eta^2\text{-}Ph_2Ppy)_2]$ (R = H [1], Me [2] or Et [3])

A suspension of the appropriate carboxylate-bridged $[Ru\{\mu\text{-}\eta^2\text{-}OC(R)O\}(CO)_2]_n$ polymer (1.50mmol) and Ph_2Ppy (395mg; 1.50mmol) in absolute ethanol (15cm^3) was refluxed for 45 minutes. The suspension gradually dissolved and was replaced by a yellow-orange precipitate, which was separated by filtration, washed with cold (0°C) absolute ethanol (5 cm^3), diethyl ether (5cm^3) and then dried *in vacuo*. for 1 hour. In cases where the precipitate had not formed after 45 minutes (for R = H), the reaction was stopped and the solvent removed carefully under reduced pressure to effect precipitation of the products. Although all products were sufficiently pure not to require further crystallisation, highly crystalline material could be isolated from a slowly evaporating dichloromethane-ethanol (1:1, vol:vol) solution of the product.

Yields: **[1]** 62%, **[2]** 76%, **[3]** 73%.

3.5.2 Synthesis of $[Ru_2\{\mu\text{-}\eta^2\text{-}OC(R)O\}_2(CO)_4(\eta^1\text{-}Ph_2Pquin)_2]$ (R = H [4], Me [5] or Et [6])

A suspension of the appropriate carboxylate-bridged $[Ru\{\mu\text{-}\eta^2\text{-}OC(R)O\}(CO)_2]_n$ polymer (1.5mmol) and Ph_2Pquin (470mg; 1.5mmol) in toluene (10cm^3) was refluxed whilst gently bubbling CO through the solution for 3 hours. The suspension gradually dissolved, yielding a bright yellow solution from which the product precipitated. This yellow product was filtered off, washed with diethyl ether (2 x 5cm^3) and dried *in vacuo.* for 2 hours. The products, in all cases, were sufficiently pure so as not to require further crystallisation. Yield: **[4]** 78%, **[5]** 88%, **[6]** 70%.

3.5.3 Synthesis of $[Ru_2\{\mu\text{-}\eta^2\text{-}OC(R)O\}_2(CO)_4(\eta^1\text{-}Ph_2Pbipy)_2]$ (R = H [7], Me [8] or Et [9])

A suspension of the appropriate carboxylate-bridged $[Ru\{\mu\text{-}\eta^2\text{-}OC(R)O\}(CO)_2]_n$ polymer (0.60mmol) and Ph_2Pbipy (205mg; 0.60mmol) in 1-butanol (15cm^3) was refluxed for 3 hours. The suspension gradually dissolved, leaving a clear brown-orange solution at the end of the reaction. The hot solution was filtered quickly and then carefully evaporated down to *ca.* 5cm^3 under reduced pressure, yielding the product as a dark orange powder. This was filtered in air, washed with cold (0°C) 1-butanol (2cm^3), diethyl ether (10cm^3) and dried *in vacuo.* for 12 hours at 40°C to effectively remove any residual 1-butanol. The product was then recrystallised from a slowly evaporating saturated acetone-ethanol (1:1, vol:vol) solution of the compound.

Yield: **[7]** 58%, **[8]** 69%, **[9]** 67%.

3.5.4 Synthesis of $[Ru_2\{\mu\text{-}\eta^2\text{-}OC(R)O\}(CO)_4(\mu\text{-}Ph_2Ppy)_2](PF_6)$ (R = H [10], Me [11] or Et [12])

A suspension of the appropriate carboxylate-bridged $[Ru\{\mu\text{-}\eta^2\text{-}OC(R)O\}(CO)_2]_n$ polymer (0.46mmol), Ph_2Ppy (125mg; 0.46mmol) and NH_4PF_6 (75mg; 0.46mmol) in toluene (15 cm^3) was refluxed whilst gently bubbling CO through the solution for 4 hours (for **[11]** and **[12]**) or 6 hours (for **[10]**). During this time the solution turned orange (corresponding to the formation of the η^1 pendant species) and then became clear yellow with the concomitant formation of a bright yellow precipitate. The suspension was cooled to room temperature, the solid isolated by filtration, washed with diethyl ether (2 x 5cm^3) and dried *in vacuo*. Further product was obtained by reducing the volume of the filtrate to *ca.* 3cm^3, then cooling it at -25°C for 12 hours. The combined products were then recrystallised from a slowly evaporating saturated dichloroethane-ethanol (1:1, vol:vol) solution to afford the bright yellow crystalline product, isolated in the manner described above.

Yield: **[10]** 63%, **[11]** 72%, **[12]** 67%.

3.5.5 Synthesis of $[Ru_2\{\mu\text{-}\eta^2\text{-}OC(R)O\}(CO)_4(\mu\text{-}Ph_2Pquin)_2](PF_6)$ (R = H [13], Me [14] or Et [15])

A suspension of the appropriate carboxylate-bridged $[Ru\{\mu\text{-}\eta^2\text{-}OC(R)O\}(CO)_2]_n$ polymer (0.46mmol), Ph_2Pquin (144mg; 0.46mmol) and excess NH_4PF_6 (300mg; 1.84mmol) in toluene (15cm^3) was refluxed whilst gently bubbling CO through the solution for 8 hours. During this time, the suspension gradually dissolved, yielding a yellow solution from which a yellow precipitate began to separate. On completion of the reaction, the solution was cooled and the product carefully isolated by filtration. It was washed with diethyl ether (2 x 5cm^3) and then dried *in vacuo*. Note: No further product could be isolated from the mother liquor; instead reduction of the solvent volume yielded the η^1 pendant precursors **[4]** - **[6]**.

Yield: **[13]** 9%, **[14]** 13%, **[15]** 4%.

3.5.6 Synthesis of $[Ru_2\{\mu\text{-}\eta^2\text{-}OC(R)O\}(CO)_2(\mu\text{-}Ph_2Pbipy)_2](PF_6)$ (R = H [16], Me [17] or Et [18])

A suspension of the appropriate carboxylate-bridged $[Ru\{\mu\text{-}\eta^2\text{-}OC(R)O\}(CO)_2]_n$ polymer (0.60mmol) and Ph_2Pbipy (205mg; 0.60mmol) in 1-butanol ($10cm^3$) was carefully refluxed at 120°C under nitrogen for 24 hours. The colour of the solution gradually changed from orange-yellow through to dark brown. The reaction solution was cooled to room temperature and filtered under nitrogen. A hot solution of NH_4PF_6 (106mg; 0.65mmol) in 1-butanol was then added dropwise with stirring to precipitate the brown product. This was isolated by filtration, washed with diethyl ether (5 x $5cm^3$) and dried *in vacuo* for 12 hours at 40°C to effectively remove any residual 1-butanol. Recrystallisation of the product from acetonitrile-diethyl ether (1:1, vol:vol) at -25°C afforded the analytically pure product as dark brown needles.

Yield: **[16]** 71%, **[17]** 81%, **[18]** 64%.

3.5.7 Synthesis of $[Ru_2(\mu\text{-}Ph_2Ppy)_2(\mu\text{-}CO)_2(NCMe)_4](PF_6)_2$ [19]

Method 1: An acetonitrile solution ($5cm^3$) of Ph_2Ppy (17mg; 0.06mmol) and $[Ru_2(CO)_4(NCMe)_6](PF_6)_2$ (25mg; 0.03mmol) was refluxed at 85°C for 24 hours. During the reflux, the solution changed colour from yellow to orange-red. After cooling the orange-red solution to room temperature, it was filtered and concentrated under reduced pressure to *ca.* $1cm^3$. Diethyl ether ($1cm^3$) was then carefully added dropwise and the mixture transferred to a fridge set at -25°C for 24 hours. The orange-red crystals of the title compound were isolated by carefully decanting off the mother-liquor and washing the crystals with a little cold (0°C) diethyl ether ($1cm^3$). They were then dried *in vacuo* for 2 hours.

Yield : 72%

Method 2: The same quantities of reagents were refluxed, this time in ethanol, for 4 hours. An ochre-coloured powder precipitated from solution. This was filtered off and recrystallised from acetonitrile-ether (1:1, vol:vol) at -25°C for 24 hours. The orange-red crystalline product was isolated in a similar fashion to that described in method 1.

Yield : 54%

3.5.8 Synthesis of $[Ru_2(CO)_4(NCMe)_4(\eta^1\text{-}Ph_2Pquin)_2](PF_6)_2$ [20]

Although this product was formed from numerous attempts at synthesising a Ph_2Pquin ligand-bridged complex, including analogous methods in refluxing solvents to those used with the Ph_2Ppy ligand in 3.5.7, the highest yielding synthesis is reported here. Reaction vessels were covered with aluminium foil throughout this preparation in order to minimise exposure to light.

A CH_2Cl_2 solution ($2cm^3$) of Ph_2Pquin (23mg; 0.070mmol) was added with stirring to a CH_2Cl_2 solution ($2cm^{-3}$) of $[Ru_2(CO)_4(NCMe)_6](PF_6)_2$ (30mg; 0.035mmol). After 3 hours stirring at room temperature, diethyl ether ($5cm^3$) was added and a yellow powder precipitated from solution. The yield of the product was increased by leaving the suspension at -25°C overnight. After careful filtration and washing with diethyl ether ($2cm^3$) the product was dried *in vacuo*. for an hour. The product was sufficiently pure so as not to require further crystallisation.

Yield : 78%

3.5.9 General synthesis of $[Ru_2(\mu\text{-}Ph_2Pbipy)_2(CO)_2(NCR)_2](PF_6)_2$ (R = Me [21], Et [22] or Ph [23])

A solution of Ph_2Pbipy (22mg; 0.06mmol) and $[Ru_2(CO)_4(NCMe)_6](PF_6)_2$ (25mg; 0.03mmol) in the appropriate nitrile solvent ($3cm^3$) was refluxed for 24 hours (in the case of MeCN), 10 hours (in the case of EtCN) or 6 hours (in the case of PhCN). During this time, the colour of the solution changed to deep purple from yellow. After cooling the solution to room temperature, it was concentrated under reduced pressure to *ca.* 1cm^3. Diethyl ether (2cm^3) was then added and the mixture transferred to a fridge set at -25°C for 12 hours. This afforded the crude product as a microcrystalline precipitate which was redissolved in the appropriate nitrile solvent, filtered through glass microfibre and transferred to a vapour diffusion apparatus. Through the slow diffusion of diethyl ether into this solution, single needle-like crystals of the complex were grown. These were isolated by carefully decanting off the mother-liquor and washing with diethyl ether (2 x 1cm^3). Finally, they were then dried *in vacuo.* for an hour.

Yield : 70% **[21]**, 73% **[22]**, 61% **[23]**

3.5.10 Synthesis of $[Ru_2(\mu\text{-}Ph_2Pbipy)_2(CO)_4](PF_6)_2$ [24]

An acetone solution (5cm^3) of Ph_2Pbipy (22mg; 0.06mmol) and $[Ru_2(CO)_4(NCMe)_6](PF_6)_2$ (25mg; 0.03mmol) was refluxed for 24 hours, during which time the solution became a purple-red colour. The solution was filtered, concentrated to *ca.* 2cm^3 under reduced pressure and then refiltered through glass microfibre into a vapour diffusion apparatus. Slow diffusion of diethyl ether vapour into this solution produced, after approximately two days, an amorphous purple-red precipitate. The mother liqour was subsequently carefully removed and the purple-red air-stable product washed with cold (0°C) diethyl ether (2 x 1cm^3). The compound was then thoroughly dried *in vacuo.* for 4 hours. Microanalysis confirmed that the product was sufficiently pure so as not to require further recrystallisation.

Yield : 65%

3.5.11 Single crystal X-ray diffraction study of $[Ru_2\{\mu\text{-}\eta^2\text{-}OC(Me)O\}_2(CO)_4(\eta^1\text{-}Ph_2Ppy)_2]$ [2]

Orange-yellow lobe shaped crystals of **[2]** were grown by slow evaporation of a saturated dichloroethane-ethanol (1:1, vol:vol) solution of the compound. The general approach used for the intensity data collection is described in Appendix A. All aromatic rings were refined as rigid phenyl groups. Subsequent to this, tentative assignments for N(1) and N(2) were made (see Fig 3.1) on the basis of (i) their temperature factors as carbons were lower than any of those for the corresponding carbon atoms on the other rings and (ii) the C-N bond distances were more correct for these assignments than for any other. The crystallographic data are given in Table 3.14, the interatomic distances in Table 3.15, the interatomic angles in Table 3.16, the fractional coordinates in Table 3.17 and the anisotropic thermal parameters in Table 3.18. The observed and calculated structure factors may be found on microfiche in an envelope fixed to the inside back cover.

Table 3.14

Crystal data and details of the crystallographic analysis for $[Ru_2\{\mu\text{-}\eta^2\text{-}OC(Me)O\}_2(CO)_4(\eta^1\text{-}Ph_2Ppy)_2]$

Formula	$Ru_2C_{42}H_{34}N_2O_8P_2$
Molecular Mass	958.83
Crystal System	Triclinic
Space Group	$P\bar{1}$
a(Å)	9.484(2)
b(Å)	13.146(3)
c(Å)	16.838(6)
α(°)	82.097(2)
β(°)	87.853(2)
γ(°)	77.617(2)
V(Å^3)	2031.10
Z	2
D_c(g.cm^{-3})	1.568
F(000)	964
λ(Mo-Kα)(Å)	0.71069
Scan mode	ω - 2θ
ω scan angle	$0.53 + 0.35\tan\theta$
Horizontal Aperture width (mm)	$2.7 + 0.1\tan\theta$
Scattering range (°)	$2 \leq \theta \leq 23$
μ (cm^{-1})	8.64
Absorption corrections	Semi empirical[103]
Measured intensities	5872
Unique intensities	5230
Unique intensities with [I > 3σ(I)]	4582
Structure solution	Direct & Fourier methods
Weighting scheme	$1/(\sigma^2(F) + 0.00043F^2)$
$R = \Sigma(F_o\text{-}F_c)/\Sigma F_o$	0.0731
$R_w = \Sigma_w{}^{1/2}(F_o\text{-}F_c)/\Sigma_w{}^{1/2}F_o$	0.0862
$(\Delta/\sigma)_{max}$	1.39
$\Delta\rho_{max}$(eÅ^{-3})	2.792
Number of parameters	457

Table 3.15: Interatomic distances (Å) for

$[Ru_2\{\mu\text{-}\eta^2\text{-}OC(Me)O\}_2(CO)_4(\eta^1\text{-}Ph_2Ppy)_2]$

Ru(1)-Ru(2)	2.719(1)	Ru(1)-P(1)	2.410(2)
Ru(1)-O(1)	2.112(7)	Ru(1)-O(3)	2.052(6)
Ru(1)-C(39)	1.806(13)	Ru(1)-C(40)	1.800(12)
Ru(2)-P(2)	2.411(2)	Ru(2)-O(2)	2.114(6)
Ru(2)-O(4)	2.065(6)	Ru(2)-C(41)	1.831(12)
Ru(2)-C(42)	1.795(9)	P(1)-C(1)	1.807(5)
P(1)-C(7)	1.810(5)	P(1)-C(13)	1.830(9)
P(2)-C(18)	1.812(5)	P(2)-C(24)	1.832(5)
P(2)-C(30)	1.841(9)	N(1)-C(13)	1.399(13)
N(1)-C(17)	1.388(13)	N(2)-C(30)	1.360(13)
N(2)-C(34)	1.362(14)	O(1)-C(35)	1.280(11)
O(2)-C(35)	1.222(10)	O(3)-C(37)	1.262(13)
O(4)-C(37)	1.289(13)	O(5)-C(39)	1.138(15)
O(6)-C(40)	1.24(2)	O(7)-C(41)	1.164(13)
O(8)-C(42)	1.218(13)	C(1)-C(2)	1.395(0)
C(1)-C(6)	1.395(0)	C(2)-C(3)	1.395(0)
C(3)-C(4)	1.395(0)	C(4)-C(5)	1.395(0)
C(5)-C(6)	1.395(0)	C(7)-C(8)	1.395(0)
C(7)-C(12)	1.395(0)	C(8)-C(9)	1.395(0)
C(9)-C(10)	1.395(0)	C(10)-C(11)	1.395(0)
C(11)-C(12)	1.395(0)	C(13)-C(14)	1.391(13)
C(14)-C(15)	1.397(15)	C(15)-C(16)	1.35(2)
C(16)-C(17)	1.40(2)	C(18)-C(19)	1.395(0)
C(18)-C(23)	1.395(0)	C(19)-C(20)	1.395(0)
C(20)-C(21)	1.395(0)	C(21)-C(22)	1.395(0)
C(22)-C(23)	1.395(0)	C(24)-C(25)	1.395(0)
C(24)-C(29)	1.395(0)	C(25)-C(26)	1.395(0)
C(26)-C(27)	1.395(0)	C(27)-C(28)	1.395(0)
C(28)-C(29)	1.395(0)	C(30)-C(31)	1.375(13)
C(31)-C(32)	1.428(14)	C(32)-C(33)	1.37(2)
C(33)-C(34)	1.43(2)	C(35)-C(36)	1.516(13)
C(37)-C(38)	1.56(2)		

Table 3.16: Interatomic angles (°) for $[\mathrm{Ru_2}\{\mu\text{-}\eta^2\text{-OC(Me)O}\}_2(\mathrm{CO})_4(\eta^1\text{-Ph_2Ppy})_2]$

Ru(2)-Ru(1)-P(1)	169.5(1)	Ru(2)-Ru(1)-O(1)	83.5(2)
P(1)-Ru(1)-O(1)	89.9(2)	Ru(2)-Ru(1)-O(3)	84.1(2)
P(1)-Ru(1)-O(3)	87.2(2)	O(1)-Ru(1)-O(3)	85.4(3)
Ru(2)-Ru(1)-C(39)	92.6(4)	P(1)-Ru(1)-C(39)	94.3(4)
O(1)-Ru(1)-C(39)	175.3(5)	O(3)-Ru(1)-C(39)	96.9(6)
Ru(2)-Ru(1)-C(40)	89.9(4)	P(1)-Ru(1)-C(40)	98.4(4)
O(1)-Ru(1)-C(40)	90.3(6)	O(3)-Ru(1)-C(40)	173.0(6)
C(39)-Ru(1)-C(40)	87.0(8)	Ru(1)-Ru(2)-P(2)	176.6(1)
Ru(1)-Ru(2)-O(2)	82.7(2)	P(2)-Ru(2)-O(2)	93.9(2)
Ru(1)-Ru(2)-O(4)	84.4(2)	P(2)-Ru(2)-O(4)	95.5(2)
O(2)-Ru(2)-O(4)	83.9(3)	Ru(1)-Ru(2)-C(41)	93.1(3)
P(2)-Ru(2)-C(41)	90.3(3)	O(2)-Ru(2)-C(41)	174.4(4)
O(4)-Ru(2)-C(41)	92.1(4)	Ru(1)-Ru(2)-C(42)	88.3(3)
P(2)-Ru(2)-C(42)	91.6(3)	O(2)-Ru(2)-C(42)	91.7(4)
O(4)-Ru(2)-C(42)	171.9(4)	C(41)-Ru(2)-C(42)	91.8(5)
Ru(1)-P(1)-C(1)	111.4(2)	Ru(1)-P(1)-C(7)	119.0(2)
C(1)-P(1)-C(7)	102.1(3)	Ru(1)-P(1)-C(13)	115.9(3)
C(1)-P(1)-C(13)	104.2(4)	C(7)-P(1)-C(13)	102.5(4)
Ru(2)-P(2)-C(18)	118.0(2)	Ru(2)-P(2)-C(24)	119.3(2)
C(18)-P(2)-C(24)	104.1(3)	Ru(2)-P(2)-C(30)	109.1(3)
C(18)-P(2)-C(30)	102.0(4)	C(24)-P(2)-C(30)	101.8(3)
C(13)-N(1)-C(17)	117.5(10)	C(30)-N(2)-C(34)	119.2(11)
Ru(1)-O(1)-C(35)	123.3(6)	Ru(2)-O(2)-C(35)	125.5(6)
Ru(1)-O(3)-C(37)	120.9(7)	Ru(2)-O(4)-C(37)	119.6(7)
P(1)-C(1)-C(2)	116.6(2)	P(1)-C(1)-C(6)	123.2(2)
C(2)-C(1)-C(6)	120.0(0)	C(1)-C(2)-C(3)	120.0(0)
C(2)-C(3)-C(4)	120.0(0)	C(3)-C(4)-C(5)	120.0(0)
C(4)-C(5)-C(6)	120.0(0)	C(1)-C(6)-C(5)	120.0(0)
P(1)-C(7)-C(8)	117.5(2)	P(1)-C(7)-C(12)	122.4(2)
C(8)-C(7)-C(12)	120.0(0)	C(7)-C(8)-C(9)	120.0(0)
C(8)-C(9)-C(10)	120.0(0)	C(9)-C(10)-C(11)	120.0(0)
C(10)-C(11)-C(12)	120.0(0)	C(7)-C(12)-C(11)	120.0(0)
P(1)-C(13)-N(1)	116.4(7)	P(1)-C(13)-C(14)	122.3(7)
N(1)-C(13)-C(14)	121.3(9)	C(13)-C(14)-C(15)	118.1(10)
C(14)-C(15)-C(16)	122.6(11)	C(15)-C(16)-C(17)	118.3(10)

Table 3.16 / cont.

N(1)-C(17)-C(16)	122.2(11)	P(2)-C(18)-C(19)	117.7(2)
P(2)-C(18)-C(23)	122.3(2)	C(19)-C(18)-C(23)	120.0(0)
C(18)-C(19)-C(20)	120.0(0)	C(19)-C(20)-C(21)	120.0(0)
C(20)-C(21)-C(22)	120.0(0)	C(21)-C(22)-C(23)	120.0(0)
C(18)-C(23)-C(22)	120.0(0)	P(2)-C(24)-C(25)	121.6(2)
P(2)-C(24)-C(29)	118.4(2)	C(25)-C(24)-C(29)	120.0(0)
C(24)-C(25)-C(26)	120.0(0)	C(25)-C(26)-C(27)	120.0(0)
C(26)-C(27)-C(28)	120.0(0)	C(27)-C(28)-C(29)	120.0(0)
C(24)-C(29)-C(28)	120.0(0)	P(2)-C(30)-N(2)	111.7(7)
P(2)-C(30)-C(31)	123.8(8)	N(2)-C(30)-C(31)	124.5(9)
C(30)-C(31)-C(32)	116.9(11)	C(31)-C(32)-C(33)	119.1(12)
C(32)-C(33)-C(34)	121.4(11)	N(2)-C(34)-C(33)	118.9(13)
O(1)-C(35)-O(2)	124.7(9)	O(1)-C(35)-C(36)	116.9(8)
O(2)-C(35)-C(36)	118.4(9)	O(3)-C(37)-O(4)	130.0(10)
O(3)-C(37)-C(38)	113.8(11)	O(4)-C(37)-C(38)	116.1(10)
Ru(1)-C(39)-O(5)	177(2)	Ru(1)-C(40)-O(6)	168(2)
Ru(2)-C(41)-O(7)	176.8(10)	Ru(2)-C(42)-O(8)	172.6(9)

Table 3.17: Fractional coordinates (x 10^4) and isotropic thermal factors ($Å^2$, x 10^3) for [$Ru_2\{\mu-\eta^2-OC(Me)O\}_2(CO)_4(\eta^1-Ph_2Ppy)_2$]

	x/a	y/b	z/c	U_{eq}
Ru(1)	821(1)	858(1)	2231(1)	59(1)
Ru(2)	-947(1)	2748(1)	2377(1)	56(1)
P(1)	2348(3)	-875(2)	2366(1)	45(1)
P(2)	-2620(3)	4368(2)	2543(1)	43(1)
N(1)	1875(12)	-1406(8)	3978(6)	89(3)
N(2)	-2125(11)	5157(7)	1041(5)	77(3)
O(1)	-790(7)	258(5)	2928(5)	75(2)
O(2)	-2274(7)	1794(5)	3000(4)	64(2)
O(3)	1625(9)	1030(6)	3308(4)	80(2)
O(4)	25(8)	2582(6)	3478(4)	71(2)
O(5)	2916(16)	1822(8)	1225(10)	219(6)
O(6)	-454(25)	674(12)	652(8)	276(8)
O(7)	1226(9)	3925(6)	1600(6)	95(3)
O(8)	-2339(14)	2772(9)	798(7)	144(4)
C(1)	4005(6)	-888(5)	1797(4)	55(2)
C(2)	4918(6)	-279(5)	2026(4)	81(3)
C(3)	6159(6)	-182(5)	1577(4)	115(5)
C(4)	6488(6)	-693(5)	899(4)	104(4)
C(5)	5575(6)	-1302(5)	670(4)	114(5)
C(6)	4333(6)	-1399(5)	1119(4)	89(4)
C(7)	1695(7)	-1933(4)	2020(4)	46(2)
C(8)	782(7)	-1680(4)	1359(4)	81(3)
C(9)	291(7)	-2470(4)	1047(4)	115(5)
C(10)	714(7)	-3512(4)	1396(4)	76(3)
C(11)	1628(7)	-3765(4)	2057(4)	76(3)
C(12)	2118(7)	-2975(4)	2369(4)	63(3)
C(13)	2948(10)	-1435(7)	3383(5)	52(2)
C(14)	4381(12)	-1907(9)	3558(7)	72(3)
C(15)	4726(14)	-2345(10)	4348(7)	88(4)
C(16)	3729(15)	-2333(9)	4940(7)	77(3)
C(17)	2296(14)	-1849(10)	4752(6)	77(3)
C(18)	-4306(5)	4288(5)	3065(4)	53(2)
C(19)	-5048(5)	3549(5)	2872(4)	72(3)
C(20)	-6353(5)	3456(5)	3255(4)	93(4)

Table 3.17 / cont.

C(21)	-6916(5)	4103(5)	3832(4)	99(4)
C(22)	-6173(5)	4843(5)	4026(4)	98(4)
C(23)	-4869(5)	4935(5)	3642(4)	68(3)
C(24)	-1985(7)	5392(4)	2975(4)	51(2)
C(25)	-2364(7)	6447(4)	2649(4)	71(3)
C(26)	-1851(7)	7204(4)	2991(4)	98(4)
C(27)	-959(7)	6906(4)	3660(4)	92(4)
C(28)	-580(7)	5852(4)	3987(4)	115(5)
C(29)	-1093(7)	5095(4)	3644(4)	83(3)
C(30)	-3248(11)	5053(7)	1550(5)	53(2)
C(31)	-4678(12)	5439(8)	1361(6)	65(3)
C(32)	-4985(16)	5991(10)	575(8)	91(4)
C(33)	-3867(21)	6101(10)	58(7)	98(5)
C(34)	-2404(19)	5676(11)	287(7)	98(5)
C(35)	-1957(10)	838(7)	3154(5)	52(2)
C(36)	-3030(12)	283(8)	3627(7)	75(3)
C(37)	1016(13)	1762(10)	3696(6)	74(3)
C(38)	1636(16)	1675(12)	4554(8)	105(4)
C(39)	2083(17)	1455(9)	1598(10)	112(4)
C(40)	-93(20)	795(10)	1327(8)	121(5)
C(41)	350(13)	3488(8)	1890(7)	65(3)
C(42)	-1728(11)	2693(8)	1434(5)	56(3)

$$U_{eq} = \frac{1}{3} \Sigma_i \Sigma_j U_{ij} a_i^* a_j^* (a_i . a_j)$$

Table 3.18:Anisotropic thermal factors (Å^2 , x 10^3) for

$[Ru_2\{\mu\text{-}\eta^2\text{-}OC(Me)O\}_2(CO)_4(\eta^1\text{-}Ph_2Ppy)_2]$

	U(11)	U(22)	U(33)	U(23)	U(13)	U(12)
Ru(1)	64(1)	35(1)	73(1)	-6(1)	24(1)	-3(1)
Ru(2)	60(1)	35(1)	65(1)	0(1)	19(1)	-1(1)
P(1)	45(1)	39(1)	48(1)	-10(1)	2(1)	-3(1)
P(2)	45(1)	38(1)	44(1)	-8(1)	0(1)	-2(1)
N(1)	92(8)	103(8)	72(7)	-9(6)	9(6)	-24(6)
N(2)	89(7)	82(6)	59(6)	7(5)	-5(5)	-24(5)
O(1)	51(4)	47(4)	120(6)	7(4)	15(4)	-12(3)
O(2)	63(4)	43(4)	81(5)	-4(3)	24(4)	-5(3)
O(3)	107(6)	67(5)	68(5)	-43(4)	-36(4)	6(4)
O(4)	77(5)	83(5)	40(4)	-4(3)	-22(3)	12(4)
O(5)	242(15)	66(6)	311(19)	6(8)	229(15)	-7(8)
O(6)	488(30)	156(13)	124(11)	-65(9)	-106(15)	115(16)
O(7)	93(6)	56(5)	131(8)	-1(5)	46(6)	-22(4)
O(8)	164(11)	131(9)	129(10)	-52(8)	-28(9)	16(8)
C(1)	53(6)	51(5)	57(6)	-3(4)	10(5)	-5(5)
C(2)	60(7)	126(10)	72(7)	-24(7)	11(6)	-46(7)
C(3)	72(9)	175(16)	111(11)	-21(11)	18(8)	-53(10)
C(4)	84(10)	116(12)	108(11)	-20(9)	37(8)	-16(8)
C(5)	131(13)	116(12)	98(11)	-27(9)	62(10)	-37(10)
C(6)	96(9)	101(9)	79(8)	-43(7)	39(7)	-30(7)
C(7)	44(5)	36(5)	56(5)	-9(4)	-1(4)	-5(4)
C(8)	106(10)	54(6)	91(8)	-18(6)	-53(8)	-21(6)
C(9)	123(14)	91(10)	138(14)	-31(9)	-50(11)	-23(9)
C(10)	75(8)	52(6)	108(9)	-24(6)	2(7)	-16(6)
C(11)	66(8)	51(6)	113(10)	-14(6)	2(7)	-17(5)
C(12)	67(7)	45(6)	75(7)	-8(5)	-1(5)	-6(5)
C(13)	55(6)	51(5)	48(5)	-10(4)	10(4)	-4(4)
C(14)	69(7)	72(7)	68(7)	-9(6)	-7(6)	6(6)
C(15)	82(8)	102(10)	72(8)	-10(7)	-23(7)	3(7)
C(16)	93(9)	84(8)	52(6)	-6(6)	-5(6)	-13(7)
C(17)	86(9)	99(9)	46(6)	1(6)	-3(6)	-22(7)
C(18)	43(5)	51(5)	59(6)	3(4)	2(4)	-3(4)
C(19)	54(7)	69(7)	91(8)	9(6)	-15(6)	-20(5)
C(20)	54(7)	76(8)	141(12)	14(8)	10(7)	-16(6)
C(21)	57(8)	82(9)	144(13)	10(9)	16(8)	-5(7)

Table 3.18 / cont.

C(22)	83(9)	93(9)	93(9)	11(7)	28(7)	14(7)
C(23)	54(6)	73(7)	68(7)	-8(5)	17(5)	2(5)
C(24)	47(6)	55(6)	52(5)	-19(4)	13(4)	-11(4)
C(25)	68(7)	52(6)	97(8)	-29(6)	4(6)	-11(5)
C(26)	89(10)	73(8)	147(13)	-53(9)	23(9)	-27(7)
C(27)	86(9)	101(10)	108(10)	-58(9)	11(8)	-39(8)
C(28)	122(13)	134(14)	108(11)	-53(10)	-44(10)	-39(11)
C(29)	84(9)	94(9)	67(7)	-26(6)	-28(6)	6(7)
C(30)	73(7)	47(5)	44(5)	-6(4)	-7(5)	-18(5)
C(31)	65(7)	59(6)	66(7)	-2(5)	-23(6)	-1(5)
C(32)	124(11)	76(8)	72(8)	6(7)	-48(8)	-24(8)
C(33)	171(16)	75(8)	55(7)	5(6)	-27(9)	-43(9)
C(34)	152(15)	92(9)	57(8)	8(7)	-19(9)	-46(10)
C(35)	54(6)	50(6)	52(5)	-7(4)	-4(4)	-14(5)
C(36)	76(8)	64(7)	85(8)	-10(6)	29(6)	-24(6)
C(37)	76(8)	97(9)	57(6)	-11(6)	-3(6)	-32(7)
C(38)	115(11)	119(11)	78(8)	-11(8)	-21(7)	-18(9)
C(39)	136(12)	40(6)	146(13)	-6(7)	85(11)	-7(7)
C(40)	221(18)	62(8)	65(8)	15(6)	-69(9)	5(9)
C(41)	77(8)	42(5)	71(7)	-7(5)	14(6)	-7(5)
C(42)	72(7)	61(6)	40(5)	-19(4)	-12(5)	-14(5)

3.5.12 Single crystal X-ray diffraction study of $[Ru_2\{\mu\text{-}\eta^2\text{-}OC(H)O\}(CO)_4(\mu\text{-}Ph_2Ppy)_2](PF_6)$ [10]

Yellow block-like crystals of **[10]** were grown by slow evaporation of a saturated acetone-ethanol (1:1, vol:vol) solution of the compound. The general approach used for the intensity data collection is described in Appendix A. The crystallographic data are given in Table 3.19, the interatomic distances in Table 3.20, the interatomic angles in Table 3.21, the fractional coordinates in Table 3.22 and the anisotropic thermal parameters in Table 3.23. The observed and calculated structure factors may be found on microfiche in an envelope fixed to the inside back cover.

Table 3.19

Crystal data and details of the crystallographic analysis for $[Ru_2\{\mu\text{-}\eta^2\text{-}OC(H)O\}(CO)_4(\mu\text{-}Ph_2Ppy)_2](PF_6)$

Formula	$Ru_2C_{39}H_{29}N_2O_6P_3F_6$
Molecular Mass	1030.72
Crystal System	Monoclinic
Space Group	$P2_1/n$
a(Å)	12.979(4)
b(Å)	13.146(3)
c(Å)	19.922(5)
β(°)	108.933(2)
V(Å^3)	3968.00
Z	4
D_c(g.cm^{-3})	1.725
F(000)	2048
λ(Mo-Kα)(Å)	0.71069
Scan mode	ω - 2θ
ω scan angle	0.40 + 0.35tanθ
Horizontal Aperture width (mm)	2.7 + 0.1tanθ
Scattering range (°)	$2 \leq \theta \leq 23$
μ (cm^{-1})	9.11
Absorption corrections	Semi empirical[103]
Measured intensities	5927
Unique intensities	4887
Unique intensities with $[I > 3\sigma(I)]$	4067
Structure solution	Direct & Fourier methods
Weighting scheme	$1/(\sigma^2(F) + 0.00075F^2)$
$R = \Sigma(F_o\text{-}F_c)/\Sigma F_o$	0.0476
$R_w = \Sigma_w½\,(F_o\text{-}F_c)/\ \Sigma_w½F_o$	0.0532
$(\Delta/\sigma)_{max}$	0.028
$\Delta\rho_{max}$(eÅ^{-3})	0.844
Number of parameters	353

Table 3.20: Interatomic distances (Å) for $[Ru_2\{\mu\text{-}\eta^2\text{-}OC(H)O\}(CO)_4(\mu\text{-}Ph_2Ppy)_2](PF_6)$

Ru(1)-Ru(2)	2.731(1)	Ru(1)-P(1)	2.285(2)
Ru(1)-N(2)	2.179(6)	Ru(1)-O(3)	2.125(5)
Ru(1)-C(35)	1.949(9)	Ru(1)-C(36)	1.831(9)
Ru(2)-P(2)	2.295(2)	Ru(2)-N(1)	2.177(6)
Ru(2)-O(6)	2.147(5)	Ru(2)-C(37)	1.954(9)
Ru(2)-C(38)	1.844(9)	P(1)-C(1)	1.843(8)
P(1)-C(7)	1.819(8)	P(1)-C(13)	1.842(8)
P(2)-C(18)	1.831(8)	P(2)-C(24)	1.811(8)
P(2)-C(30)	1.831(8)	N(1)-C(13)	1.339(9)
N(1)-C(17)	1.337(10)	N(2)-C(30)	1.363(9)
N(2)-C(34)	1.349(10)	O(1)-C(35)	1.127(10)
O(2)-C(36)	1.154(9)	O(3)-C(39)	1.243(9)
O(4)-C(37)	1.123(10)	O(5)-C(38)	1.145(9)
O(6)-C(39)	1.276(10)	C(1)-C(2)	1.393(11)
C(1)-C(6)	1.401(12)	C(2)-C(3)	1.409(13)
C(3)-C(4)	1.364(14)	C(4)-C(5)	1.420(14)
C(5)-C(6)	1.404(14)	C(7)-C(8)	1.415(11)
C(7)-C(12)	1.365(12)	C(8)-C(9)	1.393(12)
C(9)-C(10)	1.371(15)	C(10)-C(11)	1.385(15)
C(11)-C(12)	1.427(13)	C(13)-C(14)	1.372(11)
C(14)-C(15)	1.418(12)	C(15)-C(16)	1.377(12)
C(16)-C(17)	1.393(12)	C(18)-C(19)	1.407(11)
C(18)-C(23)	1.397(11)	C(19)-C(20)	1.382(12)
C(20)-C(21)	1.385(13)	C(21)-C(22)	1.372(13)
C(22)-C(23)	1.431(12)	C(24)-C(25)	1.402(11)
C(24)-C(29)	1.404(11)	C(25)-C(26)	1.403(12)
C(26)-C(27)	1.366(13)	C(27)-C(28)	1.392(13)
C(28)-C(29)	1.415(12)	C(30)-C(31)	1.362(11)
C(31)-C(32)	1.405(11)	C(32)-C(33)	1.368(11)
C(33)-C(34)	1.378(11)	P(3)-F(1)	1.537(7)
P(3)-F(2)	1.540(7)	P(3)-F(3)	1.563(7)
P(3)-F(4)	1.548(8)	P(3)-F(5)	1.600(7)
P(3)-F(6)	1.550(7)		

Table 3.21: Interatomic angles (°) for $[Ru_2\{\mu\text{-}\eta^2\text{-}OC(H)O\}(CO)_4(\mu\text{-}Ph_2Ppy)_2](PF_6)$

Ru(2)-Ru(1)-P(1)	84.8(1)	Ru(2)-Ru(1)-N(2)	89.0(1)
P(1)-Ru(1)-N(2)	168.2(2)	Ru(2)-Ru(1)-O(3)	82.4(1)
P(1)-Ru(1)-O(3)	88.7(1)	N(2)-Ru(1)-O(3)	80.6(2)
Ru(2)-Ru(1)-C(35)	176.4(3)	P(1)-Ru(1)-C(35)	92.7(3)
N(2)-Ru(1)-C(35)	93.1(3)	O(3)-Ru(1)-C(35)	95.1(3)
Ru(2)-Ru(1)-C(36)	91.4(2)	P(1)-Ru(1)-C(36)	91.7(2)
N(2)-Ru(1)-C(36)	98.5(3)	O(3)-Ru(1)-C(36)	173.7(3)
C(35)-Ru(1)-C(36)	91.2(4)	Ru(1)-Ru(2)-P(2)	83.5(1)
Ru(1)-Ru(2)-N(1)	89.4(2)	P(2)-Ru(2)-N(1)	170.1(2)
Ru(1)-Ru(2)-O(6)	81.5(1)	P(2)-Ru(2)-O(6)	90.6(2)
N(1)-Ru(2)-O(6)	81.4(2)	Ru(1)-Ru(2)-C(37)	173.6(3)
P(2)-Ru(2)-C(37)	91.6(3)	N(1)-Ru(2)-C(37)	94.9(3)
O(6)-Ru(2)-C(37)	94.4(3)	Ru(1)-Ru(2)-C(38)	93.7(2)
P(2)-Ru(2)-C(38)	93.1(2)	N(1)-Ru(2)-C(38)	94.3(3)
O(6)-Ru(2)-C(38)	173.6(3)	C(37)-Ru(2)-C(38)	90.7(4)
Ru(1)-P(1)-C(1)	115.0(3)	Ru(1)-P(1)-C(7)	120.1(3)
C(1)-P(1)-C(7)	103.6(4)	Ru(1)-P(1)-C(13)	110.5(2)
C(1)-P(1)-C(13)	101.2(3)	C(7)-P(1)-C(13)	104.4(4)
Ru(2)-P(2)-C(18)	114.0(3)	Ru(2)-P(2)-C(24)	120.5(3)
C(18)-P(2)-C(24)	105.2(3)	Ru(2)-P(2)-C(30)	110.9(2)
C(18)-P(2)-C(30)	100.7(4)	C(24)-P(2)-C(30)	103.3(3)
Ru(2)-N(1)-C(13)	124.2(5)	Ru(2)-N(1)-C(17)	117.5(5)
C(13)-N(1)-C(17)	118.2(7)	Ru(1)-N(2)-C(30)	124.0(5)
Ru(1)-N(2)-C(34)	118.5(5)	C(30)-N(2)-C(34)	117.4(6)
Ru(1)-O(3)-C(39)	120.7(5)	Ru(2)-O(6)-C(39)	120.1(5)
P(1)-C(1)-C(2)	121.7(6)	P(1)-C(1)-C(6)	117.2(6)
C(2)-C(1)-C(6)	121.1(8)	C(1)-C(2)-C(3)	118.9(8)
C(2)-C(3)-C(4)	121.0(10)	C(3)-C(4)-C(5)	120.4(10
C(4)-C(5)-C(6)	119.2(10)	C(1)-C(6)-C(5)	119.3(9)
P(1)-C(7)-C(8)	116.5(6)	P(1)-C(7)-C(12)	123.2(6)
C(8)-C(7)-C(12)	120.4(8)	C(7)-C(8)-C(9)	118.2(8)
C(8)-C(9)-C(10)	121.1(10)	C(9)-C(10)-C(11)	121.6(11
C(10)-C(11)-C(12)	117.5(10)	C(7)-C(12)-C(11)	121.1(9)
P(1)-C(13)-N(1)	116.8(5)	P(1)-C(13)-C(14)	120.6(6)
N(1)-C(13)-C(14)	122.5(7)	C(13)-C(14)-C(15)	119.7(8)

Table 3.21 / cont.

C(14)-C(15)-C(16)	117.1(9)	C(15)-C(16)-C(17)	119.4(9)
N(1)-C(17)-C(16)	122.9(8)	P(2)-C(18)-C(19)	117.2(6)
P(2)-C(18)-C(23)	122.0(6)	C(19)-C(18)-C(23)	120.7(8)
C(18)-C(19)-C(20)	121.7(8)	C(19)-C(20)-C(21)	117.6(9)
C(20)-C(21)-C(22)	122.6(10)	C(21)-C(22)-C(23)	120.6(9)
C(18)-C(23)-C(22)	116.9(8)	P(2)-C(24)-C(25)	118.2(6)
P(2)-C(24)-C(29)	121.3(6)	C(25)-C(24)-C(29)	120.5(7)
C(24)-C(25)-C(26)	120.0(8)	C(25)-C(26)-C(27)	118.6(9)
C(26)-C(27)-C(28)	123.4(9)	C(27)-C(28)-C(29)	118.3(9)
C(24)-C(29)-C(28)	119.1(8)	P(2)-C(30)-N(2)	115.1(5)
P(2)-C(30)-C(31)	121.7(6)	N(2)-C(30)-C(31)	123.2(7)
C(30)-C(31)-C(32)	118.6(7)	C(31)-C(32)-C(33)	118.3(8)
C(32)-C(33)-C(34)	120.2(8)	N(2)-C(34)-C(33)	122.0(7)
Ru(1)-C(35)-O(1)	171.2(9)	Ru(1)-C(36)-O(2)	178.4(7)
Ru(2)-C(37)-O(4)	167.5(9)	Ru(2)-C(38)-O(5)	177.2(7)
O(3)-C(39)-O(6)	126.8(7)	F(1)-P(3)-F(2)	90.5(5)
F(1)-P(3)-F(3)	179.1(5)	F(2)-P(3)-F(3)	89.3(5)
F(1)-P(3)-F(4)	90.7(5)	F(2)-P(3)-F(4)	177.9(5)
F(3)-P(3)-F(4)	89.5(5)	F(1)-P(3)-F(5)	88.9(5)
F(2)-P(3)-F(5)	89.1(4)	F(3)-P(3)-F(5)	90.2(5)
F(4)-P(3)-F(5)	89.2(4)	F(1)-P(3)-F(6)	91.1(4)
F(2)-P(3)-F(6)	89.8(5)	F(3)-P(3)-F(6)	89.7(5)
F(4)-P(3)-F(6)	92.0(5)	F(5)-P(3)-F(6)	178.9(5)

Table 3.22: Fractional coordinates (x 10^4) and isotropic thermal factors ($Å^2$, x 10^3) for $[Ru_2\{\mu\text{-}\eta^2\text{-}OC(H)O\}(CO)_4(\mu\text{-}Ph_2Ppy)_2](PF_6)$

	x/a	y/b	z/c	U_{eq}
Ru(1)	219(1)	1593(1)	3011(1)	37(1)
Ru(2)	-550(1)	1141(1)	1616(1)	38(1)
P(1)	1395(2)	2407(1)	2666(1)	41(1)
P(2)	-2069(2)	766(1)	1892(1)	39(1)
N(1)	1048(5)	1392(4)	1526(3)	43(2)
N(2)	-753(5)	613(3)	3253(3)	39(1)
O(1)	1181(6)	2187(5)	4550(4)	89(2)
O(2)	-1399(5)	2963(4)	2751(3)	67(2)
O(3)	1285(4)	581(3)	3072(3)	48(1)
O(4)	-1672(7)	556(5)	93(4)	104(3)
O(5)	-1438(5)	2806(4)	1095(4)	70(2)
O(6)	239(4)	6(3)	2049(3)	50(1)
C(1)	2739(6)	2557(5)	3344(4)	48(2)*
C(2)	3281(7)	3310(5)	3428(5)	58(2)*
C(3)	4329(8)	3373(6)	3932(6)	74(3)*
C(4)	4808(9)	2712(7)	4338(6)	81(3)*
C(5)	4247(9)	1949(7)	4269(6)	81(3)*
C(6)	3195(8)	1881(6)	3776(5)	70(3)*
C(7)	993(6)	3442(5)	2335(4)	46(2)*
C(8)	705(7)	3988(5)	2799(5)	57(2)*
C(9)	377(8)	4783(6)	2561(5)	73(3)*
C(10)	322(9)	5031(7)	1893(6)	89(3)*
C(11)	633(9)	4517(7)	1438(6)	85(3)*
C(12)	966(8)	3701(6)	1678(5)	64(2)*
C(13)	1782(6)	1902(5)	1955(4)	42(2)*
C(14)	2797(7)	2021(5)	1899(5)	58(2)*
C(15)	3084(8)	1616(6)	1354(5)	66(3)*
C(16)	2337(7)	1072(6)	932(5)	63(2)*
C(17)	1326(7)	983(5)	1028(5)	56(2)*
C(18)	-2834(6)	-88(5)	1357(4)	50(2)*
C(19)	-2237(7)	-783(5)	1277(5)	58(2)*
C(20)	-2737(8)	-1457(6)	879(5)	72(3)*
C(21)	-3859(9)	-1434(6)	573(6)	75(3)*
C(22)	-4473(8)	-773(6)	646(5)	71(3)*
C(23)	-3967(7)	-68(5)	1053(5)	59(2)*

Table 3.22 / cont.

C(24)	-3086(6)	1526(5)	1902(4)	41(2)*
C(25)	-3591(7)	1970(5)	1277(4)	53(2)*
C(26)	-4351(8)	2587(6)	1269(5)	65(2)*
C(27)	-4574(8)	2749(6)	1881(5)	67(3)*
C(28)	-4099(7)	2321(6)	2512(5)	62(2)*
C(29)	-3347(7)	1687(5)	2520(4)	53(2)*
C(30)	-1691(6)	314(5)	2781(4)	41(2)*
C(31)	-2292(6)	-296(5)	2942(4)	50(2)*
C(32)	-1932(7)	-634(5)	3629(5)	58(2)*
C(33)	-954(7)	-375(5)	4088(4)	53(2)*
C(34)	-386(6)	249(5)	3895(4)	52(2)*
C(35)	859(7)	1908(6)	4004(5)	57(2)
C(36)	-780(6)	2428(5)	2858(4)	45(2)
C(37)	-1168(8)	708(6)	653(5)	62(2)
C(38)	-1092(7)	2175(6)	1312(4)	48(2)
C(39)	1017(7)	6(5)	2638(5)	53(2)
P(3)	7604(2)	1175(2)	5092(1)	67(1)
F(1)	6500(6)	1026(6)	5202(4)	143(3)
F(2)	7459(8)	2113(4)	5142(4)	143(3)
F(3)	8735(6)	1330(6)	4993(5)	147(3)
F(4)	7790(7)	235(5)	5066(5)	136(3)
F(5)	8173(6)	1149(4)	5935(4)	119(2)
F(6)	7050(6)	1219(6)	4277(4)	135(3)

* isotropic temperature factor.

$$U_{eq} = \frac{1}{3}\Sigma_i\Sigma_j U_{ij}a_i^*a_j^*(a_i.a_j)$$

Table 3.23: Anistropic thermal factors (Å^2 , x 10^3) for

$[Ru_2\{\mu\text{-}\eta^2\text{-}OC(H)O\}(CO)_4(\mu\text{-}Ph_2Ppy)_2](PF_6)$

	U(11)	U(22)	U(33)	U(23)	U(13)	U(12)
Ru(1)	39(1)	36(1)	35(1)	-3(1)	12(1)	-2(1)
Ru(2)	41(1)	38(1)	36(1)	-4(1)	15(1)	-3(1)
P(1)	41(1)	38(1)	48(1)	-6(1)	18(1)	-4(1)
P(2)	39(1)	41(1)	37(1)	-2(1)	11(1)	-4(1)
N(1)	48(4)	44(4)	44(4)	-2(3)	24(3)	-1(3)
N(2)	48(4)	40(3)	29(3)	7(3)	12(3)	2(3)
O(1)	86(5)	117(6)	53(4)	-33(4)	10(4)	-9(4)
O(2)	65(4)	55(4)	83(5)	-12(3)	27(4)	10(3)
O(3)	51(3)	41(3)	52(3)	2(3)	15(3)	8(3)
O(4)	137(7)	124(7)	45(4)	-26(4)	22(4)	-57(6)
O(5)	71(4)	50(4)	91(5)	15(4)	29(4)	9(3)
O(6)	58(3)	36(3)	59(4)	-6(3)	21(3)	4(3)
C(35)	55(5)	69(6)	43(5)	-9(5)	12(4)	-9(5)
C(36)	45(5)	48(5)	45(5)	-12(4)	20(4)	-8(4)
C(37)	76(6)	68(6)	51(6)	-16(5)	33(5)	-27(5)
C(38)	48(5)	57(6)	44(5)	-3(4)	21(4)	-9(4)
C(39)	51(5)	48(5)	63(6)	-4(5)	24(5)	1(4)
P(3)	60(2)	75(2)	66(2)	-3(1)	19(1)	9(1)
F(1)	82(5)	227(10)	127(6)	40(6)	44(4)	17(5)
F(2)	225(9)	77(5)	133(7)	12(5)	65(7)	38(5)
F(3)	83(5)	205(9)	167(8)	-31(7)	58(5)	-34(5)
F(4)	167(7)	92(5)	150(7)	-20(5)	54(6)	13(5)
F(5)	129(6)	125(6)	80(5)	8(4)	3(4)	6(5)
F(6)	108(6)	218(9)	65(4)	7(5)	11(4)	-16(6)

3.5.13 Single crystal X-ray diffraction study of $[Ru_2\{\mu-\eta^2-OC(Me)O\}(CO)_2(\mu-Ph_2Pbipy)_2](PF_6)$ [17]

Dark brown prismatic crystals of [17] were grown by slow evaporation of a saturated acetone-ethanol (1:1, vol:vol) solution of the compound. The general approach used for the intensity data collection is described in Appendix A. The crystallographic data are given in Table 3.24, the interatomic distances in Table 3.25, the interatomic angles in Table 3.26, the fractional coordinates in Table 3.27 and the anisotropic thermal parameters in Table 3.28. The observed and calculated structure factors may be found on microfiche in an envelope fixed to the inside back cover.

Table 3.24

Crystal data and details of the crystallographic analysis for $[Ru_2\{\mu\text{-}\eta^2\text{-}OC(Me)O\}(CO)_2(\mu\text{-}Ph_2Pbipy)_2](PF_6)$

Formula	$Ru_2C_{48}H_{37}N_4O_4P_3F_6$
Molecular Mass	1142.90
Crystal System	Triclinic
Space Group	$P\bar{1}$
a(Å)	9.985(6)
b(Å)	14.743(13)
c(Å)	17.249(12)
α(°)	91.341(7)
β(°)	89.995(6)
γ(°)	90.034(7)
V($Å^3$)	2538.43
Z	2
D_c($g.cm^{-3}$)	1.495
F(000)	1128
λ(Mo-Kα)(Å)	0.71069
Scan mode	ω - 2θ
ω scan angle	1.00 + 0.35tanθ
Horizontal Aperture width (mm)	2.7 + 0.1tanθ
Scattering range (°)	$2 \leq \theta \leq 23$
μ (cm^{-1})	7.47
Absorption corrections	Semi empirical[103]
Measured intensities	6961
Unique intensities	5561
Unique intensities with [I > 3σ(I)]	3681
Structure solution	Direct & Fourier methods
Weighting scheme	$1/(\sigma^2(F) + 0.01683F^2)$
$R = \Sigma(F_o-F_c)/\Sigma F_o$	0.0853
$R_w = \Sigma_w½ (F_o-F_c)/ \Sigma_w½F_o$	0.0926
$(\Delta/\sigma)_{max}$	0.456
$\Delta\rho_{max}(eÅ^{-3})$	1.928
Number of parameters	384

Table 3.25: Interatomic distances (Å) for

$[Ru_2\{\mu\text{-}\eta^2\text{-}OC(Me)O\}(CO)_2(\mu\text{-}Ph_2Pbipy)_2](PF_6)$

Ru(1)-Ru(2)	2.687(2)	Ru(1)-P(1)	2.253(5)
Ru(1)-O(1)	2.176(13)	Ru(1)-N(3)	2.123(15)
Ru(1)-N(4)	2.193(15)	Ru(1)-C(47)	1.79(2)
Ru(2)-P(2)	2.242(5)	Ru(2)-O(2)	2.161(12)
Ru(2)-N(1)	2.152(13)	Ru(2)-N(2)	2.199(14)
Ru(2)-C(48)	1.79(2)	P(1)-C(1)	1.84(2)
P(1)-C(7)	1.82(2)	P(1)-C(13)	1.88(2)
P(2)-C(23)	1.83(2)	P(2)-C(29)	1.82(2)
P(2)-C(35)	1.88(2)	O(1)-C(45)	1.25(2)
O(2)-C(45)	1.25(2)	O(3)-C(47)	1.14(2)
O(4)-C(48)	1.17(2)	N(1)-C(13)	1.30(2)
N(1)-C(17)	1.33(2)	N(2)-C(18)	1.37(3)
N(2)-C(22)	1.33(3)	N(3)-C(35)	1.33(2)
N(3)-C(39)	1.34(3)	N(4)-C(40)	1.34(3)
N(4)-C(44)	1.37(3)	C(1)-C(2)	1.31(3)
C(1)-C(6)	1.48(3)	C(2)-C(3)	1.40(3)
C(3)-C(4)	1.46(4)	C(4)-C(5)	1.38(3)
C(5)-C(6)	1.39(3)	C(7)-C(8)	1.42(3)
C(7)-C(12)	1.37(3)	C(8)-C(9)	1.40(4)
C(9)-C(10)	1.37(4)	C(10)-C(11)	1.37(4)
C(11)-C(12)	1.47(4)	C(13)-C(14)	1.36(3)
C(14)-C(15)	1.46(3)	C(15)-C(16)	1.36(3)
C(16)-C(17)	1.45(3)	C(17)-C(18)	1.44(3)
C(18)-C(19)	1.38(3)	C(19)-C(20)	1.38(4)
C(20)-C(21)	1.48(11)	C(21)-C(22)	1.35(10)
C(23)-C(24)	1.34(3)	C(23)-C(28)	1.49(3)
C(24)-C(25)	1.40(3)	C(25)-C(26)	1.45(3)
C(26)-C(27)	1.40(4)	C(27)-C(28)	1.37(3)
C(29)-C(30)	1.38(3)	C(29)-C(34)	1.43(3)
C(30)-C(31)	1.43(3)	C(31)-C(32)	1.37(4)
C(32)-C(33)	1.33(4)	C(33)-C(34)	1.43(3)
C(35)-C(36)	1.32(3)	C(36)-C(37)	1.43(3)
C(37)-C(38)	1.42(3)	C(38)-C(39)	1.40(3)
C(39)-C(40)	1.47(3)	C(40)-C(41)	1.40(3)
C(41)-C(42)	1.38(4)	C(42)-C(43)	1.36(3)

Table 3.25 / cont.

C(43)-C(44)	1.40(3)	C(45)-C(46)	1.46(3)
P(3)-F(1)	1.51(3)	P(3)-F(2)	1.45(3)
P(3)-F(3)	1.46(3)	P(3)-F(4)	1.45(3)
P(3)-F(5)	1.52(3)	P(3)-F(6)	1.44(3)

Table 3.26: Interatomic angles (°) for

$[Ru_2\{\mu\text{-}\eta^2\text{-}OC(Me)O\}(CO)_2(\mu\text{-}Ph_2Pbipy)_2](PF_6)$

Ru(2)-Ru(1)-P(1)	83.2(1)	Ru(2)-Ru(1)-O(1)	83.3(3)
P(1)-Ru(1)-O(1)	89.5(4)	Ru(2)-Ru(1)-N(3)	92.9(4)
P(1)-Ru(1)-N(3)	171.3(4)	O(1)-Ru(1)-N(3)	82.4(5)
Ru(2)-Ru(1)-N(4)	163.8(4)	P(1)-Ru(1)-N(4)	106.1(4)
O(1)-Ru(1)-N(4)	83.5(5)	N(3)-Ru(1)-N(4)	76.0(5)
Ru(2)-Ru(1)-C(47)	95.6(7)	P(1)-Ru(1)-C(47)	91.0(7)
O(1)-Ru(1)-C(47)	178.7(7)	N(3)-Ru(1)-C(47)	97.1(8)
N(4)-Ru(1)-C(47)	97.5(8)	Ru(1)-Ru(2)-P(2)	82.9(1)
Ru(1)-Ru(2)-O(2)	83.0(3)	P(2)-Ru(2)-O(2)	89.4(4)
Ru(1)-Ru(2)-N(1)	93.2(4)	P(2)-Ru(2)-N(1)	171.7(4)
O(2)-Ru(2)-N(1)	82.8(5)	Ru(1)-Ru(2)-N(2)	163.7(4)
P(2)-Ru(2)-N(2)	106.4(4)	O(2)-Ru(2)-N(2)	83.7(6)
N(1)-Ru(2)-N(2)	75.7(6)	Ru(1)-Ru(2)-C(48)	96.3(6)
P(2)-Ru(2)-C(48)	94.0(7)	O(2)-Ru(2)-C(48)	176.5(7)
N(1)-Ru(2)-C(48)	93.7(8)	N(2)-Ru(2)-C(48)	96.4(8)
Ru(1)-P(1)-C(1)	116.7(6)	Ru(1)-P(1)-C(7)	120.2(7)
C(1)-P(1)-C(7)	104.0(9)	Ru(1)-P(1)-C(13)	111.6(6)
C(1)-P(1)-C(13)	100.9(8)	C(7)-P(1)-C(13)	100.6(9)
Ru(2)-P(2)-C(23)	117.1(6)	Ru(2)-P(2)-C(29)	119.5(7)
C(23)-P(2)-C(29)	103.4(9)	Ru(2)-P(2)-C(35)	113.4(6)
C(23)-P(2)-C(35)	99.7(8)	C(29)-P(2)-C(35)	100.7(9)
Ru(1)-O(1)-C(45)	120.2(12)	Ru(2)-O(2)-C(45)	121.6(11
Ru(2)-N(1)-C(13)	123.5(11)	Ru(2)-N(1)-C(17)	113.7(11
C(13)-N(1)-C(17)	121(2)	Ru(2)-N(2)-C(18)	114.5(12
Ru(2)-N(2)-C(22)	125.3(14)	C(18)-N(2)-C(22)	120(2)
Ru(1)-N(3)-C(35)	126.0(12)	Ru(1)-N(3)-C(39)	116.2(12
C(35)-N(3)-C(39)	117(2)	Ru(1)-N(4)-C(40)	114.3(12
Ru(1)-N(4)-C(44)	126.7(14)	C(40)-N(4)-C(44)	119(2)
P(1)-C(1)-C(2)	126(2)	P(1)-C(1)-C(6)	114.5(14
C(2)-C(1)-C(6)	120(2)	C(1)-C(2)-C(3)	124(2)
C(2)-C(3)-C(4)	117(2)	C(3)-C(4)-C(5)	120(2)
C(4)-C(5)-C(6)	121(3)	C(1)-C(6)-C(5)	118(2)
P(1)-C(7)-C(8)	116(2)	P(1)-C(7)-C(12)	122(2)
C(8)-C(7)-C(12)	123(2)	C(7)-C(8)-C(9)	121(2)
C(8)-C(9)-C(10)	117(3)	C(9)-C(10)-C(11)	124(3)

Table 3.26 / cont.

C(10)-C(11)-C(12)	120(3)	C(7)-C(12)-C(11)	116(2)
P(1)-C(13)-N(1)	113.9(13)	P(1)-C(13)-C(14)	121.3(14)
N(1)-C(13)-C(14)	125(2)	C(13)-C(14)-C(15)	117(2)
C(14)-C(15)-C(16)	119(2)	C(15)-C(16)-C(17)	118(2)
N(1)-C(17)-C(16)	121(2)	N(1)-C(17)-C(18)	120(2)
C(16)-C(17)-C(18)	119(2)	N(2)-C(18)-C(17)	114(2)
N(2)-C(18)-C(19)	120(2)	C(17)-C(18)-C(19)	126(2)
C(18)-C(19)-C(20)	119(2)	C(19)-C(20)-C(21)	122(5)
C(20)-C(21)-C(22)	112(7)	N(2)-C(22)-C(21)	128(5)
P(2)-C(23)-C(24)	126(2)	P(2)-C(23)-C(28)	114.7(14)
C(24)-C(23)-C(28)	120(2)	C(23)-C(24)-C(25)	121(2)
C(24)-C(25)-C(26)	120(2)	C(25)-C(26)-C(27)	119(2)
C(26)-C(27)-C(28)	121(2)	C(23)-C(28)-C(27)	120(2)
P(2)-C(29)-C(30)	124(2)	P(2)-C(29)-C(34)	118(2)
C(30)-C(29)-C(34)	118(2)	C(29)-C(30)-C(31)	122(2)
C(30)-C(31)-C(32)	117(3)	C(31)-C(32)-C(33)	125(3)
C(32)-C(33)-C(34)	118(3)	C(29)-C(34)-C(33)	120(2)
P(2)-C(35)-N(3)	110.9(13)	P(2)-C(35)-C(36)	123(2)
N(3)-C(35)-C(36)	126(2)	C(35)-C(36)-C(37)	118(2)
C(36)-C(37)-C(38)	119(2)	C(37)-C(38)-C(39)	116(2)
N(3)-C(39)-C(38)	124(2)	N(3)-C(39)-C(40)	116(2)
C(38)-C(39)-C(40)	120(2)	N(4)-C(40)-C(39)	116(2)
N(4)-C(40)-C(41)	121(2)	C(39)-C(40)-C(41)	122(2)
C(40)-C(41)-C(42)	119(3)	C(41)-C(42)-C(43)	122(3)
C(42)-C(43)-C(44)	117(2)	N(4)-C(44)-C(43)	122(2)
O(1)-C(45)-O(2)	127(2)	O(1)-C(45)-C(46)	116(2)
O(2)-C(45)-C(46)	117(2)	Ru(1)-C(47)-O(3)	177(2)
Ru(2)-C(48)-O(4)	177(2)	F(1)-P(3)-F(2)	86(2)
F(1)-P(3)-F(3)	172(2)	F(2)-P(3)-F(3)	100(3)
F(1)-P(3)-F(4)	87(2)	F(2)-P(3)-F(4)	172(3)
F(3)-P(3)-F(4)	86(2)	F(1)-P(3)-F(5)	83(3)
F(2)-P(3)-F(5)	91(2)	F(3)-P(3)-F(5)	94(3)
F(4)-P(3)-F(5)	84(2)	F(1)-P(3)-F(6)	91(3)
F(2)-P(3)-F(6)	87(3)	F(3)-P(3)-F(6)	93(2)
F(4)-P(3)-F(6)	98(3)	F(5)-P(3)-F(6)	173(3)

Table 3.27: Fractional coordinates (x 10^4) and isotropic thermal factors ($Å^2$, x 10^3) for $[Ru_2\{\mu\text{-}\eta^2\text{-}OC(Me)O\}(CO)_2(\mu\text{-}Ph_2Pbipy)_2](PF_6)$

	x/a	y/b	z/c	U_{eq}
Ru(1)	565(2)	6764(1)	7945(1)	29(1)
Ru(2)	565(2)	8237(1)	7056(1)	30(1)
P(1)	257(5)	6025(3)	6800(3)	34(1)
P(2)	274(5)	8968(3)	8199(3)	37(1)
O(1)	2711(13)	6788(8)	7724(8)	41(3)
O(2)	2696(12)	8202(8)	7272(8)	38(3)
O(3)	-2320(15)	6787(10)	8274(10)	60(4)
O(4)	-2338(16)	8161(12)	6716(10)	65(5)
N(1)	1117(13)	7473(10)	6027(8)	26(3)
N(2)	1108(17)	9276(10)	6218(10)	40(4)
N(3)	1139(15)	7521(10)	8953(9)	35(4)
N(4)	1106(16)	5725(9)	8778(9)	36(4)
C(1)	932(19)	4868(12)	6714(11)	35(4)*
C(2)	250(22)	4142(14)	6508(13)	51(5)*
C(3)	772(26)	3261(18)	6518(16)	70(7)*
C(4)	2187(26)	3164(17)	6703(16)	64(7)*
C(5)	2939(27)	3927(18)	6890(16)	75(7)*
C(6)	2364(23)	4789(15)	6918(14)	57(6)*
C(7)	-1411(21)	5930(14)	6383(12)	46(5)*
C(8)	-2371(25)	5459(17)	6832(15)	63(6)*
C(9)	-3681(29)	5337(19)	6563(17)	78(8)*
C(10)	-3999(30)	5704(20)	5864(18)	87(8)*
C(11)	-3110(28)	6173(19)	5423(17)	73(8)*
C(12)	-1714(25)	6287(16)	5678(15)	62(6)*
C(13)	1176(18)	6593(12)	5993(10)	34(4)*
C(14)	1825(20)	6100(14)	5430(12)	44(5)*
C(15)	2500(22)	6612(15)	4831(14)	55(6)*
C(16)	2435(22)	7537(14)	4854(13)	51(5)*
C(17)	1708(19)	7967(12)	5493(11)	38(5)*
C(18)	1628(22)	8940(14)	5534(13)	49(5)*
C(19)	1924(24)	9523(16)	4945(15)	61(6)*
C(20)	1646(32)	10438(21)	5052(19)	88(9)*
C(21)	1075(97)	10814(68)	5783(65)	135(48)*
C(22)	878(22)	10160(15)	6307(13)	50(6)*

Table 3.27 / cont.

C(23)	944(19)	10121(12)	8292(11)	38(5)*
C(24)	236(25)	10863(16)	8491(15)	64(7)*
C(25)	823(28)	11725(19)	8497(17)	77(8)*
C(26)	2235(27)	11824(18)	8309(16)	69(7)*
C(27)	2976(27)	11050(18)	8092(16)	71(7)*
C(28)	2383(22)	10211(14)	8070(13)	52(6)*
C(29)	-1398(20)	9073(13)	8604(12)	41(5)*
C(30)	-1782(26)	8724(17)	9307(16)	68(7)*
C(31)	-3121(27)	8810(18)	9589(16)	70(7)*
C(32)	-3996(30)	9303(20)	9150(18)	84(9)*
C(33)	-3718(26)	9640(18)	8460(16)	68(7)*
C(34)	-2384(23)	9551(16)	8167(14)	56(6)*
C(35)	1183(18)	8424(12)	9024(10)	34(4)*
C(36)	1784(22)	8898(14)	9581(13)	50(5)*
C(37)	2440(25)	8410(17)	10177(15)	67(7)*
C(38)	2400(25)	7448(16)	10149(14)	60(6)*
C(39)	1710(21)	7050(14)	9521(12)	43(5)*
C(40)	1631(22)	6054(14)	9442(13)	49(5)*
C(41)	1925(27)	5483(19)	10055(17)	75(8)*
C(42)	1700(26)	4563(18)	9957(16)	69(7)*
C(43)	1167(24)	4208(16)	9289(14)	60(6)*
C(44)	906(25)	4809(16)	8694(15)	63(6)*
C(45)	3263(19)	7502(15)	7507(12)	40(5)
C(46)	4719(23)	7489(16)	7483(16)	65(7)
C(47)	-1204(19)	6770(14)	8124(12)	38(5)
C(48)	-1186(21)	8211(12)	6834(14)	43(5)
P(3)	6780(8)	2499(6)	7499(4)	71(2)
F(1)	5659(43)	2946(34)	7957(20)	286(19)
F(2)	6715(54)	1781(23)	8055(19)	264(19)
F(3)	7789(28)	2131(38)	6967(17)	294(22)
F(4)	6640(49)	3222(21)	6949(19)	238(17)
F(5)	5619(45)	2079(35)	7049(22)	300(21)
F(6)	7760(41)	2924(47)	8002(18)	356(29)

* isotropic temperature factor.

$$U_{eq} = \frac{1}{3} \Sigma_i \Sigma_j U_{ij} a_i^* a_j^* (a_i . a_j)$$

Table 3.28: Anistropic thermal factors (Å^2 , x 10^3) for

$[Ru_2\{\mu-\eta^2-OC(Me)O\}(CO)_2(\mu-Ph_2Pbipy)_2](PF_6)$

	U(11)	U(22)	U(33)	U(23)	U(13)	U(12)
Ru(1)	27(1)	28(1)	32(1)	-1(1)	-1(1)	1(1)
Ru(2)	25(1)	30(1)	34(1)	-1(1)	-3(1)	4(1)
P(1)	30(3)	32(3)	41(3)	-2(2)	-4(2)	-1(2)
P(2)	33(3)	34(3)	45(3)	-5(2)	-1(2)	5(2)
O(1)	41(8)	25(7)	56(9)	-4(6)	7(7)	0(6)
O(2)	23(7)	25(7)	65(9)	4(6)	-12(7)	5(5)
O(3)	40(10)	61(10)	79(12)	-14(8)	23(9)	6(7)
O(4)	43(11)	94(13)	58(11)	14(9)	1(8)	6(9)
N(1)	8(7)	45(9)	24(8)	-6(7)	0(6)	2(6)
N(2)	45(11)	26(8)	50(11)	15(7)	-4(8)	-1(7)
N(3)	31(10)	37(9)	36(9)	-6(7)	-11(7)	4(7)
N(4)	59(11)	11(7)	38(9)	-1(6)	4(8)	-6(7)
C(45)	23(11)	52(13)	45(12)	-8(10)	7(9)	-10(10)
C(46)	49(17)	54(14)	94(19)	23(13)	1(14)	5(12)
C(47)	7(11)	56(12)	52(13)	-6(10)	-11(9)	6(8)
C(48)	20(12)	35(11)	75(16)	2(10)	25(11)	1(8)
P(3)	69(5)	87(5)	56(4)	15(4)	-3(4)	-1(4)
F(1)	277(45)	406(57)	173(31)	-12(36)	79(30)	197(43)
F(2)	489(70)	175(30)	132(27)	71(24)	-42(33)	-71(36)
F(3)	118(21)	636(88)	123(22)	-88(37)	30(17)	92(33)
F(4)	400(59)	163(26)	155(29)	79(23)	22(31)	31(30)
F(5)	316(51)	400(65)	181(35)	-34(42)	-105(34)	-164(47)
F(6)	242(40)	717(114)	103(22)	-126(43)	6(23)	-222(55)

3.5.14 Single crystal X-ray diffraction study of [Ru_2(μ-Ph_2Ppy)$_2$(μ-CO)$_2$(NCMe)$_4$](PF_6)$_2$ [19]

A single orange-red prismatic crystal of the title compound **[19]** was grown in an nmr tube by carefully layering diethyl ether onto an acetonitrile solution of the complex and allowing the solutions to interdiffuse at room temperature. The general approach used for the intensity data collection is described in Appendix A. The crystallographic data are given in Table 3.29, the interatomic distances in Table 3.30, the interatomic angles in Table 3.31, the fractional coordinates in Table 3.32 and the anisotropic thermal parameters in Table 3.33. The observed and calculated structure factors may be found on microfiche in an envelope fixed to the inside back cover.

Table 3.29

Crystal data and details of the crystallographic analysis for $[Ru_2(\mu\text{-}Ph_2Ppy)_2(\mu\text{-}CO)_2(NCMe)_4](PF_6)_2$

Formula	$Ru_2C_{44}H_{40}N_6O_2P_4F_{12}$
Molecular Mass	1238.86
Crystal System	Triclinic
Space Group	$P\bar{1}$
a(Å)	10.405(2)
b(Å)	10.669(2)
c(Å)	11.776(1)
α(°)	69.34(1)
β(°)	80.15(1)
γ(°)	84.25(2)
V($Å^3$)	1204.06
Z	1
D_c($g.cm^{-3}$)	1.708
F(000)	618
λ(Mo-Kα)(Å)	0.71069
Scan mode	ω - 2θ
ω scan angle	$0.47 + 0.35\tan\theta$
Horizontal Aperture width (mm)	$2.7 + 0.1\tan\theta$
Scattering range (°)	$2 \leq \theta \leq 23$
μ (cm^{-1})	8.44
Absorption corrections	Semi empirical[103]
Measured intensities	3528
Unique intensities	3243
Unique intensities with $[I > 3\sigma(I)]$	3077
Structure solution	Direct & Fourier methods
Weighting scheme	$1/(\sigma^2(F) + 0.00620F^2)$
$R = \Sigma(F_o\text{-}F_c)/\Sigma F_o$	0.0357
$R_w = \Sigma_w{}^{1/2}(F_o\text{-}F_c)/\Sigma_w{}^{1/2}F_o$	0.0449
$(\Delta/\sigma)_{max}$	0.134
$\Delta\rho_{max}$($eÅ^{-3}$)	0.758
Number of parameters	316

Table 3.30: Interatomic distances (Å) for

$[Ru_2(\mu\text{-}Ph_2Ppy)_2(\mu\text{-}CO)_2(NCMe)_4](PF_6)_2$

Ru-P(1)	2.272(1)	Ru-N(2)	2.161(3)
Ru-N(3)	2.174(3)	Ru-C(22)	2.009(4)
Ru-N(1′)	2.195(3)		
Ru-Ru′	2.677(0)	P(1)-C(1)	1.830(3)
P(1)-C(7)	1.834(3)	P(1)-C(13)	1.838(3)
O-C(22)	1.181(4)	N(1)-C(13)	1.356(4)
N(1)-C(17)	1.348(5)	N(2)-C(18)	1.126(5)
N(3)-C(20)	1.123(5)	C(1)-C(2)	1.389(5)
C(1)-C(6)	1.385(5)	C(2)-C(3)	1.378(6)
C(3)-C(4)	1.378(7)	C(4)-C(5)	1.374(7)
C(5)-C(6)	1.406(6)	C(7)-C(8)	1.380(5)
C(7)-C(12)	1.375(5)	C(8)-C(9)	1.410(6)
C(9)-C(10)	1.371(6)	C(10)-C(11)	1.392(7)
C(11)-C(12)	1.410(6)	C(13)-C(14)	1.384(6)
C(14)-C(15)	1.373(6)	C(15)-C(16)	1.378(6)
C(16)-C(17)	1.391(6)	C(18)-C(19)	1.458(6)
C(20)-C(21)	1.480(5)	P(2)-F(1)	1.576(4)
P(2)-F(2)	1.599(3)	P(2)-F(3)	1.569(4)
P(2)-F(4)	1.583(4)	P(2)-F(5)	1.576(3)
P(2)-F(6)	1.576(3)		

Table 3.31: Interatomic angles (°) for $[Ru_2(\mu\text{-}Ph_2Ppy)_2(\mu\text{-}CO)_2(NCMe)_4](PF_6)_2$

P(1)-Ru-N(2)	90.3(1)	P(1)-Ru-N(3)	92.8(1)
N(2)-Ru-N(3)	80.7(1)	P(1)-Ru-C(22)	88.9(1)
N(3)-Ru-C(22)	170.9(1)	N(2)-Ru-C(22)	90.3(1)
Ru'-Ru-P(1)	89.1(1)	Ru'-Ru-N(1')	92.6(1)
Ru'-Ru-N(2)	141.5(1)	Ru'-Ru-N(3)	137.7(1)
Ru-Ru'-C(22)	48.3(1)	Ru'-C(22)-O	140.2(1)
Ru'-Ru-C(22)	47.5(1)	P(1)-Ru-N(1)	79.0(1)
Ru-P(1)-C(1)	113.8(1)	Ru-P(1)-C(7)	116.3(1)
C(1)-P(1)-C(7)	108.4(2)	Ru-P(1)-C(13)	114.4(1)
C(1)-P(1)-C(13)	100.8(2)	C(7)-P(1)-C(13)	101.2(2)
C(13)-N(1)-C(17)	117.1(3)	Ru-N(2)-C(18)	163.2(3)
N(1')-Ru-N(2)	89.6(2)	N(1')-Ru-N(3)	84.7(2)
N(1')-Ru-C(22)	90.8(3)		
Ru-N(3)-C(20)	170.8(3)	P(1)-C(1)-C(2)	119.5(3)
P(1)-C(1)-C(6)	120.5(3)	C(2)-C(1)-C(6)	119.7(3)
C(1)-C(2)-C(3)	120.4(4)	C(2)-C(3)-C(4)	120.0(4)
C(3)-C(4)-C(5)	120.6(4)	C(4)-C(5)-C(6)	119.7(4)
C(1)-C(6)-C(5)	119.5(4)	P(1)-C(7)-C(8)	116.1(3)
P(1)-C(7)-C(12)	124.4(3)	C(8)-C(7)-C(12)	119.3(3)
C(7)-C(8)-C(9)	120.9(4)	C(8)-C(9)-C(10)	119.5(4)
C(9)-C(10)-C(11)	120.3(4)	C(10)-C(11)-C(12)	119.4(4)
C(7)-C(12)-C(11)	120.5(4)	P(1)-C(13)-N(1)	117.7(3)
P(1)-C(13)-C(14)	119.3(3)	N(1)-C(13)-C(14)	122.8(3)
C(13)-C(14)-C(15)	119.5(4)	C(14)-C(15)-C(16)	118.4(4)
C(15)-C(16)-C(17)	119.6(4)	N(1)-C(17)-C(16)	122.4(4)
N(2)-C(18)-C(19)	177.9(4)	N(3)-C(20)-C(21)	178.3(4)
Ru-C(22)-O	135.5(3)	F(1)-P(2)-F(2)	88.3(2)
F(1)-P(2)-F(3)	90.6(3)	F(2)-P(2)-F(3)	90.7(2)
F(1)-P(2)-F(4)	89.9(2)	F(2)-P(2)-F(4)	176.6(2)
F(3)-P(2)-F(4)	92.2(3)	F(1)-P(2)-F(5)	90.8(3)
F(2)-P(2)-F(5)	88.9(2)	F(3)-P(2)-F(5)	178.6(3)
F(4)-P(2)-F(5)	88.3(2)	F(1)-P(2)-F(6)	179.8(1)
F(2)-P(2)-F(6)	91.6(2)	F(3)-P(2)-F(6)	89.6(3)
F(4)-P(2)-F(6)	90.1(2)	F(5)-P(2)-F(6)	89.1(2)

Table 3.32: Fractional coordinates (x 10^4) and isotropic thermal factors ($Å^2$, x 10^3) for $[Ru_2(\mu\text{-}Ph_2Ppy)_2(\mu\text{-}CO)_2(NCMe)_4](PF_6)_2$

	x/a	y/b	z/c	U_{eq}
Ru	993(1)	4116(1)	4934(1)	25(1)
P(1)	698(1)	3238(1)	7017(1)	29(1)
O	-1651(3)	3246(3)	5006(3)	47(1)
N(1)	-1282(3)	5127(3)	7079(3)	32(1)
N(2)	3085(3)	3858(4)	4896(3)	36(1)
N(3)	1287(4)	2149(4)	4746(3)	39(1)
C(1)	-17(4)	1589(4)	7637(4)	35(1)
C(2)	-1345(5)	1492(5)	8068(4)	49(1)
C(3)	-1922(6)	276(6)	8443(6)	67(1)
C(4)	-1174(6)	-858(5)	8417(5)	69(2)
C(5)	140(6)	-785(5)	7990(5)	58(1)
C(6)	730(5)	457(4)	7582(4)	43(1)
C(7)	2130(4)	3156(4)	7761(3)	33(1)
C(8)	2700(5)	4358(5)	7506(4)	48(1)
C(9)	3857(5)	4400(6)	7962(5)	55(1)
C(10)	4432(5)	3230(6)	8652(5)	56(1)
C(11)	3873(5)	2010(5)	8911(5)	58(1)
C(12)	2711(4)	1987(5)	8456(4)	47(1)
C(13)	-491(4)	4191(4)	7777(4)	34(1)
C(14)	-619(5)	3854(5)	9037(4)	49(1)
C(15)	-1610(5)	4448(5)	9628(4)	57(1)
C(16)	-2438(5)	5386(6)	8936(5)	52(1)
C(17)	-2248(5)	5709(4)	7669(4)	41(1)
C(18)	4092(4)	3441(5)	5095(4)	42(1)
C(19)	5380(4)	2895(6)	5400(5)	62(1)
C(20)	1596(4)	1130(5)	4691(4)	41(1)
C(21)	1999(7)	-229(5)	4659(6)	69(2)
C(22)	-939(4)	4054(4)	4981(4)	30(1)
P(2)	4399(1)	-1573(2)	7748(1)	56(1)
F(1)	3461(5)	-1280(5)	8836(4)	113(1)
F(2)	4704(5)	-3037(4)	8680(4)	101(1)
F(3)	5574(5)	-1012(6)	8069(5)	144(2)
F(4)	4010(5)	-143(4)	6842(4)	103(1)
F(5)	3244(4)	-2154(4)	7406(4)	99(1)

Table 3.32 / cont.

F(6)	5335(5)	-1867(5)	6660(4)	109(1)

$$U_{eq} = \frac{1}{3}\Sigma_i\Sigma_j U_{ij}a_i^*a_j^*(a_i.a_j)$$

Table 3.33:Anisotropic thermal factors (Å^2 , x 10^3) for

$[Ru_2(\mu\text{-}Ph_2Ppy)_2(\mu\text{-}CO)_2(NCMe)_4](PF_6)_2$

	U(11)	U(22)	U(33)	U(23)	U(13)	U(12)
Ru	21(1)	23(1)	31(1)	-10(1)	-2(1)	5(1)
P(1)	26(1)	25(1)	32(1)	-8(1)	-4(1)	5(1)
O	33(2)	36(2)	76(2)	-22(2)	-15(1)	-2(1)
N(1)	28(2)	29(2)	37(2)	-13(2)	-1(1)	8(1)
N(2)	25(2)	42(2)	43(2)	-18(2)	-3(2)	5(2)
N(3)	42(2)	26(2)	47(2)	-14(2)	-1(2)	3(2)
C(1)	38(2)	30(2)	36(2)	-8(2)	-6(2)	-1(2)
C(2)	39(3)	47(3)	53(3)	-7(2)	-5(2)	-5(2)
C(3)	56(3)	62(4)	76(4)	-12(3)	-6(3)	-23(3)
C(4)	83(4)	46(3)	70(4)	-7(3)	-7(3)	-27(3)
C(5)	70(4)	45(3)	53(3)	-9(2)	-14(3)	-4(3)
C(6)	54(3)	30(2)	43(3)	-7(2)	-14(2)	1(2)
C(7)	31(2)	38(2)	29(2)	-13(2)	-5(2)	4(2)
C(8)	49(3)	47(3)	54(3)	-23(2)	-14(2)	-4(2)
C(9)	59(3)	62(3)	53(3)	-27(3)	-17(2)	-1(2)
C(10)	49(3)	77(4)	52(3)	-30(3)	-16(2)	-3(3)
C(11)	54(3)	64(3)	59(3)	-18(3)	-24(3)	9(3)
C(12)	39(2)	51(3)	51(3)	-14(2)	-15(2)	5(2)
C(13)	32(2)	30(2)	38(2)	-13(2)	-2(2)	5(2)
C(14)	46(3)	59(3)	36(2)	-12(2)	-7(2)	15(2)
C(15)	66(3)	61(3)	37(3)	-18(2)	-4(2)	22(3)
C(16)	52(3)	61(3)	42(3)	-26(2)	6(2)	10(2)
C(17)	41(2)	38(2)	42(3)	-16(2)	2(2)	6(2)
C(18)	35(3)	47(3)	47(3)	-22(2)	0(2)	0(2)
C(19)	29(2)	80(4)	79(4)	-31(3)	-14(2)	12(2)
C(20)	40(2)	34(3)	51(3)	-20(2)	-6(2)	5(2)
C(21)	98(4)	27(3)	88(4)	-29(3)	-18(3)	16(3)
C(22)	24(2)	31(2)	35(2)	-12(2)	-3(2)	5(2)
P(2)	49(1)	55(1)	73(1)	-33(1)	-15(1)	13(1)
F(1)	135(4)	91(3)	97(3)	-38(2)	22(3)	14(3)
F(2)	115(3)	72(3)	122(3)	-33(2)	-61(3)	39(2)
F(3)	114(4)	192(6)	163(5)	-86(4)	-32(3)	-65(4)
F(4)	118(4)	69(2)	101(3)	-10(2)	-1(3)	2(2)
F(5)	82(3)	98(3)	124(3)	-32(3)	-51(2)	-2(2)
F(6)	103(3)	146(4)	101(3)	-82(3)	-14(2)	40(3)

3.3.15 Single crystal X-ray diffraction study of [Ru_2(μ-Ph_2Pbipy)$_2$(CO)$_2$(NCEt)$_2$](PF_6)$_2$ [22]

A single, purple, needle-shaped crystal was grown by slow diffusion of diethyl ethyl vapour into a saturated propionitrile solution of the complex. Due to inherent loss of solvent from the crystal, it was mounted on a fibre inside a 3mm glass capillary. The general approach used for the intensity data collection is described in Appendix A. The crystallographic data are given in Table 3.34, the interatomic distances in Table 3.35, the interatomic angles in Table 3.36, the fractional coordinates in Table 3.37 and the anisotropic thermal parameters in Table 3.38. The observed and calculated structure factors may be found on microfiche in an envelope fixed to the inside back cover.

Table 3.34

Crystal data and details of the crystallographic analysis for $[Ru_2(\mu\text{-}Ph_2Pbipy)_2(CO)_2(NCEt)_2](PF_6)_2$

Formula	$Ru_2C_{52}H_{44}N_6O_2P_4F_{12}$
Molecular Mass	1338.98
Crystal System	Orthorhombic
Space Group	Pccn
a(Å)	18.416(6)
b(Å)	19.573(5)
c(Å)	16.442(3)
V(Å^3)	5926.73
Z	4
D_c(g.cm^{-3})	1.500
F(000)	2680
λ(Mo-Kα)(Å)	0.71069
Scan mode	ω - 2θ
ω scan angle	$0.80 + 0.35\tan\theta$
Horizontal Aperture width (mm)	$2.7 + 0.1\tan\theta$
Scattering range (°)	$2 \leq \theta \leq 23$
μ (cm^{-1})	6.92
Absorption corrections	Semi empirical[103]
Measured intensities	5286
Unique intensities	3240
Unique intensities with $[I > 3\sigma(I)]$	2067
Structure solution	Direct & Fourier methods
Weighting scheme	$1/(\sigma^2(F) + 0.00522F^2)$
$R = \Sigma(F_o - F_c)/\Sigma F_o$	0.0782
$R_w = \Sigma_w{}^{1/2}(F_o - F_c)/\Sigma_w{}^{1/2}F_o$	0.0853
$(\Delta/\sigma)_{max}$	0.098
$\Delta\rho_{max}$(eÅ^{-3})	0.883
Number of parameters	207

Table 3.35: Interatomic distances (Å) for

$[Ru_2(\mu\text{-}Ph_2Pbipy)_2(CO)_2(NCEt)_2](PF_6)_2$

Ru-P(1)	2.272(4)	Ru-N(3)	2.090(13)
Ru-C(23)	1.82(2)	Ru-Ru′	2.765(2)
Ru-N(1′)	2.20(6)	Ru-N(2′)	2.05(6)
P(1)-C(1)	1.82(2)	P(1)-C(7)	1.82(2)
P(1)-C(13)	1.814(14)	O(1)-C(23)	1.15(2)
N(1)-C(13)	1.35(2)	N(1)-C(17)	1.32(2)
N(2)-C(18)	1.37(2)	N(2)-C(22)	1.35(2)
N(3)-C(24)	1.15(2)	C(1)-C(2)	1.41(2)
C(1)-C(6)	1.41(2)	C(2)-C(3)	1.44(3)
C(3)-C(4)	1.47(3)	C(4)-C(5)	1.37(3)
C(5)-C(6)	1.40(3)	C(7)-C(8)	1.42(2)
C(7)-C(12)	1.41(2)	C(8)-C(9)	1.43(2)
C(9)-C(10)	1.40(2)	C(10)-C(11)	1.44(2)
C(11)-C(12)	1.41(2)	C(13)-C(14)	1.44(2)
C(14)-C(15)	1.43(2)	C(15)-C(16)	1.39(2)
C(16)-C(17)	1.43(2)	C(17)-C(18)	1.44(2)
C(18)-C(19)	1.42(2)	C(19)-C(20)	1.41(3)
C(20)-C(21)	1.40(2)	C(21)-C(22)	1.41(3)
C(24)-C(25)	1.49(3)	C(25)-C(26)	1.52(3)
P(2)-F(1)	1.549(14)	P(2)-F(2)	1.60(2)
P(2)-F(3)	1.53(2)	P(2)-F(4)	1.56(2)
P(2)-F(5)	1.532(14)	P(2)-F(6)	1.54(2)

Table 3.36: Interatomic angles (°) for $[Ru_2(\mu\text{-}Ph_2Pbipy)_2(CO)_2(NCEt)_2](PF_6)_2$

P(1)-Ru-N(3)	176.0(4)	P(1)-Ru-C(23)	91.5(5)
N(1')-Ru-Ru'	95.9(2)	N(2')-Ru-Ru'	169.0(2)
N(1')-Ru-N(2')	74.7(2)	N(1')-Ru-P(1)	107.5(2)
N(1')-Ru-C(23)	176.1(6)	N(1')-Ru-N(3)	69.2(4)
N(2')-Ru-P(1)	95.7(2)	N(2')-Ru-C(23)	106.3(6)
N(2')-Ru-N(3)	84.5(4)		
N(3)-Ru-C(23)	92.3(6)	Ru-P(1)-C(1)	117.9(5)
Ru-P(1)-C(7)	113.9(5)	C(1)-P(1)-C(7)	102.4(7)
Ru-P(1)-C(13)	116.4(5)	C(1)-P(1)-C(13)	102.7(7)
C(7)-P(1)-C(13)	101.2(7)	C(13)-N(1)-C(17)	122.5(12
C(18)-N(2)-C(22)	120.1(13)	Ru-N(3)-C(24)	177.7(14
P(1)-C(1)-C(2)	117.2(12)	P(1)-C(1)-C(6)	121.9(13
C(2)-C(1)-C(6)	121(2)	C(1)-C(2)-C(3)	119(2)
C(2)-C(3)-C(4)	118(2)	C(3)-C(4)-C(5)	122(2)
C(4)-C(5)-C(6)	119(2)	C(1)-C(6)-C(5)	121(2)
P(1)-C(7)-C(8)	120.8(12)	P(1)-C(7)-C(12)	119.5(12
C(8)-C(7)-C(12)	119(2)	C(7)-C(8)-C(9)	121(2)
C(8)-C(9)-C(10)	119(2)	C(9)-C(10)-C(11)	120(2)
C(10)-C(11)-C(12)	120(2)	C(7)-C(12)-C(11)	120.4(14
P(1)-C(13)-N(1)	118.9(10)	P(1)-C(13)-C(14)	120.5(10
N(1)-C(13)-C(14)	120.5(12)	C(13)-C(14)-C(15)	116.7(13
C(14)-C(15)-C(16)	121(2)	C(15)-C(16)-C(17)	117.7(13
N(1)-C(17)-C(16)	121.2(13)	N(1)-C(17)-C(18)	116.5(13
C(16)-C(17)-C(18)	122.3(13)	N(2)-C(18)-C(17)	117.0(14
N(2)-C(18)-C(19)	120.7(14)	C(17)-C(18)-C(19)	122.4(14
C(18)-C(19)-C(20)	119(2)	C(19)-C(20)-C(21)	118(2)
C(20)-C(21)-C(22)	120(2)	N(2)-C(22)-C(21)	121(2)
Ru-C(23)-O(1)	174(2)	N(3)-C(24)-C(25)	175(2)
C(24)-C(25)-C(26)	108(2)	F(1)-P(2)-F(2)	89.4(9)
F(1)-P(2)-F(3)	90.7(11)	F(2)-P(2)-F(3)	88.2(10
F(1)-P(2)-F(4)	88.5(9)	F(2)-P(2)-F(4)	175.3(11
F(3)-P(2)-F(4)	96.0(12)	F(1)-P(2)-F(5)	178.0(13
F(2)-P(2)-F(5)	91.0(10)	F(3)-P(2)-F(5)	87.4(12

Table 3.36 / cont.

F(4)-P(2)-F(5)	91.3(10)	F(1)-P(2)-F(6)	89.5(13
F(2)-P(2)-F(6)	89.8(11)	F(3)-P(2)-F(6)	178.0(12
F(4)-P(2)-F(6)	86.0(12)	F(5)-P(2)-F(6)	92.4(14

Table 3.37: Fractional coordinates (x 10^4) and isotropic thermal factors ($Å^2$, x 10^3) for $[Ru_2(\mu\text{-}Ph_2Pbipy)_2(CO)_2(NCEt)_2](PF_6)_2$

	x/a	y/b	z/c	U_{eq}
Ru	8203(1)	2583(1)	6853(1)	43
P(1)	8152(2)	1455(2)	6143(2)	42(1)
O(1)	8162(8)	1647(8)	8228(6)	98(4)
N(1)	6781(6)	1619(6)	5914(6)	40(3)*
N(2)	5721(6)	2240(7)	6622(7)	47(3)*
N(3)	8227(7)	3669(8)	7443(8)	58(3)*
C(1)	8301(8)	473(9)	6571(9)	53(4)*
C(2)	8845(9)	421(11)	7068(10)	65(5)*
C(3)	8983(12)	-345(14)	7415(13)	102(7)*
C(4)	8522(14)	-1025(15)	7258(14)	111(8)*
C(5)	7987(13)	-947(13)	6788(13)	97(7)*
C(6)	7853(10)	-188(11)	6473(11)	74(5)*
C(7)	8769(8)	1451(9)	5402(9)	49(4)*
C(8)	9407(9)	1055(10)	5478(9)	60(5)*
C(9)	9919(10)	1120(11)	4932(11)	75(5)*
C(10)	9798(9)	1609(11)	4324(10)	68(5)*
C(11)	9152(9)	2025(10)	4245(9)	61(5)*
C(12)	8643(8)	1927(9)	4777(9)	52(4)*
C(13)	7360(7)	1289(8)	5654(8)	42(4)*
C(14)	7348(8)	797(9)	5007(9)	54(4)*
C(15)	6694(8)	624(10)	4706(10)	59(5)*
C(16)	6103(7)	953(9)	5006(9)	49(4)*
C(17)	6173(8)	1449(9)	5640(8)	44(4)*
C(18)	5593(8)	1807(9)	6003(9)	48(4)*
C(19)	4915(10)	1711(11)	5743(10)	72(5)*
C(20)	4370(11)	2068(12)	6129(12)	87(6)*
C(21)	4521(10)	2501(10)	6761(10)	75(5)*
C(22)	5199(8)	2551(9)	7013(9)	61(4)*
C(23)	8173(9)	1971(10)	7675(10)	59(4)*
C(24)	8218(9)	4262(11)	7776(10)	66(5)*
C(25)	8194(11)	5067(13)	8140(13)	98(7)*
C(26)	8828(12)	5147(14)	8610(15)	112(8)*
P(2)	4277(3)	952(4)	3618(3)	86(2)
F(1)	3829(9)	193(10)	3472(9)	165(6)

Table 3.37 / cont.

F(2)	3742(9)	1494(9)	3176(9)	155(6)
F(3)	4662(9)	815(12)	2905(9)	174(6)
F(4)	4753(9)	408(11)	4094(11)	194(7)
F(5)	4737(11)	1694(11)	3740(11)	229(8)
F(6)	3873(14)	1112(14)	4322(10)	238(10)

* isotropic temperature factor.

$$U_{eq} = \frac{1}{3} \Sigma_i \Sigma_j U_{ij} a_i^* a_j^* (a_i . a_j)$$

Table 3.38: Anisotropic thermal factors (Å^2 , x 10^3) for

[Ru_2(μ-Ph_2Pbipy)$_2$(CO)$_2$(NCEt)$_2$](PF_6)$_2$

	U(11)	U(22)	U(33)	U(23)	U(13)	U(12)
Ru	55(1)	47(1)	28(1)	1(1)	-7(1)	-11(1)
P(1)	46(2)	46(2)	34(2)	3(2)	-3(2)	-1(2)
O(1)	149(14)	115(10)	30(7)	27(7)	-40(8)	-51(10)
P(2)	95(4)	100(4)	63(4)	5(3)	-9(4)	-35(4)
F(1)	207(17)	162(13)	126(12)	42(11)	-63(12)	-103(12)
F(2)	185(17)	140(12)	139(14)	13(11)	-33(12)	29(11)
F(3)	148(14)	225(18)	148(14)	28(13)	89(12)	22(13)
F(4)	175(16)	186(16)	220(18)	109(15)	-130(15)	-73(13)
F(5)	303(25)	174(15)	211(21)	31(14)	-113(19)	-174(17)
F(6)	319(31)	283(25)	110(14)	0(16)	65(16)	122(23)

CHAPTER FOUR

MONONUCLEAR RUTHENIUM COMPLEXES CONTAINING PENDANT PHOSPHORUSPYRIDYL OR PHOSPHORUSBIPYRIDYL LIGANDS: POTENTIAL PRECURSORS FOR THE SYNTHESIS OF LIGAND-BRIDGED HETERODINUCLEAR COMPOUNDS

4.1. Introduction

The proliferation of studies involving dinuclear ligand-bridged transition metal complexes and their chemistry has, to a large extent, been centred on systems with two like metals in identical coordination environments. These dimers may or may not have metal-metal bonds, with their attractiveness lying in the fact that they react with unsaturated substrates or small molecules by processes in which both metals participate simultaneously to give new substrate reactivities of the type fundamental to certain areas of catalysis.[138,139] Considerable attention has been focused on the use of dppm as a bridging ligand for these homodinuclear complexes.[7] Phosphoruspyridyl ligands (eg. Ph_2Ppy), like triphenylphosphine, can coordinate in a monodentate fashion through the phosphorus atom only (see section 1.5.1). In addition, the phosphoruspyridyl ligand has a nitrogen atom positioned so that it can bind to a second metal atom (see section 1.5.3 b)). This presents the possibility of holding two unlike metal atoms together, allowing the two individual metal centers to perform separate, unique functions over and above those of homodinuclear complexes. The same is true of the Ph_2Pbipy ligand, except that there are two nitrogen atoms positioned to bind in a chelating fashion to a second metal atom. With this in mind and coupled with our interest in ruthenium in low oxidation states, it was decided to synthesise mononuclear ruthenium complexes containing pendant phosphoruspyridyl or phosphorusbipyridyl ligands for use as precursors for the synthesis of a range of heterodinuclear ligand-bridged products with or without metal-metal interactions. Until now few studies have been undertaken in this area, due firstly to the lack of suitable precursors, secondly due to the fact that analagous reactions involving dppm result only in substitution products of $[Ru_3(CO)_{12}]$ [140-142] and chelated ruthenium(II) complexes [143] and thirdly due to the fact that complexes of ruthenium in low oxidation states tend to be coordinatively saturated, inhibiting access to the metal. However, Balch *et al* [80] have synthesised

Ph_2Ppy analogues of the disubstituted triphenylphosphine ruthenium(0) and (II) species $[Ru(CO)_3(\eta^1\text{-}PPh_3)_2]$ and $[Ru(CO)_2Cl_2(\eta^1\text{-}PPh_3)_2]$ respectively; these are shown below.

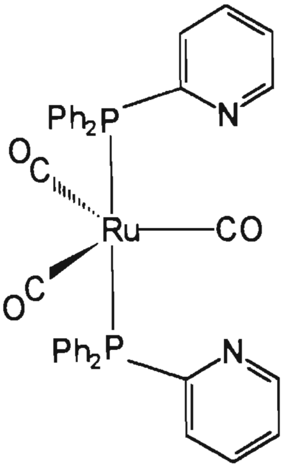

$[Ru(CO)_3(\eta^1\text{-}Ph_2Ppy)_2]$

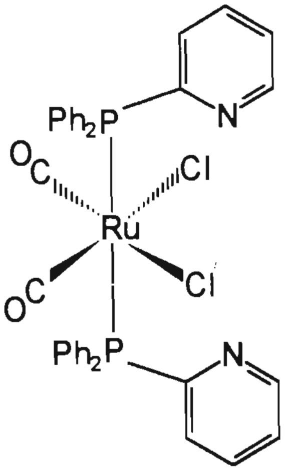

$[Ru(CO)_2Cl_2(\eta^1\text{-}Ph_2Ppy)_2]$

Reactions of $[Ru(CO)_3(\eta^1\text{-}Ph_2Ppy)_2]$ with $[Pd(1,5\text{-}cod)Cl_2]$ (1,5-cod = 1,5-cyclooctadiene) or $[Ru(CO)_2Cl_2(\eta^1\text{-}Ph_2Ppy)_2]$ with $[Pd_2(dba)_3]$ (dba = dibenzylideneacetone) afforded the desired complex $[RuPd(\mu\text{-}Ph_2Ppy)_2(CO)_2Cl_2]$, but in very low yields [80]. No further studies in this area have been reported, however.

This chapter describes the synthesis of novel mononuclear ruthenium complexes containing pendant Ph_2Pbipy ligands. The reactions of these and equivalent complexes of Ph_2Ppy with various transition metal precursors were then performed in an attempt to synthesise heterodinuclear ligand-bridged complexes stabilised to fragmentation, with priority being given to metals of group 11, despite their preference for softer donors, due to the measure of success which has been experienced in related areas of research.[16,144]

4.2. Synthesis of mononuclear ruthenium(0) complexes of Ph_2Ppy and Ph_2Pbipy

Scheme 4.1 summarises the essential features of the chemistry discussed in this section.

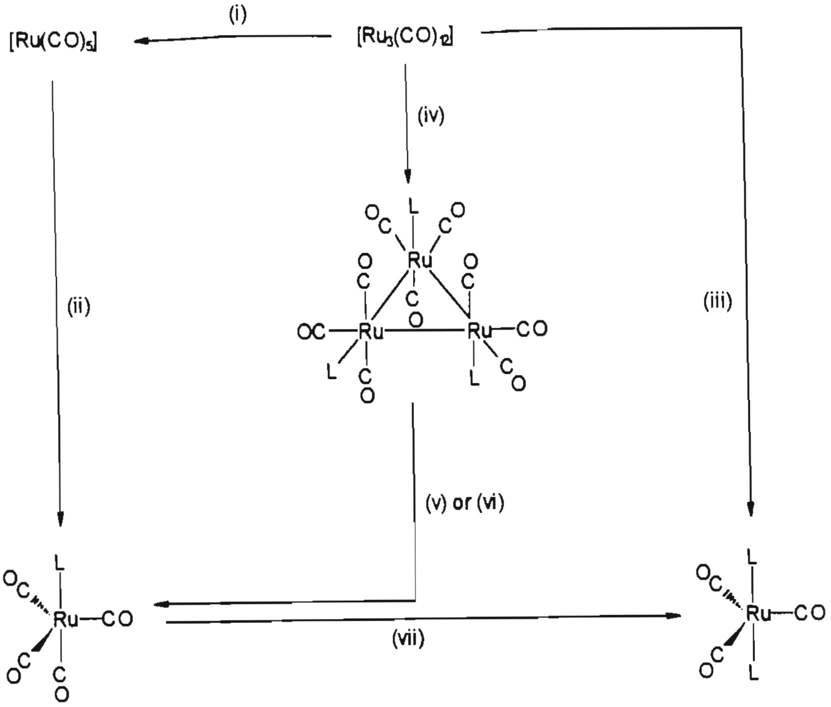

Scheme 4.1 : The reaction pathways for the synthesis of mononuclear ruthenium (0) complexes of Ph_2Ppy and Ph_2Pbipy (L).

KEY
(i) hν, n-hexane, CO, 25°C
(ii) 1.0 eq. L, CO, 25°C
(iii) 6.0 eq. L, hν(2M $NaNO_2$), n-hexane, 25°C
(iv) 3.0 eq. L, MeOH, Δ
(v) $Ph_2CO^{\bullet-}$, thf, 40°C
(vi) hν, thf, CO, 25°C
(vii) $Ph_2CO^{\bullet-}$, thf, 40°C, L

4.2.1 Synthesis of $[Ru(CO)_4(\eta^1\text{-}L)]$ (L = Ph_2Ppy [25] or Ph_2Pbipy [26])

Three routes to $[Ru(CO)_4(\eta^1\text{-}L)]$ (L = Ph_2Ppy **[25]** or Ph_2Pbipy **[26]**) have been developed. The first and most efficient involves the reaction of the respective ligand with the binary carbonyl $[Ru(CO)_5]$.[145] This highly unstable pentacarbonyl ruthenium (0) monomer is generated *in situ* by photolysis of $[Ru_3(CO)_{12}]$ under CO pressure at room temperature using a procedure adapted from the literature [146-148] (see experimental section). The addition of three equivalents of ligand (per $[Ru_3(CO)_{12}]$ unit) under CO pressure results in a change in the colour of the $[Ru(CO)_5]$ solution from colourless to pale yellow. The reaction is monitored by means of infra-red spectroscopy and is terminated when all of the bands due to the $[Ru(CO)_5]$ (Figure 4.1 a)) are replaced by those of the desired product (Figure 4.1 b)). Related studies have shown [146] that the reaction proceeds at the same limiting rate irrespective of the nature of the substituting ligand and the concentration of CO.

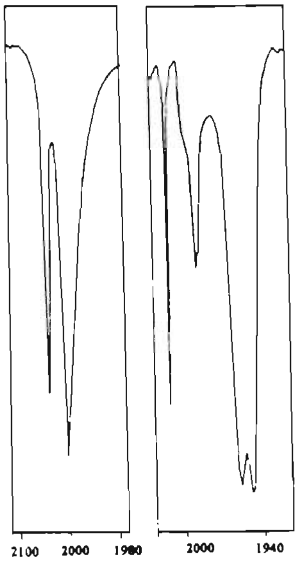

(a) (b)

Figure 4.1 : IR spectra (n-hexane) of a) [Ru(CO)$_5$] and b) [Ru(CO)$_4$(η^1-L)] (L = Ph$_2$Ppy or Ph$_2$Pbipy)

The second and third methods involve the initial synthesis of the trinuclear complexes [Ru$_3$(CO)$_9$(η^1-L)$_3$] (L = Ph$_2$Ppy) [80] as well as of the novel purple Ph$_2$Pbipy analogue **[27]**. Treatment of these trinuclear complexes with trace quantities of sodium benzophenoneketyl in warm thf leads to their respective solutions turning from purple to yellow, from which the desired product can be isolated. Alternatively, irradiation of thf solutions of the above trinuclear precursors under gentle CO pressure affords the complexes in almost quatitative yield.

Complex **[25]** is a pale yellow to beige powder while **[26]** is isolated as a pale yellow oil. Both species are soluble in most organic solvents and are moderately air sensitive.

The infra-red spectra for both complexes are identical, exhibiting four sharp carbonyl peaks, similar to that of the trimethylphosphite complex [Ru(CO)$_4${P(OCH$_3$)$_3$}].[149] This differs from the three expected for a trigonal bipyramidal molecule of the type M(CO)$_4$L with L axial (C_{3v} symmetry) [150], for example [Ru(CO)$_4$(η^1-PPh$_3$)], and can be associated with the reduction of symmetry due to the presence of the ligand, as well as the possible presence in solution of equatorial isomers of the complex. Complex **[25]** has been characterised by C, H and N microanalysis. ^{31}P{^{1}H} nmr spectra comprise

Table 4.1 : The spectroscopic parameters for the ruthenium(0) complexes$^{(a)}$

Complex	ν (CO), cm^{-1} $^{(b)}$	$^{31}P\{^1H\}$ nmr , $^{(c)}$ δ	Analysis : Found (calculated) % %C	%H	%N
[25] $[Ru(CO)_4(\eta^1\text{-}Ph_2Ppy)]$	2062(s) 1990(m) 1958(vs) 1950(vs)	48.51(s)	53.21(52.95)	2.81(2.96)	3.30(2.96)
[26] $[Ru(CO)_4(\eta^1\text{-}Ph_2Pbipy)]$	2064(s) 1991(m) 1958(vs) 1953(vs)	49.72(s)			
[27] $[Ru_3(CO)_9(\eta^1\text{-}Ph_2Pbipy)_3]$	1970(vs) (recorded in CH_2Cl_2)	39.70(s)	56.80(57.14)	3.22(3.26)	5.61(5.33)
[28] $[Ru(CO)_3(\eta^1\text{-}Ph_2Ppy)_2]$	1897(vs)	57.80(s)	62.59(62.45)	4.23(3.97)	3.59(3.94)
[29] $[Ru(CO)_3(\eta^1\text{-}Ph_2Pbipy)_2]$	1906(vs)	58.25(s)	65.50(65.20)	3.90(3.96)	5.92(6.47)

(a) : ^1H nmr data are omitted since spectra simply comprise complex resonance patterns in the region δ 8.7 - 6.7 (for complexes of Ph_2Ppy) or 9.1 - 7.0 (for complexes of Ph_2Pbipy), corresponding to ligand protons.

(b) : Recorded in n-hexane unless otherwise specified. Designation : vs = very strong, s = strong, m = medium.

(c) : Measured in CD_2Cl_2. Designation : s = singlet.

singlets at δ 48.51 and 49.72 respectively (downfield from H_3PO_4, external standard); both **[25]** and **[26]** have similar ^1H nmr spectra.

Table 4.1 lists the salient spectroscopic data for both mononuclear complexes, as well as those for the trisubstituted Ph_2Pbipy derivative **[27]** which is used as a precursor in the synthesis of **[25]** and **[26]**. ^1H nmr spectral details have not been included since all spectra contain complex resonance patterns corresponding to the aromatic portions of the relevant ligand.

4.2.2 Synthesis of $[Ru(CO)_3(\eta^1\text{-}L)_2]$ (L = Ph_2Ppy [28] or Ph_2Pbipy [29])

A convenient route to $[Ru(CO)_3(\eta^1\text{-}Ph_2Ppy)_2]$ **[28]** has already been described in the literature [80] but was suitably modified to improve the yield, especially for the low-yielding **[29]**. Irradiation of a thoroughly stirred, deoxygenated n-hexane solution of $[Ru_3(CO)_{12}]$ and six equivalents of ligand through a 2M $NaNO_2$ filter solution (maintained at room temperature through the use of a concentric outer jacket through which tap water circulates) for 5 hours affords the product in good yield which is isolated as a pale yellow (in the case of **[28]**) or yellow-brown (in the case of **[29]**) precipitate. Longer reaction times tend not to improve yields, but rather increase the chances of condensation back to the $[Ru_3(CO)_9(\eta^1\text{-}L)_3]$ species or loss of ligand to the $[Ru(CO)_4(\eta^1\text{-}L)]$ species. The choice of wavelength in this reaction is essential, since shorter, higher energy wavelengths (< 395nm) induce immediate condensation; hence the use of the $NaNO_2$ filter (λ_{cutoff} = 390nm).

A second route to the products involves the reaction of $[Ru(CO)_4(\eta^1\text{-}L)]$ (L = Ph_2Ppy **[28]** or Ph_2Pbipy **[29]**) with an equivalent of the appropriate ligand in the presence of the catalyst sodium benzophenoneketyl, under gentle heat. The result is that decarbonylation of an axial carbonyl occurs accompanied by the preferential formation of the stable tricarbonyl derivative in low yields.

The appearance of a single terminal stretching peak at 1897 cm^{-1} (for **[28]**) and 1906cm^{-1} (for **[29]**) in the infra-red spectrum of $[Ru(CO)_3(\eta^1\text{-}L)_2]$ (L = Ph_2Ppy or Ph_2Pbipy) is consistent with the structure depicted in Scheme 4.1, with two apical ligands and three equatorial carbonyls, similar to that established for the analagous triphenylphosphine complex.[151] The $^{31}P\{^1H\}$ nmr spectrum for **[29]** contains a singlet at δ 58.25 (downfield from H_3PO_4, external standard) and corresponds closely to that for the known **[28]** (57.8 ppm). C, H and N microanalyses are consistent with the above formulations. Table 4.1 summarises the above spectroscopic data, but again omits ^{1}H nmr data since complex resonance patterns in the regions δ 8.7-6.7 (for complexes of Ph_2Ppy) or 9.1-7.0 (for complexes of Ph_2Pbipy), corresponding to the shifts of aromatic ligand protons, are the only observed features.

4.3 Synthesis of mononuclear ruthenium(II) complexes of dppm, Ph_2Ppy and Ph_2Pbipy

Another large category of mononuclear ruthenium complexes is that involving ruthenium in the +2 oxidation state. A widely utilised precursor for the synthesis of a range of ruthenium(II) species is the chloride-bridged complex $[Ru_2(\mu\text{-}Cl)_2(Cl)_2(CO)_6]$.[152] Its chloride bridges are easily cleaved by thf or other ligands such as nitriles or pyridine,[153] affording labile adducts such as $[(thf)Ru(CO)_3Cl_2]$. These adducts are useful for the synthesis of cis- or trans-$[Ru(CO)_2Cl_2L_2]$ (L = PPh_3 or pyridine).[154]

4.3.1 Synthesis of $[Ru(CO)Cl(\eta^2\text{-dppm})_2][Ru(CO)_3Cl_3]$ [30]

In preliminary studies designed to elucidate the behaviour of bidentate ligands with the $[Ru_2(\mu\text{-}Cl)_2(Cl)_2(CO)_6]$ precursor, reaction of two equivalents of dppm (per dimer unit) with this dimer in refluxing toluene under nitrogen was found to afford a pale yellow precipitate as product in excellent yield. The solid state (KBr disc) infra-red spectrum of this species (Fig. 4.2) reveals four peaks in the ν(CO) region at relatively high wavenumbers.

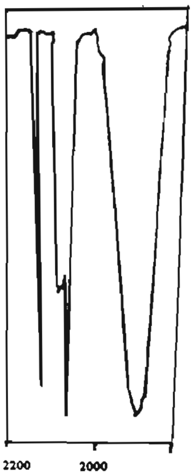

Figure 4.2 : Infra-red spectrum (KBr disk) of [30]

The presence of four carbonyl bands is indicative of a mixture of products but this is not consistent with the $^{31}P\{^1H\}$ nmr spectral data. A singlet at δ -7.12 confirms the presence of a single complex in which all of the phosphorus atoms are equivalent, unless there is a rapid interconversion of the species involved. The fact that two molar equivalents of dppm were added (per dimeric unit) would suggest the presence of a monomer with one chelating dppm, together with two carbonyl and two chloride ligands (given the neutrality of the complex) completing the octahedral configuration around the ruthenium. However, this compound, in cis- form would give rise to two terminal carbonyl bands. In the trans- form, only one band would result. $^{31}P\{^1H\}$ nmr data precludes the possibility of two equally abundant isomeric forms. The only possibility left is for the complex to comprise a carbonyl cation and a carbonyl anion in which the dppm ligands are present in either the cation or the anion, eg. $[Ru(CO)Cl(\eta^2\text{-dppm})_2][Ru(CO)_3Cl_3]$ (below), but not in both, eg. $[Ru(CO)_3Cl(\eta^2\text{-dppm})][Ru(CO)Cl_3(\eta^2\text{-dppm})]$ since, similar to the situation for the mixture of compounds, the latter would give rise to two singlets in its $^{31}P\{^1H\}$ nmr spectrum. An X-ray diffraction study has subsequently established this to be the case (see section 4.3.3).

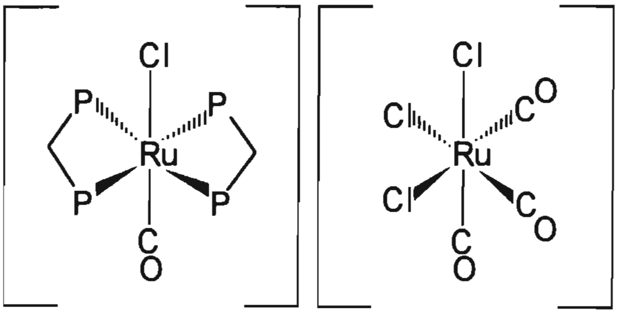

$[Ru(CO)Cl(\eta^2\text{-dppm})_2][Ru(CO)_3Cl_3]$

The broad stretch at 1977cm^{-1} is assigned to the $[Ru(CO)Cl(\eta^1\text{-dppm})_2]^+$ cation, in comparison with the carbonyl band appearing for the analogous dppe cationic complex at 1950cm^{-1}.[155] The three remaining bands are thus assignable to the carbonyl ligands of the anion. Presumably, these occur at higher wavenumbers because of the presence of three π-accepting CO's rather than one. The ^1H nmr spectrum exhibits

Table 4.2 : The spectroscopic parameters for the ruthenium(II) complexes

Complex	ν (CO), cm$^{-1\ (a)}$	$^{31}P\{^1H\}$ nmr, $^{(b)}$ δ	^1H nmr, $^{(c)}$ δ	Analysis : Found (calculated) %		
				%C	%H	%N
[30] $[Ru(CO)Cl(\eta^2\text{-dppm})_2][Ru(CO)_3Cl_3]$	2124(s) 2058(s) 2048(vs) 1977(brs)	-7.12(s)	8.00 - 7.22(m, 40H, dppm) 5.17(q, 4H, -CH$_2$-)	52.78(53.04)	3.66(3.47)	-
[31] $[Ru(CO)_2Cl_2(\eta^1\text{-}Ph_2Ppy)_2]$	2064(vs) 1998(vs)	20.87(s)		57.75(57.30)	3.59(3.74)	3.37(3.71)
[32] $[Ru(CO)_2Cl_2(\eta^1\text{-}Ph_2Pbipy)_2]$	2064(vs) 2004(vs)	19.54(s)		60.72(60.83)	3.41(3.77)	6.19(6.17)

(a) : Recorded in the solid state as KBr disks. Designation : vs = very strong, s = strong, brs = broad-strong.

(b) : Recorded in CD_2Cl_2. Designation : s = singlet.

(c) : Recorded in CD_2Cl_2. Designation : m = multiplet, q = quintet. Note : Data for compounds **[31]** and **[32]** are omitted since spectra simply comprise complex resonance patterns at δ 9.02 - 7.35 and 8.65 - 7.35 respectively, corresponding to phosphine ligand protons.

complex resonance patterns between δ 8.00 - 7.22 assigned to the phenyl protons as well as an unresolved multiplet at δ 5.17. The latter feature is attributable to the methylene protons of the dppm ligands, since it is assumed that the chelate dppm lacks rigidity in solution, therefore giving poor resolution. Table 4.2 lists the above spectroscopic parameters.

4.3.2 Synthesis of $[Ru(CO)_2Cl_2(\eta^1\text{-}L)_2]$ (L = Ph_2Ppy [31] or Ph_2Pbipy [32])

A novel, higher yielding route to $[Ru(CO)_2Cl_2(\eta^1\text{-}Ph_2Ppy)_2]$ **[31]** than that reported in literature has been developed and applied successfully to the synthesis of its Ph_2Pbipy analogue **[32]**. Balch *et al.*[80] have reacted the complex $[Ru(CO)_3(\eta^1\text{-}Ph_2Ppy)_2]$ (**[28]** in this thesis) with a steam of dichlorine gas in gently refluxing dichloromethane, affording the product in 76% yield. However, the method developed in this study in this work involves a simpler synthesis using the $[Ru_2(\mu\text{-}Cl)_2(Cl)_2(CO)_6]$ precursor discussed earlier, and affords the product in 84% yield.

Thus, the refluxing of a suspension of $[Ru_2(\mu\text{-}Cl)_2(Cl)_2(CO)_6]$ and four equivalents of ligand (per dimeric unit) in toluene for two hours affords the product in microcrystalline form as a white (in the case of **[31]**) or pale yellow (in the case of **[32]**) precipitate in excellent yields. Cleavage of the halogen bridges and loss of carbon monoxide from the dimeric precursor is effected during the reaction. It also appears that the same product is formed when the reaction is repeated with two equivalents of ligand, but the yields are more than halved.

The infra-red spectrum for **[31]** is consistent with that reported in the literature,[80] exhibiting two strong bands of equal intensity at 2064 and 1988cm^{-1}; that for the Ph_2Pbipy analogue **[32]** is virtually identical. This corresponds to two mutually cis carbonyl ligands, identical with the products obtained by other workers under different conditions.[151,153,154] The $^{31}P\{^1H\}$ and ^1H nmr spectra for both complexes are as expected; the former exhibits singlets at approximately 20 ppm (downfield from H_3PO_4, external standard) for both complexes while the latter comprise complex resonance patterns in the aromatic region attributable to the relevant ligand protons. C, H and N microanalyses have confirmed the stoichiometry of both products.

A single crystal X-ray diffraction study of **[31]** has confirmed that its structure is as expected. Table 4.2 lists the spectroscopic parameters for the complexes.

4.3.3 Crystal structure determination of $[Ru(CO)Cl(\eta^2\text{-dppm})_2][Ru(CO)_3Cl_3]$ [30]

A perspective drawing of $[Ru(CO)Cl(\eta^2\text{-dppm})_2][Ru(CO)_3Cl_3]$ **[30]** is shown in Figure 4.3 together with the atom labelling scheme. The coordination sphere of the ruthenium atom in the cation consists of two mutually trans chelating dppm ligands in the equatorial plane with the remaining two axial sites occupied by a chlorine atom and a carbonyl group. The anion consists of two groups of three facially orientated chlorine atoms and carbonyl groups.

The geometry around each ruthenium atom is pseudo-octahedral , but the distortion of the octahedral cofiguration is more pronounced in the case of the cation. As far as the cation is concerned, a large degree of angular distortion is observed within the chelate ring and about the ruthenium atom. Thus the intrachelate P-Ru-P angles are distorted away from the ideal 90°, being pinched inwards to 70.1(1)° for both chelate rings, while the extrachelate P-Ru-P angles are bent to correspondingly higher angles of 105.9(1)° [for P(1)-Ru(1)-P(4)] and 112.7(1)° [for P(2)-Ru(1)-P(3)]. The difference in the extrachelate angles probably arises from the twist of the dppm MP_2C skeletons out of an exactly equatorial plane, the dihedral angle between the two mean planes through the two MP_2C chelates being rather substantial (29.8°). Within the chelate ring itself, all angles are slightly compressed. The P(1)-C(13)-P(2) and P(3)-C(38)-P(4) angles are 94.6(5)° and 95.6(5)° whilst the intrachelate C-P-Ru angles range from 92.3(4)° [for Ru(1)-P(3)-C(38)] to 94.1(3)° [for Ru(1)-P(1)-C(13)].This compression is alleviated to some extent by the slight increase in the intrachelate P-C distances ; for example, the P(2)-C(13) bond distance of 1.862(10)Å is considerably longer than the corresponding distance in dppm-monodentate or bridged complexes (see section 1.1). The chelating mode of coordination of the dppm ligands is the same as that found in related complexes of similar stereochemistry and established structure, one of which is the rhodium complex trans-$[RhHCl(\eta^2\text{-dppm})_2]$.[156] The remaining CO and Cl ligands of the cation of **[30]** are orientated in a near-linear fashion [Cl(1)-Ru(1)-C(51) = 175.1(3)°] at the axial sites of the octahedron.

As far as the anion is concerned, all angles about the octahedral ruthenium atom are approximately 90°. A noticeable difference is that the Ru(2)-C distances are

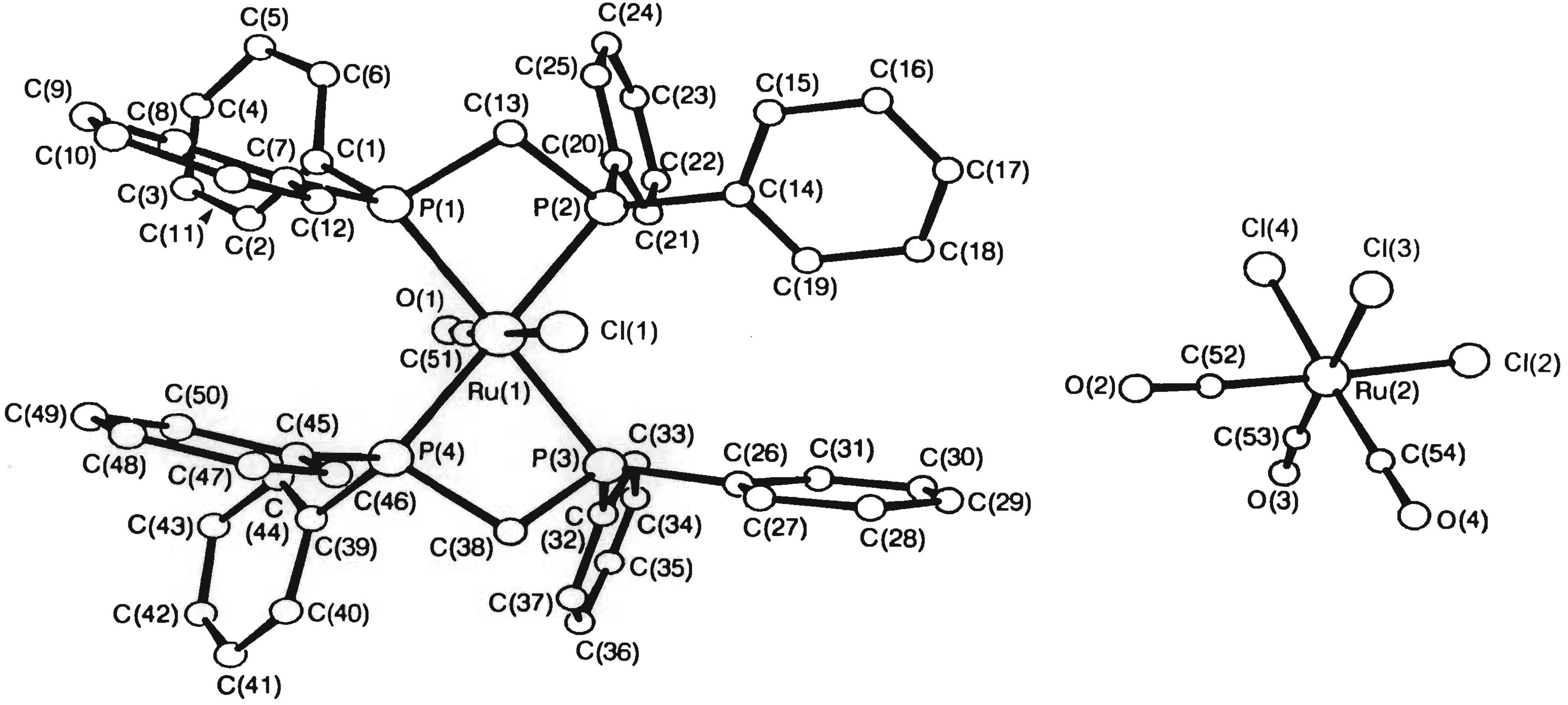
C(24)
C(5)
C(25)
C(6)
C(23)
C(15)
C(16)
C(9)
C(8)
C(4)
C(13)
C(20)
C(22)
C(17)
C(10)
C(7)
C(1)
C(14)
C(3)
P(1)
P(2)
C(11)
C(2)
C(12)
C(21)
C(18)
C(19)
Cl(4)
Cl(3)
O(1)
Cl(1)
C(51)
Ru(1)
C(52)
Cl(2)
O(2)
Ru(2)
C(50)
C(49)
C(45)
C(33)
C(53)
C(54)
P(4)
P(3)
C(26)
C(31)
C(30)
C(48)
C(47)
C(46)
C(29)
O(3)
O(4)
C
C
C(43)
(44)
C(39)
C(34)
C(38)
(32)
C(27)
C(28)
C(35)
C(37)
C(42)
C(40)
C(36)
C(41)

considerably longer that those for Ru(1)-C(51). This can be interpreted in terms of the low electron density on the ruthenium(II) atom being shared by three carbonyl ligands instead of just one. This also supports the infra-red carbonyl band assignment made in section 4.3.1

4.3.4 Crystal structure determination of [Ru(CO)$_2$Cl$_2$(η^1-Ph$_2$Ppy)$_2$] [31]

The molecular geometry of the neutral [Ru(CO)$_2$Cl$_2$(η^1-Ph$_2$Ppy)$_2$] **[31]** molecule is depicted in Figure 4.4 and shows the atom labelling scheme. The coordination sphere around the octahedral ruthenium atom consists of two mutually trans Ph$_2$Ppy ligands occupying the axial sites and bonded in a P-monodentate fashion. There are two mutually cis carbonyl ligands and two chlorine atoms in the equatorial plane. The two phosphine ligands are connected through the ruthenium atom in a near-linear fashion [P(1)-Ru(1)-P(2) = 173.9(3)°] while, in the equatorial plane, the minimally distorted C(35)-Ru-C(36) and C(35)-Ru-Cl(1) angles are 91.5(10)° and 91.4(7)° respectively. The overall structure is thus very regular. The nitrogens are tentatively assigned on the basis of reasons outlined later (section 4.6.6). Assigned as they are, it is interesting to note that the pyridine rings are cis disposed with respect to each other. All remaining bond lengths and angles are as expected.

4.4 Attempted syntheses of heterodinuclear complexes of ruthenium(0) and ruthenium(II).

The preparation of heteronuclear complexes has, for the most part been accomplished through reactions in which chance plays a major role. A great number of complexes have been prepared by reacting a number of reagents together, usually under vigorous conditions and while many interesting complexes have been prepared, a definite need exists for the development of a systematic approach to their synthesis. This work attempts to do this by eliminating possible side reactions through the use of mononuclear metal complexes containing bi- or tridentate ligands bonded in a pendant

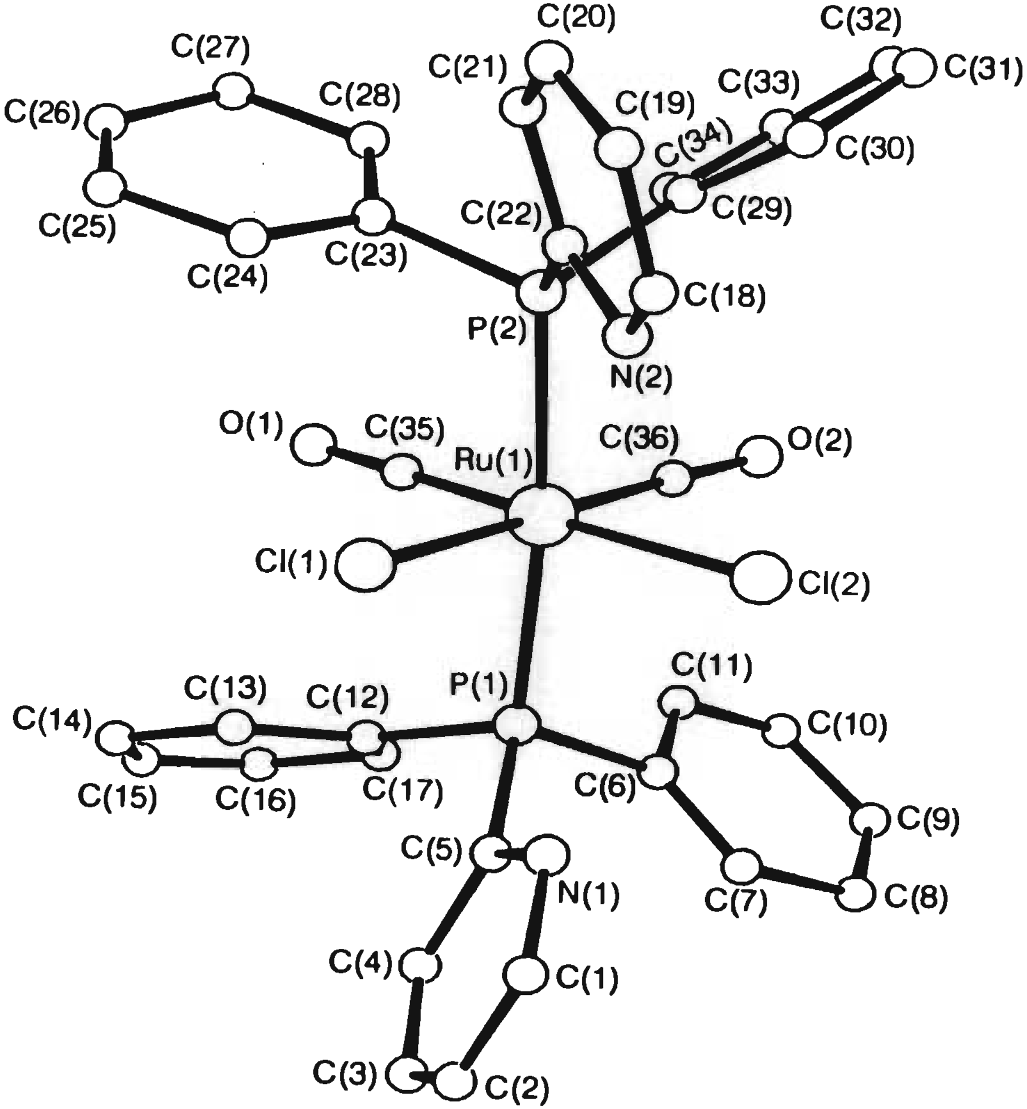
C(20)
C(32)
C(27)
C(21)
C(31)
C(33)
C(28)
C(26)
C(19)
C(34)
C(30)
C(22)
C(29)
C(25)
C(24)
C(23)
C(18)
P(2)
N(2)
O(1)
C(35)
C(36)
O(2)
Ru(1)
Cl(1)
Cl(2)
C(11)
C(13)
C(12)
P(1)
C(14)
C(10)
C(15)
C(16)
C(17)
C(6)
C(9)
C(5)
N(1)
C(7)
C(8)
C(4)
C(1)
C(3)
C(2)

fashion through one donor atom only. In this way the chance factor is reduced to a degree since donor atoms are favourably positioned for coordination to other atoms. This approach has had a measure of success, particularly in the synthesis and characterisation of mixed Cu(I)-, Ag(I)-, Au(I)-, Hg(II)- and Rh(I)-Pt(II) acetylide complexes containing bridging dppm.[16,157,158] However, the results described below show that there are more criteria involved than simply the correct positioning of the atoms when phosphoruspyridyl and related ligands are utilised in such a fashion.

4.4.1 Using the metal-containing ligands [Ru(CO)$_4$(η^1-L)] (L = Ph$_2$Ppy [25] or Ph$_2$Pbipy [26]) and [Ru(CO)$_3$(η^1-L)$_2$] (L = Ph$_2$Ppy [28] or Ph$_2$Pbipy [29]) as precursors

Reaction of [Ru(CO)$_3$(η^1-Ph$_2$Ppy)$_2$] **[28]** with a half equivalent of [Rh$_2$(CO)$_4$(μ-Cl)$_2$] in CH_2Cl_2 for 24 hours at room temperature produced a purple-brown solution whose infra-red spectrum contained seven terminal carbonyl stretching bands at 2115(w), 2095(s), 2045(vs), 1994(vs), 1956(s), 1904(m) and 1807(vs). Addition of methanol to the resultant solution afforded a brown-red precipitate whose infra-red spectrum (KBr disk), in the CO stretching region, comprised solely of the band at 1807cm^{-1}. A $^{31}P\{^1H\}$ nmr spectrum (CD_2Cl_2) exhibited a doublet consistent with an AA'XX' spin system - a pair of equally intense doublets due to one-bond and two-bond rhodium-phosphorus coupling. Single crystals of the complex were grown from CH_2Cl_2/MeOH and the structure elucidated by means of X-ray crystallography. Cell parameters were : *Crystal System, Triclinic; Space group, P1; a = 10.000(3)Å; b = 12.579(3)Å; c = 13.878(4)Å; α = 93.18(2)°; β = 107.14(3)°; γ = 99.84(3)°; V = 1633.3(9)Å³; Z = 2.* These parameters correspond to those for the dirhodium complex [Rh$_2$(μ-CO)Cl$_2$(μ-Ph$_2$Ppy)$_2$], previously prepared by Balch *et al.*[86] and illustrated in section 1.5.3.b.i). Not only were both ligands abstracted from the ruthenium atom, but a metal-metal bond, not present in the [Rh$_2$(CO)$_4$(μ-Cl)$_2$] starting material, was formed between the rhodium atoms. Reaction of [Ru(CO)$_4$(η^1-Ph$_2$Ppy)] **[25]** with half an equivalent of [Rh$_2$(CO)$_4$(μ-Cl)$_2$] afforded the same product, only in lower yields.

Since a common feature to all known reactions of metal-containing ligands is their reaction with species containing one or more transition-metal halide bonds,[80,159] it was anticipated that reaction of the species [Ru(CO)$_4$(η^1-Ph$_2$Ppy)$_2$] **[25]** or [Ru(CO)$_3$(η^1-

$Ph_2Ppy)_2]$ **[28]** with transition metal halides would lead to desired products of the core formulation below.

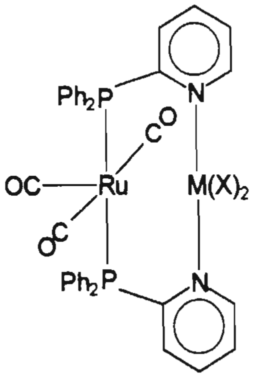

Reactions of **[28]** with one equivalent of $MCl_2.xH_2O$ (M = Mn, Co or Ni) in CH_2Cl_2/MeOH (3:1, vol:vol) mixtures were closely monitored by means of infra-red spectroscopy. The characteristic strong band at 1897cm^{-1} corresponding to the equivalent carbonyl ligands of **[28]** were replaced in a few hours by two sharp bands at 2064(vs) and 2002(vs)cm^{-1}. Reduction of the solvent volume under reduced pressure led to the precipitation of a white product which analysed for $[Ru(CO)_2Cl_2(\eta^1\text{-}Ph_2Ppy)_2]$ **[31]** (see infra-red assignment in Table 4.2). In this case, although the ligand was not stripped off the ruthenium atom, oxidation proceeded fairly effectively with the simultaneous loss of a carbonyl ligand and the coordination of two chloride ligands. Vigorous drying of the $MnCl_2.4H_2O$ compound did not appear to influence the reaction in any way; if anything, it increased the rate of oxidation. The reactions of **[25]** with these transition metal halides were also monitored. Once again, in all cases, all bands characteristic of the ruthenium(0) monomer (see Fig. 4.1) were replaced by two bands at *ca.* 2066(vs) and 2005(vs)cm^{-1}. The $^{31}P\{^1H\}$ nmr spectrum of the resultant product revealed a singlet corresponding to equivalent phosphorus atoms. Initial speculation was that this product was simply the analogous $[Ru(CO)_2Cl_2(\eta^1\text{-}Ph_2Ppy)_2]$ complex. However, an X-ray diffraction study of a single crystal, grown from hot 2-methoxyethanol, revealed the complex to be the known $[Ru(CO)_2Cl_2(\eta^2\text{-}Ph_2Ppy)]$,[76] containing a somewhat strained, chelating Ph_2Ppy ligand. Cell parameters were: *Crystal system, Orthorhombic; Space group,* $P2_12_12_1$; $a = 8.456(2)Å$; $b = 15.127(5)Å$; $c = 15.658(6)Å$, $V = 2003.0(11)Å^3$; $Z = 4$. These are similar to those determined for the compound by Balch *et al.*[76] The crystal structure is shown in Figure 1.10 a).

Addition of silver(I) salts ($AgPF_6$, $AgBF_4$ and $AgCF_3SO_3$) to both **[25]** and **[28]** in acetonitrile led to the immediate oxidation of the ruthenium complex with the deposition of silver metal.

The analogous ruthenium(0) species containing pendant Ph_2Pbipy ligands were reacted with metal precursors that would respond favourably to chelation of one (in the case of $[Ru(CO)_4(\eta^1\text{-}Ph_2Pbipy)]$ **[26]**) or two (in the case of $[Ru(CO)_3(\eta^1\text{-}Ph_2Pbipy)_2]$ **[29]**) bipyridyl moieties, *viz.* Ag(I) and Cu(I) species. Addition of these cations, it was hoped, would lead to species of the core stucture shown below.

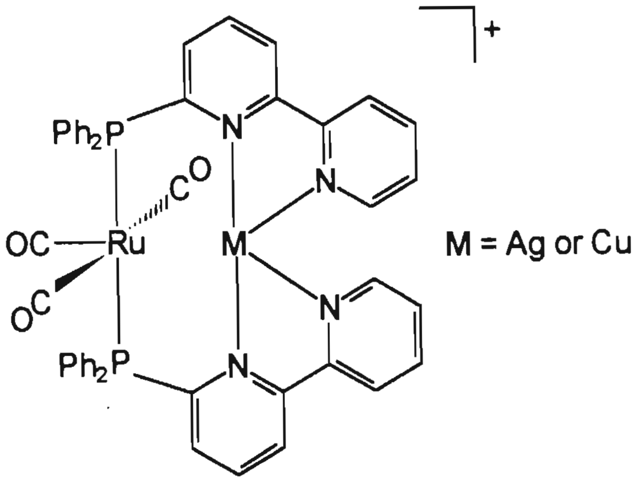

Addition of $AgPF_6$ or $AgSbF_6$ salts to **[26]** or **[29]** in acetonitrile in equimolar proportions caused immediate precipitation of silver metal accompanied by oxidation of the ruthenium complex. The same occured in CH_2Cl_2. Continous stirring at room temperature for 24 hours caused further precipitation of a silver mirror on the inside of the flask. Under identical conditions, the Cu(I) salt $[Cu(CH_3CN)_4](PF_6)$[160] was reacted with the ruthenium monomer, affording an orange solution from which the dimeric $[Cu_2(\mu\text{-}Ph_2Pbipy)_2(CH_3CN)_2](PF_6)_2$ was isolated by addition of diethyl ether. This previously synthesised complex [161] contains two copper(I) atoms bridged by two mutually trans Ph_2Pbipy ligands in a "head-to-tail" fashion. There is, however, no metal-metal bond present. Thus, as for the rhodium case described above, a stable ligand-bridged dimer has been formed at the expense of the complex that we wish to remain intact, through the systematic abstraction of the pendant Ph_2Pbipy ligands.

Reaction of **[26]** with equimolar quantities of $MCl_2.xH_2O$ (M = Mn or Co) under the same conditions as those for the Ph_2Ppy derivatives afforded the complex $[Ru(CO)_2(Cl)_2(\eta^1\text{-}Ph_2Pbipy)_2]$ **[32]** in the same way, characterised by the appearance of two equally intense terminal carbonyl bands at 2064(vs) and 2002(vs)cm^{-1} in its infra-red spectrum.

4.4.2 Using the metal-containing ligands $[Ru(CO)_2Cl_2(\eta^1\text{-}L)_2]$ (L = Ph_2Ppy [31] or Ph_2Pbipy [32]) as precursors.

In attempts to form mixed ruthenium(II)-silver(I) ligand-bridged complexes, one equivalent of $AgPF_6$ was added to solutions of $[Ru(CO)_2Cl_2(\eta^1\text{-}Ph_2Ppy)_2]$ **[31]** or $[Ru(CO)_2Cl_2(\eta^1\text{-}Ph_2Pbipy)_2]$ **[32]**. Immediate precipitation of AgCl occurred, corresponding to the abstraction of one chloride ligand from the relevant ruthenium complex. It was subsequently found that it was possible to abstract both chloride ligands through the addition of two equivalents of $AgPF_6$ under fairly vigorous conditions (i.e. refluxing acetonitrile). Once the AgCl was isolated by filtration, the pale yellow mother-liquors were treated with a further equivalent of $AgPF_6$ in the hope that the conditions were now favourable for the formation of a heteronuclear dimer, since it was apparent that the ligands were still attached to the ruthenium(II) atom. Instead, these reactions afforded two novel and interesting silver(I) dimers bridged by the respective ligand in a "head-to-tail" fashion, through the stepwise abstraction of the ligand, shown below.

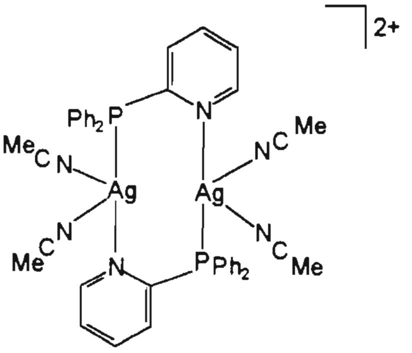

$[Ag_2(\mu\text{-}Ph_2Ppy)_2(CH_3CN)_4]^{2+}$

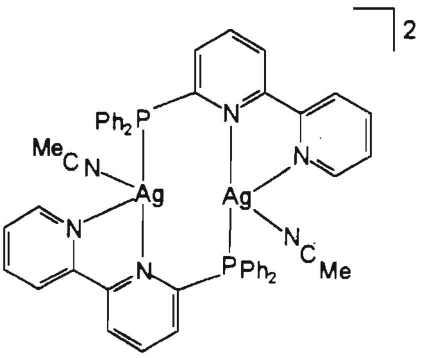

$[Ag_2(\mu\text{-}Ph_2Pbipy)_2(CH_3CN)_2]^{2+}$

These products were cleanly isolated after prolonged (15 hours) reaction at room temperature through reduction of solvent volume, addition of diethyl ether and cooling at -25°C for 2 hours.The novel Ph_2Ppy derivative is exactly analagous to that for the known copper complex [83] and has since been synthesised by alternative routes and its chemistry studied.[84] The Ph_2Pbipy derivative is even more interesting being more electron-rich and its synthesis from alternative precursors, as well as its chemistry, is reported in chapter five.

Likewise, reaction of the precursors **[31]** and **[32]** with $[Cu(CH_3CN)_4]PF_6$ afforded known dinuclear copper products of the form $[Cu_2(\mu\text{-}Ph_2Ppy)_2(CH_3CN)_4](PF_6)_2$ [83] and $[Cu_2(\mu\text{-}Ph_2Pbipy)_2(CH_3CN)_2](PF_6)_2$.[161] The only difference observed was that there was no initial precipitation of chloride salt.

4.5 Conclusion

With the ultimate object of making a series of heterodinuclear ligand-bridged compounds, a series of novel ruthenium(0) and ruthenium(II) monomeric complexes containing phosphoruspyridyl and phosphorusbipyridyl ligands bonded in a P-monodentate fashion have been successfully synthesised via a number of routes. In addition, some known complexes (**[28]** and **[31]**) have been resynthesised via more efficient, higher-yielding methods. The versatility of the $[Ru_3(CO)_{12}]$ complex has been demonstrated by the synthesis of the ruthenium(0) species mentioned above, either through the substitution of its photochemically generated $[Ru(CO)_5]$ derivative with the respective ligand or by direct interaction with the ligand under fairly forcing conditions.

The halide-bridged ruthenium(II) dimer $[Ru_2(\mu\text{-}Cl)_2(Cl)_2(CO)_6]$ has proved to be an excellent precursor for the synthesis of mononuclear ruthenium(II) complexes containing pendant phosphoruspyridyl or phosphorusbipyridyl ligands. The reactions proceed smoothly through the fissioning of the chloride bridges of the dimer with subsequent formation of the monomers in good yields.

All attempts to utilise these species as precursors for heterodinuclear ligand-bridged compound formation failed, however. Treatment of the ruthenium(0) precursors with silver salts effected immediate oxidation of the ruthenium atom, not surprising in view of the fact that silver(I) salts have been used in the past as oxidising agents for diruthenium(0) diphosphazane ligand-bridged species[162,163]. Oxidation also occurred upon reaction with transition metal chlorides, yielding octahedral ruthenium(II) monomers of the core structure shown by **[31]**, for example. In certain instances, abstraction of the relevant ligand from the monomeric complex occurred. The rhodium

(I) dimer $[Rh_2(CO)_4(\mu\text{-}Cl)_2]$ abstracted Ph_2Ppy from **[28]** to form a stable metal-metal bonded dirhodium(I) bridged species. Likewise, reaction of the ruthenium(II) precursors with Ag^+ and Cu^+ resulted in ligand abstraction and formation of the corresponding group 11 metal dimer. At the outset, the attempts to form heterodinuclear complexes from ruthenium(II) precursors containing pendant ligands would have been considered futile in view of the inherent electron deficiency on the ruthenium.

However, an important result that emerged during the course of these investigations was that silver(I) has a great affinity for phosphoruspyridyl and phosphorusbipyridyl ligands. An immediate priority was then to investigate the reactions of the Ph_2Pbipy ligand with appropriate silver(I) precursors in the hope that the complex cation $[Ag_2(\mu\text{-}Ph_2Pbipy)_2(CH_3CN)_2]^{2+}$ (see above diagram) could be directly synthesised and its chemistry extensively studied. These results are described in Chapter five.

4.6 Experimental

General experimental details and sources of chemicals are outlined in Appendices A and B respectively.

4.6.1 General synthesis of $[Ru(CO)_4(\eta^1\text{-}L)]$ (L = Ph_2Ppy [25] or Ph_2Pbipy [26])

Method 1: $[Ru(CO)_5]$ was prepared photochemically from $[Ru_3(CO)_{12}]$ in n-hexane through modification of a literature procedure. [146] A solution of $[Ru_3(CO)_{12}]$ (100mg ; 0.16mmol) in freshly distilled (Na wire) n-hexane ($300cm^3$) was purged with CO gas for 30 minutes to ensure complete deoxygenation. The solution was then irradiated with a high-pressure Hg lamp (580W) for 25 minutes, whilst maintaining the CO pressure, or until all the bands due to $[Ru_3(CO)_{12}]$ - 2065(vs), 2035(vs) and 2012(m) - were replaced by those due to $[Ru(CO)_5]$ - 2038(s) and 2002(vs). The yield was assumed to be quantitative. Following this, the lamp was switched off and the relevant amount of ligand (0.49mmol) was added as a solid under CO pressure. The resultant solution was stirred for 4 hours under a slow CO purge. During this time, the colour of the solution darkened slightly to yellow. In the case of **[25]**, the solvent was removed under reduced pressure to a small volume (1.0cm^3) the precipitate isolated by filtration, washed with cold n-hexane (3cm^3) and dried *in vacuo* for 1 hour.

Yield: 88%.

In the case of **[26]**, the solvent was removed completely under reduced pressure, affording the product as a pale yellow oil which crystallised partially at -25°C.

Yield: approx. 50%

Method 2: $[Ru_3(CO)_9(\eta^1\text{-}Ph_2Ppy)_3]$ was synthesised via the literature method [80] while its Ph_2Pbipy analogue **[27]** was synthesised in the identical manner. A quantity of the triruthenium species (0.15mmol) was dissolved in thf (15cm^3) and the purple solution purged with CO to ensure efficient deoxygenation (45 min.). Irradiation, whilst maintaining the CO purge, slowly changed to colour of the solution to yellow (~ 4 hours). The lamp was then switched off and the thf removed under reduced pressure. The oily residue was then washed with cold (0°C) n-hexane (5cm^3) to yield the beige powder (in the case of **[25]**), which was isolated by filtration, or the yellow oil (in the case of **[26]**), which was isolated by thorough washing (2 x 5cm^3 cold n-hexane aliquots).

Yield: **[25]** 59% , Yield: **[26]** approx. 40%

Method 3: Addition of freshly prepared sodium benzophenoneketyl (0.1cm^3) to a warm (40°C) thf solution (10cm^3) of the appropriate trinuclear ruthenium adduct (0.1mmol) caused the gradual conversion from the purple Ru_3 precursor to the desired tetracarbonyl monomer (12 hours). The work up was the same as for method 2.

Yield: **[25]** 51%, **[26]** approx. 22%.

4.6.2 General synthesis of $[Ru(CO)_3(\eta^1\text{-}L)_2]$ (L = Ph_2Ppy [28] or Ph_2Pbipy [29])

Method 1: A freshly distilled n-hexane solution (250cm^3) was thoroughly degassed by means of at least three freeze-pump-thaw cycles. $[Ru_3(CO)_{12}]$ (200mg; 0.31mmol) and the appropriate amount of ligand (1.9mmol) was then added as a solid and the resulting yellow solution purged with argon gas for 20 minutes to ensure thorough deoxygenation. The flask was then immersed in a glass bath containing a 2M $NaNO_2$ solution (λ_{cutoff} = 395nm) cooled by means of a glass concentric outer jacket through which tap water flowed. This ensured that the reaction temperature was maintained at approximately 25°C. Irradiation of the thoroughly stirred solution with a high-pressure

Hg lamp (580W) afforded the product as an off-white (**[28]**) or yellow-brown (**[29]**) solid after 5 hours. The product was filtered off under nitrogen, washed with a small amount of cold (0°C) n-hexane and dried *in vacuo* for 2 hours. Both products could be recrystallised from CH_2Cl_2/Et_2O at -25°C.

Yield: **[28]** 84%, **[29]** 36%.

Method 2 : A quantity of $[Ru(CO)_4(\eta^1\text{-}L)]$ (**[25]** or **[26]**) was prepared in the manner described in method 2 of section 4.6.1. To the resultant yellow solution was added an equivalent (per ruthenium atom) of the appropriate ligand as well as a quantity of freshly prepared sodium benzophenoneketyl catalyst ($0.25cm^3$). Gentle heating at 40°C produced an orange solution after approximately one hour. This solution was evaporated to dryness under reduced pressure and then redissolved in methanol ($3cm^3$). The solution was then left to stand at -25°C for 12 hours, affording pale yellow plates of the product, isolated by decanting the mother-liquor, washing the crystals with cold (-30°C) methanol ($2cm^3$) and drying *in vacuo* for an hour.

Yield : **[28]** 38% , **[29]** 24%

4.6.3 Synthesis of $[Ru(CO)Cl(\eta^2\text{-dppm})_2]$ $[Ru(CO)_3Cl_3]$ [30]

A suspension of the halide-bridged dimer $[Ru(CO)_3Cl_2]_2$ (120mg; 0.23mmol) and dppm (183mg; 0.46mmol) in toluene ($20cm^3$) was refluxed under nitrogen for 2 hours. The yellow precipitate which formed during this time was filtered off, washed with toluene ($5cm^3$) and diethyl ether ($10cm^3$) and dried *in vacuo* for 1 hour. Further product was isolated from the mother-liqour, through its evaporation under reduced pressure to *ca.* $2cm^3$. Allowing the solution to stand at room temperature for a day afforded crystalline products that were isolated in the manner described above.

Yield: 96%.

4.6.4 General synthesis of $[Ru(CO)_2Cl_2(\eta^1\text{-}L)_2]$ (L = Ph_2Ppy [31] or Ph_2Pbipy [32])

A suspension of the halide-bridged dimer $[Ru(CO)_3Cl_2]_2$ (100mg; 0.20mmol) and the appropriate ligand (0.8mmol) in toluene ($20cm^3$) was refluxed for 2 hours. The solution was then cooled to 0°C (ice-water bath) and the resultant pale yellow crystalline precipitate filtered quickly, washed with a cold (0°C) toluene ($2cm^3$) and dried *in vacuo* for 1 hour. More product was isolated from the filtrate through its evaporation under reduced pressure to *ca.* 2cm^3. The pale yellow material, isolated by cooling this solution to -25°C overnight, was collected in the fashion described above. Yield: **[31]** 78%, **[32]** 61%.

4.6.5 Single crystal X-ray diffraction study of [Ru(CO)Cl(η^2-dppm)$_2$][Ru(CO)$_3$Cl$_3$] [30]

A single pale yellow block-shaped crystal was grown from a hot saturated ethanol solution of the compound by slow cooling to room temperature. The general approach used for the intensity data collection is described in Appendix A. The crystallographic data are given in Table 4.3, the interatomic distances in Table 4.4, the interatomic angles in Table 4.5, the fractional coordinates in Table 4.6 and the anistropic thermal parameters in Table 4.7. The observed and calculated structure factors may be found on microfiche in an envelope fixed to the inside back cover.

Table 4.3

Crystal data and details of the crystallographic analysis for $[Ru(CO)Cl(\eta^2\text{-dppm})_2][Ru(CO)_3Cl_3]$

Formula	$Ru_2C_{54}H_{44}O_4P_4Cl_2$
Molecular Mass	1153.88
Crystal System	Monoclinic
Space Group	$P2_1/n$
a(Å)	13.322(3)
b(Å)	17.620(2)
c(Å)	26.644(3)
β(°)	104.704(7)
V($Å^3$)	5368.30
Z	4
D_c($g.cm^{-3}$)	1.428
F(000)	2328
λ(Mo-Kα)(Å)	0.71069
Scan mode	ω - 2θ
ω scan angle	$0.45 + 0.35\tan\theta$
Horizontal Aperture width (mm)	$2.7 + 0.1\tan\theta$
Scattering range (°)	$2 \leq \theta \leq 23$
μ (cm^{-1})	8.42
Absorption corrections	Semi empirical[103]
Measured intensities	8044
Unique intensities	6956
Unique intensities with [$I > 3\sigma(I)$]	5339
Structure solution	Direct Methods
Weighting scheme	$1/(\sigma^2(F) + 0.00052F^2)$
$R = \Sigma(F_o-F_c)/\Sigma F_o$	0.0672
$R_w = \Sigma_w½ (F_o-F_c)/ \Sigma_w½F_o$	0.0748
$(\Delta/\sigma)_{max}$	1.28
$\Delta\rho_{max}$($eÅ^{-3}$)	2.919
Number of parameters	323

Table 4.4 : Interatomic distances (Å) for $[Ru(CO)Cl(\eta^2\text{-dppm})_2][Ru(CO)_3Cl_3]$

Ru(1)-P(1)	2.376(3)	Ru(1)-P(2)	2.386(3)
Ru(1)-P(3)	2.401(3)	Ru(1)-P(4)	2.371(3)
Ru(1)-Cl(1)	2.432(3)	Ru(1)-C(51)	1.823(11)
P(1)-C(1)	1.811(10)	P(1)-C(7)	1.832(10)
P(1)-C(13)	1.860(10)	P(2)-C(13)	1.862(10)
P(2)-C(14)	1.826(10)	P(2)-C(20)	1.819(10)
P(3)-C(26)	1.806(11)	P(3)-C(32)	1.815(11)
P(3)-C(38)	1.854(12)	P(4)-C(38)	1.843(12)
P(4)-C(39)	1.827(12)	P(4)-C(45)	1.812(10)
O(1)-C(51)	1.143(12)	C(1)-C(2)	1.382(15)
C(1)-C(6)	1.387(15)	C(2)-C(3)	1.42(2)
C(3)-C(4)	1.32(2)	C(4)-C(5)	1.39(2)
C(5)-C(6)	1.47(2)	C(7)-C(8)	1.37(2)
C(7)-C(12)	1.36(2)	C(8)-C(9)	1.44(2)
C(9)-C(10)	1.37(2)	C(10)-C(11)	1.42(2)
C(11)-C(12)	1.42(2)	C(14)-C(15)	1.38(2)
C(14)-C(19)	1.34(2)	C(15)-C(16)	1.41(2)
C(16)-C(17)	1.38(2)	C(17)-C(18)	1.41(2)
C(18)-C(19)	1.49(2)	C(20)-C(21)	1.37(2)
C(20)-C(25)	1.400(15)	C(21)-C(22)	1.42(2)
C(22)-C(23)	1.41(2)	C(23)-C(24)	1.35(2)
C(24)-C(25)	1.42(2)	C(26)-C(27)	1.39(2)
C(26)-C(31)	1.390(15)	C(27)-C(28)	1.43(2)
C(28)-C(29)	1.42(2)	C(29)-C(30)	1.38(2)
C(30)-C(31)	1.44(2)	C(32)-C(33)	1.392(15)
C(32)-C(37)	1.40(2)	C(33)-C(34)	1.39(2)
C(34)-C(35)	1.25(3)	C(35)-C(36)	1.46(3)
C(36)-C(37)	1.47(2)	C(39)-C(40)	1.42(2)
C(39)-C(44)	1.35(2)	C(40)-C(41)	1.42(2)
C(41)-C(42)	1.37(2)	C(42)-C(43)	1.33(2)
C(43)-C(44)	1.48(2)	C(45)-C(46)	1.379(15)
C(45)-C(50)	1.40(2)	C(46)-C(47)	1.43(2)
C(47)-C(48)	1.40(2)	C(48)-C(49)	1.40(2)
C(49)-C(50)	1.46(2)	Ru(2)-Cl(2)	2.396(3)
Ru(2)-Cl(3)	2.424(3)	Ru(2)-Cl(4)	2.404(3)

Table 4.4 / cont.

Ru(2)-C(52)	1.864(14)	Ru(2)-C(53)	1.864(15)
Ru(2)-C(54)	1.829(14)	O(2)-C(52)	1.14(2)
O(3)-C(53)	1.16(2)	O(4)-C(54)	1.163(15)

Table 4.5 : Interatomic angles (°) for [Ru(CO)Cl(η^2-dppm)$_2$][Ru(CO)$_3$Cl$_3$]

P(1)-Ru(1)-P(2)	70.1(1)	P(1)-Ru(1)-P(3)	172.5(1)
P(2)-Ru(1)-P(3)	112.7(1)	P(1)-Ru(1)-P(4)	105.9(1)
P(2)-Ru(1)-P(4)	169.4(1)	P(3)-Ru(1)-P(4)	70.1(1)
P(1)-Ru(1)-Cl(1)	88.8(1)	P(2)-Ru(1)-Cl(1)	83.8(1)
P(3)-Ru(1)-Cl(1)	84.6(1)	P(4)-Ru(1)-Cl(1)	86.3(1)
P(1)-Ru(1)-C(51)	92.9(3)	P(2)-Ru(1)-C(51)	92.5(3)
P(3)-Ru(1)-C(51)	94.0(3)	P(4)-Ru(1)-C(51)	97.7(3)
Cl(1)-Ru(1)-C(51)	175.1(3)	Ru(1)-P(1)-C(1)	116.5(3)
Ru(1)-P(1)-C(7)	127.2(3)	C(1)-P(1)-C(7)	102.2(5)
Ru(1)-P(1)-C(13)	94.1(3)	C(1)-P(1)-C(13)	108.9(5)
C(7)-P(1)-C(13)	106.3(5)	Ru(1)-P(2)-C(13)	93.7(3)
Ru(1)-P(2)-C(14)	125.1(3)	C(13)-P(2)-C(14)	107.3(5)
Ru(1)-P(2)-C(20)	119.0(3)	C(13)-P(2)-C(20)	106.4(5)
C(14)-P(2)-C(20)	103.1(5)	Ru(1)-P(3)-C(26)	126.7(4)
Ru(1)-P(3)-C(32)	116.4(4)	C(26)-P(3)-C(32)	104.3(5)
Ru(1)-P(3)-C(38)	92.3(4)	C(26)-P(3)-C(38)	106.5(5)
C(32)-P(3)-C(38)	108.5(5)	Ru(1)-P(4)-C(38)	93.5(4)
Ru(1)-P(4)-C(39)	123.4(4)	C(38)-P(4)-C(39)	104.4(5)
Ru(1)-P(4)-C(45)	120.0(4)	C(38)-P(4)-C(45)	109.4(5)
C(39)-P(4)-C(45)	103.8(5)	P(1)-C(1)-C(2)	117.2(8)
P(1)-C(1)-C(6)	122.2(8)	C(2)-C(1)-C(6)	120.5(10
C(1)-C(2)-C(3)	120.8(11)	C(2)-C(3)-C(4)	118.6(13
C(3)-C(4)-C(5)	124(2)	C(4)-C(5)-C(6)	116.9(13
C(1)-C(6)-C(5)	118.4(11)	P(1)-C(7)-C(8)	120.1(8)
P(1)-C(7)-C(12)	118.7(9)	C(8)-C(7)-C(12)	121.2(11
C(7)-C(8)-C(9)	119.7(12)	C(8)-C(9)-C(10)	120.2(13
C(9)-C(10)-C(11)	119.1(14)	C(10)-C(11)-C(12)	120(2)
C(7)-C(12)-C(11)	120.0(13)	P(1)-C(13)-P(2)	94.6(5)
P(2)-C(14)-C(15)	120.5(9)	P(2)-C(14)-C(19)	117.3(10
C(15)-C(14)-C(19)	121.9(12)	C(14)-C(15)-C(16)	121(2)
C(15)-C(16)-C(17)	120(2)	C(16)-C(17)-C(18)	120(2)
C(17)-C(18)-C(19)	118(2)	C(14)-C(19)-C(18)	119(2)
P(2)-C(20)-C(21)	118.7(9)	P(2)-C(20)-C(25)	120.2(8)
C(21)-C(20)-C(25)	121.0(11)	C(20)-C(21)-C(22)	119.4(12
C(21)-C(22)-C(23)	119.5(14)	C(22)-C(23)-C(24)	120.6(14

Table 4.5 / cont.

C(23)-C(24)-C(25)	120.6(14)	C(20)-C(25)-C(24)	118.8(11
P(3)-C(26)-C(27)	120.4(9)	P(3)-C(26)-C(31)	119.0(9)
C(27)-C(26)-C(31)	120.4(11)	C(26)-C(27)-C(28)	120.1(13
C(27)-C(28)-C(29)	119(2)	C(28)-C(29)-C(30)	122(2)
C(29)-C(30)-C(31)	118.8(13)	C(26)-C(31)-C(30)	120.6(11
P(3)-C(32)-C(33)	117.4(9)	P(3)-C(32)-C(37)	122.2(9)
C(33)-C(32)-C(37)	120.3(11)	C(32)-C(33)-C(34)	121.7(11
C(33)-C(34)-C(35)	118(2)	C(34)-C(35)-C(36)	126(2)
C(35)-C(36)-C(37)	114(2)	C(32)-C(37)-C(36)	117.8(12
P(3)-C(38)-P(4)	95.6(5)	P(4)-C(39)-C(40)	117.1(10
P(4)-C(39)-C(44)	121.6(10)	C(40)-C(39)-C(44)	121.3(13
C(39)-C(40)-C(41)	117(2)	C(40)-C(41)-C(42)	121(2)
C(41)-C(42)-C(43)	124(2)	C(42)-C(43)-C(44)	116(2)
C(39)-C(44)-C(43)	120.6(13)	P(4)-C(45)-C(46)	122.6(8)
P(4)-C(45)-C(50)	116.2(8)	C(46)-C(45)-C(50)	121.1(10
C(45)-C(46)-C(47)	120.8(11)	C(46)-C(47)-C(48)	119.2(13
C(47)-C(48)-C(49)	120.8(14)	C(48)-C(49)-C(50)	119.1(14
C(45)-C(50)-C(49)	118.9(12)	Ru(1)-C(51)-O(1)	178.2(9)
Cl(2)-Ru(2)-Cl(3)	92.9(1)	Cl(2)-Ru(2)-Cl(4)	90.4(1)
Cl(3)-Ru(2)-Cl(4)	93.0(1)	Cl(2)-Ru(2)-C(52)	177.6(4)
Cl(3)-Ru(2)-C(52)	85.0(4)	Cl(4)-Ru(2)-C(52)	88.3(4)
Cl(2)-Ru(2)-C(53)	85.7(4)	Cl(3)-Ru(2)-C(53)	178.5(4)
Cl(4)-Ru(2)-C(53)	86.6(4)	C(52)-Ru(2)-C(53)	96.4(6)
Cl(2)-Ru(2)-C(54)	87.5(4)	Cl(3)-Ru(2)-C(54)	86.8(4)
Cl(4)-Ru(2)-C(54)	177.9(4)	C(52)-Ru(2)-C(54)	93.7(6)
C(53)-Ru(2)-C(54)	93.6(6)	Ru(2)-C(52)-O(2)	176.8(13
Ru(2)-C(53)-O(3)	174.3(13)	Ru(2)-C(54)-O(4)	179.0(12

Table 4.6 : Fractional coordinates (x 10^4) and isotropic thermal factors (Å^2, x10^3) for [Ru(CO)Cl(η^2-dppm)$_2$][Ru(CO)$_3$Cl$_3$]

	x/a	y/b	z/c	U_{eq}
Ru(1)	6130(1)	150(1)	8097(1)	31(1)
P(1)	6939(2)	1218(2)	8639(1)	33(1)
P(2)	5219(2)	1280(1)	7717(1)	33(1)
P(3)	5516(2)	-944(2)	7504(1)	42(1)
P(4)	7282(2)	-883(2)	8400(1)	41(1)
Cl(1)	7108(2)	408(2)	7378(1)	47(1)
O(1)	4772(6)	-105(5)	8897(4)	63(2)*
C(1)	6551(7)	1438(5)	9301(4)	39(2)*
C(2)	6651(9)	869(7)	9714(5)	54(3)*
C(3)	6431(10)	1008(8)	10262(6)	69(3)*
C(4)	6066(11)	1681(9)	10355(6)	84(4)*
C(5)	5984(11)	2296(9)	9979(7)	80(4)*
C(6)	6220(9)	2157(7)	9412(5)	59(3)*
C(7)	8327(7)	1442(5)	8848(4)	39(2)*
C(8)	8796(10)	1651(7)	9408(5)	64(3)*
C(9)	9874(10)	1863(8)	9561(6)	72(4)*
C(10)	10444(11)	1809(8)	9157(6)	77(4)*
C(11)	9942(13)	1596(10)	8577(7)	93(5)*
C(12)	8875(11)	1385(8)	8437(6)	75(4)*
C(13)	6325(8)	1912(6)	8063(4)	39(2)*
C(14)	4808(7)	1532(6)	6943(4)	38(2)*
C(15)	4850(11)	2275(9)	6767(7)	79(4)*
C(16)	4464(14)	2478(10)	6176(8)	105(5)*
C(17)	4026(12)	1933(9)	5766(7)	88(4)*
C(18)	3897(15)	1185(11)	5946(9)	119(6)*
C(19)	4384(13)	983(10)	6567(7)	93(5)*
C(20)	4129(8)	1582(6)	7995(4)	40(2)*
C(21)	3331(10)	1083(7)	7971(6)	66(3)*
C(22)	2472(12)	1311(9)	8182(7)	84(4)*
C(23)	2439(11)	2053(8)	8397(6)	82(4)*
C(24)	3223(11)	2544(8)	8411(6)	75(4)*
C(25)	4086(9)	2325(7)	8198(5)	54(3)*
C(26)	5084(8)	-973(6)	6716(5)	47(3)*
C(27)	5797(10)	-913(8)	6377(6)	70(4)*

Table 4.6 / cont.

C(28)	5443(13)	-899(9)	5751(7)	94(5)*
C(29)	4355(12)	-906(9)	5491(7)	89(5)*
C(30)	3649(11)	-974(8)	5824(6)	75(4)*
C(31)	4025(9)	-993(7)	6453(5)	56(3)*
C(32)	4610(8)	-1552(6)	7748(4)	44(3)*
C(33)	3702(9)	-1221(7)	7821(5)	55(3)*
C(34)	2954(10)	-1642(8)	7996(6)	66(3)*
C(35)	3060(20)	-2345(16)	8027(12)	282(10)*
C(36)	4023(12)	-2761(9)	8067(7)	87(4)*
C(37)	4805(10)	-2322(7)	7867(5)	63(3)*
C(38)	6815(9)	-1397(6)	7704(5)	53(3)*
C(39)	7150(9)	-1566(7)	8958(5)	53(3)*
C(40)	7583(12)	-2299(9)	8934(7)	85(4)*
C(41)	7431(14)	-2837(11)	9351(8)	112(6)*
C(42)	6960(13)	-2635(11)	9779(8)	105(5)*
C(43)	6608(13)	-1938(10)	9837(7)	101(5)*
C(44)	6687(10)	-1380(8)	9383(6)	73(4)*
C(45)	8670(8)	-738(6)	8543(4)	40(2)*
C(46)	9182(9)	-726(7)	8104(5)	58(3)*
C(47)	10267(10)	-564(8)	8232(6)	70(4)*
C(48)	10807(12)	-398(9)	8810(7)	85(4)*
C(49)	10304(11)	-419(8)	9264(7)	83(4)*
C(50)	9196(10)	-585(7)	9126(6)	67(3)*
C(51)	5298(8)	-19(6)	8589(4)	41(3)*
Ru(2)	107(1)	125(1)	3804(1)	46(1)
Cl(2)	-1430(3)	302(3)	3029(2)	86(1)
Cl(3)	1045(3)	1109(2)	3436(1)	60(1)
Cl(4)	-538(3)	997(2)	4410(1)	71(1)
O(2)	2058(9)	10(6)	4775(5)	107(4)*
O(3)	-1187(8)	-1058(6)	4214(5)	98(3)*
O(4)	860(9)	-943(6)	3018(5)	100(3)*
C(52)	1313(11)	31(7)	4405(6)	67(4)*
C(53)	-646(11)	-621(8)	4075(6)	72(4)*
C(54)	559(10)	-528(8)	3320(6)	65(3)*

* isotropic temperature factor.

$$U_{eq} = \frac{1}{3} \Sigma_i \Sigma_j U_{ij} a_i^* a_j^* (a_i . a_j)$$

Table 4.7 : Anisotropic thermal factors ($Å^2$, x10^3) for $[Ru(CO)Cl(\eta^2\text{-dppm})_2][Ru(CO)_3Cl_3]$

	U(11)	U(22)	U(33)	U(23)	U(13)	U(12)
Ru(1)	26(1)	33(1)	32(1)	1(1)	5(1)	0(1)
P(1)	27(1)	39(1)	32(1)	-1(1)	8(1)	-1(1)
P(2)	27(1)	35(1)	37(1)	3(1)	7(1)	-1(1)
P(3)	36(1)	38(2)	46(2)	-3(1)	1(1)	1(1)
P(4)	35(1)	40(2)	43(2)	2(1)	3(1)	7(1)
Cl(1)	43(1)	59(2)	43(2)	-2(1)	17(1)	-1(1)
Ru(2)	49(1)	45(1)	43(1)	2(1)	9(1)	1(1)
Cl(2)	56(2)	139(4)	54(2)	10(2)	-2(2)	-2(2)
Cl(3)	75(2)	43(2)	68(2)	0(1)	29(2)	-3(1)
Cl(4)	90(2)	70(2)	59(2)	-2(2)	29(2)	18(2)

4.6.6 Single crystal X-ray diffraction study of [Ru(CO)$_2$Cl$_2$(η^1-Ph$_2$Ppy)$_2$] [31]

A colourless block-shaped crystal was grown by slow evaporation of a saturated acetonitrile solution of the complex. The general approach used for the intensity data collection is described in Appendix A. All aromatic rings were refined originally as rigid phenyl groups so that tentative assignments for the nitrogen atoms could later be made.The nitrogen atoms were assigned as they are since (i) their temperature factors as carbon atoms were lower than any of those for the corresponding carbon atoms on the other rings and (ii) the C-N bond distances were more correct for these assignments than for any other. The crystallographic data are given in Table 4.8, the interatomic distances in Table 4.9, the interatomic angles in Table 4.10, the fractional coordinates in Table 4.11 and the anistropic thermal parameters in Table 4.12. The observed and calculated structure factors may be found on microfiche in an envelope fixed to the inside back cover.

Table 4.8

Crystal data and details of the crystallographic analysis for $[Ru(CO)_2Cl_2(\eta^1\text{-}Ph_2Ppy)_2]$

Formula	$RuC_{36}H_{28}N_2O_2P_2Cl_2$
Molecular Mass	754.55
Crystal System	Orthorhombic
Space Group	Pbca
a(Å)	16.493(2)
b(Å)	21.134(5)
c(Å)	19.537(5)
V(Å^3)	6809.90
Z	8
D_c(g.cm^{-3})	1.472
F(000)	3056
λ(Mo-Kα)(Å)	0.71069
Scan mode	ω - 2θ
ω scan angle	$0.55 + 0.35\tan\theta$
Horizontal Aperture width (mm)	$2.7 + 0.1\tan\theta$
Scattering range (°)	$2 \leq \theta \leq 23$
μ (cm^{-1})	7.37
Absorption corrections	Semi empirical[103]
Measured intensities	5241
Unique intensities	4314
Unique intensities with $[I > 3\sigma(I)]$	2836
Structure solution	Direct & Fourier Methods
Weighting scheme	$1/(\sigma^2(F) + 0.00054F^2)$
$R = \Sigma(F_o\text{-}F_c)/\Sigma F_o$	0.1098
$R_w = \Sigma_w ½ (F_o\text{-}F_c)/ \Sigma_w ½ F_o$	0.1198
$(\Delta/\sigma)_{max}$	1.94
$\Delta\rho_{max}$(eÅ^{-3})	0.936
Number of parameters	206

Table 4.9 : Interatomic distances (Å) for [$Ru(CO)_2Cl_2(\eta^1\text{-}Ph_2Ppy)_2$]

Ru(1)-P(1)	2.414(8)	Ru(1)-P(2)	2.420(8)
Ru(1)-Cl(1)	2.421(5)	Ru(1)-Cl(2)	2.446(5)
Ru(1)-C(35)	1.81(2)	Ru(1)-C(36)	1.83(3)
P(1)-C(5)	1.79(2)	P(1)-C(6)	1.80(2)
P(1)-C(12)	1.82(2)	P(2)-C(22)	1.82(2)
P(2)-C(23)	1.82(2)	P(2)-C(29)	1.78(2)
N(1)-C(1)	1.42(3)	N(1)-C(5)	1.36(3)
N(2)-C(18)	1.41(3)	N(2)-C(22)	1.36(3)
O(1)-C(35)	1.13(2)	O(2)-C(36)	1.17(3)
C(1)-C(2)	1.38(3)	C(2)-C(3)	1.41(3)
C(3)-C(4)	1.43(3)	C(4)-C(5)	1.52(3)
C(6)-C(7)	1.34(3)	C(6)-C(11)	1.43(3)
C(7)-C(8)	1.48(3)	C(8)-C(9)	1.42(4)
C(9)-C(10)	1.37(4)	C(10)-C(11)	1.31(3)
C(12)-C(13)	1.44(3)	C(13)-C(14)	1.37(3)
C(14)-C(15)	1.39(4)	C(15)-C(16)	1.35(4)
C(18)-C(19)	1.36(3)	C(19)-C(20)	1.35(3)
C(20)-C(21)	1.41(3)	C(21)-C(22)	1.42(3)
C(23)-C(24)	1.37(3)	C(23)-C(28)	1.39(3)
C(24)-C(25)	1.47(4)	C(25)-C(26)	1.31(4)
C(26)-C(27)	1.50(4)	C(27)-C(28)	1.55(4)
C(29)-C(30)	1.35(3)	C(29)-C(34)	1.36(3)
C(30)-C(31)	1.43(3)	C(31)-C(32)	1.29(3)
C(32)-C(33)	1.40(4)	C(33)-C(34)	1.39(4)

Table 4.10 : Interatomic angles (°) for $[Ru(CO)_2Cl_2(\eta^1\text{-}Ph_2Ppy)_2]$

P(1)-Ru(1)-P(2)	173.9(3)	P(1)-Ru(1)-Cl(1)	88.3(2
P(2)-Ru(1)-Cl(1)	86.6(2)	P(1)-Ru(1)-Cl(2)	89.3(2
P(2)-Ru(1)-Cl(2)	94.4(2)	Cl(1)-Ru(1)-Cl(2)	94.1(2
P(1)-Ru(1)-C(35)	89.9(7)	P(2)-Ru(1)-C(35)	86.9(7
Cl(1)-Ru(1)-C(35)	91.4(7)	Cl(2)-Ru(1)-C(35)	174.4(7
P(1)-Ru(1)-C(36)	92.8(8)	P(2)-Ru(1)-C(36)	92.5(8
Cl(1)-Ru(1)-C(36)	176.9(7)	Cl(2)-Ru(1)-C(36)	83.0(7
C(35)-Ru(1)-C(36)	91.5(10)	Ru(1)-P(1)-C(5)	118.8(7
Ru(1)-P(1)-C(6)	114.4(7)	C(5)-P(1)-C(6)	102.5(1
Ru(1)-P(1)-C(12)	110.9(7)	C(5)-P(1)-C(12)	102.8(1
C(6)-P(1)-C(12)	106.1(10)	Ru(1)-P(2)-C(22)	120.3(7
Ru(1)-P(2)-C(23)	111.2(7)	C(22)-P(2)-C(23)	102.8(9
Ru(1)-P(2)-C(29)	114.0(8)	C(22)-P(2)-C(29)	100.9(1
C(23)-P(2)-C(29)	106.1(10)	C(1)-N(1)-C(5)	123(2)
C(18)-N(2)-C(22)	120(2)	N(1)-C(1)-C(2)	120(2)
C(1)-C(2)-C(3)	119(2)	C(2)-C(3)-C(4)	123(2)
C(3)-C(4)-C(5)	115(2)	P(1)-C(5)-N(1)	125(2)
P(1)-C(5)-C(4)	115.6(14)	N(1)-C(5)-C(4)	119(2)
P(1)-C(6)-C(7)	124(2)	P(1)-C(6)-C(11)	114(2)
C(7)-C(6)-C(11)	121(2)	C(6)-C(7)-C(8)	122(2)
C(7)-C(8)-C(9)	113(3)	C(8)-C(9)-C(10)	122(3)
C(9)-C(10)-C(11)	124(3)	C(6)-C(11)-C(10)	117(2)
P(1)-C(12)-C(13)	116(2)	C(12)-C(13)-C(14)	122(2)
C(13)-C(14)-C(15)	118(3)	C(14)-C(15)-C(16)	121(3)
N(2)-C(18)-C(19)	121(2)	C(18)-C(19)-C(20)	120(3)
C(19)-C(20)-C(21)	121(2)	C(20)-C(21)-C(22)	118(2)
P(2)-C(22)-N(2)	122(2)	P(2)-C(22)-C(21)	118(2)
N(2)-C(22)-C(21)	120(2)	P(2)-C(23)-C(24)	117(2)
P(2)-C(23)-C(28)	120(2)	C(24)-C(23)-C(28)	123(2)
C(23)-C(24)-C(25)	121(2)	C(24)-C(25)-C(26)	121(3)
C(25)-C(26)-C(27)	122(3)	C(26)-C(27)-C(28)	116(3)
C(23)-C(28)-C(27)	117(3)	P(2)-C(29)-C(30)	129(2)
P(2)-C(29)-C(34)	115(2)	C(30)-C(29)-C(34)	116(2)
C(29)-C(30)-C(31)	124(2)	C(30)-C(31)-C(32)	118(2)
C(31)-C(32)-C(33)	121(3)	C(32)-C(33)-C(34)	119(3)

Table 4.10 / cont.

C(29)-C(34)-C(33)	122(3)	Ru(1)-C(35)-O(1)	177(2)
Ru(1)-C(36)-O(2)	175(2)		

Table 4.11 : Fractional coordinates (x 10^4) and isotropic thermal factors ($Å^2$, x10^3) for [Ru(CO)$_2$Cl$_2$(η^1-Ph$_2$Ppy)$_2$]

	x/a	y/b	z/c	U_{eq}
Ru(1)	3534(1)	1334(1)	997(1)	41(1)
P(1)	2644(4)	463(3)	728(4)	0(2)
P(2)	4326(5)	2279(3)	1204(4)	0(2)
N(1)	1484(13)	680(9)	1750(10)	54(5)*
N(2)	3587(15)	2636(11)	2433(13)	74(7)*
Cl(1)	2350(3)	2008(2)	1071(3)	54(1)
Cl(2)	3484(4)	1026(3)	2204(3)	67(1)
O(1)	3680(11)	1604(9)	-474(10)	97(6)*
O(2)	5019(14)	518(11)	1043(11)	128(8)*
C(1)	710(15)	619(11)	2056(12)	69(7)*
C(2)	101(13)	291(10)	1727(11)	62(6)*
C(3)	266(15)	-7(12)	1094(12)	73(7)*
C(4)	1029(14)	54(11)	748(12)	66(6)*
C(5)	1671(11)	429(9)	1128(9)	47(5)*
C(6)	3057(12)	-305(9)	913(10)	49(5)*
C(7)	2752(13)	-705(10)	1381(11)	61(6)*
C(8)	3138(18)	-1319(13)	1533(15)	95(9)*
C(9)	3866(18)	-1413(14)	1162(15)	96(9)*
C(10)	4122(18)	-997(15)	666(15)	96(9)*
C(11)	3787(14)	-447(12)	552(12)	70(7)*
C(12)	2393(12)	456(9)	-179(10)	50(5)*
C(13)	1899(15)	971(12)	-421(12)	73(7)*
C(14)	1662(16)	1014(14)	-1091(14)	90(8)*
C(15)	1876(19)	523(15)	-1532(16)	101(9)*
C(16)	2385(22)	59(17)	-1331(17)	125(11)*
C(17)	2319(16)	2(13)	4387(14)	87(8)*
C(18)	3439(16)	3060(13)	2975(13)	83(7)*
C(19)	3774(14)	3650(12)	2971(12)	74(7)*
C(20)	4217(16)	3845(12)	2429(14)	84(8)*
C(21)	4393(15)	3436(11)	1881(12)	72(7)*
C(22)	4042(12)	2822(9)	1889(10)	48(5)*
C(23)	4342(12)	2788(9)	454(9)	47(5)*
C(24)	3676(15)	3158(12)	348(13)	80(7)*
C(25)	3604(19)	3550(14)	-273(16)	105(10)*

UNIVERSITY OF NATAL LIBRARY

PIETERMARITZBURG

Donation accepted for stock. Please input as an order and forward for accessioning and receipting.

Supplier DONATN

Vote CHEM

SAPSE number /5

Provenance

9505/2832

Special bookplate
required?

Any other instructions

Initials

Table 4.11 / cont.

C(26)	4175(21)	3540(16)	-740(17)	111(10)*
C(27)	4968(21)	3211(16)	-622(17)	121(11)*
C(28)	5015(18)	2793(14)	28(15)	97(9)*
C(29)	5361(12)	2127(10)	1415(10)	55(6)*
C(30)	5743(14)	2215(10)	2019(11)	64(6)*
C(31)	6573(16)	2060(12)	2136(12)	78(7)*
C(32)	6971(17)	1786(14)	1651(15)	96(9)*
C(33)	6584(20)	1616(16)	1042(17)	115(10)*
C(34)	5803(15)	1836(12)	918(12)	76(7)*
C(35)	3645(12)	1502(10)	94(11)	54(6)*
C(36)	4436(15)	828(11)	992(12)	68(6)*

* isotropic temperature factor.

$$U_{eq} = \frac{1}{3} \Sigma_i \Sigma_j U_{ij} a_i^* a_j^* (a_i . a_j)$$

Table 4.12 : Anisotropic thermal factors ($Å^2$, x10^3) for $[Ru(CO)_2Cl_2(\eta^1\text{-}Ph_2Ppy)_2]$

	U(11)	U(22)	U(33)	U(23)	U(13)	U(12)
Ru(1)	40(1)	40(1)	43(1)	-2(1)	0(1)	3(1)
P(1)	0(4)	0(4)	0(4)	-3(3)	5(3)	-3(4)
P(2)	0(4)	0(4)	0(4)	-5(3)	-1(3)	2(3)
Cl(1)	45(3)	49(3)	68(3)	-2(3)	1(3)	5(2)
Cl(2)	77(4)	73(4)	49(3)	9(3)	-6(3)	7(3)

CHAPTER FIVE

DINUCLEAR Ph_2Pbipy LIGAND-BRIDGED DERIVATIVES OF SILVER(I)

5.1 Introduction

While many studies of the coordination behaviour of neutral nitrogen and phosphorus donor ligands towards various silver(I) precursors have been conducted, only a small number of them have been concerned with bidentate phosphine ligands. This is surprising in the light of the fact that bidentate phosphines have been reacted with a wide range of other metals and also that there are many suitable silver starting materials, available through simple synthetic procedures or from commercial sources.

Bau *et al.*[28] have synthesised the neutral nitrate complex $[Ag_2(\mu\text{-dppm})_2(NO_3)_2]$, which contains two bridging dppm ligands trans disposed with respect to each other. Also coordinated to each silver atom is a nitrate anion, each bonded to the silver atom in an asymmetric, bidentate fashion through two of its oxygen atoms.

Schmidbaur *et al.*[164] have revealed that reaction of 2-diphenylphosphinopyridine with AgCl affords the tetrameric complex $[Ag(\mu\text{-Cl})(\eta^1\text{-}Ph_2Ppy)]_4$. An X-ray diffraction analysis of the crystal and molecular structure of this compound confirms that the Ph_2Ppy ligands are bonded to Ag atom through the P atoms only *i.e.* in a pendant fashion.

This chapter describes the synthesis of a range of Ph_2Pbipy ligand-bridged derivatives of silver(I) and their reactions with a range of anionic and neutral donor ligands.

5.2 Reactions of Ph_2Pbipy with silver(I) precursors

A detailed literature study has revealed two excellent tetrahedral silver(I) precursors; $[Ag(NCMe)_4]ClO_4$ [165], isostructural with $[Cu(NCMe)_4]ClO_4$ [166], and $[Ag(1,5\text{-cod})_2]BF_4$.[167] The latter compound, although more difficult to synthesise, proved easier to use, being more readily isolated at room temperature in contrast to the former complex. Significantly, it also gave better yields of product.

5.2.1 Synthesis of $[Ag_2(\mu\text{-}Ph_2Pbipy)_2(NCMe)_2](PF_6)_2$ [33]

Reaction of either $[Ag(NCMe)_4]X$ or $[Ag(1,5\text{-cod})_2]X$ ($X = PF_6^-$, BF_4^- of ClO_4^-) with an equimolar quantity of Ph_2Pbipy in acetonitrile was found to afford, in reasonable yield, the novel homobimetallic complex $[Ag_2(\mu\text{-}Ph_2Pbipy)_2(NCMe)_2](PF_6)_2$ **[33]** according to Scheme 5.1. The reaction involving $[Ag(1,5\text{-cod})_2]X$ can be performed at room temperature, whereas that with the tetra-acetonitrile adduct needs to be carried out at -15°C, since $[Ag(NCMe)_4]X$ is only stable at this temperature. As a result, the former reaction generally gives better yields.

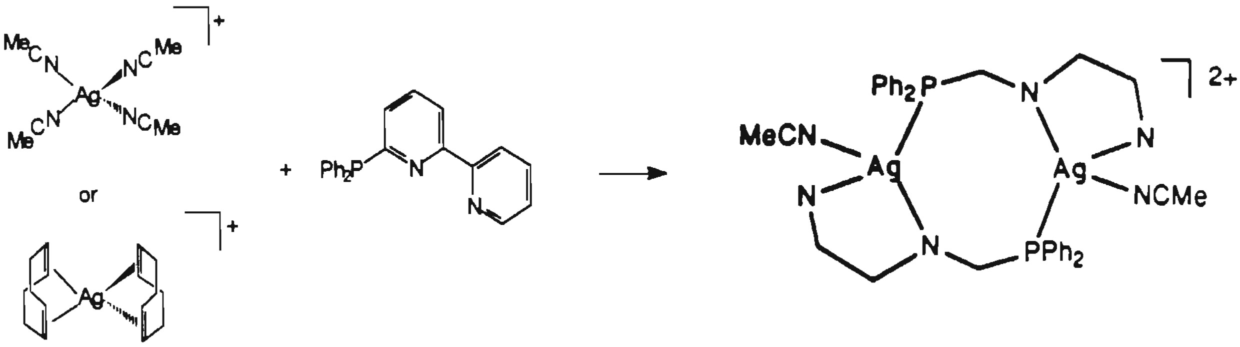

Scheme 5.1 Synthesis of $[Ag_2(\mu\text{-}Ph_2Pbipy)_2(NCMe)_2]X_2$

The product is an air-stable, moderately light-sensitive, pale yellow crystalline material soluble in most organic solvents but insoluble in diethyl ether, toluene and alkanes. Solutions of the complex show no sensitivity to light.

Table 5.1 lists the analytical and spectroscopic parameters for the complex. The infra-red spectrum (in KBr) of the complex exhibits the expected bands due to the Ph_2Pbipy ligand. From this spectrum, it is possible to ascertain the mode of coordination of the Ph_2Pbipy ligand. Coordination of the bipyridine nitrogens, in general, are characterised by a shift to higher wavenumbers of the C-N stretching bands, whilst the $P\text{-}C_{bipy,ph}$ stretching bands are shifted to higher wavenumbers on coordination of the phosphorus atom. A distinct shift in both these sets of bands is observed, attributable to coordination of both the phosphorus

Table 5.1 The analytical and spectroscopic parameters for $[Ag_2(\mu\text{-}Ph_2Pbipy)_2(NCMe)_2](PF_6)_2$ [33]

$^{31}P\{^1H\}$ nmr [(a)]			^1H nmr [(b)]	Infra-red[(c)]		Analysis Found (Calculated) %		
δ	$^1J(^{107}Ag\text{-}^{31}P)$ (approx. Hz)	$^1J(^{109}Ag\text{-}^{31}P)$	δ	ν(C≡N)	ν(P-F)	%C	%H	%N
32.38	669	761	8.83-7.41(m, 34H, Ph_2Pbipy) 2.81(s,6H, $C\underline{H}_3CN$)	2280(vw)	840(vs)	45.00(45.45)	3.29(3.18)	6.44(6.63)

(a) : Recorded in acetone-d_6 (in ppm) relative to H_3PO_4 at temperatures between 25 and -89°C. Accuracy in ^1J coupling constants not better than ± 0.5 Hz.

(b) : Recorded in acetone-d_6 at 25°C.

(c) : Recorded in the solid state as a KBr disk. Ph_2Pbipy ligand bands (see Figure 5.1) are omitted. Designation : vs = very strong, vw = very weak.

atom and the bipyridine moiety. In addition, a characteristic band at ~840 cm^{-1} is assigned to the P-F stretch within the PF$_6^-$ counter anion, while the C≡N stretch expected for the nitrile ligands is barely detectable at ~2280 cm^{-1}.

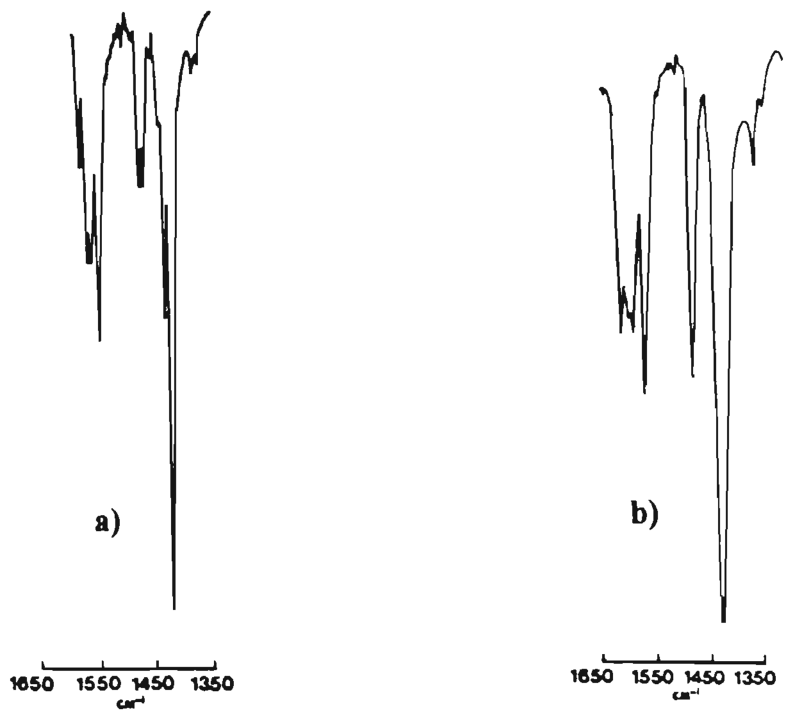

Figure 5.1 Infrared spectra (KBr disk) of a) Ph$_2$Pbipy and b) [33]

The ^{1}H nmr spectrum of **[33]** in acetone-d$_6$ at ambient (25°C) temperature exhibits characteristic resonance patterns in the aromatic region, attributable to the ligand protons. A comparison of the integrals confirms the expected presence of two Ph$_2$Pbipy and two acetonitrile ligands. The Ph$_2$Pbipy ligand resonances cannot unambiguously be assigned to specific protons due in part to overlap between phenyl proton and bipyridine proton shifts and also to the broad, unresolved nature of the multiplets that result.

The ^{31}P{^{1}H} nmr spectrum of the product in acetone-d$_6$ exhibits a complex doublet of multiplets centred at δ 32.38, downfield from H$_3$PO$_4$, external standard, as shown in Figure 5.2. Naturally occurring silver consists of almost equal amounts of the isotopes ^{107}Ag and ^{109}Ag, both with spin I = ½. Due to a 15% larger magnetogyric ratio(μ), the less abundant (48.18%) ^{109}Ag is the more receptive to nmr observation, but only by a factor of approximately 1.4.[168-170] Assigning an exact splitting pattern to the observed spectrum is complicated by the presence of these two isotopes. This can be rationalised in terms of the chemical environments pertaining to the phosphorus atoms coupled with the two silver

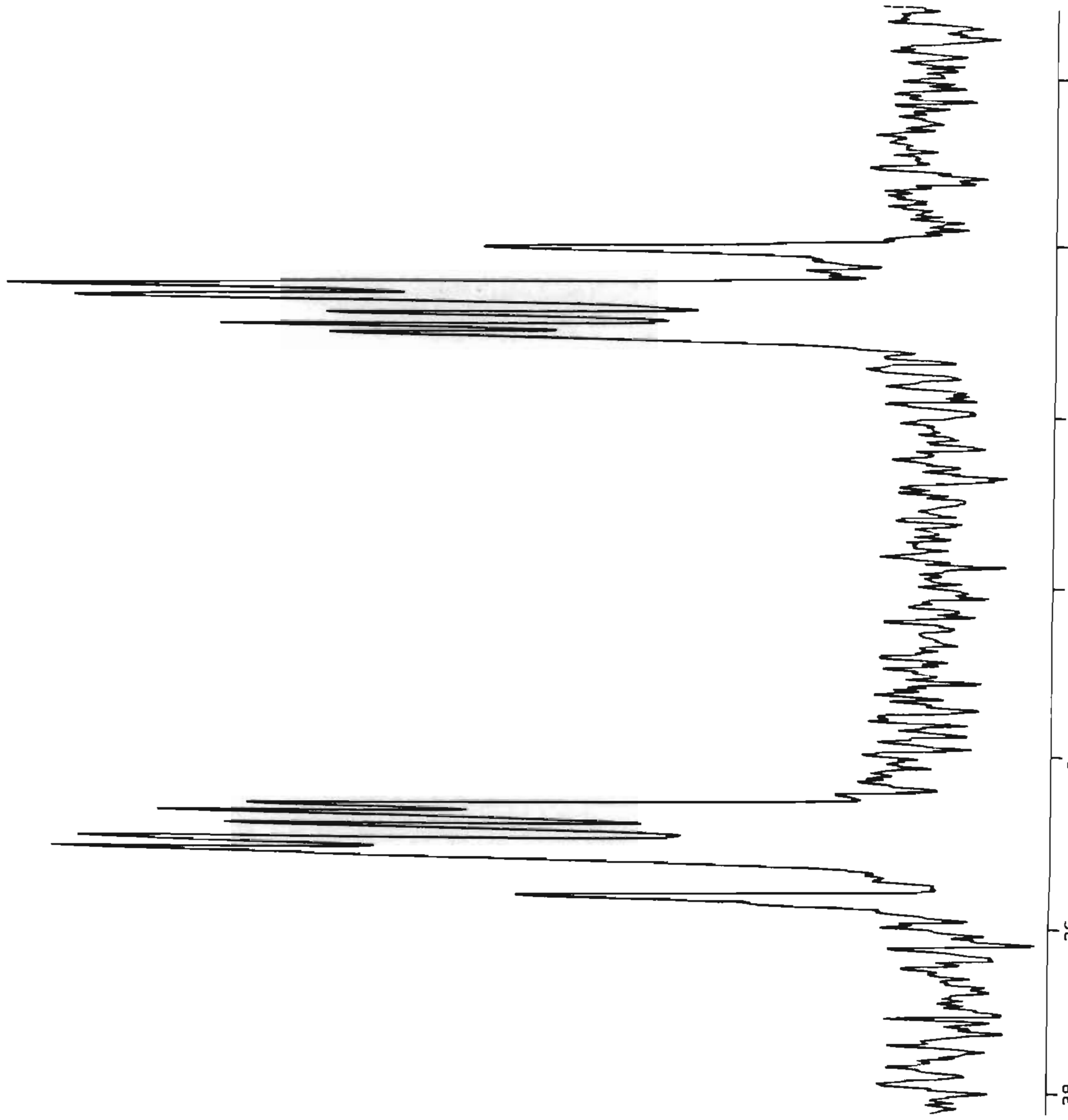
26
28
30
32
34
36
38
PPM

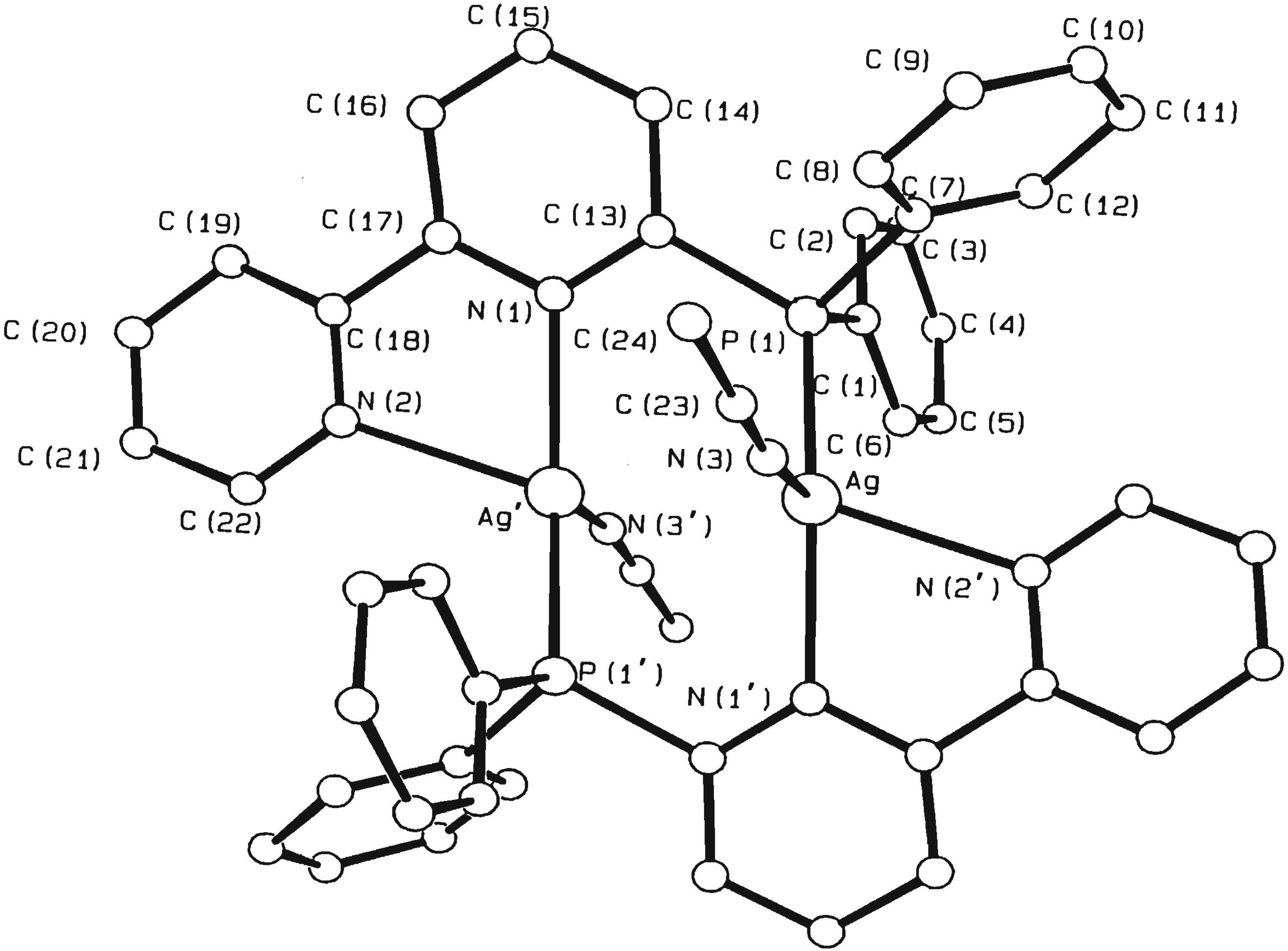
C (15)
C (10)
C (9)
C (16)
C (14)
C (11)
C (8)
C (7)
C (12)
C (19)
C (17)
C (13)
C (2)
C (3)
C (20)
N (1)
C (24)
P (1)
C (4)
C (18)
C (1)
N (2)
C (23)
C (5)
C (21)
N (3)
C (6)
Ag
C (22)
Ag'
N (3')
N (2')
P (1')
N (1')

bipyridine fragment of the ligand. The large degree of distortion is somewhat greater than that found for the equivalent angle in $[Ag_2(\mu\text{-dppm})_2(NO_3)_2]$ [28] [138.3(1)°] and is directly attributable to the differing steric requirements of the respective ligands and in particular the bipyridine fragment of the Ph_2Pbipy ligand. The remaining angles around each silver atom are close to those expected for tetrahedral coordination. (See Table 5.13)

The Ag-P bond distance of 2.379(3)Å is in slightly shorter than others reported in the literature[28,164,173]; for example, the Ag-P bond distances in $[Ag_2(\mu\text{-dppm})_2(NO_3)_2]$ [28] range from 2.417(2) to 2.436(2)Å while those for $[Ag(\mu\text{-Cl})(\eta^1\text{-}Ph_2Ppy)]_4$ range from 2.387(5) to 2.429(5)Å. The Ag -N(3) bond distance [2.437(13)Å] is significantly longer than the range of Ag-N distances found in the $[Ag(CH_3CN)_4]^+$ cation [2.18 - 2.30Å].[166] Rotation about the interannular C(17)-C(18) bond (see dihedral angle below) results in the Ag-N(1′) bond distance [2.311(5)Å] being slightly shorter than that for Ag-N(2′) [2.417(5)Å].

The eight-membered Ag-P-C-N-Ag′-P-C-N ring adopts a distorted, puckered conformation, which is impossible to assign as either "chair-chair" or "chair-boat" (Figure 5.3) due to the P(1)-Ag-Ag′-N(1) twist of 24.3°. Within the bipyridine group itself, the dihedral angle between the mean-planes through the non-hydrogen atoms of each pyridine ring is 16.6°, significantly different from that of the free uncoordinated ligand (7.7°).

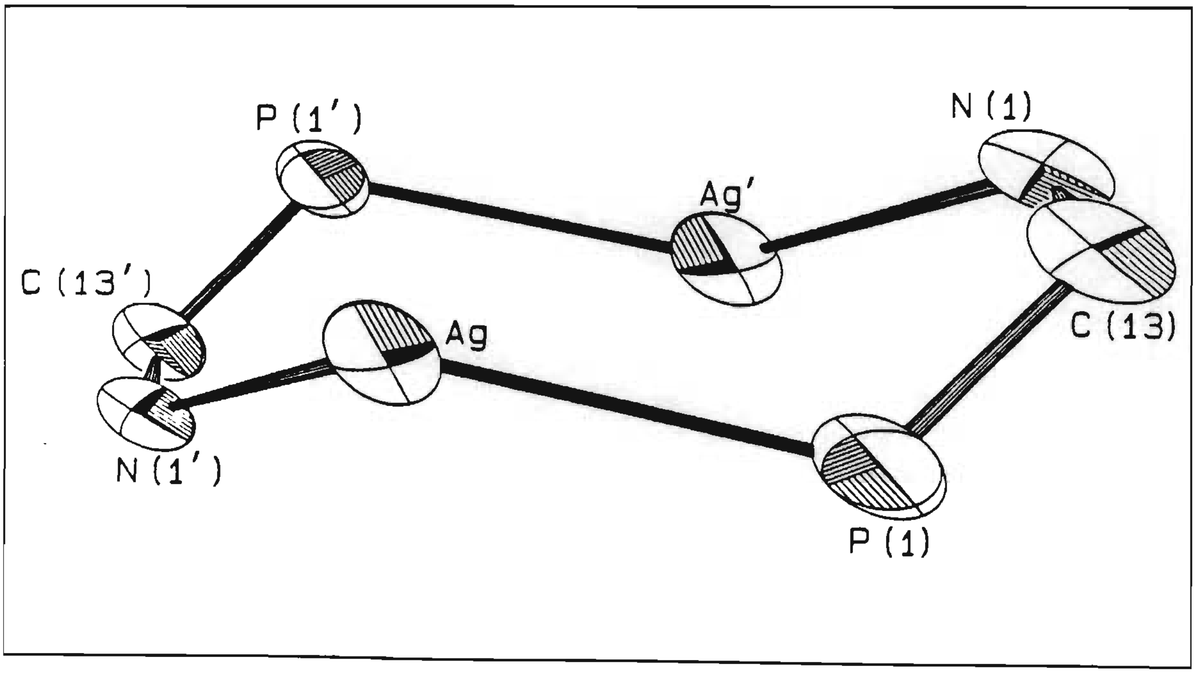

Figure 5.4 A view of the eight-membered AgPCNAgPCN ring of the cation of [33], showing the puckered conformation.

Another noticeable feature of the structure is how the acetonitrile ligands are bent at angle of approximately 19.8° away from the Ag-N(3) vector.

5.3 The chemistry of $[Ag_2(\mu\text{-}Ph_2Pbipy)_2(NCMe)_2](PF_6)_2$ [33]

5.3.1 The substitution behaviour of $[Ag_2(\mu\text{-}Ph_2Pbipy)_2(NCMe)_2]^{2+}$

The acetonitrile ligands bound to the silver atoms in the $[Ag_2(\mu\text{-}Ph_2Pbipy)_2(NCMe)_2]^{2+}$ cation were found to be labile and to be readily replaced by a series of other polar, weakly-donating solvent ligands. In addition, isocyanide ligands such as 2,6-dimethylphenyl (Xylyl) isocyanide have been shown to substitute for the acetonitrile ligands. Scheme 5.2 illustrates the reversible nature of the substitutions discussed in this section.

5.3.1.1 Synthesis of the solvento derivatives $[Ag_2(\mu\text{-}Ph_2Pbipy)_2(S)_2](X)_2$ (S = PhCN and X = BF_4 [34], S = py and X = PF_6[35] or S = EtOH and X = BF_4 [36])

It was found that it is possible to substitute the acetonitrile ligands in the $[Ag_2(\mu\text{-}Ph_2Pbipy)_2(NCMe)_2]^{2+}$ complex cation by simply dissolving the appropriate salt (under reflux in the case of EtOH) in the appropriate solvent. Addition of diethyl ether precipitates the pale yellow products $[Ag_2(\mu\text{-}Ph_2Pbipy)_2(NCPh)_2](BF_4)_2$ **[34]** and $[Ag_2(\mu\text{-}Ph_2Pbipy)_2(py)_2](PF_6)_2$ **[35]**, while cooling the hot ethanolic solution affords the pale yellow $[Ag_2(\mu\text{-}Ph_2Pbipy)_2(EtOH)_2](BF_4)_2$ **[36]**, all in excellent yields. All of the derivatives can be converted back to **[33]** by treatment with acetonitrile and isolation in a similar fashion. All complexes show very similar solubilities and mimic those of **[33]**.

Tables 5.2 and 5.3 respectively list the analytical and spectroscopic data for the complexes. All complexes have microanalyses consistent with their formulation. The infra-red spectra contain characteristic Ph_2Pbipy ligand bands as shown in Figure 5.1 as well as bands attributable to the relevant counter-anion. The ^1H nmr spectra contain characteristic Ph_2Pbipy peaks which, in the case of **[34]** and **[35]**, obscure those of the ligands that have replaced the acetonitrile ligands *viz.* PhCN and pyridine respectively. Therefore, comparison of intensity ratios (integrals) is not possible. In the ^1H nmr spectrum (CD_2Cl_2) of **[36]** the presence of a hydroxy singlet, as well as a triplet and a quartet corresponding to methyl and methylene protons respectively, confirm the presence of coordinated ethanol; the shifts of the latter two sets of resonances (δ 1.32 and 3.84 respectively) are slightly

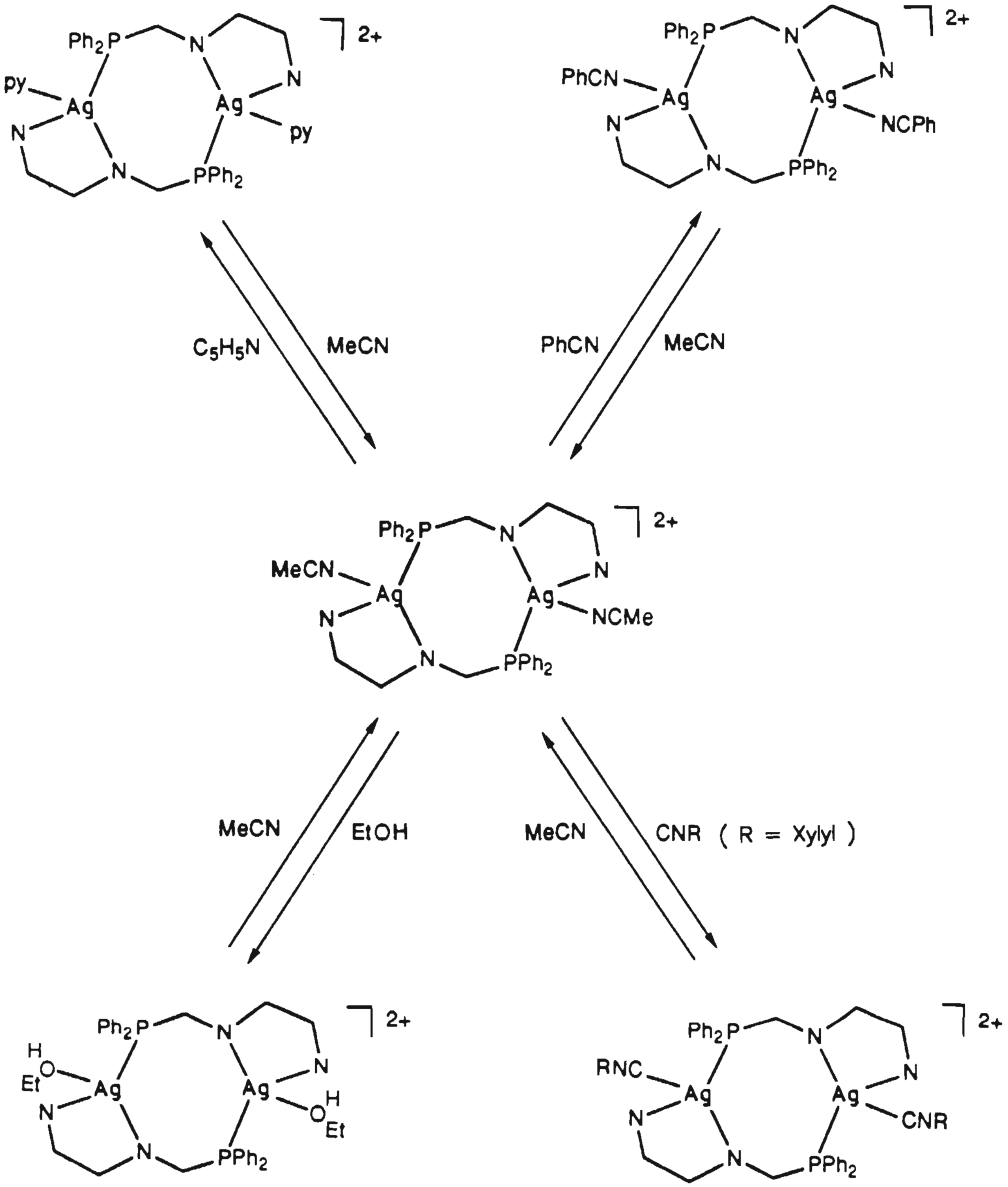
Ph₂P
N
2+
py
Ag
Ag
N
N
py
N
PPh₂
PhCN
NCPh
C₅H₅N
MeCN
PhCN
MeCN
MeCN
NCMe
MeCN
EtOH
MeCN
CNR (R = Xylyl)
H
O
Et
RNC
CNR

Scheme 5.2 The substitution behaviour of $[Ag_2(\mu\text{-}Ph_2Pbipy)_2(NCMe)_2]^{2+}$

Table 5.2 Physical and microanalytical data

	Complex	Colour	M:g.mol^{-1}	Analysis : Found (Calculated) %		
				%C	%H	%N
[34]	$[Ag_2(\mu\text{-}Ph_2Pbipy)_2(NCPh)_2](BF_4)_2$	pale yellow	1276.32	54.95(54.58)	3.63(3.47)	5.98(6.58)
[35]	$[Ag_2(\mu\text{-}Ph_2Pbipy)_2(py)_2](PF_6)_2$	pale yellow	1344.60	48.21(48.24)	3.10(3.30)	5.87(6.25)
[36]	$[Ag_2(\mu\text{-}Ph_2Pbipy)_2(EtOH)_2](BF_4)_2$	pale yellow	1162.21	49.89(49.61)	3.86(3.99)	5.19(4.82)
[37]	$[Ag_2(\mu\text{-}Ph_2Pbipy)_2(CNXylyl)_2](ClO_4)_2$	white	1357.72	54.42(54.85)	3.82(3.86)	5.94(6.19)

Table 5.3 Infra-red, ^1H and $^{31}P\{^1H\}$ nmr spectroscopic data

Complex	IR[(a)]	δ ^1H nmr (ppm)[(b)]	$^{31}P\{^1H\}$nmr[(e)]		
			δ	$^1J(^{107}Ag-^{31}P)$ (Hz)	$^1J(^{109}Ag-^{31}P)$ (Hz)
[34]	1057(vs)	(c)	32.35	660	761
[35]	839(vs)	(d)	24.68	583	725
[36]	1056(vs)	3.84(q, 4H, $CH_3C\underline{H_2}OH$) 1.32(t, 6H, $C\underline{H_3}CH_2OH$) 1.56(s,2H, $CH_3CH_2O\underline{H}$)	30.08	618	724
[37]	2168(s) 1091(vs)	2.12(s, 12H, Xylyl $C\underline{H_3}$)	21.55	(f)	

(a) : Recorded in the solid state as KBr disks. Only bands other than those corresponding to Ph_2Pbipy or aromatic ligands are listed. Designation : s = strong, vs = very strong

(b) : Recorded in CD_2Cl_2 unless otherwise stated. Only shifts arising from protons other than those of the Ph_2Pbipy ligand (see Table 5.1) are reported.

(c) : NCPh protons shifts obscured by ligand resonances.

(d) : Pyridine proton shifts obscured by ligand resonances.

(e) : Recorded in CD_2Cl_2 unless otherwise stated. All spectra exhibit characteristic splitting pattern for head to tail silver dimers discussed in the text. δ (in ppm) relative to H_3PO_4. Accuracy in coupling constants not greater than ± 0.5 Hz.

(f) : Not possible to accurately record coupling constants due to partial collapse of pattern arising from fluxionality of isocyanide ligands.

downfield of those for uncoordinated ethanol (δ 1.20 and 3.70 respectively) while the singlet for the hydroxy proton occurs at 1.56 ppm. When the spectrum is recorded in CD_3CN, peaks attributable to free ethanol solvent appear, presumably due to substitution of the ethanol by the deuterated solvent.

All $^{31}P\{^1H\}$ nmr spectra (Table 5.3) exhibit the characteristic complex splitting discussed in section 5.2.1. These patterns are centred at δ values which correlate well with that of the parent complex **[33]**, and have approximate ^1J coupling constants that are consistent with the $\mu(^{109}Ag)/\ \mu(^{107}Ag)$ ratio of 1.49. This also implies that the Ph_2Pbipy ligands remain bonded to the dimer in a head-to tail manner, at least on the nmr time scale.

5.3.1.2 Crystal structure determination of $[Ag_2(\mu\text{-}Ph_2Pbipy)_2(py)_2](PF_6)_2$ [35]

The crystal structure of the cation of $[Ag_2(\mu\text{-}Ph_2Pbipy)_2(py)_2](PF_6)_2$ **[35]** is shown in Figure 5.5, together with the atom labelling scheme. The cation contains a crystallographically imposed centre of symmetry midway between the two silver atoms which are bridged by two Ph_2Pbipy ligands in a head-to-tail fashion. The pseudo-tetrahedral coordination around each silver atom is completed by a pyridine ligand bonded to the silver atom in a σ fashion through its nitrogen atom. A noticeable feature of this structure is the substantial increase in Ag....Ag separation from that of the parent complex **[33]** (i.e. [4.092(1)Å as opposed to 2.973(2)Å]). As a result, the angles around each silver atom more closely approximate tetrahedral geometry than do those found in **[33]**(see Table 5.18). The P(1)-Ag-N(3) angle of 113.4(0)° is marginally greater than the corresponding angle in **[33]** (105.8(3)°], while the substantially distorted P(1)-Ag-N(1′) angle in **[33]** [168.3(3)°] is reduced to 118.6(1)°. Once again, the angle subtended by the two nitrogen atoms of the bipyridine fragment at each silver atom is determined by the chelating geometry of the bipyridyl ligand and at 69.3(2°) is substantially smaller than the idealised tetrahedral value. It can also be noted that the plane defined by the non-hydrogen atoms of the pyridine ligand is nearly parallel to that defined by the non-hydrogen atoms of the phenyl ring containing C(1) (dihedral angle = 7.6°). However, the distance between these mean planes (approximately 5.7Å) is too great to support any form of stabilising π-interaction. The Ag-P bond distance of 2.398(0)Å corresponds more closely than **[33]** to those found in literature,[28,164,173] which range from 2.387(5)Å to 2.436(2)Å while the Ag-N(3) bond distance [2.333(1)Å] is shorter than that for **[33]** [2.437(13)°], reflecting the

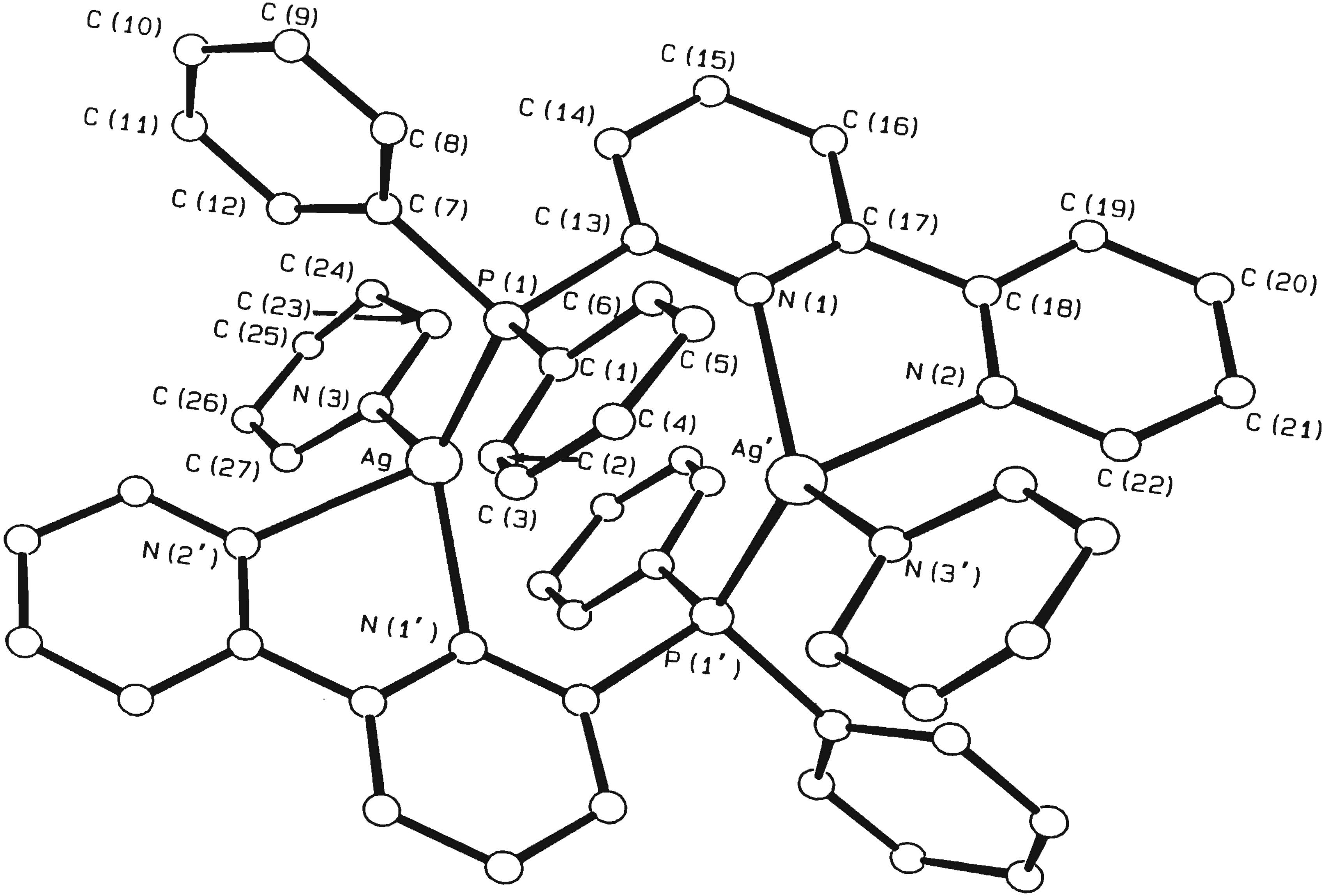
C (10)
C (9)
C (15)
C (14)
C (16)
C (11)
C (8)
C (12)
C (7)
C (13)
C (17)
C (19)
C (24)
P (1)
C (20)
C (6)
N (1)
C (18)
C (23)
C (25)
C (1)
C (5)
N (2)
C (26)
N (3)
C (4)
C (21)
Ag'
Ag
C (2)
C (27)
C (22)
C (3)
N (2')
N (3')
N (1')
P (1')

greater σ character of the Ag-N(3) bond. It is however, analogous to those observed in the $[Ag(py)_4]^+$ cation, [166] which range from 2.322(3)Å to 2.240(1)Å. As in **[33]**, the eight-membered core adopts a distorted conformation which, due to torsional factors within the ligand, is impossible to assign as either "chair-chair" or "chair-boat". However, the torsion angle of 41.5° [P(1)-Ag-Ag'-N(1)] is almost double that of the parent complex, a result of the aforementioned twisting of the phosphorus atom away from the pyridine ligand. In contrast to this unusually high torsion angle, the dihedral angle between the mean-planes through the non-hydrogen atoms of each pyridine ring of the bipyridine fragment is a small 6.7°; indeed, this is even smaller than that found in the free, uncoordinated ligand. This has the result that there is only marginal difference between the Ag-N(1') and Ag-N(2') bond distances, in contrast to those of **[33]**.

5.3.1.3 Crystal structure determination of $[Ag_2(\mu\text{-}Ph_2Pbipy)_2(EtOH)_2](BF_4)_2$ [36]

The molecular geometry of $[Ag_2(\mu\text{-}Ph_2Pbipy)_2(EtOH)_2](BF_4)_2$ **[36]** is shown in Figure 5.6. A crystallographically imposed centre of symmetry is located midway between the two silver atoms bridged by the two Ph_2Pbipy ligands. The pseudo-tetrahedral geometry around each silver atom is completed by the coordination of an ethanol molecule bonded through its oxygen atom. A fluorine atom of the BF_4^- anion is sufficiently close to the O atom to be considered as weakly interacting. O....F hydrogen bonding is not uncommon and the O....F(2) hydrogen-bond length of 2.681(1)Å in this molecule is less than that observed for 2-fluoroethanol, in which the O....F hydrogen bond length is 2.820(3)Å.[174]

The non-bonded Ag.....Ag separation is 2.984(1)Å which is very similar to that of the parent complex **[33]**[2.973(2)Å]. As for the latter complex, the distortions of the angles around each silver atom from that of an ideal tetrahedral geometry vary greatly. The short bite bipyridine fragment of the Ph_2Pbipy ligand subtends a small angle of 70.5(2)° at each silver atom while the P(1)-Ag-N(1') angle is expanded to the relatively large value of 151. 9(2)°. The remaining angles around each silver atom exhibit less marked distortion.

The Ag-P bond distance of 2.973(1)Å is somewhat larger than that for **[33]**.The 19.6° twist involving the P(1)-Ag-Ag'-N(1) angle is, however, somewhat reduced from that of **[33]**. In addition, a degree of interannular rotation about the C(17)-C(18) bond induces a dihedral angle of 9.3° between the mean planes through the non-hydrogen atoms defined by each pyridine ring of the bipyridine fragment; moreover, this rotation causes the Ag-N(1')

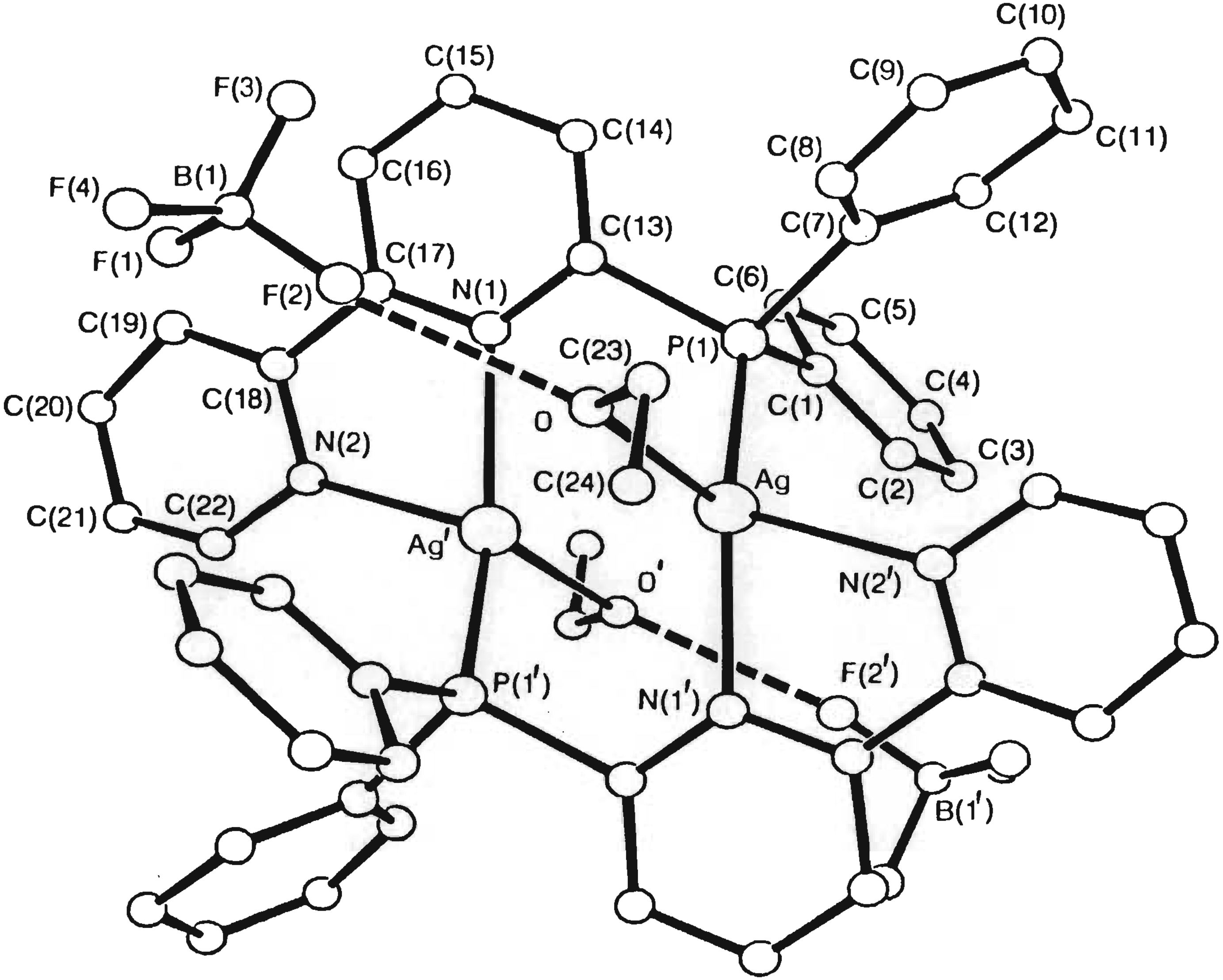
C(10)
C(15)
C(9)
F(3)
C(14)
C(11)
C(8)
C(16)
B(1)
F(4)
C(13)
C(7)
C(12)
F(1)
C(17)
C(6)
F(2)
N(1)
C(5)
C(19)
C(23)
P(1)
C(4)
C(1)
C(20)
C(18)
O
C(3)
N(2)
Ag
C(24)
C(2)
C(21)
C(22)
Ag'
O'
N(2')
F(2')
P(1')
N(1')
B(1')

bond length of 2.316(3)Å to be somewhat shorter than the 2.351(3)Å for Ag-N(2′). The complex as a whole is presumed to be more stable than its parent **[33]** since, as mentioned above, the dihedral angle within the ligand is less (a result of less steric strain) and the difference in bond length between Ag-N(2′) and Ag-N(1′) is reduced from approximately 0.1Å (for **[33]**) to approximately 0.035Å. Although the eight-membered core still adopts the characteristic distorted conformation, it is significantly less puckered.

5.3.1.4 Synthesis of the isocyanide derivative $[Ag_2(\mu\text{-}Ph_2Pbipy)_2(CNXylyl)_2](ClO_4)_2$ [37] (Xylyl = 2,6-dimethylphenyl)

As the atomic number increases across any given row of the periodic table, transition metals' d electrons become more tightly held. As a result, there are very few isolable carbonyls beyond group 10. The carbonyl chemistry of silver is almost nonexistent with only two reports of complexes formed; the first [175] describes the formation of silver carbonyl from silver atoms and CO in a matrix at 20K while the second complex $[Ag(CO)\{B(OTeF_5)_4\}]$ [176] shows the metals' very weak π-donor character in its C≡O stretch frequency of 2204cm^{-1}, an extremely high value indicating little CO π* population. On the other hand, direct reaction of silver salts with isocyanides (isoelectronic with CO) leads to a range of stable silver isocyanide complexes,[177-180] easily identified through the presence of ν(NC) stretching peaks.

Treatment of **[33]** (ClO_4^- salt) with 2,6-dimethylphenyl (Xylyl) isocyanide in dichloromethane affords a clear, colourless solution from which colourless crystals separate in moderate yield on addition of diethyl ether. Improved yields can be obtained through an alternative route *viz.* the direct reaction of $[Ag(CNXylyl)_3]PF_6$ [180] with an equimolar quantity of Ph_2Pbipy in dichloromethane and isolation of the product in the same fashion. Tables 5.2 and 5.3 give the spectroscopic parameters for the complex. The most noticeable feature of its infra-red spectrum is the distinctive ν(NC) stretching band centred at 2168 cm^{-1}, well within the range (2150 - 2250 cm^{-1}) expected for terminal isocyanide ligands bonded through their carbon atoms.[178] Peaks assigned to P-C and C-N vibrations within the Ph_2Pbipy ligand are observed (see Figure 5.1) as well as a perchlorate stretch at 1091cm^{-1}, typical of that expected for an uncoordinated anion.[181]

In the ^{1}H nmr spectrum, resonances due to aromatic protons of the isocyanide ligand (*ca.* 7.4ppm [180]) are obscured by those of the Ph_2Pbipy ligands at δ 8.59 -7.05. However, a sharp singlet at 2.12 ppm attributable to methyl protons of the isocyanide ligand has the correct intensity ratio when integrated against all aromatic protons. As with a host of dimeric metal-carbonyls, fluxionality of the isoelectronic isocyanide ligands about the silver dimer is thought to occur based on $^{31}P\{^{1}H\}$ nmr evidence. The characteristic splitting pattern observed for **[33]** discussed in section 5.2.1 collapses in this case into two broad, featureless bands centred at approximately 21.55 ppm and for which realistic J(Ag-P) coupling constants are impossible to assign.

Nevertheless, correct microanalysis consistent with the perchlorate salts' formation has been obtained.

As with complexes **[34]**-**[36]**, the complex is readily converted back to the parent **[33]** by simply dissolving it in excess acetonitrile and isolating the product in the manner described. The yield is near quantitative.

5.3.2 Reactions of $[Ag_2(\mu\text{-}Ph_2Pbipy)_2(NCMe)_2]^{2+}$ with anionic ligands

The labile acetonitrile ligands bound to the silver atoms of the $[Ag_2(\mu\text{-}Ph_2Pbipy)_2(NCMe)_2]^{2+}$ cation are readily substituted by a range of anionic ligands resulting either in neutral products in which the anionic ligands are bound in a terminal fashion, or monocationic complexes containing the anion as a bridging ligand. Scheme 5.3 illustrates the essential features of the chemistry described in this section.

5.3.2.1 Synthesis of the neutral species $[Ag_2(\mu\text{-}Ph_2Pbipy)_2(X)_2]$ (X = Cl^- [38], Br^- [39], I^- [40], CN^- [41], $PhC{\equiv}C^-$ [42] or NO_3^- [43])

Reaction of $[Ag_2(\mu\text{-}Ph_2Pbipy)_2(NCMe)_2](PF_6)_2$ **[33]** with a two-fold excess of the appropriate tetra-alkylammonium halide salt in CH_2Cl_2 at room temperature affords the neutral complexes $[Ag_2(\mu\text{-}Ph_2Pbipy)_2(X)_2]$ (X = Cl^- **[38]**, Br^- **[39]**, I^- **[40]**) in good yields. All three complexes precipitate immediately as white powders and are isolated by decanting the supernatant liquor and by washing the product with CH_2Cl_2. The derivatives are very insoluble in all common organic solvents but are partially soluble in hot dimethylsulphoxide. This essentially precludes the effective recording of ^{1}H and $^{31}P\{^{1}H\}$

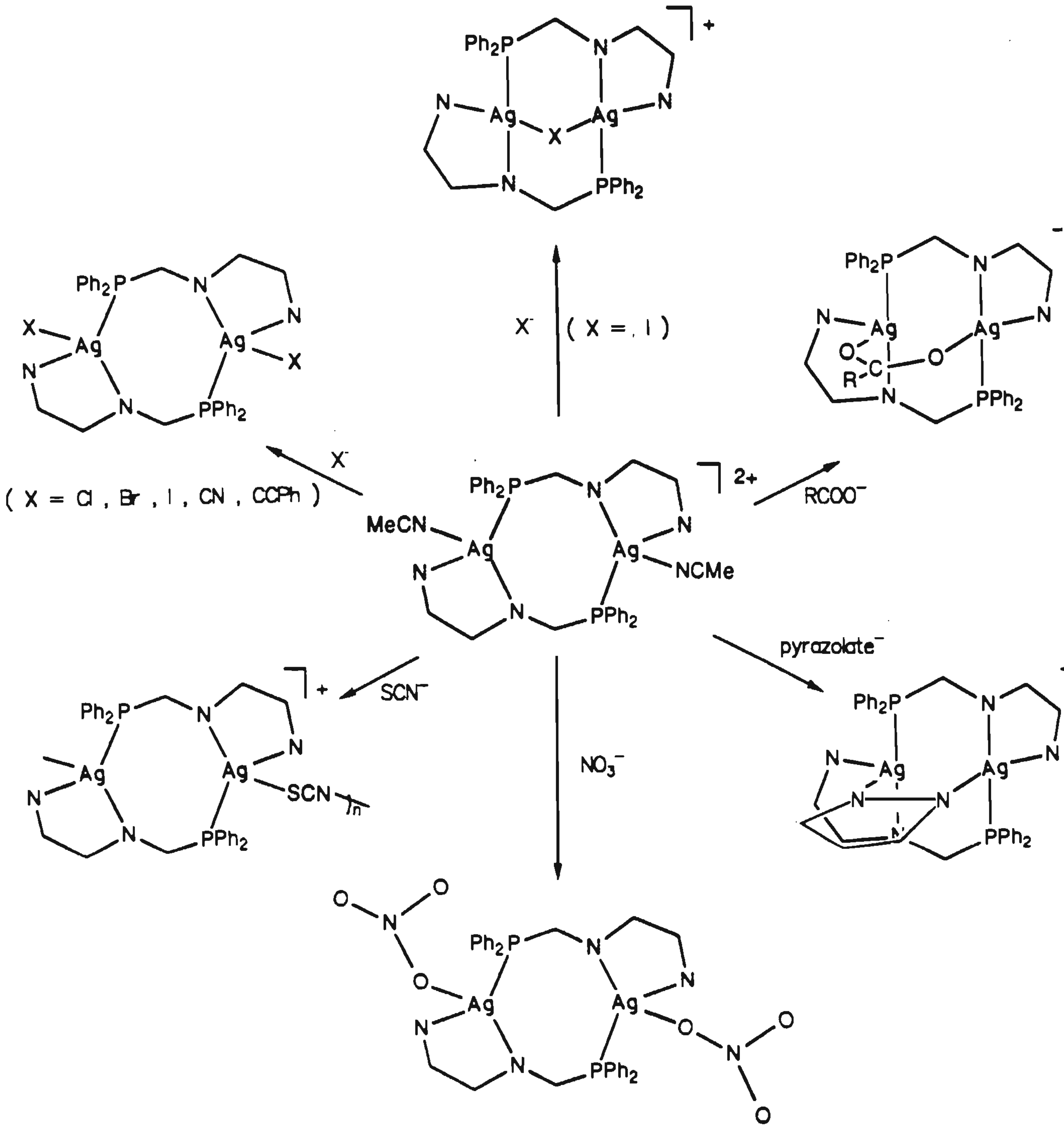

Ph2P
N
Ag
X
PPh2
+
X⁻
(X = , I)
(X = Cl , Br , I , CN , CCPh)
MeCN
NCMe
2+
RCOO⁻
O
C
R
pyrazolate⁻
SCN⁻
SCN
n
NO3⁻
O

Scheme 5.3 The reactions of $[Ag_2(\mu\text{-}Ph_2Pbipy)_2(NCMe)_2]^{2+}$ with anionic ligands

Table 5.4 Physical and microanalytical data

	Complex	Colour	M:g.mol^{-1}	Analysis : Found (Calculated) %		
				%C	%H	%N
[38]	$[Ag_2(\mu\text{-}Ph_2Pbipy)_2(Cl)_2]$	white	967.37	54.98(54.63)	4.04(3.54)	5.67(5.79)
[39]	$[Ag_2(\mu\text{-}Ph_2Pbipy)_2(Br)_2].CH_2Cl_2$	white	1140.80	49.90(50.50)$^{(a)}$	2.97(3.39)	5.40(5.23)
[40]	$[Ag_2(\mu\text{-}Ph_2Pbipy)_2(I)_2]$	white	1150.27	45.82(45.94)	2.71(2.92)	4.53(4.87)
[41]	$[Ag_2(\mu\text{-}Ph_2Pbipy)_2(CN)_2]$	white	948.50	58.24(58.25)	3.35(3.61)	8.52(8.86)
[42]	$[Ag_2(\mu\text{-}Ph_2Pbipy)_2(C{\equiv}CPh)_2]$	pale yellow	1098.72	66.31(65.59)	4.31(4.04)	4.83(5.10)
[43]	$[Ag_2(\mu\text{-}Ph_2Pbipy)_2(NO_3)_2]$	pale yellow	1020.47	51.95(51.76)	3.84(3.36)	8.08(8.24)
[44]	$[Ag_2(\mu\text{-}Ph_2Pbipy)_2(\mu\text{-}I)](BF_4)$	white	1110.17	47.51(47.60)	3.89(3.09)	4.78(5.05)
[45]	$[Ag_2(\mu\text{-}Ph_2Pbipy)_2\{\mu\text{-}OC(Me)O\}](PF_6)$	pale yellow	1099.47	49.68(50.25)	3.20(3.30)	4.78(5.10)
[46]	$[Ag_2(\mu\text{-}Ph_2Pbipy)_2\{\mu\text{-}OC(Ph)O\}](PF_6)$	pale yellow	1162.54	52.12(52.69)	3.78(3.38)	4.64(4.82)
[47]	$[Ag_2(\mu\text{-}Ph_2Pbipy)_2(\mu\text{-}pyz)](BF_4)$	pale yellow	1050.34	53.22(53.75)	3.84(3.55)	7.51(8.00)
[48]	$\{[Ag_2(\mu\text{-}Ph_2Pbipy)_2(\mu'\text{-}SCN)](BF_4)\}_n$	yellow	1041.35	51.71(51.90)	3.00(3.29)	6.24(6.73)

(a) : Calculated values for **[39]** include a CH_2Cl_2 molecule.

Table 5.5 Infra-red, ^{1}H and ^{31}P{^{1}H} nmr spectroscopic data

Complex	IR$^{(a)}$	δ ^{1}H nmr (ppm)$^{(b)}$	^{31}P{^{1}H}nmr$^{(g)}$ δ	^{1}J(^{107}Ag-^{31}P) (Hz)	^{1}J(^{109}Ag-^{31}P) (Hz)
[38]		(c)	(c)		
[39]		(c)	(c)		
[40]		(c)	(c)		
[41]	2156(m) 2144(vs)		29.61	616	717
[42]	2120(w)	(d)	30.07	627	743
[43]	789(s) 748(s) 694(s)	recorded in CD_3OD	30.25	626	730
[44]	1051(vs)		24.12	588	702
[45]	1574(vs) 841(vs)	1.84(s, 3H, $C\underline{H}_3CO_2$)	20.57	598	710
[46]	1562(vs) 840(vs)	(e)	21.76	607	698
[47]	1054(vs)	(f)	24.00	611	721
[48]	2087(vs) 1058(vs)	(c)	(c)		

(a) : Recorded in the solid state as KBr disks. Only bands other than those corresponding to Ph_2Pbipy or aromatic ligands are listed. Designation : s = strong, vs = very strong, w = weak.

(b) : Recorded in CD_2Cl_2 unless otherwise stated. Only shifts arising from protons other than those of the Ph_2Pbipy ligand (see Table 5.1) are reported.

(c) : Product too insoluble to record.
(d) : $C\equiv CPh$ proton shifts obscured by Ph_2Pbipy ligand resonances.
(e) : Benzoate proton shifts obscured by Ph_2Pbipy ligand resonances.
(f) : Pyrazolate proton shifts obscured by Ph_2Pbipy ligand resonances.
(g) : Recorded in CD_2Cl_2 unless otherwise stated. All spectra exhibit characteristic splitting pattern for head to tail silver dimers discussed in the text. δ (in ppm) relative to H_3PO_4. Accuracy in coupling constants not greater than ± 0.5 Hz.

nmr spectra, as well as the chance of obtaining single crystals suitable for X-ray diffraction studies. However, the powders obtained yield satisfactory microanalyses consistent with their formulae (Table 5.4), while their solid state (KBr disk) infra-red spectra (Table 5.5) are characterised by the absence of counter-anion bands at ~838 cm^{-1} (for PF_6^-) or ~1050 cm^{-1} (for BF_4^-), confirming the coordination of two anionic ligands in a terminal fashion. The ν(N-C) and ν(P-C) stretching bands of the Ph_2Pbipy ligand remain unaffected.

Treatment of **[33]** with two equivalents of KCN in CH_2Cl_2 affords a pale yellow, clear solution after 24 hours stirring at room temperature. Upon addition of diethyl ether pale yellow needles of $[Ag_2(\mu\text{-}Ph_2Pbipy)_2(CN)_2]$ **[41]** separate from the solution in moderate (60%) yield. This highly crystalline complex, soluble in dichloromethane and acetone, has been characterised by microanalysis (Table 5.4) and the appearance of two C≡N stretching bands at 2156(m) and 2144(vs)cm^{-1} in its infra-red spectrum (Table 5.5) corresponding to two coordinated CN^- ligands, bonded to the silver atoms through their carbon atoms. Like those of complexes **[38]**-**[40]**, the counter-anion peak attributable to BF_4^- at ~1050 cm^{-1} is not present while the bands corresponding to the Ph_2Pbipy ligands remain as they are for the parent complex. The remaining characterisation data is as specified in Table 5.5.

Two methods for the synthesis of the neutral phenylacetylide derivative $[Ag_2(\mu\text{-}Ph_2Pbipy)_2(C{\equiv}CPh)_2]$ **[42]** have been developed. The first involves the addition of two equivalents of LiC≡CPh (0.1M in thf) to **[33]** in CH_2Cl_2 at room temperature. Prolonged reaction affords an orange solution from which a light yellow, feathery precipitate is obtained on treatment with a $MeOH{:}Et_2O$ (1:1, vol:vol) solution. The second method involves the initial synthesis and isolation of the $[Ag(C{\equiv}CPh)]_n$ polymer,[182] which is dissolved in the minimum amount of pyridine and reacted with an equivalent of Ph_2Pbipy in warm (30°C) methanol. The product **[42]** separates from solution as a pale yellow microcrystalline powder. Both methods provide yields of the product in excess of 90%. The compound exhibits a band at 2120 cm^{-1} in its infra-red spectrum (Table 5.5), which is very weak and assigned to the C≡C stretching vibration, as well as the characteristic ligand bands mentioned previously. Resonances in the aromatic region of the ^1H nmr spectrum due to the phenylacetylide protons are obscured by those due to Ph_2Pbipy ligand protons and it is thus impossible to estimate relative intensities.

As for **[42]**, two methods for the synthesis of $[Ag_2(\mu\text{-}Ph_2Pbipy)_2(NO_3)_2]$ **[43]** have been developed. Addition of a two-fold excess KNO_3 to **[33]** in acetone at room temperature results in the precipitation of the pale yellow, microcrystalline product **[43]** in good yield after 24 hours. Alternatively, the product can be formed through the treatment of $AgNO_3$ with an equivalent of Ph_2Pbipy in acetone; the product precipitates from solution in a similar fashion. This latter method tends to give better yields. The complex is soluble in warm methanol and acetonitrile and has a satisfactory microanalysis (Table 5.4). An infra-red spectrum (KBr disk, Table 5.5) exhibits characteristic ν(C-P) and ν(C-N) stretching bands as well as three equally intense bands at 789(s), 748(s) and 694(s)cm^{-1}, attributable to the N-O stretch within the nitrate ligands. On the basis of work carried out by Yamaguchi *et al*,[183] it is proposed that the nitrate binds to the silver atom in a symmetric fashion through one of its oxygen atoms only and not in an asymmetric, bidentate fashion similar to that found in $[Ag_2(\mu\text{-}dppm)_2(NO_3)_2]$.[28] Remaining characterisation data are as specified in Table 5.5. The molecular structure of **[43]** has been elucidated through the use of single crystal X-ray diffraction studies.

5.3.2.2 Crystal structure determination of $[Ag_2(\mu\text{-}Ph_2Pbipy)_2(NO_3)_2]$ [43]

The molecular geometry of $[Ag_2(\mu\text{-}Ph_2Pbipy)_2(NO_3)_2]$ **[43]**, which possesses a crystallographically imposed centre of symmetry midway between the two silver atoms, is depicted in Figure 5.7. The structure consists of neutral, dimeric molecular units separated in the crystal lattice by a methanol molecule. The two silver atoms in each dimer are bridged by a pair of Ph_2Pbipy ligands in a head-to-tail fashion. In addition, each silver atom is terminally bound by a single nitrate anion in a symmetric, monodentate fashion through one of the latter's oxygen atoms; this completes the preferred tetrahedral geometry at each silver atom.

A noticeable feature of this complex is the short Ag....Ag separation of 2.935(2)Å, a distance slightly shorter than that of the parent complex $[Ag_2(\mu\text{-}Ph_2Pbipy)_2(NCMe)_2](PF_6)_2$ **[33]** [2.973(2)Å]. The structure shows that this may, in part, be due to the tendency of the nitrate anion to bridge across the two silver atoms, when one considers the relative positioning of O(3) and Ag′(3.333(2)Å apart), thereby pulling the silver atoms closer together. As in **[33]**, there is a significant amount of distortion from ideal tetrahedral

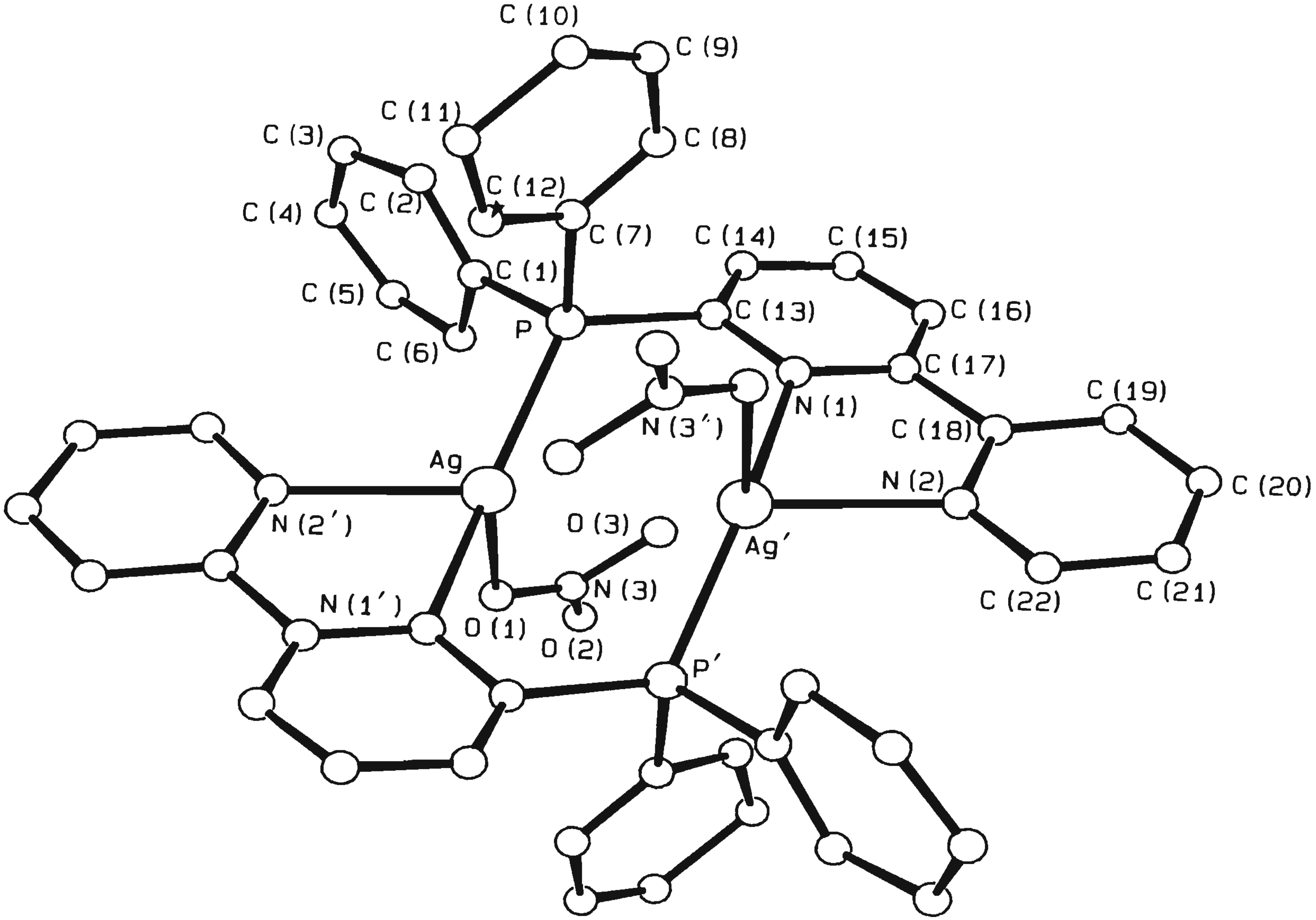
C (10)
C (9)
C (11)
C (8)
C (3)
C (12)
C (4)
C (2)
C (7)
C (14)
C (15)
C (1)
C (5)
C (13)
C (16)
P
C (6)
C (17)
N (1)
C (19)
N (3′)
C (18)
Ag
N (2)
C (20)
N (2′)
O (3)
Ag′
N (3)
C (22)
C (21)
N (1′)
O (1)
O (2)
P′

geometry around each silver atom. The large P-Ag-N(1′) angle of 153.8(1)° effectively compensates for the much smaller angle of 70.1(1)° subtended at the silver atom by the two nitrogen atoms of the bipyridine fragment. The remaining angles around each silver atom are all reasonably close to that expected for tetrahedral coordination (see Table 5.28). N(3)-O bond angles within the nitrate anion are all very close to 120° such that the moiety retains its planarity upon coordination to the silver.

This mode of coordination of the nitrate anion is not unusual, being similar to that proposed by Yamaguchi *et al.*[183] for the $Ag^+NO_3^-$ ion pair. In addition, monodentate perchlorate bonding is found in the crystal structure of $AgClO_4$.[184] The observed Ag-O bond distance in **[43]** of 2.422(8)Å is comparable to those found in $[Ag_2(\mu\text{-dppm})_2(NO_3)_2]$ [28] and $[Ag(PPh_3)(NO_3)]$ [185] [2.416(5)Å and 2.438(7)Å respectively]; both contain nitrate ligands bound to the silver atom in a chelating fashion through two of their oxygen atoms.

The Ag-P bond distance of 2.378(3)Å is identical to that of the parent complex **[33]**, and closely resembles, for example, those found in $[Ag(\mu\text{-Cl})(\eta^1\text{-Ph}_2\text{Ppy})]_4$[164] which range from 2.387(5) to 2.429(5)Å.

A degree of rotation about the interannular C(17)-C(18) bond, which is necessary in order for the bipyridine fragment to coordinate to a metal atom preferring tetrahedral coordination geometry, has the result that the Ag-N(2′) bond [2.392(2)Å] is longer than that for Ag-N(1′) [2.322(2)Å]. In addition, the dihedral angle between the mean planes through the non-hydrogen atoms of each pyridine ring of the bipyridine fragment is 13.9°. Of interest is the large P(1)-Ag-Ag′-N(1) torsion angle of 46.0°; indeed, this is the largest degree of torsion within the AgPCNAg core thus far observed and is attributed to the shorter Ag....Ag separation and the steric restrictions which that imposes upon the coordination of the Ph_2Pbipy ligand. Nevertheless, the AgPCNAgPCN eight-membered core still adopts the characteristic puckered conformation shown in Figure 5.8.

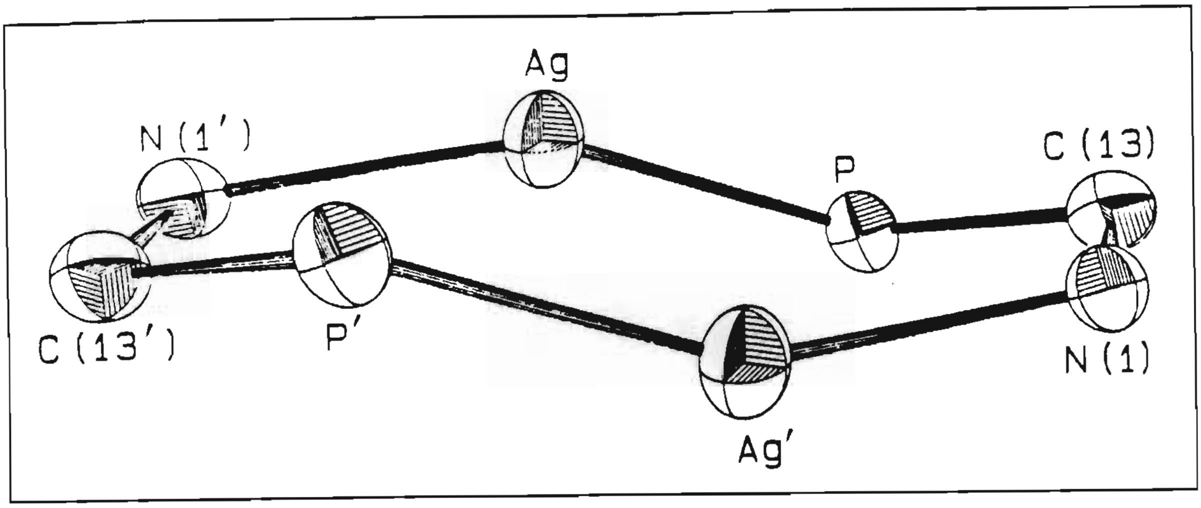

Figure 5.8: A view of the eight-membered AgPCNAgPCN ring of [43], showing the distorted conformation

5.3.2.3 Synthesis of the monocationic species $[Ag_2(\mu\text{-}Ph_2Pbipy)_2(\mu\text{-}L)]X$ ($L = I^-$ and $X = BF_4^-$ [44], $L = OC(Me)O^-$ and $X = PF_6^-$ [45], $L = OC(Ph)O^-$ and $X = PF_6^-$ [46] or L = pyrazolate and $X = BF_4^-$ [47])

Reaction of the BF_4^- salt of **[33]** with one equivalent of tetrabutylammonium iodide in acetone at 0°C affords a clear, pale yellow solution from which the colourless crystalline product $[Ag_2(\mu\text{-}Ph_2Pbipy)_2(\mu\text{-}I)](BF_4)$ **[44]** can be precipitated by the addition of ethanol. Unlike the insoluble, neutral diiodide mentioned in 5.3.2.1, this complex is soluble in most organic solvents, as well as warm methanol and acetonitrile, but insoluble in ethers and alkanes. Its infra-red spectrum (Table 5.5) is characterised by a ν(B-F) stretching band at 1051 cm^{-1}, attributable to the BF_4^- anion, and characteristic ligand bands. In addition to a satisfactory microanalysis (Table 5.4), the complex has ^1H nmr and $^{31}P\{^1H\}$ nmr spectra as outlined in Table 5.5. The structure of the cation of **[44]** has been elucidated by means of X-ray diffraction techniques (see section 5.3.2.4).

The synthesis of $[Ag_2(\mu\text{-}Ph_2Pbipy)_2\{\mu\text{-}OC(Me)O\}](PF_6)$ **[45]** and $[Ag_2(\mu\text{-}Ph_2Pbipy)_2\{\mu\text{-}OC(Ph)O\}](PF_6)$ **[46]** are carried out in an analogous fashion; indeed, both complexes can be synthesised via two procedures. Addition of one equivalent of the appropriate sodium carboxylate salt to the PF_6^- salt of **[33]** in acetone at room temperature, followed by addition of diethyl ether at -25°C, affords the relevant complex as a pale yellow, microcrystalline powder. Alternatively, treatment of Ph_2Pbipy with one equivalent of the appropriate silver carboxylate in acetone produces a clear yellow solution. Displacement of the carboxylate counterion occurs by subsequent treatment with one equivalent of NH_4PF_6; the PF_6^- salts precipitate as pale yellow, microcrystalline powders at -25°C in the presence of diethyl ether. The yields of the products synthesised by the latter method are significantly better than those using the former method. The complexes are soluble in all common organic solvents, but insoluble in ethers and ethanol. The analogous formate-bridged derivative could not be isolated, which is not particularly surprising in view of the instability of silver formate itself. Both complexes have acceptable microanalytical results. The infra-red spectral details are summarised in Table 5.5. Complex **[45]** shows, in its infra-red spectrum, a P-F stretching band of frequency 841 cm^{-1} (assignable to the PF_6^- counterion), characteristic ligand bands and an intense band at 1574 cm^{-1}, attributable to the acetate bridge; that for the silver acetate itself occurs at 1581 cm^{-1}. Similarly, for the benzoate derivative **[46]**, an intense broad band at 1562 cm^{-1} confirms the presence of a bridging benzoate moiety. The ^1H nmr and $^{31}P\{^1H\}$ nmr spectral details for both complexes are also given in Table 5.5. The peak intensities attributable to the acetate protons of **[45]**, when compared with those of the Ph_2Pbipy ligand protons, confirm the presence of one acetate ligand whilst those of the benzoate bridge of **[46]** are apparently obscured by the aromatic resonances of the protons of Ph_2Pbipy. The proposed molecular structures of **[45]** and **[46]** have been confirmed using X-ray diffraction techniques (see sections 5.3.2.5 and 5.3.2.6 respectively).

Reaction of solid sodium pyrazolate (Na^+pyz^-) with an equimolar quantity of the BF_4^- salt of **[33]** in methanol at 30°C leads to the separation of a white solid, identified as $NaBF_4$, from a pale-yellow solution of $[Ag_2(\mu\text{-}Ph_2Pbipy)_2(\mu\text{-}pyz)](BF_4)$ **[47]**. The complex precipitates as pale-yellow rhombs (which lose solvent immediately) by filtration of the $NaBF_4$ and allowing the filtrate to evaporate slowly in air. The product has similar solubilities to those of the carboxylate-bridged species. The appearance of a strong B-F stretching band, in its infra-red spectrum (Table 5.5), at 1054 cm^{-1}, confirms the existence of a cationic species for which BF_4^- is the counter-anion. The bands attributable to the pyrazolate bridge are no doubt masked by those of the Ph_2Pbipy ligand. On the basis of microanalytical results (Table 5.4) and ^1H nmr and $^{31}P\{^1H\}$nmr spectra (Table 5.5), the structure shown in Scheme 5.3 is proposed, with a four-membered Ag-N-N-Ag pyrazolate bridge.

5.3.2.4 Crystal structure determination of $[Ag_2(\mu\text{-}Ph_2Pbipy)_2(\mu\text{-}I)]^+$

The molecular geometry of the $[Ag_2(\mu\text{-}Ph_2Pbipy)_2(\mu\text{-}I)]^+$ cation is depicted in Figure 5.9. The molecule consists of two silver atoms bridged, not only by a pair of Ph_2Pbipy ligands in a head-to-tail fashion, but by an iodide ligand as well, so completing the pseudo-tetrahedral coordination around each silver atom. The two silver atoms are linked to the iodide atom through closed three-centre bonding.

Upon coordination of the bridging iodide, the first effect is for the Ag....Ag separation to decrease from 2.973(2)Å to 2.920(3)Å and the second is for the eight-membered AgPCNAgPCN core to bend away from the bridging iodide, such that it adopts the "chair-chair" conformation in the solid state illustrated in Figure 5.10.

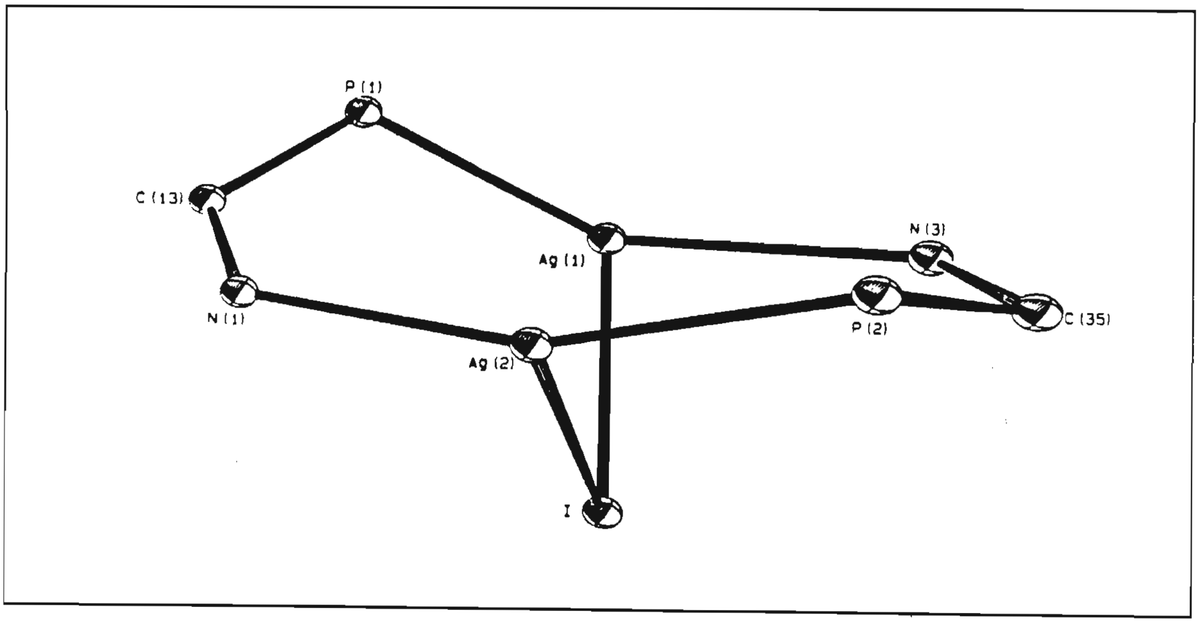

Figure 5.10: A view of the eight-membered AgPCNAgPCN core of the $[Ag_2(\mu\text{-}Ph_2Pbipy)_2(\mu\text{-}I)]^+$ cation, showing the distortion away from the bridging iodide and the resultant "chair-chair" conformation.

Despite this distortion, the range of angles around each silver atom is not as great as that for the parent complex **[33]**. The largest angles are the inter-ligand P-Ag-N angles [P(1)-Ag(1)-N(3) = 138.5(5)° and P(2)-Ag(2)-N(1) = 156.4(5)] but both are significantly reduced from the corresponding angle in **[33]** [168.3(3)°], while the small angles

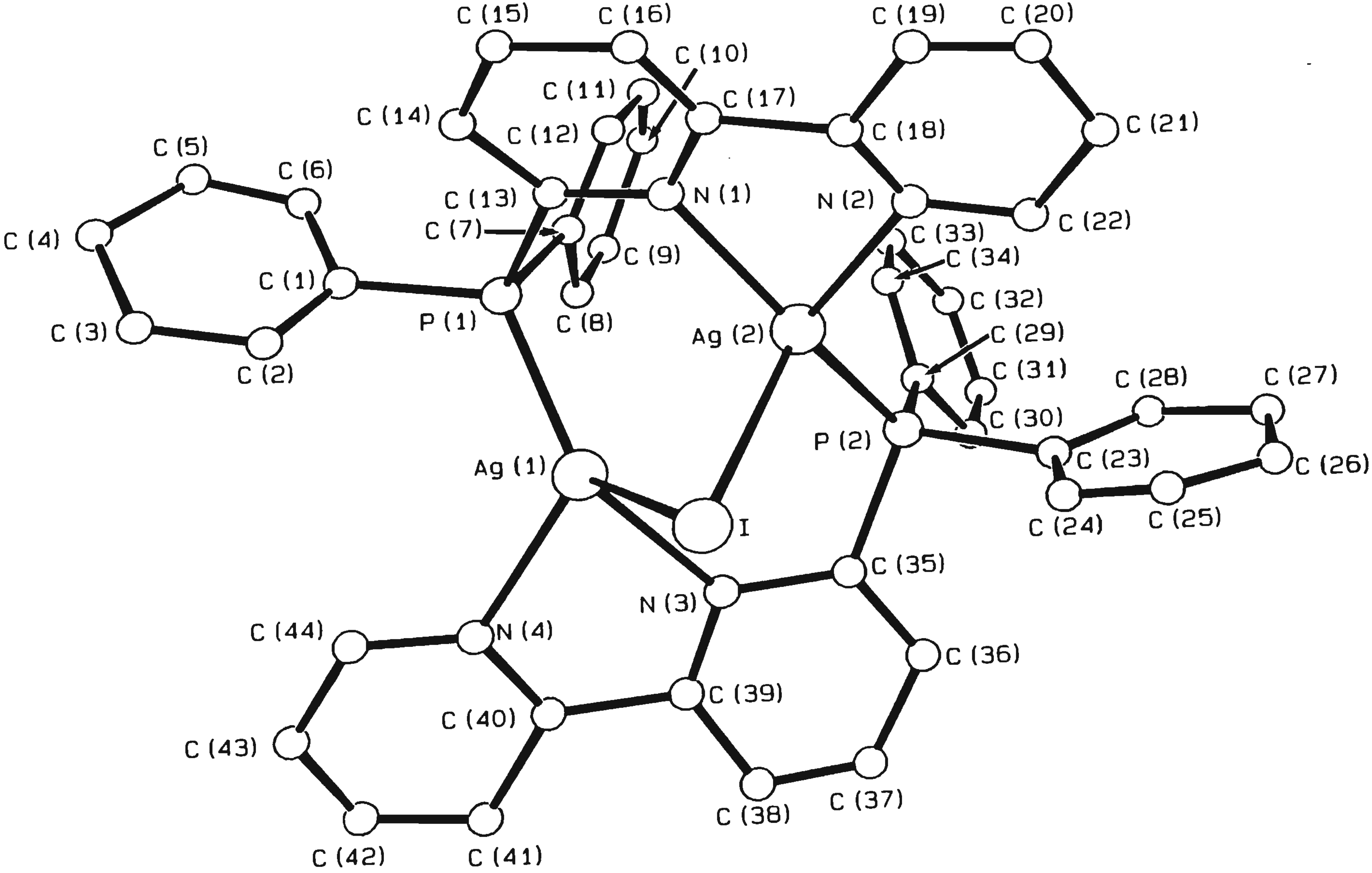
C (15)
C (16)
C (19)
C (20)
C (10)
C (11)
C (17)
C (14)
C (12)
C (18)
C (21)
C (5)
C (6)
C (13)
N (1)
N (2)
C (22)
C (4)
C (7)
C (33)
C (9)
C (34)
C (1)
C (32)
C (3)
P (1)
C (8)
Ag (2)
C (29)
C (2)
C (31)
C (28)
C (27)
C (30)
P (2)
Ag (1)
C (23)
C (26)
C (24)
C (25)
I
C (35)
N (3)
C (44)
N (4)
C (36)
C (39)
C (40)
C (43)
C (38)
C (37)
C (42)
C (41)

subtended at each silver atom by the two nitrogen atoms of the bipyridine moiety [N(1)-Ag-(2)-N(2) = 69.4(8)° and N(3)-Ag(1)-N(4) = 71.0(7)°] are approximately the same as those for **[33]** [71.1(3)°]. The remaining angles around each silver atom are significantly closer to that expected for tetrahedral coordination (Table 5.33). In addition, all angles involving Ag(1), Ag(2) and I are close to 60°.

The Ag-I bond distances differ to a significant degree [Ag(1)-I = 2.719(3)Å and Ag(2)-I = 2.855(3)Å] and are a little longer than that found for AgI itself [2.544(8)Å].[185] This gives an idea of the asymmetry present in the complex but it is unclear why there is such a difference in the two Ag-I bond lengths. The differing bond distances have the effect that the iodine atom is closer to the bipyridine fragment containing N(3) and N(4) than that containing N(1) and N(2). This might explain why the dihedral angle between the mean planes though the non-hydrogen atoms defined by each pyridine ring containing N(3) and N(4) is 14.0° whilst that between the planes defined by each pyridine ring containing N(1) and N(2) is a mere 5.2°. In an opposing sense, the P(1)-Ag(1)-Ag(2)-N(1) torsion angle of 29.2° contrasts with that for P(2)-Ag(2)-Ag(1)-N(3) which is only 13.3°. These torsion angles have the result that the Ag(1)-P(1) bond distance of 2.385(7)Å is significantly longer than that for Ag(2)-P(2) of 2.366(7)Å. Moreover, both distances are a little less than the range cited in the literature [2.387(5)Å to 2.436(2)Å].[28,164,173]

5.3.2.5 Crystal structure determination of $[Ag_2(\mu\text{-}Ph_2Pbipy)_2\{\mu\text{-}OC(Me)O\}](PF_6)$ [45]

The molecular geometry of the asymmetric $[Ag_2(\mu\text{-}Ph_2Pbipy)_2\{\mu\text{-}OC(Me)O\}]^+$ cation is depicted in Figure 5.11. The structure consists of discrete cations and anions separated in the lattice by three water molecules and one acetone molecule per dimer unit. As in previous structures, the two silver atoms are held in place by a pair of Ph_2Pbipy ligands, orientated in a head-to-tail fashion. Furthermore, they are bridged by an acetate anion, bonded in a μ-η^2- fashion through its oxygen atoms.

As for the iodide-bridged complex **[44]**, the eight-membered AgPCNAgPCN core is bent away from the bridging acetate and has the same characteristic "chair-chair" conformation. The Ag....Ag non-bonded distance of 2.988(2)Å is a little longer than that of the parent complex **[33]** [2.973(2)Å], implying that the three-membered OCO bridge does not pull the silver atoms closer together, as does the single-membered iodide bridge of complex **[44]**.

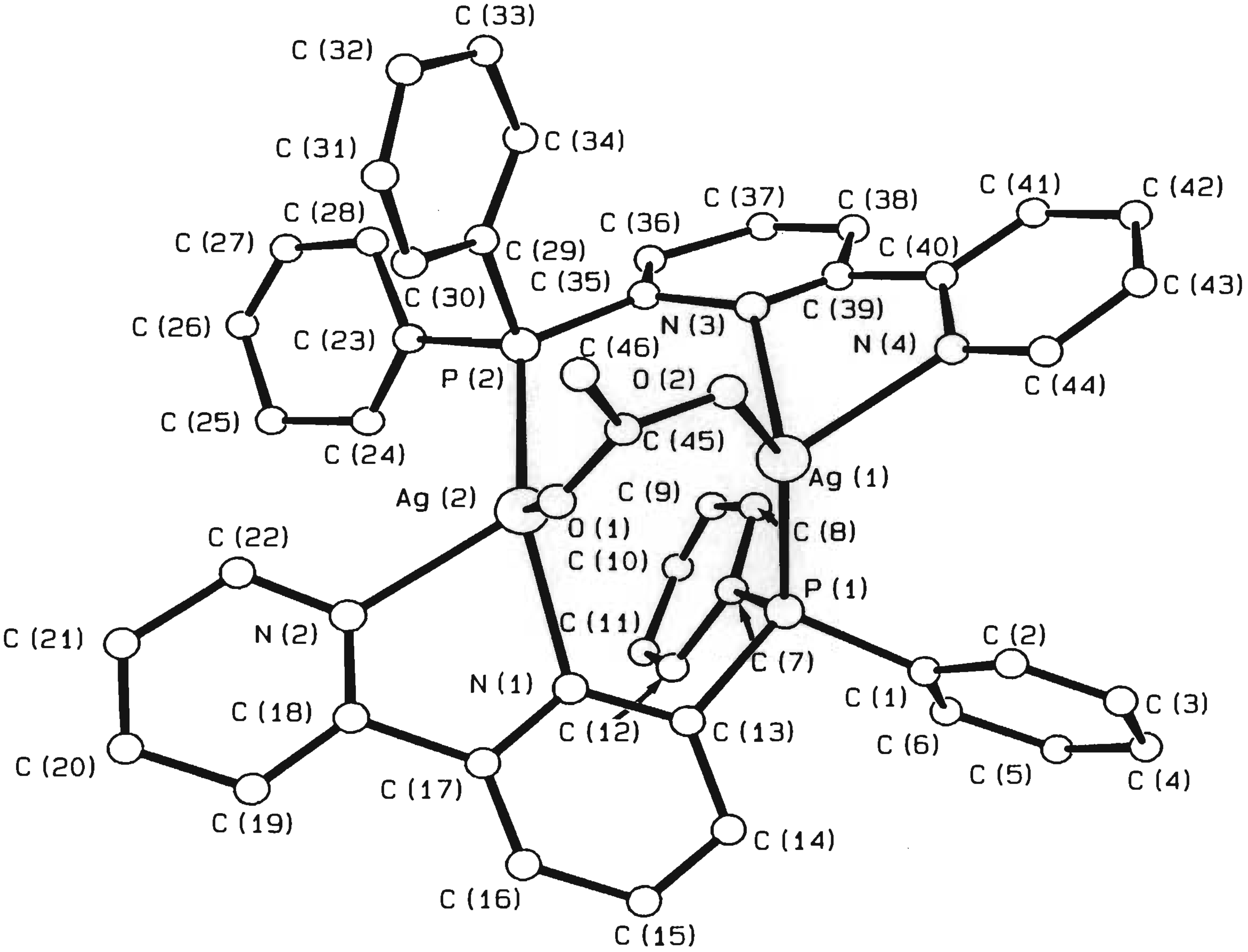
C (33)
C (32)
C (31)
C (34)
C (28)
C (27)
C (29)
C (36)
C (37)
C (38)
C (41)
C (42)
C (30)
C (35)
C (40)
C (43)
C (26)
C (23)
P (2)
C (46)
N (3)
C (39)
N (4)
O (2)
C (44)
C (25)
C (24)
C (45)
Ag (1)
Ag (2)
C (9)
O (1)
C (8)
C (22)
C (10)
P (1)
C (21)
N (2)
C (11)
C (2)
C (7)
N (1)
C (1)
C (3)
C (18)
C (12)
C (13)
C (6)
C (20)
C (5)
C (4)
C (17)
C (19)
C (14)
C (16)
C (15)

The greatest extent of distortion away from tetrahedral geometry at the silver atoms occurs for the P(1)-Ag(1)-N(3) [114.3(5)°] and P(2)-Ag-(2)-N(1) [153.8(5)°] angles, but neither of these are as pronounced as the 168.3(3)° observed in complex **[33]**. Compensating for this expansion are the much smaller N(3)-Ag(1)-N(4) [69.2(6)°] and N(1)-Ag(2)-N(2) [70.8(6)°] angles subtended at Ag(1) and Ag(2) respectively by the nitrogen atoms of the relevant bipyridine fragment. The remaining angles around each silver atom lie within these ranges of distortions and are given in Table 5.38.

The acetate bridge is twisted at an angle [O(1)-Ag(2)-Ag(1)-O(2)] of 23.3° away from the Ag-Ag vector and towards the Ph_2Pbipy ligand containing P(2). This latter feature has the result that the dihedral angle through the mean planes defined by the non-hydrogen atoms of the pyridine rings containing N(3) and N(4) is a substantial 30.5°. Associated with this large twist is a relatively small P(2)-Ag(2)-Ag(1)-N(3) torsion angle of 9.4°. In contrast, the dihedral angle between the mean planes defined by the pyridine groups containing N(1) and N(2) is only 9.8° compared with the torsional twist involving the P(1)-Ag-(1)-Ag(2)-N(1) angle which is a relatively large 30.2°. Interatomic bond distances within the complex closely resemble those of **[33]** (Table 5.37). There is a marked difference between the Ag-O bond distances and this gives an indication of the asymmetry present within the cation; that of Ag(1)-O(2) is 2.236(17)Å while that of Ag(2)-O(1) is 2.480(18)Å.

5.3.2.6 Crystal structure determination of $[Ag_2(\mu\text{-}Ph_2Pbipy)_2\{\mu\text{-}OC(Ph)O\}](PF_6)$ [46]

A perspective view of the $[Ag_2(\mu\text{-}Ph_2Pbipy)_2\{\mu\text{-}OC(Ph)O\}]^+$ cation is given in Figure 5.12. The crystal lattice consists of discrete cations and anions separated by two acetone molecules per dimer unit. The complex closely resembles the μ-acetate species **[45]**, with the two silver atoms bridged by a pair of Ph_2Pbipy ligands as well as a benzoate anion bonded in a $\mu\text{-}\eta^2$-fashion through its oxygen atoms.

The view shown in Fig. 5.12 gives an indication of the extent of asymmetry within the complex. The benzoate bridge coordinates to the dimer with a O(1)-Ag(1)-Ag(2)-O(2) torsion angle of 25.4°. Within the benzoate moiety, a degree of interannular rotation about the C(45)-C(46) bond has the result that the plane defined by the carbon atoms of the phenyl ring is twisted at an angle of 18.2° away from the plane defined by the O(1)-C(45)-O(2) triad. The non-bonded Ag....Ag separation [2.945(1)Å] is shorter than the

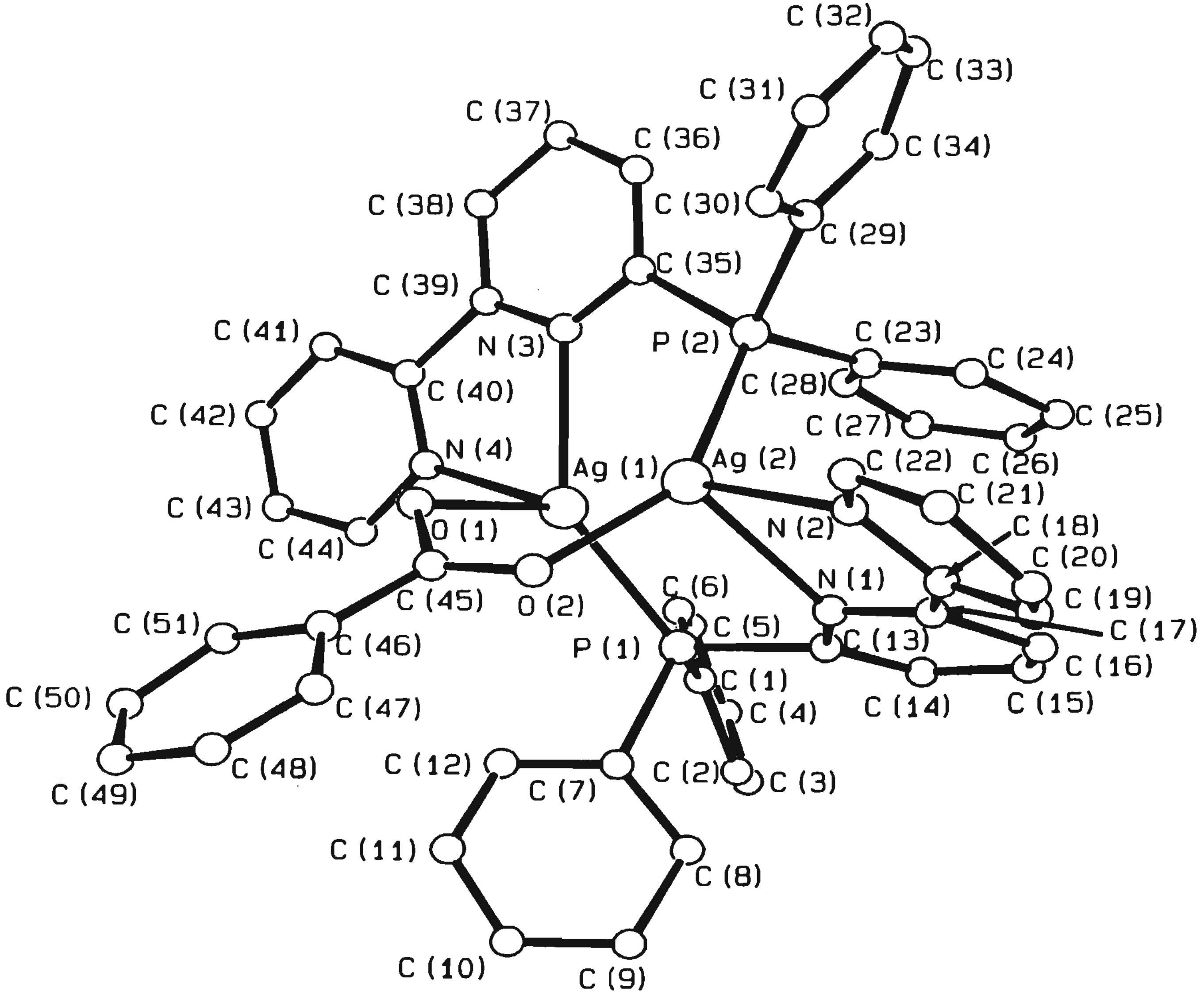
C (32)
C (33)
C (31)
C (37)
C (36)
C (34)
C (38)
C (30)
C (29)
C (39)
C (35)
C (41)
N (3)
P (2)
C (23)
C (24)
C (28)
C (40)
C (42)
C (27)
C (25)
N (4)
Ag (1)
Ag (2)
C (22)
C (26)
C (21)
C (43)
N (2)
0 (1)
C (18)
C (44)
C (20)
N (1)
C (45)
0 (2)
C (6)
C (19)
C (17)
C (51)
C (5)
C (46)
P (1)
C (13)
C (16)
C (1)
C (50)
C (47)
C (4)
C (14)
C (15)
C (12)
C (48)
C (2)
C (3)
C (7)
C (49)
C (11)
C (8)
C (10)
C (9)

corresponding distance in the acetate complex **[45]** [2.988(2)Å] as well as that for the parent complex **[33]** [2.973(2)Å].

The angles around each silver atom are distorted to varying extents away from tetrahedral geometry with the largest occurring at the Ag(1) atom for the P(1)-Ag(1)-N(3) angle of 141.6(1)°. The analogous angle at Ag(2) [P(2)-Ag(2)-N(1)] is substantially less at 104.3(1)°. Indeed, the greatest deviation at Ag(2) is the P(2)-Ag(2)-O(2) angle [144.8(1)°]. The much smaller angles subtended at each silver atom by the two nitrogen atoms of the relevant bipyridine fragment [N(1)-Ag(2)-N(2) = 68.4(2)° and N(3)-Ag(1)-N(4) = 70.1(2)°] effectively compensate for the larger angles. The two bridging Ph_2Pbipy ligands exhibit contrasting torsional characteristics. The dihedral angle between the mean planes defined by the non-hydrogen atoms of the pyridine rings containing N(1) and N(2) which is 27.3°, while that between the rings containing N(3) and N(4) is only 6.2°. In contrast, the P(1)-Ag(1)-Ag(2)-N(1) torsion angle is 11.5° while that for P(2)-Ag(2)-Ag(1)-N(3) is a substantial 26.8°.

The Ag-P bond distances of 2.371(2)Å [Ag(1)-P(1)] and 2.396(1)Å [Ag(2)-P(2)] correspond more closely to the parent **[33]** than those of the analogous acetate complex **[45]**. However, the asymmetry present within the complex closely resembles that of **[45]** in that the Ag-O distances are significantly different [Ag(1)-O(1) = 2.369(4)Å and Ag(2)-O(2) = 2.241(4)Å]. Remaining bond angles and distances are presented in Tables 5.43 and 5.42 respectively.

5.3.2.7 Synthesis of the monocationic polymer $\{[Ag_2(\mu\text{-}Ph_2Pbipy)_2(\mu'\text{-}SCN)](BF_4)\}_n$ [48]

Addition of an equivalent of tetrabutylammonium thiocyanate to $[Ag_2(\mu\text{-}Ph_2Pbipy)_2(NCMe)_2](BF_4)_2$ in CH_2Cl_2, affords a clear yellow solution from which, upon addition of n-heptane, yellow rhombs can be isolated. These crystals are totally insoluble in all solvents, including CH_2Cl_2 from which they are isolated. Presumably, the soluble species is some sort of solvento species and the product, therefore, a polymeric material, most likely comprising dimeric units linked through thiocyanate ligands (see Scheme 5.3). This follows in the light of the known tendency for AgSCN to have the linear chain structure shown below.[186]

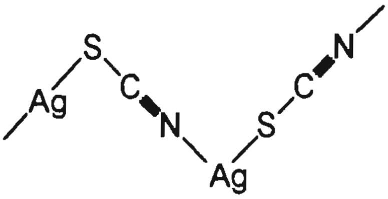

Its solid-state (KBr disk) infra-red spectrum (Table 5.5) exhibits an intense band at 2087 cm^{-1} attributed to the μ-SCN ligand. Furthermore, in addition to the characteristic Ph_2Pbipy ligand bands (Figure 5.1a)), a broad band at 1058 cm^{-1} assigned to the BF_4^- counter-anion confirms the cationic nature of the product. Microanalytical results (Table 5.4) are consistent with the compounds stoichiometry. Insolubility precludes the measurement of its ^1H or $^{31}P\{^1H\}$ nmr spectra. The complex resembles those polymers discussed in later sections involving heterocyclic nitrogen ligands.

5.3.3 Reactions of $[Ag_2(\mu\text{-}Ph_2Pbipy)_2(NCMe)_2]^{2+}$ with substituted pyridines.

The labile acetonitrile ligands bound to the silver atoms of the $[Ag_2(\mu\text{-}Ph_2Pbipy)_2(NCMe)_2]^{2+}$ cation are readily substituted by a range of substituted pyridines. Depending on the nature of the substituted pyridine, either dicationic dinuclear units containing pendant pyridine ligands or monocationic polymers in which the pyridine ligand bridges across adjacent dimers, are formed. The top portion of Scheme 5.4 illustrates the reactions carried out.

5.3.3.1 Synthesis of the dicationic complexes $[Ag_2(\mu\text{-}Ph_2Pbipy)_2(\eta^1\text{-}Rpy)_2](BF_4)_2$ (R = 4-cyano [49] or 4-vinyl [50]) and $[Ag_2(\mu\text{-}Ph_2Pbipy)_2(\eta^1\text{-}pbpz)_2](BF_4)_2$ [51] (pbpz = pyrido-[2,3-b]pyrazine).

Reaction of the BF_4^- salt of **[33]** with excess Rpy (R = 4-cyano or 4-vinyl) in CH_2Cl_2 affords yellow solutions from which $[Ag_2(\mu\text{-}Ph_2Pbipy)_2(\eta^1\text{-}Rpy)_2](BF_4)_2$ (R = 4-cyano **[49]** or 4-vinyl **[50]**) are isolated as crystalline white precipitates at -25°C after reduction of the solvent volume and addition of diethyl ether. Both complexes are very soluble in most organic solvents, but insoluble in ethers and alcohols. The characterisation of the complexes was achieved using methods analogous to that for the pyridine complex **[35]** mentioned in 5.3.1.1. Physical and microanalytical data are presented in Table 5.6. In their respective infra-red spectra (Table 5.7) the B-F stretching bands at 1048 and 1052 cm^{-1} respectively confirm that the products retain their ionic character. For complex **[49]**, an additional

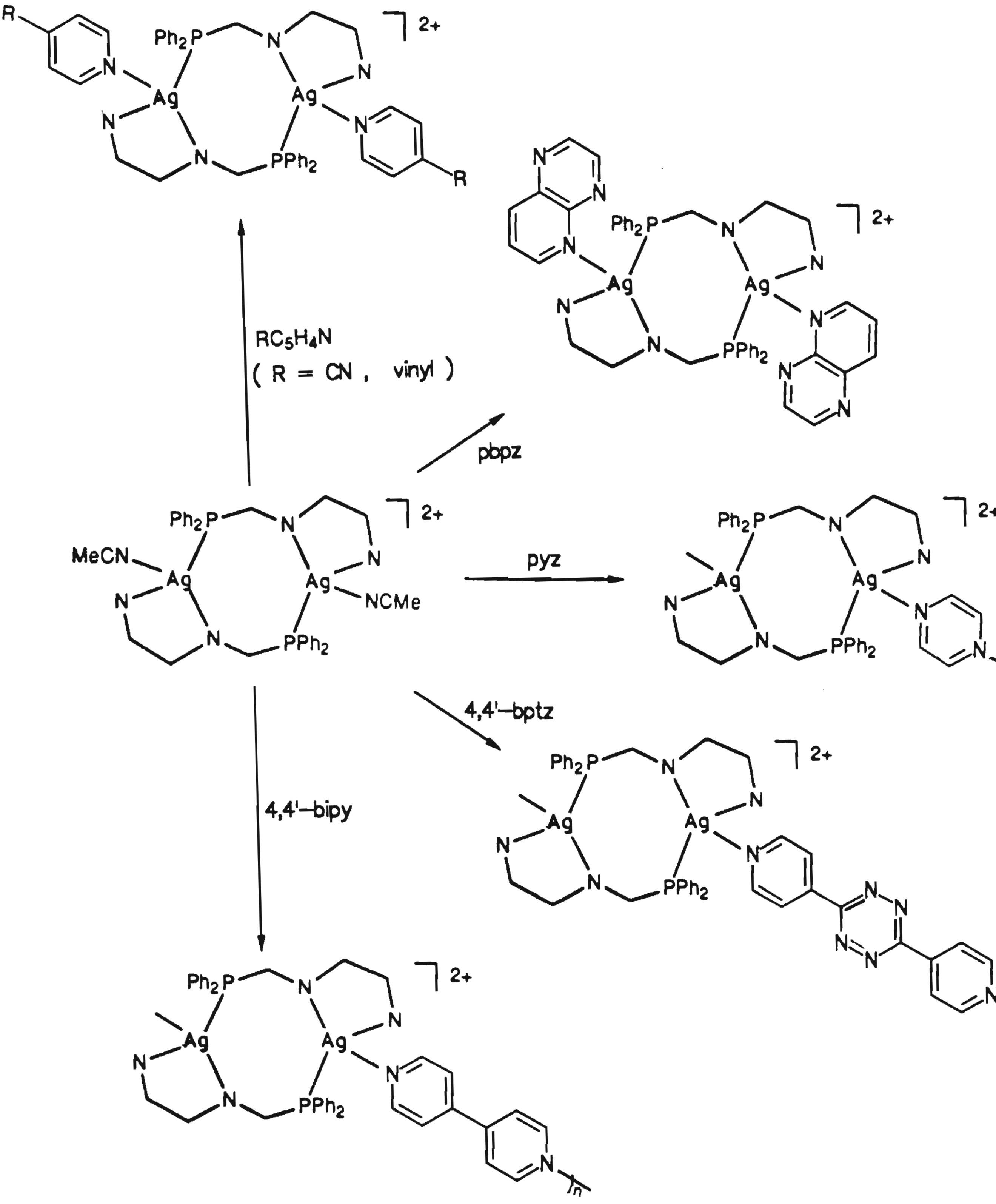

R
Ph2P
N
N
Ag
Ag
N
N
N
PPh2
R
2+
RC5H4N
(R = CN , vinyl)
pbpz
pyz
4,4'–bptz
4,4'–bipy
MeCN
NCMe
n

Scheme 5.4 The reactions of $[Ag_2(\mu\text{-}Ph_2Pbipy)_2(NCMe)_2]^{2+}$ with substituted pyridines

Table 5.6 Physical and microanalytical data

	Complex	Colour	M:g.mol^{-1}	Analysis : Found (Calculated) %		
				%C	%H	%N
[49]	$[Ag_2(\mu\text{-}Ph_2Pbipy)_2(\eta^1\text{-4-cyanopy})_2](BF_4)_2$	white	1278.29	52.10(52.62)	3.14(3.31)	8.34(8.77)
[50]	$[Ag_2(\mu\text{-}Ph_2Pbipy)_2(\eta^1\text{-4-vinylpy})_2](BF_4)_2$	white	1280.35	54.13(54.41)	3.98(3.78)	6.02(6.56)
[51]	$[Ag_2(\mu\text{-}Ph_2Pbipy)_2(\eta^1\text{-pbpz})_2](BF_4)_2$	yellow	1332.35	52.00(52.29)	3.38(3.33)	10.30(10.52)
[52]	$\{[Ag_2(\mu\text{-}Ph_2Pbipy)_2(\mu'\text{-pz})_2](PF_6)_2\}_n$	white	1226.48	45.21(45.52)	3.11(3.02)	6.65(6.64)

Table 5.7 Infra-red, ^{1}H and ^{31}P{^{1}H} nmr spectroscopic data

Complex	IR(a)	δ ^{1}H nmr (ppm) (b)	^{31}P{^{1}H}nmr (g)		
			δ	$^{1}J(^{107}\text{Ag-}^{31}\text{P})$ (Hz)	$^{1}J(^{109}\text{Ag-}^{31}\text{P})$ (Hz)
[49]	1048(vs)	(c)	22.35	580	711
[50]	1052(vs)	(d)	24.78	584	725
[51]	1051(vs)	(e)	23.44	609	745
[52]	839(vs)	Recorded in acetone-d_6 (f)	24.68 recorded in acetone-d_6	583	727

(a) : Recorded in the solid state as KBr disks. Only bands other than those corresponding to Ph_2Pbipy or aromatic ligands are listed. Designation : vs = very strong

(b) : Recorded in CD_2Cl_2 unless otherwise stated. Only shifts arising from protons other than those of the Ph_2Pbipy ligand (see Table 5.1) are reported.

(c) : 4-cyanopyridine proton shifts obscured by Ph_2Pbipy ligand resonances.

(d) : 4-vinylpyridine proton shifts partially obscured by Ph_2Pbipy ligand resonances.

(e) : Pbpz proton shifts obscured by Ph_2Pbipy ligand resonances.

(f) : Pz proton shifts obscured by Ph_2Pbipy ligand resonances.

(g) : Recorded in CD_2Cl_2 unless otherwise stated. All spectra exhibit characteristic splitting pattern for head to tail silver dimers discussed in the text. δ (in ppm) relative to H_3PO_4. Accuracy in coupling constants not greater than ± 0.5 Hz.

ν(C≡N) stretching band occurring at 2123 cm^{-1}, albeit weak, is consistent with the presence of the 4-cyanopyridine ligand. ^{1}H or ^{31}P{^{1}H} nmr data for both complexes are presented in Table 5.7. In their ^{1}H nmr spectra, resonances due to protons bound to the aromatic pyridine portions are obscured by those of the Ph$_2$Pbipy ligand protons. The vinyllic protons of **[50]** exhibit shifts (distorted doublet of doublets due to the methylene protons and an obscured feature presumably due to the proton of the vinyllic-CH) which are characteristically downfield. The crystal structure of **[51]** has been solved through X-ray diffraction techniques (5.3.3.2)

$[Ag_2(\mu\text{-}Ph_2Pbipy)_2(\eta^1\text{-}pbpz)_2](BF_4)_2$ **[51]** is synthesised by the addition of two equivalents of pyrido[2,3-b]pyrazine (pbpz), below, to the BF_4^- salt of **[33]** in CH_2Cl_2 at room temperature.

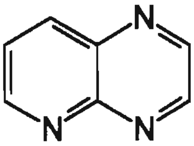

Prolonged interaction affords a pale yellow solution from which golden-yellow crystals of **[51]** can be isolated by addition of diethyl ether and cooling the resultant mixture to -25°C. The reaction was initially carried out with one equivalent of pbpz, with the intention of forming a pbpz ligand-bridged polymer similar to the form of the thiocyanate derivative **[48]** or those polymers described later in the text; the same product, above, resulted. The product's infra-red spectrum (Table 5.7) contains the characteristic broad, intense band at ~1051 cm^{-1} attributable to the BF_4^- counter-anion, while the compound's microanalysis (Table 5.6) is consistent with its stoichiometry. The remaining ^{1}H or ^{31}P{^{1}H} nmr spectral characterisation data are outlined in Table 5.7. The molecular geometry of **[51]** has been elucidated through the use of X-ray diffraction techniques.

5.3.3.2 Crystal structure determination of $[Ag_2(\mu\text{-}Ph_2Pbipy)_2(\eta^1\text{-4-vinylpy})_2](BF_4)_2$ [50]

The molecular geometry of the $[Ag_2(\mu\text{-}Ph_2Pbipy)_2(\eta^1\text{-4-vinylpy})_2]^{2+}$ dication resembles that of the pyridine complex **[35]**, and is shown in Figure 5.13. A crystallographically imposed centre of symmetry is located midway between the two silver atoms. The two silver atoms are linked by a pair of Ph$_2$Pbipy ligands which bridge the dimer in a head-to-tail fashion. In

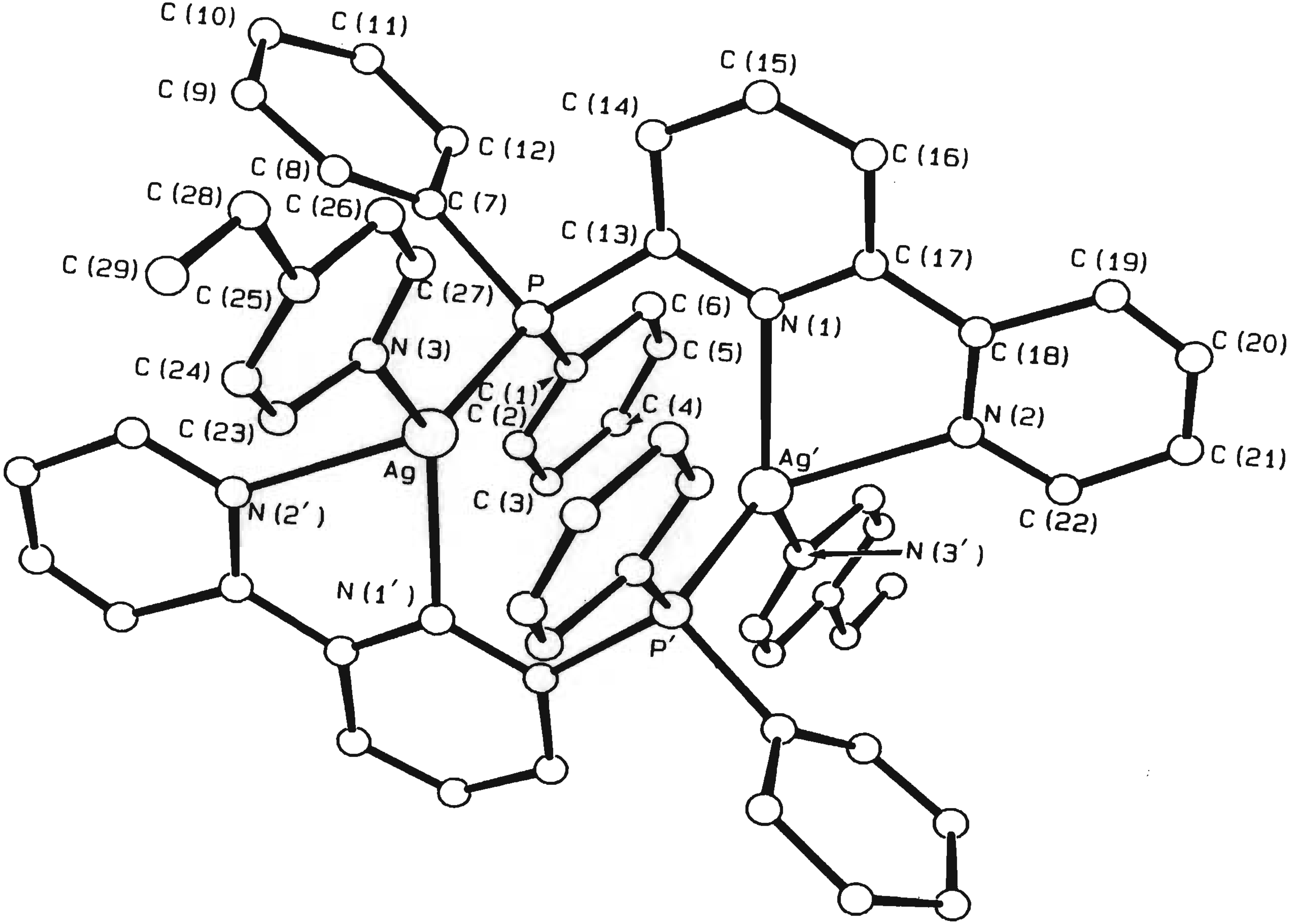
C (10)
C (11)
C (15)
C (9)
C (14)
C (12)
C (16)
C (8)
C (28)
C (26)
C (7)
C (13)
C (17)
C (19)
C (29)
C (25)
C (27)
P
C (6)
C (5)
N (1)
C (18)
C (20)
C (24)
N (3)
C (1)
C (2)
C (4)
N (2)
C (23)
Ag
Ag′
C (21)
C (3)
C (22)
N (2′)
N (3′)
N (1′)
P′

addition, a 4-vinylpyridine molecule is terminally bound in a monodentate fashion through its nitrogen atom to each silver atom, completing the coordination at the latter.

Like the pyridine complex **[35]**, the non-bonded Ag....Ag distance of 4.012(1)Å is substantially larger than that for the parent complex **[33]** [2.973(2)Å]. The angles around each silver atom are distorted to varying extents from the ideal tetrahedral angle of 109.5°. The largest extent of distortion occurs for the N(1)-Ag′-N(3′) angle of 124.4(9)°. Other angles are less distorted (Table 5.48). The smallest angle is the 69.2(4)° angle subtended at the silver atom by the two nitrogen atoms of the bipyridine fragment of the Ph_2Pbipy ligand. The latter once again compensates effectively for the distortions which are significantly greater than 109.5°.

The eight-membered AgPCNAgPCN core, similar to others discussed above, exhibits torsional puckering which results in it adopting neither a “chair-chair” nor a “chair-boat” conformation. This torsional puckering is a result of the large P-Ag-Ag′-N(1) twist of 41.6° in order to alleviate steric interference between the phosphorus atom, its phenyl substituents and the vinylpyridine protons. In contrast, the dihedral angle between the mean planes through the non-hydrogen atoms of the pyridine rings containing N(1) and N(2) is a small 10.9°.

Despite the large torsion angle, the Ag-P bond distance of 2.392(3)Å corresponds well with the 2.398(0)Å obtained in the pyridine analogue, **[35]** as does the Ag-N(3) bond distance of 2.355(9)Å. The latter distance is slightly longer than the maximum distance [2.340(1)Å] found in the $[Ag(py)_4]^+$cation. [166] All relevant bond distances and angles are summarised in Tables 5.47 and 5.48 respectively.

5.3.3.3 Crystal structure determination of $[Ag_2(\mu\text{-}Ph_2Pbipy)_2(\eta^1\text{-}pbpz)_2](BF_4)_2$ [51]

Figure 5.14 illustrates the molecular geometry of the $[Ag_2(\mu\text{-}Ph_2Pbipy)_2(\eta^1\text{-}pbpz)_2]^{2+}$ cation. As for all other dimers discussed thus far which possess, in addition to the two bridging Ph_2Pbipy ligands, two identical ligands bonded to the two remaining coordination sites on the silver atoms in a pendant, monodentate fashion, there is a crystallographically imposed centre of symmetry situated midway between the two silver atoms. The two pbpz ligands are bound to the two silver atoms through their pyrido-nitrogen atoms (found in the literature [187,188] to be the most basic nitrogen of pbpz), while the pyrazino-nitrogens remain

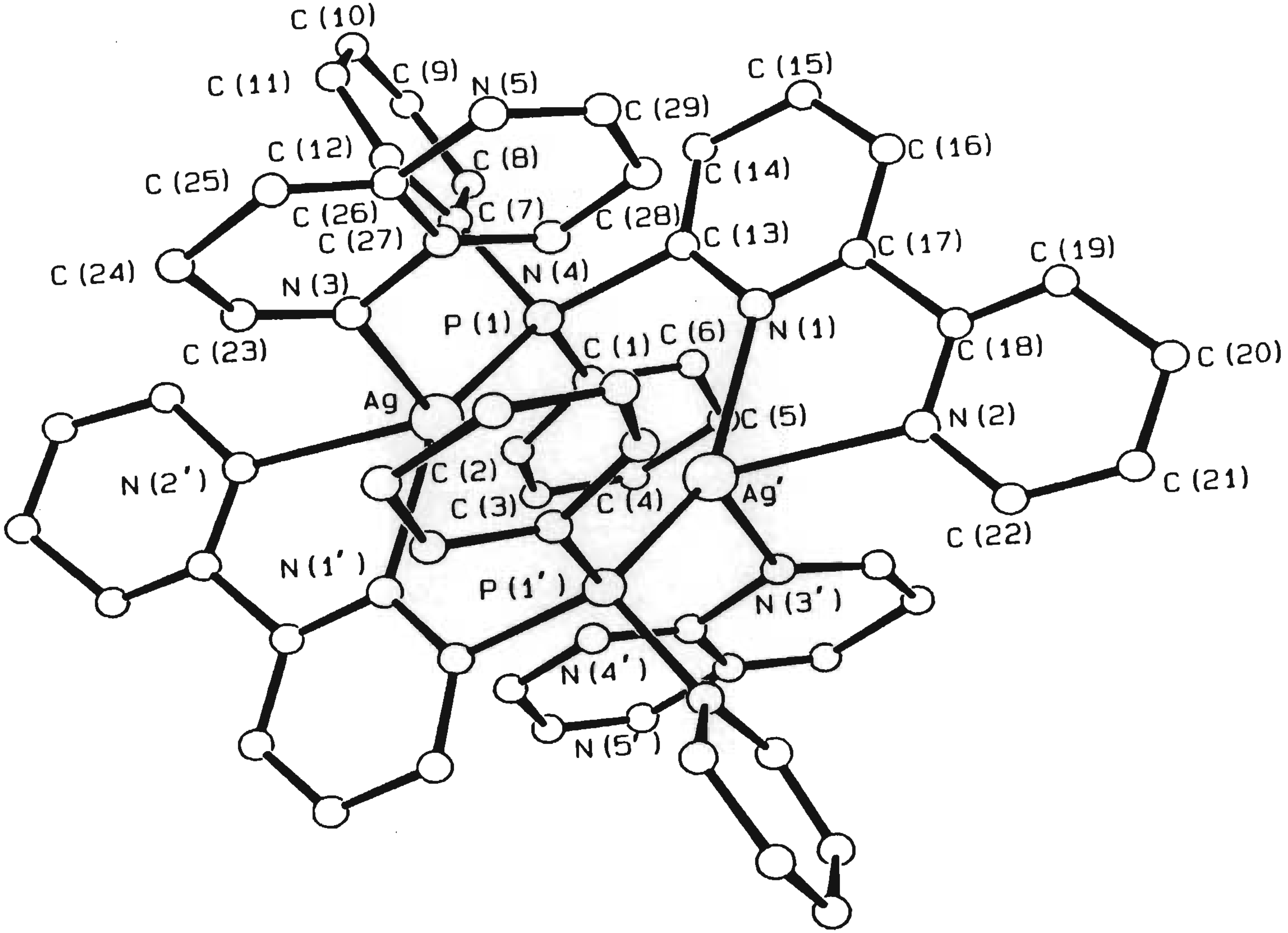
C (10)
C (11)
C (9)
N (5)
C (29)
C (15)
C (12)
C (8)
C (16)
C (25)
C (14)
C (26)
C (7)
C (28)
C (27)
C (13)
C (17)
C (19)
C (24)
N (4)
N (3)
P (1)
C (1)
C (6)
N (1)
C (18)
C (23)
C (20)
Ag
C (5)
N (2)
C (2)
N (2')
C (4)
Ag'
C (21)
C (3)
C (22)
N (1')
P (1')
N (3')
N (4')
N (5')

unbonded. They complete the coordination geometry at each silver atom. This monodentate form of bonding has been suggested before [189] but not structurally proven, as pbpz has a preference to bond in a bridging fashion through two of its nitrogen atoms; in addition, it has been known to chelate to a metal atom.[189]

The non-bonded Ag....Ag separation of 3.125(1)Å is marginally larger than that of the parent complex **[33]** [2.973(2)Å] but is shorter than the corresponding distances in both the 4-vinylpyridine **[50]** [4.012(1)Å] and pyridine **[35]** [4.092(1)Å] complexes.

Angles around each silver atom are distorted to some extent; the smallest is the 69.4(2)° subtended by the two nitrogen atoms of the pyridine fragment, while the largest is once again the P(1)-Ag-N(1′) angle of 145.1(2)°. However, this range of distortions is not as large as that found in **[33]** [71.3(3°) to 168.3(3)°] despite the presence of greater overall steric crowding around each silver atom. The ligands themselves twist at an angle [P(1)-Ag-Ag′-N(1)] of 30.2(1)° and this, somewhat surprisingly, correlates well with that observed in **[33]** [24.3(2)°]. The dihedral angle between the mean planes through the non-hydrogen atoms of each pyridine ring of the bipyridyl fragment is 7.06(4)°, even less than that obtained for the free, uncoordinated Ph_2Pbipy ligand [7.7(3)°].

The Ag-P bond distance of 2.386(2)Å is in good agreement with that found for **[33]** [2.398(2)Å] while the Ag-N(3) distance of 2.403(7)Å is significantly longer than the 2.333(1)Å found in the pyridine analogue **[35]** as well as the 2.355(9)Å found in the 4-vinylpyridine derivative **[50]**, the latter feature being attributed to the weaker donor nature of pbpz.

5.3.3.4 Synthesis of the dicationic polymer $\{[Ag_2(\mu\text{-}Ph_2Pbipy)_2(\mu'\text{-}pz)](PF_6)_2\}_n$ [52] (pz = pyrazine)

Reaction of the parent complex **[33]** (hexafluorophosphate salt) with excess pyrazine, illustrated in Scheme 5.4, in CH_2Cl_2 at room temperature afforded a white precipitate which was isolated by filtration and characterised as the polymeric complex $\{[Ag_2(\mu\text{-}Ph_2Pbipy)_2(\mu'\text{-}pz)](PF_6)_2\}_n$ **[52]**. The complex forms in excellent yield and is soluble in nitrile donor solvents, and partially so in weak donor solvents such as acetone and methanol. It is insoluble in all other solvents. Single crystals grown from an acetone solution cooled to -25°C for 24 hours lost incorporated solvent immediately. However, in subsequent X-ray diffraction studies involving ligands related to pyrazine (*e.g.* 4,4′-

bipyridine), the compounds polymeric nature has been confirmed. The product which is isolated from the CH_2Cl_2 solution is analytically pure (Table 5.6), provided it is washed thoroughly with diethyl ether after filtration. A solid state (KBr disk) infra-red spectrum exhibits characteristic Ph_2Pbipy ν(C-N) and ν(C-P) bands (see Figure 5.1) as well as an intense band at 839 cm^{-1} which is attributed to the PF_6^- anion of the complex, confirming the products ionic character. Details of the ^1H and $^{31}P\{^1H\}$ nmr spectra are presented in Table 5.7.

5.3.4 Reactions of $[Ag_2(\mu\text{-}Ph_2Pbipy)_2(NCMe)_2]^{2+}$ with bipyridines and substituted bipyridines.

Owing to the importance of bipyridyl-type ligands in inorganic and analytical chemistry, especially in the photochemistry of coordination compounds,[190] there have been numerous studies on developing ligands related to bipyridine.[191] This section describes, in the first instance, the reaction of $[Ag_2(\mu\text{-}Ph_2Pbipy)_2(NCMe)_2]^{2+}$ (BF_4^- salt of **[33]**) with 2,2′-bipyridine and in the second, reactions involving the $[Ag_2(\mu\text{-}Ph_2Pbipy)_2(NCMe)_2]^{2+}$ cation and bipyridyl-type N-heterocyclic ligands containing planar conjugated π systems.

The labile acetonitrile ligands on the $[Ag_2(\mu\text{-}Ph_2Pbipy)_2(NCMe)_2]^{2+}$ cation are readily substituted by N-heterocyclic ligands. The reactions produce either dimers bridged in a head-to-head fashion by the two Ph_2Pbipy ligands(i.e. both phosphorus atoms bonded to the same silver atom) and which contain the N-heterocycle chelating at one silver atom, light and air stable polymers in which the N-heterocycle bridges between successive dimers or, in one case, a head-to-head bonded tetrameric complex. The reactions are summarised in the remaining part of Scheme 5.4 as well as Scheme 5.5.

5.3.4.1 Synthesis of the head-to-head complexes $[Ag_2(\mu\text{-}Ph_2Pbipy)_2(\eta^2\text{-}L)](BF_4)_2$ [L = 2,2′-bipy [53], 1,10-phen [54] and bpd [55] {bpd = 2,3-bis(2-pyridyl)pyrazine}]

The addition of an equivalent of solid 2,2′-bipyridine to $[Ag_2(\mu\text{-}Ph_2Pbipy)_2(NCMe)_2]BF_4$ in acetone solution at room temperature produces a clear, yellow solution from which a pale-yellow crystalline material can be isolated through reduction of solvent volume under reduced pressure and addition of diethyl ether. The product has identical solubilities to those of **[33]** and is air and light stable. Improved yields of the product can be achieved

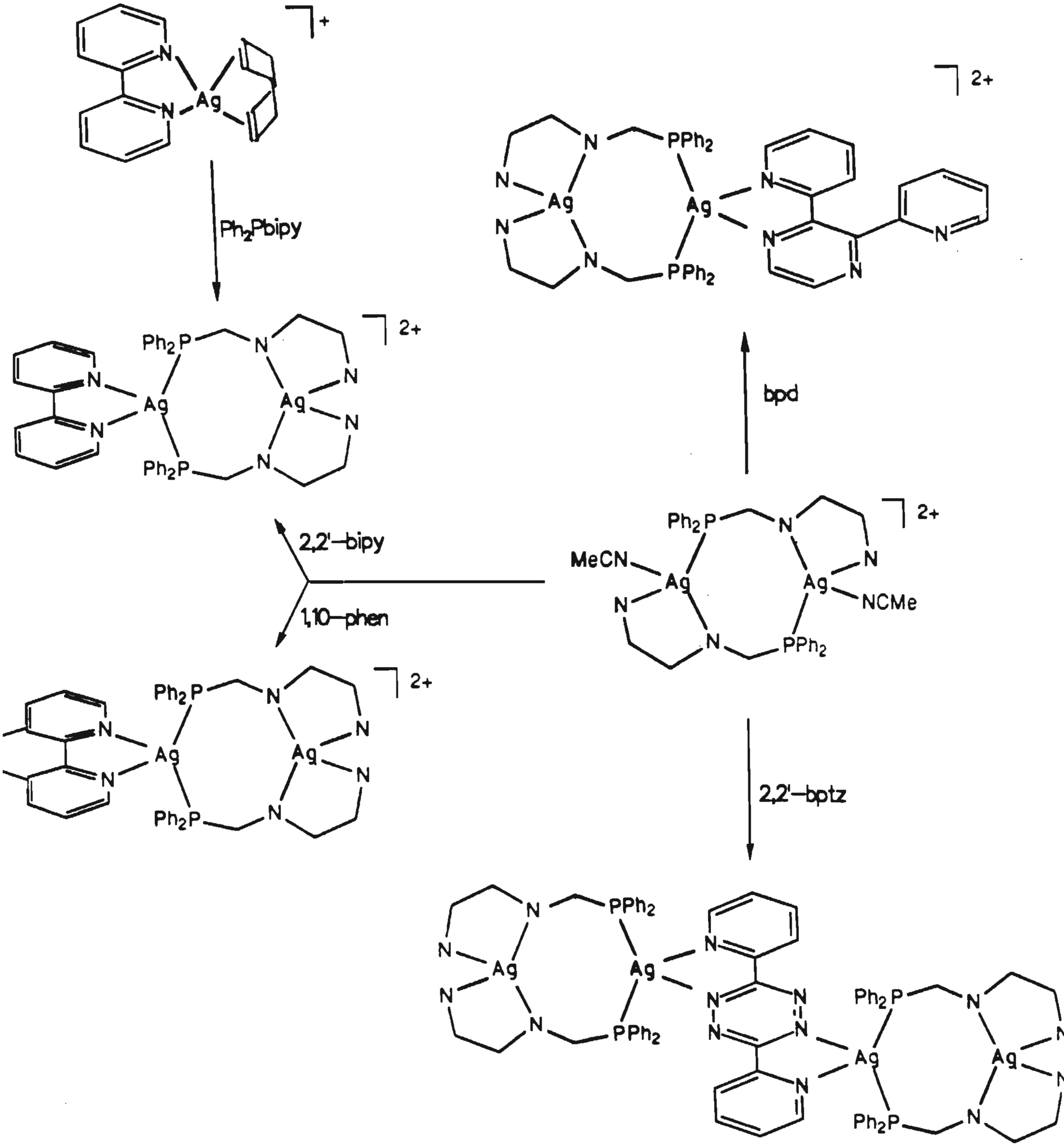
+
Ph₂Pbipy
2+
2+
bpd
2,2'–bipy
1,10–phen
2+
2+
2,2'–bptz
MeCN
NCMe
Ag
N
PPh₂
Ph₂P

Scheme 5.5 The reactions of $[Ag_2(\mu\text{-}Ph_2Pbipy)_2(NCMe)_2]^{2+}$ with bipyridines and substituted bipyridines

Table 5.8 Physical and microanalytical data

	Complex	Colour	M:g.mol^{-1}	Analysis : Found (Calculated) %		
				%C	%H	%N
[53]	$[Ag_2(\mu\text{-}Ph_2Pbipy)_2(\eta^2\text{-}2,2'\text{-bipy})](BF_4)_2$	pale yellow	1226.26	52.57(52.89)	3.30(3.45)	6.81(6.85)
[54]	$[Ag_2(\mu\text{-}Ph_2Pbipy)_2(\eta^2\text{-}1,10\text{-phen})](BF_4)_2$	yellow	1250.28	53.99(53.80)	3.82(3.39)	6.64(6.72)
[55]	$[Ag_2(\mu\text{-}Ph_2Pbipy)_2(\eta^2\text{-bpd})](BF_4)_2$	pale yellow	1304.33	53.23(53.41)	3.12(3.40)	8.76(8.59)
[56]	$\{[Ag_2(\mu\text{-}Ph_2Pbipy)_2(\mu'\text{-}4,4'\text{-bipy})](PF_6)_2\}_n$	white	1342.58	47.98(48.31)	3.34(3.15)	5.93(6.26)
[57]	$\{[Ag_2(\mu\text{-}Ph_2Pbipy)_2(\mu'\text{-}4,4'\text{-bptz})](PF_6)_2\}_n$	scarlet	1306.31	51.00(51.49)	3.19(3.24)	10.05(10.72)
[58]	$[\{Ag_2(\mu\text{-}Ph_2Pbipy)_2\}_2(\mu'\text{-}2,2'\text{-bptz})](BF_4)_4$	purple	2376.38	50.14(50.54)	3.69(3.22)	8.26(8.25)

Table 5.9 Infra-red, ^{1}H and ^{31}P{^{1}H} nmr spectroscopic data

Complex	IR(a)	δ ^{1}H nmr (ppm) (b)	^{31}P{^{1}H}nmr (c)		
			δ	^{1}J(^{107}Ag-^{31}P) (Hz)	^{1}J(^{109}Ag-^{31}P) (Hz)
[53]	1061(vs)	Recorded in acetone-d_6	21.02	483	673 (d)
[54]	1058(vs)		21.78	490	675 (d)
[55]	1060(vs)		21.43	503	671 (d)
[56]	839(vs)		23.21	598	743 (e)
[57]	1057(vs)		23.32	610	749 (e)
[58]	1058(vs)		20.16	472	641 (d)

(a) : Recorded in the solid state as KBr disks. Only bands other than those corresponding to Ph_2Pbipy or aromatic ligands are listed. Designation : vs = very strong.

(b) : Recorded in CD_2Cl_2 unless otherwise stated. All spectra comprise characteristic resonances due to the Ph_2Pbipy ligand, which obscure those of the relevant N-heterocycle.

(c) : Recorded in CD_2Cl_2 unless otherwise stated.

(d) : These spectra exhibit characteristic splitting pattern for head to head silver dimers discussed in the text. δ (in ppm), relative to H_3PO_4, is quoted for the approximate mid-point of the central peak of the coarse triplet. Accuracy in coupling constants not greater than ± 5Hz.

(e) : These spectra exhibit characteristic splitting pattern for head to tail silver dimers discussed in the text. δ (in ppm) relative to H_3PO_4. Accuracy in coupling constants not greater than ± 0.5 Hz.

through a second method; i.e. the reaction of $[Ag(\eta^2\text{-}2,2'\text{-bipy})(cod)]BF_4$, generated *in situ* by the reaction of one equivalent of 2,2′-bipyridine with $[Ag(cod)_2](BF_4)$,[167] with one molar equivalent of Ph_2Pbipy. Prolonged interaction in this manner, followed by the addition of petroleum spirits (60-80°C), affords the highly crystalline title compound **[53]**. The infrared spectrum (Table 5.9) consists of characteristic coordinated Ph_2Pbipy ligand bands (see Figure 5.1) superimposed on which are C-N stretching bands attributable to the 2,2′-bipyridine ligand, as well as an intense B-F stretching band at 1061 cm^{-1} due to the BF_4^- counter-anion. On the basis of $^{31}P\{^1H\}$ nmr evidence presented below, it is presumed that rearrangement of the Ph_2Pbipy ligands, from the head-to-tail orientation present in **[33]** to a head-to-head situation (i.e. one in which both phosphorus atoms of both bridging ligands bind to the same silver atom), occurs in order for 2,2′-bipyridine to chelate at one of the silver atoms. The $^{31}P\{^1H\}$ nmr spectrum (Table 5.9) comprises a very coarse, broad triplet centred at 21.02 ppm, relative to H_3PO_4, external standard. This poorly resolved spectrum is presumed to arise from the overlap of two A_2XY sub-spectra, each one resulting from the coupling of two chemically and magnetically equivalent phosphorus atoms (A_2) with the two chemically and magnetically *in*equivalent silver atoms of the dimer (XY). As for complex **[33]**, the pattern is further complicated by the presence of two isotopes of silver (see section 5.2.1). It is presumed, in this case, that the difference between the $^1J(^{107}Ag/^{109}Ag\text{-}^{31}P)$ and $^3J(^{107}Ag/^{109}Ag\text{-}^{31}P)$ coupling constants are sufficiently small to cause overlap of the central resonances, thereby producing the observed broad central peak and hence the pseudo-triplet. Assigning approximate $^1J(^{107}Ag/^{109}Ag\text{-}^{31}P)$ coupling constants is possible on the same grounds as those presented for the head to tail complex **[33]** in section 5.2.1. and these are presented in Table 5.9.

This structural assignment for **[53]** has subsequently been confirmed through the use of X-ray diffraction techniques (5.3.4.3).

In a similar fashion, reaction of the BF_4^- salt of **[33]** with an equivalent of 1,10-phenanthroline, sterically more rigid than 2,2′-bipyridine, affords the darker yellow product $[Ag_2(\mu\text{-}Ph_2Pbipy)_2(\eta^2\text{-}1,10\text{-phen})](BF_4)_2$ **[54]** which precipitates partially from the acetone solution. The complex forms in lower yield than that for the bipyridine analogue but has similar solubilities. The same type of Ph_2Pbipy ligand rearrangement occurs in order to incorporate 1,10-phenanthroline into the complex. Its microanalytical and spectroscopic characterisation data are presented in Tables 5.8 and 5.9 respectively and are analogous to those of the 2,2′-bipyridine complex **[53]**.

In view of the ability of the Ph_2Pbipy ligands to rearrange around the disilver unit, it was envisaged that polycyclic derivatives of 2,2′-bipyridine, in which further nitrogen centres are introduced, such as 2,3-bis(2-pyridyl)pyrazine (bpd), below, could possibly react with **[33]** to form higher nuclearity clusters (such as tetrameric systems).

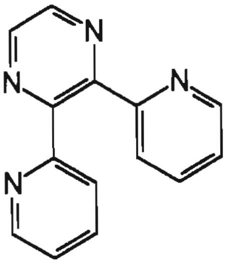

Reaction of **[33]** with half an equivalent (in an attempt to form a tetrameric system) of bpd in acetone indeed induces rearrangement of the Ph_2Pbipy ligands; this was monitored through the convenient use of $^{31}P\{^1H\}$ nmr (as presented in Table 5.9). During approximately 8 hours stirring at room temperature, the characteristic splitting pattern of the head to tail precursor (section 5.2.1) slowly converted to the coarse, broad triplet observed for the head-to-head complexes and discussed above. The pale-yellow solid, whose solubilities are similar to those of **[53]** and **[54]**, has a microanalysis (Table 5.8) that is consistent with one bpd ligand per dimeric unit. This would suggest that the bpd ligand chelates to one silver through only two of its nitrogen atoms in the same way that 2,2′-bipyridine itself does, while the other two nitrogen atoms remain unbonded. It is presumed that the formation of a tetrameric, head-to-head system with bpd bridging between dimers is sterically hindered, in view of the close proximity of the phenyl groups on the phosphorus atoms in such a conformation. The proposed dimeric structure of $[Ag_2(\mu\text{-}Ph_2Pbipy)_2(\eta^2\text{-}bpd)](BF_4)_2$ **[55]** is illustrated in Scheme 5.5 and is similar to that observed for **[53]** and **[54]**. Yields of the product are improved by reacting one equivalent of bpd with **[33]** in acetone. The remaining characterisation data for the complex fall in line with the structural assignment outlined above and are presented in Tables 5.8 and 5.9.

5.3.4.2 Crystal structure determination of $[Ag_2(\mu\text{-}Ph_2Pbipy)_2(\eta^2\text{-}2,2'\text{-bipy})](BF_4)_2$ [53]

The molecular structure of the $[Ag_2(\mu\text{-}Ph_2Pbipy)_2(\eta^2\text{-}2,2'\text{-bipy})]^{2+}$ cation has been solved and is presented in Figure 5.15. The cation consists of a disilver unit which is bridged by a pair of Ph_2Pbipy ligands bound in a head-to-head fashion (i.e. the phosphorus atoms of both Ph_2Pbipy ligands bind to the same silver atom whilst their bipyridine fragments chelate at the second). This mode of coordination facilitates the chelation of 2,2′-bipyridine at the former silver atom. Pseudo-tetrahedral geometry is maintained at each silver atom.

As a result of the strain introduced at Ag(2), discussed below, due to the chelation of the bipyridyl fragments, the Ag....Ag non-bonded distance of 3.674(1)Å is significantly longer than that observed in the parent complex **[33]** [2.973(2)Å]. Again, the eight-membered AgPCNAgPCN core adopts a puckered conformation due to torsional factors within the ligands and is impossible to ascribe as being either "chair-chair" or "chair-boat" when viewed down the Ag....Ag vector. Since there is no centre of symmetry between the silver atoms, there are two different PAgAgN torsion angles; that for P(1)-Ag(1)-Ag(2)-N(1) is a substantial 44.5° while that for P(2)-Ag(1)-Ag(2)-N(4) is marginally larger at 48.4°. These two torsion angles are the largest thus far encountered and can be rationalised in terms of the strain existing at Ag(2) and the necessity for each Ph_2Pbipy ligand to twist into a conformation suitable to allow their bipyridine portions to coordinate in a pseudo-tetrahedral manner to Ag(2), such that steric repulsions involving their protons are minimised. It is plain to see this torsion in the complex as well as how distorted (from ideal tetrahedral geometry) the angles around Ag(2) are. Of these, the two largest are N(1)-Ag(2)-N(4) [150.3(4)°] and N(1)-Ag(2)-N(3) [130.2(4)°]; compensating effectively for these are the significantly smaller N(1)-Ag(2)-N(2) [70.9(5)°] and N(3)-Ag(2)-N(4) [70.3(4)°] angles. The angles about Ag(1) do not exhibit such a range of distortions, the small angle subtended by N(5) and N(6) at the silver atom of 68.1(4)° being the only distortion requiring comment. The remaining bond angles at Ag(1) and Ag(2) are presented in Table 5.58.

Contrasting with the torsion about the silver dimeric unit is the fact that the bipyridine fragments of the Ph_2Pbipy ligands and the 2,2′-bipyridine ligand chelated at Ag(1) exhibit very little twist of their respective pyridine rings. The interannular rotation about C(17)-C(18) is only slight, such that the dihedral angle between the mean planes through the non-

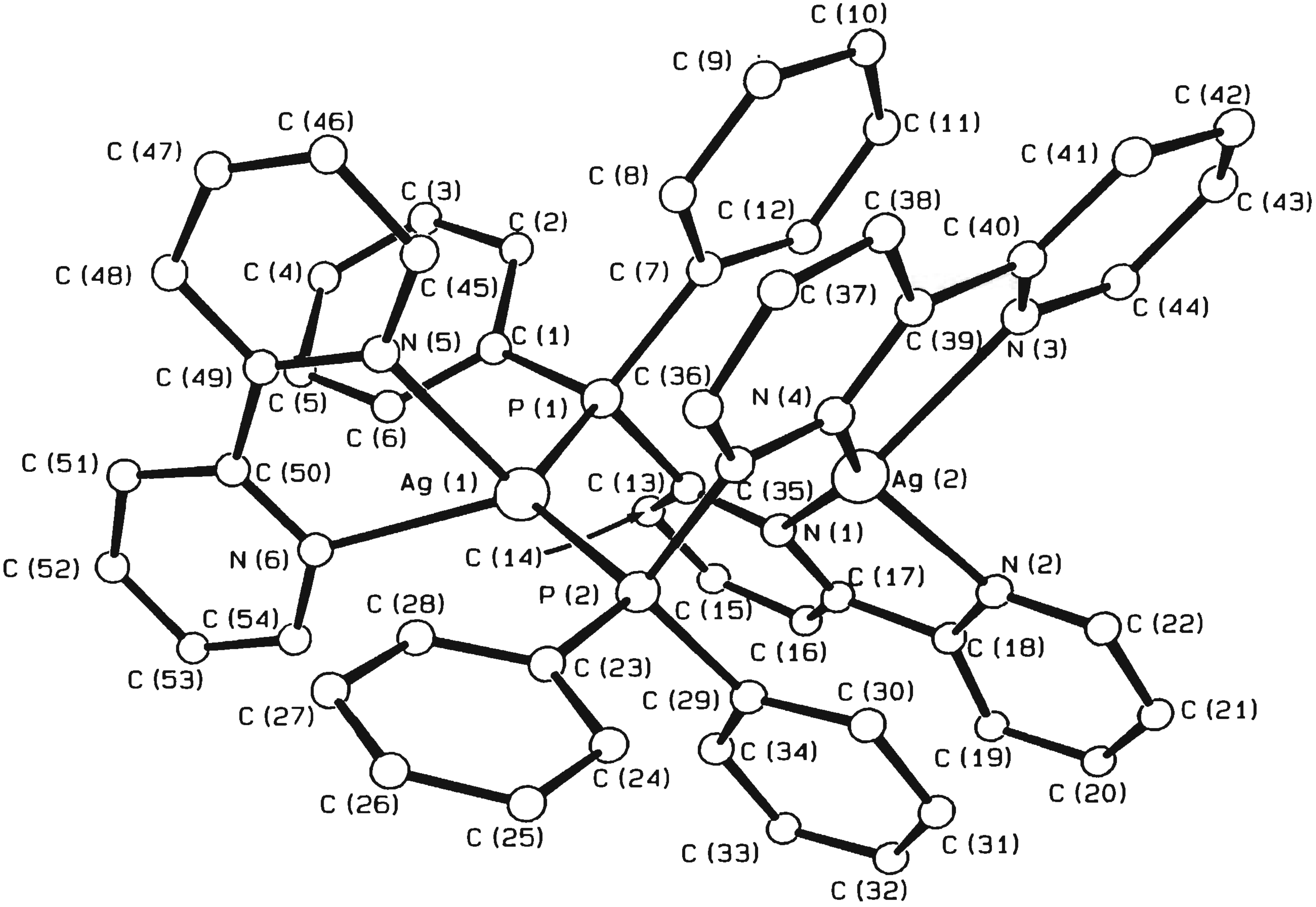
C (10)
C (9)
C (42)
C (11)
C (46)
C (47)
C (41)
C (8)
C (3)
C (38)
C (43)
C (12)
C (2)
C (40)
C (48)
C (4)
C (7)
C (45)
C (37)
C (44)
C (1)
N (5)
C (39)
N (3)
C (49)
C (36)
C (5)
N (4)
P (1)
C (6)
C (51)
C (50)
Ag (1)
C (13)
Ag (2)
C (35)
N (1)
C (14)
C (52)
N (6)
N (2)
C (17)
P (2)
C (28)
C (54)
C (15)
C (22)
C (16)
C (18)
C (53)
C (23)
C (30)
C (29)
C (27)
C (21)
C (34)
C (19)
C (24)
C (20)
C (26)
C (31)
C (25)
C (33)
C (32)

hydrogen atoms defined by the pyridine rings containing N(1) and N(2) is only 7.0° while that resulting from rotation involving the pyridine rings containing N(3) and N(4) is also small at 6.4°. Both values are smaller than that for the free, uncoordinated Ph_2Pbipy ligand [7.7(3)°]. The dihedral angle involving the two pyridyl planes of the coordinated 2,2′-bipyridine ligand is also an undistorted 7.0°.

The Ag-P bond distances are similar [Ag(1)-P(1) = 2.454(3)Å and Ag(1)-P(2) = 2.416(3)Å] but somewhat longer than that observed in the parent complex **[33]** [2.379(3)Å]. The remaining bond lengths are presented in Table 5.57.

5.2.4.3 Synthesis of the polymeric complexes $\{[Ag_2(\mu\text{-}Ph_2Pbipy)_2(\mu'\text{-}4,4'\text{-}bipy)](PF_6)_2\}_n$ [56] and $\{[Ag_2(\mu\text{-}Ph_2Pbipy)_2(\mu'\text{-}4,4'\text{-}bptz)](PF_6)_2\}_n$ [57] [4,4′-bptz = 3,6-bis(4-pyridyl)-1,2,4,5-tetrazine]

N-heterocyclic ligands containing planar conjugated π systems are capable of bridging two metal atoms and have received increasing attention in various areas of chemistry.[192-195] In this context, it was envisaged that 4,4′-bipyridine and the related brightly coloured C_2N_4(1,2,4,5-tetrazine) derivative 4,4′-bptz, below, would function as good bridging ligands between dimeric silver units, forming polymeric species in much the same way as pyrazine does (section 5.3.3.4).

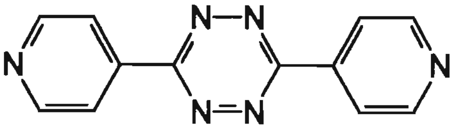

Dropwise addition of one equivalent of 4,4′-bipyridine (dihydrate) to $[Ag_2(\mu\text{-}Ph_2Pbipy)_2(NCMe)_2](PF_6)_2$ **[33]** at room temperature in CH_2Cl_2 immediately produces, in quantitative yield, a white precipitate which analyses for $\{[Ag_2(\mu\text{-}Ph_2Pbipy)_2(\mu'\text{-}4,4'\text{-}bipy)](PF_6)_2\}_n$ **[56]** (Table 5.8). The product was isolated pure by filtration and thorough washing of the filtered precipitate. It is soluble in donor solvents such as acetone, acetonitrile and methanol as well as hot dichloroethane. Single crystals of the complex were grown from the latter solvent and its polymeric nature confirmed through the use of X-ray diffraction techniques (5.3.4.4). Its infra-red spectrum contains a characteristically intense band at 839 cm^{-1} due to the PF_6^- anion, as well as distinguishing bands attributable to the Ph_2Pbipy ligand superimposed on which are those due to the 4,4′-bipy ligand. The remaining physical and spectroscopic characterisation data are presented in Tables 5.8 and 5.9 respectively.

Although identical methodology is employed in the synthesis of the 4,4′-bptz analogue $\{[Ag_2(\mu\text{-}Ph_2Pbipy)_2(\mu'\text{-}4,4'\text{-}bptz)](PF_6)_2\}_n$ **[57]**, there is no initial precipitation of product as found for the 4,4′-bipyridine complex. It is only upon addition of ethanol to the solution, followed by controlled cooling to -25°C, that the product precipitates as a scarlet, highly crystalline material in moderate (63%) yield. The complex is readily soluble in most organic solvents except chloroform, presumably due to the formation of solvento species, but insoluble in ethers and alkanes. Like **[56]**, its microanalysis (Table 5.8) is consistent with its stoichiometry while confirmation of its ionic character is derived from the presence, in its infra-red spectrum (Table 5.9) of a ν(B-F) stretching band attributable to the BF_4^- counter-anion. While complete spectroscopic characterisation has been carried out, its polymeric nature has been elucidated through the use of X-ray diffraction techniques (5.3.4.5) and shows it to consist, as postulated, of dimeric $\{Ag_2(Ph_2Pbipy)_2\}$ units linked in the crystal lattice through the heterocyclic 4,4′-bptz ligand.

5.3.4.4 Crystal structure determination of $\{[Ag_2(\mu\text{-}Ph_2Pbipy)_2(\mu'\text{-}4,4'\text{-}bipy)](PF_6)_2\}_n$ [56]

The crystal structure of the cation of $\{[Ag_2(\mu\text{-}Ph_2Pbipy)_2(\mu'\text{-}4,4'\text{-}bipy)](PF_6)_2\}_n$ **[56]** is shown in Figure 5.16 shows how the 4,4′-bipyridine ligands bind in a terminal fashion to the silver atoms and how the second nitrogen atom of each bipyridine ligand is coordinated to the silver atom of the next $\{Ag_2(Ph_2Pbipy)_2\}$ unit. A crystallographically imposed centre of symmetry is located midway between the two rings making up the 4,4′-bipyridine ligand along its interannular C(25)-C(25″) bond. There is thus no dihedral angle between the two planes defined by the non-hydrogen atoms of each pyridine ring. A second centre of inversion is located midway between the silver atoms of the disilver unit. The silver dimer is held intact by the presence of a pair of Ph_2Pbipy ligands bridging in a head-to-tail fashion.

The coordination of the 4,4′-bipyridine ligand is sterically analogous to that of the pyridine ligand in **[35]**. The result is that there is a substantial increase in the non-bonded Ag....Ag separation [4.092(1)Å] from that of the starting complex **[33]** [2.973(2)Å]. This increase presumably compensates for the strain present in the dimeric unit; the P-Ag-Ag′-N(1)

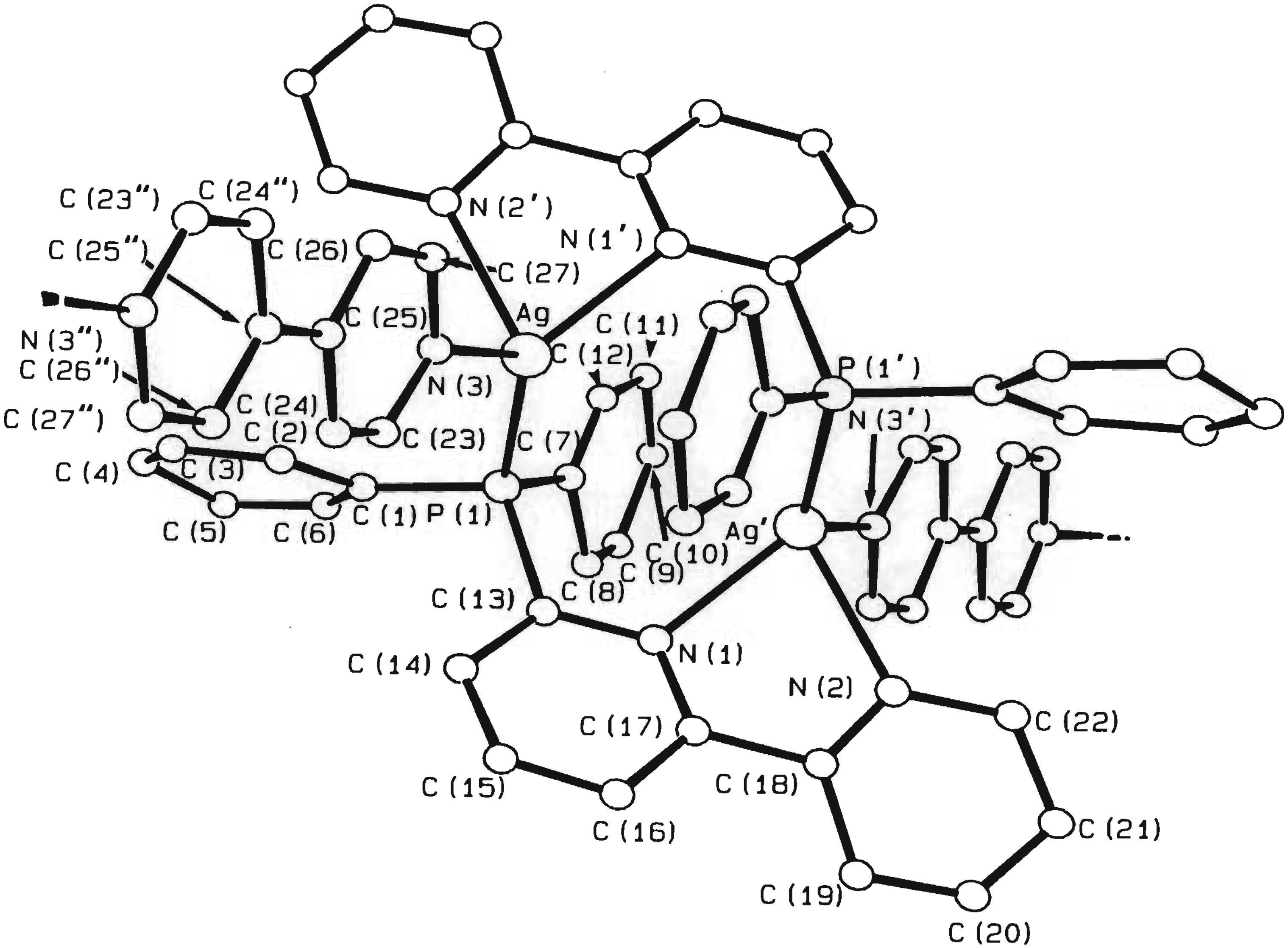
C (23")
C (24")
N (2')
N (1')
C (26)
C (27)
C (25")
C (25)
Ag
C (11)
N (3")
C (12)
C (26")
N (3)
P (1')
N (3')
C (27")
C (24)
C (2)
C (23)
C (7)
C (4)
C (3)
C (5)
C (6)
C (1)
P (1)
C (10)
Ag'
C (9)
C (13)
C (8)
N (1)
C (14)
N (2)
C (17)
C (22)
C (18)
C (15)
C (16)
C (21)
C (19)
C (20)

torsion angle of 41.1° is far greater than the 24.3° observed in **[33]**. Despite the fact that such large torsion angles are almost always accompanied by small intra-ligand dihedral angles between pyridino-planes of the bipyridine fragment, the relevant dihedral angle in this case is a surprisingly twisted 27.9°. This twist is presumably a result of the small angle subtended at the silver atom [70.2(1)°] by the two nitrogen atoms of the bipyridine moiety. The remaining angles at each silver atom suffer less distortion than the parent complex **[33]** [*e.g.* P(1)-Ag-N(1′) = 118.7(1)° as opposed to 168.3(3)°]. Bond distances involving the silver atom are all as expected and are presented in Table 5.62.

Figure 5.17 shows a crystallographic packing diagram for the polymeric **[56]** about the triclinic unit cell. Of interest in this case is the relative positioning of the dimer itself (on the centre of symmetry at the corners of the unit cell) and the 4,4′-bipy ligand (on the centre of symmetry at the centre of the unit cell). The polymer packs in such a way that the PF_6^- anions are located in the crystallographic "holes" created above and below the relatively uncrowded 4,4′-bipy portions of the polymer. Another interesting feature is that the repeating unit is staggered across the unit cell parallel to the plane defined by the [a] and [c] axes and at an angle of 45° to both. The staggered arrangement has the result that no direct electronic interaction between adjacent 4,4′-bipy ligands can occur, since the ligands don't bind to the same silver and there is no metal-metal bond.

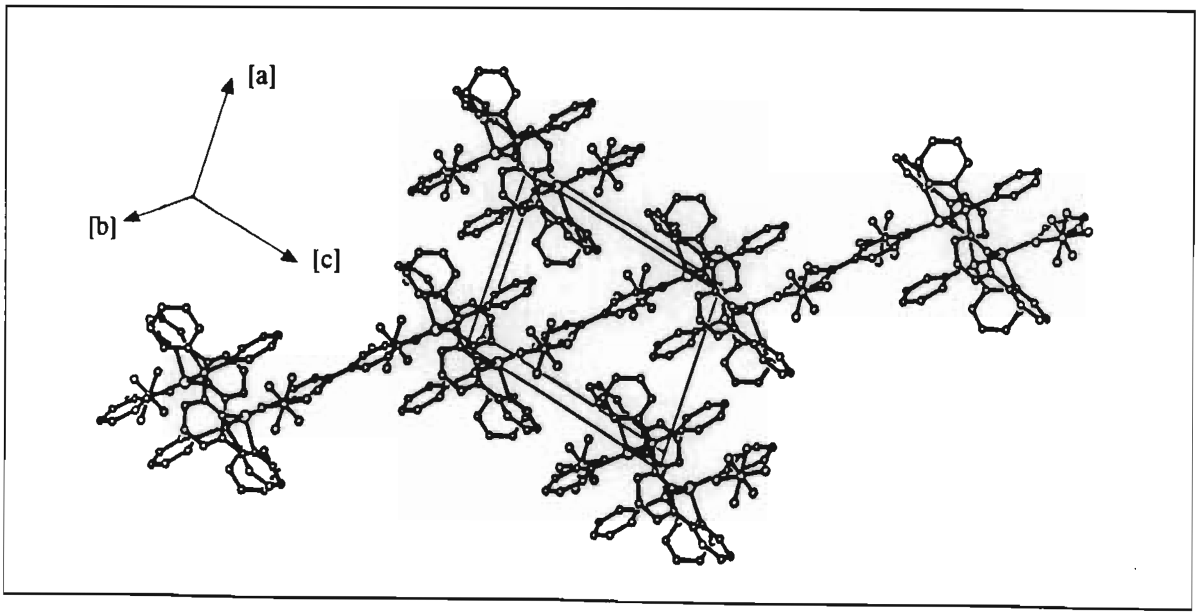

Figure 5.17 Crystallographic packing diagram for {[Ag$_2$(μ-Ph$_2$Pbipy)$_2$(μ′-4,4′-bipy)](PF$_6$)$_2$}$_n$ [56]

5.3.4.5 Crystal structure determination of {[Ag_2(μ-Ph_2Pbipy)$_2$(μ'-4,4'-bptz)](BF_4)$_2$}$_n$

The molecular geometry of the cation of the BF_4^- salt of {[Ag_2(μ-Ph_2Pbipy)$_2$(μ'-4,4'-bptz)](PF_6)$_2$}$_n$ **[57]** is illustrated in Figure 5.18 and shows how the 4,4'-bptz ligands bridge between successive dimeric units. As for the 4,4'-bipy analogue, there are two crystallographically imposed centres of inversion within the molecule; one midway between the two silver atoms and the other located in the middle of the azine ring of the bptz ligand. Figure 5.19 gives the crystallographic packing diagram for the polymer and shows how these inversion centres are related with respect to the entire unit cell. The coordination of the 4,4'-bptz ligand satisfies the preference that Ag^+ adopts a tetrahedral coordination geometry.

Within the dimeric unit, as for the parent complex **[33]**, the P-Ag-N(1') angle is substantially distorted to 144.8(4)°. Compensating for this is the much smaller angle subtended at the silver atom by the two nitrogen atoms of the bipyridine fragment [N(1)-Ag'-N(2) = 69.8(5)°]. All other angles around the silver atoms are reasonably close to that required for tetrahedral coordination (109.5°).

The non-bonded Ag....Ag separation of 3.012(3)Å is noticeably shorter than that for **[56]** [4.092(1)Å] and correlates well with that of the parent **[33]** [2.973(2)Å]. As observed in the pyridine **[35]**, the 4-vinylpyridine **[50]** and 4,4'-bipy **[56]** complexes, the bulky nature of the pyridino-substituent on the silver atom causes the bipyridine ring to twist away from it in order to minimise steric repulsions. This incurs a rather large P-Ag-Ag'-N(1) torsion angle of 38.9° which contrasts with the small dihedral angle (7.6°) between the mean planes through the non-hydrogen atoms defined by the pyridine rings of the bipyridine fragment of Ph_2Pbipy. The structure shows, too, how the 1,2,4,5 -tetrazine ring of the 4,4'-bptz ligand twists at an angle of 31.4° away from the planes defined by the non-hydrogen atoms of the pyridine ring containing N(3). This is rationalised on the basis of steric repulsions experienced by the nitrogen lone-pair electrons and the hydrogen atoms bonded to the adjacent pyridine ring.

The crystallographic packing diagram (Figure 5.20) shows how the 4,4'-bptz ligands are linked in a staggered fashion through the silver dimer across the monoclinic unit cell parallel to the [b] axis and in the plane of the [b] and [c] axes. The dimeric silver unit is located on

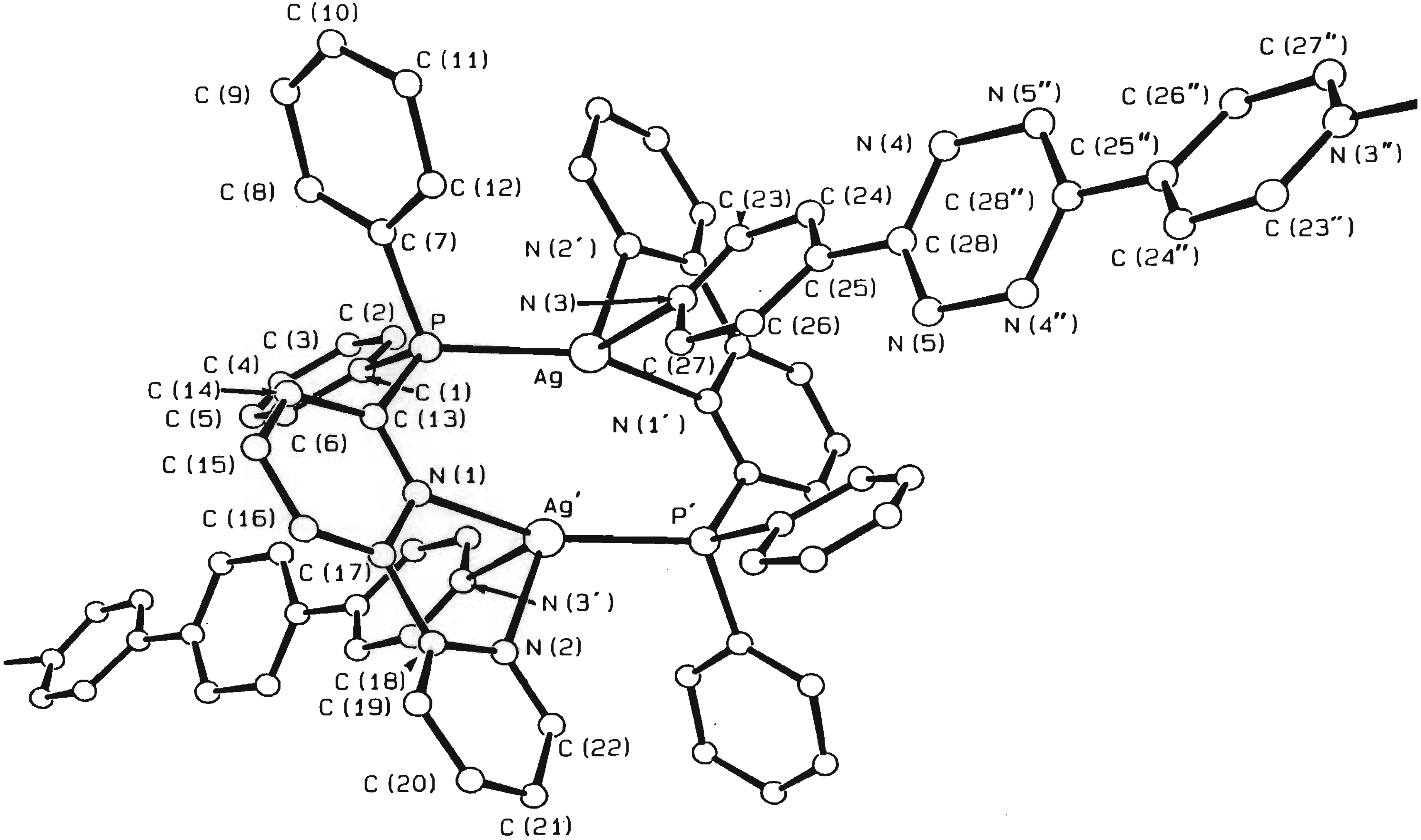
C (10)
C (11)
C (9)
C (8)
C (12)
C (7)
C (2)
P
C (3)
C (4)
C (14)
C (1)
C (5)
C (13)
C (6)
C (15)
N (1)
C (16)
Ag'
P'
C (17)
N (3')
C (18)
N (2)
C (19)
C (22)
C (20)
C (21)
N (2')
N (3)
Ag
C (27)
N (1')
C (23)
C (24)
C (25)
C (26)
C (28)
N (4)
N (5)
N (5")
N (4")
C (28")
C (25")
C (26")
C (27")
N (3")
C (23")
C (24")

the centre on inversion at the centre of the unit cell, halfway along the [b] and [c] axes, while the 4,4′-bptz ligand sits on the centre of inversion located midway along the [c] axis. The two BF_4^- anions for each repeating unit fit into the "holes" existing above and below the 4,4′-bptz ligand in the crystal lattice; more specifically, those above and below the tetrazine moiety.

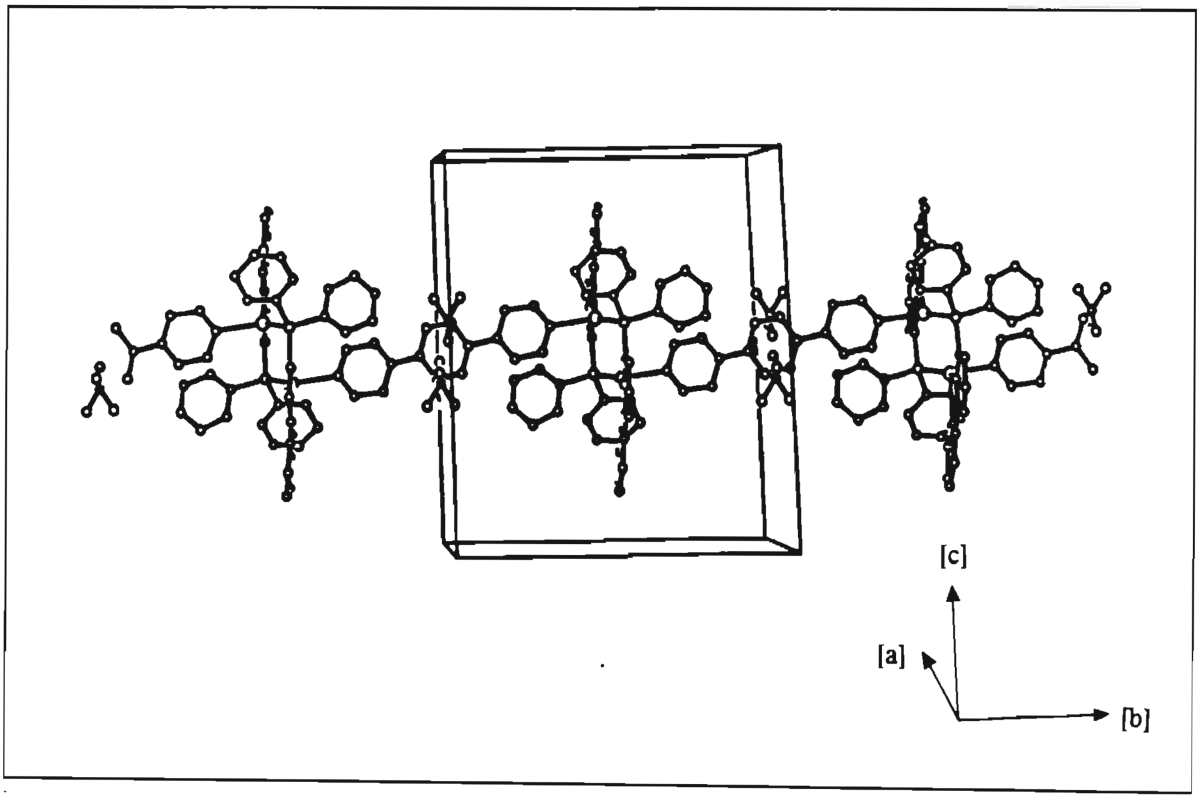

Figure 5.20 Crystallographic packing diagram for $\{[Ag_2(\mu\text{-}Ph_2Pbipy)_2(\mu'\text{-}4,4'\text{-}bptz)](BF_4)_2\}_n$

5.3.4.6 Synthesis of the tetranuclear complex $[\{Ag_2(\mu\text{-}Ph_2Pbipy)_2\}_2(\mu'\text{-}2,2'\text{-}bptz)](BF_4)_4$ [58] [2,2′-bptz = 3,6-bis-(2-pyridyl)-1,2,4,5-tetrazine]

The 2,2′analogue of 4,4′-bptz, depicted below, provides two sites at which chelation can occur. Moreover, these sites should be sufficiently far from one another (unlike bpd, for example) to induce rearrangement of the Ph_2Pbipy ligands in two adjacent dimeric silver units, thereby facilitating the formation of a tetranuclear head-to-head adduct essentially free of steric interference.

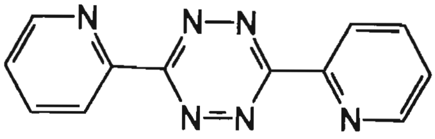

Slow, dropwise addition of a CH_2Cl_2 solution of 2,2'-bptz to **[33]** in CH_2Cl_2 at 10°C (water bath) affords a royal-purple coloured solution from which purple needles are isolated through the addition of ethanol and slow evaporation of the resultant solution. Reactions carried out at higher temperatures (>30°C) tend to precipitate a highly insoluble blue material, presumably the polymeric $\{[Ag(\mu\text{-}2,2'\text{-bptz})]PF_6\}_n$ adduct. The purple crystals isolated from the reaction at 10°C suffered from immediate solvent loss while crystals grown from a dichlorethane:ethanol solution proved to be too thin for an adequate search and data collection. No other solvent system provided suitable crystals. On the basis of microanalytical (Table 5.8) and spectroscopic (Table 5.9) data, the complex is proposed to be the tetranuclear complex $[\{Ag_2(\mu\text{-}Ph_2Pbipy)_2\}_2(\mu\text{-}2,2'\text{-bptz})](BF_4)_4$ **[58]** and is illustrated in Scheme 5.5. The observed coarse pseudo-triplet pattern (discussed in section 5.3.4.1) in the compounds $^{31}P\{^1H\}$ nmr spectrum provides evidence for the rearrangement of the Ph_2Pbipy ligands about the silver dimer into a head-to-head orientation.

Complex **[58]** exhibits, in its infra-red spectrum, an intense band at 1058 cm^{-1} which is assigned to the BF_4^- anion. In addition, characteristic N-C and P-C stretching bands attributable to the Ph_2Pbipy ligands are observed, superimposed on which are the ν(N-C) bands arising from vibrations within the 2,2'-bptz ligand. ^1H nmr data is presented in Table 5.9 and needs no further comment.

5.4 Structural trends in dimeric $Ag_2(\mu\text{-}Ph_2Pbipy)_2$ units

Table 5.10 outlines the essential features of all structures discussed in this chapter. The complexes shown therein vary considerably, both in terms of the structure of the dimeric unit and in terms of the nature of the ligand completing the tetrahedral coordination around the silver atom. Despite the obvious differences, certain trends exist with respect to the torsion within the Ph_2Pbipy ligands and the non-bonded Ag....Ag separations. The core structure illustrated below shows the basic "head-to-tail" arrangement of the ligands about the silver dimer. Certain listings on Table 5.10 refer directly back to this diagram.

Table 5.10 Structural features of silver compounds characterised through X-ray diffraction

Complex cation	Ag...Ag (Å)	Ag-P$^{(a)}$ (Å)	P_A-Ag-$N_B$$^{(a)}$ (°)	Dihedral angle(s) (°) $Ph_2Pbipy(s)$	Dihedral angle(s) (°) Other ligands	Torsion angle P_A-Ag-Ag-N_A	Torsion angle P_B-Ag-Ag-N_B
[33]: $[Ag_2(\mu\text{-}Ph_2Pbipy)_2(NCMe)_2]^{2+}$	2.973(2)	2.379(3)	168.3(3)	16.6(9)		24.3(2)	
[35]: $[Ag_2(\mu\text{-}Ph_2Pbipy)_2(py)_2]^{2+}$	4.092(1)	2.398(0)	113.4(0)	6.6(1)		41.5(1)	
[36]: $[Ag_2(\mu\text{-}Ph_2Pbipy)_2(EtOH)_2]^{2+}$	2.984(1)	2.973(1)	151.9(2)	9.3(2)		19.6(2)	
[43]: $[Ag_2(\mu\text{-}Ph_2Pbipy)_2(NO_3)_2]$	2.935(2)	2.378(3)	153.8(1)	13.9(2)		46.0(4)	
[44]: $[Ag_2(\mu\text{-}Ph_2Pbipy)_2(\mu\text{-}I)]^{+}$	2.920(3)	2.385(7) 2.366(7)	138.5(5) 156.4(5)	5.2(8) 14.0(8)		13.3(5)	29.2(5)
[45]: $[Ag_2(\mu\text{-}Ph_2Pbipy)_2\{\mu\text{-}OC(Me)O\}]^{+}$	2.988(2)	2.350(6) 2.372(6)	114.3(5) 153.8(5)	9.8(5) 30.5(3)		30.2(5)	9.4(5)
[46]: $[Ag_2(\mu\text{-}Ph_2Pbipy)_2\{\mu\text{-}OC(Ph)O\}]^{+}$	2.945(1)	2.371(2) 2.396(1)	141.6(1) 104.3(1)	27.3(3) 6.2(2)		11.5(1)	26.8(1)
[50]: $[Ag_2(\mu\text{-}Ph_2Pbipy)_2(\eta^1\text{-}4\text{-}vinylpy)_2]^{2+}$	4.012(1)	2.392(3)	124.4(9)	10.9(2)		41.6(2)	
[51]: $[Ag_2(\mu\text{-}Ph_2Pbipy)_2(\eta^1\text{-}pbpz)_2]^{2+}$	3.125(1)	2.386(2)	145.1(2)	7.1(4)		30.2(1)	
[53]: $[Ag_2(\mu\text{-}Ph_2Pbipy)_2(\eta^2\text{-}2,2'\text{-}bipy)]^{2+}$	3.674(1)	2.454(3) 2.416(3)	(b)	7.0(9) 6.4(4)	7.0(7)	44.5(5)	48.4(6)
[56]: $\{[Ag_2(\mu\text{-}Ph_2Pbipy)_2(\mu'\text{-}4,4'\text{-}bipy)]^{2+}\}_n$	4.092(1)	2.375(1)	118.7(1)	27.9(4)	(c)	41.1(1)	
[57]: $\{[Ag_2(\mu\text{-}Ph_2Pbipy)_2(\mu'\text{-}4,4'\text{-}bptz)]^{2+}\}_n$	3.012(3)	2.379(5)	144.8(4)	7.6(7)	31.4(6)	38.9(4)	

(a) : Two values are given for molecules not containing a centre of inversion between the silver atoms.

(b) : Head to head complex.

(c) : Centre of inversion relates one half of 4,4'-bipyridine to the other, such that there is zero resultant dihedral angle.

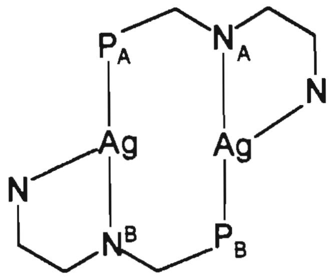

The parent complex $[Ag_2(\mu\text{-}Ph_2Pbipy)_2(NCMe)_2](PF_6)_2$ **[33]** has a non-bonded Ag....Ag separation of 2.973(2)Å. It seems to be generally the case that when more bulky ligands, such as pyridine or any of its derivatives, substitute for the labile acetonitrile ligands in **[33]**, the non-bonded separation increases substantially. This is in order to facilitate coordination of the bulkier ligands such that the steric repulsions are minimised. A result of this is that the Ph_2Pbipy bridging ligands twist somewhat across the dimeric unit and in so doing create tighter P_A-Ag-N_B angles and more pronounced P_A-Ag-Ag-N_A torsion angles. However, it does not appear to affect the Ag-P bond distances in any way.

Another interesting trend observed is that relief of strain within the Ph_2Pbipy ligands, a result of the necessary tetrahedral coordination about the silver atoms, occurs through either a twist of the ligand about the Ag....Ag vector (P_A-Ag-Ag-N_A torsion angle) or a degree of rotation about the interannular bipyridine bond (dihedral angle), but *not* both. In other words, the larger the torsion angle, the smaller the dihedral angle between the mean planes through the non-hydrogen atoms defined by the pyridine rings of the bipyridine fragment. Furthermore, it seems that when terminal substitution occurs, a torsional twist is favoured over a dihedral rotation, while the reverse is true of ligands that opt to bridge across the dimer, such as iodide or carboxylate,

5.5 Conclusion

This work has significantly extended the known types of silver(I) dimers bridged by binucleating ligands. The affinity that silver(I) has for phosphoruspyridyl and related ligands, as discovered through studies described in Chapter Four, has been demonstrated effectively by the coordination of Ph_2Pbipy in a head-to-tail bridging fashion across two silver(I) atoms, thereby stabilising the dimer to fragmentation.

The versatile complex $[Ag_2(\mu\text{-}Ph_2Pbipy)_2(NCMe)_2](PF_6)_2$ **[33]** has been synthesised and the acetonitrile ligands have been shown to be labile towards substitution by various anionic and N-heterocyclic nucleophiles, resulting in a range of neutral, mono- and dicationic complexes. Certain of these complexes are polymeric in the solid state. Furthermore, **[33]** reacts readily with a range of donor solvents.

The structures of a number of these complexes have been unambiguously elucidated through the use of X-ray diffraction studies on suitable single crystals. This has enabled us to confirm that the Ph_2Pbipy ligands do bridge in an asymmetric, head-to-head fashion without a great deal of steric strain. This mode of coordination comes about through the systematic rearrangement of the ligands from a head-to-tail coordination mode. A number of trends have emerged with regards to the structural features of the complexes studied. This has deepened our understanding of the preferred coordination modes and torsional characteristics of this highly versatile ligand.

5.6 Experimental

General experimental details and sources of chemicals are outlined in appendices A and B respectively.

5.6.1 Synthesis of $[Ag_2(\mu\text{-}Ph_2Pbipy)_2(NCMe)_2](PF_6)_2$ [33]

An acetonitrile solution ($10cm^3$) of Ph_2Pbipy (130mg; 0.37mmol) was added dropwise to a solution ($15cm^3$) of either $[Ag(1,5\text{-}cod)_2](PF_6)$ (150 mg; 0.37mmol) or $[Ag(NCMe)_4](PF_6)$ (138mg; 0.37mmol) in acetonitrile ($15cm^3$), the latter generated *in situ* by dissolving $AgPF_6$ in acetonitrile at -15°C. The resultant solution was stirred for 15 hours at room temperature and then evaporated to *ca.* $5cm^3$ under reduced pressure. Diethyl ether ($\pm 7cm^3$) was then added carefully to precipitate the product as pale yellow crystals. Further product was obtained by cooling the solution to -25°C and keeping it at this temperature for 2 hours. It was isolated by filtration and washed with diethyl ether ($5cm^3$) and dried *in vacuo*.

Yield: 74%.

5.6.2 Synthesis of $[Ag_2(\mu\text{-}Ph_2Pbipy)_2(S)_2](BF_4)_2$ (S = PhCN [34] and EtOH [36]) and $[Ag_2(\mu\text{-}Ph_2Pbipy)_2(py)_2](PF_6)_2$ [35]

A quantity of the appropriate salt of **[33]** (0.07mmol) was dissolved in the minimum amount of the appropriate solvent at room temperature. In the case of the synthesis of **[36]**, the precursor dissolved in refluxing solvent. By reducing the volume of the solvent under reduced pressure (in the case of **[34]** and **[35]**) and carefully adding diethyl ether, the relevant complex was isolated in quantitative yield. Cooling the warm solution of **[33]** in EtOH to room temperature afforded highly crystalline **[36]**, also in near quantitative yield. All three products were isolated through careful filtration, washed thoroughly (diethyl ether) and dried *in vacuo* for an hour.

Yield: **[34]**, **[35]** and **[36]** 94%

5.6.3 Synthesis of the isocyanide complex $[Ag_2(\mu\text{-}Ph_2Pbipy)_2(CNXylyl)_2](ClO_4)_2$ [37] (Xylyl = 2,6-dimethylphenyl)

Method 1: A solution of $[Ag(CNXylyl)_3](ClO_4)$ (75mg; 0.13 mmol) in CH_2Cl_2 ($5cm^3$) was mixed with a solution of Ph_2Pbipy (50mg; 0.13mmol) in CH_2Cl_2 ($5cm^3$). The resultant clear, very pale-yellow solution was stirred for 6 hours, evaporated under reduced pressure to *ca.* $3cm^3$ and filtered through glass microfibre. Diethyl ether ($3cm^3$) was added to the filtrate, yielding (at -25°C) colourless rhombs of the title complex. These were isolated by filtration and washed thoroughly with diethyl ether ($10cm^3$), to ensure complete removal of all isocyanide residues and dried *in vacuo* for 2 hours.

Yield: 59%

Method 2: A solution of a two fold excess of CNXylyl in CH_2Cl_2 ($5cm^3$) was added dropwise to a solution of the ClO_4^- salt of **[33]** (100mg; 0.10mmol) in CH_2Cl_2 ($5cm^3$) and the resultant clear, pale-yellow solution stirred for 24 hours. Reduction of the solvent volume under reduced pressure, filtration through glass microfibre and addition of diethyl ether afforded the colourless microcrystalline product. This was isolated in an analogous manner to that described in method 1.

Yield: 47%

5.6.4 Synthesis of the neutral complexes $[Ag_2(\mu\text{-}Ph_2Pbipy)_2(X)_2]$ ($X = Cl^-$ [38], Br^- [39] and I^- [40]

To a solution of the appropriate tetraalkylammonium halide (R_4NX) salt (R = Me, X = Cl; R = Et, X = Br and R = Bu, X = I) (0.20mmol) in CH_2Cl_2 (3cm^3) was added a CH_2Cl_2 solution (5cm^3) of **[33]** (100mg; 0.09mmol) at room temperature. Immediate precipitation of the relevant dihalide occurred. The compounds were isolated by carefully decanting the mother liquor and washing the precipitate with three successive quantities (5cm^3) of CH_2Cl_2 and diethyl ether. Improved yields of the bromide complex **[39]** were obtained by adding solid KBr to the CH_2Cl_2 solution of **[33]**(PF_6^- salt). In this case, precipitation occurred more slowly and during the time it took for KBr to completely react in the CH_2Cl_2 (*ca.* 4 hours). Analogous methods were followed for its isolation. After the washing, the complexes were dried thoroughly *in vacuo*.

Yield: **[38]** 61%, **[39]** 58%, **[40]** 39%

5.6.5 Synthesis of the neutral cyanide complex $[Ag_2(\mu\text{-}Ph_2Pbipy)_2(CN)_2]$ [41]

When a CH_2Cl_2 solution (10cm^3) of **[33]** (50mg; 0.05mmol) was stirred with a two-fold excess of solid KCN (0.14mmol), a pale-yellow clear solution resulted after approximately 8 hours reaction at room temperature. Colourless crystals of the title compound were obtained by evaporation of the solution to *ca.* 2cm^3 under reduced pressure, addition of diethyl ether (5cm^3) and cooling the resultant mixture to -25°C. The material was filtered, washed with a little diethyl ether (2cm^3) and dried *in vacuo*.

Yield: 60%

5.6.6 Synthesis of the neutral phenylacetylide complex $[Ag_2(\mu\text{-}Ph_2Pbipy)_2(C{\equiv}CPh)_2]$ [42]

Method 1: A solution of $LiC{\equiv}CPh$ (0.25cm^3; 0.25mmol; 0.1M in thf) was added under strictly oxygen-free conditions to **[33]** (100 mg; 0.10mmol) in CH_2Cl_2 (8cm^3). The orange solution that resulted was stirred for 15 hours at room temperature, reduced in volume to *ca.* 3cm^3 and filtered through glass microfibre. A MeOH:Et$_2$O (1:1, vol:vol) mixture (3cm^3) was added to afford the product, at -25°C, as a pale-yellow, feathery precipitate. This was isolated by filtration, washed with diethyl ether and dried *in vacuo* for 2 hours.

Yield: 92%

Method 2: A solution of Ph_2Pbipy (163mg; 0.48mmol) in warm (35°C) methanol ($10cm^3$) was added to a solution of $[Ag(C{\equiv}CPh)]_n$ (100mg; 0.48mmol) in pyridine ($1cm^3$). Immediate precipitation of the pale-yellow product occurred and this was isolated in the manner described in method 1.

Yield: 96%

5.6.7 Synthesis of the neutral nitrate complex $[Ag_2(\mu\text{-}Ph_2Pbipy)_2(NO_3)_2]$ [43]

Method 1: An acetone solution ($5cm^3$) of Ph_2Pbipy (205mg; 0.60mmol) was added dropwise over a period of 3 min. to $AgNO_3$ (100mg; 0.60mmol) in acetone ($25cm^3$) at room temperature. The title compound precipitated immediately from solution as a finely divided pale-yellow powder. Stirring was continued for 5 hours and the yield of the product maximised by concentrating the volume of the solvent under reduced pressure to *ca.* $10cm^3$. It was filtered off, washed with acetone ($5cm^3$) and dried *in vacuo* for 4 hours.

Yield: 88%

Method 2: Excess solid KNO_3 (20mg; 0.2mmol) was added to a solution of **[33]** (100mg; 0.09 mmol) in acetone ($20cm^3$) and the resultant pale-yellow solution stirred at room temperature for 24 hours. After this time, a small amount of pale-yellow precipitate had formed. The yield was increased by reducing the volume of the solvent under reduced pressure to *ca.* $10cm^3$ and the powder isolated as described in method 1.

Yield: 62%

5.6.8 Synthesis of the iodide complex $[Ag_2(\mu\text{-}Ph_2Pbipy)_2(\mu\text{-}I)](BF_4)$ [44]

A solution of tetrabutylammonium iodide (17mg; 0.10mmol) in acetone ($5cm^3$) was added slowly to a solution of the BF_4^- salt of **[33]** (100mg; 0.10mmol) in acetone ($5cm^3$) at 0°C (ice-water bath). The clear, pale-yellow solution was gently stirred at this temperature for 15 hours. The solution was then allowed to warm to room temperature and evaporated under reduced pressure to *ca.* $3cm^3$. Ethanol ($3cm^3$) was added and the solution allowed to evaporate in air for 2 days, affording a colourless, microcrystalline precipitate. This was filtered on a frit, washed with cold (0°C) ethanol ($2cm^3$) and dried *in vacuo*.

Yield: 53%

5.6.9 Synthesis of the carboxylato derivatives $[Ag_2(\mu\text{-}Ph_2Pbipy)_2\{\mu\text{-}OC(R)O\}](PF_6)$ (R=Me [45], Ph [46])

Method 1: A solution of Ph_2Pbipy (205mg; 0.60mmol) in acetone (5cm^3) was added dropwise to a suspension of the appropriate silver carboxylate (0.06mmol) in acetone(10cm^3). The suspension slowly dissolved, yielding a clear, yellow solution. A solution of NH_4PF_6 (98mg; 0.60mmol) in acetone (5cm^3) was then added and the resultant solution stirred for 15 hours at room temperature. The volume of the solution was concentrated under reduced pressure to *ca.* 3cm^3 and diethyl ether (2cm^3) added, which resulted in the compound being precipitated as pale-yellow crystals. They were isolated in the usual manner through filtration, washing with diethyl ether and drying *in vacuo* for 4 hours.

Yield: **[45]** 80%, **[46]** 62%

Method 2: A solid sample of the appropriate sodium carboxylate salt (0.15mmol) was added to a solution of **[33]** (100mg; 0.10mmol) in acetone (5cm^3) at room temperature. After stirring the resultant clear, pale yellow solution at room temperature for 24 hours, the product was isolated in the manner described in method 1.

Yield : **[45]** 60%, **[46]** 46%

5.6.10 Synthesis of the pyrazolate complex $[Ag_2(\mu\text{-}Ph_2Pbipy)_2(\mu\text{-}pyz)](BF_4)$ [47]

Solid sodium pyrazolate (10mg; 0.11mmol), prepared by reaction of sodium metal with pyrazole in thf as outlined in Appendix B, was added to a solution of the BF_4^- salt of **[33]** (115mg; 0.11mmol) in methanol (5cm^3), under strictly oxygen-free conditions. Immediate precipitation of a white powder occurred ($NaBF_4$). This was separated from the solution using standard filtration techniques. The volume of the filtrate was reduced to *ca.* 2cm^3 and diethyl ether (3cm^3) was added to precipitate the product as a pale yellow microcrystalline material. This was isolated by filtration, washed with a little diethyl ether (1cm^3) and dried *in vacuo* for an hour.

Yield: 59%

5.6.11 Synthesis of the polymeric complex $\{[Ag_2(\mu\text{-}Ph_2Pbipy)_2(\mu'\text{-}SCN)](BF_4)\}_n$ [48]

Treatment of a solution of the BF_4^- salt of **[33]** (75mg; 0.07mmol) in CH_2Cl_2 (3cm^3) with a solution of tetrabutylammonium thiocyanate (21mg; 0.07mmol) in CH_2Cl_2 (1cm^3) produced a yellow solution at room temperature. Yellow rhombs of the title compound were isolated by adding n-heptane (5cm^3) to this solution and allowing the mixture to evaporate slowly in air. The crystals were totally insoluble in all solvents. They were washed with diethyl ether (1cm^3) and dried *in vacuo* for an hour.

Yield: 32%

5.6.12 Synthesis of the complexes $[Ag_2(\mu\text{-}Ph_2Pbipy)_2(\eta^1\text{-}L)_2](BF_4)_2$ (L = 4-cyanopyridine [49], 4-vinylpyridine [50] and pyrido-[2,3-b]pyrazine{pbpz} [51])

A twice molar quantity of the appropriate donor ligand (0.15mmol of 4-cyanopyridine, excess of liquid 4-vinylpyridine or 0.15mmol of pbpz) was added to to a solution of the BF_4^- salt of **[33]** (75mg; 0.07mmol) in CH_2Cl_2 (5cm^3). The relevant solution was stirred for 24 hours, then filtered through glass microfibre and evaporated under reduced pressure to *ca.* 1cm^3. The addition of diethyl ether (1cm^3) to this solution afforded the required complex at -25°C as colourless powders, in the case of **[49]** and **[50]**, or as a yellow microcrystalline solid in the case of **[51]**. All three were isolated by decanting the mother-liquor, washing the product thoroughly with diethyl ether (3 x 1cm^3) and drying *in vacuo*.

Yield: **[49]** 53%, **[50]** 69%, **[51]** 76%

5.6.13 Synthesis of the pyrazine polymer $\{[Ag_2(\mu\text{-}Ph_2Pbipy)_2(\mu'\text{-}pz)](PF_6)_2\}_n$ [52]

A solution of pyrazine (4mg; 0.04mmol) in CH_2Cl_2 (1cm^3) was added dropwise to a solution of **[33]** (50mg; 0.04mmol) in CH_2Cl_2 (5cm^3) at room temperature. A white powder precipitated immediately. This was isolated by carefully decanting the mother liquor, washing the solid material with CH_2Cl_2 (2 x 1cm^3) and diethyl ether (2cm^3), and drying the analytically pure product *in vacuo* for 2 hours.

Yield: 91%

5.6.14 Synthesis of the head-to-head complex $[Ag_2(\mu\text{-}Ph_2Pbipy)_2(\eta^2\text{-}2,2'\text{-bipy})](BF_4)_2$ [53]

Method 1: A solution of 2,2′-bipyridine (80mg; 0.50mmol) in acetone (5cm^3) was added dropwise over 3 minutes to an acetone solution (8cm^3) of $[Ag(1,5\text{-cod})_2](BF_4)$ (200mg; 0.50mmol). This solution was stirred for 4 hours, filtered and reduced in volume to 5cm^3. During this preparation, some white material, which analysed as $[Ag(1,5\text{-cod})(2,2'\text{-bipy})](BF_4)$, precipitated from solution. A solution of Ph_2Pbipy (172mg; 0.50mmol) in acetone (4cm^3) was added to this solution at room temperature. The solution changed colour to yellow over 15 hours. The solution was concentrated under reduced pressure to *ca.* 3cm^3 and filtered through glass microfibre. Diethyl ether (3cm^3) was added and the compound precipitated as pale yellow needles at -25° C. These were isolated by filtration, washed with diethyl ether (2cm^3) and dried *in vacuo*.

Yield: 68%

Method 2: A solution of 2,2′-bipyridine (13mg; 0.08mmol) in acetone (2cm^3) was added dropwise to a solution of the BF_4^- salt of **[33]** (96mg; 0.08mmol) in acetone (2cm^3). The pale-yellow solution that resulted from stirring at room temperature for 24 hours was reduced in volume to *ca.* 2cm^3 and the pale-yellow title compound isolated in an analogous manner to that described in method 1.

Yield: 52%

5.6.15 Synthesis of the head-to-head complexes $[Ag_2(\mu\text{-}Ph_2Pbipy)(\eta^2\text{-}L)](BF_4)_2$ (L = 1,10-phen [54] and 2,3-bis(2-pyridyl)pyrazine{bpd}[55])

A solution of the relevant chelating ligand (0.12mmol) in CH_2Cl_2 (5cm^3) was added dropwise to a solution of the BF_4^- salt of **[33]** (120mg; 0.12mmol) in CH_2Cl_2 (5cm^3). After 15 hours stirring at room temperature the product, in the case of the reaction involving 1,10-phen, had partially precipitated from solution. The precipitation was completed by the addition of diethyl ether (3cm^3). In the case of the reaction involving bpd, the product was precipitated from the clear yellow solution by evaporating the solution under reduced pressure to *ca.* 2cm^3, adding ethanol (5cm^3) and allowing the solution to evaporate slowly in air, affording the product as a pale-yellow microcrystalline powder. In both cases, the product was isolated in the usual fashion by filtration, washing the product with diethyl ether (2 x 1cm^3) and drying in *in vacuo* for 2 hours.

Yield: **[54]** 58%, **[55]** 89%

5.6.16 Synthesis of the polymeric complexes $\{[Ag_2(\mu\text{-}Ph_2Pbipy)_2(\mu'\text{-}L)](PF_6)_2\}_n$ (L = 4,4′-bipy [56] and 3,6-bis(4-pyridyl)-1,2,4,5-tetrazine{4,4′-bptz}[57])

A solution of the relevant N-heterocycle (0.07mmol) in CH_2Cl_2 (10cm^3) was added dropwise to a solution of **[33]** (75mg; 0.07mmol) in CH_2Cl_2 (5cm^3) at room temperature. In the case of the reaction involving 4,4′-bipy, the title compound (white) precipitated immediately from solution and was isolated by filtering, washing the filtered solid with cold (0°C) CH_2Cl_2 (2cm^3) and drying *in vacuo*. for an hour. In the case of the reaction involving 4,4′-bptz, no initial precipitation occurred. The purple-red solution was stirred for 15 hours and evaporated under reduced to *ca.* 3cm^3. Ethanol (5cm^3) was added and the solution cooled to -25°C for 12 hours, affording highly crystalline scarlet needles of the title complex which were isolated in a similar fashion to that described for the isolation of the 4,4′-bipyridine polymer.

Yield : **[56]** 80%, **[57]** 63%

5.6.17 Synthesis of the tetranuclear complex $[\{Ag_2(\mu\text{-}Ph_2Pbipy)_2\}_2(\mu\text{-}2,2'\text{-}bptz)](BF_4)_4$ [58] (2,2′-bptz = 3,6-(2-pyridyl)-1,2,4,5-tetrazine)

A solution of 2,2′-bptz (13mg; 0.05mmol) in CH_2Cl_2 was added slowly over a 10 minute period to a solution of the BF_4^- salt of **[33]** (100mg; 0.10mmol) in CH_2Cl_2 (5cm^3) at 10°C. The solution turned a royal-purple colour and the solution was stirred at this temperature for a further 24 hours. The reaction was carried out at 10°C in order to avoid formation of the blue $\{[Ag(\mu\text{-}2,2'\text{-}bptz)]BF_4\}_n$ polymer. The resultant solution was evaporated under reduced pressure to *ca.* 5cm^3 and carefully filtered through glass microfibre. Ethanol (5cm^3) was added and the solution allowed to evaporate slowly in air, affording purple needles which were isolated by decanting off the mother liquor, washing with diethyl ether (3 x 1cm^3) and drying *in vacuo*. for 2 hours.

Yield: 31%

5.6.18 Single crystal X-ray diffraction study of $[Ag_2(\mu\text{-}Ph_2Pbipy)_2(NCMe)_2](PF_6)_2$ [33]

A pale-yellow needle was grown by slow evaporation of a saturated acetonitrile solution of the complex. Crystals grown in this manner tended to slowly lose incorporated solvent. As a precaution, therefore, the crystal was mounted on a glass fibre sealed inside a 0.3mm capillary tube. The general approach used for the intensity data collection is described in Appendix A. The crystallographic data are given in Table 5.11, the interatomic distances in Table 5.12, the interatomic angles in Table 5.13, the fractional coordinates in Table 5.14 and the anisotropic thermal parameters in Table 5.15. The observed and calculated structure factors may be found on microfiche in an envelope fixed to the inside back cover.

Table 5.11

Crystal data and details of the crystallographic analysis for $[Ag_2(\mu\text{-}Ph_2Pbipy)_2(NCMe)_2](PF_6)_2$

Formula	$Ag_2C_{48}H_{40}N_6P_4F_{12}$
Molecular Mass	1268.50
Crystal System	Monoclinic
Space Group	$P2_1/c$
a(Å)	9.814(2)
b(Å)	12.161(4)
c(Å)	21.497(4)
β(°)	99.38(2)
V(Å^3)	2531.15
Z	2
D_c(g.cm^{-3})	1.664
F(000)	1264
λ(Mo-Kα)(Å)	0.71069
Scan mode	ω - 2θ
ω scan angle	$0.70 + 0.35\tan\theta$
Horizontal Aperture width (mm)	$2.7 + 0.1\tan\theta$
Scattering range (°)	$2 \leq \theta \leq 23$
μ (cm^{-1})	9.72
Absorption corrections	Semi empirical[103]
Measured intensities	3825
Unique intensities	2845
Unique intensities with $[I > 3\sigma(I)]$	1862
Structure solution	Direct & Fourier methods
Weighting scheme	$1/(\sigma^2(F) + 0.00083F^2)$
$R = \Sigma(F_o\text{-}F_c)/\Sigma F_o$	0.0567
$R_w = \Sigma_w \frac{1}{2}(F_o\text{-}F_c)/\Sigma_w \frac{1}{2}F_o$	0.0573
$(\Delta/\sigma)_{max}$	0.120
$\Delta\rho_{max}$(eÅ^{-3})	0.590
Number of parameters	205

Table 5.12 : Interatomic distances (Å) for $[Ag_2(\mu\text{-}Ph_2Pbipy)_2(NCMe)_2](PF_6)_2$

Ag-P(1)	2.379(3)	Ag-N(3)	2.437(13)
Ag-Ag'	2.973(2)	P(1)-C(1)	1.816(12)
Ag'-N(1)	2.311(5)	Ag'-N(2)	2.417(5)
P(1)-C(7)	1.829(12)	P(1)-C(13)	1.830(12)
N(1)-C(13)	1.330(14)	N(1)-C(17)	1.362(13)
N(2)-C(18)	1.326(14)	N(2)-C(22)	1.35(2)
N(3)-C(23)	1.11(2)	C(1)-C(2)	1.38(2)
C(1)-C(6)	1.40(2)	C(2)-C(3)	1.43(2)
C(3)-C(4)	1.40(2)	C(4)-C(5)	1.37(2)
C(5)-C(6)	1.44(2)	C(7)-C(8)	1.40(2)
C(7)-C(12)	1.38(2)	C(8)-C(9)	1.41(2)
C(9)-C(10)	1.34(2)	C(10)-C(11)	1.38(2)
C(11)-C(12)	1.48(2)	C(13)-C(14)	1.41(2)
C(14)-C(15)	1.39(2)	C(15)-C(16)	1.39(2)
C(16)-C(17)	1.404(15)	C(17)-C(18)	1.49(2)
C(18)-C(19)	1.42(2)	C(19)-C(20)	1.40(2)
C(20)-C(21)	1.35(2)	C(21)-C(22)	1.41(2)
C(23)-C(24)	1.54(2)	P(2)-F(1)	1.603(10)
P(2)-F(2)	1.576(11)	P(2)-F(3)	1.547(9)
P(2)-F(4)	1.552(11)	P(2)-F(5)	1.585(11)
P(2)-F(6)	1.591(10)		

Table 5.13 : Interatomic angles (°) for $[Ag_2(\mu\text{-}Ph_2Pbipy)_2(NCMe)_2](PF_6)_2$

P(1)-Ag-N(3)	105.8(3)	Ag-P(1)-C(1)	117.0(4)
P(1')-Ag'-N(1)	168.3(3)	P(1')-Ag'-N(2)	109.3(3)
N(1)-Ag'-N(2)	71.1(3)	N(1)-Ag'-N(3')	96.5(3)
N(2)-Ag'-N(3')	94.2(4)		
Ag-P(1)-C(7)	107.5(4)	C(1)-P(1)-C(7)	105.6(5)
Ag-P(1)-C(13)	119.9(4)	C(1)-P(1)-C(13)	102.1(5)
Ag'-N(1)-C(13)	123.8(5)	Ag'-N(1)-C(17)	118.1(5)
Ag'-N(2)-C(18)	113.9(2)	Ag'-N(2)-C(22)	122.9(2)
C(7)-P(1)-C(13)	103.2(5)	C(13)-N(1)-C(17)	117.9(10
C(18)-N(2)-C(22)	122.0(11)	Ag-N(3)-C(23)	160.2(12
P(1)-C(1)-C(2)	121.1(9)	P(1)-C(1)-C(6)	117.5(9)
C(2)-C(1)-C(6)	121.4(11)	C(1)-C(2)-C(3)	120.5(12
C(2)-C(3)-C(4)	118.7(13)	C(3)-C(4)-C(5)	120(2)
C(4)-C(5)-C(6)	122(2)	C(1)-C(6)-C(5)	117.0(12
P(1)-C(7)-C(8)	116.8(9)	P(1)-C(7)-C(12)	120.5(10
C(8)-C(7)-C(12)	122.4(12)	C(7)-C(8)-C(9)	118.6(12
C(8)-C(9)-C(10)	120.5(14)	C(9)-C(10)-C(11)	123(2)
C(10)-C(11)-C(12)	117.9(14)	C(7)-C(12)-C(11)	117.4(12
P(1)-C(13)-N(1)	114.5(8)	P(1)-C(13)-C(14)	121.7(10
N(1)-C(13)-C(14)	123.7(11)	C(13)-C(14)-C(15)	117.5(11
C(14)-C(15)-C(16)	120.1(12)	C(15)-C(16)-C(17)	118.3(12
N(1)-C(17)-C(16)	122.5(11)	N(1)-C(17)-C(18)	116.4(10
C(16)-C(17)-C(18)	121.0(11)	N(2)-C(18)-C(17)	119.0(11
N(2)-C(18)-C(19)	121.4(12)	C(17)-C(18)-C(19)	119.4(11
C(18)-C(19)-C(20)	115.3(13)	C(19)-C(20)-C(21)	123(2)
C(20)-C(21)-C(22)	119(2)	N(2)-C(22)-C(21)	119.3(13
N(3)-C(23)-C(24)	179(2)	F(1)-P(2)-F(2)	89.6(6)
F(1)-P(2)-F(3)	178.7(7)	F(2)-P(2)-F(3)	91.7(7)
F(1)-P(2)-F(4)	90.1(7)	F(2)-P(2)-F(4)	89.4(7)
F(3)-P(2)-F(4)	89.7(7)	F(1)-P(2)-F(5)	88.8(7)
F(2)-P(2)-F(5)	90.8(7)	F(3)-P(2)-F(5)	91.3(7)
F(4)-P(2)-F(5)	179.0(7)	F(1)-P(2)-F(6)	88.4(6)
F(2)-P(2)-F(6)	177.9(7)	F(3)-P(2)-F(6)	90.3(6)
F(4)-P(2)-F(6)	89.7(6)	F(5)-P(2)-F(6)	90.0(7)

Table 5.14 : Fractional coordinates (x 10^4) and isotropic thermal factors ($Å^2$, x10^3) for $[Ag_2(\mu\text{-}Ph_2Pbipy)_2(NCMe)_2](PF_6)_2$

	x/a	y/b	z/c	U_{eq}
Ag	779(1)	926(1)	4774(1)	55(1)
P(1)	-259(3)	1790(3)	5573(1)	44(1)
N(1)	-867(9)	-30(8)	6167(4)	43(2)
N(2)	-1380(10)	-2238(9)	5981(5)	60(3)
N(3)	3168(12)	575(11)	5247(6)	95(4)
C(1)	-1950(12)	2403(9)	5332(5)	47(3)*
C(2)	-2643(13)	2907(11)	5767(6)	63(4)*
C(3)	-3971(14)	3401(11)	5568(6)	70(4)*
C(4)	-4572(15)	3321(13)	4935(7)	87(5)*
C(5)	-3880(17)	2809(14)	4511(8)	95(5)*
C(6)	-2540(14)	2321(10)	4695(6)	63(4)*
C(7)	870(12)	2920(10)	5895(5)	49(3)*
C(8)	2151(12)	2631(10)	6250(5)	58(3)*
C(9)	3093(14)	3475(12)	6465(6)	70(4)*
C(10)	2775(15)	4530(12)	6327(7)	74(4)*
C(11)	1539(16)	4857(13)	5973(7)	85(5)*
C(12)	516(12)	3995(11)	5741(6)	61(3)*
C(13)	-504(11)	1015(10)	6276(5)	48(3)*
C(14)	-415(12)	1526(10)	6872(6)	55(3)*
C(15)	-727(13)	891(11)	7367(6)	62(3)*
C(16)	-1117(12)	-201(11)	7266(6)	58(3)*
C(17)	-1211(11)	-628(9)	6654(5)	47(3)*
C(18)	-1625(12)	-1788(10)	6514(5)	52(3)*
C(19)	-2342(15)	-2371(13)	6935(7)	76(4)*
C(20)	-2645(16)	-3470(14)	6775(8)	88(5)*
C(21)	-2331(15)	-3943(12)	6249(7)	81(4)*
C(22)	-1694(14)	-3299(12)	5834(7)	70(4)*
C(23)	4109(16)	494(12)	5611(7)	70(4)*
C(24)	5396(17)	388(14)	6122(7)	93(5)*
P(2)	-3078(4)	1453(4)	2719(2)	79(1)
F(1)	-1812(10)	1250(10)	2347(5)	141(4)
F(2)	-2598(12)	435(10)	3154(5)	146(4)
F(3)	-4314(11)	1670(9)	3067(6)	152(4)
F(4)	-3998(11)	676(8)	2255(5)	145(4)
F(5)	-2118(12)	2246(11)	3185(5)	158(4)

Table 5.14 / cont.

F(6)	-3534(10)	2461(8)	2261(4)	117(3)

* isotropic temperature factor.

$$U_{eq} = \frac{1}{3} \Sigma_i \Sigma_j U_{ij} a_i^* a_j^* (a_i . a_j)$$

Table 5.15 : Anisotropic thermal factors (Å^2 , x10^3) for [Ag_2(μ-Ph_2Pbipy)$_2$(NCMe)$_2$](PF_6)$_2$

	U(11)	U(22)	U(33)	U(23)	U(13)	U(12)
Ag	61(1)	59(1)	49(1)	-6(1)	24(1)	-5(1)
P(1)	49(2)	48(2)	38(2)	-4(2)	12(1)	-4(2)
N(1)	49(6)	46(6)	36(5)	4(5)	14(5)	2(5)
N(2)	66(7)	52(7)	65(7)	-6(6)	20(6)	4(6)
N(3)	57(8)	124(12)	98(10)	-19(8)	-7(7)	21(8)
P(2)	70(3)	103(3)	66(3)	6(3)	16(2)	8(3)
F(1)	114(8)	189(11)	129(8)	45(8)	48(7)	50(8)
F(2)	142(9)	147(9)	149(9)	87(8)	23(7)	9(8)
F(3)	127(9)	156(10)	200(11)	-19(9)	108(9)	2(8)
F(4)	126(8)	103(8)	182(11)	-45(7)	-48(8)	33(7)
F(5)	157(10)	209(13)	98(7)	-9(8)	-6(7)	-80(10)
F(6)	120(8)	109(8)	121(8)	30(7)	15(6)	25(6)

5.6.19 Single crystal X-ray diffraction study of $[Ag_2(\mu\text{-}Ph_2Pbipy)_2(py)_2](PF_6)_2$ [35]

A pale-yellow block-shaped crystal was grown by slow evaporation of a saturated pyridine solution of the complex. The general approach used for the intensity data collection is described in Appendix A. The phenyl groups of the Ph_2Pbipy ligands were refined as rigid groups. The crystallographic data are given in Table 5.16, the interatomic distances in Table 5.17, the interatomic angles in Table 5.18, the fractional coordinates in Table 5.19 and the anisotropic thermal parameters in Table 5.20. The observed and calculated structure factors may be found on microfiche in an envelope fixed to the inside back cover.

Table 5.16

Crystal data and details of the crystallographic analysis for $[Ag_2(\mu\text{-}Ph_2Pbipy)_2(py)_2](PF_6)_2$

Formula	$Ag_2C_{54}H_{44}N_6P_4F_{12}$
Molecular Mass	1344.60
Crystal System	Triclinic
Space Group	$P\bar{1}$
a(Å)	11.527(2)
b(Å)	11.546(2)
c(Å)	11.760(3)
α(°)	80.60(2)
β(°)	62.88(2)
γ(°)	89.35(1)
V(Å^3)	1370.72
Z	1
D_c(g.cm^{-3})	1.629
F(000)	1344
λ(Mo-Kα)(Å)	0.71069
Scan mode	ω - 2θ
ω scan angle	0.65 + 0.35tanθ
Horizontal Aperture width (mm)	2.7 + 0.1tanθ
Scattering range (°)	$2 \leq \theta \leq 23$
μ (cm^{-1})	9.03
Absorption corrections	Semi empirical[103]
Measured intensities	4022
Unique intensities	3516
Unique intensities with [I > 3σ(I)]	3057
Structure solution	Direct & Fourier methods
Weighting scheme	$1/(\sigma^2(F) + 0.10298F^2)$
$R = \Sigma(F_o-F_c)/\Sigma F_o$	0.0462
$R_w = \Sigma_w½ (F_o-F_c)/ \Sigma_w½F_o$	0.0555
$(\Delta/\sigma)_{max}$	0.412
$\Delta\rho_{max}$(eÅ^{-3})	0.855
Number of parameters	328

Table 5.17 : Interatomic distances (Å) for $[Ag_2(\mu\text{-}Ph_2Pbipy)_2(py)_2](PF_6)_2$

Ag-P(1)	2.398(0)	Ag-N(3)	2.333(1)
Ag-Ag′	4.092(1)	Ag-N(1′)	2.392(2)
Ag-N(2′)	2.371(2)		
P(1)-C(1)	1.802(1)	P(1)-C(7)	1.821(1)
P(1)-C(13)	1.837(1)	N(1)-C(13)	1.348(2)
N(1)-C(17)	1.336(2)	N(2)-C(18)	1.338(2)
N(2)-C(22)	1.342(2)	N(3)-C(23)	1.350(3)
N(3)-C(27)	1.331(3)	C(1)-C(2)	1.395(0)
C(1)-C(6)	1.395(0)	C(2)-C(3)	1.395(0)
C(3)-C(4)	1.395(0)	C(4)-C(5)	1.395(0)
C(5)-C(6)	1.395(0)	C(7)-C(8)	1.395(0)
C(7)-C(12)	1.395(0)	C(8)-C(9)	1.395(0)
C(9)-C(10)	1.395(0)	C(10)-C(11)	1.395(0)
C(11)-C(12)	1.395(0)	C(13)-C(14)	1.371(2)
C(14)-C(15)	1.384(3)	C(15)-C(16)	1.380(3)
C(16)-C(17)	1.397(2)	C(17)-C(18)	1.489(2)
C(18)-C(19)	1.390(2)	C(19)-C(20)	1.382(3)
C(20)-C(21)	1.349(3)	C(21)-C(22)	1.400(2)
C(23)-C(24)	1.445(5)	C(24)-C(25)	1.410(7)
C(25)-C(26)	1.275(8)	C(26)-C(27)	1.433(5)
P(2)-F(1)	1.547(2)	P(2)-F(2)	1.508(3)
P(2)-F(3)	1.536(2)	P(2)-F(4)	1.534(2)
P(2)-F(5)	1.538(1)	P(2)-F(6)	1.545(2)

Table 5.18 : Interatomic angles (°) for $[Ag_2(\mu\text{-}Ph_2Pbipy)_2(py)_2](PF_6)_2$

P(1)-Ag-N(3)	113.4(0)	Ag-P(1)-C(1)	114.6(0)
N(1′)-Ag-N(2′)	69.3(2)	N(1′)-Ag-P(1)	118.6(1)
N(2′)-Ag-P(1)	119.0(2)	N(2′)-Ag-N(3)	96.2(1)
N(1′)-Ag-N(3)	126.5(2)	Ag-N(2′)-C(18′)	118.2(4)
Ag-N(1′)-C(17′)	117.4(4)	Ag-N(1′)-C(13′)	124.1(3)
Ag-P(1)-C(7)	112.0(0)	C(1)-P(1)-C(7)	103.1(0)
Ag-P(1)-C(13)	117.9(0)	C(1)-P(1)-C(13)	105.5(1)
C(7)-P(1)-C(13)	102.1(1)	C(13)-N(1)-C(17)	117.8(1)
C(18)-N(2)-C(22)	118.9(1)	Ag-N(3)-C(23)	116.9(2)
Ag-N(3)-C(27)	121.7(2)	C(23)-N(3)-C(27)	121.4(2)
P(1)-C(1)-C(2)	116.7(0)	P(1)-C(1)-C(6)	123.0(0)
C(2)-C(1)-C(6)	120.0(0)	C(1)-C(2)-C(3)	120.0(0)
C(2)-C(3)-C(4)	120.0(0)	C(3)-C(4)-C(5)	120.0(0)
C(4)-C(5)-C(6)	120.0(0)	C(1)-C(6)-C(5)	120.0(0)
P(1)-C(7)-C(8)	121.2(0)	P(1)-C(7)-C(12)	118.8(0)
C(8)-C(7)-C(12)	120.0(0)	C(7)-C(8)-C(9)	120.0(0)
C(8)-C(9)-C(10)	120.0(0)	C(9)-C(10)-C(11)	120.0(0)
C(10)-C(11)-C(12)	120.0(0)	C(7)-C(12)-C(11)	120.0(0)
P(1)-C(13)-N(1)	115.5(1)	P(1)-C(13)-C(14)	121.1(1)
N(1)-C(13)-C(14)	123.4(1)	C(13)-C(14)-C(15)	118.5(2)
C(14)-C(15)-C(16)	119.3(2)	C(15)-C(16)-C(17)	118.6(2)
N(1)-C(17)-C(16)	122.3(2)	N(1)-C(17)-C(18)	116.9(1)
C(16)-C(17)-C(18)	120.7(1)	N(2)-C(18)-C(17)	117.2(1)
N(2)-C(18)-C(19)	122.0(2)	C(17)-C(18)-C(19)	120.8(2)
C(18)-C(19)-C(20)	118.1(2)	C(19)-C(20)-C(21)	120.7(2)
C(20)-C(21)-C(22)	118.3(2)	N(2)-C(22)-C(21)	121.9(2)
N(3)-C(23)-C(24)	121.3(4)	C(23)-C(24)-C(25)	113.4(4)
C(24)-C(25)-C(26)	125.2(5)	C(25)-C(26)-C(27)	119.5(5)
N(3)-C(27)-C(26)	119.1(4)	F(1)-P(2)-F(2)	93.2(2)
F(1)-P(2)-F(3)	178.6(2)	F(2)-P(2)-F(3)	85.6(2)
F(1)-P(2)-F(4)	87.8(1)	F(2)-P(2)-F(4)	178.6(2)
F(3)-P(2)-F(4)	93.4(2)	F(1)-P(2)-F(5)	88.8(1)

Table 5.18 / cont.

F(2)-P(2)-F(5)	87.6(1)	F(3)-P(2)-F(5)	91.8(1)
F(4)-P(2)-F(5)	91.4(1)	F(1)-P(2)-F(6)	89.1(1)
F(2)-P(2)-F(6)	90.8(2)	F(3)-P(2)-F(6)	90.2(1)
F(4)-P(2)-F(6)	90.2(2)	F(5)-P(2)-F(6)	177.3(1)

Table 5.19 : Fractional coordinates (x 10^4) and isotropic thermal factors ($Å^2$, x10^3) for $[Ag_2(\mu\text{-}Ph_2Pbipy)_2(py)_2](PF_6)_2$

	x/a	y/b	z/c	U_{eq}
Ag	747(1)	4481(1)	8232(1)	48(1)
P(1)	1302(1)	3575(1)	9887(1)	39(1)
N(1)	-823(4)	3417(4)	12232(4)	39(1)
N(2)	-2449(5)	4779(4)	13872(4)	50(1)
N(3)	-254(6)	3164(6)	7585(7)	71(2)
C(1)	2105(4)	4563(3)	10388(3)	43(1)
C(2)	2867(4)	5522(3)	9456(3)	62(2)
C(3)	3612(4)	6266(3)	9734(3)	86(2)
C(4)	3595(4)	6051(3)	10944(3)	84(2)
C(5)	2833(4)	5093(3)	11876(3)	74(2)
C(6)	2088(4)	4349(3)	11598(3)	58(2)
C(7)	2471(3)	2464(3)	9340(4)	45(1)
C(8)	3250(3)	2115(3)	9941(4)	62(2)
C(9)	4136(3)	1261(3)	9503(4)	79(2)
C(10)	4243(3)	755(3)	8464(4)	78(2)
C(11)	3465(3)	1103(3)	7862(4)	73(2)
C(12)	2578(3)	1958(3)	8300(4)	58(2)
C(13)	-12(5)	2754(5)	11397(5)	43(1)
C(14)	-160(8)	1549(6)	11617(7)	72(2)
C(15)	-1230(10)	985(7)	12722(9)	103(2)
C(16)	-2095(9)	1645(7)	13576(8)	86(2)
C(17)	-1844(6)	2866(6)	13306(6)	54(1)
C(18)	-2706(6)	3613(6)	14233(5)	50(1)
C(19)	-3710(7)	3106(7)	15434(7)	70(2)
C(20)	-4451(7)	3844(8)	16268(7)	77(2)
C(21)	-4177(6)	5020(8)	15939(7)	66(2)
C(22)	-3174(6)	5478(7)	14703(6)	61(2)
C(23)	-985(10)	2234(8)	8489(14)	116(4)
C(24)	-1569(15)	1322(12)	8165(26)	170(7)
C(25)	-1319(23)	1530(20)	6856(33)	208(12)
C(26)	-662(17)	2426(22)	6013(20)	172(7)
C(27)	-84(10)	3301(12)	6372(11)	117(4)
P(2)	3333(3)	1502(2)	13886(2)	85(1)
F(1)	2692(9)	2656(6)	13707(7)	155(3)

Table 5.19 / cont.

F(2)	2139(13)	737(9)	14193(12)	219(4)
F(3)	3949(11)	341(6)	14053(7)	199(3)
F(4)	4551(9)	2261(9)	13599(11)	205(4)
F(5)	2741(8)	1539(5)	15344(5)	141(2)
F(6)	3868(10)	1485(7)	12422(6)	175(3)

$$U_{eq} = \frac{1}{3} \Sigma_i \Sigma_j U_{ij} a_i^* a_j^* (a_i . a_j)$$

Table 5.20 : Anisotropic thermal factors (Å^2 , x10^3) for $[Ag_2(\mu\text{-}Ph_2Pbipy)_2(py)_2](PF_6)_2$

	U(11)	U(22)	U(33)	U(23)	U(13)	U(12)
Ag	52(1)	47(1)	41(1)	0(1)	-21(1)	0(1)
P(1)	39(1)	38(1)	36(1)	-1(1)	-14(1)	2(1)
N(1)	33(2)	40(2)	36(2)	3(2)	-11(2)	-5(2)
N(2)	42(3)	61(3)	38(3)	-6(2)	-12(2)	-3(2)
N(3)	61(4)	72(4)	95(5)	-28(4)	-44(4)	5(3)
C(1)	36(3)	45(3)	45(3)	-6(3)	-16(3)	1(2)
C(2)	48(4)	61(4)	67(4)	-6(3)	-19(3)	-10(3)
C(3)	61(5)	80(5)	107(7)	-5(5)	-33(5)	-23(4)
C(4)	80(5)	79(5)	116(7)	-20(5)	-64(6)	-7(4)
C(5)	70(5)	88(5)	82(5)	-15(4)	-51(4)	1(4)
C(6)	57(4)	70(4)	59(4)	-9(3)	-39(3)	5(3)
C(7)	37(3)	40(3)	47(3)	0(3)	-13(3)	5(2)
C(8)	55(4)	55(4)	72(4)	-8(3)	-28(4)	15(3)
C(9)	80(5)	62(5)	91(6)	-12(4)	-36(5)	25(4)
C(10)	75(5)	65(5)	85(6)	-16(4)	-28(5)	25(4)
C(11)	63(5)	67(4)	78(5)	-25(4)	-19(4)	15(4)
C(12)	56(4)	52(4)	56(4)	-11(3)	-15(3)	0(3)
C(13)	43(3)	39(3)	40(3)	3(2)	-16(3)	-3(2)
C(14)	76(5)	40(4)	72(5)	2(3)	-14(4)	-7(3)
C(15)	112(7)	50(4)	90(6)	1(4)	-3(6)	-11(4)
C(16)	85(6)	56(4)	69(5)	5(4)	0(4)	-22(4)
C(17)	49(4)	58(4)	45(4)	5(3)	-18(3)	-4(3)
C(18)	39(3)	67(4)	36(3)	-2(3)	-14(3)	-5(3)
C(19)	50(4)	92(5)	47(4)	-4(4)	-8(3)	-12(4)
C(20)	48(4)	113(7)	51(4)	-4(4)	-9(3)	-21(4)
C(21)	43(4)	106(6)	48(4)	-17(4)	-20(3)	-2(4)
C(22)	47(4)	86(5)	50(4)	-20(4)	-21(3)	2(3)
C(23)	80(6)	66(5)	208(12)	-14(7)	-77(7)	-8(5)
C(24)	105(10)	85(8)	326(26)	-38(13)	-104(15)	-8(7)
C(25)	167(19)	174(20)	395(45)	-178(28)	-185(28)	72(15)
C(26)	132(13)	272(23)	178(16)	-136(17)	-96(12)	45(13)
C(27)	95(7)	182(11)	121(8)	-76(8)	-75(7)	19(7)
P(2)	128(2)	49(1)	55(1)	-6(1)	-24(1)	8(1)
F(1)	242(9)	110(5)	133(5)	-19(4)	-104(6)	62(5)
F(2)	271(13)	163(8)	255(12)	-40(8)	-145(10)	-53(9)

Table 5.20 / cont.

F(3)	259(11)	101(5)	119(5)	14(4)	1(6)	63(6)
F(4)	136(7)	188(9)	242(11)	6(8)	-60(7)	-25(6)
F(5)	218(8)	105(4)	74(3)	-12(3)	-45(4)	8(5)
F(6)	276(11)	139(6)	83(4)	-24(4)	-59(6)	57(6)

5.6.20 Single crystal X-ray diffraction study of $[Ag_2(\mu\text{-}Ph_2Pbipy)_2(EtOH)_2](BF_4)_2$ [36]

A pale-yellow block-shaped crystal was grown by slow evaporation of a saturated ethanol solution of the complex. The general approach used for the intensity data collection is described in Appendix A. The crystallographic data are given in Table 5.21, the interatomic distances in Table 5.22, the interatomic angles in Table 5.23, the fractional coordinates in Table 5.24 and the anisotropic thermal parameters in Table 5.25. The observed and calculated structure factors may be found on microfiche in an envelope fixed to the inside back cover.

Table 5.21

Crystal data and details of the crystallographic analysis for $[Ag_2(\mu\text{-}Ph_2Pbipy)_2(EtOH)_2](BF_4)_2$

Formula	$Ag_2C_{48}H_{46}N_4O_2P_2B_2F_8$
Molecular Mass	1162.21
Crystal System	Triclinic
Space Group	$P\bar{1}$
a(Å)	10.777(2)
b(Å)	11.556(20
c(Å)	11.570(3)
α(°)	104.48(2)
β(°)	102.83(2)
γ(°)	111.13(1)
V(Å^3)	1221.08
Z	1
D_c(g.cm^{-3})	1.580
F(000)	1168
λ(Mo-Kα)(Å)	0.71069
Scan mode	ω - 2θ
ω scan angle	0.52 + 0.35tanθ
Horizontal Aperture width (mm)	2.7 + 0.1tanθ
Scattering range (°)	$2 \leq \theta \leq 23$
μ (cm^{-1})	9.26
Absorption corrections	Semi empirical[103]
Measured intensities	3599
Unique intensities	3162
Unique intensities with $[I > 3\sigma(I)]$	2748
Structure solution	Direct & Fourier methods
Weighting scheme	$1/(\sigma^2(F) + 0.00085F^2)$
$R = \Sigma(F_o\text{-}F_c)/\Sigma F_o$	0.0438
$R_w = \Sigma_w{}^{1/2}(F_o\text{-}F_c)/\Sigma_w{}^{1/2}F_o$	0.0474
$(\Delta/\sigma)_{max}$	0.104
$\Delta\rho_{max}$(eÅ^{-3})	1.513
Number of parameters	307

Table 5.22 : Interatomic distances (Å) for $[Ag_2(\mu\text{-}Ph_2Pbipy)_2(EtOH)_2](BF_4)_2$

Ag-P(1)	2.379(1)	Ag-O	2.494(6)
Ag-N(1′)	2.316(4)	P(1)-C(1)	1.820(6)
Ag-N(2′)	2.351(5)		
P(1)-C(7)	1.824(6)	P(1)-C(13)	1.824(6)
N(1)-C(13)	1.354(7)	N(1)-C(17)	1.354(7)
N(2)-C(18)	1.344(8)	N(2)-C(22)	1.342(9)
O-C(23)	1.412(13)	C(1)-C(2)	1.397(8)
C(1)-C(6)	1.380(8)	C(2)-C(3)	1.397(10)
C(3)-C(4)	1.376(10)	C(4)-C(5)	1.365(10)
C(5)-C(6)	1.405(10)	C(7)-C(8)	1.378(9)
C(7)-C(12)	1.382(9)	C(8)-C(9)	1.403(10)
C(9)-C(10)	1.377(11)	C(10)-C(11)	1.365(11)
C(11)-C(12)	1.400(9)	C(13)-C(14)	1.386(9)
C(14)-C(15)	1.374(10)	C(15)-C(16)	1.384(10)
C(16)-C(17)	1.400(9)	C(17)-C(18)	1.483(9)
C(18)-C(19)	1.367(9)	C(19)-C(20)	1.404(11)
C(20)-C(21)	1.350(11)	C(21)-C(22)	1.392(10)
C(23)-C(24)	1.35(2)	B(1)-F(1)	1.362(12)
B(1)-F(2)	1.272(11)		

Table 5.23 : Interatomic angles (°) for [Ag_2(μ-Ph_2Pbipy)$_2$(EtOH)$_2$](BF_4)$_2$

P(1)-Ag-O	100.9(2)	Ag-P(1)-C(1)	118.2(2
N(1')-Ag-N(2')	70.5(2)	N(1')-Ag-P	151.9(2
N(2')-Ag-P	116.6(2)	N(1')-Ag-O	105.5(2
N(2')-Ag-O	95.2(2)		
Ag-P(1)-C(7)	108.3(2)	C(1)-P(1)-C(7)	104.2(3
Ag-P(1)-C(13)	116.9(2)	C(1)-P(1)-C(13)	103.0(3
C(7)-P(1)-C(13)	104.7(3)	C(13)-N(1)-C(17)	119.1(5
C(18)-N(2)-C(22)	119.3(6)	Ag-O-C(23)	132.0(7
P(1)-C(1)-C(2)	117.0(5)	P(1)-C(1)-C(6)	123.1(5
C(2)-C(1)-C(6)	119.9(6)	C(1)-C(2)-C(3)	119.1(6
C(2)-C(3)-C(4)	121.3(7)	C(3)-C(4)-C(5)	118.8(7
C(4)-C(5)-C(6)	121.7(6)	C(1)-C(6)-C(5)	119.1(6
P(1)-C(7)-C(8)	118.1(5)	P(1)-C(7)-C(12)	122.5(5
C(8)-C(7)-C(12)	119.1(6)	C(7)-C(8)-C(9)	120.6(7
C(8)-C(9)-C(10)	119.3(7)	C(9)-C(10)-C(11)	120.6(6
C(10)-C(11)-C(12)	119.9(7)	C(7)-C(12)-C(11)	120.3(6
P(1)-C(13)-N(1)	112.7(4)	P(1)-C(13)-C(14)	125.0(5
N(1)-C(13)-C(14)	122.2(6)	C(13)-C(14)-C(15)	118.6(6
C(14)-C(15)-C(16)	120.1(6)	C(15)-C(16)-C(17)	119.0(6
N(1)-C(17)-C(16)	120.9(6)	N(1)-C(17)-C(18)	116.7(5
C(16)-C(17)-C(18)	122.5(5)	N(2)-C(18)-C(17)	116.5(5
N(2)-C(18)-C(19)	121.7(6)	C(17)-C(18)-C(19)	121.7(6
C(18)-C(19)-C(20)	118.2(7)	C(19)-C(20)-C(21)	120.8(7
C(20)-C(21)-C(22)	117.9(7)	N(2)-C(22)-C(21)	122.2(7
O-C(23)-C(24)	118.6(13)	F(1)-B(1)-F(2)	117.8(1

Table 5.24 : Fractional coordinates (x 10^4) and isotropic thermal factors ($Å^2$, x10^3) for $[Ag_2(\mu\text{-}Ph_2Pbipy)_2(EtOH)_2](BF_4)_2$

	x/a	y/b	z/c	U_{eq}
Ag	5162(1)	4241	3840	47
P(1)	6088(2)	6457(1)	3866(1)	39
N(1)	6679(5)	7688(4)	6330(4)	40(1)
N(2)	5430(6)	7462(5)	8089(5)	55(1)
O	7378(6)	4147(7)	4929(6)	96(2)
C(1)	4844(6)	7065(6)	3247(5)	41(1)
C(2)	3548(7)	6120(7)	2311(7)	59(2)
C(3)	2594(8)	6546(8)	1750(7)	67(2)
C(4)	2889(8)	7873(8)	2124(7)	64(2)
C(5)	4140(9)	8780(7)	3068(7)	66(2)
C(6)	5147(7)	8397(6)	3630(6)	56(2)
C(7)	7189(6)	6585(6)	2868(6)	41(1)
C(8)	8259(8)	6198(8)	3113(7)	66(2)
C(9)	9047(8)	6151(8)	2302(9)	76(2)
C(10)	8771(8)	6533(7)	1275(7)	63(2)
C(11)	7716(8)	6920(8)	1023(7)	68(2)
C(12)	6925(8)	6960(7)	1830(6)	60(2)
C(13)	7241(6)	7781(6)	5401(6)	42(1)
C(14)	8529(7)	8815(7)	5615(7)	62(2)
C(15)	9266(7)	9765(7)	6817(7)	66(2)
C(16)	8689(7)	9713(7)	7769(6)	57(2)
C(17)	7371(6)	8661(6)	7497(6)	44(1)
C(18)	6649(7)	8562(6)	8445(6)	47(1)
C(19)	7162(9)	9567(7)	9599(7)	71(2)
C(20)	6364(10)	9437(9)	10407(7)	80(2)
C(21)	5131(9)	8344(8)	10056(7)	72(2)
C(22)	4674(9)	7361(8)	8868(7)	70(2)
C(23)	8094(14)	3417(13)	4491(14)	126(4)
C(24)	7602(18)	2128(14)	4381(15)	160(5)
B(1)	9928(10)	7018(10)	8224(10)	74(2)
F(1)	9400(11)	7671(9)	8977(8)	181(4)
F(2)	9049(10)	6021(9)	7228(7)	220(3)
F(3)	9310(9)	2063(7)	2156(8)	175(3)
F(4)	9393(13)	3373(12)	1043(9)	234(5)

Table 5,24 / cont.

$$U_{eq} = \frac{1}{3} \Sigma_i \Sigma_j U_{ij} a_i^* a_j^* (a_i \cdot a_j)$$

Table 5.25 : Anisotropic thermal factors ($Å^2$, $x10^3$) for
$[Ag_2(\mu\text{-}Ph_2Pbipy)_2(EtOH)_2](BF_4)_2$

	U(11)	U(22)	U(33)	U(23)	U(13)	U(12)
Ag	57(1)	35(1)	49(1)	15(1)	27(1)	14(1)
P(1)	43(1)	36(1)	40(1)	15(1)	21(1)	14(1)
N(1)	44(3)	39(3)	36(3)	18(2)	13(2)	17(2)
N(2)	60(3)	55(3)	46(3)	16(3)	24(3)	18(3)
O	85(4)	126(5)	78(4)	25(4)	15(3)	63(4)
C(1)	43(3)	43(3)	40(3)	18(3)	19(3)	17(3)
C(2)	47(4)	57(4)	64(4)	16(3)	19(3)	17(3)
C(3)	53(4)	75(5)	70(5)	22(4)	18(4)	30(4)
C(4)	61(5)	76(5)	66(5)	28(4)	27(4)	37(4)
C(5)	90(6)	65(5)	71(5)	34(4)	41(5)	51(4)
C(6)	62(4)	50(4)	60(4)	17(3)	25(4)	28(3)
C(7)	44(3)	37(3)	45(3)	16(3)	22(3)	16(3)
C(8)	66(5)	81(5)	80(5)	43(4)	44(4)	42(4)
C(9)	68(5)	82(5)	102(6)	39(5)	52(5)	42(4)
C(10)	61(4)	63(4)	59(4)	16(4)	34(4)	20(4)
C(11)	64(5)	91(6)	54(4)	28(4)	33(4)	32(4)
C(12)	70(5)	75(5)	53(4)	33(4)	36(4)	37(4)
C(13)	44(3)	43(3)	42(3)	21(3)	17(3)	18(3)
C(14)	57(4)	52(4)	61(4)	18(3)	24(4)	8(3)
C(15)	54(4)	55(4)	66(5)	11(4)	21(4)	7(3)
C(16)	51(4)	51(4)	55(4)	15(3)	13(3)	16(3)
C(17)	45(3)	39(3)	44(3)	15(3)	11(3)	15(3)
C(18)	58(4)	43(3)	38(3)	13(3)	12(3)	25(3)
C(19)	107(6)	57(4)	43(4)	13(3)	30(4)	30(4)
C(20)	117(7)	72(5)	44(4)	11(4)	33(5)	40(5)
C(21)	100(6)	75(5)	53(4)	25(4)	39(4)	44(5)
C(22)	87(6)	75(5)	53(4)	21(4)	38(4)	34(4)
C(23)	125(9)	128(10)	162(12)	68(9)	60(9)	78(8)
C(24)	210(16)	113(10)	170(13)	64(10)	109(12)	52(10)
B(1)	69(6)	64(5)	86(7)	26(5)	26(6)	26(5)
F(1)	286(11)	240(10)	204(8)	157(8)	184(9)	204(9)
F(2)	185(8)	162(7)	112(6)	-19(5)	-3(6)	-59(6)
F(3)	196(8)	125(6)	165(7)	41(5)	118(6)	6(5)
F(4)	317(13)	321(14)	165(8)	95(9)	53(8)	260(12)

5.6.21 Single crystal X-ray diffraction study of [Ag_2(μ-Ph_2Pbipy)$_2$ (NO_3)$_2$].MeOH [43]

A pale-yellow block-shaped crystal was grown by cooling a hot, saturated methanolic solution of the complex to room temperature. The general approach used for the intensity data collection is described in Appendix A. The crystallographic data are given in Table 5.26, the interatomic distances in Table 5.27, the interatomic angles in Table 5.28, the fractional coordinates in Table 5.29 and the anisotropic thermal parameters in Table 5.30. The observed and calculated structure factors may be found on microfiche in an envelope fixed to the inside back cover.

Table 5.26

Crystal data and details of the crystallographic analysis for $[Ag_2(\mu\text{-}Ph_2Pbipy)_2(NO_3)_2].MeOH$

Formula	$Ag_2C_{45}H_{38}N_6O_7P_2$
Molecular Mass	1052.52
Crystal System	Monoclinic
Space Group	$P2_1/c$
a(Å)	9.917(3)
b(Å)	19.952(3)
c(Å)	11.585(2)
β(°)	112.99(2)
V(Å^3)	2292.25
Z	2
D_c(g.cm^{-3})	1.525
F(000)	1060
λ(Mo-Kα)(Å)	0.71069
Scan mode	ω - 2θ
ω scan angle	1.20 + 0.35tanθ
Horizontal Aperture width (mm)	3.0 + 0.1tanθ
Scattering range (°)	$2 \leq \theta \leq 23$
μ (cm^{-1})	9.61
Absorption corrections	Semi empirical[103]
Measured intensities	3202
Unique intensities	2489
Unique intensities with [I > 3σ(I)]	1819
Structure solution	Direct & Fourier methods
Weighting scheme	$1/(\sigma^2(F) + 0.01732F^2)$
$R = \Sigma(F_o\text{-}F_c)/\Sigma F_o$	0.052
$R_w = \Sigma_w\frac{1}{2}(F_o\text{-}F_c)/\Sigma_w\frac{1}{2}F_o$	0.056
$(\Delta/\sigma)_{max}$	0.452
$\Delta\rho_{max}$(eÅ^{-3})	0.690
Number of parameters	169

Table 5.27 : Interatomic distances (Å) for $[Ag_2(\mu\text{-}Ph_2Pbipy)_2(NO_3)_2]$

Ag-P	2.378(3)	Ag-O(1)	2.422(8)
Ag-O(4)	1.300(5)	Ag-N(1′)	2.322(2)
Ag-N(2′)	2.393(2)		
P-C(1)	1.828(11)	P-C(7)	1.834(11)
P-C(13)	1.851(11)	N(1)-C(13)	1.324(13)
N(1)-C(17)	1.367(14)	N(2)-C(18)	1.36(2)
N(2)-C(22)	1.33(2)	N(3)-O(1)	1.238(12)
N(3)-O(2)	1.213(13)	N(3)-O(3)	1.258(13)
C(1)-C(2)	1.37(2)		
C(1)-C(6)	1.38(2)	C(2)-C(3)	1.40(2)
C(3)-C(4)	1.39(2)	C(4)-C(5)	1.38(2)
C(5)-C(6)	1.42(2)	C(7)-C(8)	1.37(2)
C(7)-C(12)	1.38(2)	C(8)-C(9)	1.44(2)
C(9)-C(10)	1.37(2)	C(10)-C(11)	1.35(2)
C(11)-C(12)	1.42(2)	C(13)-C(14)	1.38(2)
C(14)-C(15)	1.39(2)	C(15)-C(16)	1.38(2)
C(16)-C(17)	1.42(2)	C(16)-C(23)	1.5(8)
C(17)-C(18)	1.46(2)	C(18)-C(19)	1.42(2)
C(19)-C(20)	1.37(2)	C(20)-C(21)	1.37(2)
C(21)-C(22)	1.41(2)		

Table 5.28 : Interatomic angles (°) for [$Ag_2(\mu\text{-}Ph_2Pbipy)_2(NO_3)_2$]

P-Ag-O(1)	112.5(2)	P-Ag-O(4)	92(17)
N(1')-Ag-N(2')	70.1(1)	N(1')-Ag-P	153.8(1)
Ag-P-C(1)	107.1(4)	N(2')-Ag-P	113.3(1)
N(1')-Ag-O(1)	111.2(3)	N(2')-Ag-O(1)	108.8(4)
Ag-P-C(7)	117.0(4)	C(1)-P-C(7)	104.7(5)
Ag-P-C(13)	118.7(4)	C(1)-P-C(13)	103.7(5)
C(7)-P-C(13)	104.1(5)	C(13)-N(1)-C(17)	118.2(9)
C(18)-N(2)-C(22)	119.5(10)	O(1)-N(3)-O(2)	121.1(12
O(1)-N(3)-O(3)	118.8(10)	O(2)-N(3)-O(3)	119.9(10
Ag-O(1)-N(3)	114.5(7)	Ag-O(1)-O(4)	31(14)
N(3)-O(1)-O(4)	116(17)	P-C(1)-C(2)	123.4(9)
P-C(1)-C(6)	116.8(9)	C(2)-C(1)-C(6)	119.8(12
C(1)-C(2)-C(3)	120.0(13)	C(2)-C(3)-C(4)	121(2)
C(3)-C(4)-C(5)	120(2)	C(4)-C(5)-C(6)	119(2)
C(1)-C(6)-C(5)	120.9(13)	P-C(7)-C(8)	122.2(9)
P-C(7)-C(12)	115.1(10)	C(8)-C(7)-C(12)	122.7(12
C(7)-C(8)-C(9)	118.6(13)	C(8)-C(9)-C(10)	118(2)
C(9)-C(10)-C(11)	122(2)	C(10)-C(11)-C(12)	121(2)
C(7)-C(12)-C(11)	117(2)	P-C(13)-N(1)	111.8(7)
P-C(13)-C(14)	122.9(9)	N(1)-C(13)-C(14)	125.3(10
C(13)-C(14)-C(15)	116.5(11)	C(14)-C(15)-C(16)	120.9(12
C(15)-C(16)-C(17)	118.6(11)	C(15)-C(16)-C(23)	94(22)
C(17)-C(16)-C(23)	147(22)	N(1)-C(17)-C(16)	120.3(10
N(1)-C(17)-C(18)	117.9(10)	C(16)-C(17)-C(18)	121.8(10
N(2)-C(18)-C(17)	116.1(10)	N(2)-C(18)-C(19)	120.6(10
C(17)-C(18)-C(19)	123.2(10)	C(18)-C(19)-C(20)	118.2(12
C(19)-C(20)-C(21)	121.6(13)	C(20)-C(21)-C(22)	117.3(13
N(2)-C(22)-C(21)	122.8(12)	Ag-O(4)-O(1)	106(35)

Table 5.29 : Fractional coordinates (x 10^4) and isotropic thermal factors ($Å^2$, x10^3) for [$Ag_2(\mu\text{-}Ph_2Pbipy)_2(NO_3)_2$]

	x/a	y/b	z/c	U_{eq}
Ag	944(1)	590	467(1)	38
P	424(3)	252(1)	2220(2)	31(1)
N(1)	-1981(8)	-450(4)	1001(8)	30(2)
N(2)	-3111(10)	-1257(5)	-1031(8)	46(2)
N(3)	-1930(10)	1443(5)	-761(9)	47(2)
O(1)	-674(8)	1470(5)	-740(9)	66(2)
O(2)	-2807(11)	1887(6)	-1232(12)	108(4)
O(3)	-2322(8)	922(5)	-364(9)	66(2)
C(1)	709(10)	984(5)	3237(9)	33(2)*
C(2)	1639(13)	987(6)	4474(11)	49(3)*
C(3)	1842(16)	1576(8)	5181(14)	76(4)*
C(4)	1132(15)	2163(7)	4632(14)	71(4)*
C(5)	187(17)	2165(8)	3385(15)	79(4)*
C(6)	-20(13)	1565(7)	2686(12)	58(3)*
C(7)	1598(11)	-399(5)	3236(10)	38(3)*
C(8)	1086(14)	-854(7)	3856(13)	61(3)*
C(9)	2066(17)	-1361(8)	4603(15)	82(5)*
C(10)	3487(18)	-1356(9)	4693(16)	87(5)*
C(11)	3983(18)	-895(9)	4099(16)	91(5)*
C(12)	3024(16)	-406(7)	3310(14)	71(4)*
C(13)	-1459(10)	-24(5)	1950(9)	32(2)*
C(14)	-2198(12)	194(6)	2672(10)	44(3)*
C(15)	-3610(13)	-48(6)	2349(11)	51(3)*
C(16)	-4191(12)	-513(6)	1405(11)	49(3)*
C(17)	-3338(11)	-719(5)	731(10)	38(3)*
C(18)	-3882(11)	-1205(5)	-286(10)	38(3)*
C(19)	-5123(13)	-1619(6)	-498(11)	56(3)*
C(20)	-5531(14)	-2063(7)	-1479(12)	60(4)*
C(21)	-4759(14)	-2120(7)	-2234(12)	61(4)*
C(22)	-3537(13)	-1695(7)	-1972(12)	58(3)*
O(4)	695(784)	1217(211)	634(476)	3165(234)*
C(23)	4359(713)	-559(281)	1547(548)	2679(229)*

* isotropic temperature factor.

$$U_{eq} = \frac{1}{3} \Sigma_i \Sigma_j U_{ij} a_i^* a_j^* (a_i . a_j)$$

Table 5.30 : Anisotropic thermal factors ($Å^2$, $x10^3$) for $[Ag_2(\mu\text{-}Ph_2Pbipy)_2(NO_3)_2]$

	U(11)	U(22)	U(33)	U(23)	U(13)	U(12)
Ag	34(1)	42(1)	42(1)	-3(1)	20(1)	-9(1)
P	26(1)	37(2)	34(2)	-3(1)	14(1)	-1(1)
N(1)	16(4)	32(5)	41(5)	3(4)	9(3)	-2(3)
N(2)	41(5)	51(6)	40(6)	-19(5)	8(4)	-24(4)
N(3)	29(5)	57(7)	51(6)	12(5)	11(5)	10(5)
O(1)	36(5)	63(6)	101(7)	36(5)	30(5)	11(4)
O(2)	75(7)	112(9)	148(10)	88(9)	56(7)	59(7)
O(3)	35(4)	80(7)	86(7)	34(6)	26(4)	2(4)

5.6.22 Single crystal X-ray diffraction study of $[Ag_2(\mu\text{-}Ph_2Pbipy)_2(\mu\text{-}I)]BF_4$

A single, block-shaped crystal was grown by carefully cooling a hot, saturated methanol solution of the complex to room temperature. The general approach used for the intensity data collection is described in Appendix A. Considerable difficulty was experienced in locating the BF_4^- ions. Inspection of a contoured difference Fourier map phased on the atoms of the cation indicated that the anion is disordered both in terms of position and orientation; indeed, the residual electron density, though clearly associated with the BF_4^- anion, is so ill defined that it was impossible to define alternative positions for the anion. When the BF_4^- anion was refined as a rigid group with the boron fixed in alternative positions the refinement i) did not converge and ii) led to physically unreasonable temperature factors for the constituent atoms. The correct procedure at this stage would have been to carry out a low temperature data collection; however, no facilities were available. Finally, it was decided to simply refine the atoms of the cation, though it must be said that this is not good practice and leads to uncertainty in the standard errors for the bonding parameters of the cation. The standard errors quoted are from the least-squares refinement but probably should be at least doubled. However, the overall stereochemistry of the cation is not in doubt. The crystallographic data are given in Table 5.31, the interatomic distances in Table 5.32, the interatomic angles in Table 5.33, the fractional coordinates in Table 5.34 and the anisotropic thermal parameters in Table 5.35. The observed and calculated structure factors may be found on microfiche in an envelope fixed to the inside back cover.

Table 5.31

Crystal data and details of the crystallographic analysis for $[Ag_2(\mu\text{-}Ph_2Pbipy)_2(\mu\text{-}I)]BF_4$ [(a)]

Formula	$Ag_2C_{44}H_{34}N_4P_2IBF_4$
Molecular Mass	1110.25
Crystal System	Monoclinic
Space Group	C2/c
a(Å)	27.582(9)
b(Å)	22.286(7)
c(Å)	14.523(5)
β(°)	105.73(3)
V(Å^3)	8927.18
Z	8
D_c(g.cm^{-3})	1.65
F(000)	2176
λ(Mo-Kα)(Å)	0.71069
Scan mode	ω - 2θ
ω scan angle	0.42 + 0.35tanθ
Horizontal Aperture width (mm)	3.0 + 0.1tanθ
Scattering range (°)	$2 \leq \theta \leq 23$
μ (cm^{-1})	16.58
Absorption corrections	Semi empirical[103]
Measured intensities	6448
Unique intensities	4862
Unique intensities with [I > 3σ(I)]	3425
Structure solution	Direct & Fourier methods
Weighting scheme	$1/(\sigma^2(F) + 0.28765F^2)$
$R = \Sigma(F_o\text{-}F_c)/\Sigma F_o$	0.119
$R_w = \Sigma_w{}^{1/2}(F_o\text{-}F_c)/\Sigma_w{}^{1/2}F_o$	0.130
$(\Delta/\sigma)_{max}$	0.015
$\Delta\rho_{max}$(eÅ^{-3})	1.850
Number of parameters	258

(a) : Structure solved for cation only due to inherent anion disorder at 25°C.

Table 5:32 : Interatomic distances (Å) for $[Ag_2(\mu\text{-}Ph_2Pbipy)_2(\mu\text{-}I)]^+$

I-Ag(1)	2.719(3)	I-Ag(2)	2.855(3)
Ag(1)-Ag(2)	2.920(3)	Ag(1)-P(1)	2.385(7)
Ag(1)-N(3)	2.49(2)	Ag(1)-N(4)	2.29(2)
Ag(2)-P(2)	2.366(7)	Ag(2)-N(1)	2.34(2)
Ag(2)-N(2)	2.37(2)	P(1)-C(1)	1.79(3)
P(1)-C(7)	1.76(3)	P(1)-C(13)	1.81(3)
P(2)-C(23)	1.80(3)	P(2)-C(29)	1.84(2)
P(2)-C(35)	1.85(3)	N(1)-C(13)	1.37(3)
N(1)-C(17)	1.35(3)	N(2)-C(18)	1.26(3)
N(2)-C(22)	1.31(5)	N(3)-C(35)	1.43(3)
N(3)-C(39)	1.34(3)	N(4)-C(40)	1.34(3)
N(4)-C(44)	1.35(4)	C(1)-C(2)	1.34(4)
C(1)-C(6)	1.40(4)	C(2)-C(3)	1.30(5)
C(3)-C(4)	1.53(6)	C(4)-C(5)	1.40(6)
C(5)-C(6)	1.40(6)	C(7)-C(8)	1.48(5)
C(7)-C(12)	1.40(5)	C(8)-C(9)	1.27(5)
C(9)-C(10)	1.56(7)	C(10)-C(11)	1.28(7)
C(11)-C(12)	1.46(7)	C(13)-C(14)	1.27(4)
C(14)-C(15)	1.50(5)	C(15)-C(16)	1.44(5)
C(16)-C(17)	1.33(4)	C(17)-C(18)	1.49(4)
C(18)-C(19)	1.38(4)	C(19)-C(20)	1.22(5)
C(20)-C(21)	1.38(5)	C(21)-C(22)	1.53(5)
C(23)-C(24)	1.26(4)	C(23)-C(28)	1.46(4)
C(24)-C(25)	1.48(5)	C(25)-C(26)	1.28(5)
C(26)-C(27)	1.32(5)	C(27)-C(28)	1.40(5)
C(29)-C(30)	1.30(4)	C(29)-C(34)	1.41(4)
C(30)-C(31)	1.35(4)	C(31)-C(32)	1.33(5)
C(32)-C(33)	1.36(5)	C(33)-C(34)	1.40(5)
C(35)-C(36)	1.27(3)	C(36)-C(37)	1.41(4)
C(37)-C(38)	1.37(4)	C(38)-C(39)	1.36(3)
C(39)-C(40)	1.54(4)	C(40)-C(41)	1.39(4)
C(41)-C(42)	1.40(4)	C(42)-C(43)	1.47(5)
C(43)-C(44)	1.46(5)		

Table 5.33 . Interatomic angles (°) for $[Ag_2(\mu\text{-}Ph_2Pbipy)_2(\mu\text{-}I)]^+$

Ag(1)-I-Ag(2)	63.1(1)	I-Ag(1)-Ag(2)	60.7(1)
I-Ag(1)-P(1)	118.2(2)	Ag(2)-Ag(1)-P(1)	79.4(2)
I-Ag(1)-N(3)	86.6(5)	Ag(2)-Ag(1)-N(3)	86.5(5)
P(1)-Ag(1)-N(3)	138.5(5)	I-Ag(1)-N(4)	109.4(5)
Ag(2)-Ag(1)-N(4)	156.4(5)	P(1)-Ag(1)-N(4)	122.4(6)
N(3)-Ag(1)-N(4)	71.0(7)	I-Ag(2)-Ag(1)	56.2(1)
I-Ag(2)-P(2)	97.9(2)	Ag(1)-Ag(2)-P(2)	87.3(2)
I-Ag(2)-N(1)	99.2(5)	Ag(1)-Ag(2)-N(1)	88.8(5)
P(2)-Ag(2)-N(1)	156.4(5)	I-Ag(2)-N(2)	106.1(7)
Ag(1)-Ag(2)-N(2)	150.2(6)	P(2)-Ag(2)-N(2)	120.8(6)
N(1)-Ag(2)-N(2)	69.4(8)	Ag(1)-P(1)-C(1)	119.3(9)
Ag(1)-P(1)-C(7)	114.1(11)	C(1)-P(1)-C(7)	103.3(13
Ag(1)-P(1)-C(13)	113.6(9)	C(1)-P(1)-C(13)	99.8(13
C(7)-P(1)-C(13)	104.6(13)	Ag(2)-P(2)-C(23)	103.1(9)
Ag(2)-P(2)-C(29)	122.8(8)	C(23)-P(2)-C(29)	107.1(11
Ag(2)-P(2)-C(35)	117.4(8)	C(23)-P(2)-C(35)	100.6(12
C(29)-P(2)-C(35)	103.3(11)	Ag(2)-N(1)-C(13)	122(2)
Ag(2)-N(1)-C(17)	117(2)	C(13)-N(1)-C(17)	121(2)
Ag(2)-N(2)-C(18)	119(2)	Ag(2)-N(2)-C(22)	119(2)
C(18)-N(2)-C(22)	122(3)	Ag(1)-N(3)-C(35)	125.9(14
Ag(1)-N(3)-C(39)	112(2)	C(35)-N(3)-C(39)	118(2)
Ag(1)-N(4)-C(40)	120(2)	Ag(1)-N(4)-C(44)	122(2)
C(40)-N(4)-C(44)	117(2)	P(1)-C(1)-C(2)	118(2)
P(1)-C(1)-C(6)	122(2)	C(2)-C(1)-C(6)	119(3)
C(1)-C(2)-C(3)	124(3)	C(2)-C(3)-C(4)	119(4)
C(3)-C(4)-C(5)	118(4)	C(4)-C(5)-C(6)	118(4)
C(1)-C(6)-C(5)	122(4)	P(1)-C(7)-C(8)	122(3)
P(1)-C(7)-C(12)	124(3)	C(8)-C(7)-C(12)	114(3)
C(7)-C(8)-C(9)	125(4)	C(8)-C(9)-C(10)	115(4)
C(9)-C(10)-C(11)	126(5)	C(10)-C(11)-C(12)	113(5)
C(7)-C(12)-C(11)	126(4)	P(1)-C(13)-N(1)	116(2)
P(1)-C(13)-C(14)	124(3)	N(1)-C(13)-C(14)	121(3)
C(13)-C(14)-C(15)	121(3)	C(14)-C(15)-C(16)	116(3)
C(15)-C(16)-C(17)	118(3)	N(1)-C(17)-C(16)	123(3)
N(1)-C(17)-C(18)	117(2)	C(16)-C(17)-C(18)	120(3)

Table 5.33 / cont.

N(2)-C(18)-C(17)	117(2)	N(2)-C(18)-C(19)	121(2)
C(17)-C(18)-C(19)	122(2)	C(18)-C(19)-C(20)	119(3)
C(19)-C(20)-C(21)	130(4)	C(20)-C(21)-C(22)	107(3)
N(2)-C(22)-C(21)	121(4)	P(2)-C(23)-C(24)	118(2)
P(2)-C(23)-C(28)	120(2)	C(24)-C(23)-C(28)	123(3)
C(23)-C(24)-C(25)	119(3)	C(24)-C(25)-C(26)	119(4)
C(25)-C(26)-C(27)	121(4)	C(26)-C(27)-C(28)	125(4)
C(23)-C(28)-C(27)	113(3)	P(2)-C(29)-C(30)	128(2)
P(2)-C(29)-C(34)	116(2)	C(30)-C(29)-C(34)	116(2)
C(29)-C(30)-C(31)	129(3)	C(30)-C(31)-C(32)	116(3)
C(31)-C(32)-C(33)	120(4)	C(32)-C(33)-C(34)	122(4)
C(29)-C(34)-C(33)	116(3)	P(2)-C(35)-N(3)	111(2)
P(2)-C(35)-C(36)	127(2)	N(3)-C(35)-C(36)	122(2)
C(35)-C(36)-C(37)	119(3)	C(36)-C(37)-C(38)	121(3)
C(37)-C(38)-C(39)	119(2)	N(3)-C(39)-C(38)	122(2)
N(3)-C(39)-C(40)	118(2)	C(38)-C(39)-C(40)	120(2)
N(4)-C(40)-C(39)	117(2)	N(4)-C(40)-C(41)	127(2)
C(39)-C(40)-C(41)	116(2)	C(40)-C(41)-C(42)	114(3)
C(41)-C(42)-C(43)	125(3)	C(42)-C(43)-C(44)	111(3)
N(4)-C(44)-C(43)	125(3)		

Table 5.34 : Fractional coordinates (x 10^4) and isotropic thermal factors ($Å^2$, x10^3) for $[Ag_2(\mu\text{-}Ph_2Pbipy)_2(\mu\text{-}I)]^+$

	x/a	y/b	z/c	U_{eq}
I	3329(1)	4046(1)	4593(2)	82(1)
Ag(1)	3983(1)	3534(1)	3721(2)	44(1)
Ag(2)	2902(1)	3347(1)	2923(1)	47(1)
P(1)	3956(3)	2472(3)	3516(5)	44(2)
P(2)	2934(2)	4084(3)	1768(4)	37(1)
N(1)	2994(8)	2392(9)	3615(14)	39(5)
N(2)	2119(8)	2989(12)	3083(18)	63(7)
N(3)	3877(8)	4455(10)	2711(15)	44(5)
N(4)	4723(8)	4061(9)	4103(14)	42(5)
C(1)	4476(10)	2029(12)	4163(19)	48(7)*
C(2)	4705(10)	2181(12)	5071(19)	49(7)*
C(3)	5034(16)	1850(20)	5662(32)	98(12)*
C(4)	5209(17)	1271(21)	5286(33)	103(13)*
C(5)	5000(18)	1129(22)	4320(35)	111(14)*
C(6)	4618(14)	1499(17)	3787(28)	81(10)*
C(7)	3868(11)	2238(14)	2326(21)	57(8)*
C(8)	4164(15)	2495(19)	1714(30)	91(11)*
C(9)	4123(15)	2345(19)	853(30)	89(11)*
C(10)	3736(21)	1831(26)	459(39)	128(17)*
C(11)	3426(21)	1611(24)	882(41)	122(16)*
C(12)	3520(17)	1804(20)	1871(32)	99(12)*
C(13)	3452(10)	2113(12)	3892(19)	47(7)*
C(14)	3506(14)	1630(17)	4372(28)	81(10)*
C(15)	3084(14)	1374(17)	4712(26)	80(10)*
C(16)	2613(13)	1690(16)	4414(25)	72(9)*
C(17)	2590(10)	2166(12)	3857(19)	47(7)*
C(18)	2110(9)	2505(12)	3531(18)	41(6)*
C(19)	1670(10)	2309(12)	3706(19)	46(6)*
C(20)	1286(15)	2607(19)	3419(29)	89(11)*
C(21)	1209(15)	3134(18)	2903(27)	83(10)*
C(22)	1721(16)	3336(19)	2804(29)	89(11)*
C(23)	2362(10)	4504(12)	1651(19)	45(6)*
C(24)	2282(12)	4711(15)	2407(24)	67(8)*
C(25)	1799(15)	5020(19)	2348(29)	90(11)*

Table 5.34 / cont.

C(26)	1451(14)	5015(18)	1557(27)	79(10)*
C(27)	1545(15)	4825(18)	762(30)	90(11)*
C(28)	2000(12)	4570(15)	715(23)	64(8)*
C(29)	2963(9)	3896(11)	551(16)	36(6)*
C(30)	3027(10)	4256(12)	-109(19)	44(6)*
C(31)	3039(14)	4124(16)	-1011(26)	77(10)*
C(32)	2983(14)	3549(17)	-1261(28)	82(10)*
C(33)	2917(14)	3129(18)	-625(28)	84(10)*
C(34)	2906(12)	3281(14)	308(22)	62(8)*
C(35)	3408(9)	4688(11)	2134(18)	42(6)*
C(36)	3360(9)	5232(11)	1859(18)	40(6)*
C(37)	3762(11)	5633(13)	2215(20)	53(7)*
C(38)	4210(8)	5434(10)	2805(16)	31(5)*
C(39)	4259(9)	4840(11)	3026(18)	41(6)*
C(40)	4746(9)	4605(11)	3717(18)	40(6)*
C(41)	5168(10)	4971(13)	3852(20)	49(7)*
C(42)	5609(11)	4724(14)	4453(22)	60(8)*
C(43)	5643(14)	4131(17)	4902(26)	80(10)*
C(44)	5160(12)	3822(15)	4628(23)	65(8)*

* isotropic temperature factor.

$$U_{eq} = \frac{1}{3} \Sigma_i \Sigma_j U_{ij} a_i^* a_j^* (a_i . a_j)$$

Table 5.35 : Anisotropic thermal factors (Å^2 , x10^3) for $[Ag_2(\mu\text{-}Ph_2Pbipy)_2(\mu\text{-}I)]^+$

	U(11)	U(22)	U(33)	U(23)	U(13)	U(12)
I	98(2)	83(2)	71(2)	-9(1)	36(1)	-15(1)
Ag(1)	44(1)	33(1)	55(1)	-4(1)	15(1)	-14(1)
Ag(2)	46(1)	52(1)	44(1)	9(1)	15(1)	-19(1)
P(1)	42(4)	35(4)	55(4)	-7(3)	13(3)	-6(3)
P(2)	37(4)	50(4)	24(3)	0(3)	6(3)	-12(3)
N(1)	50(13)	40(12)	40(12)	-20(9)	33(10)	-23(10)
N(2)	31(12)	94(20)	70(17)	28(15)	24(12)	-13(12)
N(3)	40(12)	52(14)	44(13)	-12(10)	22(10)	-19(10)
N(4)	47(13)	45(13)	43(12)	5(10)	29(11)	-9(10)

5.6.23 Single crystal X-ray diffraction study of [Ag_2(μ-Ph_2Pbipy)$_2${μ-OC(Me)O}](PF_6).3H_2O.Me_2CO [45]

A pale yellow prism was grown by slow evaporation of a saturated acetone solution of the complex. The general approach used for the intensity data collection is described in Appendix A. The crystallographic data are given in Table 5.36, the interatomic distances in Table 5.37, the interatomic angles in Table 5.38, the fractional coordinates in Table 5.39 and the anisotropic thermal parameters in Table 5.40. The observed and calculated structure factors may be found on microfiche in an envelope fixed to the inside back cover.

Table 5.36

Crystal data and details of the crystallographic analysis for $[Ag_2(\mu\text{-}Ph_2Pbipy)_2\{\mu\text{-}OC(Me)O\}](PF_6).3H_2O.Me_2CO$

Formula	$Ag_2C_{49}H_{49}N_4O_6P_3F_6$
Molecular Mass	1212.60
Crystal System	Triclinic
Space Group	$P\bar{1}$
a(Å)	11.039(3)
b(Å)	14.789(2)
c(Å)	17.414(3)
α(°)	85.48(1)
β(°)	84.20(2)
γ(°)	87.84(2)
V(Å^3)	2842.94
Z	2
D_c(g.cm^{-3})	1.42
F(000)	1224
λ(Mo-Kα)(Å)	0.71069
Scan mode	ω - 2θ
ω scan angle	0.80 + 0.35tanθ
Horizontal Aperture width (mm)	2.7 + 0.1tanθ
Scattering range (°)	$2 \leq \theta \leq 23$
μ (cm^{-1})	8.28
Absorption corrections	Semi empirical[103]
Measured intensities	8121
Unique intensities	6336
Unique intensities with [I > 3σ(I)]	4134
Structure solution	Direct & Fourier methods
Weighting scheme	$1/(\sigma^2(F) + 0.02164F^2)$
$R = \Sigma(F_o-F_c)/\Sigma F_o$	0.104
$R_w = \Sigma_w{}^{1/2}(F_o-F_c)/\Sigma_w{}^{1/2}F_o$	0.111
$(\Delta/\sigma)_{max}$	0.528[(a)]
$\Delta\rho_{max}$(eÅ^{-3})	1.650
Number of parameters	396

(a) : Due to disorder within the acetone molecule.

Table 5.37 : Interatomic distances (Å) for $[Ag_2(\mu\text{-}Ph_2Pbipy)_2\{\mu\text{-}OC(Me)O\}](PF_6).3H_2O.Me_2CO$

Ag(1)-Ag(2)	2.988(2)	Ag(1)-P(1)	2.350(6)
Ag(1)-O(2)	2.24(2)	Ag(1)-N(3)	2.43(2)
Ag(1)-N(4)	2.35(2)	Ag(2)-P(2)	2.372(6)
Ag(2)-O(1)	2.48(2)	Ag(2)-N(1)	2.36(2)
Ag(2)-N(2)	2.36(2)	P(1)-C(1)	1.79(2)
P(1)-C(7)	1.81(2)	P(1)-C(13)	1.83(2)
P(2)-C(23)	1.85(3)	P(2)-C(29)	1.79(2)
P(2)-C(35)	1.84(2)	P(3)-F(1)	1.55(2)
P(3)-F(2)	1.49(3)	P(3)-F(3)	1.52(2)
P(3)-F(4)	1.42(3)	P(3)-F(5)	1.65(3)
P(3)-F(6)	1.50(2)	O(1)-C(45)	1.26(3)
O(2)-C(45)	1.20(3)	O(3)-C(47)	1.18(4)
N(1)-C(13)	1.31(3)	N(1)-C(17)	1.40(3)
N(2)-C(18)	1.36(3)	N(2)-C(22)	1.32(4)
N(3)-C(35)	1.32(3)	N(3)-C(39)	1.34(3)
N(4)-C(40)	1.33(3)	N(4)-C(44)	1.31(3)
C(1)-C(2)	1.38(3)	C(1)-C(6)	1.40(3)
C(2)-C(3)	1.45(3)	C(3)-C(4)	1.34(4)
C(4)-C(5)	1.48(4)	C(5)-C(6)	1.41(3)
C(7)-C(8)	1.42(3)	C(7)-C(12)	1.40(3)
C(8)-C(9)	1.38(4)	C(9)-C(10)	1.38(4)
C(10)-C(11)	1.38(4)	C(11)-C(12)	1.48(4)
C(13)-C(14)	1.41(3)	C(14)-C(15)	1.44(3)
C(15)-C(16)	1.36(3)	C(16)-C(17)	1.40(3)
C(17)-C(18)	1.44(3)	C(18)-C(19)	1.49(4)
C(19)-C(20)	1.31(5)	C(20)-C(21)	1.49(5)
C(21)-C(22)	1.41(5)	C(23)-C(24)	1.47(4)
C(23)-C(28)	1.37(4)	C(24)-C(25)	1.44(4)
C(25)-C(26)	1.34(4)	C(26)-C(27)	1.44(4)
C(27)-C(28)	1.35(4)	C(29)-C(30)	1.42(3)
C(29)-C(34)	1.48(3)	C(30)-C(31)	1.35(3)
C(31)-C(32)	1.30(4)	C(32)-C(33)	1.41(4)
C(33)-C(34)	1.34(3)	C(35)-C(36)	1.41(3)
C(36)-C(37)	1.46(4)	C(37)-C(38)	1.35(4)
C(38)-C(39)	1.36(3)	C(39)-C(40)	1.49(3)

Table 5.37 / cont.

C(40)-C(41)	1.40(3)	C(41)-C(42)	1.36(4)
C(42)-C(43)	1.32(4)	C(43)-C(44)	1.45(4)
C(45)-C(46)	1.61(4)	C(47)-C(48)	1.24(4)
C(47)-C(49)	1.53(6)		

Table 5.38 : Interatomic angles (°) for
$[Ag_2(\mu\text{-}Ph_2Pbipy)_2\{\mu\text{-}OC(Me)O\}](PF_6).3H_2O.Me_2CO$

Ag(2)-Ag(1)-P(1)	76.4(1)	Ag(2)-Ag(1)-O(2)	84.6(4)
P(1)-Ag(1)-O(2)	140.4(5)	Ag(2)-Ag(1)-N(3)	87.5(4)
P(1)-Ag(1)-N(3)	114.3(5)	O(2)-Ag(1)-N(3)	99.0(6)
Ag(2)-Ag(1)-N(4)	156.1(4)	P(1)-Ag(1)-N(4)	117.2(5)
O(2)-Ag(1)-N(4)	93.7(7)	N(3)-Ag(1)-N(4)	69.2(6)
Ag(1)-Ag(2)-P(2)	83.8(2)	Ag(1)-Ag(2)-O(1)	71.6(4)
P(2)-Ag(2)-O(1)	109.7(4)	Ag(1)-Ag(2)-N(1)	87.4(4)
P(2)-Ag(2)-N(1)	153.8(5)	O(1)-Ag(2)-N(1)	90.6(6)
Ag(1)-Ag(2)-N(2)	152.7(5)	P(2)-Ag(2)-N(2)	122.8(5)
O(1)-Ag(2)-N(2)	91.9(7)	N(1)-Ag(2)-N(2)	70.8(6)
Ag(1)-P(1)-C(1)	113.5(7)	Ag(1)-P(1)-C(7)	112.6(7)
C(1)-P(1)-C(7)	106.4(10)	Ag(1)-P(1)-C(13)	114.1(8)
C(1)-P(1)-C(13)	105.4(10)	C(7)-P(1)-C(13)	104.0(10
Ag(2)-P(2)-C(23)	113.9(8)	Ag(2)-P(2)-C(29)	113.5(7)
C(23)-P(2)-C(29)	101.9(10)	Ag(2)-P(2)-C(35)	117.0(7)
C(23)-P(2)-C(35)	106.5(11)	C(29)-P(2)-C(35)	102.3(10
F(1)-P(3)-F(2)	77(2)	F(1)-P(3)-F(3)	89(2)
F(2)-P(3)-F(3)	88(2)	F(1)-P(3)-F(4)	170(3)
F(2)-P(3)-F(4)	96(3)	F(3)-P(3)-F(4)	98(3)
F(1)-P(3)-F(5)	87(2)	F(2)-P(3)-F(5)	91(2)
F(3)-P(3)-F(5)	176(2)	F(4)-P(3)-F(5)	87(2)
F(1)-P(3)-F(6)	95(2)	F(2)-P(3)-F(6)	172(3)
F(3)-P(3)-F(6)	92(2)	F(4)-P(3)-F(6)	92(2)
F(5)-P(3)-F(6)	88.3(14)	Ag(2)-O(1)-C(45)	120(2)
Ag(1)-O(2)-C(45)	121(2)	Ag(2)-N(1)-C(13)	122.7(14
Ag(2)-N(1)-C(17)	115.7(13)	C(13)-N(1)-C(17)	121(2)
Ag(2)-N(2)-C(18)	116(2)	Ag(2)-N(2)-C(22)	121(2)
C(18)-N(2)-C(22)	123(2)	Ag(1)-N(3)-C(35)	124.1(14
Ag(1)-N(3)-C(39)	113.0(13)	C(35)-N(3)-C(39)	116(2)
Ag(1)-N(4)-C(40)	117.4(14)	Ag(1)-N(4)-C(44)	121(2)
C(40)-N(4)-C(44)	120(2)	P(1)-C(1)-C(2)	118(2)
P(1)-C(1)-C(6)	122(2)	C(2)-C(1)-C(6)	121(2)
C(1)-C(2)-C(3)	117(2)	C(2)-C(3)-C(4)	123(2)
C(3)-C(4)-C(5)	122(3)	C(4)-C(5)-C(6)	114(2)
C(1)-C(6)-C(5)	124(2)	P(1)-C(7)-C(8)	117(2)

Table 5.38 / cont.

P(1)-C(7)-C(12)	120(2)	C(8)-C(7)-C(12)	123(2)
C(7)-C(8)-C(9)	117(2)	C(8)-C(9)-C(10)	124(3)
C(9)-C(10)-C(11)	119(3)	C(10)-C(11)-C(12)	121(3)
C(7)-C(12)-C(11)	116(3)	P(1)-C(13)-N(1)	113(2)
P(1)-C(13)-C(14)	123(2)	N(1)-C(13)-C(14)	124(2)
C(13)-C(14)-C(15)	115(2)	C(14)-C(15)-C(16)	122(2)
C(15)-C(16)-C(17)	119(2)	N(1)-C(17)-C(16)	120(2)
N(1)-C(17)-C(18)	117(2)	C(16)-C(17)-C(18)	123(2)
N(2)-C(18)-C(17)	119(2)	N(2)-C(18)-C(19)	120(2)
C(17)-C(18)-C(19)	120(2)	C(18)-C(19)-C(20)	116(3)
C(19)-C(20)-C(21)	122(4)	C(20)-C(21)-C(22)	118(4)
N(2)-C(22)-C(21)	120(3)	P(2)-C(23)-C(24)	116(2)
P(2)-C(23)-C(28)	126(2)	C(24)-C(23)-C(28)	118(2)
C(23)-C(24)-C(25)	117(3)	C(24)-C(25)-C(26)	121(3)
C(25)-C(26)-C(27)	122(3)	C(26)-C(27)-C(28)	117(3)
C(23)-C(28)-C(27)	125(3)	P(2)-C(29)-C(30)	122(2)
P(2)-C(29)-C(34)	123(2)	C(30)-C(29)-C(34)	115(2)
C(29)-C(30)-C(31)	124(2)	C(30)-C(31)-C(32)	120(3)
C(31)-C(32)-C(33)	122(3)	C(32)-C(33)-C(34)	121(3)
C(29)-C(34)-C(33)	119(2)	P(2)-C(35)-N(3)	113(2)
P(2)-C(35)-C(36)	121(2)	N(3)-C(35)-C(36)	126(2)
C(35)-C(36)-C(37)	114(2)	C(36)-C(37)-C(38)	119(3)
C(37)-C(38)-C(39)	120(3)	N(3)-C(39)-C(38)	125(2)
N(3)-C(39)-C(40)	115(2)	C(38)-C(39)-C(40)	121(2)
N(4)-C(40)-C(39)	118(2)	N(4)-C(40)-C(41)	121(2)
C(39)-C(40)-C(41)	121(2)	C(40)-C(41)-C(42)	119(3)
C(41)-C(42)-C(43)	120(3)	C(42)-C(43)-C(44)	119(3)
N(4)-C(44)-C(43)	120(3)	O(1)-C(45)-O(2)	127(2)
O(1)-C(45)-C(46)	114(3)	O(2)-C(45)-C(46)	119(2)
O(3)-C(47)-C(48)	127(4)	O(3)-C(47)-C(49)	120(4)
C(48)-C(47)-C(49)	110(3)	P(3)-F(1)-F(2)	50.0(14

Table 5.39 : Fractional coordinates (x 10^4) and isotropic thermal factors ($Å^2$, x10^3) for $[Ag_2(\mu\text{-}Ph_2Pbipy)_2\{\mu\text{-}OC(Me)O\}](PF_6).3H_2O.Me_2CO$

	x/a	y/b	z/c	U_{eq}
Ag(1)	182(2)	1215(1)	2185(1)	41
Ag(2)	-1154(2)	2370(1)	3346(1)	48
P(1)	-1308(5)	255(4)	2825(3)	35(1)
P(2)	-1415(6)	3387(4)	2249(3)	40(1)
P(3)	5791(6)	1877(5)	8238(4)	59(2)
O(1)	1025(17)	2268(11)	3586(10)	59(4)
O(2)	1818(16)	1956(12)	2422(11)	59(5)
O(3)	1265(31)	4171(15)	4490(15)	121(9)
O(4)	1805(11)	3533(8)	-279(6)	27(3)
O(5)	-5113(21)	1431(24)	5051(15)	148(11)
O(6)	-5673(21)	3863(18)	5368(15)	118(8)
N(1)	-1530(17)	1024(11)	4142(10)	43(4)
N(2)	-1757(24)	2743(12)	4627(11)	64(6)
N(3)	-554(17)	2273(12)	1186(10)	45(5)
N(4)	1033(19)	849(13)	950(11)	53(5)
C(1)	-1096(20)	-904(14)	2592(12)	40(5)*
C(2)	83(23)	-1247(17)	2465(15)	57(7)*
C(3)	231(22)	-2188(17)	2287(15)	54(6)*
C(4)	-710(26)	-2716(19)	2240(17)	67(7)*
C(5)	-1983(23)	-2370(17)	2375(15)	56(7)*
C(6)	-2087(22)	-1453(16)	2544(14)	51(6)*
C(7)	-2837(19)	604(14)	2607(12)	39(5)*
C(8)	-2983(23)	957(17)	1839(15)	54(6)*
C(9)	-4155(29)	1185(21)	1665(19)	78(9)*
C(10)	-5177(29)	1059(21)	2179(19)	77(8)*
C(11)	-5042(34)	702(25)	2925(22)	95(10)*
C(12)	-3828(26)	418(19)	3161(17)	67(8)*
C(13)	-1392(21)	220(16)	3880(14)	47(6)*
C(14)	-1419(21)	-595(16)	4357(14)	49(6)*
C(15)	-1510(23)	-479(17)	5173(15)	58(7)*
C(16)	-1636(23)	355(17)	5457(15)	57(7)*
C(17)	-1686(20)	1122(15)	4937(13)	43(6)*
C(18)	-1843(24)	2033(17)	5174(15)	58(7)*
C(19)	-2240(31)	2188(23)	5999(20)	85(9)*

Table 5.39 / cont.

C(20)	-2421(35)	3033(28)	6163(23)	107(12)*
C(21)	-2337(36)	3799(27)	5556(25)	108(12)*
C(22)	-2005(32)	3594(23)	4784(21)	87(10)*
C(23)	-2790(23)	4137(17)	2362(15)	56(7)*
C(24)	-3743(26)	3838(19)	2972(17)	70(8)*
C(25)	-4786(31)	4439(24)	3098(21)	89(10)*
C(26)	-4848(30)	5244(22)	2695(19)	81(9)*
C(27)	-3948(31)	5516(22)	2069(19)	84(9)*
C(28)	-2971(23)	4950(17)	1950(15)	56(6)*
C(29)	-231(19)	4190(14)	2042(12)	39(5)*
C(30)	508(24)	4413(17)	2618(15)	58(7)*
C(31)	1426(25)	4999(18)	2483(16)	62(7)*
C(32)	1643(25)	5415(19)	1799(17)	66(7)*
C(33)	1009(24)	5224(18)	1167(15)	59(7)*
C(34)	121(23)	4617(17)	1258(15)	56(6)*
C(35)	-1436(20)	2889(15)	1314(13)	42(5)*
C(36)	-2348(24)	3142(18)	818(16)	62(7)*
C(37)	-2225(26)	2689(19)	96(16)	65(7)*
C(38)	-1259(23)	2119(17)	-50(15)	55(6)*
C(39)	-454(20)	1939(15)	488(13)	42(5)*
C(40)	603(20)	1302(15)	342(13)	42(5)*
C(41)	1176(25)	1230(19)	-405(16)	63(7)*
C(42)	2176(31)	672(23)	-504(20)	86(10)*
C(43)	2659(31)	266(22)	100(20)	86(9)*
C(44)	2031(26)	347(19)	862(17)	66(7)*
C(45)	1847(21)	2291(16)	3026(17)	51(6)
C(46)	3039(30)	2826(22)	3174(22)	94(10)
C(47)	1155(31)	3615(25)	5013(21)	85(9)*
C(48)	1163(21)	2781(15)	4979(13)	45(6)*
C(49)	1370(46)	3848(34)	5827(30)	152(17)*
F(1)	5176(32)	2190(26)	7495(17)	200(13)
F(2)	6400(32)	2737(18)	7963(32)	262(19)
F(3)	4831(30)	2431(16)	8706(19)	185(11)
F(4)	6549(50)	1638(23)	8839(27)	313(22)
F(5)	6782(23)	1302(18)	7676(15)	144(9)
F(6)	5082(27)	1025(15)	8414(18)	177(10)

* isotropic temperature factor.

$$U_{eq} = \frac{1}{3} \Sigma_i \Sigma_j U_{ij} a_i^* a_j^* (a_i . a_j)$$

Table 5.40 : Anisotropic thermal factors ($Å^2$, x10^3) for $[Ag_2(\mu\text{-}Ph_2Pbipy)_2\{\mu\text{-}OC(Me)O\}](PF_6).3H_2O.Me_2CO$

	U(11)	U(22)	U(33)	U(23)	U(13)	U(12)
Ag(1)	50(1)	42(1)	31(1)	2(1)	-1(1)	0(1)
Ag(2)	76(1)	33(1)	32(1)	6(1)	1(1)	4(1)
P(1)	43(3)	33(3)	30(3)	-1(2)	-4(2)	4(2)
P(2)	50(4)	34(3)	32(3)	6(2)	3(3)	3(3)
P(3)	52(4)	58(4)	68(5)	4(4)	-18(4)	6(3)
O(1)	75(12)	53(10)	45(10)	21(8)	-10(9)	-4(9)
O(2)	62(11)	65(11)	57(11)	-28(9)	-21(9)	8(9)
O(3)	217(31)	54(13)	85(17)	9(12)	0(17)	1(15)
O(4)	47(8)	17(6)	12(6)	12(5)	15(6)	-10(6)
O(5)	66(15)	288(38)	104(20)	-115(23)	5(13)	-11(19)
O(6)	86(16)	136(21)	128(22)	46(17)	-24(15)	-37(15)
N(1)	65(13)	32(10)	29(10)	6(8)	10(9)	-10(9)
N(2)	136(21)	27(10)	32(11)	-4(9)	-15(12)	-14(12)
N(3)	54(12)	41(10)	37(11)	-6(8)	3(9)	9(9)
N(4)	78(15)	42(11)	38(11)	-9(9)	-5(10)	27(11)
C(45)	34(14)	44(14)	73(19)	22(14)	-19(14)	-9(11)
C(46)	81(23)	83(23)	124(29)	-58(21)	7(20)	-41(18)
F(1)	203(31)	278(39)	125(23)	21(24)	-94(23)	40(29)
F(2)	176(30)	78(18)	519(74)	35(29)	-8(39)	-37(19)
F(3)	226(31)	95(17)	201(29)	13(17)	90(24)	68(19)
F(4)	467(67)	160(29)	374(56)	-80(32)	-342(56)	110(36)
F(5)	131(20)	157(23)	139(22)	-27(18)	20(16)	10(17)
F(6)	201(27)	90(16)	224(30)	-40(17)	106(24)	-66(17)

5.6.24 Single crystal X-ray diffraction study of $[Ag_2(\mu\text{-}Ph_2Pbipy)_2\{\mu\text{-}OC(Ph)O\}](PF_6).2(Me_2CO)$ [46]

A single, block shaped crystal was grown in acetone-d_6 in an nmr tube. This was transferred to a 3mm capillary containing acetone solvent, sealed in place using an Araldite glue-plug and mounted on the end of a glass fibre. This prevented immediate solvent loss, a problem inherent in crystals of the complex. The general approach used for the intensity data collection is described in Appendix A. The crystallographic data are given in Table 5.41, the interatomic distances in Table 5.42, the interatomic angles in Table 5.43, the fractional coordinates in Table 5.44 and the anisotropic thermal parameters in Table 5.45. The observed and calculated structure factors may be found on microfiche in an envelope fixed to the inside back cover.

Table 5.41

Crystal data and details of the crystallographic analysis for $[Ag_2(\mu\text{-}Ph_2Pbipy)_2\{\mu\text{-}OC(Ph)O\}](PF_6).2(Me_2CO)$

Formula	$Ag_2C_{57}H_{51}N_4O_4P_3F_6$
Molecular Mass	1278.70
Crystal System	Triclinic
Space Group	$P\bar{1}$
a(Å)	12.486(5)
b(Å)	15.068(6)
c(Å)	16.869(3)
α(°)	105.55(2)
β(°)	110.18(2)
γ(°)	95.75(3)
V($Å^3$)	3173.71
Z	2
D_c($g.cm^{-3}$)	1.34
F(000)	1292
λ(Mo-Kα)(Å)	0.71069
Scan mode	ω - 2θ
ω scan angle	$0.80 + 0.35\tan\theta$
Horizontal Aperture width (mm)	$2.7 + 0.1\tan\theta$
Scattering range (°)	$2 \leq \theta \leq 23$
μ (cm^{-1})	7.43
Absorption corrections	Semi empirical[103]
Measured intensities	8133
Unique intensities	7590
Unique intensities with $[I > 3\sigma(I)]$	7145
Structure solution	Direct & Fourier methods
Weighting scheme	$1/ (\sigma^2(F) + 0.00465F^2)$
$R = \Sigma(F_o\text{-}F_c)/\Sigma F_o$	0.055
$R_w = \Sigma_w½ (F_o\text{-}F_c)/ \Sigma_w½F_o$	0.071
$(\Delta/\sigma)_{max}$	4.18[(a)]
$\Delta\rho_{max}$($eÅ^{-3}$)	1.440
Number of parameters	487

(a) : Due to disorder within the acetone molecule.

Table 5.42 : Interatomic distances (Å) for $[Ag_2(\mu\text{-}Ph_2Pbipy)_2\{\mu\text{-}OC(Ph)O\}](PF_6).2(Me_2CO)$

Ag(1)-Ag(2)	2.945(1)	Ag(1)-P(1)	2.371(2)
Ag(1)-O(1)	2.369(4)	Ag(1)-N(3)	2.340(4)
Ag(1)-N(4)	2.375(5)	Ag(2)-P(2)	2.396(1)
Ag(2)-O(2)	2.241(4)	Ag(2)-N(1)	2.471(5)
Ag(2)-N(2)	2.383(4)	P(1)-C(1)	1.812(6)
P(1)-C(7)	1.830(5)	P(1)-C(13)	1.838(6)
P(2)-C(23)	1.833(6)	P(2)-C(29)	1.829(6)
P(2)-C(35)	1.835(5)	O(1)-C(45)	1.293(5)
O(2)-C(45)	1.239(7)	N(1)-C(13)	1.373(7)
N(1)-C(17)	1.322(7)	N(2)-C(18)	1.319(9)
N(2)-C(22)	1.339(8)	N(3)-C(35)	1.356(7)
N(3)-C(39)	1.338(6)	N(4)-C(40)	1.342(8)
N(4)-C(44)	1.306(9)	C(1)-C(2)	1.363(11)
C(1)-C(6)	1.444(8)	C(2)-C(3)	1.414(9)
C(3)-C(4)	1.347(10)	C(4)-C(5)	1.393(15)
C(5)-C(6)	1.380(11)	C(7)-C(8)	1.411(9)
C(7)-C(12)	1.377(9)	C(8)-C(9)	1.393(8)
C(9)-C(10)	1.380(11)	C(10)-C(11)	1.386(11)
C(11)-C(12)	1.363(8)	C(13)-C(14)	1.360(10)
C(14)-C(15)	1.412(10)	C(15)-C(16)	1.373(10)
C(16)-C(17)	1.370(11)	C(17)-C(18)	1.535(8)
C(18)-C(19)	1.387(8)	C(19)-C(20)	1.396(9)
C(20)-C(21)	1.348(12)	C(21)-C(22)	1.410(8)
C(23)-C(24)	1.362(10)	C(23)-C(28)	1.363(8)
C(24)-C(25)	1.448(14)	C(25)-C(26)	1.371(14)
C(26)-C(27)	1.315(13)	C(27)-C(28)	1.359(12)
C(29)-C(30)	1.358(8)	C(29)-C(34)	1.404(9)
C(30)-C(31)	1.414(11)	C(31)-C(32)	1.354(12)
C(32)-C(33)	1.435(12)	C(33)-C(34)	1.348(12)
C(35)-C(36)	1.383(8)	C(36)-C(37)	1.390(9)
C(37)-C(38)	1.364(10)	C(38)-C(39)	1.409(9)
C(39)-C(40)	1.497(8)	C(40)-C(41)	1.379(8)
C(41)-C(42)	1.366(10)	C(42)-C(43)	1.354(12)
C(43)-C(44)	1.378(10)	C(45)-C(46)	1.509(7)
C(46)-C(47)	1.406(6)	C(46)-C(51)	1.358(9)

Table 5.42 / cont.

C(47)-C(48)	1.401(9)	C(48)-C(49)	1.395(13)
C(49)-C(50)	1.341(9)	C(50)-C(51)	1.387(11)
P(3)-F(1)	1.586(5)	P(3)-F(2)	1.574(7)
P(3)-F(3)	1.572(6)	P(3)-F(4)	1.548(8)
P(3)-F(5)	1.562(7)	P(3)-F(6)	1.501(8)
O(3)-C(52)	1.240(10)	C(52)-C(53)	1.520(10)
C(52)-C(54)	1.520(13)	O(4)-C(55)	1.255(14)
C(55)-C(56)	1.54(2)	C(55)-C(57)	1.54(2)

Table 5.43 : Interatomic angles (°) for
$[Ag_2(\mu\text{-}Ph_2Pbipy)_2\{\mu\text{-}OC(Ph)O\}](PF_6).2(Me_2CO)$

Ag(2)-Ag(1)-P(1)	83.8(0)	Ag(2)-Ag(1)-O(1)	71.1(1
P(1)-Ag(1)-O(1)	116.9(1)	Ag(2)-Ag(1)-N(3)	91.4(1
P(1)-Ag(1)-N(3)	141.6(1)	O(1)-Ag(1)-N(3)	97.1(1
Ag(2)-Ag(1)-N(4)	153.2(1)	P(1)-Ag(1)-N(4)	122.7(1
O(1)-Ag(1)-N(4)	91.5(2)	N(3)-Ag(1)-N(4)	70.1(2
Ag(1)-Ag(2)-P(2)	77.7(0)	Ag(1)-Ag(2)-O(2)	84.9(1
P(2)-Ag(2)-O(2)	144.8(1)	Ag(1)-Ag(2)-N(1)	88.3(1
P(2)-Ag(2)-N(1)	104.3(1)	O(2)-Ag(2)-N(1)	105.6(2
Ag(1)-Ag(2)-N(2)	156.7(1)	P(2)-Ag(2)-N(2)	107.4(1
O(2)-Ag(2)-N(2)	100.7(1)	N(1)-Ag(2)-N(2)	68.4(2
Ag(1)-P(1)-C(1)	113.6(2)	Ag(1)-P(1)-C(7)	112.1(2
C(1)-P(1)-C(7)	104.9(3)	Ag(1)-P(1)-C(13)	118.1(2
C(1)-P(1)-C(13)	104.6(3)	C(7)-P(1)-C(13)	102.1(2
Ag(2)-P(2)-C(23)	110.2(2)	Ag(2)-P(2)-C(29)	112.5(1
C(23)-P(2)-C(29)	105.2(3)	Ag(2)-P(2)-C(35)	120.2(2
C(23)-P(2)-C(35)	103.0(2)	C(29)-P(2)-C(35)	104.3(3
Ag(1)-O(1)-C(45)	122.5(4)	Ag(2)-O(2)-C(45)	117.3(3
Ag(2)-N(1)-C(13)	122.6(4)	Ag(2)-N(1)-C(17)	114.5(4
C(13)-N(1)-C(17)	116.0(5)	Ag(2)-N(2)-C(18)	119.3(3
Ag(2)-N(2)-C(22)	122.1(5)	C(18)-N(2)-C(22)	118.0(5
Ag(1)-N(3)-C(35)	122.0(3)	Ag(1)-N(3)-C(39)	118.3(4
C(35)-N(3)-C(39)	119.7(5)	Ag(1)-N(4)-C(40)	117.3(4
Ag(1)-N(4)-C(44)	123.8(4)	C(40)-N(4)-C(44)	118.5(5
P(1)-C(1)-C(2)	125.3(4)	P(1)-C(1)-C(6)	115.9(5
C(2)-C(1)-C(6)	118.8(5)	C(1)-C(2)-C(3)	120.3(6
C(2)-C(3)-C(4)	121.9(8)	C(3)-C(4)-C(5)	118.2(7
C(4)-C(5)-C(6)	122.6(7)	C(1)-C(6)-C(5)	118.2(7
P(1)-C(7)-C(8)	121.6(4)	P(1)-C(7)-C(12)	118.9(5
C(8)-C(7)-C(12)	119.4(5)	C(7)-C(8)-C(9)	117.8(6
C(8)-C(9)-C(10)	121.5(7)	C(9)-C(10)-C(11)	119.8(6
C(10)-C(11)-C(12)	119.3(7)	C(7)-C(12)-C(11)	122.1(6
P(1)-C(13)-N(1)	111.3(4)	P(1)-C(13)-C(14)	124.5(5
N(1)-C(13)-C(14)	124.2(6)	C(13)-C(14)-C(15)	116.6(6
C(14)-C(15)-C(16)	120.2(7)	C(15)-C(16)-C(17)	117.6(6
N(1)-C(17)-C(16)	125.0(5)	N(1)-C(17)-C(18)	114.9(6

Table 5.43 / cont.

C(16)-C(17)-C(18)	120.0(5)	N(2)-C(18)-C(17)	116.4(5
N(2)-C(18)-C(19)	123.4(5)	C(17)-C(18)-C(19)	120.2(6
C(18)-C(19)-C(20)	117.6(7)	C(19)-C(20)-C(21)	120.5(6
C(20)-C(21)-C(22)	117.7(6)	N(2)-C(22)-C(21)	122.8(7
P(2)-C(23)-C(24)	117.6(4)	P(2)-C(23)-C(28)	123.2(5
C(24)-C(23)-C(28)	118.8(6)	C(23)-C(24)-C(25)	119.3(7
C(24)-C(25)-C(26)	118.8(9)	C(25)-C(26)-C(27)	119.1(9
C(26)-C(27)-C(28)	123.3(8)	C(23)-C(28)-C(27)	120.7(7
P(2)-C(29)-C(30)	116.6(5)	P(2)-C(29)-C(34)	123.1(4
C(30)-C(29)-C(34)	120.2(6)	C(29)-C(30)-C(31)	120.1(6
C(30)-C(31)-C(32)	119.9(7)	C(31)-C(32)-C(33)	119.6(9
C(32)-C(33)-C(34)	119.8(7)	C(29)-C(34)-C(33)	120.3(6
P(2)-C(35)-N(3)	114.7(4)	P(2)-C(35)-C(36)	123.5(4
N(3)-C(35)-C(36)	121.8(5)	C(35)-C(36)-C(37)	118.2(6
C(36)-C(37)-C(38)	120.4(6)	C(37)-C(38)-C(39)	118.8(6
N(3)-C(39)-C(38)	121.0(5)	N(3)-C(39)-C(40)	117.4(5
C(38)-C(39)-C(40)	121.6(5)	N(4)-C(40)-C(39)	116.2(5
N(4)-C(40)-C(41)	122.1(5)	C(39)-C(40)-C(41)	121.7(5
C(40)-C(41)-C(42)	117.6(6)	C(41)-C(42)-C(43)	120.9(6
C(42)-C(43)-C(44)	117.8(7)	N(4)-C(44)-C(43)	123.2(7
O(1)-C(45)-O(2)	123.9(4)	O(1)-C(45)-C(46)	116.3(4
O(2)-C(45)-C(46)	119.4(4)	C(45)-C(46)-C(47)	119.6(5
C(45)-C(46)-C(51)	121.2(4)	C(47)-C(46)-C(51)	119.2(5
C(46)-C(47)-C(48)	119.4(6)	C(47)-C(48)-C(49)	119.8(5
C(48)-C(49)-C(50)	119.1(8)	C(49)-C(50)-C(51)	122.1(9
C(46)-C(51)-C(50)	120.3(5)	F(1)-P(3)-F(2)	90.2(3
F(1)-P(3)-F(3)	178.8(3)	F(2)-P(3)-F(3)	89.0(4
F(1)-P(3)-F(4)	90.1(4)	F(2)-P(3)-F(4)	167.1(5
F(3)-P(3)-F(4)	90.9(4)	F(1)-P(3)-F(5)	91.9(4
F(2)-P(3)-F(5)	89.9(5)	F(3)-P(3)-F(5)	88.9(4
F(4)-P(3)-F(5)	77.2(5)	F(1)-P(3)-F(6)	89.0(3
F(2)-P(3)-F(6)	87.9(5)	F(3)-P(3)-F(6)	90.2(4
F(4)-P(3)-F(6)	105.1(6)	F(5)-P(3)-F(6)	177.6(6
O(3)-C(52)-C(53)	120.0(9)	O(3)-C(52)-C(54)	120.0(7
C(53)-C(52)-C(54)	120.0(6)	O(4)-C(55)-C(56)	116.9(1
O(4)-C(55)-C(57)	116.7(14)	C(56)-C(55)-C(57)	116.8(9

Table 5.44 : Fractional coordinates (x 10^4) and isotropic thermal factors (Å^2, x10^3) for $[Ag_2(\mu\text{-}Ph_2Pbipy)_2\{\mu\text{-}OC(Ph)O\}](PF_6).2(Me_2CO)$

	x/a	y/b	z/c	U_{eq}
Ag(1)	1180(1)	4136(1)	3099(1)	39(1)
Ag(2)	654(1)	2061(1)	2423(1)	38(1)
P(1)	1949(1)	4001(1)	1978(1)	36(1)
P(2)	2025(1)	2397(1)	3923(1)	34(1)
O(1)	-857(3)	3577(3)	2611(2)	53(1)
O(2)	-1110(3)	2202(3)	1576(3)	54(1)
N(1)	1885(4)	2157(3)	1562(3)	35(1)
N(2)	721(4)	536(3)	1581(3)	42(1)
N(3)	1687(3)	4142(3)	4572(3)	31(1)
N(4)	1090(4)	5611(3)	4007(3)	49(1)
C(1)	3059(5)	5015(4)	2212(4)	43(1)
C(2)	3426(5)	5229(4)	1600(4)	60(2)
C(3)	4324(6)	6027(5)	1865(5)	65(2)
C(4)	4834(6)	6605(5)	2717(5)	76(2)
C(5)	4467(8)	6389(6)	3348(5)	94(2)
C(6)	3612(6)	5609(4)	3134(4)	67(2)
C(7)	826(5)	3889(3)	896(3)	41(1)
C(8)	1009(5)	3568(3)	96(4)	47(1)
C(9)	94(7)	3474(4)	-701(4)	59(2)
C(10)	-946(6)	3718(4)	-712(4)	64(2)
C(11)	-1102(5)	4047(4)	82(5)	60(2)
C(12)	-221(5)	4125(4)	865(4)	46(1)
C(13)	2601(5)	2982(4)	1695(4)	42(1)
C(14)	3654(5)	3034(4)	1619(5)	61(2)
C(15)	4011(6)	2175(5)	1388(5)	69(2)
C(16)	3278(6)	1336(4)	1194(5)	57(2)
C(17)	2240(5)	1373(4)	1297(4)	44(1)
C(18)	1412(5)	461(3)	1137(3)	39(1)
C(19)	1398(6)	-380(4)	537(4)	54(1)
C(20)	604(6)	-1181(4)	402(4)	57(2)
C(21)	-118(6)	-1127(4)	843(4)	60(2)
C(22)	-28(5)	-243(4)	1446(4)	51(1)
C(23)	3522(4)	2655(3)	3982(3)	40(1)
C(24)	3964(6)	1916(5)	3654(6)	84(2)

Table 5.44 / cont.

C(25)	5098(8)	2096(7)	3607(8)	127(3)
C(26)	5686(6)	3013(7)	3877(6)	108(2)
C(27)	5218(7)	3697(6)	4193(6)	90(2)
C(28)	4155(6)	3548(5)	4242(4)	62(2)
C(29)	1949(5)	1392(4)	4329(4)	42(1)
C(30)	899(5)	781(4)	3972(4)	61(1)
C(31)	753(8)	12(5)	4283(5)	75(2)
C(32)	1661(9)	-115(5)	4937(6)	93(3)
C(33)	2775(7)	520(5)	5293(5)	79(2)
C(34)	2901(6)	1250(4)	4992(4)	67(2)
C(35)	2012(4)	3395(3)	4824(3)	36(1)
C(36)	2297(5)	3397(4)	5693(4)	49(1)
C(37)	2253(7)	4196(4)	6317(4)	63(2)
C(38)	1900(6)	4941(4)	6065(4)	56(2)
C(39)	1627(4)	4902(3)	5172(3)	39(1)
C(40)	1239(4)	5696(3)	4852(3)	36(1)
C(41)	1062(5)	6476(4)	5403(4)	48(1)
C(42)	729(6)	7175(4)	5059(5)	65(2)
C(43)	582(6)	7100(4)	4209(5)	65(2)
C(44)	787(6)	6300(4)	3706(4)	66(2)
C(45)	-1458(4)	2914(3)	1864(3)	42(1)
C(46)	-2581(4)	3093(4)	1280(3)	46(1)
C(47)	-3333(5)	2372(5)	498(4)	70(2)
C(48)	-4371(5)	2544(6)	-47(5)	85(2)
C(49)	-4635(6)	3432(7)	181(5)	79(2)
C(50)	-3893(7)	4104(7)	930(5)	98(2)
C(51)	-2860(5)	3951(4)	1479(4)	64(1)
P(3)	2137(2)	2277(1)	7825(1)	67(1)
F(1)	1861(5)	2102(4)	6798(3)	105(1)
F(2)	1651(7)	1199(5)	7616(4)	166(2)
F(3)	2387(5)	2437(5)	8838(3)	139(2)
F(4)	2881(9)	3267(5)	8061(5)	195(3)
F(5)	3391(5)	2085(6)	7998(4)	159(3)
F(6)	919(6)	2424(8)	7666(4)	209(3)
O(3)	4598(5)	-317(6)	8336(6)	204(4)
C(52)	3556(5)	-395(6)	8231(6)	148(3)
C(53)	2605(5)	-864(6)	7305(6)	219(4)

Table 5.44 / cont.

C(54)	3231(5)	23(6)	9021(6)	166(3)
O(4)	5615(11)	832(11)	6292(7)	275(6)
C(55)	6499(11)	1120(11)	7012(7)	384(10)
C(56)	6281(11)	1391(11)	7881(7)	353(10)
C(57)	7582(11)	1709(11)	7013(7)	444(14)

$$U_{eq} = \frac{1}{3} \Sigma_i \Sigma_j U_{ij} a_i^* a_j^* (a_i . a_j)$$

Table 5.45 : Anisotropic thermal factors (Å^2 , x10^3) for
[Ag_2(μ-Ph_2Pbipy)$_2${μ-OC(Ph)O}](PF_6).2(Me_2CO)

	U(11)	U(22)	U(33)	U(23)	U(13)	U(12)
Ag(1)	48(1)	37(1)	35(1)	7(1)	24(1)	10(1)
Ag(2)	42(1)	35(1)	37(1)	4(1)	19(1)	7(1)
P(1)	43(1)	30(1)	39(1)	10(1)	23(1)	6(1)
P(2)	35(1)	32(1)	35(1)	5(1)	17(1)	7(1)
O(1)	44(2)	68(2)	39(2)	-1(2)	19(2)	9(2)
O(2)	46(2)	48(2)	54(2)	6(2)	11(2)	12(2)
N(1)	44(2)	30(2)	41(2)	15(2)	24(2)	12(2)
N(2)	52(3)	30(2)	45(2)	4(2)	28(2)	6(2)
N(3)	31(2)	31(2)	33(2)	2(2)	19(2)	7(2)
N(4)	56(3)	44(3)	52(3)	12(2)	29(2)	22(2)
C(1)	50(3)	36(3)	45(3)	14(2)	22(3)	2(2)
C(2)	63(4)	62(3)	66(4)	31(3)	31(3)	5(3)
C(3)	63(4)	57(4)	80(5)	27(4)	34(3)	1(3)
C(4)	65(4)	79(5)	82(5)	33(4)	26(4)	-4(4)
C(5)	100(6)	77(5)	64(5)	-1(4)	20(4)	-44(4)
C(6)	86(4)	49(4)	54(4)	6(3)	26(3)	-13(3)
C(7)	57(3)	27(2)	42(3)	11(2)	25(2)	4(2)
C(8)	73(4)	30(3)	49(3)	13(2)	36(3)	11(3)
C(9)	91(5)	39(3)	47(3)	11(3)	29(3)	14(3)
C(10)	80(4)	54(4)	49(4)	18(3)	15(3)	11(3)
C(11)	58(4)	52(3)	72(4)	29(3)	23(3)	6(3)
C(12)	49(3)	42(3)	56(3)	22(3)	25(3)	12(2)
C(13)	49(3)	41(3)	46(3)	13(2)	31(3)	12(2)
C(14)	59(4)	60(4)	91(5)	36(3)	48(3)	19(3)
C(15)	56(4)	67(4)	110(6)	31(4)	57(4)	26(3)
C(16)	62(4)	51(4)	81(5)	23(3)	50(4)	27(3)
C(17)	53(3)	39(3)	48(3)	13(2)	30(3)	13(2)
C(18)	55(3)	32(3)	39(3)	11(2)	26(2)	18(2)
C(19)	73(4)	44(3)	50(4)	14(3)	27(3)	22(3)
C(20)	82(5)	32(3)	60(4)	9(3)	34(4)	18(3)
C(21)	83(4)	41(3)	48(4)	0(3)	27(3)	13(3)
C(22)	70(4)	30(3)	54(4)	8(2)	30(3)	5(3)
C(23)	35(2)	38(3)	39(3)	-4(2)	19(2)	3(2)
C(24)	54(4)	74(5)	120(7)	0(4)	51(4)	19(3)
C(25)	63(5)	97(7)	201(10)	-7(7)	74(6)	13(5)

Table.5.45 / cont.

C(26)	49(4)	138(8)	102(6)	-2(5)	30(4)	-18(5)
C(27)	71(4)	76(5)	100(6)	-21(4)	53(4)	-19(4)
C(28)	59(4)	58(4)	65(4)	5(3)	32(3)	1(3)
C(29)	51(3)	37(3)	36(3)	9(2)	18(2)	8(2)
C(30)	64(4)	60(4)	56(4)	3(3)	33(3)	4(3)
C(31)	103(6)	47(4)	71(5)	16(3)	41(5)	-15(4)
C(32)	138(8)	56(5)	85(5)	30(4)	43(5)	5(5)
C(33)	96(6)	58(4)	80(5)	36(4)	17(4)	23(4)
C(34)	68(4)	47(4)	70(4)	19(3)	7(3)	10(3)
C(35)	41(3)	35(3)	31(3)	6(2)	15(2)	8(2)
C(36)	74(4)	49(3)	36(3)	13(2)	33(3)	18(3)
C(37)	89(5)	64(4)	40(3)	13(3)	32(3)	25(3)
C(38)	90(4)	45(3)	41(3)	8(3)	38(3)	22(3)
C(39)	36(2)	40(3)	42(3)	9(2)	22(2)	1(2)
C(40)	34(2)	36(3)	35(3)	4(2)	17(2)	4(2)
C(41)	51(3)	41(3)	47(3)	2(2)	21(3)	15(2)
C(42)	69(4)	45(3)	74(4)	7(3)	27(3)	23(3)
C(43)	70(4)	48(4)	67(4)	8(3)	18(3)	28(3)
C(44)	94(5)	42(3)	63(4)	20(3)	26(3)	20(3)
C(45)	39(2)	51(3)	36(2)	7(2)	20(2)	11(2)
C(46)	36(2)	62(3)	40(3)	9(2)	22(2)	8(2)
C(47)	60(4)	81(4)	65(4)	26(3)	18(3)	4(3)
C(48)	52(4)	114(6)	66(4)	31(4)	4(3)	-11(4)
C(49)	54(4)	123(7)	74(5)	52(5)	22(4)	29(4)
C(50)	100(5)	154(8)	66(4)	44(5)	41(4)	84(6)
C(51)	74(4)	82(4)	51(3)	20(3)	37(3)	41(3)
P(3)	67(1)	88(1)	58(1)	35(1)	30(1)	12(1)
F(1)	137(4)	135(4)	71(3)	50(3)	57(3)	39(3)
F(2)	191(6)	133(5)	140(5)	67(4)	27(4)	-41(4)
F(3)	113(4)	245(7)	64(3)	57(4)	39(3)	24(4)
F(4)	280(10)	114(5)	140(6)	41(4)	46(6)	-47(6)
F(5)	109(4)	262(9)	139(6)	89(6)	57(4)	84(5)
F(6)	114(4)	440(13)	79(4)	54(5)	45(3)	136(6)
O(3)	132(6)	287(11)	259(12)	122(9)	105(7)	129(7)
C(52)	147(7)	138(6)	189(8)	64(6)	78(6)	76(5)
C(53)	232(12)	224(11)	157(9)	16(8)	72(9)	1(9)
C(54)	198(9)	169(8)	129(6)	36(6)	74(6)	26(7)

Table 5.45 / cont.

O(4)	146(10)	368(20)	196(11)	-35(11)	33(8)	31(11)
C(55)	208(16)	254(15)	539(34)	-55(20)	80(20)	140(14)
C(56)	303(20)	329(23)	423(28)	168(20)	94(19)	88(17)
C(57)	336(28)	729(45)	350(30)	176(26)	204(26)	209(27)

5.6.25 Single crystal X-ray diffraction study of $[Ag_2(\mu\text{-}Ph_2Pbipy)_2(\eta^1\text{-}4\text{-}vinylpy)_2](BF_4)_2$ [50]

A colourless, cube-shaped crystal was grown from a CH_2Cl_2/ EtOH:Et_2O (1: 1, vol : vol) solution of the complex at -25°C. Like the benzoate crystal, this was mounted in a 3mm glass capillary in CH_2Cl_2. The general approach used for the intensity data collection is described in Appendix A.The crystallographic data are given in Table 5.46, the interatomic distances in Table 5.47, the interatomic angles in Table 5.48, the fractional coordinates in Table 5.49 and the anisotropic thermal parameters in Table 5.50. The observed and calculated structure factors may be found on microfiche in an envelope fixed to the inside back cover.

Table 5.46

Crystal data and details of the crystallographic analysis for $[Ag_2(\mu\text{-}Ph_2Pbipy)_2(4\text{-vinylpy})_2](BF_4)_2$

Formula	$Ag_2C_{58}H_{48}N_6P_2B_2F_8$
Molecular Mass	1280.35
Crystal System	Monoclinic
Space Group	$P2_1/n$
a(Å)	9.623(3)
b(Å)	23.836(5)
c(Å)	12.486(2)
β(°)	99.92(3)
V(Å^3)	2821.06
Z	2
D_c(g.cm^{-3})	1.50
F(000)	1288
λ(Mo-Kα)(Å)	0.71069
Scan mode	ω - 2θ
ω scan angle	$0.80 + 0.35\tan\theta$
Horizontal Aperture width (mm)	$2.7 + 0.1\tan\theta$
Scattering range (°)	$2 \leq \theta \leq 23$
μ (cm^{-1})	8.05
Absorption corrections	Semi empirical[103]
Measured intensities	5184
Unique intensities	3764
Unique intensities with $[I > 3\sigma(I)]$	2386
Structure solution	Direct & Fourier methods
Weighting scheme	$1/(\sigma^2(F) + 0.00129F^2)$
$R = \Sigma(F_o\text{-}F_c)/\Sigma F_o$	0.071
$R_w = \Sigma_w½(F_o\text{-}F_c)/\Sigma_w½F_o$	0.076
$(\Delta/\sigma)_{max}$	0.926
$\Delta\rho_{max}$(eÅ^{-3})	1.020
Number of parameters	207

Table 5.47 : Interatomic distances (Å) for $[Ag_2(\mu\text{-}Ph_2Pbipy)_2(4\text{-vinylpy})_2](BF_4)_2$

Ag-P	2.392(3)	Ag-N(3)	2.354(11)
Ag-N(1′)	2.373(9)	Ag-N(2′)	2.391(11)
P-C(1)	1.823(12)	P-C(7)	1.844(13)
P-C(13)	1.821(12)	N(1)-C(13)	1.344(14)
N(1)-C(17)	1.328(14)	N(2)-C(18)	1.32(2)
N(2)-C(22)	1.37(2)	N(3)-C(23)	1.33(2)
N(3)-C(27)	1.33(2)	C(1)-C(2)	1.39(2)
C(1)-C(6)	1.38(2)	C(2)-C(3)	1.43(2)
C(3)-C(4)	1.34(2)	C(4)-C(5)	1.36(2)
C(5)-C(6)	1.44(2)	C(7)-C(8)	1.38(2)
C(7)-C(12)	1.40(2)	C(8)-C(9)	1.47(2)
C(9)-C(10)	1.41(2)	C(10)-C(11)	1.34(2)
C(11)-C(12)	1.42(2)	C(13)-C(14)	1.40(2)
C(14)-C(15)	1.41(2)	C(15)-C(16)	1.40(2)
C(16)-C(17)	1.42(2)	C(17)-C(18)	1.49(2)
C(18)-C(19)	1.41(2)	C(19)-C(20)	1.38(2)
C(20)-C(21)	1.37(2)	C(21)-C(22)	1.38(2)
C(23)-C(24)	1.42(2)	C(24)-C(25)	1.38(2)
C(25)-C(26)	1.31(2)	C(25)-C(28)	1.62(3)
C(26)-C(27)	1.42(2)	C(28)-C(29)	1.20(3)
B-F(1)	1.28(2)	B-F(2)	1.23(2)
B-F(3)	1.25(3)	B-F(4)	1.19(3)
F(3)-F(4)	1.75(3)		

Table 5.48 : Interatomic angles (°) for [Ag_2(μ-Ph_2Pbipy)$_2$(4-vinylpy)$_2$](BF_4)$_2$

P-Ag-N(3)	114.5(3)	Ag-P-C(1)	116.1(4)
N(1′)-Ag-N(2′)	69.2(4)	N(1′)-Ag-N(3)	124.5(3)
N(2′)-Ag-N(3)	93.3(4)	N(1′)-Ag-P	119.8(2)
N(2′)-Ag-P	120.9(3)		
Ag-P-C(7)	110.3(4)	C(1)-P-C(7)	104.3(5)
Ag-P-C(13)	116.2(4)	C(1)-P-C(13)	104.8(5)
C(7)-P-C(13)	103.8(5)	C(13)-N(1)-C(17)	119.5(10
C(18)-N(2)-C(22)	119.2(12)	Ag-N(3)-C(23)	120.9(10
Ag-N(3)-C(27)	119.7(9)	C(23)-N(3)-C(27)	118.9(12
P-C(1)-C(2)	116.3(10)	P-C(1)-C(6)	121.2(10
C(2)-C(1)-C(6)	122.4(12)	C(1)-C(2)-C(3)	117.5(13
C(2)-C(3)-C(4)	120(2)	C(3)-C(4)-C(5)	123(2)
C(4)-C(5)-C(6)	119(2)	C(1)-C(6)-C(5)	118.1(14
P-C(7)-C(8)	115.7(10)	P-C(7)-C(12)	121.4(10
C(8)-C(7)-C(12)	122.8(12)	C(7)-C(8)-C(9)	118(2)
C(8)-C(9)-C(10)	119(2)	C(9)-C(10)-C(11)	121(2)
C(10)-C(11)-C(12)	122(2)	C(7)-C(12)-C(11)	117.8(13
P-C(13)-N(1)	116.4(8)	P-C(13)-C(14)	120.1(10
N(1)-C(13)-C(14)	122.9(12)	C(13)-C(14)-C(15)	117.6(14
C(14)-C(15)-C(16)	120(2)	C(15)-C(16)-C(17)	117(2)
N(1)-C(17)-C(16)	122.7(13)	N(1)-C(17)-C(18)	117.3(1
C(16)-C(17)-C(18)	120.0(12)	N(2)-C(18)-C(17)	117.2(1
N(2)-C(18)-C(19)	121.6(12)	C(17)-C(18)-C(19)	121.2(1
C(18)-C(19)-C(20)	118.1(13)	C(19)-C(20)-C(21)	120.9(1
C(20)-C(21)-C(22)	118.4(14)	N(2)-C(22)-C(21)	121.7(1
N(3)-C(23)-C(24)	123(2)	C(23)-C(24)-C(25)	116(2)
C(24)-C(25)-C(26)	122(2)	C(24)-C(25)-C(28)	123(2)
C(26)-C(25)-C(28)	115(2)	C(25)-C(26)-C(27)	120(2)
N(3)-C(27)-C(26)	120.4(13)	C(25)-C(28)-C(29)	112(2)
F(1)-B-F(2)	117(2)	F(1)-B-F(3)	120(3)
F(2)-B-F(3)	110(2)	F(1)-B-F(4)	108(2)
F(2)-B-F(4)	107(4)	F(3)-B-F(4)	91(2)
B-F(3)-F(4)	43(2)	B-F(4)-F(3)	46(2)

Table 5.49 : Fractional coordinates (x 10^4) and isotropic thermal factors (Å^2, x10^3) for $[Ag_2(\mu\text{-}Ph_2Pbipy)_2(4\text{-vinylpy})_2](BF_4)_2$

	x/a	y/b	z/c	U_{eq}
Ag	341(1)	830	5014(1)	56
P	1050(3)	247(1)	3645(2)	47(1)
N(1)	-911(9)	-565(4)	3130(7)	46(2)
N(2)	-1948(11)	-1485(5)	3989(9)	67(3)
N(3)	-1304(11)	1531(5)	4339(8)	64(3)
C(1)	2315(12)	-305(5)	4128(9)	50(3)*
C(2)	3090(13)	-235(6)	5163(11)	62(3)*
C(3)	4204(15)	-623(6)	5513(12)	79(4)*
C(4)	4466(18)	-1041(8)	4853(14)	96(5)*
C(5)	3677(18)	-1132(7)	3856(14)	96(5)*
C(6)	2543(16)	-747(6)	3466(12)	79(4)*
C(7)	1937(13)	670(5)	2726(10)	57(3)*
C(8)	1732(16)	1243(7)	2766(12)	84(4)*
C(9)	2466(21)	1599(9)	2078(16)	121(6)*
C(10)	3358(17)	1341(7)	1440(14)	93(5)*
C(11)	3542(15)	784(7)	1456(12)	77(4)*
C(12)	2831(14)	424(6)	2090(10)	64(4)*
C(13)	-360(12)	-107(5)	2734(10)	50(3)*
C(14)	-947(16)	140(6)	1743(12)	78(4)*
C(15)	-2180(18)	-102(7)	1157(15)	96(5)*
C(16)	-2751(17)	-587(7)	1551(13)	85(5)*
C(17)	-2032(13)	-811(6)	2551(10)	59(3)*
C(18)	-2560(13)	-1332(5)	3004(10)	59(3)*
C(19)	-3647(14)	-1655(6)	2393(11)	64(4)*
C(20)	-4038(15)	-2145(6)	2842(12)	77(4)*
C(21)	-3396(16)	-2313(6)	3854(12)	80(4)*
C(22)	-2350(15)	-1977(6)	4418(12)	74(4)*
C(23)	-1594(16)	1949(7)	4975(13)	82(4)*
C(24)	-2648(17)	2355(7)	4620(13)	91(5)*
C(25)	-3438(16)	2275(7)	3605(13)	84(4)*
C(26)	-3196(15)	1855(7)	2985(12)	80(4)*
C(27)	-2073(14)	1478(6)	3348(11)	66(4)*
C(28)	-4714(24)	2686(10)	3075(19)	139(8)*
C(29)	-4865(28)	3072(12)	3666(22)	171(10)*

Table 5.49 / cont.

B	-3114(30)	1335(15)	-283(19)	145(9)
F(1)	-2068(13)	1312(5)	497(11)	166(4)
F(2)	-3145(14)	1726(7)	-933(13)	199(6)
F(3)	-3555(32)	897(7)	-776(18)	313(10)
F(4)	-4156(19)	1371(18)	107(15)	401(19)

* isotropic temperature factor.

$$U_{eq} = \frac{1}{3} \Sigma_i \Sigma_j U_{ij} a_i^* a_j^* (a_i . a_j)$$

Table 5.50 : Anisotropic thermal factors (Å^2 , x10^3) for $[Ag_2(\mu\text{-}Ph_2Pbipy)_2(4\text{-vinylpy})_2](BF_4)_2$

	U(11)	U(22)	U(33)	U(23)	U(13)	U(12)
Ag	61(1)	59(1)	47(1)	-2(1)	8(1)	4(1)
P	48(2)	55(2)	39(2)	0(1)	8(1)	-1(2)
N(1)	45(6)	51(6)	43(5)	-5(5)	6(4)	-1(5)
N(2)	59(7)	69(8)	72(8)	-1(6)	10(6)	-6(6)
N(3)	63(7)	71(8)	58(7)	-1(6)	11(6)	6(6)
B	133(19)	217(29)	65(14)	56(17)	-44(14)	-147(21)
F(1)	149(10)	135(10)	183(12)	28(9)	-60(9)	-20(8)
F(2)	143(11)	212(15)	214(15)	109(13)	-51(10)	-43(10)
F(3)	486(35)	140(14)	227(23)	-63(14)	-174(25)	56(17)
F(4)	134(14)	908(76)	181(18)	0(28)	83(14)	-90(26)

5.6.26 Single crystal X-ray diffraction study of $[Ag_2(\mu\text{-}Ph_2Pbipy)_2(\eta^1\text{-}pbpz)_2](BF_4)_2.H_2O$ [51]

A pale yellow needle was grown by slow evaporation of a saturated acetone : ethanol solution of the complex. The complex crystallises with two molecules in each asymmetric unit. The general approach used for the intensity data collection is described in Appendix A. The crystallographic data are given in Table 5.51, the interatomic distances in Table 5.52, the interatomic angles in Table 5.53, the fractional coordinates in Table 5.54 and the anisotropic thermal parameters in Table 5.55. The observed and calculated structure factors may be found on microfiche in an envelope fixed to the inside back cover.

Table 5.51

Crystal data and details of the crystallographic analysis for $[Ag_2(\mu\text{-}Ph_2Pbipy)_2(pbpz)_2](BF_4)_2.H_2O$

Formula	$Ag_2C_{58}H_{46}N_{10}OP_2B_2F_8$
Molecular Mass	1350.36
Crystal System	Triclinic
Space Group	$P\bar{1}$
a(Å)	11.265(2)
b(Å)	11.600(1)
c(Å)	22.208(3)
α(°)	77.85(1)
β(°)	78.68(1)
γ(°)	88.40(1)
V(Å^3)	2781.61
Z	2
D_c(g.cm^{-3})	1.61
F(000)	1356
λ(Mo-Kα)(Å)	0.71069
Scan mode	ω - 2θ
ω scan angle	0.45 + 0.35tanθ
Horizontal Aperture width (mm)	2.7 + 0.1tanθ
Scattering range (°)	$2 \leq \theta \leq 23$
μ (cm^{-1})	8.27
Absorption corrections	Semi empirical[103]
Measured intensities	7957
Unique intensities	6785
Unique intensities with [I > 3σ(I)]	5763
Structure solution	Direct & Fourier methods
Weighting scheme	$1/(\sigma^2(F) + 0.00092F^2)$
$R = \Sigma(F_o\text{-}F_c)/\Sigma F_o$	0.053
$R_w = \Sigma_w½ (F_o\text{-}F_c)/ \Sigma_w½F_o$	0.058
$(\Delta/\sigma)_{max}$	2.500[(a)]
$\Delta\rho_{max}$(eÅ^{-3})	0.812
Number of parameters	346

(a) : Due to disorder within the water molecule.

Table 5.52 : Interatomic distances (Å) for $[Ag_2(\mu\text{-}Ph_2Pbipy)_2(pbpz)_2](BF_4)_2.H_2O$

Ag(A)-P(A)	2.386(2)	Ag(A)-N(3A)	2.403(7)
Ag(A)-Ag(A′)	3.125(1)	P(A)-C(1A)	1.813(5)
Ag(A)-N(1A′)	2.367(5)	Ag(A)-N(2A′)	2.428(7)
P(A)-C(7A)	1.825(6)	P(A)-C(13A)	1.847(7)
N(1A)-C(13A)	1.321(10)	N(1A)-C(17A)	1.354(8)
N(2A)-C(18A)	1.310(10)	N(2A)-C(22A)	1.316(14)
N(3A)-C(23A)	1.344(12)	N(3A)-C(27A)	1.347(9)
N(4A)-C(27A)	1.342(11)	N(4A)-C(28A)	1.311(11)
N(5A)-C(26A)	1.384(10)	N(5A)-C(29A)	1.351(15)
C(1A)-C(2A)	1.395(6)	C(1A)-C(6A)	1.395(6)
C(2A)-C(3A)	1.395(7)	C(3A)-C(4A)	1.395(6)
C(4A)-C(5A)	1.395(6)	C(5A)-C(6A)	1.395(7)
C(7A)-C(8A)	1.395(7)	C(7A)-C(12A)	1.395(8)
C(8A)-C(9A)	1.395(8)	C(9A)-C(10A)	1.395(8)
C(10A)-C(11A)	1.395(7)	C(11A)-C(12A)	1.395(8)
C(13A)-C(14A)	1.364(11)	C(14A)-C(15A)	1.395(12)
C(15A)-C(16A)	1.357(15)	C(16A)-C(17A)	1.376(11)
C(17A)-C(18A)	1.511(12)	C(18A)-C(19A)	1.362(10)
C(19A)-C(20A)	1.42(2)	C(20A)-C(21A)	1.37(2)
C(21A)-C(22A)	1.400(13)	C(23A)-C(24A)	1.415(14)
C(24A)-C(25A)	1.298(13)	C(25A)-C(26A)	1.367(12)
C(26A)-C(27A)	1.435(12)	C(28A)-C(29A)	1.409(15)
B(1A)-F(1A)	1.247(12)	B(1A)-F(2A)	1.313(13)
B(1A)-F(3A)	1.277(15)	B(1A)-F(4A)	1.26(2)
Ag(B)-P(B)	2.393(2)	Ag(B)-N(3B)	2.395(7)
Ag(B)-Ag(B′)	3.082(1)	P(B)-C(1B)	1.808(6)
Ag(B)-N(1B′)	2.374(2)	Ag(B)-N(2B′)	2.443(2)
P(B)-C(7B)	1.829(4)	P(B)-C(13B)	1.849(7)
N(1B)-C(13B)	1.336(8)	N(1B)-C(17B)	1.337(9)
N(2B)-C(18B)	1.333(10)	N(2B)-C(22B)	1.352(10)
N(3B)-C(23B)	1.322(11)	N(3B)-C(27B)	1.334(10)
N(4B)-C(27B)	1.356(10)	N(4B)-C(28B)	1.321(13)
N(5B)-C(26B)	1.391(12)	N(5B)-C(29B)	1.348(14)
C(1B)-C(2B)	1.395(7)	C(1B)-C(6B)	1.395(6)
C(2B)-C(3B)	1.395(8)	C(3B)-C(4B)	1.395(6)

Table 5.52 / cont.

C(4B)-C(5B)	1.395(7)	C(5B)-C(6B)	1.395(8)
C(7B)-C(8B)	1.395(6)	C(7B)-C(12B)	1.395(7)
C(8B)-C(9B)	1.395(6)	C(9B)-C(10B)	1.395(7)
C(10B)-C(11B)	1.395(6)	C(11B)-C(12B)	1.395(6)
C(13B)-C(14B)	1.363(9)	C(14B)-C(15B)	1.381(12)
C(15B)-C(16B)	1.408(12)	C(16B)-C(17B)	1.403(9)
C(17B)-C(18B)	1.474(10)	C(18B)-C(19B)	1.392(12)
C(19B)-C(20B)	1.404(13)	C(20B)-C(21B)	1.356(15)
C(21B)-C(22B)	1.384(14)	C(23B)-C(24B)	1.402(15)
C(24B)-C(25B)	1.312(15)	C(25B)-C(26B)	1.413(12)
C(26B)-C(27B)	1.407(13)	C(28B)-C(29B)	1.42(2)
B(1B)-F(1B)	1.26(2)	B(1B)-F(2B)	1.26(2)
B(1B)-F(3B)	1.27(2)	B(1B)-F(4B)	1.18(2)

Table 5.53 : Interatomic angles (°) for $[Ag_2(\mu\text{-}Ph_2Pbipy)_2(pbpz)_2](BF_4)_2.H_2O$

P(A)-Ag(A)-N(3A)	115.3(2)	Ag(A)-P(A)-C(1A)	118.6(2
N(1A′)-Ag(A)-N(2A′)	69.4(2)	N(1A′)-Ag(A)-P(A)	145.1(2
N(2A′)-Ag(A)-P(A)	114.2(2)	N(2A′)-Ag(A)-N(3A)	89.7(3
N(1A′)-Ag(A)-N(3A)	99.1(2)	Ag(A)-N(2A′)-C(18A′)	117.4(3
Ag(A)-N(1A′)-C(17A′)	117.5(2)	Ag(A)-N(1A′)-C(13A′)	123.6(3
Ag(A)-P(A)-C(7A)	111.1(2)	C(1A)-P(A)-C(7A)	103.5(2
Ag(A)-P(A)-C(13A)	116.2(2)	C(1A)-P(A)-C(13A)	103.4(3
C(7A)-P(A)-C(13A)	102.1(3)	C(13A)-N(1A)-C(17A)	118.3(6
C(18A)-N(2A)-C(22A)	118.8(7)	Ag(A)-N(3A)-C(23A)	125.8(5
Ag(A)-N(3A)-C(27A)	116.6(6)	C(23A)-N(3A)-C(27A)	117.6(8
C(27A)-N(4A)-C(28A)	116.5(8)	C(26A)-N(5A)-C(29A)	118.9(9
P(A)-C(1A)-C(2A)	116.7(3)	P(A)-C(1A)-C(6A)	123.3(3
C(2A)-C(1A)-C(6A)	120.0(4)	C(1A)-C(2A)-C(3A)	120.0(4
C(2A)-C(3A)-C(4A)	120.0(4)	C(3A)-C(4A)-C(5A)	120.0(4
C(4A)-C(5A)-C(6A)	120.0(4)	C(1A)-C(6A)-C(5A)	120.0(4
P(A)-C(7A)-C(8A)	122.1(4)	P(A)-C(7A)-C(12A)	117.4(4
C(8A)-C(7A)-C(12A)	120.0(5)	C(7A)-C(8A)-C(9A)	120.0(5
C(8A)-C(9A)-C(10A)	120.0(5)	C(9A)-C(10A)-C(11A)	120.0(5
C(10A)-C(11A)-C(12A)	120.0(5)	C(7A)-C(12A)-C(11A)	120.0(5
P(A)-C(13A)-N(1A)	114.6(5)	P(A)-C(13A)-C(14A)	121.6(7
N(1A)-C(13A)-C(14A)	123.8(7)	C(13A)-C(14A)-C(15A)	116.9(9
C(14A)-C(15A)-C(16A)	120.8(8)	C(15A)-C(16A)-C(17A)	118.2(7
N(1A)-C(17A)-C(16A)	121.8(8)	N(1A)-C(17A)-C(18A)	117.3(6
C(16A)-C(17A)-C(18A)	120.9(7)	N(2A)-C(18A)-C(17A)	117.0(6
N(2A)-C(18A)-C(19A)	123.2(8)	C(17A)-C(18A)-C(19A)	119.7(7
C(18A)-C(19A)-C(20A)	117.4(9)	C(19A)-C(20A)-C(21A)	120.4(8
C(20A)-C(21A)-C(22A)	115.4(10)	N(2A)-C(22A)-C(21A)	124.7(1
N(3A)-C(23A)-C(24A)	121.8(8)	C(23A)-C(24A)-C(25A)	120.8(9
C(24A)-C(25A)-C(26A)	120.0(9)	N(5A)-C(26A)-C(25A)	122.8(9
N(5A)-C(26A)-C(27A)	118.2(8)	C(25A)-C(26A)-C(27A)	119.0(7
N(3A)-C(27A)-N(4A)	116.6(8)	N(3A)-C(27A)-C(26A)	120.8(7
N(4A)-C(27A)-C(26A)	122.6(7)	N(4A)-C(28A)-C(29A)	124.9(9
N(5A)-C(29A)-C(28A)	118.8(8)	F(1A)-B(1A)-F(2A)	110.3(9
F(1A)-B(1A)-F(3A)	104.1(9)	F(2A)-B(1A)-F(3A)	110.1(1
F(1A)-B(1A)-F(4A)	113.8(11)	F(2A)-B(1A)-F(4A)	112.9(9

Table 5.53 / cont.

F(3A)-B(1A)-F(4A)	105.1(11)	P(B)-Ag(B)-N(3B)	118.1(1
Ag(B)-P(B)-C(1B)	118.5(2)	Ag(B)-P(B)-C(7B)	112.4(2
N(1B′)-Ag(B)-N(2B′)	69.1(2)	N(1B′)-Ag(B)-P(B)	143.4(2
N(2B′)-Ag(B)-P(B)	113.0(3)	N(2B′)-Ag(B)-N(3B)	91.8(3
N(1B′)-Ag(B)-N(3B′)	97.9(1)	Ag(B)-N(2B′)-C(18B′)	114.3(2
Ag(B)-N(1B′)-C(17B′)	116.9(2)	Ag(B)-N(1B′)-C(13B′)	123.6(2
C(1B)-P(B)-C(7B)	103.2(2)	Ag(B)-P(B)-C(13B)	114.2(2
C(1B)-P(B)-C(13B)	104.6(3)	C(7B)-P(B)-C(13B)	102.1(3
C(13B)-N(1B)-C(17B)	119.2(5)	C(18B)-N(2B)-C(22B)	119.8(7
Ag(B)-N(3B)-C(23B)	124.1(6)	Ag(B)-N(3B)-C(27B)	118.1(5
C(23B)-N(3B)-C(27B)	117.8(8)	C(27B)-N(4B)-C(28B)	116.9(8
C(26B)-N(5B)-C(29B)	117.9(10)	P(B)-C(1B)-C(2B)	116.7(3
P(B)-C(1B)-C(6B)	123.3(4)	C(2B)-C(1B)-C(6B)	120.0(5
C(1B)-C(2B)-C(3B)	120.0(4)	C(2B)-C(3B)-C(4B)	120.0(4
C(3B)-C(4B)-C(5B)	120.0(5)	C(4B)-C(5B)-C(6B)	120.0(4
C(1B)-C(6B)-C(5B)	120.0(4)	P(B)-C(7B)-C(8B)	122.3(4
P(B)-C(7B)-C(12B)	117.3(3)	C(8B)-C(7B)-C(12B)	120.0(4
C(7B)-C(8B)-C(9B)	120.0(5)	C(8B)-C(9B)-C(10B)	120.0(4
C(9B)-C(10B)-C(11B)	120.0(4)	C(10B)-C(11B)-C(12B)	120.0(5
C(7B)-C(12B)-C(11B)	120.0(4)	P(B)-C(13B)-N(1B)	114.9(4
P(B)-C(13B)-C(14B)	121.8(6)	N(1B)-C(13B)-C(14B)	123.3(7
C(13B)-C(14B)-C(15B)	118.6(7)	C(14B)-C(15B)-C(16B)	119.7(7
C(15B)-C(16B)-C(17B)	117.3(7)	N(1B)-C(17B)-C(16B)	121.9(6
N(1B)-C(17B)-C(18B)	118.5(6)	C(16B)-C(17B)-C(18B)	119.6(7
N(2B)-C(18B)-C(17B)	117.1(7)	N(2B)-C(18B)-C(19B)	121.4(7
C(17B)-C(18B)-C(19B)	121.4(7)	C(18B)-C(19B)-C(20B)	118.0(9
C(19B)-C(20B)-C(21B)	120.3(10)	C(20B)-C(21B)-C(22B)	118.8(8
N(2B)-C(22B)-C(21B)	121.6(8)	N(3B)-C(23B)-C(24B)	122.1(8
C(23B)-C(24B)-C(25B)	122.5(9)	C(24B)-C(25B)-C(26B)	116.1(9
N(5B)-C(26B)-C(25B)	120.0(9)	N(5B)-C(26B)-C(27B)	120.2(8
C(25B)-C(26B)-C(27B)	119.8(8)	N(3B)-C(27B)-N(4B)	116.7(8
N(3B)-C(27B)-C(26B)	121.6(7)	N(4B)-C(27B)-C(26B)	121.6(7

Table.5.53 / cont.

N(4B)-C(28B)-C(29B)	124.2(8)	N(5B)-C(29B)-C(28B)	119.1(9)
F(1B)-B(1B)-F(2B)	106.2(10)	F(1B)-B(1B)-F(3B)	112.5(12
F(2B)-B(1B)-F(3B)	108.1(13)	F(1B)-B(1B)-F(4B)	109.1(13
F(2B)-B(1B)-F(4B)	118.3(12)	F(3B)-B(1B)-F(4B)	102.8(12

Table 5.54 : Fractional coordinates (x 10^4) and isotropic thermal factors (Å^2, x10^3) for $[Ag_2(\mu\text{-}Ph_2Pbipy)_2(pbpz)_2](BF_4)_2.H_2O$

	x/a	y/b	z/c	U_{eq}
Ag(A)	929(1)	968(1)	9(1)	52(1)
P(A)	1623(2)	-802(2)	593(1)	45(1)
N(1A)	-527(5)	-1926(5)	980(3)	43(1)
N(2A)	-2527(6)	-2384(6)	543(3)	65(2)
N(3A)	51(6)	2372(6)	619(3)	62(2)
N(4A)	-1133(7)	821(6)	1224(3)	67(2)
N(5A)	-2480(8)	2320(9)	1938(4)	89(3)
C(1A)	2444(4)	-1843(4)	167(2)	47(2)
C(2A)	3309(4)	-1372(4)	-364(2)	62(2)
C(3A)	3973(4)	-2118(4)	-718(2)	75(3)
C(4A)	3771(4)	-3334(4)	-542(2)	78(3)
C(5A)	2906(4)	-3805(4)	-11(2)	73(3)
C(6A)	2242(4)	-3059(4)	343(2)	57(2)
C(7A)	2665(4)	-477(4)	1071(2)	46(2)
C(8A)	3614(4)	-1223(4)	1206(2)	68(2)
C(9A)	4294(4)	-1018(4)	1636(2)	74(3)
C(10A)	4025(4)	-66(4)	1930(2)	73(3)
C(11A)	3077(4)	680(4)	1795(2)	72(2)
C(12A)	2396(4)	475(4)	1366(2)	63(2)
C(13A)	458(7)	-1729(6)	1184(3)	49(2)
C(14A)	609(8)	-2132(7)	1787(4)	67(2)
C(15A)	-341(9)	-2798(9)	2201(4)	79(3)
C(16A)	-1363(8)	-3020(8)	2005(4)	67(2)
C(17A)	-1424(7)	-2599(6)	1385(3)	50(2)
C(18A)	-2506(6)	-2876(6)	1129(3)	48(2)
C(19A)	-3395(8)	-3618(8)	1503(5)	75(2)
C(20A)	-4361(9)	-3899(9)	1229(6)	85(3)
C(21A)	-4381(8)	-3428(8)	612(5)	74(3)
C(22A)	-3428(9)	-2645(9)	295(5)	85(3)
C(23A)	367(9)	3517(8)	507(5)	74(3)
C(24A)	-281(10)	4306(8)	854(5)	74(3)
C(25A)	-1187(9)	3936(7)	1309(4)	64(2)
C(26A)	-1524(8)	2771(8)	1458(4)	59(2)
C(27A)	-866(8)	1978(7)	1102(4)	58(2)

Table 5.54 / cont.

C(28A)	-2006(9)	434(9)	1704(5)	79(3)
C(29A)	-2730(9)	1152(9)	2065(4)	78(3)
B(1A)	2526(8)	3909(8)	1706(4)	43(2)
F(1A)	1904(10)	3213(8)	2155(6)	219(4)
F(2A)	2210(13)	5002(8)	1724(5)	212(4)
F(3A)	3609(10)	3745(10)	1796(6)	203(4)
F(4A)	2535(13)	3661(10)	1182(6)	223(5)
Ag(B)	1008(1)	4083(1)	5067(1)	47(1)
P(B)	-795(2)	2968(2)	5587(1)	42(1)
N(1B)	7973(5)	4838(5)	5921(3)	39(1)
N(2B)	7416(6)	7100(6)	5426(3)	62(2)
N(3B)	2309(6)	4615(5)	5700(3)	53(2)
N(4B)	591(6)	5213(7)	6288(3)	63(2)
N(5B)	1965(9)	5937(8)	7078(4)	88(3)
C(1B)	-1748(4)	2502(4)	5113(2)	46(2)
C(2B)	-1167(4)	2011(4)	4612(2)	68(2)
C(3B)	-1843(4)	1622(4)	4229(2)	80(3)
C(4B)	-3101(4)	1723(4)	4345(2)	81(3)
C(5B)	-3682(4)	2213(4)	4846(2)	70(2)
C(6B)	-3005(4)	2603(4)	5229(2)	58(2)
C(7B)	-479(4)	1586(3)	6097(2)	47(2)
C(8B)	-1259(4)	610(3)	6252(2)	67(2)
C(9B)	-1051(4)	-373(3)	6700(2)	81(3)
C(10B)	-63(4)	-381(3)	6994(2)	73(2)
C(11B)	717(4)	596(3)	6840(2)	74(3)
C(12B)	509(4)	1579(3)	6391(2)	57(2)
C(13B)	-1836(6)	3699(6)	6140(3)	44(2)
C(14B)	-2343(7)	3111(7)	6730(4)	58(2)
C(15B)	-3085(8)	3722(8)	7124(4)	69(2)
C(16B)	-3297(7)	4927(7)	6910(4)	60(2)
C(17B)	-2753(6)	5445(6)	6291(3)	44(2)
C(18B)	-2964(6)	6698(6)	6040(3)	45(2)
C(19B)	-3560(8)	7423(8)	6425(5)	72(3)
C(20B)	-3775(9)	8593(8)	6145(6)	85(3)
C(21B)	-3410(9)	8988(8)	5518(5)	77(3)
C(22B)	-2795(8)	8229(7)	5164(4)	70(2)
C(23B)	3492(8)	4451(7)	5604(4)	63(2)

Table 5.54 / cont.

C(24B)	4220(8)	4780(9)	5986(5)	77(3)
C(25B)	3779(8)	5272(8)	6462(4)	63(2)
C(26B)	2513(8)	5439(7)	6577(4)	63(2)
C(27B)	1808(6)	5077(6)	6191(3)	47(2)
C(28B)	95(8)	5691(9)	6767(4)	76(3)
C(29B)	758(9)	6094(9)	7164(4)	76(3)
B(1B)	4151(8)	1553(10)	6680(5)	66(2)
F(1B)	4268(12)	455(9)	6720(5)	244(5)
F(2B)	3521(11)	1681(10)	7194(6)	253(5)
F(3B)	5158(10)	2083(15)	6603(6)	282(6)
F(4B)	3803(15)	1967(11)	6214(8)	292(7)
O(B)	5477(17)	3684(17)	2288(8)	308(8)

$$U_{eq} = \frac{1}{3} \Sigma_i \Sigma_j U_{ij} a_i^* a_j^* (a_i . a_j)$$

Table 5.55 : Anisotropic thermal factors (Å^2 , x10^3) for $[Ag_2(\mu\text{-}Ph_2Pbipy)_2(pbpz)_2](BF_4)_2.H_2O$

	U(11)	U(22)	U(33)	U(23)	U(13)	U(12)
Ag(A)	55(1)	50(1)	47(1)	2(1)	-14(1)	0(1)
P(A)	45(1)	47(1)	41(1)	-2(1)	-12(1)	1(1)
N(1A)	43(3)	42(3)	41(3)	-6(3)	-5(3)	0(3)
N(2A)	51(4)	75(5)	68(5)	-2(4)	-24(4)	-8(3)
N(3A)	66(4)	68(5)	52(4)	-13(3)	-15(4)	6(4)
N(4A)	86(5)	53(4)	60(5)	-12(4)	-13(4)	6(4)
N(5A)	85(6)	111(7)	70(5)	-26(5)	-11(5)	20(5)
C(1A)	52(4)	55(5)	40(4)	-15(3)	-18(4)	6(4)
C(2A)	62(5)	68(5)	50(5)	-6(4)	-7(4)	-4(4)
C(3A)	75(6)	91(7)	52(5)	-10(5)	-3(5)	12(5)
C(4A)	79(7)	91(7)	78(7)	-43(6)	-25(5)	25(6)
C(5A)	69(6)	73(6)	90(7)	-41(5)	-21(5)	-4(5)
C(6A)	53(5)	55(5)	62(5)	-16(4)	-2(4)	-4(4)
C(7A)	46(4)	49(4)	43(4)	-6(3)	-14(3)	-4(3)
C(8A)	64(5)	64(5)	84(6)	-17(5)	-37(5)	11(4)
C(9A)	72(6)	71(6)	81(7)	7(5)	-42(5)	-7(5)
C(10A)	70(6)	76(6)	77(6)	-4(5)	-32(5)	-15(5)
C(11A)	84(7)	76(6)	63(6)	-21(5)	-22(5)	-15(5)
C(12A)	64(5)	63(5)	59(5)	-5(4)	-10(4)	-2(4)
C(13A)	55(5)	48(4)	41(4)	-5(3)	-10(4)	2(4)
C(14A)	91(7)	62(5)	45(5)	1(4)	-21(5)	-3(5)
C(15A)	94(7)	86(7)	51(5)	7(5)	-22(5)	-27(6)
C(16A)	79(6)	67(6)	52(5)	-5(4)	-11(5)	-4(5)
C(17A)	54(5)	44(4)	49(5)	-9(4)	-4(4)	4(4)
C(18A)	44(4)	44(4)	53(5)	-10(4)	-3(4)	2(3)
C(19A)	56(5)	74(6)	90(7)	-15(5)	2(5)	-12(5)
C(20A)	59(6)	80(7)	110(9)	-25(6)	3(6)	-12(5)
C(21A)	59(5)	64(6)	97(8)	-16(5)	-8(5)	-1(4)
C(22A)	66(6)	90(7)	101(8)	-15(6)	-24(6)	-10(5)
C(23A)	82(6)	63(6)	83(7)	-13(5)	-37(5)	-3(5)
C(24A)	89(7)	62(6)	76(7)	-18(5)	-28(6)	2(5)
C(25A)	82(6)	53(5)	73(6)	-28(5)	-36(5)	17(5)
C(26A)	70(6)	70(6)	43(5)	-19(4)	-21(4)	22(4)
C(27A)	66(5)	61(5)	51(5)	-11(4)	-23(4)	12(4)
C(28A)	90(7)	79(7)	68(6)	-18(5)	-12(6)	7(6)

Table 5.55 / cont.

C(29A)	83(7)	81(7)	67(6)	-10(5)	-13(5)	2(6)
B(1A)	53(5)	51(5)	27(4)	-9(4)	-12(4)	-5(4)
F(1A)	209(10)	118(7)	253(11)	-14(7)	109(9)	33(6)
F(2A)	380(16)	101(6)	151(8)	-17(5)	-57(9)	65(8)
F(3A)	158(9)	220(11)	263(12)	-104(9)	-61(9)	-8(8)
F(4A)	338(15)	191(10)	192(10)	-75(8)	-146(11)	50(10)
Ag(B)	41(1)	49(1)	46(1)	-7(1)	-3(1)	-1(1)
P(B)	42(1)	40(1)	41(1)	-6(1)	-5(1)	1(1)
N(1B)	37(3)	40(3)	43(3)	-13(3)	-6(3)	-2(2)
N(2B)	65(4)	51(4)	64(4)	-9(3)	-2(4)	13(3)
N(3B)	63(4)	51(4)	45(4)	-6(3)	-16(3)	-6(3)
N(4B)	59(4)	85(5)	55(4)	-24(4)	-20(4)	-11(4)
N(5B)	115(7)	93(6)	74(6)	-38(5)	-40(5)	0(5)
C(1B)	53(4)	34(4)	46(4)	-6(3)	-4(4)	-6(3)
C(2B)	72(6)	80(6)	52(5)	-23(5)	-5(4)	5(5)
C(3B)	98(8)	87(7)	62(6)	-28(5)	-16(5)	-8(6)
C(4B)	105(8)	69(6)	75(7)	-3(5)	-44(6)	-15(6)
C(5B)	76(6)	61(5)	78(6)	-11(5)	-31(5)	-6(5)
C(6B)	52(5)	48(5)	72(6)	-9(4)	-13(4)	-1(4)
C(7B)	53(4)	45(4)	39(4)	-1(3)	-5(4)	-5(3)
C(8B)	76(6)	42(5)	75(6)	-2(4)	-6(5)	-2(4)
C(9B)	87(7)	58(6)	88(7)	0(5)	-10(6)	11(5)
C(10B)	93(7)	55(5)	62(6)	-4(4)	-10(5)	15(5)
C(11B)	84(7)	69(6)	64(6)	-5(5)	-14(5)	27(5)
C(12B)	63(5)	62(5)	46(4)	-8(4)	-11(4)	15(4)
C(13B)	42(4)	47(4)	43(4)	-9(3)	-7(3)	-5(3)
C(14B)	60(5)	59(5)	45(5)	-6(4)	9(4)	6(4)
C(15B)	72(6)	72(6)	54(5)	-6(5)	4(5)	4(5)
C(16B)	58(5)	64(5)	51(5)	-10(4)	3(4)	1(4)
C(17B)	34(4)	52(4)	46(4)	-14(3)	-6(3)	-3(3)
C(18B)	36(4)	47(4)	52(5)	-15(4)	-6(3)	-1(3)
C(19B)	63(5)	58(5)	97(7)	-30(5)	-5(5)	7(4)
C(20B)	76(7)	60(6)	116(9)	-31(6)	4(6)	11(5)
C(21B)	72(6)	54(5)	98(7)	-11(5)	-7(6)	5(5)
C(22B)	71(6)	53(5)	82(6)	-12(5)	-11(5)	8(4)
C(23B)	59(5)	61(5)	75(6)	-18(4)	-24(5)	7(4)
C(24B)	61(6)	81(7)	92(7)	-8(6)	-32(5)	2(5)

Table 5.55 / cont.

C(25B)	59(5)	68(5)	71(6)	-19(5)	-27(5)	-1(4)
C(26B)	75(6)	59(5)	57(5)	-9(4)	-24(4)	-3(4)
C(27B)	45(4)	55(5)	42(4)	-11(4)	-11(3)	-10(3)
C(28B)	58(5)	108(8)	65(6)	-28(5)	-10(5)	-6(5)
C(29B)	77(7)	95(7)	62(6)	-30(5)	-11(5)	3(5)
B(1B)	33(5)	70(7)	66(6)	46(6)	-4(4)	3(5)
F(1B)	330(15)	139(8)	192(10)	4(7)	68(10)	74(9)
F(2B)	242(12)	211(11)	256(12)	-97(9)	134(10)	-60(9)
F(3B)	154(9)	436(21)	239(12)	-53(13)	8(9)	-143(11)
F(4B)	420(20)	169(10)	329(18)	37(11)	-270(17)	-6(11)
O(B)	327(19)	368(23)	287(17)	-188(16)	-69(15)	39(17)

5.6.27 Single crystal X-ray diffraction study of $[Ag_2(\mu\text{-}Ph_2Pbipy)_2(\eta^2\text{-}2,2'\text{-bipy})](BF_4)_2$ [53]

A single, pale yellow rhomb was grown by slow evaporation of a saurated acetone : ethanol (1 : 1, vol : vol) solution of the complex. The general approach used for the intensity data collection is described in Appendix A. The crystallographic data are given in Table 5.56, the interatomic distances in Table 5.57, the interatomic angles in Table 5.58, the fractional coordinates in Table 5.59 and the anisotropic thermal parameters in Table 5.60. The observed and calculated structure factors may be found on microfiche in an envelope fixed to the inside back cover.

Table 5.56

Crystal data and details of the crystallographic analysis for $[Ag_2(\mu\text{-}Ph_2Pbipy)_2(\eta^2\text{-}2,2'\text{-}bipy)](BF_4)_2$

Formula	$Ag_2C_{54}H_{42}N_6P_2B_2F_8$
Molecular Mass	1226.26
Crystal System	Orthorhombic
Space Group	$P2_12_12_1$
a(Å)	13.313(8)
b(Å)	16.901(6)
c(Å)	23.457(4)
V(Å^3)	5278.20
Z	4
D_c(g.cm^{-3})	1.54
F(000)	2456
λ(Mo-Kα)(Å)	0.71069
Scan mode	ω - 2θ
ω scan angle	$0.80 + 0.35\tan\theta$
Horizontal Aperture width (mm)	$2.7 + 0.1\tan\theta$
Scattering range (°)	$2 \le \theta \le 23$
μ (cm^{-1})	8.58
Absorption corrections	Semi empirical[103]
Measured intensities	4109
Unique intensities	3770
Unique intensities with $[I > 3\sigma(I)]$	3205
Structure solution	Direct & Fourier methods
Weighting scheme	$1/(\sigma^2(F) + 0.00162F^2)$
$R = \Sigma(F_o - F_c)/\Sigma F_o$	0.059
$R_w = \Sigma_w½(F_o - F_c)/\Sigma_w½F_o$	0.064
$(\Delta/\sigma)_{max}$	0.202
$\Delta\rho_{max}$(eÅ^{-3})	0.923
Number of parameters	317

Table 5.57 : Interatomic distances (Å) for $[Ag_2(\mu\text{-}Ph_2Pbipy)_2(\eta^2\text{-}2,2'\text{-}bipy)](BF_4)_2$

Ag(1)-P(1)	2.454(3)	Ag(1)-P(2)	2.416(3)
Ag(1)-N(5)	2.426(14)	Ag(1)-N(6)	2.369(12)
Ag(2)-N(1)	2.312(11)	Ag(2)-N(2)	2.40(2)
Ag(2)-N(3)	2.368(14)	Ag(2)-N(4)	2.337(11)
P(1)-C(1)	1.784(14)	P(1)-C(7)	1.852(14)
P(1)-C(13)	1.869(14)	P(2)-C(23)	1.790(15)
P(2)-C(29)	1.81(2)	P(2)-C(35)	1.856(14)
N(1)-C(13)	1.29(2)	N(1)-C(17)	1.32(2)
N(2)-C(18)	1.34(2)	N(2)-C(22)	1.38(2)
N(3)-C(40)	1.31(2)	N(3)-C(44)	1.39(2)
N(4)-C(35)	1.35(2)	N(4)-C(39)	1.38(2)
N(5)-C(45)	1.36(2)	N(5)-C(49)	1.33(2)
N(6)-C(50)	1.32(2)	N(6)-C(54)	1.33(2)
C(1)-C(2)	1.46(2)	C(1)-C(6)	1.40(2)
C(2)-C(3)	1.37(2)	C(3)-C(4)	1.32(2)
C(4)-C(5)	1.45(3)	C(5)-C(6)	1.43(3)
C(7)-C(8)	1.36(2)	C(7)-C(12)	1.35(2)
C(8)-C(9)	1.43(2)	C(9)-C(10)	1.40(3)
C(10)-C(11)	1.38(3)	C(11)-C(12)	1.41(2)
C(13)-C(14)	1.37(2)	C(14)-C(15)	1.41(2)
C(15)-C(16)	1.34(2)	C(16)-C(17)	1.41(2)
C(17)-C(18)	1.52(2)	C(18)-C(19)	1.42(2)
C(19)-C(20)	1.50(3)	C(20)-C(21)	1.31(3)
C(21)-C(22)	1.36(3)	C(23)-C(24)	1.41(2)
C(23)-C(28)	1.36(2)	C(24)-C(25)	1.37(3)
C(25)-C(26)	1.41(3)	C(26)-C(27)	1.34(3)
C(27)-C(28)	1.48(3)	C(29)-C(30)	1.46(2)
C(29)-C(34)	1.37(2)	C(30)-C(31)	1.41(3)
C(31)-C(32)	1.35(3)	C(32)-C(33)	1.39(3)
C(33)-C(34)	1.37(2)	C(35)-C(36)	1.37(2)
C(36)-C(37)	1.37(2)	C(37)-C(38)	1.43(3)
C(38)-C(39)	1.34(2)	C(39)-C(40)	1.51(2)
C(40)-C(41)	1.40(3)	C(41)-C(42)	1.32(3)
C(42)-C(43)	1.39(3)	C(43)-C(44)	1.37(3)
C(45)-C(46)	1.40(3)	C(46)-C(47)	1.28(3)

Table 5.57 / cont.

C(47)-C(48)	1.48(3)	C(48)-C(49)	1.41(3)
C(49)-C(50)	1.48(2)	C(50)-C(51)	1.39(3)
C(51)-C(52)	1.39(3)	C(52)-C(53)	1.39(3)
C(53)-C(54)	1.37(3)	B(1)-F(1)	1.36(2)
B(1)-F(2)	1.26(2)	B(1)-F(3)	1.37(2)
B(1)-F(4)	1.31(2)	B(2)-F(5)	1.34(3)
B(2)-F(6)	1.28(3)	B(2)-F(7)	1.35(3)
B(2)-F(8)	1.47(3)		

Table 5.58 : Interatomic angles (°) for $[Ag_2(\mu\text{-}Ph_2Pbipy)_2(\eta^2\text{-}2,2'\text{-bipy})](BF_4)_2$

P(1)-Ag(1)-P(2)	128.5(1)	P(1)-Ag(1)-N(5)	107.6(3
P(2)-Ag(1)-N(5)	106.2(3)	P(1)-Ag(1)-N(6)	110.6(3
P(2)-Ag(1)-N(6)	117.6(3)	N(5)-Ag(1)-N(6)	68.1(4
N(1)-Ag(2)-N(2)	70.9(5)	N(1)-Ag(2)-N(3)	130.2(4
N(2)-Ag(2)-N(3)	96.3(5)	N(1)-Ag(2)-N(4)	150.3(4
N(2)-Ag(2)-N(4)	134.0(5)	N(3)-Ag(2)-N(4)	70.3(4
Ag(1)-P(1)-C(1)	115.9(5)	Ag(1)-P(1)-C(7)	113.4(4
C(1)-P(1)-C(7)	103.8(6)	Ag(1)-P(1)-C(13)	113.6(5
C(1)-P(1)-C(13)	104.5(6)	C(7)-P(1)-C(13)	104.4(6
Ag(1)-P(2)-C(23)	119.0(5)	Ag(1)-P(2)-C(29)	116.7(5
C(23)-P(2)-C(29)	106.8(7)	Ag(1)-P(2)-C(35)	105.0(5
C(23)-P(2)-C(35)	101.0(6)	C(29)-P(2)-C(35)	106.3(7
Ag(2)-N(1)-C(13)	125.3(9)	Ag(2)-N(1)-C(17)	117.9(9
C(13)-N(1)-C(17)	116.7(12)	Ag(2)-N(2)-C(18)	115.8(1
Ag(2)-N(2)-C(22)	124.6(13)	C(18)-N(2)-C(22)	118(2)
Ag(2)-N(3)-C(40)	118.9(11)	Ag(2)-N(3)-C(44)	121.3(1
C(40)-N(3)-C(44)	120(2)	Ag(2)-N(4)-C(35)	125.7(9
Ag(2)-N(4)-C(39)	117.2(9)	C(35)-N(4)-C(39)	116.6(1
Ag(1)-N(5)-C(45)	122.4(11)	Ag(1)-N(5)-C(49)	115.5(1
C(45)-N(5)-C(49)	121.6(14)	Ag(1)-N(6)-C(50)	117.1(1
Ag(1)-N(6)-C(54)	117.9(11)	C(50)-N(6)-C(54)	120.7(1
P(1)-C(1)-C(2)	125.0(12)	P(1)-C(1)-C(6)	118.1(1
C(2)-C(1)-C(6)	116.9(14)	C(1)-C(2)-C(3)	119(2)
C(2)-C(3)-C(4)	123(2)	C(3)-C(4)-C(5)	122(2)
C(4)-C(5)-C(6)	116(2)	C(1)-C(6)-C(5)	123(2)
P(1)-C(7)-C(8)	114.8(10)	P(1)-C(7)-C(12)	123.0(
C(8)-C(7)-C(12)	122.1(14)	C(7)-C(8)-C(9)	118.7(
C(8)-C(9)-C(10)	120(2)	C(9)-C(10)-C(11)	118(2)
C(10)-C(11)-C(12)	121(2)	C(7)-C(12)-C(11)	120(2)
P(1)-C(13)-N(1)	113.7(10)	P(1)-C(13)-C(14)	119.1(
N(1)-C(13)-C(14)	127.1(14)	C(13)-C(14)-C(15)	114.3(
C(14)-C(15)-C(16)	122(2)	C(15)-C(16)-C(17)	117(2)
N(1)-C(17)-C(16)	123(2)	N(1)-C(17)-C(18)	118.9(
C(16)-C(17)-C(18)	117.7(14)	N(2)-C(18)-C(17)	116(2)
N(2)-C(18)-C(19)	124(2)	C(17)-C(18)-C(19)	119(2)

Table 5.58 / cont.

C(18)-C(19)-C(20)	112(2)	C(19)-C(20)-C(21)	122(2)
C(20)-C(21)-C(22)	121(3)	N(2)-C(22)-C(21)	122(2)
P(2)-C(23)-C(24)	125.4(12)	P(2)-C(23)-C(28)	118.0(1
C(24)-C(23)-C(28)	117(2)	C(23)-C(24)-C(25)	125(2)
C(24)-C(25)-C(26)	116(2)	C(25)-C(26)-C(27)	124(2)
C(26)-C(27)-C(28)	116(2)	C(23)-C(28)-C(27)	122(2)
P(2)-C(29)-C(30)	125.8(12)	P(2)-C(29)-C(34)	117.3(1
C(30)-C(29)-C(34)	117(2)	C(29)-C(30)-C(31)	120(2)
C(30)-C(31)-C(32)	118(2)	C(31)-C(32)-C(33)	123(2)
C(32)-C(33)-C(34)	119(2)	C(29)-C(34)-C(33)	123(2)
P(2)-C(35)-N(4)	112.5(10)	P(2)-C(35)-C(36)	122.2(1
N(4)-C(35)-C(36)	124.8(13)	C(35)-C(36)-C(37)	117(2)
C(36)-C(37)-C(38)	121(2)	C(37)-C(38)-C(39)	117(2)
N(4)-C(39)-C(38)	122.9(13)	N(4)-C(39)-C(40)	116.1(1
C(38)-C(39)-C(40)	120.6(14)	N(3)-C(40)-C(39)	116.5(1
N(3)-C(40)-C(41)	124(2)	C(39)-C(40)-C(41)	120(2)
C(40)-C(41)-C(42)	118(2)	C(41)-C(42)-C(43)	119(2)
C(42)-C(43)-C(44)	122(2)	N(3)-C(44)-C(43)	117(2)
N(5)-C(45)-C(46)	120(2)	C(45)-C(46)-C(47)	119(2)
C(46)-C(47)-C(48)	123(3)	C(47)-C(48)-C(49)	114(2)
N(5)-C(49)-C(48)	122(2)	N(5)-C(49)-C(50)	117.8(1
C(48)-C(49)-C(50)	121(2)	N(6)-C(50)-C(49)	116.1(1
N(6)-C(50)-C(51)	124(2)	C(49)-C(50)-C(51)	120(2)
C(50)-C(51)-C(52)	114(2)	C(51)-C(52)-C(53)	123(2)
C(52)-C(53)-C(54)	117(2)	N(6)-C(54)-C(53)	121(2)
F(1)-B(1)-F(2)	116(2)	F(1)-B(1)-F(3)	105(2)
F(2)-B(1)-F(3)	107(2)	F(1)-B(1)-F(4)	110(2)
F(2)-B(1)-F(4)	112(2)	F(3)-B(1)-F(4)	107(2)
F(5)-B(2)-F(6)	117(2)	F(5)-B(2)-F(7)	111(2)
F(6)-B(2)-F(7)	114(2)	F(5)-B(2)-F(8)	108(2)
F(6)-B(2)-F(8)	108(2)	F(7)-B(2)-F(8)	96(2)

Table 5.59 : Fractional coordinates (x 10^4) and isotropic thermal factors ($Å^2$, x10^3) for $[Ag_2(\mu\text{-}Ph_2Pbipy)_2(\eta^2\text{-}2,2'\text{-}bipy)](BF_4)_2$

	x/a	y/b	z/c	U_{eq}
Ag(1)	6812(1)	8437(1)	2266(1)	51(1)
Ag(2)	7653(1)	9433(1)	958(1)	66(1)
P(1)	6602(3)	9879(2)	2238(2)	49(1)
P(2)	7450(3)	7571(2)	1531(2)	50(1)
N(1)	6119(8)	10023(6)	1139(5)	49(3)*
N(2)	6877(12)	9784(9)	69(7)	89(4)*
N(3)	9237(10)	10007(9)	760(6)	75(4)*
N(4)	8930(8)	8555(7)	1218(5)	52(3)*
N(5)	7737(10)	8115(8)	3126(6)	70(4)*
N(6)	5761(9)	7873(7)	2973(5)	58(3)*
C(1)	6062(11)	10318(9)	2858(6)	57(4)*
C(2)	6285(12)	11113(10)	3066(7)	68(4)*
C(3)	5840(13)	11376(10)	3558(8)	79(5)*
C(4)	5166(15)	10959(11)	3845(8)	84(5)*
C(5)	4883(15)	10168(11)	3672(8)	86(5)*
C(6)	5339(14)	9885(10)	3159(8)	76(5)*
C(7)	7799(10)	10422(8)	2143(6)	53(3)*
C(8)	8611(12)	10072(9)	2383(7)	65(4)*
C(9)	9568(14)	10445(11)	2326(8)	85(5)*
C(10)	9660(15)	11160(12)	2029(8)	89(5)*
C(11)	8801(14)	11490(11)	1797(8)	80(5)*
C(12)	7872(13)	11098(10)	1840(7)	75(5)*
C(13)	5792(11)	10229(9)	1638(6)	54(4)*
C(14)	4924(12)	10631(10)	1759(7)	71(4)*
C(15)	4362(13)	10850(10)	1276(7)	76(5)*
C(16)	4645(12)	10641(10)	750(7)	71(4)*
C(17)	5544(12)	10206(10)	698(7)	64(4)*
C(18)	5926(12)	10035(9)	102(7)	65(4)*
C(19)	5241(15)	10032(11)	-361(8)	88(5)*
C(20)	5752(19)	9864(15)	-919(11)	119(8)*
C(21)	6702(19)	9655(14)	-943(10)	116(7)*
C(22)	7263(16)	9602(12)	-460(9)	95(6)*
C(23)	7537(10)	6532(9)	1673(6)	56(3)*
C(24)	7778(16)	5946(12)	1268(8)	88(5)*

Table 5.59 / cont.

C(25)	7802(17)	5153(13)	1379(10)	98(6)*
C(26)	7678(17)	4929(13)	1952(10)	98(6)*
C(27)	7515(15)	5441(12)	2380(9)	96(6)*
C(28)	7398(13)	6283(9)	2219(7)	71(4)*
C(29)	6905(12)	7674(9)	830(7)	62(4)*
C(30)	7415(14)	7517(11)	290(8)	81(5)*
C(31)	6889(16)	7585(12)	-229(9)	93(6)*
C(32)	5909(17)	7799(13)	-208(10)	101(6)*
C(33)	5421(14)	7983(11)	297(8)	84(5)*
C(34)	5924(12)	7908(10)	801(7)	66(4)*
C(35)	8796(10)	7836(8)	1459(6)	50(3)*
C(36)	9543(12)	7390(9)	1695(7)	65(4)*
C(37)	10485(15)	7716(11)	1699(8)	84(5)*
C(38)	10670(12)	8478(10)	1459(7)	68(4)*
C(39)	9903(11)	8830(9)	1189(6)	56(3)*
C(40)	10051(12)	9611(10)	888(7)	72(4)*
C(41)	11020(16)	9875(12)	763(9)	93(6)*
C(42)	11114(19)	10518(16)	448(11)	122(8)*
C(43)	10269(21)	10985(15)	348(11)	124(8)*
C(44)	9315(15)	10724(12)	472(8)	87(5)*
C(45)	8751(13)	8172(10)	3158(7)	71(5)*
C(46)	9244(19)	8079(15)	3683(12)	119(8)*
C(47)	8714(19)	8015(16)	4138(12)	118(8)*
C(48)	7613(18)	7880(14)	4127(10)	107(7)*
C(49)	7182(11)	7968(9)	3583(7)	58(4)*
C(50)	6083(12)	7903(10)	3505(7)	65(4)*
C(51)	5461(18)	7833(14)	3976(10)	108(7)*
C(52)	4444(19)	7800(14)	3840(10)	111(7)*
C(53)	4090(17)	7785(13)	3284(10)	98(6)*
C(54)	4789(13)	7807(10)	2858(8)	79(5)*
B(1)	6747(13)	6955(10)	5513(7)	54(4)*
F(1)	6710(10)	6786(7)	6080(5)	119(4)*
F(2)	5936(10)	7170(8)	5286(6)	122(4)*
F(3)	7393(15)	7582(12)	5470(8)	182(7)*
F(4)	7166(16)	6366(11)	5241(8)	184(7)*
B(2)	6565(19)	3705(15)	3425(11)	93(7)*
F(5)	5619(10)	3781(7)	3238(5)	113(4)*

Table 5.59 / cont.

F(6)	7104(11)	4333(9)	3441(6)	136(5)*
F(7)	6600(17)	3268(13)	3905(9)	202(8)*
F(8)	7076(14)	3128(11)	3056(8)	171(6)*

* isotropic temperature factor.

$$U_{eq} = \tfrac{1}{3} \Sigma_i \Sigma_j U_{ij} a_i^* a_j^* (a_i . a_j)$$

Table 5.60 : Anisotropic thermal factors (Å^2 , x10^3) for
[Ag_2(μ-Ph_2Pbipy)$_2$(η^2-2,2′-bipy)]$(BF_4)_2$

	U(11)	U(22)	U(33)	U(23)	U(13)	U(12)
Ag(1)	58(1)	46(1)	50(1)	-2(1)	5(1)	4(1)
Ag(2)	53(1)	69(1)	75(1)	11(1)	0(1)	14(1)
P(1)	53(2)	44(2)	51(2)	-4(2)	-1(2)	3(2)
P(2)	55(2)	42(2)	53(2)	-4(2)	13(2)	-2(2)

5.6.28 Single crystal X-ray diffration study of $\{[Ag_2(\mu\text{-}Ph_2Pbipy)_2(\mu'\text{-}4,4'\text{-}bipy)](PF_6)_2\}_n$ [56]

A colourless, single block-shaped crystal was grown by the slow cooling of a hot, saturated dichloroethane solution of the complex. The general approach used for the intensity data collection is described in Appendix A. The crystallographic data are given in Table 5.61, the interatomic distances in Table 5.62, the interatomic angles in Table 5.63, the fractional coordinates in Table 5.64 and the anisotropic thermal parameters in Table 5.65. The observed and calculated structure factors may be found on microfiche in an envelope fixed to the inside back cover.

Table 5.61

Crystal data and details of the crystallographic analysis for $\{[Ag_2(\mu\text{-}Ph_2Pbipy)_2(\mu'\text{-}4,4'\text{-bipy})](PF_6)_2\}_n$

Formula	$Ag_2C_{54}H_{42}N_6P_4F_{12}$
Molecular Mass	1342.58
Crystal System	Triclinic
Space Group	$P\bar{1}$
a(Å)	9.670(2)
b(Å)	10.730(2)
c(Å)	13.162(3)
α(°)	89.65(2)
β(°)	78.17(1)
γ(°)	84.79(2)
V($Å^3$)	1332.31
Z	1
D_c($g.cm^{-3}$)	1.67
F(000)	670
λ(Mo-Kα)(Å)	0.71069
Scan mode	$\omega - 2\theta$
ω scan angle	$0.80 + 0.35\tan\theta$
Horizontal Aperture width (mm)	$2.7 + 0.1\tan\theta$
Scattering range (°)	$2 \leq \theta \leq 23$
μ (cm^{-1})	9.27
Absorption corrections	Semi empirical[103]
Measured intensities	3740
Unique intensities	3387
Unique intensities with [$I > 3\sigma(I)$]	3026
Structure solution	Direct & Fourier methods
Weighting scheme	$1/ (\sigma^2(F) + 0.00073F^2)$
$R = \Sigma(F_o-F_c)/\Sigma F_o$	0.038
$R_w = \Sigma_w\frac{1}{2} (F_o-F_c)/ \Sigma_w\frac{1}{2}F_o$	0.042
$(\Delta/\sigma)_{max}$	0.185
$\Delta\rho_{max}(eÅ^{-3})$	0.599
Number of parameters	328

Table 5.62 : Interatomic distances (Å) for $\{[Ag_2(\mu\text{-}Ph_2Pbipy)_2(\mu'\text{-}4,4'\text{-}bipy)](PF_6)_2\}_n$

Ag-P(1)	2.375(1)	Ag-N(3)	2.310(4)
Ag-N(1′)	2.373(3)	Ag-N(2′)	2.404(5)
P(1)-C(1)	1.828(3)	P(1)-C(7)	1.808(3)
P(1)-C(13)	1.834(5)	N(1)-C(13)	1.351(6)
N(1)-C(17)	1.344(6)	N(2)-C(18)	1.310(8)
N(2)-C(22)	1.335(7)	N(3)-C(23)	1.333(7)
N(3)-C(27)	1.346(7)	C(1)-C(2)	1.395(0)
C(1)-C(6)	1.395(0)	C(2)-C(3)	1.395(0)
C(3)-C(4)	1.395(0)	C(4)-C(5)	1.395(0)
C(5)-C(6)	1.395(0)	C(7)-C(8)	1.395(0)
C(7)-C(12)	1.395(0)	C(8)-C(9)	1.395(0)
C(9)-C(10)	1.395(0)	C(10)-C(11)	1.395(0)
C(11)-C(12)	1.395(0)	C(13)-C(14)	1.378(7)
C(14)-C(15)	1.390(8)	C(15)-C(16)	1.394(9)
C(16)-C(17)	1.385(8)	C(17)-C(18)	1.494(7)
C(18)-C(19)	1.409(8)	C(19)-C(20)	1.364(10)
C(20)-C(21)	1.398(12)	C(21)-C(22)	1.392(10)
C(23)-C(24)	1.366(7)	C(24)-C(25)	1.395(7)
C(25)-C(26)	1.396(7)	C(25)-C(25)	1.494(10)
C(26)-C(27)	1.378(7)	P(2)-F(1)	1.574(4)
P(2)-F(2)	1.595(4)	P(2)-F(3)	1.584(4)
P(2)-F(4)	1.551(4)	P(2)-F(5)	1.570(4)
P(2)-F(6)	1.573(4)		

Table 5.63 : Interatomic angles (°) for $\{[Ag_2(\mu\text{-}Ph_2Pbipy)_2(\mu'\text{-}4,4'\text{-}bipy)](PF_6)_2\}_n$

P(1)-Ag-N(3)	122.0(1)	Ag-P(1)-C(1)	108.0(1
N(1')-Ag-N(2')	70.2(1)	N(1')-Ag-P	118.7(1
N(1')-Ag-N(3)	118.2(2)	N(2')-Ag-P	118.6(1
N(2')-Ag-N(3)	90.6(2)		
Ag-P(1)-C(7)	118.2(1)	C(1)-P(1)-C(7)	104.6(2
Ag-P(1)-C(13)	113.6(2)	C(1)-P(1)-C(13)	106.0(2
C(7)-P(1)-C(13)	105.4(2)	C(13)-N(1)-C(17)	117.8(4
C(18)-N(2)-C(22)	119.1(5)	Ag-N(3)-C(23)	122.9(3
Ag-N(3)-C(27)	119.6(3)	C(23)-N(3)-C(27)	117.3(4
P(1)-C(1)-C(2)	117.6(1)	P(1)-C(1)-C(6)	122.2(1
C(2)-C(1)-C(6)	-11.1(0)	C(1)-C(2)-C(3)	-11.1(0
C(2)-C(3)-C(4)	-11.1(0)	C(3)-C(4)-C(5)	-11.1(0
C(4)-C(5)-C(6)	-11.1(0)	C(1)-C(6)-C(5)	-11.1(0
P(1)-C(7)-C(8)	122.5(1)	P(1)-C(7)-C(12)	117.1(1
C(8)-C(7)-C(12)	-11.1(0)	C(7)-C(8)-C(9)	-11.1(0
C(8)-C(9)-C(10)	-11.1(0)	C(9)-C(10)-C(11)	-11.1(0
C(10)-C(11)-C(12)	-11.1(0)	C(7)-C(12)-C(11)	-11.1(0
P(1)-C(13)-N(1)	115.0(4)	P(1)-C(13)-C(14)	121.6(4
N(1)-C(13)-C(14)	123.0(5)	C(13)-C(14)-C(15)	119.2(5
C(14)-C(15)-C(16)	118.0(6)	C(15)-C(16)-C(17)	119.5(5
N(1)-C(17)-C(16)	122.4(5)	N(1)-C(17)-C(18)	116.1(5
C(16)-C(17)-C(18)	121.5(5)	N(2)-C(18)-C(17)	118.0(5
N(2)-C(18)-C(19)	123.5(6)	C(17)-C(18)-C(19)	118.5(6
C(18)-C(19)-C(20)	117.3(8)	C(19)-C(20)-C(21)	120.0(7
C(20)-C(21)-C(22)	118.1(7)	N(2)-C(22)-C(21)	122.0(8
N(3)-C(23)-C(24)	124.1(5)	C(23)-C(24)-C(25)	119.2(5
C(24)-C(25)-C(26)	117.0(5)	C(25)-C(26)-C(27)	120.0(5
N(3)-C(27)-C(26)	122.3(5)	F(1)-P(2)-F(2)	90.0(2
F(1)-P(2)-F(3)	178.3(2)	F(2)-P(2)-F(3)	88.5(2
F(1)-P(2)-F(4)	90.5(2)	F(2)-P(2)-F(4)	179.1(3
F(3)-P(2)-F(4)	91.1(2)	F(1)-P(2)-F(5)	89.5(3
F(2)-P(2)-F(5)	89.2(3)	F(3)-P(2)-F(5)	89.8(2
F(4)-P(2)-F(5)	91.5(3)	F(1)-P(2)-F(6)	90.1(3
F(2)-P(2)-F(6)	88.1(3)	F(3)-P(2)-F(6)	90.6(3
F(4)-P(2)-F(6)	91.2(3)	F(5)-P(2)-F(6)	177.3(3

Table 5.64 : Fractional coordinates (x 10^4) and isotropic thermal factors ($Å^2$, x10^3) for $\{[Ag_2(\mu\text{-}Ph_2Pbipy)_2(\mu'\text{-}4,4'\text{-}bipy)](PF_6)_2\}_n$

	x/a	y/b	z/c	U_{eq}
Ag	10145	-285	8445	45
P(1)	8847(1)	1508(1)	9335(1)	37
N(1)	10175(4)	2279(4)	10800(3)	38(1)
N(2)	11006(5)	1515(5)	12597(3)	55(1)
N(3)	12018(4)	-127(4)	7060(3)	45(1)
C(1)	8020(3)	2430(3)	8409(2)	43(1)
C(2)	8720(3)	2378(3)	7370(2)	65(2)
C(3)	8085(3)	2980(3)	6618(2)	73(2)
C(4)	6749(3)	3636(3)	6905(2)	69(2)
C(5)	6049(3)	3688(3)	7944(2)	72(2)
C(6)	6685(3)	3086(3)	8696(2)	60(2)
C(7)	7401(3)	1274(3)	10409(2)	43(1)
C(8)	6773(3)	2228(3)	11115(2)	57(1)
C(9)	5558(3)	2037(3)	11855(2)	73(2)
C(10)	4971(3)	893(3)	11890(2)	77(2)
C(11)	5600(3)	-61(3)	11185(2)	75(2)
C(12)	6815(3)	130(3)	10444(2)	57(1)
C(13)	9955(5)	2552(5)	9839(4)	41(1)
C(14)	10638(6)	3449(5)	9228(4)	53(1)
C(15)	11615(7)	4098(6)	9600(5)	67(2)
C(16)	11823(7)	3839(6)	10600(5)	62(2)
C(17)	11073(5)	2945(5)	11178(4)	45(1)
C(18)	11256(6)	2637(6)	12254(4)	51(1)
C(19)	11629(8)	3581(8)	12860(5)	81(2)
C(20)	11770(9)	3280(10)	13844(6)	96(3)
C(21)	11545(8)	2076(10)	14214(5)	94(3)
C(22)	11160(7)	1218(8)	13557(5)	76(2)
C(23)	12704(6)	899(5)	6875(4)	50(1)
C(24)	13847(6)	1002(5)	6086(4)	47(1)
C(25)	14371(5)	-28(5)	5434(4)	41(1)
C(26)	13669(6)	-1111(5)	5630(4)	56(1)
C(27)	12522(6)	-1133(5)	6445(4)	56(1)
P(2)	7385(2)	5065(1)	13517(1)	51
F(1)	8324(5)	4308(4)	12562(3)	93(1)

Table 5.64 / cont.

F(2)	6897(5)	6092(4)	12750(3)	87(1)
F(3)	6411(5)	5845(4)	14457(3)	92(1)
F(4)	7868(6)	4082(4)	14271(3)	111(2)
F(5)	6097(5)	4321(4)	13410(4)	105(1)
F(6)	8658(5)	5853(5)	13582(4)	101(1)

$$U_{eq} = \frac{1}{3} \Sigma_i \Sigma_j U_{ij} a_i^* a_j^* (a_i . a_j)$$

Table 5.65 : Anisotropic thermal factors (Å^2 , x10^3) for
{[Ag_2(μ-Ph_2Pbipy)$_2$(μ′-4,4′-bipy)](PF_6)$_2$}$_n$

	U(11)	U(22)	U(33)	U(23)	U(13)	U(12)
Ag	48(1)	53(1)	31(1)	-1(1)	1(1)	-3(1)
P(1)	35(1)	48(1)	26(1)	2(1)	-4(1)	-4(1)
N(1)	34(2)	47(2)	31(2)	-5(2)	-6(2)	2(2)
N(2)	50(3)	85(4)	31(2)	-2(2)	-9(2)	-11(2)
N(3)	41(3)	52(3)	38(2)	2(2)	4(2)	-2(2)
C(1)	37(3)	53(3)	39(3)	3(2)	-9(2)	-7(2)
C(2)	73(4)	83(4)	37(3)	10(3)	-13(3)	-1(3)
C(3)	83(5)	86(5)	56(4)	19(3)	-29(4)	-6(4)
C(4)	73(5)	75(4)	66(4)	15(3)	-31(4)	-9(4)
C(5)	65(4)	79(4)	79(5)	17(4)	-32(4)	-3(3)
C(6)	49(4)	70(4)	64(4)	9(3)	-16(3)	-1(3)
C(7)	34(3)	66(3)	30(3)	3(2)	-5(2)	-6(2)
C(8)	50(3)	77(4)	37(3)	-6(3)	0(3)	5(3)
C(9)	45(4)	121(6)	47(4)	-1(4)	2(3)	9(4)
C(10)	44(4)	140(7)	46(4)	5(4)	0(3)	-15(4)
C(11)	51(4)	123(6)	57(4)	18(4)	-12(3)	-37(4)
C(12)	48(3)	84(4)	42(3)	11(3)	-11(3)	-21(3)
C(13)	36(3)	49(3)	35(3)	-4(2)	-2(2)	0(2)
C(14)	56(4)	53(3)	50(3)	3(3)	-5(3)	-11(3)
C(15)	69(4)	68(4)	64(4)	4(3)	-12(3)	-22(3)
C(16)	60(4)	66(4)	65(4)	-6(3)	-13(3)	-21(3)
C(17)	39(3)	53(3)	41(3)	-13(2)	-7(2)	1(2)
C(18)	39(3)	71(4)	44(3)	-16(3)	-9(2)	-3(3)
C(19)	83(5)	107(6)	59(4)	-32(4)	-32(4)	-8(4)
C(20)	100(6)	124(7)	69(5)	-22(5)	-31(5)	-12(5)
C(21)	85(5)	161(9)	42(4)	-16(5)	-29(4)	-9(5)
C(22)	62(4)	125(6)	43(4)	-4(4)	-13(3)	-5(4)
C(23)	48(3)	49(3)	46(3)	-4(2)	3(3)	-1(3)
C(24)	43(3)	45(3)	44(3)	-1(2)	8(2)	3(2)
C(25)	43(3)	44(3)	31(3)	-1(2)	0(2)	-1(2)
C(26)	58(4)	54(3)	47(3)	-11(3)	14(3)	-17(3)
C(27)	58(4)	53(3)	49(3)	-6(3)	9(3)	-9(3)
P(2)	60(1)	55(1)	40(1)	-1(1)	-11(1)	-4(1)
F(1)	101(3)	107(3)	61(2)	-19(2)	-4(2)	24(3)
F(2)	101(3)	85(3)	76(3)	14(2)	-28(2)	6(2)

Table 5.65 / cont.

F(3)	101(3)	93(3)	68(3)	-21(2)	14(2)	-7(2)
F(4)	159(5)	103(3)	71(3)	32(2)	-36(3)	13(3)
F(5)	101(3)	90(3)	130(4)	-23(3)	-27(3)	-30(3)
F(6)	76(3)	123(4)	112(4)	-6(3)	-27(3)	-36(3)

5.6.29 Single crystal X-ray diffraction study of $\{[Ag_2(\mu\text{-}Ph_2Pbipy)_2(\mu'\text{-}4,4'\text{-}bptz)](BF_4)_2\}_n$ [57]

A scarlet, prismatic crystal was grown by slow evaporation of a saturated dichloroethane solution of the complex. The general approach used for the intensity data collection is described in Appendix A. The crystallographic data are given in Table 5.66, the interatomic distances in Table 5.67, the interatomic angles in Table 5.68, the fractional coordinates in Table 5.69 and the anisotropic thermal parameters in Table 5.70. The observed and calculated structure factors may be found on microfiche in an envelope fixed to the inside back cover.

Table 5.66

Crystal data and details of the crystallographic analysis for $\{[Ag_2(\mu\text{-}Ph_2Pbipy)_2(\mu'\text{-}4,4'\text{-}bptz)](BF_4)_2\}_n$

Formula	$Ag_2C_{56}H_{42}N_{10}P_2B_2F_8$
Molecular Mass	1306.31
Crystal System	Monoclinic
Space Group	$P2_1/n$
a(Å)	12.593(4)
b(Å)	16.832(6)
c(Å)	18.126(5)
β(°)	104.62(4)
$V(Å^3)$	3681.05
Z	2
$D_c(g.cm^{-3})$	1.20
F(000)	1468
λ(Mo-Kα)(Å)	0.71069
Scan mode	$\omega - 2\theta$
ω scan angle	$0.46 + 0.35\tan\theta$
Horizontal Aperture width (mm)	$2.7 + 0.1\tan\theta$
Scattering range (°)	$2 \leq \theta \leq 23$
$\mu\ (cm^{-1})$	6.43
Absorption corrections	Semi empirical[103]
Measured intensities	5497
Unique intensities	4154
Unique intensities with $[I > 3\sigma(I)]$	2821
Structure solution	Direct & Fourier methods
Weighting scheme	$1/(\sigma^2(F) + 0.04701F^2)$
$R = \Sigma(F_o-F_c)/\Sigma F_o$	0.110
$R_w = \Sigma_w{}^{1/2}(F_o-F_c)/\Sigma_w{}^{1/2}F_o$	0.116
$(\Delta/\sigma)_{max}$	0.492
$\Delta\rho_{max}(eÅ^{-3})$	1.530
Number of parameters	238

Table 5.67 : Interatomic distances (Å) for $\{[Ag_2(\mu\text{-}Ph_2Pbipy)_2(\mu'\text{-}4,4'\text{-}bptz)_2](BF_4)_2\}_n$

Ag-P	2.379(5)	Ag-N(3)	2.39(2)
Ag-N(1′)	2.365(2)	Ag-N(2′)	2.374(3)
P-C(1)	1.79(2)		
P-C(7)	1.81(2)	P-C(13)	1.84(2)
N(1)-C(13)	1.33(2)	N(1)-C(17)	1.34(2)
N(2)-C(18)	1.36(2)	N(2)-C(22)	1.36(3)
N(3)-C(23)	1.31(3)	N(3)-C(27)	1.31(3)
N(4)-C(28)	1.36(3)	N(5)-C(28)	1.27(2)
N(4)-N(5′′)	1.36(2)	N(5)-N(4′′)	1.36(2)
N(5′′)-C(28′′)	1.27(3)	N(4′′)-C(28′′)	1.36(3)
C(1)-C(2)	1.43(3)	C(1)-C(6)	1.39(3)
C(2)-C(3)	1.43(4)	C(3)-C(4)	1.39(5)
C(4)-C(5)	1.35(4)	C(5)-C(6)	1.43(3)
C(7)-C(8)	1.37(3)	C(7)-C(12)	1.44(3)
C(8)-C(9)	1.38(3)	C(9)-C(10)	1.31(3)
C(10)-C(11)	1.44(3)	C(11)-C(12)	1.47(3)
C(13)-C(14)	1.36(3)	C(14)-C(15)	1.39(3)
C(15)-C(16)	1.35(3)	C(16)-C(17)	1.47(3)
C(17)-C(18)	1.44(3)	C(18)-C(19)	1.37(3)
C(19)-C(20)	1.45(3)	C(20)-C(21)	1.37(3)
C(21)-C(22)	1.43(3)	C(23)-C(24)	1.44(4)
C(24)-C(25)	1.32(3)	C(25)-C(26)	1.40(3)
C(25)-C(28)	1.48(3)	C(26)-C(27)	1.41(3)
B-F(1)	1.35(3)	B-F(2)	1.29(4)
B-F(3)	1.25(3)	B-F(4)	1.27(4)
F(3)-F(4)	1.55(5)		

Table 5.68 : Interatomic angles (°) for {[Ag$_2$(μ-Ph$_2$Pbipy)$_2$(μ'-4,4'-bptz)$_2$](BF$_4$)$_2$}$_n$

P-Ag-N(3)	115.0(4)	Ag-P-C(1)	116.4(7
N(1')-Ag-N(2')	69.8(5)	N(1')-Ag-N(3)	99.8(5
N(1')-Ag-P	144.8(4)	N(2')-Ag-N(3)	99.2(6
N(2')-Ag-P	107.8(5)		
Ag-P-C(7)	109.5(7)	C(1)-P-C(7)	100.1(9
Ag-P-C(13)	118.7(6)	C(1)-P-C(13)	105.6(9
C(7)-P-C(13)	104.2(9)	C(13)-N(1)-C(17)	120(2)
C(18)-N(2)-C(22)	119(2)	Ag-N(3)-C(23)	119(2)
Ag-N(3)-C(27)	119.8(14)	C(23)-N(3)-C(27)	121(2)
P-C(1)-C(2)	114(2)	P-C(1)-C(6)	123(2)
C(2)-C(1)-C(6)	122(2)	C(1)-C(2)-C(3)	120(2)
C(2)-C(3)-C(4)	113(3)	C(3)-C(4)-C(5)	130(4)
C(4)-C(5)-C(6)	116(3)	C(1)-C(6)-C(5)	119(2)
P-C(7)-C(8)	124(2)	P-C(7)-C(12)	115(2)
C(8)-C(7)-C(12)	121(2)	C(7)-C(8)-C(9)	121(2)
C(8)-C(9)-C(10)	121(2)	C(9)-C(10)-C(11)	124(2)
C(10)-C(11)-C(12)	115(2)	C(7)-C(12)-C(11)	118(2)
P-C(13)-N(1)	112.9(13)	P-C(13)-C(14)	123(2)
N(1)-C(13)-C(14)	124(2)	C(13)-C(14)-C(15)	119(2)
C(14)-C(15)-C(16)	119(2)	C(15)-C(16)-C(17)	121(2)
N(1)-C(17)-C(16)	117(2)	N(1)-C(17)-C(18)	122(2)
C(16)-C(17)-C(18)	121(2)	N(2)-C(18)-C(17)	114(2)
N(2)-C(18)-C(19)	123(2)	C(17)-C(18)-C(19)	123(2)
C(18)-C(19)-C(20)	118(2)	C(19)-C(20)-C(21)	118(2)
C(20)-C(21)-C(22)	120(2)	N(2)-C(22)-C(21)	121(2)
N(3)-C(23)-C(24)	121(2)	C(23)-C(24)-C(25)	119(2)
C(24)-C(25)-C(26)	120(2)	C(24)-C(25)-C(28)	122(2)
C(26)-C(25)-C(28)	118(2)	C(25)-C(26)-C(27)	118(2)
N(3)-C(27)-C(26)	121(2)	N(4)-C(28)-N(5)	127(2)
N(4)-C(28)-C(25)	114(2)	N(5)-C(28)-C(25)	119(2)
N(4)-C(28)-N(5)	127(2)	N(5)-N(4'')-C(28'')	116(2)
N(4'')-C(28'')-N(5'')	127(2)	N(4)-N(5'')-C(28'')	117(2)
F(1)-B-F(2)	113(3)	F(1)-B-F(3)	111(3)
F(2)-B-F(3)	121(4)	F(1)-B-F(4)	115(3)
F(2)-B-F(4)	116(4)	F(3)-B-F(4)	76(3)
B-F(3)-F(4)	53(2)	B-F(4)-F(3)	51(2)

Table 5.69 : Fractional coordinates (x 10^4) and isotropic thermal factors ($Å^2$, x10^3) for $\{[Ag_2(\mu\text{-}Ph_2Pbipy)_2(\mu'\text{-}4,4'\text{-}bptz)_2](BF_4)_2\}_n$

	x/a	y/b	z/c	U_{eq}
Ag	9566(1)	9595(1)	9231(1)	41
P	8026(4)	352(3)	9346(3)	38(1)
N(1)	8609(11)	336(8)	10877(8)	35(3)
N(2)	10468(13)	398(10)	12085(9)	52(4)
N(3)	9429(14)	-1804(9)	9411(9)	51(4)
N(4)	9499(16)	-4762(10)	9269(11)	67(5)
N(5)	10292(15)	-4452(10)	10573(11)	63(5)
C(1)	7981(16)	1373(12)	9054(12)	53(5)*
C(2)	8348(18)	1510(14)	8386(13)	63(6)*
C(3)	8307(28)	2298(21)	8080(20)	110(10)*
C(4)	7951(28)	2864(21)	8516(21)	115(10)*
C(5)	7737(22)	2791(16)	9200(16)	81(7)*
C(6)	7702(18)	1994(13)	9470(12)	61(5)*
C(7)	6772(16)	-12(12)	8667(11)	47(5)*
C(8)	6035(17)	460(13)	8146(12)	60(5)*
C(9)	5131(18)	135(14)	7607(13)	62(6)*
C(10)	4995(19)	-635(14)	7550(14)	68(6)*
C(11)	5707(21)	-1202(16)	8052(15)	78(7)*
C(12)	6654(17)	-860(14)	8643(13)	63(6)*
C(13)	7705(15)	358(12)	10275(11)	46(4)*
C(14)	6651(18)	330(13)	10336(13)	60(5)*
C(15)	6500(19)	289(13)	11066(13)	62(6)*
C(16)	7395(20)	347(14)	11685(14)	69(6)*
C(17)	8521(14)	354(11)	11597(10)	41(4)*
C(18)	9487(14)	336(11)	12258(10)	41(4)*
C(19)	9416(17)	243(12)	12996(12)	56(5)*
C(20)	10433(21)	152(16)	13614(15)	74(7)*
C(21)	11421(18)	240(13)	13443(13)	63(6)*
C(22)	11431(19)	336(14)	12662(14)	68(6)*
C(23)	9549(20)	-2286(15)	8873(15)	72(7)*
C(24)	9627(20)	-3129(16)	8999(15)	78(7)*
C(25)	9628(16)	-3411(13)	9679(12)	52(5)*
C(26)	9436(19)	-2896(14)	10236(14)	69(6)*
C(27)	9343(18)	-2077(14)	10067(13)	66(6)*

Table 5.69 / cont.

C(28)	9822(15)	-4262(11)	9880(11)	42(4)*
B	7406(21)	-5217(15)	10766(15)	54(6)*
F(1)	6294(15)	-5283(15)	10488(11)	145(8)
F(2)	7898(20)	-5177(36)	10230(18)	388(26)
F(3)	7669(26)	-4768(29)	11334(23)	279(17)
F(4)	7849(32)	-5676(30)	11327(27)	299(19)
O(1)	6476(16)	-3124(10)	9022(14)	104(6)
O(2)	8829(18)	-1968(12)	12005(11)	108(6)
O(3)	4412(26)	1839(20)	-160(20)	187(12)*

* isotropic temperature factor.

$$U_{eq} = \frac{1}{3} \Sigma_i \Sigma_j U_{ij} a_i^* a_j^* (a_i . a_j)$$

Table 5.70 : Anisotropic thermal factors (Å^2 , x10^3) for
{[Ag_2(μ-Ph_2Pbipy)$_2$(μ′-4,4′- bptz)$_2$](BF_4)$_2$}$_n$

	U(11)	U(22)	U(33)	U(23)	U(13)	U(12)
Ag	47(1)	39(1)	39(1)	-1(1)	15(1)	2(1)
P	46(3)	35(2)	34(2)	1(2)	11(2)	5(2)
N(1)	38(8)	33(8)	34(7)	1(6)	11(6)	3(6)
N(2)	55(10)	62(10)	38(8)	0(8)	11(7)	2(9)
N(3)	70(11)	27(8)	57(11)	-7(7)	21(9)	-7(8)
N(4)	80(13)	48(11)	73(13)	5(10)	22(11)	5(10)
N(5)	74(13)	38(11)	73(13)	-4(9)	16(10)	6(8)
F(1)	94(12)	262(28)	80(11)	13(14)	24(9)	-39(14)
F(2)	82(16)	933(107)	173(27)	-163(45)	74(17)	-89(31
F(3)	139(22)	421(59)	235(35)	-233(41)	-13(23)	-3(32)
F(4)	203(33)	372(55)	272(46)	203(46)	-12(30)	-79(39)
O(1)	107(14)	49(10)	169(20)	-5(12)	60(14)	5(9)
O(2)	146(18)	106(14)	90(13)	20(12)	65(13)	51(13)

APPENDIX A : GENERAL EXPERIMENTAL DETAILS

A.1 Instrumentation

Carbon, hydrogen and nitrogen analyses were performed by the Microanalytical Laboratory of the Chemistry Department at the University of Natal in Pietermaritzburg and by Analytische Laboratorien, Gummersbach, Germany.

All infra-red spectra were recorded as KBr disks(unless otherwise specified) on a Shimadzu Fourier-Transform IR 4300 spectrometer.

$^{31}P\{^{1}H\}$ nmr spectra were recorded locally on a Varian FT-80A spectrometer and at the University of Sussex (Mols) using a multinuclear Bruker 200MHz spectrometer. ^{1}H nmr spectra were recorded on a Gemini 200MHz spectrometer. Deuterated solvents were employed in all cases.

A.2 Experimental techniques

All reactions, unless otherwise stated, were performed under an atmosphere of dry dinitrogen using standard Schlenk techniques.

Solvents

The solvents were freshly distilled and dried before use using standard procedures [196] except for propionitrile and 1-butanol which were used in Analar Grade purity without further purification.

Photochemical cell

The ultraviolet reactor consisted of a halogen 580W lamp encased in an evacuated quartz tube. No external cooling was provided since is was necessary to harness the full intensity of radiation.

A.3 Crystal structure determinations

Data collection

The intensities of the reflections were measured at 22°C with an Enraf-Nonius CAD-4 diffractometer using graphite monochromated Mo-K_α radiation.

Cell constants were obtained by fitting the setting angles of 25 high-order reflections($\theta > 12°$). Three standard reflections were measured every hour to check on any possible decomposition of the crystal. An ω-2θ scan with a variable speed up to a maximum of 5.49° .min^{-1} was used. The ω-angle changed as $a_\omega + b_\omega\tan\theta$(°), the horizontal aperture as $a_h + b_h\tan\theta$(mm), but was limited to the range 1, 3-5, 9mm. The vertical slit was fixed at 4mm. Optical values of a_ω, b_ω, a_h and b_h were determined for each crystal by a critical evaluation of peak shape for several reflections with different of θ using the program OTPLOT (Omega-Theta plot; Enraf-Nonius diffractometer control program, 1988D). Where applicable, a linear decay correction was applied using the mean value of linear curves fitted through three intensity control reflections, measured at regular time intervals. Data were corrected for Lorentz and polarisation effects and where possible absorption by the psi-scan (empirical) method.[197]

Structural solution and refinement

Direct methods or the Patterson function were used to solve the phase problem. Once a suitable phasing model was found, succesive applications of Fourier and difference Fourier techniques allowed the location of the remaining non-hydrogen atoms. In general, hydrogen atoms were not located but, where the location of a hydrogen atom was particularly important, a difference Fourier, calculated with the low angle reflections weighted relative to the high angle reflections, was employed. Weighted full-matrix least-squares methods were always used to refine the structure; the weighting scheme was chosen so as to find the smallest variation of the mean value of $\omega(F_o-F_c)^2$ as a function of the magnitude of F_o. R, R_w and the weighting scheme are defined as follows:

$$R = \frac{\Sigma|F_o - F_c|}{\Sigma|F_o|} \qquad R_w = \frac{\Sigma_{\omega}\tfrac{1}{2}|F_o - F_c|}{\Sigma_{\omega}\tfrac{1}{2}|F_o|}$$

$$\omega = 1/[\sigma^2 F + gF^2]$$

Scattering factor data were taken from reference 198. For all these calculations, the programs SHELX-76 [199] and SHELX-86 [200] were employed. The crystal structures were plotted using the program ORTEP [201] while the tabulation of the inter-atomic bond distances and angles, the fractional coordinates and the thermal parameters was achieved using the program TABLES.[202]

APPENDIX B : SOURCES OF CHEMICALS

B.1 Commercially available chemicals

The following chemicals and solvents were all purchased from the indicated supplier and, except for the solvents, were all used without further purification.

(i) Chemicals obtained from **Fluka AG**:

Silver acetate, silver hexafluorophosphate, silver tetrafluoroborate, silver perchlorate (monohydrate), $RuCl_3.xH_2O$, 4-cyanopyridine, 4-vinylpyridine, 2-aminopyridine, CH_3I, 2,6-dimethylphenyl isocyanide, benzonitrile, 2-chloroquinoline, pyrazole.

(ii) Chemicals obtained from **British Drug Houses Ltd.**:

absolute ethanol, methanol, diethyl ether, AR acetone.

(iii) Chemicals obtained from **E.Merck**:

silver nitrate, ammonium hexafluorophosphate, CD_3OD, acetone-d_6, CD_2Cl_2, $CDCl_3$, silver benzoate, NaH(80% in paraffin).

(iv) Chemicals obtained from **Strem Chemicals**:

$TlPF_6$, $Ru_3(CO)_{12}$, $ClPPh_2$, dppm, 2,2′-bipy.

(v) Chemicals obtained from **Holpro Analytics Pty Ltd.**:

formic acid, glacial acetic acid, propionic acid.

(vi) Chemicals obtained from **Riedel de Haen**:

Propionitrile, 1-butanol, tetrahydrofuran.

(vii) Chemicals obtained from **SAARchem.**:

P_2O_5, $MnCl_2.6H_2O$, $CoCl_2.4H_2O$, Li metal, $MgSO_4$, KNO_3, KCN, CuI, pyridine, $POCl_3$, PCl_5, $K_3[Fe(CN)_6]$, Na metal, KBr, acetonitrile.

(viii) Chemicals obtained from **Aldrich Chemical Company Inc.**:

1,5-cyclo-octadiene, $LiC{\equiv}CPh$ (0.1M in thf), $Bu_4NCl.xH_2O$, $Bu_4NBr.xH_2O$, Bu_4NI, Bu_4NSCN, 2-bromopyridine, 2,3-bis(2-pyridyl)pyrazine, 1,10-phenanthroline.

(ix) Chemicals obtained from **Janssen Chimica**:

pyrido-[2,3-b]pyrazine.

(x) Chemicals obtained from **PGM Chemicals**:

$Ru_3(CO)_{12}$.

B.2 Chemicals synthesised by published methods

The following chemicals were synthesised by literature methods:

$[Ru_2(\mu\text{-}Cl)_2(Cl)_2(CO)_6]$ [152], $[Ag(C{\equiv}CPh)]_n$ [182], $[Ag(CNXylyl)_3]^+$ [180] and 2,2′-bptz [203]. 4,4′-bptz was synthesised by adaption of a method used by Case *et al.*[204] to synthesise 2,2′-bptz. Sodium pyrazolate was prepared by reacting equivalent amounts of pyrazole and NaH in thf. Reduction of the solvent volume and addition of diethyl ether precipitated the white solid at -25°C.

Sodium benzophenone ketyl solution was prepared in inert, anhydrous conditions under reflux in thf. Dry syringes were used to transfer aliqouts of the solution to the reaction vessels under nitrogen.

$[Ag(1,5\text{-}cod)_2](X)$ ($X = BF_4$, PF_6 and ClO_4) was synthesised, using the appropriate silver(I) salt, by adaption of the procedure by Albinati *et al.*[167]

In all preparations of silver complexes, the appropriate salt of $[Ag_2(\mu\text{-}Ph_2Pbipy)_2(NCMe)_2]^{2+}$ was utilised, usually prepared from the corresponding $[Ag(1,5\text{-}cod)_2]^+$ salt.

APPENDIX C : PUBLICATION LIST

The following is a list of publications and proceedings which have emerged as a result of work carried out during this project.

1. J.S Field, R.J.Haines, C.J.Parry and S.H.Sookraj; Synthesis and molecular structure of the potentially binucleating tridentate ligand 6-diphenylphosphino-2,2′-bipyridine; *S. Afr. J. Chem.*,1993, **46**, 70.
2. J.S.Field, R.J.Haines, C.J.Parry and S.H.Sookraj; Dicopper(I) complexes of the novel phophorusbipyridyl ligand 6-diphenylphosphino-2,2′-bipyridine; *Polyhedron*, 1993, **12**, 2425.
3. J.S.Field, R.J.Haines, C.P.Kubiak, C.J.Parry, S.Reiser, S.Sookraj and R.E.Wittrig; Development of homogenous electrocatalysts based on copper for the reduction of carbon dioxide; Special publication No. 131, Proceeding of the first international conference on the Chemistry of the Copper and Zinc Triads, University of Edinburgh, Scotland. Page 160.

REFERENCES

1. F.A.Cotton and G.Wilkinson in *'Advanced Inorganic Chemistry'*, Fifth Ed., John Wiley and sons, USA (1988).

2a). See, for example, *'Comprehensive Organometallic Chemistry'*, E.W.Abel, F.G.A.Stone, G.W.Wilkinson (Ed) , Pergamon, Oxford (1982).

b). H.B.Kagan, *ibid*, Volume 8, Pergamon, Oxford (1982), 466.

3. J.A.Osborn, F.H.Jardine, J.F.Young, G.Wilkinson, *J.Chem.Soc.(A)*1966, 1711.

4. G.W.Parshall, *Acc. Chem. Res.*, 1970, **3**, 139; 1975, **8**, 113.

5. D.M.A.Minahan, W.E.Hill, C.A.McAuliffe, *Coord. Chem. Rev.*, 1984, **55**, 31.

6. C.A.McAuliffe and W.A.Levason in *'Phosphine, Arsine and Stibine Complexes of the Transition Elements'*, Elsevier, Amsterdam, 1979.

7. R.J.Puddephatt, *Chem. Soc. Rev.*, 1983, 12(2), 99.

8. M.G.B. Drew, A.P.Wolters, I.B.Tomkins, *J. Chem. Soc. Dalton Trans.*, 1977, 974.

9. Lj. Manojlovic-Muir, K.W.Muir, *J. Organomet.Chem.*, 1981, **219**, 129.

10. M.M.Olmstead, C-L.Lee. A.L.Balch, *Inorg. Chem.*, 1982, **21**, 2712.

11. C.Ercolani, J.V.Quagliano, L.M.Vallarino, *Inorg. Chim. Acta.*, 1973, 7, 413.

12. K.K.Chow, C.A.McAuliffe, *Inorg. Chim. Acta.*, 1974, **10**, 195.

13. W.Levason, C.A.McAuliffe, F.P McCullough, *Inorg. Chem.*, 1977, **16**, 2911.

14. J.A.Connor, J.P.Day, E.M.Jones, G.K.McEwen, *J. Chem. Soc. Dalton Trans.*, 1973, 347.

15. D.M.McEwan, P.G.Pringle, B.L.Shaw, *J. Chem. Soc. Chem. Commun.*, 1982, 1240.

16. G.R.Cooper, A.T.Hutton, C.R.Langrick, D.M.McEwan, P.G.Pringle, B.L.Shaw, *J.Chem Soc. Dalton Trans.*, 1984, 855.

17. S.J. Cooper, M.P.Brown, R.J.Puddephatt, *Inorg. Chem.*, 1981, **20**, 1374.

18. M.P.Brown, R.J.Puddephatt, M.Rashidi, K.R.Seddon, *J. Chem. Soc. Dalton Trans.*, 1977, 951.

19. A.F.M.J.Van der Ploeg, G.Van Koten, *Inorg. Chim. Acta.*,1981, **51**, 225.

20. K-K.Cheung, T-F.Lai, K-S.Mok, *J.Chem. Soc.(A)* 1971, 1644.

21. F.Glockling, F.J.Ivan Pollock, *J. Chem. Soc. Dalton Trans.*, 1975, 2259.

22. C-L.Lee, C.T.Hunt, A.L.Balch, *Inorg. Chem.*, 1981, **20**, 2498.

23. R.J.Puddephatt, M.A.Tomson, Lj.Manojlovic-Muir, K.W.Muir, A.A.Frew, M.P.Brown, *J. Chem. Soc. Chem. Commun.*, 1981, 805.

24. C-M.Che, H-L.Kwong, V.W-W.Yam, K-C.Cho, *J. Chem. Soc. Chem Commun.*, 1989, 885.

25. S.Al-Baker, W.E.Hill, C.A.McAuliffe, *J. Chem. Soc. Dalton Trans.*, 1985, 2655.

26. E.W.Stern, P.K.Maples, *J. Catal.*, 1972, **27**, 120.

27. M.C.Grossel, M.P.Brown, C.D.Nelson, A.Yavari, E.Kallas, R.P.Moulding, K.R.Seddon, *J. Organomet. Chem.*, 1982, **232**, C13.

28. D.M.Ho, R.Bau, *Inorg. Chem.*, 1983, **22**, 4073.

29. A.L.Balch, *J. Am. Chem. Soc.*, 1976, **98**, 8049.

30. J.T.Mague, S.H.de Vries, *Inorg. Chem.*, 1980, **19**, 3743.

31. P.G.Pringle, B.L.Shaw, *J. Chem. Soc. Chem. Commun.*, 1982, 581.

32. R.J.Puddephatt, M.A.Tomson, *J. Organomet. Chem.*, 1981, **238**, 231.

33. A.L.Balch, C.T.Hunt, C-L.Lee, M.M.Olmstead, J.P.Farr, *J. Am. Chem. Soc.*, 1981, **103**, 3764.

34. M.P.Brown, R.J.Puddephatt, M.Rashidi, K.R.Seddon, *J. Chem. Soc. Dalton Trans.*, 1978, 1540.

35. A.R.Sanger, *J. Chem. Soc. Dalton Trans.*, 1981, 228.

36. L.B.Anderson, T.J.Barder, R.A.Walton, *Inorg. Chem.*, 1985, **24**, 1421.

37. K.G.Caulton, P.Adair, *J. Organomet. Chem.*, 1976, **114**, C11.

38. A.L.Balch, L.S.Benner, *J. Organomet. Chem.*,1977, **135**, 339.

39. L.S.Benner, M.M.Olmstead, A.L.Balch, *J. Organomet. Chem.*, 1978, **159**, 289.

40. L.B.Anderson, F.A.Cotton, K.R.Dunbar, L.R.Falvello, A.C.Price, A.H.Reid, R.A.Walton, *Inorg. Chem.*, 1987, **26**, 2717.

41. W.Levason, C.A.McAuliffe, *Adv. Inorg. Chem. Radiochem.*, 1972, **14**, 173.

42. D.M.A.Minahan, W.E.Hill, C.A.McAuliffe, *Coord. Chem. Rev.*, 1984, **55**, 31.

43. M.W.Anker, R.Colton, I.B.Tomkins, *Aust. J. Chem.*, 1968, **21**, 1143.

44. R.B.King, A.Efraty, *Inorg. Chem.*, 1969, **8**, 2374.

45. J.Chatt, R.S.Coffey, *J.Chem. Soc.(A)* 1969, 1963.

46. C.A.McAuliffe, D.W.Meek, *Inorg. Chem.*, 1969, **8**, 904.

47. G.J.Palenik, M.Mathew, W.L.Steffen, G.Beran, *J. Am. Chem. Soc.*, 1975, **97**, 1059.

48. A.R.Sanger, *J. Chem. Soc. Dalton Trans.*, 1977, 1971.

49. F.Cariati, L.Naldini, *Gazz. Chim. Ital.*, 1965, **95**, 3.

50. A.Sacco, R.Ugo, *J. Chem. Soc.(London)*, 1964, 3274.

51.W.Hieber, A.Zeidler, *Z. Anorg. Allg. Chem.*, 1964, **329**, 92.

52. J.Chatt, H.R.Watson, *Proc. Chem. Soc.(London),* 1961,4980.

53. J.Chatt, G.Booth, *J. Chem. Soc.(A)* 1969, 2131.

54. A.V.Butcher, J.Chatt, *J.Chem. Soc.(A)* 1970, 2652.

55a) J.Chatt, R.G.Hayter, *Proc. Chem. Soc.(London)*, 1961, 896.

b) J.Chatt, R.G.Hayter, *ibid.*, 1961, 2605.

c) J.Chatt, R.G.Hayter, *ibid.*, 1963, 6017.

56. R.J.Haines, A.L.DuPreez, *J. Organomet. Chem.*, 1970, **21**, 181.

57. C.A.McAuliffe, R.V(D).Parish, P.D.Randall, *J. Chem. Soc. Dalton Trans.*, 1979, 1730.

58. F.A.Cotton, G.G.Stanley, R.A.Walton, *Inorg. Chem.*, 1978, **17**, 2099.

59. N.Kuhn, M.Winter, *J. Organomet. Chem.*, 1982, **229**, C33.

60. M.S.Balakrishna, V.Sreenivasa Reddy, S.S.Krishnamurthy, J.F.Nixon, J.C.T.R. Burckett St Laurent, *Coord. Chem. Rev.*, 1994, **129**, 44.

61. D.S.Payne, J.A.A. Mokuolu, J.C.Speakman, *J. Chem. Soc. Chem. Commun.*, 1965, 599.

62. T.K.Prakasha in his Ph.D Thesis, Indian Institute of Science, Bangalore, 1990.

63. J.Ellerman, K.Geibel, L.Mader, M.Moll, *Chem. Ber.*, 1981, **114**, 2322.

64. H.Schmidbaur, F.E.Wagner, A. Wohlleben-Hammer, *Chem. Ber.*, 1979, **112**, 496.

65. J.Ellerman, F.A.Knoch, K.J.Meier, *Z. Naturforsch., Teil B.*, 1990, **45**, 1657.

66. J.Ellerman, K.J.Meier, *Z Anorg. Allg. Chem.*, 1991, **603**, 77.

67. J.Ellerman, E.F.Hohenberger, W.Kehr. A.Puerzer, G.Thiele, *Z Anorg. Allg. Chem.*, 1980, **464**, 45.

68. R.Uson, J.Fornies, R.Navarro, M.Tomas, C.Fortuno, J.I.Cebollada, *Polyhedron,* 1989, **8**, 1045.

69a). G.de Leeuw, J.S.Field, R.J.Haines, B.McCulloch, E.Meintjies, C.Monberg, G.M.Olivier, P.Ramdial, C.N.Sampson, B.Sigwarth, N.D.Steen, K.G.Moodley, *J. Organomet. Chem.*, 1982, **228**, C66.

b).G.de Leeuw, J.S.Field, R.J.Haines, B.McCulloch, E.Meintjies, C.Monberg, G.M.Olivier, P.Ramdial, C.N.Sampson, B.Sigwarth, N.D.Steen, K.G.Moodley, *ibid.*,1984, **275**, 99.

c). D.W.Engel, K.G.Moodley, L.Subramony, R.J.Haines, *J. Organomet. Chem.*, 1988, **349**, 393.

70. D.R.Derringer, P.E.Fanwick, J.Moran, R.A.Walton, *Inorg. Chem.*, 1989, **28**, 1384.

71a). E.H.Wong, R.M.Ravanelle, E.J.Gabe, F.L.Lee, L.Prasad, *J. Organomet. Chem.*, 1982,

233, 321.

b). E.H.Wong, F.C.Bradley, E.J.Gabe, *J. Organomet. Chem.*, 1983, **244**, 235.

72. E.H.Wong, F.C.Bradley, L.Prasad, E.J.Gabe, *J. Organomet. Che.*, 1984, **263**, 167.

73. V.Riero, M.A.Ruiz, *J. Chem. Soc. Dalton Trans.*, 1986, 2617.

74. G.Bruno, S.Lo Schiavo, E.Rotondo, C.G.Arena, F.Faraone, *Organometallics.*, 1989, **8**, 886.

75. J.P.Farr, M.M.Olmstead, A.L.Balch, *Inorg. Chem.*, 1983, **22**, 1229.

76. M.M.Olmstead, A.Maissonet, J.P.Farr, A.L.Balch, *Inorg. Chem.*, 1981, **20**, 4060.

77. Z-Z.Zhang, H-K.Wang, Y-J.Shen, H-G.Wang, R.J.Wang, *J. Organomet. Chem.*, 1990, **381**, 45.

78. C.G.Arena, F.Faraone, M.Fochi, M.Lanfranchi, C.Mealli, R.Seeber, A.Tiripicchio, *J. Chem. Soc. Dalton Trans.*, 1992, 1847.

79. G.R.Newkome, *Chem. Rev.*, 1993, **93**, 2067.

80. A.Maissonet, J.P.Farr, M.M.Olmstead, C.T.Hunt, A.L.Balch, *Inorg. Chem.*, 1982, **21**, 3961.

81. H.J.Wasserman, D.C.Moody, R.T.Paine, R.R.Ryan, K.V.Salazar, *J. Chem. Soc. Chem. Commun.*, 1984, 533.

82. C.D.Landsberg, M.Sc. Thesis, University of Natal, Pietermaritzburg, 1993.

83. E.Lastra, M.Pilar Gamasa, J.Gimeno, M.Lanfranchi, A.Tiripicchio, *J Chem. Soc. Dalton Trans.*, 1989, 1499.

84. J.S.Field, R.J.Haines, P.Harden, C.J.Parry, unpublished work.

85. N.W.Alcock, P.Moore, P.A.Lampe, K.F.Mok, *J. Chem. Soc. Dalton Trans.*, 1982, 207.

86. J.P.Farr, M.M.Olmstead, C.T.Hunt, A.L.Balch, *Inorg. Chem.*, 1981, **20**, 1182.

87. J.P.Farr, M.M.Olmstead, F.E.Wood, A.L.Balch, *J. Am. Chem. Soc.*, 1983, **105**, 792.

88. Z-Z.Zhang, H-P.Xi, W-J.Zhao, K-Y.Jiang, R.J.Wang, H-G.Wang, *J. Organomet. Chem.*, 1993, **454**, 221.

89. W.S.Schauerte, M.Sc. Thesis, University of Natal, Pietermaritzburg, 1992.

90. J.S.Field, R.J.Haines, K.Lea, W.S.Schauerte, D.Wood, unpublished work.

91. E.C.Constable, *Adv. Inorg. Chem. Radiochem.*, 1986, **30**, 69; 1989, **34**, 1.

92. M.R.M.Bruce, E.Megehee, B.P.Sullivan, H.H.Thorp, T.R.O'Toole, A.Downard, J.R.Pugh, T.J.Meyer, *Inorg. Chem.*, 1992, **31**, 4864.

93. J.R.Pugh, M.R.M.Bruce, B.P.Sullivan, T.J.Meyer, *Inorg. Chem.*, 1991, **30**, 86.

94.C.M.Bollinger, N.Story, B.P.Sullivan, T.J.Meyer, *Inorg. Chem.*, 1988, **27**, 4582.

95. B.Durham, T.J.Meyer, *J. Am. Chem. Soc.*, 1978, **100**, 6286.

96. J.-M.Lehn, R.Ziessel, *J. Organomet. Chem.*, 1990, **382**, 157.

97. C.Kutal, A.J.Corbin, G.Ferraudi, *Organometallics*, 1987, **6**, 553.

98. R.Ziessel, *Tetrahedron Lett.*, 1989, **30**, 463.

99. F.H.Case, *J. Org. Chem.*, 1966, **31**, 2398.

100. J.S.Field, R.J.Haines, C.J.Parry, S.H.Sookraj, *Polyhedron*, 1993, **12**, 2425; C.J.Parry, S.H.Sookraj, unpublished work.

101. L.L.Merrit, E.D.Schroeder, *Acta Crystallogr.*, 1956, **9**, 801.

102. D.D.Perrin, W.L.F.Armarego, D.R.Perrin in '*Purification of Laboratory Chemicals*', 2nd Edn., Pergamon Press, New York, 1980.

103. A.C.T North, D.C.Philips, F.S.Mathews, *Acta Crystallogr.,Sect. A.*, 1968, **24**, 351.

104. R.Poilblanc, *Inorg. Chim. Acta,* 1982, **62**, 75.

105. B.R.Sutherland, M.Cowie,*Organometallics*, 1985, **4**, 1801.

106. T.G.Schenck, J.M.Downes, C.R.C.Milne, P.B.Mackenzie, H.Boucher, J.Whelan, B.Bosnich, *Inorg. Chem.*, 1985, **24**, 2334.

107. J.R.Moss, W.A.G.Graham, *J. Chem. Soc. Dalton Trans.*, 1977, 95.

108. H.A.Mirza, J.J.Vittal, R.J.Puddephatt, *Inorg. Chem.*, 1993, **32**, 1327.

109. S.F.Woollam in his Ph.D Thesis, University of Natal, Pietermaritzburg, 1991.

110. R.J.Haines in his review '*Binuclear complexes of Ruthenium and Osmium containing metal-metal bonds*' submitted for publication in '*Comprehensive Organometallic Chemistry*', Pergamon, Oxford, (1995).

111. W.W.Porterfield in ' *Inorganic Chemistry: A Unified approach*', 2nd Ed., Academic Press, California, 1993, 316.

112. M.A.Bennet, M.I.Bruce,T.W.Matheson in ' *Comprehensive Organometallic Chemistry*', F.G.A.Stone,E.W.Abel (Ed), Volume 4, Pergamon, Oxford, (1982), 651.

113. G.R.Crooks, B.F.G.Johnson, J.Lewis, I.G.Williams, G.Gamlen, *J. Chem. Soc., (A)*, 1969, 2761.

114. M.Bianchi, U.Matteoli, P.Ferdiani, F.Piacenti, M.Nardeli, G.Pelizzi, *Chem. Ind. (Milan).*, 1981, **63**, 475.

115. M.Bianchi, P.Ferdiani, U.Matteoli, G.Menchi, F.Piacenti, G.Pettrucci, *J. Organomet. Chem.*, 1983, **259**, 207.

116. D.S.Bohle, H.Vahrenkamp, *Inorg. Chem.*, 1990, **29**, 1097.

117. S.J.Sherlock, M.Cowie, E.Singleton, M.M.de V.Steyn, *Organometallics*, 1988, **7**, 1663.

118. E.Singleton, P.H.Van Rooyen, M.M.de V.Steyn, *S. Afr. J. Chem.*, 1989, **42**, 57.

119. R.W.Hilts, S.J.Sherlock, M.Cowie, E.Singleton, M.M.de V.Steyn, *Inorg. Chem.*, 1990, **29**, 3161.

120. W.G.Klemperer, B.Zhong, *Inorg. Chem.*, 1993, **32**, 5821.

121. A.J.Deeming, N.P.Randle, M.B.Hursthouse, R.J.Short, *J. Chem. Soc. Dalton Trans.*, 1987, 2473.

122. M.M.de V.Steyn in her Ph.D Thesis, University of South Africa, Pretoria, 1989.

123. J.G.Bullitt, F.A.Cotton, *Inorg. Chim. Acta*, 1971, **5**, 406.

124. M.Spohn, T.Vogt, J.Stahle, *Z. Naturforsch.*, 1986, **41B**, 1373.

125. H.Schumann, J.Opitz, J.Pickardt, *J. Organomet. Chem.*, 1977, **128**, 253.

126. M.Rotem, I.Goldberg, U.Schmueli, Y.Shvo, *J. Organomet. Chem.*, 1986, **314**, 185.

127. R.Mason, K.M.Thomas, D.F.Gill, B.L.Shaw, *J. Organomet. Chem.*, 1972, **40**, C67.

128. J.A.Cabeza, C.Landazuri, L.A.Oro, A.Tiripicchio, M.Tiripicchio-Camellini, *J. Organomet. Chem.*, 1987, **322**, C16.

129. S.J.Sherlock, M.Cowie, E.Singleton, M.M.de V.Steyn, *J. Organomet. Chem.*,1989, **361**, 353.

130. M.M.de V.Steyn, E.Singleton, S.Hietkamp, D.C.Liles, *J. Chem. Soc. Dalton Trans.*, 1990, 2991.

131. K-B.Shiu, W-N.Guo, S-M.Peng, M-C.Cheng, *Inorg. Chem.*, 1994, **33**, 3010.

132. K-B.Shiu, S-M.Peng, M-C.Cheng, *J. Organomet. Chem.*, 1993, **452**, 143.

133. G.G.Christoph, Y-B.Koh, *J. Am. Chem. Soc.*, 1974, **101**, 1422.

134. B.R.Sutherland, M.Cowie, *Organometallics*, 1984, **3**, 1869.

135.A.A.Chalmers, D.C.Liles, E.Meintjies, H.E.Oosthuizen, J.A.Pretorius, E.Singleton, *J. Chem. Soc.Chem. Commun.*, 1985, 1340.

136. C.J.Parry, F.A.Ajulu, Unpublished work, 1994.

137. M.-N.Collomb-Dunand-Sauthier, A.Deronzier, R.Ziessel, *J. Chem. Soc. Chem. Commun.*, 1994, 189.

138. A.L.Balch in '*Heterogenous Catalysis with Metal Phosphine complexes*', L.H.Pignolet (Ed.), Plenum Press, New York, 1983, page 167.

139. A.R.Sanger in '*Heterogenous Catalysis with Metal Phosphine complexes*', L.H.Pignolet

(Ed.), Plenum Press, New York, 1983, page 216.

140. F.A.Cotton, B.E.Hanson, *Inorg. Chem.*, 1977, **16**, 3369.

141. G.Lavigne, J.-J. Bonnet, *Inorg. Chem.*, 1981, **20**, 2713.

142. G.Lavigne, N. Lugan, J.-J.Bonnet, *Nouv. J. Chem.*, 1981, **5**, 423.

143. J.T.Mague, J.P.Mitchener, *Inorg. Chem.*, 1972, **11**, 2714.

144. G.Smith, D.J.Cole-Hamilton, A.C.Gregory, N.G.Gooden, *Polyhedron*, 1982, **1**, 97.

145. B.F.G.Johnson, J.Lewis, M.V.Twigg, *J. Organomet. Chem.*, 1974, **67**, C75.

146. R.Huq, A.J.Poë, S. Chawla, *Inorg. Chim. Acta*, 1980, **38**, 121.

147. P.Yarrow, P.C.Ford, *J. Organomet. Chem.*, 1981, **214**, 115.

148. M.F.Desrosiers, D.A.Wink, R.Trautman, A.E.Friedman, P.C.Ford, *J. Amer. Chem. Soc.*, 1986, **108**, 1917.

149. R.E.Cobbledick, F.W.B.Einstein, R.K.Pomeroy, E.R.Spetch, *J. Organomet. Chem.*, 1980, **195**, 77.

150. D.J.Cane, W.A.G.Graham, L.Vancea, *Canad. J. Chem.*, 1978, **56**, 1538.

151. J.P.Collman, R.W.Roper, *J. Amer. Chem. Soc.*, 1965, **87**, 4008.

152. A.Mantovani, S. Cenini, *Inorg. Synth.*, 1976, **16**, 51.

153. E.Benedetti, G.Braca, G.Sbrana, F.Salvetti, B.Grassi, *J. Organomet. Chem.*, 1972, **37**, 361.

154. M.I.Bruce, F.G.A.Stone, *J. Chem. Soc.(A)*, 1967, 1238.

155. M.M.Taqui Khan, R.Mohiuddin, *Polyhedron*, 1983, **2**, 1247.

156. M.Cowie, S.K.Dwight, *Inorg. Chem.*, 1979, **18**, 1209.

157. C.R.Langrick, D.M.McEwan, P.G.Pringle, B.L.Shaw, *J. Chem. Soc. Dalton Trans.*, 1983, 2487.

158. D.M.McEwan, P.G.Pringle, B.L.Shaw, *J. Chem. Soc. Dalton Trans.*, 1982, 859.

159. J.P.Farr, M.M.Olmstead, N.M.Rutherford, F.E.Wood, A.L.Balch, *Organometallics*, 1983, **2**, 1758.

160. G.J.Kubas, *Inorg. Synth.*, 1979, **19**, 90.

161. S.H.Sookraj, Ph.D Thesis, University of Natal, 1994.

162. J.S.Field, R.J.Haines, U.Honrath, J.Sundermeyer, S.F.Woollam, *J. Organomet. Chem.*, 1990, **395**, C9.

163. D.W.Engel, J.S.Field, R.J.Haines, U.Honrath, E.C.Horsfield, J.Sundermeyer, S.F.Woollam, *J. Chem. Soc. Dalton Trans.*, in press.

164. Y.Inoguçhi, B.Milewski-Mahrla, D.Neugebauer, P.G.Jones, H.Schmidbaur, *Chem. Ber.*, 1983, **116**, 1487.

165. K.Nilsson, Å.Oskarsson, *Acta Chim. Scand.*, 1984, **38(A)**, 79.

166. K.Nilsson,Å.Oskarsson, *Acta Cim. Scand.*, 1982, **36(A)**, 605.

167. A.Albinati, S.V.Mielle, G.Carturan, *J. Organomet. Chem.*, 1979, **182**, 269.

168. R.Garth-Kidd, R.J.Goodfellow in '*Nmr and the Periodic Table*', R.K.Harris, B.E.Mann (Ed.), Academic Press, London, 1978, 258.

169. J.G.Verkade, J.A.Mosbo in '*Phophorus-31 nmr Spectroscopy in Stereochemical Analysis*', J.G.Verkade, L.D.Quin (Ed.), VCH Publishers inc., Deerfield Beach, Florida, 1987, Chapter 13, page 441.

170. C.Brevard, P.Granger in '*Handbook of High Resolution multinuclear nmr*', Wiley Interscience, New York, 1981.

171. E.L.Meutterties, C.W.Allegranti, *J. Amer. Chem. Soc.*, 1972, **94**, 6386.

172. F.M.J.Van der Ploeg, G.Van Koten, *Inorg. Chim. Acta*, 1981, **51**, 225.

173. A.A.M.Aly, D.Neugebauer, O.Orama, U.Schubert, H.Schmidbaur, *Angew. Chem., Int. Ed. (Engl.)*, 1978, **17**, 125.

174. M.Igarashi, M.Yamaha, *Bull. Chem. Soc. Japan*, 1956, **29**, 871.

175. J.S.Ogden, *J. Chem. Soc. Chem. Commun.*, 1971, 978.

176. W.W.Porterfield in '*Inorganic Chemistry: A Unified Approach*', 2nd Ed. Academic Pres California, 1993, 648.

177. F.Klages, K.Moenkemeyer, R.Heinle, *Chem. Ber.*, 1952, **85**, 109.

178. F.A.Cotton, F.Zingales, *J. Am. Chem. Soc.*, 1961, **83**, 351.

179. G.Minghetti, F.Bonati, M.Massoblio, *Inorg. Chem.*, 1975, **14**, 1974.

180. Y.Yamamoyo, K.Aoki, H.Yamazaki, *Inorg. Chim. Acta*, 1982, **68**, 75.

181. K.Nakamoto in '*Infra-red and Raman Spectra of Inorganic and Coordination compounds*', 3rd Ed., Wiley Interscience, New York, 1978.

182. S.J.Huang, V.Paneccasio, F.DiBattista, D.Picker, G.Wilson, *J. Org. Chem.*, 1975, **4** 125.

183. T.Yamaguchi, G.Johansson, B.Holmberg, M.Maeda, H.Ohtaki, *Acta Chim. Scand.* 1984, **38(A)**, 437.

184. H.J.Berthold, W.Ludwig, R.Wartchlow, *Z. Kristallogr.*, 1976, **144**, 116.

185. R.A.Stein, C.Knobler, *Inorg. Chem.*, 1977, **16**, 242.

186. R.F.Barrow, E.Morgan, C.V.Wright, *Proc. Chem. Soc.*, 1959, 303.

187. H.J.Stoklosa, J.R.Wasson, E.V.Brown, H.W.Richardson, W.E.Hatfield, *Inorg. Chem.*, 1973, **14**, 2378.

188. J.A.Zoltewicz, L.W.Deady, *Tetrahedron*, 1972, **28**, 1983.

189. R.J.Staniewicz, R.F.Sympson, D.G.Hendriker, *Inorg. Chem.*, 1977, **16**, 2166.

190. V.Balzani, F.Bolletta, N.T.Gondolfi, M.Maestri, *Top. Curr. Chem.*, 1978, **75**, 1.

191. S.Ernst, W.Kaim, *Angew. Chem. Int. Ed. (Engl.)*, 1985, **24**, 430.

192. W.Kaim, S.Kohlmann, *Inorg. Chem.*, 1990, **29**, 1898.

193. A.J.Blacker, J.Jazwinski, J.-M.Lehn, *Helv. Chim. Acta*, 1987, **70**, 1.

194. D.K.Smith, G.A.Lane, M.S.Wrighton, *J. Amer. Chem. Soc.*, 1986, **108**, 3522.

195. O.Schneider, M.Hanack, *Angew. Chem. Int. Ed. (Engl.)*, 1983, **95**, 804.

196. D.D.Perrin, W.L.F.Armarego, D.Perrin in '*Purification of Laboratory Chemicals*', Pergamon Press, Oxford, 1966.

197. A.C.T.North, D.C.Phillips, F.S.Mathews, *Acta Crystallogr., Sect A*, 1968, **24**, 351.

198. "*International Tables for X-ray Crystallography*', Kynoch Press, Birmingham, 1974, **4**, pp 99, 149.

199. G.M.Sheldrick, SHELX-76, Program for Crystal Structure Determination, University of Cambridge, 1976.

200. G.M.Sheldrick, SHELX-86, Program for Crystal Structure Determination, University of Göttingen, 1986.

201. C.K.Johnson, ORTEP-II, A Fortran Thermal-Ellipsoid Plot Program for Crystal Structure Illustrations, Oak Ridge National Laboratory, Tennessee, 1976.

202. D.C.Liles, TABLES, Program for Tabulation for Crystallographic data, Council for Scientific and Industrial Research (Pretoria), 1988.

203. J.F.Geldard, F.Lions, *J. Org. Chem.*, 1965, **30**, 318.

204. W.A.Butte, F.H.Case, *J. Org. Chem.*, 1961, **26**, 4690.